Scanning

Nuclear Scanning Optimization for Medical Applications

Lead Guest Editor: Danilo Pelusi
Guest Editors: S N Sivanandam and P. Vijayakumar

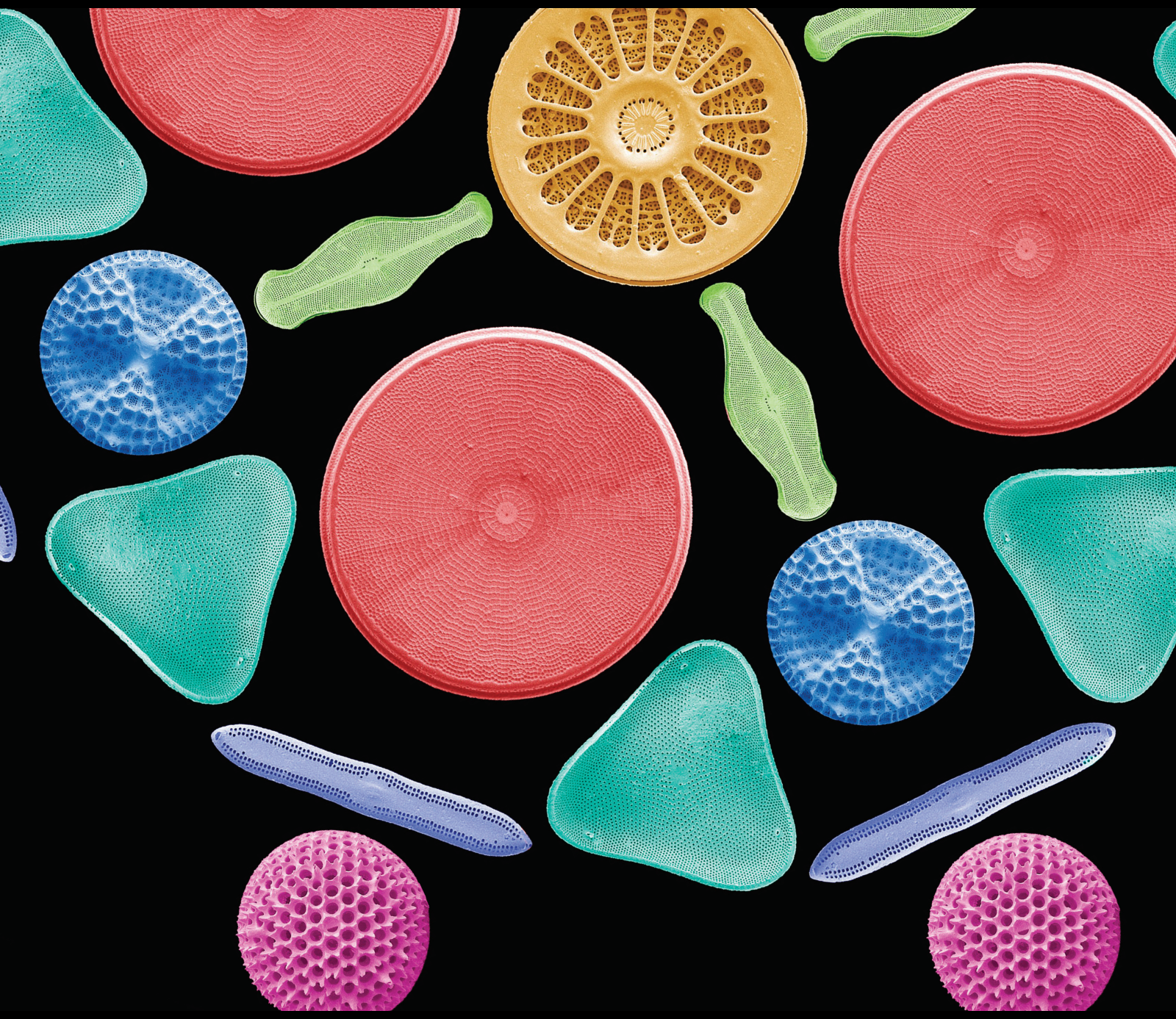

Nuclear Scanning Optimization for Medical Applications

Scanning

Nuclear Scanning Optimization for Medical Applications

Lead Guest Editor: Danilo Pelusi
Guest Editors: S N Sivanandam and P. Vijayakumar

Contents

Retracted: Diagnostic Value of Color Doppler Ultrasonography in Subacute Thyroiditis
Scanning
Retraction (1 page), Article ID 9801545, Volume 2023 (2023)

Retracted: Management Strategies and Imaging Observation of Early and Delayed Intelligent Treatment of Meniscus Sports Injury under Knee Osteoarthroscopy
Scanning
Retraction (1 page), Article ID 9795735, Volume 2023 (2023)

Retracted: Optimal Modeling and Simulation of the Relationship between Athletes' High-Intensity Training and Sports Injuries
Scanning
Retraction (1 page), Article ID 9784601, Volume 2023 (2023)

Retracted: Effect of Running Exercise on Brain Functional Magnetic Resonance Characteristics of College Students with Depression
Scanning
Retraction (1 page), Article ID 9782180, Volume 2023 (2023)

Retracted: 3D Convolutional Neural Network Framework with Deep Learning for Nuclear Medicine
Scanning
Retraction (1 page), Article ID 9765894, Volume 2023 (2023)

Retracted: Observation on the Effect of MRI Image Scanning on Knee Pain in Football Injury
Scanning
Retraction (1 page), Article ID 9760450, Volume 2023 (2023)

Retracted: Diagnostic Value of Endoscopic Narrow-Band Imaging Technique in Early Gastric Cancer and Precancerous Lesions
Scanning
Retraction (1 page), Article ID 9894170, Volume 2023 (2023)

Retracted: Clinical Analysis of Echocardiography and Serum IL-6 and TNF-α Changes in Pregnant Women with Hypertension
Scanning
Retraction (1 page), Article ID 9897839, Volume 2023 (2023)

Retracted: Effect of Rehabilitation Physical Training on PE Teaching Sports Injury under Ultrasonic Examination
Scanning
Retraction (1 page), Article ID 9879863, Volume 2023 (2023)

Retracted: Intervention of Fluency and Anxiety in Mindfulness Training of Shooting
Scanning
Retraction (1 page), Article ID 9871261, Volume 2023 (2023)

Contents

Retracted: Diagnostic Value of Spiral CT and Magnetic Resonance Imaging Scanning in Gastric Cancer and Precancerous Lesions
Scanning
Retraction (1 page), Article ID 9896178, Volume 2023 (2023)

Retracted: Unsupervised Hyperspectral Microscopic Image Segmentation Using Deep Embedded Clustering Algorithm
Scanning
Retraction (1 page), Article ID 9890786, Volume 2023 (2023)

Retracted: Predictive Model of Cerebral Vasospasm in Subarachnoid Hemorrhage Based on Regression Equation
Scanning
Retraction (1 page), Article ID 9872786, Volume 2023 (2023)

Retracted: Image Effect Observation of Acanthopanax senticosus on Antifatigue Activity after Exercise
Scanning
Retraction (1 page), Article ID 9869713, Volume 2023 (2023)

Retracted: Clinical Observation of MRI Image in Floating Needle Therapy for Cervical Spondylosis of Cervical Type
Scanning
Retraction (1 page), Article ID 9864261, Volume 2023 (2023)

Retracted: Clinical Characteristics and Mathematical Analysis of Curative Effect of Hemodialysis in Curing Poisoning Caused by Snakebite
Scanning
Retraction (1 page), Article ID 9862750, Volume 2023 (2023)

Retracted: Observation on the Effect of Rehabilitative Physical Training on Ice and Snow Sports Injury under Ultrasound Examination
Scanning
Retraction (1 page), Article ID 9857053, Volume 2023 (2023)

Retracted: Application of Scanning Magnetic Resonance Imaging in the Diagnosis of Prenatal Placental Implantation and Related Care
Scanning
Retraction (1 page), Article ID 9836370, Volume 2023 (2023)

Retracted: Exploring the Clinical Point Selection Rules of Acupuncture and Moxibustion in the Treatment of Infantile Enuresis Based on Data Mining Technology
Scanning
Retraction (1 page), Article ID 9835940, Volume 2023 (2023)

Contents

Retracted: Effect of Rehabilitation Training Based on Automatic Extraction Algorithm on Knee Anterior Cruciate Ligament Injury Caused by Exercise
Scanning
Retraction (1 page), Article ID 9765738, Volume 2023 (2023)

Retracted: Research and Implementation of Robot Vision Scanning Tracking Algorithm Based on Deep Learning
Scanning
Retraction (1 page), Article ID 9765484, Volume 2023 (2023)

Retracted: Application of Ultrasound Combined with Magnetic Resonance Imaging in the Diagnosis and Grading of Patients with Prenatal Placenta Accreta
Scanning
Retraction (1 page), Article ID 9859421, Volume 2023 (2023)

[Retracted] Evaluation of Pelvic Floor Dysfunction by Pelvic Floor Ultrasonography after Total Hysterectomy for Cervical Cancer
Dan-dan Liu, Jing Xin, Wei Liu, Yan-feng Zhang, and Peishan Li
Research Article (4 pages), Article ID 5914344, Volume 2022 (2022)

[Retracted] Sports Injury Risk Prevention and MRI Image Performance of Athletes in Physical Education
Jun Yang
Research Article (7 pages), Article ID 1166314, Volume 2022 (2022)

[Retracted] Diagnostic Value of Color Doppler Ultrasonography in Subacute Thyroiditis
Yonggang Chen, Shulan Zhu, Huabin Chen, Liting Yao, Jingmian Zhou, Yi Xu, Biqin Lin, and Xiaoping Chen
Research Article (7 pages), Article ID 7456622, Volume 2022 (2022)

[Retracted] Effect of Rehabilitation Physical Training on PE Teaching Sports Injury under Ultrasonic Examination
Wangda Li
Research Article (6 pages), Article ID 1470303, Volume 2022 (2022)

[Retracted] Application of Low-Dose CT and MRI in the Evaluation of Soft Tissue Injury in Tibial Plateau Fractures
Yinping Qi, Peipei He, Jianping Zhu, Yanan Wang, Hong Zhao, and Junbo Chen
Research Article (6 pages), Article ID 7686485, Volume 2022 (2022)

[Retracted] Optimal Modeling and Simulation of the Relationship between Athletes' High-Intensity Training and Sports Injuries
Youcheng Zhang and Yuanyuan Chang
Research Article (7 pages), Article ID 8447453, Volume 2022 (2022)

Contents

[Retracted] Changes of Volume Parameters in the Treatment of Graves Ophthalmopathy by Endoscopic Transethmoidal Decompression of the Orbital Inner Wall Combined with Fat Decompression
Weina Fu
Research Article (6 pages), Article ID 8149247, Volume 2022 (2022)

[Retracted] The Effect of CT Imaging Technology in the Diagnosis of Thoracic and Cardiac Surgery Diseases
Min Yang, Hongbo Qian, Dafa Zhang, and Yingjing Gui
Research Article (7 pages), Article ID 9385451, Volume 2022 (2022)

[Retracted] Influence of Comprehensive Nursing Intervention Combined with WeChat Platform Propaganda and Education of ERAS Concept on Postoperative Functional Recovery of Patients with Gallbladder Polyps
Yan Zhang, Dongmei Guo, Xiaocui Yang, Xiaojing Sun, Yajuan Dong, Jun Zhang, Yujiao Gao, Zhanhua Guo, Haikun Zhou, and Quanfu Li
Research Article (7 pages), Article ID 6919130, Volume 2022 (2022)

[Retracted] High-Intensity Injury Recognition Pattern of Sports Athletes Based on the Deep Neural Network
Nan Chen and Yang Zhang
Research Article (6 pages), Article ID 2794225, Volume 2022 (2022)

[Retracted] Sports Medical Image Modeling of Injury Prevention in Wushu Training
Yuanyuan Feng
Research Article (6 pages), Article ID 5201952, Volume 2022 (2022)

[Retracted] Observation on the Effect of Rehabilitative Physical Training on Ice and Snow Sports Injury under Ultrasound Examination
Yang Wang and Yongzhi Zhou
Research Article (7 pages), Article ID 2931686, Volume 2022 (2022)

[Retracted] Effect of Running Exercise on Brain Functional Magnetic Resonance Characteristics of College Students with Depression
Wangda Li and Jun Yang
Research Article (8 pages), Article ID 7558807, Volume 2022 (2022)

[Retracted] Effect of Foot and Hand Massage on Abdominal Pain of Cesarean Section Incision under Ultrasound Guidance
Yu Qing Wang, Rongrong Jiang, and Jianmin Pan
Research Article (7 pages), Article ID 8356256, Volume 2022 (2022)

[Retracted] Sports Medical Image Modeling of Injury Prevention in Dance Learning and Sports Training
Renying Fei
Research Article (7 pages), Article ID 7027007, Volume 2022 (2022)

Contents

[Retracted] Scanning Imaging Study of Patients with Parkinson's Disease Lower Urinary Tract Dysfunction Based on Linear Equation
Yong Liu, Jiasheng Han, Xuguang Guo, Lei Fang, and Ting Liu
Research Article (6 pages), Article ID 9506328, Volume 2022 (2022)

[Retracted] The Pathogenesis and Influencing Factors of Adult Hypertension Based on Structural Equation Scanning
Yaqiong Wu, Guangyu Ma, Nana Feng, Zhiqiang Zhang, Sijie Zhang, and Xingtao Li
Research Article (6 pages), Article ID 2663604, Volume 2022 (2022)

[Retracted] Observation on the Effect of MRI Image Scanning on Knee Pain in Football Injury
Weidong Yu
Research Article (6 pages), Article ID 7348978, Volume 2022 (2022)

[Retracted] Clinical Observation of MRI Image in Floating Needle Therapy for Cervical Spondylosis of Cervical Type
Xianqiang Liu, Zhenyi Tang, Botao Wang, and Yongshuai Chen
Research Article (10 pages), Article ID 1340192, Volume 2022 (2022)

[Retracted] Effect of Core Muscle Strength Training Combined with Taijiquan on Bone Mineral Density Measured by Quantitative CT Scanning in the Elderly
Mingliang Zhong
Research Article (7 pages), Article ID 6942081, Volume 2022 (2022)

[Retracted] Observation on the Effect of Shoulder Pain Caused by Volleyball Training Injury Based on MRI Image Scanning
Kesen Li and Nan Fu
Research Article (5 pages), Article ID 4368871, Volume 2022 (2022)

[Retracted] Diagnostic Value of Magnetic Resonance Susceptibility-Weighted Imaging Scanning in Different Types of Early Prostate Cancer
Ruihui Gao, Jiayuan Liu, and Hengcheng Zhu
Research Article (6 pages), Article ID 4884646, Volume 2022 (2022)

[Retracted] The Diagnostic Value of Scanning in the Injury of Triceps Crus of Volleyball Players
Jinfeng Zhao and Jianxin Liu
Research Article (7 pages), Article ID 2203065, Volume 2022 (2022)

[Retracted] Diagnostic Value of Spiral CT and Magnetic Resonance Imaging Scanning in Gastric Cancer and Precancerous Lesions
Yaolan Zhen, Qing Xie, and Lei Liu
Research Article (6 pages), Article ID 3627385, Volume 2022 (2022)

Contents

Hindawi
Scanning
Volume 2023, Article ID 9896168, 1 page
https://doi.org/10.1155/2023/9896168

Retraction

Retracted: Diagnostic Efficacy of CT Radiomic Features in Pulmonary Invasive Mucinous Adenocarcinoma

Scanning

Received 12 December 2023; Accepted 12 December 2023; Published 13 December 2023

This article has been retracted by Hindawi, as publisher, following an investigation undertaken by the publisher [1]. This investigation has uncovered evidence of systematic manipulation of the publication and peer-review process. We cannot, therefore, vouch for the reliability or integrity of this article.

Please note that this notice is intended solely to alert readers that the peer-review process of this article has been compromised.

Wiley and Hindawi regret that the usual quality checks did not identify these issues before publication and have since put additional measures in place to safeguard research integrity.

We wish to credit our Research Integrity and Research Publishing teams and anonymous and named external researchers and research integrity experts for contributing to this investigation.

The corresponding author, as the representative of all authors, has been given the opportunity to register their agreement or disagreement to this retraction. We have kept a record of any response received.

References

[1] A. Sheng, P. Zhou, Y. Ye, K. Sun, and Z. Yang, "Diagnostic Efficacy of CT Radiomic Features in Pulmonary Invasive Mucinous Adenocarcinoma," *Scanning*, vol. 2022, Article ID 5314225, 8 pages, 2022.

Hindawi
Scanning
Volume 2023, Article ID 9892518, 1 page
https://doi.org/10.1155/2023/9892518

Retraction

Retracted: Balance Analysis of Peripheral Neuropathy in Type 2 Diabetes Mellitus Based on Logistic Regression Equation

Scanning

Received 12 December 2023; Accepted 12 December 2023; Published 13 December 2023

This article has been retracted by Hindawi, as publisher, following an investigation undertaken by the publisher [1]. This investigation has uncovered evidence of systematic manipulation of the publication and peer-review process. We cannot, therefore, vouch for the reliability or integrity of this article.

Please note that this notice is intended solely to alert readers that the peer-review process of this article has been compromised.

Wiley and Hindawi regret that the usual quality checks did not identify these issues before publication and have since put additional measures in place to safeguard research integrity.

We wish to credit our Research Integrity and Research Publishing teams and anonymous and named external researchers and research integrity experts for contributing to this investigation.

The corresponding author, as the representative of all authors, has been given the opportunity to register their agreement or disagreement to this retraction. We have kept a record of any response received.

References

[1] L. Zhang, Q. Du, M. Yao, M. Wang, and B. Ge, "Balance Analysis of Peripheral Neuropathy in Type 2 Diabetes Mellitus Based on Logistic Regression Equation," *Scanning*, vol. 2022, Article ID 2113758, 7 pages, 2022.

Hindawi
Scanning
Volume 2023, Article ID 9876203, 1 page
https://doi.org/10.1155/2023/9876203

Retraction

Retracted: Diagnostic Value of Specialist Systems in Sports Knee Injuries

Scanning

Received 12 December 2023; Accepted 12 December 2023; Published 13 December 2023

This article has been retracted by Hindawi, as publisher, following an investigation undertaken by the publisher [1]. This investigation has uncovered evidence of systematic manipulation of the publication and peer-review process. We cannot, therefore, vouch for the reliability or integrity of this article.

Please note that this notice is intended solely to alert readers that the peer-review process of this article has been compromised.

Wiley and Hindawi regret that the usual quality checks did not identify these issues before publication and have since put additional measures in place to safeguard research integrity.

We wish to credit our Research Integrity and Research Publishing teams and anonymous and named external researchers and research integrity experts for contributing to this investigation.

The corresponding author, as the representative of all authors, has been given the opportunity to register their agreement or disagreement to this retraction. We have kept a record of any response received.

References

[1] X. Chen, A. Yu, N. Cai, S. Wei, and Y. Tong, "Diagnostic Value of Specialist Systems in Sports Knee Injuries," *Scanning*, vol. 2022, Article ID 1892877, 7 pages, 2022.

Hindawi
Scanning
Volume 2023, Article ID 9869615, 1 page
https://doi.org/10.1155/2023/9869615

Retraction

Retracted: Intravoxel Incoherent Motion Diffusion-Weighted Imaging and 3D-ASL to Assess the Value of Ki-67 Labeling Index and Grade in Glioma

Scanning

Received 12 December 2023; Accepted 12 December 2023; Published 13 December 2023

This article has been retracted by Hindawi, as publisher, following an investigation undertaken by the publisher [1]. This investigation has uncovered evidence of systematic manipulation of the publication and peer-review process. We cannot, therefore, vouch for the reliability or integrity of this article.

Please note that this notice is intended solely to alert readers that the peer-review process of this article has been compromised.

Wiley and Hindawi regret that the usual quality checks did not identify these issues before publication and have since put additional measures in place to safeguard research integrity.

We wish to credit our Research Integrity and Research Publishing teams and anonymous and named external researchers and research integrity experts for contributing to this investigation.

The corresponding author, as the representative of all authors, has been given the opportunity to register their agreement or disagreement to this retraction. We have kept a record of any response received.

References

[1] J. Zhou, H. Li, X. Ma, M. Jin, X. Meng, and G. Zhang, "Intravoxel Incoherent Motion Diffusion-Weighted Imaging and 3D-ASL to Assess the Value of Ki-67 Labeling Index and Grade in Glioma," *Scanning*, vol. 2022, Article ID 8429659, 7 pages, 2022.

Hindawi
Scanning
Volume 2023, Article ID 9859036, 1 page
https://doi.org/10.1155/2023/9859036

Retraction

Retracted: Application of Low-Dose CT and MRI in the Evaluation of Soft Tissue Injury in Tibial Plateau Fractures

Scanning

Received 12 December 2023; Accepted 12 December 2023; Published 13 December 2023

This article has been retracted by Hindawi, as publisher, following an investigation undertaken by the publisher [1]. This investigation has uncovered evidence of systematic manipulation of the publication and peer-review process. We cannot, therefore, vouch for the reliability or integrity of this article.

Please note that this notice is intended solely to alert readers that the peer-review process of this article has been compromised.

Wiley and Hindawi regret that the usual quality checks did not identify these issues before publication and have since put additional measures in place to safeguard research integrity.

We wish to credit our Research Integrity and Research Publishing teams and anonymous and named external researchers and research integrity experts for contributing to this investigation.

The corresponding author, as the representative of all authors, has been given the opportunity to register their agreement or disagreement to this retraction. We have kept a record of any response received.

References

[1] Y. Qi, P. He, J. Zhu, Y. Wang, H. Zhao, and J. Chen, "Application of Low-Dose CT and MRI in the Evaluation of Soft Tissue Injury in Tibial Plateau Fractures," *Scanning*, vol. 2022, Article ID 7686485, 6 pages, 2022.

Hindawi
Scanning
Volume 2023, Article ID 9853252, 1 page
https://doi.org/10.1155/2023/9853252

Retraction

Retracted: Evaluation of Pelvic Floor Dysfunction by Pelvic Floor Ultrasonography after Total Hysterectomy for Cervical Cancer

Scanning

Received 12 December 2023; Accepted 12 December 2023; Published 13 December 2023

This article has been retracted by Hindawi, as publisher, following an investigation undertaken by the publisher [1]. This investigation has uncovered evidence of systematic manipulation of the publication and peer-review process. We cannot, therefore, vouch for the reliability or integrity of this article.

Please note that this notice is intended solely to alert readers that the peer-review process of this article has been compromised.

Wiley and Hindawi regret that the usual quality checks did not identify these issues before publication and have since put additional measures in place to safeguard research integrity.

We wish to credit our Research Integrity and Research Publishing teams and anonymous and named external researchers and research integrity experts for contributing to this investigation.

The corresponding author, as the representative of all authors, has been given the opportunity to register their agreement or disagreement to this retraction. We have kept a record of any response received.

References

[1] D.-d. Liu, J. Xin, W. Liu, Y.-f. Zhang, and P. Li, "Evaluation of Pelvic Floor Dysfunction by Pelvic Floor Ultrasonography after Total Hysterectomy for Cervical Cancer," *Scanning*, vol. 2022, Article ID 5914344, 4 pages, 2022.

Hindawi
Scanning
Volume 2023, Article ID 9847959, 1 page
https://doi.org/10.1155/2023/9847959

Retraction

Retracted: Application of Moving Target Information Perception Technology in Intelligent Supervision System

Scanning

Received 12 December 2023; Accepted 12 December 2023; Published 13 December 2023

This article has been retracted by Hindawi, as publisher, following an investigation undertaken by the publisher [1]. This investigation has uncovered evidence of systematic manipulation of the publication and peer-review process. We cannot, therefore, vouch for the reliability or integrity of this article.

Please note that this notice is intended solely to alert readers that the peer-review process of this article has been compromised.

Wiley and Hindawi regret that the usual quality checks did not identify these issues before publication and have since put additional measures in place to safeguard research integrity.

We wish to credit our Research Integrity and Research Publishing teams and anonymous and named external researchers and research integrity experts for contributing to this investigation.

The corresponding author, as the representative of all authors, has been given the opportunity to register their agreement or disagreement to this retraction. We have kept a record of any response received.

References

[1] M. Zhu, "Application of Moving Target Information Perception Technology in Intelligent Supervision System," *Scanning*, vol. 2022, Article ID 5192601, 7 pages, 2022.

Hindawi
Scanning
Volume 2023, Article ID 9839032, 1 page
https://doi.org/10.1155/2023/9839032

Retraction

Retracted: Intelligent Scanning Detection System of Muscle Exercise Fatigue Based on Surface Electromyography

Scanning

Received 12 December 2023; Accepted 12 December 2023; Published 13 December 2023

This article has been retracted by Hindawi, as publisher, following an investigation undertaken by the publisher [1]. This investigation has uncovered evidence of systematic manipulation of the publication and peer-review process. We cannot, therefore, vouch for the reliability or integrity of this article.

Please note that this notice is intended solely to alert readers that the peer-review process of this article has been compromised.

Wiley and Hindawi regret that the usual quality checks did not identify these issues before publication and have since put additional measures in place to safeguard research integrity.

We wish to credit our Research Integrity and Research Publishing teams and anonymous and named external researchers and research integrity experts for contributing to this investigation.

The corresponding author, as the representative of all authors, has been given the opportunity to register their agreement or disagreement to this retraction. We have kept a record of any response received.

References

[1] W. Wang, "Intelligent Scanning Detection System of Muscle Exercise Fatigue Based on Surface Electromyography," *Scanning*, vol. 2022, Article ID 9163978, 7 pages, 2022.

Hindawi
Scanning
Volume 2023, Article ID 9814192, 1 page
https://doi.org/10.1155/2023/9814192

Retraction

Retracted: Changes of Volume Parameters in the Treatment of Graves Ophthalmopathy by Endoscopic Transethmoidal Decompression of the Orbital Inner Wall Combined with Fat Decompression

Scanning

Received 12 December 2023; Accepted 12 December 2023; Published 13 December 2023

This article has been retracted by Hindawi, as publisher, following an investigation undertaken by the publisher [1]. This investigation has uncovered evidence of systematic manipulation of the publication and peer-review process. We cannot, therefore, vouch for the reliability or integrity of this article.

Please note that this notice is intended solely to alert readers that the peer-review process of this article has been compromised.

Wiley and Hindawi regret that the usual quality checks did not identify these issues before publication and have since put additional measures in place to safeguard research integrity.

We wish to credit our Research Integrity and Research Publishing teams and anonymous and named external researchers and research integrity experts for contributing to this investigation.

The corresponding author, as the representative of all authors, has been given the opportunity to register their agreement or disagreement to this retraction. We have kept a record of any response received.

References

[1] W. Fu, "Changes of Volume Parameters in the Treatment of Graves Ophthalmopathy by Endoscopic Transethmoidal Decompression of the Orbital Inner Wall Combined with Fat Decompression," *Scanning*, vol. 2022, Article ID 8149247, 6 pages, 2022.

Hindawi
Scanning
Volume 2023, Article ID 9801545, 1 page
https://doi.org/10.1155/2023/9801545

Retraction

Retracted: Diagnostic Value of Color Doppler Ultrasonography in Subacute Thyroiditis

Scanning

Received 12 December 2023; Accepted 12 December 2023; Published 13 December 2023

This article has been retracted by Hindawi, as publisher, following an investigation undertaken by the publisher [1]. This investigation has uncovered evidence of systematic manipulation of the publication and peer-review process. We cannot, therefore, vouch for the reliability or integrity of this article.

Please note that this notice is intended solely to alert readers that the peer-review process of this article has been compromised.

Wiley and Hindawi regret that the usual quality checks did not identify these issues before publication and have since put additional measures in place to safeguard research integrity.

We wish to credit our Research Integrity and Research Publishing teams and anonymous and named external researchers and research integrity experts for contributing to this investigation.

The corresponding author, as the representative of all authors, has been given the opportunity to register their agreement or disagreement to this retraction. We have kept a record of any response received.

References

[1] Y. Chen, S. Zhu, H. Chen et al., "Diagnostic Value of Color Doppler Ultrasonography in Subacute Thyroiditis," *Scanning*, vol. 2022, Article ID 7456622, 7 pages, 2022.

Hindawi
Scanning
Volume 2023, Article ID 9795735, 1 page
https://doi.org/10.1155/2023/9795735

Retraction

Retracted: Management Strategies and Imaging Observation of Early and Delayed Intelligent Treatment of Meniscus Sports Injury under Knee Osteoarthroscopy

Scanning

Received 12 December 2023; Accepted 12 December 2023; Published 13 December 2023

This article has been retracted by Hindawi, as publisher, following an investigation undertaken by the publisher [1]. This investigation has uncovered evidence of systematic manipulation of the publication and peer-review process. We cannot, therefore, vouch for the reliability or integrity of this article.

Please note that this notice is intended solely to alert readers that the peer-review process of this article has been compromised.

Wiley and Hindawi regret that the usual quality checks did not identify these issues before publication and have since put additional measures in place to safeguard research integrity.

We wish to credit our Research Integrity and Research Publishing teams and anonymous and named external researchers and research integrity experts for contributing to this investigation.

The corresponding author, as the representative of all authors, has been given the opportunity to register their agreement or disagreement to this retraction. We have kept a record of any response received.

References

[1] T. Deng, X. Li, Z. Guo et al., "Management Strategies and Imaging Observation of Early and Delayed Intelligent Treatment of Meniscus Sports Injury under Knee Osteoarthroscopy," *Scanning*, vol. 2022, Article ID 8716823, 6 pages, 2022.

Hindawi
Scanning
Volume 2023, Article ID 9784601, 1 page
https://doi.org/10.1155/2023/9784601

Retraction

Retracted: Optimal Modeling and Simulation of the Relationship between Athletes' High-Intensity Training and Sports Injuries

Scanning

Received 12 December 2023; Accepted 12 December 2023; Published 13 December 2023

This article has been retracted by Hindawi, as publisher, following an investigation undertaken by the publisher [1]. This investigation has uncovered evidence of systematic manipulation of the publication and peer-review process. We cannot, therefore, vouch for the reliability or integrity of this article.

Please note that this notice is intended solely to alert readers that the peer-review process of this article has been compromised.

Wiley and Hindawi regret that the usual quality checks did not identify these issues before publication and have since put additional measures in place to safeguard research integrity.

We wish to credit our Research Integrity and Research Publishing teams and anonymous and named external researchers and research integrity experts for contributing to this investigation.

The corresponding author, as the representative of all authors, has been given the opportunity to register their agreement or disagreement to this retraction. We have kept a record of any response received.

References

[1] Y. Zhang and Y. Chang, "Optimal Modeling and Simulation of the Relationship between Athletes' High-Intensity Training and Sports Injuries," *Scanning*, vol. 2022, Article ID 8447453, 7 pages, 2022.

Hindawi
Scanning
Volume 2023, Article ID 9782180, 1 page
https://doi.org/10.1155/2023/9782180

Retraction

Retracted: Effect of Running Exercise on Brain Functional Magnetic Resonance Characteristics of College Students with Depression

Scanning

Received 12 December 2023; Accepted 12 December 2023; Published 13 December 2023

This article has been retracted by Hindawi, as publisher, following an investigation undertaken by the publisher [1]. This investigation has uncovered evidence of systematic manipulation of the publication and peer-review process. We cannot, therefore, vouch for the reliability or integrity of this article.

Please note that this notice is intended solely to alert readers that the peer-review process of this article has been compromised.

Wiley and Hindawi regret that the usual quality checks did not identify these issues before publication and have since put additional measures in place to safeguard research integrity.

We wish to credit our Research Integrity and Research Publishing teams and anonymous and named external researchers and research integrity experts for contributing to this investigation.

The corresponding author, as the representative of all authors, has been given the opportunity to register their agreement or disagreement to this retraction. We have kept a record of any response received.

References

[1] W. Li and J. Yang, "Effect of Running Exercise on Brain Functional Magnetic Resonance Characteristics of College Students with Depression," *Scanning*, vol. 2022, Article ID 7558807, 8 pages, 2022.

Hindawi
Scanning
Volume 2023, Article ID 9765894, 1 page
https://doi.org/10.1155/2023/9765894

Retraction

Retracted: 3D Convolutional Neural Network Framework with Deep Learning for Nuclear Medicine

Scanning

Received 12 December 2023; Accepted 12 December 2023; Published 13 December 2023

This article has been retracted by Hindawi, as publisher, following an investigation undertaken by the publisher [1]. This investigation has uncovered evidence of systematic manipulation of the publication and peer-review process. We cannot, therefore, vouch for the reliability or integrity of this article.

Please note that this notice is intended solely to alert readers that the peer-review process of this article has been compromised.

Wiley and Hindawi regret that the usual quality checks did not identify these issues before publication and have since put additional measures in place to safeguard research integrity.

We wish to credit our Research Integrity and Research Publishing teams and anonymous and named external researchers and research integrity experts for contributing to this investigation.

The corresponding author, as the representative of all authors, has been given the opportunity to register their agreement or disagreement to this retraction. We have kept a record of any response received.

References

[1] P. Manimegalai, R. Suresh Kumar, P. Valsalan, R. Dhanagopal, P. T. Vasanth Raj, and J. Christhudass, "3D Convolutional Neural Network Framework with Deep Learning for Nuclear Medicine," *Scanning*, vol. 2022, Article ID 9640177, 9 pages, 2022.

Hindawi
Scanning
Volume 2023, Article ID 9760450, 1 page
https://doi.org/10.1155/2023/9760450

Retraction

Retracted: Observation on the Effect of MRI Image Scanning on Knee Pain in Football Injury

Scanning

Received 12 December 2023; Accepted 12 December 2023; Published 13 December 2023

This article has been retracted by Hindawi, as publisher, following an investigation undertaken by the publisher [1]. This investigation has uncovered evidence of systematic manipulation of the publication and peer-review process. We cannot, therefore, vouch for the reliability or integrity of this article.

Please note that this notice is intended solely to alert readers that the peer-review process of this article has been compromised.

Wiley and Hindawi regret that the usual quality checks did not identify these issues before publication and have since put additional measures in place to safeguard research integrity.

We wish to credit our Research Integrity and Research Publishing teams and anonymous and named external researchers and research integrity experts for contributing to this investigation.

The corresponding author, as the representative of all authors, has been given the opportunity to register their agreement or disagreement to this retraction. We have kept a record of any response received.

References

[1] W. Yu, "Observation on the Effect of MRI Image Scanning on Knee Pain in Football Injury," *Scanning*, vol. 2022, Article ID 7348978, 6 pages, 2022.

Hindawi
Scanning
Volume 2023, Article ID 9894170, 1 page
https://doi.org/10.1155/2023/9894170

Retraction

Retracted: Diagnostic Value of Endoscopic Narrow-Band Imaging Technique in Early Gastric Cancer and Precancerous Lesions

Scanning

Received 17 October 2023; Accepted 17 October 2023; Published 18 October 2023

This article has been retracted by Hindawi following an investigation undertaken by the publisher [1]. This investigation has uncovered evidence of one or more of the following indicators of systematic manipulation of the publication process:

(1) Discrepancies in scope

(2) Discrepancies in the description of the research reported

(3) Discrepancies between the availability of data and the research described

(4) Inappropriate citations

(5) Incoherent, meaningless and/or irrelevant content included in the article

(6) Peer-review manipulation

The presence of these indicators undermines our confidence in the integrity of the article's content and we cannot, therefore, vouch for its reliability. Please note that this notice is intended solely to alert readers that the content of this article is unreliable. We have not investigated whether authors were aware of or involved in the systematic manipulation of the publication process.

In addition, our investigation has also shown that one or more of the following human-subject reporting requirements has not been met in this article: ethical approval by an Institutional Review Board (IRB) committee or equivalent, patient/participant consent to participate, and/or agreement to publish patient/participant details (where relevant).

Wiley and Hindawi regrets that the usual quality checks did not identify these issues before publication and have since put additional measures in place to safeguard research integrity.

We wish to credit our own Research Integrity and Research Publishing teams and anonymous and named external researchers and research integrity experts for contributing to this investigation.

The corresponding author, as the representative of all authors, has been given the opportunity to register their agreement or disagreement to this retraction. We have kept a record of any response received.

References

[1] X. Huang, R. Chen, and L. Zhao, "Diagnostic Value of Endoscopic Narrow-Band Imaging Technique in Early Gastric Cancer and Precancerous Lesions," *Scanning*, vol. 2022, Article ID 9205150, 6 pages, 2022.

Hindawi
Scanning
Volume 2023, Article ID 9897839, 1 page
https://doi.org/10.1155/2023/9897839

Retraction

Retracted: Clinical Analysis of Echocardiography and Serum IL-6 and TNF-α Changes in Pregnant Women with Hypertension

Scanning

Received 10 October 2023; Accepted 10 October 2023; Published 11 October 2023

This article has been retracted by Hindawi following an investigation undertaken by the publisher [1]. This investigation has uncovered evidence of one or more of the following indicators of systematic manipulation of the publication process:

(1) Discrepancies in scope

(2) Discrepancies in the description of the research reported

(3) Discrepancies between the availability of data and the research described

(4) Inappropriate citations

(5) Incoherent, meaningless and/or irrelevant content included in the article

(6) Peer-review manipulation

The presence of these indicators undermines our confidence in the integrity of the article's content and we cannot, therefore, vouch for its reliability. Please note that this notice is intended solely to alert readers that the content of this article is unreliable. We have not investigated whether authors were aware of or involved in the systematic manipulation of the publication process.

In addition, our investigation has also shown that one or more of the following human-subject reporting requirements has not been met in this article: ethical approval by an Institutional Review Board (IRB) committee or equivalent, patient/participant consent to participate, and/or agreement to publish patient/participant details (where relevant).

Wiley and Hindawi regrets that the usual quality checks did not identify these issues before publication and have since put additional measures in place to safeguard research integrity.

We wish to credit our own Research Integrity and Research Publishing teams and anonymous and named external researchers and research integrity experts for contributing to this investigation.

The corresponding author, as the representative of all authors, has been given the opportunity to register their agreement or disagreement to this retraction. We have kept a record of any response received.

References

[1] Y. Liu, X. Hou, M. Yu, and J. Zhou, "Clinical Analysis of Echocardiography and Serum IL-6 and TNF-α Changes in Pregnant Women with Hypertension," *Scanning*, vol. 2022, Article ID 9299746, 7 pages, 2022.

Hindawi
Scanning
Volume 2023, Article ID 9879863, 1 page
https://doi.org/10.1155/2023/9879863

Retraction

Retracted: Effect of Rehabilitation Physical Training on PE Teaching Sports Injury under Ultrasonic Examination

Scanning

Received 3 October 2023; Accepted 3 October 2023; Published 4 October 2023

This article has been retracted by Hindawi following an investigation undertaken by the publisher [1]. This investigation has uncovered evidence of one or more of the following indicators of systematic manipulation of the publication process:

(1) Discrepancies in scope

(2) Discrepancies in the description of the research reported

(3) Discrepancies between the availability of data and the research described

(4) Inappropriate citations

(5) Incoherent, meaningless and/or irrelevant content included in the article

(6) Peer-review manipulation

The presence of these indicators undermines our confidence in the integrity of the article's content and we cannot, therefore, vouch for its reliability. Please note that this notice is intended solely to alert readers that the content of this article is unreliable. We have not investigated whether authors were aware of or involved in the systematic manipulation of the publication process.

In addition, our investigation has also shown that one or more of the following human-subject reporting requirements has not been met in this article: ethical approval by an Institutional Review Board (IRB) committee or equivalent, patient/participant consent to participate, and/or agreement to publish patient/participant details (where relevant).

Wiley and Hindawi regrets that the usual quality checks did not identify these issues before publication and have since put additional measures in place to safeguard research integrity.

We wish to credit our own Research Integrity and Research Publishing teams and anonymous and named external researchers and research integrity experts for contributing to this investigation.

The corresponding author, as the representative of all authors, has been given the opportunity to register their agreement or disagreement to this retraction. We have kept a record of any response received.

References

[1] W. Li, "Effect of Rehabilitation Physical Training on PE Teaching Sports Injury under Ultrasonic Examination," *Scanning*, vol. 2022, Article ID 1470303, 6 pages, 2022.

Hindawi
Scanning
Volume 2023, Article ID 9871261, 1 page
https://doi.org/10.1155/2023/9871261

Retraction

Retracted: Intervention of Fluency and Anxiety in Mindfulness Training of Shooting

Scanning

Received 3 October 2023; Accepted 3 October 2023; Published 4 October 2023

This article has been retracted by Hindawi following an investigation undertaken by the publisher [1]. This investigation has uncovered evidence of one or more of the following indicators of systematic manipulation of the publication process:

(1) Discrepancies in scope

(2) Discrepancies in the description of the research reported

(3) Discrepancies between the availability of data and the research described

(4) Inappropriate citations

(5) Incoherent, meaningless and/or irrelevant content included in the article

(6) Peer-review manipulation

The presence of these indicators undermines our confidence in the integrity of the article's content and we cannot, therefore, vouch for its reliability. Please note that this notice is intended solely to alert readers that the content of this article is unreliable. We have not investigated whether authors were aware of or involved in the systematic manipulation of the publication process.

In addition, our investigation has also shown that one or more of the following human-subject reporting requirements has not been met in this article: ethical approval by an Institutional Review Board (IRB) committee or equivalent, patient/participant consent to participate, and/or agreement to publish patient/participant details (where relevant).

Wiley and Hindawi regrets that the usual quality checks did not identify these issues before publication and have since put additional measures in place to safeguard research integrity.

We wish to credit our own Research Integrity and Research Publishing teams and anonymous and named external researchers and research integrity experts for contributing to this investigation.

The corresponding author, as the representative of all authors, has been given the opportunity to register their agreement or disagreement to this retraction. We have kept a record of any response received.

References

[1] W. Liu, "Intervention of Fluency and Anxiety in Mindfulness Training of Shooting," *Scanning*, vol. 2022, Article ID 6069561, 5 pages, 2022.

Hindawi
Scanning
Volume 2023, Article ID 9859742, 1 page
https://doi.org/10.1155/2023/9859742

Retraction

Retracted: The Diagnostic Value of Scanning in the Injury of Triceps Crus of Volleyball Players

Scanning

Received 3 October 2023; Accepted 3 October 2023; Published 4 October 2023

This article has been retracted by Hindawi following an investigation undertaken by the publisher [1]. This investigation has uncovered evidence of one or more of the following indicators of systematic manipulation of the publication process:

(1) Discrepancies in scope

(2) Discrepancies in the description of the research reported

(3) Discrepancies between the availability of data and the research described

(4) Inappropriate citations

(5) Incoherent, meaningless and/or irrelevant content included in the article

(6) Peer-review manipulation

The presence of these indicators undermines our confidence in the integrity of the article's content and we cannot, therefore, vouch for its reliability. Please note that this notice is intended solely to alert readers that the content of this article is unreliable. We have not investigated whether authors were aware of or involved in the systematic manipulation of the publication process.

In addition, our investigation has also shown that one or more of the following human-subject reporting requirements has not been met in this article: ethical approval by an Institutional Review Board (IRB) committee or equivalent, patient/participant consent to participate, and/or agreement to publish patient/participant details (where relevant).

Wiley and Hindawi regrets that the usual quality checks did not identify these issues before publication and have since put additional measures in place to safeguard research integrity.

We wish to credit our own Research Integrity and Research Publishing teams and anonymous and named external researchers and research integrity experts for contributing to this investigation.

The corresponding author, as the representative of all authors, has been given the opportunity to register their agreement or disagreement to this retraction. We have kept a record of any response received.

References

[1] J. Zhao and J. Liu, "The Diagnostic Value of Scanning in the Injury of Triceps Crus of Volleyball Players," *Scanning*, vol. 2022, Article ID 2203065, 7 pages, 2022.

Hindawi
Scanning
Volume 2023, Article ID 9853105, 1 page
https://doi.org/10.1155/2023/9853105

Retraction

Retracted: Sports Medical Image Modeling of Injury Prevention in Wushu Training

Scanning

Received 3 October 2023; Accepted 3 October 2023; Published 4 October 2023

This article has been retracted by Hindawi following an investigation undertaken by the publisher [1]. This investigation has uncovered evidence of one or more of the following indicators of systematic manipulation of the publication process:

(1) Discrepancies in scope

(2) Discrepancies in the description of the research reported

(3) Discrepancies between the availability of data and the research described

(4) Inappropriate citations

(5) Incoherent, meaningless and/or irrelevant content included in the article

(6) Peer-review manipulation

The presence of these indicators undermines our confidence in the integrity of the article's content and we cannot, therefore, vouch for its reliability. Please note that this notice is intended solely to alert readers that the content of this article is unreliable. We have not investigated whether authors were aware of or involved in the systematic manipulation of the publication process.

Wiley and Hindawi regrets that the usual quality checks did not identify these issues before publication and have since put additional measures in place to safeguard research integrity.

We wish to credit our own Research Integrity and Research Publishing teams and anonymous and named external researchers and research integrity experts for contributing to this investigation.

The corresponding author, as the representative of all authors, has been given the opportunity to register their agreement or disagreement to this retraction. We have kept a record of any response received.

References

[1] Y. Feng, "Sports Medical Image Modeling of Injury Prevention in Wushu Training," *Scanning*, vol. 2022, Article ID 5201952, 6 pages, 2022.

Hindawi
Scanning
Volume 2023, Article ID 9829873, 1 page
https://doi.org/10.1155/2023/9829873

Retraction

Retracted: Effect of Foot and Hand Massage on Abdominal Pain of Cesarean Section Incision under Ultrasound Guidance

Scanning

Received 3 October 2023; Accepted 3 October 2023; Published 4 October 2023

This article has been retracted by Hindawi following an investigation undertaken by the publisher [1]. This investigation has uncovered evidence of one or more of the following indicators of systematic manipulation of the publication process:

(1) Discrepancies in scope

(2) Discrepancies in the description of the research reported

(3) Discrepancies between the availability of data and the research described

(4) Inappropriate citations

(5) Incoherent, meaningless and/or irrelevant content included in the article

(6) Peer-review manipulation

The presence of these indicators undermines our confidence in the integrity of the article's content and we cannot, therefore, vouch for its reliability. Please note that this notice is intended solely to alert readers that the content of this article is unreliable. We have not investigated whether authors were aware of or involved in the systematic manipulation of the publication process.

In addition, our investigation has also shown that one or more of the following human-subject reporting requirements has not been met in this article: ethical approval by an Institutional Review Board (IRB) committee or equivalent, patient/participant consent to participate, and/or agreement to publish patient/participant details (where relevant).

Wiley and Hindawi regrets that the usual quality checks did not identify these issues before publication and have since put additional measures in place to safeguard research integrity.

We wish to credit our own Research Integrity and Research Publishing teams and anonymous and named external researchers and research integrity experts for contributing to this investigation.

The corresponding author, as the representative of all authors, has been given the opportunity to register their agreement or disagreement to this retraction. We have kept a record of any response received.

References

[1] Y. Q. Wang, R. Jiang, and J. Pan, "Effect of Foot and Hand Massage on Abdominal Pain of Cesarean Section Incision under Ultrasound Guidance," *Scanning*, vol. 2022, Article ID 8356256, 7 pages, 2022.

Hindawi
Scanning
Volume 2023, Article ID 9826840, 1 page
https://doi.org/10.1155/2023/9826840

Retraction

Retracted: Discuss the Application of Data Services in Data Health Management of High-Risk Pregnant and Lying-In Women in Smart Medical Care

Scanning

Received 3 October 2023; Accepted 3 October 2023; Published 4 October 2023

This article has been retracted by Hindawi following an investigation undertaken by the publisher [1]. This investigation has uncovered evidence of one or more of the following indicators of systematic manipulation of the publication process:

(1) Discrepancies in scope

(2) Discrepancies in the description of the research reported

(3) Discrepancies between the availability of data and the research described

(4) Inappropriate citations

(5) Incoherent, meaningless and/or irrelevant content included in the article

(6) Peer-review manipulation

The presence of these indicators undermines our confidence in the integrity of the article's content and we cannot, therefore, vouch for its reliability. Please note that this notice is intended solely to alert readers that the content of this article is unreliable. We have not investigated whether authors were aware of or involved in the systematic manipulation of the publication process.

In addition, our investigation has also shown that one or more of the following human-subject reporting requirements has not been met in this article: ethical approval by an Institutional Review Board (IRB) committee or equivalent, patient/participant consent to participate, and/or agreement to publish patient/participant details (where relevant).

Wiley and Hindawi regrets that the usual quality checks did not identify these issues before publication and have since put additional measures in place to safeguard research integrity.

We wish to credit our own Research Integrity and Research Publishing teams and anonymous and named external researchers and research integrity experts for contributing to this investigation.

The corresponding author, as the representative of all authors, has been given the opportunity to register their agreement or disagreement to this retraction. We have kept a record of any response received.

References

[1] L. Shen, W. Shi, L. Cai, J. An, and Q. Ling, "Discuss the Application of Data Services in Data Health Management of High-Risk Pregnant and Lying-In Women in Smart Medical Care," *Scanning*, vol. 2022, Article ID 5957697, 7 pages, 2022.

Hindawi
Scanning
Volume 2023, Article ID 9819368, 1 page
https://doi.org/10.1155/2023/9819368

Retraction

Retracted: Scanning Imaging Study of Patients with Parkinson's Disease Lower Urinary Tract Dysfunction Based on Linear Equation

Scanning

Received 3 October 2023; Accepted 3 October 2023; Published 4 October 2023

This article has been retracted by Hindawi following an investigation undertaken by the publisher [1]. This investigation has uncovered evidence of one or more of the following indicators of systematic manipulation of the publication process:

(1) Discrepancies in scope

(2) Discrepancies in the description of the research reported

(3) Discrepancies between the availability of data and the research described

(4) Inappropriate citations

(5) Incoherent, meaningless and/or irrelevant content included in the article

(6) Peer-review manipulation

The presence of these indicators undermines our confidence in the integrity of the article's content and we cannot, therefore, vouch for its reliability. Please note that this notice is intended solely to alert readers that the content of this article is unreliable. We have not investigated whether authors were aware of or involved in the systematic manipulation of the publication process.

In addition, our investigation has also shown that one or more of the following human-subject reporting requirements has not been met in this article: ethical approval by an Institutional Review Board (IRB) committee or equivalent, patient/participant consent to participate, and/or agreement to publish patient/participant details (where relevant).

Wiley and Hindawi regrets that the usual quality checks did not identify these issues before publication and have since put additional measures in place to safeguard research integrity.

We wish to credit our own Research Integrity and Research Publishing teams and anonymous and named external researchers and research integrity experts for contributing to this investigation.

The corresponding author, as the representative of all authors, has been given the opportunity to register their agreement or disagreement to this retraction. We have kept a record of any response received.

References

[1] Y. Liu, J. Han, X. Guo, L. Fang, and T. Liu, "Scanning Imaging Study of Patients with Parkinson's Disease Lower Urinary Tract Dysfunction Based on Linear Equation," *Scanning*, vol. 2022, Article ID 9506328, 6 pages, 2022.

Hindawi
Scanning
Volume 2023, Article ID 9785215, 1 page
https://doi.org/10.1155/2023/9785215

Retraction

Retracted: Effect of Core Muscle Strength Training Combined with Taijiquan on Bone Mineral Density Measured by Quantitative CT Scanning in the Elderly

Scanning

Received 3 October 2023; Accepted 3 October 2023; Published 4 October 2023

This article has been retracted by Hindawi following an investigation undertaken by the publisher [1]. This investigation has uncovered evidence of one or more of the following indicators of systematic manipulation of the publication process:

(1) Discrepancies in scope

(2) Discrepancies in the description of the research reported

(3) Discrepancies between the availability of data and the research described

(4) Inappropriate citations

(5) Incoherent, meaningless and/or irrelevant content included in the article

(6) Peer-review manipulation

The presence of these indicators undermines our confidence in the integrity of the article's content and we cannot, therefore, vouch for its reliability. Please note that this notice is intended solely to alert readers that the content of this article is unreliable. We have not investigated whether authors were aware of or involved in the systematic manipulation of the publication process.

In addition, our investigation has also shown that one or more of the following human-subject reporting requirements has not been met in this article: ethical approval by an Institutional Review Board (IRB) committee or equivalent, patient/participant consent to participate, and/or agreement to publish patient/participant details (where relevant).

Wiley and Hindawi regrets that the usual quality checks did not identify these issues before publication and have since put additional measures in place to safeguard research integrity.

We wish to credit our own Research Integrity and Research Publishing teams and anonymous and named external researchers and research integrity experts for contributing to this investigation.

The corresponding author, as the representative of all authors, has been given the opportunity to register their agreement or disagreement to this retraction. We have kept a record of any response received.

References

[1] M. Zhong, "Effect of Core Muscle Strength Training Combined with Taijiquan on Bone Mineral Density Measured by Quantitative CT Scanning in the Elderly," *Scanning*, vol. 2022, Article ID 6942081, 7 pages, 2022.

Hindawi
Scanning
Volume 2023, Article ID 9781403, 1 page
https://doi.org/10.1155/2023/9781403

Retraction

Retracted: The Effect of CT Imaging Technology in the Diagnosis of Thoracic and Cardiac Surgery Diseases

Scanning

Received 3 October 2023; Accepted 3 October 2023; Published 4 October 2023

This article has been retracted by Hindawi following an investigation undertaken by the publisher [1]. This investigation has uncovered evidence of one or more of the following indicators of systematic manipulation of the publication process:

(1) Discrepancies in scope

(2) Discrepancies in the description of the research reported

(3) Discrepancies between the availability of data and the research described

(4) Inappropriate citations

(5) Incoherent, meaningless and/or irrelevant content included in the article

(6) Peer-review manipulation

The presence of these indicators undermines our confidence in the integrity of the article's content and we cannot, therefore, vouch for its reliability. Please note that this notice is intended solely to alert readers that the content of this article is unreliable. We have not investigated whether authors were aware of or involved in the systematic manipulation of the publication process.

In addition, our investigation has also shown that one or more of the following human-subject reporting requirements has not been met in this article: ethical approval by an Institutional Review Board (IRB) committee or equivalent, patient/participant consent to participate, and/or agreement to publish patient/participant details (where relevant).

Wiley and Hindawi regrets that the usual quality checks did not identify these issues before publication and have since put additional measures in place to safeguard research integrity.

We wish to credit our own Research Integrity and Research Publishing teams and anonymous and named external researchers and research integrity experts for contributing to this investigation.

The corresponding author, as the representative of all authors, has been given the opportunity to register their agreement or disagreement to this retraction. We have kept a record of any response received.

References

[1] M. Yang, H. Qian, D. Zhang, and Y. Gui, "The Effect of CT Imaging Technology in the Diagnosis of Thoracic and Cardiac Surgery Diseases," *Scanning*, vol. 2022, Article ID 9385451, 7 pages, 2022.

Hindawi
Scanning
Volume 2023, Article ID 9757214, 1 page
https://doi.org/10.1155/2023/9757214

Retraction

Retracted: Influence of Comprehensive Nursing Intervention Combined with WeChat Platform Propaganda and Education of ERAS Concept on Postoperative Functional Recovery of Patients with Gallbladder Polyps

Scanning

Received 3 October 2023; Accepted 3 October 2023; Published 4 October 2023

This article has been retracted by Hindawi following an investigation undertaken by the publisher [1]. This investigation has uncovered evidence of one or more of the following indicators of systematic manipulation of the publication process:

(1) Discrepancies in scope

(2) Discrepancies in the description of the research reported

(3) Discrepancies between the availability of data and the research described

(4) Inappropriate citations

(5) Incoherent, meaningless and/or irrelevant content included in the article

(6) Peer-review manipulation

The presence of these indicators undermines our confidence in the integrity of the article's content and we cannot, therefore, vouch for its reliability. Please note that this notice is intended solely to alert readers that the content of this article is unreliable. We have not investigated whether authors were aware of or involved in the systematic manipulation of the publication process.

Wiley and Hindawi regrets that the usual quality checks did not identify these issues before publication and have since put additional measures in place to safeguard research integrity.

We wish to credit our own Research Integrity and Research Publishing teams and anonymous and named external researchers and research integrity experts for contributing to this investigation.

The corresponding author, as the representative of all authors, has been given the opportunity to register their agreement or disagreement to this retraction. We have kept a record of any response received.

References

[1] Y. Zhang, D. Guo, X. Yang et al., "Influence of Comprehensive Nursing Intervention Combined with WeChat Platform Propaganda and Education of ERAS Concept on Postoperative Functional Recovery of Patients with Gallbladder Polyps," *Scanning*, vol. 2022, Article ID 6919130, 7 pages, 2022.

Hindawi
Scanning
Volume 2023, Article ID 9756591, 1 page
https://doi.org/10.1155/2023/9756591

Retraction

Retracted: Sports Injury Risk Prevention and MRI Image Performance of Athletes in Physical Education

Scanning

Received 3 October 2023; Accepted 3 October 2023; Published 4 October 2023

This article has been retracted by Hindawi following an investigation undertaken by the publisher [1]. This investigation has uncovered evidence of one or more of the following indicators of systematic manipulation of the publication process:

(1) Discrepancies in scope

(2) Discrepancies in the description of the research reported

(3) Discrepancies between the availability of data and the research described

(4) Inappropriate citations

(5) Incoherent, meaningless and/or irrelevant content included in the article

(6) Peer-review manipulation

The presence of these indicators undermines our confidence in the integrity of the article's content and we cannot, therefore, vouch for its reliability. Please note that this notice is intended solely to alert readers that the content of this article is unreliable. We have not investigated whether authors were aware of or involved in the systematic manipulation of the publication process.

Wiley and Hindawi regrets that the usual quality checks did not identify these issues before publication and have since put additional measures in place to safeguard research integrity.

We wish to credit our own Research Integrity and Research Publishing teams and anonymous and named external researchers and research integrity experts for contributing to this investigation.

The corresponding author, as the representative of all authors, has been given the opportunity to register their agreement or disagreement to this retraction. We have kept a record of any response received.

References

[1] J. Yang, "Sports Injury Risk Prevention and MRI Image Performance of Athletes in Physical Education," *Scanning*, vol. 2022, Article ID 1166314, 7 pages, 2022.

Hindawi
Scanning
Volume 2023, Article ID 9896178, 1 page
https://doi.org/10.1155/2023/9896178

Retraction

Retracted: Diagnostic Value of Spiral CT and Magnetic Resonance Imaging Scanning in Gastric Cancer and Precancerous Lesions

Scanning

Received 20 June 2023; Accepted 20 June 2023; Published 21 June 2023

This article has been retracted by Hindawi following an investigation undertaken by the publisher [1]. This investigation has uncovered evidence of one or more of the following indicators of systematic manipulation of the publication process:

(1) Discrepancies in scope

(2) Discrepancies in the description of the research reported

(3) Discrepancies between the availability of data and the research described

(4) Inappropriate citations

(5) Incoherent, meaningless and/or irrelevant content included in the article

(6) Peer-review manipulation

The presence of these indicators undermines our confidence in the integrity of the article's content and we cannot, therefore, vouch for its reliability. Please note that this notice is intended solely to alert readers that the content of this article is unreliable. We have not investigated whether authors were aware of or involved in the systematic manipulation of the publication process.

In addition, our investigation has also shown that one or more of the following human-subject reporting requirements has not been met in this article: ethical approval by an Institutional Review Board (IRB) committee or equivalent, patient/participant consent to participate, and/or agreement to publish patient/participant details (where relevant).

Wiley and Hindawi regrets that the usual quality checks did not identify these issues before publication and have since put additional measures in place to safeguard research integrity.

We wish to credit our own Research Integrity and Research Publishing teams and anonymous and named external researchers and research integrity experts for contributing to this investigation.

The corresponding author, as the representative of all authors, has been given the opportunity to register their agreement or disagreement to this retraction. We have kept a record of any response received.

References

[1] Y. Zhen, Q. Xie, and L. Liu, "Diagnostic Value of Spiral CT and Magnetic Resonance Imaging Scanning in Gastric Cancer and Precancerous Lesions," *Scanning*, vol. 2022, Article ID 3627385, 6 pages, 2022.

Hindawi
Scanning
Volume 2023, Article ID 9890786, 1 page
https://doi.org/10.1155/2023/9890786

Retraction

Retracted: Unsupervised Hyperspectral Microscopic Image Segmentation Using Deep Embedded Clustering Algorithm

Scanning

Received 20 June 2023; Accepted 20 June 2023; Published 21 June 2023

This is article has been retracted by Hindawi following an investigation undertaken by the publisher [1]. This is investigation has uncovered evidence of one or more of the following indicators of systematic manipulation of the publication process:

(1) Discrepancies in scope

(2) Discrepancies in the description of the research reported

(3) Discrepancies between the availability of data and the research described

(4) Inappropriate citations

(5) Incoherent, meaningless and/or irrelevant content included in the article

(6) Peer-review manipulation

The presence of these indicators undermines our confidence in the integrity of the article's content and we cannot, therefore, vouch for its reliability. Please note that this notice is intended solely to alert readers that the content of this article is unreliable. We have not investigated whether authors were aware of or involved in the systematic manipulation of the publication process.

Wiley and Hindawi regrets that the usual quality checks did not identify these issues before publication and have since put additional measures in place to safeguard research integrity.

We wish to credit our own Research Integrity and Research Publishing teams and anonymous and named external researchers and research integrity experts for contributing to this investigation.

The corresponding author, as the representative of all authors, has been given the opportunity to register their agreement or disagreement to this retraction. We have kept a record of any response received.

References

[1] P. Ajay, B. Nagaraj, R. A. Kumar, R. Huang, and P. Ananthi, "Unsupervised Hyperspectral Microscopic Image Segmentation Using Deep Embedded Clustering Algorithm," *Scanning*, vol. 2022, Article ID 1200860, 9 pages, 2022.

Hindawi
Scanning
Volume 2023, Article ID 9872786, 1 page
https://doi.org/10.1155/2023/9872786

Retraction

Retracted: Predictive Model of Cerebral Vasospasm in Subarachnoid Hemorrhage Based on Regression Equation

Scanning

Received 20 June 2023; Accepted 20 June 2023; Published 21 June 2023

This article has been retracted by Hindawi following an investigation undertaken by the publisher [1]. This investigation has uncovered evidence of one or more of the following indicators of systematic manipulation of the publication process:

(1) Discrepancies in scope

(2) Discrepancies in the description of the research reported

(3) Discrepancies between the availability of data and the research described

(4) Inappropriate citations

(5) Incoherent, meaningless and/or irrelevant content included in the article

(6) Peer-review manipulation

The presence of these indicators undermines our confidence in the integrity of the article's content and we cannot, therefore, vouch for its reliability. Please note that this notice is intended solely to alert readers that the content of this article is unreliable. We have not investigated whether authors were aware of or involved in the systematic manipulation of the publication process.

In addition, our investigation has also shown that one or more of the following human-subject reporting requirements has not been met in this article: ethical approval by an Institutional Review Board (IRB) committee or equivalent, patient/participant consent to participate, and/or agreement to publish patient/participant details (where relevant).

Wiley and Hindawi regrets that the usual quality checks did not identify these issues before publication and have since put additional measures in place to safeguard research integrity.

We wish to credit our own Research Integrity and Research Publishing teams and anonymous and named external researchers and research integrity experts for contributing to this investigation.

The corresponding author, as the representative of all authors, has been given the opportunity to register their agreement or disagreement to this retraction. We have kept a record of any response received.

References

[1] J. Li, K. Zhou, L. Wang, and Q. Cao, "Predictive Model of Cerebral Vasospasm in Subarachnoid Hemorrhage Based on Regression Equation," *Scanning*, vol. 2022, Article ID 3397967, 6 pages, 2022.

Hindawi
Scanning
Volume 2023, Article ID 9869713, 1 page
https://doi.org/10.1155/2023/9869713

Retraction

Retracted: Image Effect Observation of Acanthopanax senticosus on Antifatigue Activity after Exercise

Scanning

Received 20 June 2023; Accepted 20 June 2023; Published 21 June 2023

This article has been retracted by Hindawi following an investigation undertaken by the publisher [1]. This investigation has uncovered evidence of one or more of the following indicators of systematic manipulation of the publication process:

(1) Discrepancies in scope

(2) Discrepancies in the description of the research reported

(3) Discrepancies between the availability of data and the research described

(4) Inappropriate citations

(5) Incoherent, meaningless and/or irrelevant content included in the article

(6) Peer-review manipulation

The presence of these indicators undermines our confidence in the integrity of the article's content and we cannot, therefore, vouch for its reliability. Please note that this notice is intended solely to alert readers that the content of this article is unreliable. We have not investigated whether authors were aware of or involved in the systematic manipulation of the publication process.

Wiley and Hindawi regrets that the usual quality checks did not identify these issues before publication and have since put additional measures in place to safeguard research integrity.

We wish to credit our own Research Integrity and Research Publishing teams and anonymous and named external researchers and research integrity experts for contributing to this investigation.

The corresponding author, as the representative of all authors, has been given the opportunity to register their agreement or disagreement to this retraction. We have kept a record of any response received.

References

[1] X. Zhang and W. Zhu, "Image Effect Observation of Acanthopanax senticosus on Antifatigue Activity after Exercise," *Scanning*, vol. 2022, Article ID 7588680, 7 pages, 2022.

Hindawi
Scanning
Volume 2023, Article ID 9864261, 1 page
https://doi.org/10.1155/2023/9864261

Retraction

Retracted: Clinical Observation of MRI Image in Floating Needle Therapy for Cervical Spondylosis of Cervical Type

Scanning

Received 20 June 2023; Accepted 20 June 2023; Published 21 June 2023

This article has been retracted by Hindawi following an investigation undertaken by the publisher [1]. This investigation has uncovered evidence of one or more of the following indicators of systematic manipulation of the publication process:

(1) Discrepancies in scope

(2) Discrepancies in the description of the research reported

(3) Discrepancies between the availability of data and the research described

(4) Inappropriate citations

(5) Incoherent, meaningless and/or irrelevant content included in the article

(6) Peer-review manipulation

The presence of these indicators undermines our confidence in the integrity of the article's content and we cannot, therefore, vouch for its reliability. Please note that this notice is intended solely to alert readers that the content of this article is unreliable. We have not investigated whether authors were aware of or involved in the systematic manipulation of the publication process.

In addition, our investigation has also shown that one or more of the following human-subject reporting requirements has not been met in this article: ethical approval by an Institutional Review Board (IRB) committee or equivalent, patient/participant consent to participate, and/or agreement to publish patient/participant details (where relevant).

Wiley and Hindawi regrets that the usual quality checks did not identify these issues before publication and have since put additional measures in place to safeguard research integrity.

We wish to credit our own Research Integrity and Research Publishing teams and anonymous and named external researchers and research integrity experts for contributing to this investigation.

The corresponding author, as the representative of all authors, has been given the opportunity to register their agreement or disagreement to this retraction. We have kept a record of any response received.

References

[1] X. Liu, Z. Tang, B. Wang, and Y. Chen, "Clinical Observation of MRI Image in Floating Needle Therapy for Cervical Spondylosis of Cervical Type," *Scanning*, vol. 2022, Article ID 1340192, 10 pages, 2022.

Hindawi
Scanning
Volume 2023, Article ID 9862750, 1 page
https://doi.org/10.1155/2023/9862750

Retraction

Retracted: Clinical Characteristics and Mathematical Analysis of Curative Effect of Hemodialysis in Curing Poisoning Caused by Snakebite

Scanning

Received 20 June 2023; Accepted 20 June 2023; Published 21 June 2023

This article has been retracted by Hindawi following an investigation undertaken by the publisher [1]. This investigation has uncovered evidence of one or more of the following indicators of systematic manipulation of the publication process:

(1) Discrepancies in scope

(2) Discrepancies in the description of the research reported

(3) Discrepancies between the availability of data and the research described

(4) Inappropriate citations

(5) Incoherent, meaningless and/or irrelevant content included in the article

(6) Peer-review manipulation

The presence of these indicators undermines our confidence in the integrity of the article's content and we cannot, therefore, vouch for its reliability. Please note that this notice is intended solely to alert readers that the content of this article is unreliable. We have not investigated whether authors were aware of or involved in the systematic manipulation of the publication process.

Wiley and Hindawi regrets that the usual quality checks did not identify these issues before publication and have since put additional measures in place to safeguard research integrity.

We wish to credit our own Research Integrity and Research Publishing teams and anonymous and named external researchers and research integrity experts for contributing to this investigation.

The corresponding author, as the representative of all authors, has been given the opportunity to register their agreement or disagreement to this retraction. We have kept a record of any response received.

References

[1] G. Huang, B. Chen, Y. Luo, L. Chen, S. Wu, and S. Wang, "Clinical Characteristics and Mathematical Analysis of Curative Effect of Hemodialysis in Curing Poisoning Caused by Snakebite," *Scanning*, vol. 2022, Article ID 2312972, 7 pages, 2022.

Hindawi
Scanning
Volume 2023, Article ID 9857053, 1 page
https://doi.org/10.1155/2023/9857053

Retraction

Retracted: Observation on the Effect of Rehabilitative Physical Training on Ice and Snow Sports Injury under Ultrasound Examination

Scanning

Received 20 June 2023; Accepted 20 June 2023; Published 21 June 2023

This article has been retracted by Hindawi following an investigation undertaken by the publisher [1]. This investigation has uncovered evidence of one or more of the following indicators of systematic manipulation of the publication process:

(1) Discrepancies in scope

(2) Discrepancies in the description of the research reported

(3) Discrepancies between the availability of data and the research described

(4) Inappropriate citations

(5) Incoherent, meaningless and/or irrelevant content included in the article

(6) Peer-review manipulation

The presence of these indicators undermines our confidence in the integrity of the article's content and we cannot, therefore, vouch for its reliability. Please note that this notice is intended solely to alert readers that the content of this article is unreliable. We have not investigated whether authors were aware of or involved in the systematic manipulation of the publication process.

In addition, our investigation has also shown that one or more of the following human-subject reporting requirements has not been met in this article: ethical approval by an Institutional Review Board (IRB) committee or equivalent, patient/participant consent to participate, and/or agreement to publish patient/participant details (where relevant).

Wiley and Hindawi regrets that the usual quality checks did not identify these issues before publication and have since put additional measures in place to safeguard research integrity.

We wish to credit our own Research Integrity and Research Publishing teams and anonymous and named external researchers and research integrity experts for contributing to this investigation.

The corresponding author, as the representative of all authors, has been given the opportunity to register their agreement or disagreement to this retraction. We have kept a record of any response received.

References

[1] Y. Wang and Y. Zhou, "Observation on the Effect of Rehabilitative Physical Training on Ice and Snow Sports Injury under Ultrasound Examination," *Scanning*, vol. 2022, Article ID 2931686, 7 pages, 2022.

Hindawi
Scanning
Volume 2023, Article ID 9836370, 1 page
https://doi.org/10.1155/2023/9836370

Retraction

Retracted: Application of Scanning Magnetic Resonance Imaging in the Diagnosis of Prenatal Placental Implantation and Related Care

Scanning

Received 20 June 2023; Accepted 20 June 2023; Published 21 June 2023

This article has been retracted by Hindawi following an investigation undertaken by the publisher [1]. This investigation has uncovered evidence of one or more of the following indicators of systematic manipulation of the publication process:

(1) Discrepancies in scope

(2) Discrepancies in the description of the research reported

(3) Discrepancies between the availability of data and the research described

(4) Inappropriate citations

(5) Incoherent, meaningless and/or irrelevant content included in the article

(6) Peer-review manipulation

The presence of these indicators undermines our confidence in the integrity of the article's content and we cannot, therefore, vouch for its reliability. Please note that this notice is intended solely to alert readers that the content of this article is unreliable. We have not investigated whether authors were aware of or involved in the systematic manipulation of the publication process.

In addition, our investigation has also shown that one or more of the following human-subject reporting requirements has not been met in this article: ethical approval by an Institutional Review Board (IRB) committee or equivalent, patient/participant consent to participate, and/or agreement to publish patient/participant details (where relevant).

Wiley and Hindawi regrets that the usual quality checks did not identify these issues before publication and have since put additional measures in place to safeguard research integrity.

We wish to credit our own Research Integrity and Research Publishing teams and anonymous and named external researchers and research integrity experts for contributing to this investigation.

The corresponding author, as the representative of all authors, has been given the opportunity to register their agreement or disagreement to this retraction. We have kept a record of any response received.

References

[1] Q. Lin, B. Li, S. Chen et al., "Application of Scanning Magnetic Resonance Imaging in the Diagnosis of Prenatal Placental Implantation and Related Care," *Scanning*, vol. 2022, Article ID 4883989, 7 pages, 2022.

Hindawi
Scanning
Volume 2023, Article ID 9835940, 1 page
https://doi.org/10.1155/2023/9835940

Retraction

Retracted: Exploring the Clinical Point Selection Rules of Acupuncture and Moxibustion in the Treatment of Infantile Enuresis Based on Data Mining Technology

Scanning

Received 20 June 2023; Accepted 20 June 2023; Published 21 June 2023

This article has been retracted by Hindawi following an investigation undertaken by the publisher [1]. This investigation has uncovered evidence of one or more of the following indicators of systematic manipulation of the publication process:

(1) Discrepancies in scope

(2) Discrepancies in the description of the research reported

(3) Discrepancies between the availability of data and the research described

(4) Inappropriate citations

(5) Incoherent, meaningless and/or irrelevant content included in the article

(6) Peer-review manipulation

The presence of these indicators undermines our confidence in the integrity of the article's content and we cannot, therefore, vouch for its reliability. Please note that this notice is intended solely to alert readers that the content of this article is unreliable. We have not investigated whether authors were aware of or involved in the systematic manipulation of the publication process.

Wiley and Hindawi regrets that the usual quality checks did not identify these issues before publication and have since put additional measures in place to safeguard research integrity.

We wish to credit our own Research Integrity and Research Publishing teams and anonymous and named external researchers and research integrity experts for contributing to this investigation.

The corresponding author, as the representative of all authors, has been given the opportunity to register their agreement or disagreement to this retraction. We have kept a record of any response received.

References

[1] C. Ma, N. Li, and X. Zhang, "Exploring the Clinical Point Selection Rules of Acupuncture and Moxibustion in the Treatment of Infantile Enuresis Based on Data Mining Technology," *Scanning*, vol. 2022, Article ID 7928052, 6 pages, 2022.

Hindawi
Scanning
Volume 2023, Article ID 9831918, 1 page
https://doi.org/10.1155/2023/9831918

Retraction

Retracted: Prediction of Renal Function Damage in Patients with Essential Hypertension Based on Stepwise Regression Equation Scanning by AASI

Scanning

Received 20 June 2023; Accepted 20 June 2023; Published 21 June 2023

This article has been retracted by Hindawi following an investigation undertaken by the publisher [1]. This investigation has uncovered evidence of one or more of the following indicators of systematic manipulation of the publication process:

(1) Discrepancies in scope

(2) Discrepancies in the description of the research reported

(3) Discrepancies between the availability of data and the research described

(4) Inappropriate citations

(5) Incoherent, meaningless and/or irrelevant content included in the article

(6) Peer-review manipulation

The presence of these indicators undermines our confidence in the integrity of the article's content and we cannot, therefore, vouch for its reliability. Please note that this notice is intended solely to alert readers that the content of this article is unreliable. We have not investigated whether authors were aware of or involved in the systematic manipulation of the publication process.

In addition, our investigation has also shown that one or more of the following human-subject reporting requirements has not been met in this article: ethical approval by an Institutional Review Board (IRB) committee or equivalent, patient/participant consent to participate, and/or agreement to publish patient/participant details (where relevant).

Wiley and Hindawi regrets that the usual quality checks did not identify these issues before publication and have since put additional measures in place to safeguard research integrity.

We wish to credit our own Research Integrity and Research Publishing teams and anonymous and named external researchers and research integrity experts for contributing to this investigation.

The corresponding author, as the representative of all authors, has been given the opportunity to register their agreement or disagreement to this retraction. We have kept a record of any response received.

References

[1] Y. Wu, G. Ma, H. Sun, S. Zhang, and X. Li, "Prediction of Renal Function Damage in Patients with Essential Hypertension Based on Stepwise Regression Equation Scanning by AASI," *Scanning*, vol. 2022, Article ID 4728921, 6 pages, 2022.

Hindawi
Scanning
Volume 2023, Article ID 9823960, 1 page
https://doi.org/10.1155/2023/9823960

Retraction

Retracted: The Pathogenesis and Influencing Factors of Adult Hypertension Based on Structural Equation Scanning

Scanning

Received 20 June 2023; Accepted 20 June 2023; Published 21 June 2023

This article has been retracted by Hindawi following an investigation undertaken by the publisher [1]. This investigation has uncovered evidence of one or more of the following indicators of systematic manipulation of the publication process:

(1) Discrepancies in scope

(2) Discrepancies in the description of the research reported

(3) Discrepancies between the availability of data and the research described

(4) Inappropriate citations

(5) Incoherent, meaningless and/or irrelevant content included in the article

(6) Peer-review manipulation

The presence of these indicators undermines our confidence in the integrity of the article's content and we cannot, therefore, vouch for its reliability. Please note that this notice is intended solely to alert readers that the content of this article is unreliable. We have not investigated whether authors were aware of or involved in the systematic manipulation of the publication process.

In addition, our investigation has also shown that one or more of the following human-subject reporting requirements has not been met in this article: ethical approval by an Institutional Review Board (IRB) committee or equivalent, patient/participant consent to participate, and/or agreement to publish patient/participant details (where relevant).

Wiley and Hindawi regrets that the usual quality checks did not identify these issues before publication and have since put additional measures in place to safeguard research integrity.

We wish to credit our own Research Integrity and Research Publishing teams and anonymous and named external researchers and research integrity experts for contributing to this investigation.

The corresponding author, as the representative of all authors, has been given the opportunity to register their agreement or disagreement to this retraction. We have kept a record of any response received.

References

[1] Y. Wu, G. Ma, N. Feng, Z. Zhang, S. Zhang, and X. Li, "The Pathogenesis and Influencing Factors of Adult Hypertension Based on Structural Equation Scanning," *Scanning*, vol. 2022, Article ID 2663604, 6 pages, 2022.

Hindawi
Scanning
Volume 2023, Article ID 9821689, 1 page
https://doi.org/10.1155/2023/9821689

Retraction

Retracted: High-Intensity Injury Recognition Pattern of Sports Athletes Based on the Deep Neural Network

Scanning

Received 20 June 2023; Accepted 20 June 2023; Published 21 June 2023

This article has been retracted by Hindawi following an investigation undertaken by the publisher [1]. This investigation has uncovered evidence of one or more of the following indicators of systematic manipulation of the publication process:

(1) Discrepancies in scope

(2) Discrepancies in the description of the research reported

(3) Discrepancies between the availability of data and the research described

(4) Inappropriate citations

(5) Incoherent, meaningless and/or irrelevant content included in the article

(6) Peer-review manipulation

The presence of these indicators undermines our confidence in the integrity of the article's content and we cannot, therefore, vouch for its reliability. Please note that this notice is intended solely to alert readers that the content of this article is unreliable. We have not investigated whether authors were aware of or involved in the systematic manipulation of the publication process.

In addition, our investigation has also shown that one or more of the following human-subject reporting requirements has not been met in this article: ethical approval by an Institutional Review Board (IRB) committee or equivalent, patient/participant consent to participate, and/or agreement to publish patient/participant details (where relevant).

Wiley and Hindawi regrets that the usual quality checks did not identify these issues before publication and have since put additional measures in place to safeguard research integrity.

We wish to credit our own Research Integrity and Research Publishing teams and anonymous and named external researchers and research integrity experts for contributing to this investigation.

The corresponding author, as the representative of all authors, has been given the opportunity to register their agreement or disagreement to this retraction. We have kept a record of any response received.

References

[1] N. Chen and Y. Zhang, "High-Intensity Injury Recognition Pattern of Sports Athletes Based on the Deep Neural Network," *Scanning*, vol. 2022, Article ID 2794225, 6 pages, 2022.

Hindawi
Scanning
Volume 2023, Article ID 9817461, 1 page
https://doi.org/10.1155/2023/9817461

Retraction

Retracted: Research on Influencing Factors of Clinical Efficacy of Meniscus Resection Based on Logistic Regression Analysis

Scanning

Received 20 June 2023; Accepted 20 June 2023; Published 21 June 2023

This article has been retracted by Hindawi following an investigation undertaken by the publisher [1]. This investigation has uncovered evidence of one or more of the following indicators of systematic manipulation of the publication process:

(1) Discrepancies in scope

(2) Discrepancies in the description of the research reported

(3) Discrepancies between the availability of data and the research described

(4) Inappropriate citations

(5) Incoherent, meaningless and/or irrelevant content included in the article

(6) Peer-review manipulation

The presence of these indicators undermines our confidence in the integrity of the article's content and we cannot, therefore, vouch for its reliability. Please note that this notice is intended solely to alert readers that the content of this article is unreliable. We have not investigated whether authors were aware of or involved in the systematic manipulation of the publication process.

In addition, our investigation has also shown that one or more of the following human-subject reporting requirements has not been met in this article: ethical approval by an Institutional Review Board (IRB) committee or equivalent, patient/participant consent to participate, and/or agreement to publish patient/participant details (where relevant).

Wiley and Hindawi regrets that the usual quality checks did not identify these issues before publication and have since put additional measures in place to safeguard research integrity.

We wish to credit our own Research Integrity and Research Publishing teams and anonymous and named external researchers and research integrity experts for contributing to this investigation.

The corresponding author, as the representative of all authors, has been given the opportunity to register their agreement or disagreement to this retraction. We have kept a record of any response received.

References

[1] X. Mao, Q. Hong, R. You, Y. Lu, and F. Zhao, "Research on Influencing Factors of Clinical Efficacy of Meniscus Resection Based on Logistic Regression Analysis," *Scanning*, vol. 2022, Article ID 4606139, 2022.

Hindawi
Scanning
Volume 2023, Article ID 9816104, 1 page
https://doi.org/10.1155/2023/9816104

Retraction

Retracted: Image Observation Study on Improving the Effectiveness of Muscle Strength Training for Sprinters

Scanning

Received 20 June 2023; Accepted 20 June 2023; Published 21 June 2023

This article has been retracted by Hindawi following an investigation undertaken by the publisher [1]. This investigation has uncovered evidence of one or more of the following indicators of systematic manipulation of the publication process:

(1) Discrepancies in scope

(2) Discrepancies in the description of the research reported

(3) Discrepancies between the availability of data and the research described

(4) Inappropriate citations

(5) Incoherent, meaningless and/or irrelevant content included in the article

(6) Peer-review manipulation

The presence of these indicators undermines our confidence in the integrity of the article's content and we cannot, therefore, vouch for its reliability. Please note that this notice is intended solely to alert readers that the content of this article is unreliable. We have not investigated whether authors were aware of or involved in the systematic manipulation of the publication process.

In addition, our investigation has also shown that one or more of the following human-subject reporting requirements has not been met in this article: ethical approval by an Institutional Review Board (IRB) committee or equivalent, patient/participant consent to participate, and/or agreement to publish patient/participant details (where relevant).

Wiley and Hindawi regrets that the usual quality checks did not identify these issues before publication and have since put additional measures in place to safeguard research integrity.

We wish to credit our own Research Integrity and Research Publishing teams and anonymous and named external researchers and research integrity experts for contributing to this investigation.

The corresponding author, as the representative of all authors, has been given the opportunity to register their agreement or disagreement to this retraction. We have kept a record of any response received.

References

[1] Y. Zou and L. Han, "Image Observation Study on Improving the Effectiveness of Muscle Strength Training for Sprinters," *Scanning*, vol. 2022, Article ID 4987782, 7 pages, 2022.

Hindawi
Scanning
Volume 2023, Article ID 9809430, 1 page
https://doi.org/10.1155/2023/9809430

Retraction

Retracted: Diagnostic Value of Magnetic Resonance Susceptibility-Weighted Imaging Scanning in Different Types of Early Prostate Cancer

Scanning

Received 20 June 2023; Accepted 20 June 2023; Published 21 June 2023

This article has been retracted by Hindawi following an investigation undertaken by the publisher [1]. This investigation has uncovered evidence of one or more of the following indicators of systematic manipulation of the publication process:

(1) Discrepancies in scope

(2) Discrepancies in the description of the research reported

(3) Discrepancies between the availability of data and the research described

(4) Inappropriate citations

(5) Incoherent, meaningless and/or irrelevant content included in the article

(6) Peer-review manipulation

The presence of these indicators undermines our confidence in the integrity of the article's content and we cannot, therefore, vouch for its reliability. Please note that this notice is intended solely to alert readers that the content of this article is unreliable. We have not investigated whether authors were aware of or involved in the systematic manipulation of the publication process.

In addition, our investigation has also shown that one or more of the following human-subject reporting requirements has not been met in this article: ethical approval by an Institutional Review Board (IRB) committee or equivalent, patient/participant consent to participate, and/or agreement to publish patient/participant details (where relevant).

Wiley and Hindawi regrets that the usual quality checks did not identify these issues before publication and have since put additional measures in place to safeguard research integrity.

We wish to credit our own Research Integrity and Research Publishing teams and anonymous and named external researchers and research integrity experts for contributing to this investigation.

The corresponding author, as the representative of all authors, has been given the opportunity to register their agreement or disagreement to this retraction. We have kept a record of any response received.

References

[1] R. Gao, J. Liu, and H. Zhu, "Diagnostic Value of Magnetic Resonance Susceptibility-Weighted Imaging Scanning in Different Types of Early Prostate Cancer," *Scanning*, vol. 2022, Article ID 4884646, 6 pages, 2022.

Hindawi
Scanning
Volume 2023, Article ID 9803893, 1 page
https://doi.org/10.1155/2023/9803893

Retraction

Retracted: Observation on the Effect of Shoulder Pain Caused by Volleyball Training Injury Based on MRI Image Scanning

Scanning

Received 20 June 2023; Accepted 20 June 2023; Published 21 June 2023

This article has been retracted by Hindawi following an investigation undertaken by the publisher [1]. This investigation has uncovered evidence of one or more of the following indicators of systematic manipulation of the publication process:

(1) Discrepancies in scope

(2) Discrepancies in the description of the research reported

(3) Discrepancies between the availability of data and the research described

(4) Inappropriate citations

(5) Incoherent, meaningless and/or irrelevant content included in the article

(6) Peer-review manipulation

The presence of these indicators undermines our confidence in the integrity of the article's content and we cannot, therefore, vouch for its reliability. Please note that this notice is intended solely to alert readers that the content of this article is unreliable. We have not investigated whether authors were aware of or involved in the systematic manipulation of the publication process.

In addition, our investigation has also shown that one or more of the following human-subject reporting requirements has not been met in this article: ethical approval by an Institutional Review Board (IRB) committee or equivalent, patient/participant consent to participate, and/or agreement to publish patient/participant details (where relevant).

Wiley and Hindawi regrets that the usual quality checks did not identify these issues before publication and have since put additional measures in place to safeguard research integrity.

We wish to credit our own Research Integrity and Research Publishing teams and anonymous and named external researchers and research integrity experts for contributing to this investigation.

The corresponding author, as the representative of all authors, has been given the opportunity to register their agreement or disagreement to this retraction. We have kept a record of any response received.

References

[1] K. Li and N. Fu, "Observation on the effect of shoulder pain caused by volleyball training injury based on MRI image scanning," *Scanning*, vol. 2022, Article ID 4368871, 5 pages, 2022.

Hindawi
Scanning
Volume 2023, Article ID 9794806, 1 page
https://doi.org/10.1155/2023/9794806

Retraction

Retracted: Application of Color Doppler Ultrasound in Microscopic Imaging Diagnosis of Adenomyosis

Scanning

Received 20 June 2023; Accepted 20 June 2023; Published 21 June 2023

This article has been retracted by Hindawi following an investigation undertaken by the publisher [1]. This investigation has uncovered evidence of one or more of the following indicators of systematic manipulation of the publication process:

(1) Discrepancies in scope

(2) Discrepancies in the description of the research reported

(3) Discrepancies between the availability of data and the research described

(4) Inappropriate citations

(5) Incoherent, meaningless and/or irrelevant content included in the article

(6) Peer-review manipulation

The presence of these indicators undermines our confidence in the integrity of the article's content and we cannot, therefore, vouch for its reliability. Please note that this notice is intended solely to alert readers that the content of this article is unreliable. We have not investigated whether authors were aware of or involved in the systematic manipulation of the publication process.

In addition, our investigation has also shown that one or more of the following human-subject reporting requirements has not been met in this article: ethical approval by an Institutional Review Board (IRB) committee or equivalent, patient/participant consent to participate, and/or agreement to publish patient/participant details (where relevant).

Wiley and Hindawi regrets that the usual quality checks did not identify these issues before publication and have since put additional measures in place to safeguard research integrity.

We wish to credit our own Research Integrity and Research Publishing teams and anonymous and named external researchers and research integrity experts for contributing to this investigation.

The corresponding author, as the representative of all authors, has been given the opportunity to register their agreement or disagreement to this retraction. We have kept a record of any response received.

References

[1] J. Zhu, S. Liu, and D. Gao, "Application of Color Doppler Ultrasound in Microscopic Imaging Diagnosis of Adenomyosis," *Scanning*, vol. 2022, Article ID 2366871, 7 pages, 2022.

Hindawi
Scanning
Volume 2023, Article ID 9792567, 1 page
https://doi.org/10.1155/2023/9792567

Retraction

Retracted: Sports Medical Image Modeling of Injury Prevention in Dance Learning and Sports Training

Scanning

Received 20 June 2023; Accepted 20 June 2023; Published 21 June 2023

This article has been retracted by Hindawi following an investigation undertaken by the publisher [1]. This investigation has uncovered evidence of one or more of the following indicators of systematic manipulation of the publication process:

(1) Discrepancies in scope

(2) Discrepancies in the description of the research reported

(3) Discrepancies between the availability of data and the research described

(4) Inappropriate citations

(5) Incoherent, meaningless and/or irrelevant content included in the article

(6) Peer-review manipulation

The presence of these indicators undermines our confidence in the integrity of the article's content and we cannot, therefore, vouch for its reliability. Please note that this notice is intended solely to alert readers that the content of this article is unreliable. We have not investigated whether authors were aware of or involved in the systematic manipulation of the publication process.

Wiley and Hindawi regrets that the usual quality checks did not identify these issues before publication and have since put additional measures in place to safeguard research integrity.

We wish to credit our own Research Integrity and Research Publishing teams and anonymous and named external researchers and research integrity experts for contributing to this investigation.

The corresponding author, as the representative of all authors, has been given the opportunity to register their agreement or disagreement to this retraction. We have kept a record of any response received.

References

[1] R. Fei, "Sports Medical Image Modeling of Injury Prevention in Dance Learning and Sports Training," *Scanning*, vol. 2022, Article ID 7027007, 7 pages, 2022.

Hindawi
Scanning
Volume 2023, Article ID 9765738, 1 page
https://doi.org/10.1155/2023/9765738

WILEY | Hindawi

Retraction

Retracted: Effect of Rehabilitation Training Based on Automatic Extraction Algorithm on Knee Anterior Cruciate Ligament Injury Caused by Exercise

Scanning

Received 20 June 2023; Accepted 20 June 2023; Published 21 June 2023

This article has been retracted by Hindawi following an investigation undertaken by the publisher [1]. This investigation has uncovered evidence of one or more of the following indicators of systematic manipulation of the publication process:

(1) Discrepancies in scope

(2) Discrepancies in the description of the research reported

(3) Discrepancies between the availability of data and the research described

(4) Inappropriate citations

(5) Incoherent, meaningless and/or irrelevant content included in the article

(6) Peer-review manipulation

The presence of these indicators undermines our confidence in the integrity of the article's content and we cannot, therefore, vouch for its reliability. Please note that this notice is intended solely to alert readers that the content of this article is unreliable. We have not investigated whether authors were aware of or involved in the systematic manipulation of the publication process.

In addition, our investigation has also shown that one or more of the following human-subject reporting requirements has not been met in this article: ethical approval by an Institutional Review Board (IRB) committee or equivalent, patient/participant consent to participate, and/or agreement to publish patient/participant details (where relevant).

Wiley and Hindawi regrets that the usual quality checks did not identify these issues before publication and have since put additional measures in place to safeguard research integrity.

We wish to credit our own Research Integrity and Research Publishing teams and anonymous and named external researchers and research integrity experts for contributing to this investigation.

The corresponding author, as the representative of all authors, has been given the opportunity to register their agreement or disagreement to this retraction. We have kept a record of any response received.

References

[1] S. Zhu and J. Gao, "Effect of Rehabilitation Training Based on Automatic Extraction Algorithm on Knee Anterior Cruciate Ligament Injury Caused by Exercise," *Scanning*, vol. 2022, Article ID 8304071, 7 pages, 2022.

Hindawi
Scanning
Volume 2023, Article ID 9765484, 1 page
https://doi.org/10.1155/2023/9765484

Retraction

Retracted: Research and Implementation of Robot Vision Scanning Tracking Algorithm Based on Deep Learning

Scanning

Received 20 June 2023; Accepted 20 June 2023; Published 21 June 2023

This article has been retracted by Hindawi following an investigation undertaken by the publisher [1]. This investigation has uncovered evidence of one or more of the following indicators of systematic manipulation of the publication process:

(1) Discrepancies in scope

(2) Discrepancies in the description of the research reported

(3) Discrepancies between the availability of data and the research described

(4) Inappropriate citations

(5) Incoherent, meaningless and/or irrelevant content included in the article

(6) Peer-review manipulation

The presence of these indicators undermines our confidence in the integrity of the article's content and we cannot, therefore, vouch for its reliability. Please note that this notice is intended solely to alert readers that the content of this article is unreliable. We have not investigated whether authors were aware of or involved in the systematic manipulation of the publication process.

Wiley and Hindawi regrets that the usual quality checks did not identify these issues before publication and have since put additional measures in place to safeguard research integrity.

We wish to credit our own Research Integrity and Research Publishing teams and anonymous and named external researchers and research integrity experts for contributing to this investigation.

The corresponding author, as the representative of all authors, has been given the opportunity to register their agreement or disagreement to this retraction. We have kept a record of any response received.

References

[1] H. Guo, W. Li, N. Zhou, H. Sun, and Z. Han, "Research and Implementation of Robot Vision Scanning Tracking Algorithm Based on Deep Learning," *Scanning*, vol. 2022, Article ID 3330427, 8 pages, 2022.

Hindawi
Scanning
Volume 2023, Article ID 9859421, 1 page
https://doi.org/10.1155/2023/9859421

Retraction

Retracted: Application of Ultrasound Combined with Magnetic Resonance Imaging in the Diagnosis and Grading of Patients with Prenatal Placenta Accreta

Scanning

Received 20 June 2023; Accepted 20 June 2023; Published 21 June 2023

This article has been retracted by Hindawi following an investigation undertaken by the publisher [1]. This investigation has uncovered evidence of one or more of the following indicators of systematic manipulation of the publication process:

(1) Discrepancies in scope

(2) Discrepancies in the description of the research reported

(3) Discrepancies between the availability of data and the research described

(4) Inappropriate citations

(5) Incoherent, meaningless and/or irrelevant content included in the article

(6) Peer-review manipulation

The presence of these indicators undermines our confidence in the integrity of the article's content and we cannot, therefore, vouch for its reliability. Please note that this notice is intended solely to alert readers that the content of this article is unreliable. We have not investigated whether authors were aware of or involved in the systematic manipulation of the publication process.

In addition, our investigation has also shown that one or more of the following human-subject reporting requirements has not been met in this article: ethical approval by an Institutional Review Board (IRB) committee or equivalent, patient/participant consent to participate, and/or agreement to publish patient/participant details (where relevant).

Wiley and Hindawi regrets that the usual quality checks did not identify these issues before publication and have since put additional measures in place to safeguard research integrity.

We wish to credit our own Research Integrity and Research Publishing teams and anonymous and named external researchers and research integrity experts for contributing to this investigation.

The corresponding author, as the representative of all authors, has been given the opportunity to register their agreement or disagreement to this retraction. We have kept a record of any response received.

References

[1] X. Zhang, F. Liu, and X. Wang, "Application of Ultrasound Combined with Magnetic Resonance Imaging in the Diagnosis and Grading of Patients with Prenatal Placenta Accreta," *Scanning*, vol. 2022, Article ID 1199210, 7 pages, 2022.

Hindawi
Scanning
Volume 2023, Article ID 9853252, 1 page
https://doi.org/10.1155/2023/9853252

Retraction

Retracted: Evaluation of Pelvic Floor Dysfunction by Pelvic Floor Ultrasonography after Total Hysterectomy for Cervical Cancer

Scanning

Received 12 December 2023; Accepted 12 December 2023; Published 13 December 2023

This article has been retracted by Hindawi, as publisher, following an investigation undertaken by the publisher [1]. This investigation has uncovered evidence of systematic manipulation of the publication and peer-review process. We cannot, therefore, vouch for the reliability or integrity of this article.

Please note that this notice is intended solely to alert readers that the peer-review process of this article has been compromised.

Wiley and Hindawi regret that the usual quality checks did not identify these issues before publication and have since put additional measures in place to safeguard research integrity.

We wish to credit our Research Integrity and Research Publishing teams and anonymous and named external researchers and research integrity experts for contributing to this investigation.

The corresponding author, as the representative of all authors, has been given the opportunity to register their agreement or disagreement to this retraction. We have kept a record of any response received.

References

[1] D.-d. Liu, J. Xin, W. Liu, Y.-f. Zhang, and P. Li, "Evaluation of Pelvic Floor Dysfunction by Pelvic Floor Ultrasonography after Total Hysterectomy for Cervical Cancer," *Scanning*, vol. 2022, Article ID 5914344, 4 pages, 2022.

Hindawi
Scanning
Volume 2022, Article ID 5914344, 4 pages
https://doi.org/10.1155/2022/5914344

Research Article

Evaluation of Pelvic Floor Dysfunction by Pelvic Floor Ultrasonography after Total Hysterectomy for Cervical Cancer

Dan-dan Liu,[1] **Jing Xin**,[2] **Wei Liu**,[3] **Yan-feng Zhang**,[4] **and Peishan Li**[5]

[1]*Obstetrics and Gynecology Department, Laishan Branch of Yantai Yuhuangding Hospital, Yantai, Shandong 264003, China*
[2]*Obstetric Center, Qingdao Eighth People's Hospital, Qingdao, Shandong 266000, China*
[3]*Health Management Division, Qingdao Eighth People's Hospital, Qingdao, Shandong 266000, China*
[4]*Surgery, Laishan Branch of Yantai Yuhuangding Hospital, Yantai, Shandong 264003, China*
[5]*Operation Room, Laishan Branch of Yantai Yuhuangding Hospital, Yantai, Shandong 264003, China*

Correspondence should be addressed to Peishan Li; 0107034@yzpc.edu.cn

Received 2 August 2022; Revised 6 September 2022; Accepted 14 September 2022; Published 28 September 2022

Academic Editor: Danilo Pelusi

Objective. To study the value of pelvic floor ultrasonography in evaluating pelvic floor dysfunction (PFD) after total hysterectomy for cervical cancer. *Methods*. All the enrolled patients were given 4D pelvic floor ultrasound examination before and after surgery. The results of ultrasonic examination and the parameters of four-dimensional ultrasonic examination before and after surgery were analyzed, and the quality of life of the patients before and after surgery was evaluated. *Results*. Postoperatively, the posterior angle of bladder and urethra, the rotation angle of urethra, the decreased value of bladder neck, and the distance between bladder neck and pubic symphysis were $(122.60 \pm 9.53)^{\circ}$, $(136.47 \pm 14.67)^{\circ}$, $(58.90 \pm 18.19)^{\circ}$, (18.14 ± 7.32) mm, and (2.76 ± 0.46) cm, significantly greater than the preoperative $(89.90 \pm 9.59)^{\circ}$, $(107.30 \pm 9.96)^{\circ}$, $(27.59 \pm 10.96)^{\circ}$, (13.27 ± 5.69) mm, and (2.24 ± 0.21) cm ($P < 0.05$). Postoperative detrusor muscle thickness, bladder neck movement, residual urine volume, and bladder rotation angle (4.48 ± 0.82) mm, (0.64 ± 0.17) cm, (12.82 ± 2.69) ml, $(12.11 \pm 2.43)^{\circ}$ were significantly higher than those of preoperative (3.70 ± 0.64) mm, (0.43 ± 0.18) cm, (4.83 ± 1.07) ml, $(4.30 - 1.19)^{\circ}$ ($P < 0.05$). The scores of emotional function, psychological function, social function, and physiological function were (2.35 ± 0.75) points, (2.45 ± 0.66) points, (2.30 ± 0.77) points, and (2.19 ± 0.71) points, significantly higher than those of (1.01 ± 0.50) points, (1.25 ± 0.54) points, and (1.00 ± 0.57) points before surgery, (1.05 ± 0.46) ($P < 0.05$). *Conclusions*. The application of pelvic floor ultrasonography to detect pelvic floor dysfunction after total hysterectomy can clearly display the anatomical structure of the pelvic floor, which is conducive to disease prevention and treatment. Four-dimensional pelvic floor ultrasound can clearly show the postoperative pelvic floor function, which is worthy of clinical promotion and reference.

1. Introduction

Cervical cancer (CC) is one of the most common gynecological malignant tumors, and its incidence is second only to breast cancer and currently ranks second in the global gynecological malignant tumors, which seriously threatens women's life and health. According to statistics, one-third of the total number of global cases happened in China each year [1]. At the same time, with the increase of HPV infection rate, the incidence of cervical cancer increases significantly and gradually tends to be younger. The current treatment of cervical cancer is based on the International Federation of Gynecology Obstetrics (FIGO) staging with the options of operation in the early stage, such as extensive hysterectomy plus pelvic lymph node dissection [2, 3]. As the number of cancer survivors continues to increase, the quality of life (QOL) of these survivors is an important consideration for healthcare providers, such as pelvic floor dysfunction [4]. In recent years, with the development of 3D multisection and 4D dynamic image acquisition techniques and their powerful data postprocessing capacity, pelvic floor ultrasound has begun to be applied in clinical practice. The 4D view off-machine analysis can be exploited to reconstruct 3D plane image, measured in the corresponding

physiological action state with easy operation, reliable inspection data, and low cost [5]. However, there are few studies on the effect of 4D pelvic floor ultrasound in the diagnosis of pelvic floor function after cervical cancer surgery. We hypothesized that four-dimensional pelvic floor ultrasound can be complementary or alternative route to improve the comprehensive diagnosis of the extent of anatomical structure of the pelvic floor.

1.1. Patients. A total of 119 patients who underwent hysterectomy cervical cancer surgery in our hospital from January 2019 to August 2020 were identified as potential candidate, including 68 patients with stage I cervical cancer and 51 patients with stage II cervical cancer. The ethics committee of the hospital recorded this study; all patients acknowledged the purpose and the procedures of this research and signed informed consent.

1.2. The Inclusion Criteria. (1) Mean age was (52.87 ± 3.82) years (range 42-67) years; (2) mean body mass index was (22.60 ± 0.91) kg/m^2. (3) 12weeks after surgery (4) without symptom of pelvic organ prolapses or history of pelvic surgery in the past (5) no other related treatments were received after surgery (6)have ultrasound examinations before and after surgery.

1.3. The Exclusion Criteria. (1) Patients with hypertension liver and kidney dysfunction and other serious underlying diseases. (2) Patients with a history of pelvic surgery, urinary surgery, nervous system, and infectious diseases. (3) Those patients who did not agree to participant in this study.

2. Methods

The ultrasonic images were collected using a GE Voluson E8 Color Doppler Ultrasound Machine equipped with RIC 5–9-D Probes. The working frequency was 5 to 10 MHz. 4D View 10.0 camera analysis software was used to reconstruct the data, and the instrument was set to pelvic floor ultrasound examination. Prior to the image collection, feces of the patients must be removed. The amount of residual urine in the bladder must be about 50 mL. The volume probe was outsourced to sterile protective sleeve, which was coated with disinfectant and chelating agent on both the inside and outside. The probe was firmly placed in the perineum of the patient to store the images including the midsagittal plane of the urethra, vagina, bladder neck, rectal junction, and pubic symphysis. The angle of urethral rotation, the vertical distance between the bladder neck and the lower symphysis pubis (BSD), the degree of bladder neck depression (BND), and the posterior horn of bladder and urethral angle were also measured at both the resting and maximum Valsalva action state. The reference value of the posterior angle of the bladder and urethra is 90° to 120°, and the reference value of the urethral rotation angle is 30° to 45°. All detections were repeated 3 times.

2.1. Diagnostic Criteria. Stress urinary incontinence diagnostic criteria: (1) BND ≥ 2.0 cm in the maximal Valsalva state; the posterior angle of the bladder and urethra ≥ 120° and the bladder neck rotation angle ≥ 20° in the maximal Valsalva state; (2) caused by sneezing, coughing, and laughter urine overflow occurs when there is increased pressure in the abdomen. The diagnostic criteria for pelvic organ prolapse are: the vertical distance between the lowest point of the pelvic organ and the lower part of the pubic symphysis detected by ultrasound of the perineal pelvic floor is greater than 1 cm. The posterior angle of the bladder and urethra is greater than or equal to 140°, and the rotation angle of the urethra is less than 45°. Combined with the changes in the anatomical structure of the pelvic floor, clinical manifestations, and the characteristics of this transperineal four-dimensional pelvic floor ultrasound imaging, the results were obtained. The four-dimensional pelvic floor ultrasound was used to detect stress urine. Four items of incontinence, bladder prolapse, uterine prolapse, and rectal prolapse were used as diagnostic indicators. The comparison of four-dimensional pelvic floor ultrasound examination parameters of pelvic floor dysfunction after cervical cancer hysterectomy in different states uses SF-36 to evaluate the quality of life [6]. SF-36 includes four aspects: emotional function, mental function, social function, and physiological function. According to the severity of the impact of symptoms on daily life, patients are divided into no effect (0 points), mildly affected (1 point), moderately affected (2 points), and severely affected (3 points), the higher the score, the worse the quality of life.

2.2. Statistical Analysis. Statistical analysis was performed using SPSS 23.0 software. Continuous data were expressed as mean ± standard deviation, group t-test was used for comparison between two groups. Chi-square test was used for the comparison of binary data. Multiple logistic regression analyses were conducted to identify the potential risks. In this present study, $P < 0.05$ was considered that the differences were statistically significant.

2.3. Results of Four-Dimensional Pelvic Floor Ultrasound Diagnosis. Among 119 patients with cervical cancer who underwent hysterectomy, 57 cases (47.90%) of bladder prolapse were found by four-dimensional pelvic floor ultrasonography, 22 cases (18.49%) of rectal prolapse, 7 cases (5.88%) of uterine prolapse, and 33 cases (27.73%) of stress urinary incontinence.

2.4. Comparison of Parameter Values of Four-Dimensional Ultrasonography before and after Surgery. After surgery, urinary tract rotation angle, the vertical distance between the bladder neck and the pubic symphysis (BSD), the bladder neck reduction (BND) in the resting state and the posterior angle of the bladder and urethra in the maximum Valsalva state were significantly higher t ($P < 0.05$).As shown in Table 1.

2.5. Changes of Lower Urinary Tract in Patients before and after Surgery. As shown in Table 2, the degree of bladder neck motion, bladder residual urine volume, bladder rotation angle, and bladder detrusor thickness were significantly improved after surgery ($P < 0.05$).

Table 1: Comparison of parameter values of four-dimensional ultrasonography before and after surgery ($\bar{X} \pm s$).

Group	n	BSD (cm)	BND (mm)	URA (°)	PUVA resting (°)	PUVA Valsalva (°)
Pre	119	2.12 ± 0.32	13.24 ± 5.59	27.58 ± 10.99	89.89 ± 9.61	107.27 ± 9.94
Post	119	2.76 ± 0.54*	18.18 ± 7.32*	58.90 ± 18.22*	122.62 ± 9.51*	136.42 ± 14.65*
t		11.123	5.851	16.057	26.408	17.962
P		≤0.001	≤0.001	≤0.001	≤0.001	≤0.001

*$P < 0.05$.

Table 2: Changes of lower urinary tract in patients before and after surgery ($\bar{X} \pm s$).

Group Pre	n 119	BNM (cm)	RBV (mL)	BRA (°)	DWT (mm)
Post	119	0.43 ± 0.18	4.83 ± 1.07	4.30 ± 1.19	3.70 ± 0.64
t		0.64 ± 0.17*	12.82 ± 2.69*	12.11 ± 2.43*	4.48 ± 0.82*
P		9.253	30.107	31.488	8.180
		≤0.001	≤0.001	≤0.001	≤0.001

*$P < 0.05$.

Table 3: Comparison of the quality of life of the two groups of patients before and after surgery ($\bar{X} \pm s$).

Group Pre	n 119	Emotion function	Mental function	Social function	Physiological function
Post	119	1.02 ± 0.52	1.20 ± 0.52	1.20 ± 0.58	1.00 ± 0.52
t		2.34 ± 0.76*	2.42 ± 0.71*	2.38 ± 0.81*	2.18 ± 0.74*
P		16.637	15.122	12.921	14.232
		≤0.001	≤0.001	≤0.001	≤0.001

*$P < 0.05$.

2.6. Comparison of the Quality of Life of the Two Groups of Patients before and after Surgery. As shown in Table 3, the scores of the patients after operation were higher than before operation ($P < 0.05$), that means the quality of life after operation was worse.

3. Discussion

From the perspective of human anatomy, the female pelvic cavity involves the cervix, uterus, and supporting tissues, as well as part of the pelvic lymph nodes and vagina, which can play important role in undertaking and supporting to ensure the normal state of pelvic organs [7]. Pelvic floor dysfunction can lead to pelvic floor dysfunction diseases such as stress urinary incontinence and pelvic organ prolapse. According to research reports, childbirth and surgery are the main causes of pelvic floor dysfunction. The hysterectomy not only needs to cut off the main and sacral ligaments in the center of the pelvic floor but also needs to push down the bladder and rectum, which causes about 20% patients have symptoms of urinary and stool disorders and incontinence [8].

At present, the clinical methods for evaluating the structural and functional changes of the female pelvic floor mainly include clinical staging, urodynamic examination, and acupressure test, while the imaging methods used for the examination of female pelvic floor dysfunction mainly include CT, ultrasound, and nuclear magnetic resonance [9]. Although MRI technology has high contrast resolution and good impact space, it is difficult to repeat observation due to its high cost, long inspection time, and cannot dynamically observe pelvic function. CT is difficult to be accepted by patients because of its radiation, ultrasound because of its minimally invasive, nonradiation, dynamic observation, and other characteristics, it is widely used in clinical examination and diagnosis [10, 11]. Four-dimensional pelvic floor ultrasound is a new inspection method, which is real-time dynamic imaging based on three-dimensional ultrasound [12]. Clinical studies have shown that four-dimensional pelvic floor ultrasound for pelvic floor dysfunction can dynamically observe the three-dimensional image of the pelvic floor and pelvic floor muscles in real time through three-dimensional stereo imaging, making up for the insufficiency of two-dimensional plane ultrasound, making clinical diagnosis more intuitive and

Hindawi
Scanning
Volume 2023, Article ID 9756591, 1 page
https://doi.org/10.1155/2023/9756591

Retraction

Retracted: Sports Injury Risk Prevention and MRI Image Performance of Athletes in Physical Education

Scanning

Received 3 October 2023; Accepted 3 October 2023; Published 4 October 2023

This article has been retracted by Hindawi following an investigation undertaken by the publisher [1]. This investigation has uncovered evidence of one or more of the following indicators of systematic manipulation of the publication process:

(1) Discrepancies in scope

(2) Discrepancies in the description of the research reported

(3) Discrepancies between the availability of data and the research described

(4) Inappropriate citations

(5) Incoherent, meaningless and/or irrelevant content included in the article

(6) Peer-review manipulation

The presence of these indicators undermines our confidence in the integrity of the article's content and we cannot, therefore, vouch for its reliability. Please note that this notice is intended solely to alert readers that the content of this article is unreliable. We have not investigated whether authors were aware of or involved in the systematic manipulation of the publication process.

Wiley and Hindawi regrets that the usual quality checks did not identify these issues before publication and have since put additional measures in place to safeguard research integrity.

We wish to credit our own Research Integrity and Research Publishing teams and anonymous and named external researchers and research integrity experts for contributing to this investigation.

The corresponding author, as the representative of all authors, has been given the opportunity to register their agreement or disagreement to this retraction. We have kept a record of any response received.

References

[1] J. Yang, "Sports Injury Risk Prevention and MRI Image Performance of Athletes in Physical Education," *Scanning*, vol. 2022, Article ID 1166314, 7 pages, 2022.

Hindawi
Scanning
Volume 2022, Article ID 1166314, 7 pages
https://doi.org/10.1155/2022/1166314

Research Article

Sports Injury Risk Prevention and MRI Image Performance of Athletes in Physical Education

Jun Yang

School of Physical Education, Ankang University, Ankang, Shaanxi 725099, China

Correspondence should be addressed to Jun Yang; 0107020@yzpc.edu.cn

Received 25 July 2022; Revised 27 August 2022; Accepted 13 September 2022; Published 28 September 2022

Academic Editor: Danilo Pelusi

In order to effectively prevent athletes' injury during sports training in physical education, a method of risk prevention of sports injury based on MRI technology was proposed. This method solves the problem of injury prevention in sports training by studying the association analysis algorithm in data mining technology and the research of MRI technology. The experimental results show that the average prediction error of CT and US is about 5%, so it can be considered that the model can predict accurately. *Conclusion*. The method of risk prevention of sports injury based on MRI technology can effectively prevent the injury of athletes in the process of sports training and reduce the injury rate of athletes.

1. Introduction

In order to better play their own strength in the training process, athletes often exert too much force, which will cause the occurrence of sports injury. Sports injury caused by athlete training is often a convoluted complex, and such sports injury is generally accompanied. Players need rehabilitation training; light weight sports injury can cause sports career to come to an end. Many excellent athletes because of injury had to say goodbye to the sports career ahead of time. It can be said that sports injury has become a problem that many athletes have to face. Therefore, the athlete injury prevention is very important in the process of movement [1].

Medical imaging is a device-dependent discipline. Medical imaging equipment, especially CT MR equipment, is driven by the most rapid and cutting-edge technology in natural science and is developing at a veritable speed with each passing day [2–4]. At each stage of the development of medical imaging, it will have an important and sometimes epoch-making impact on other clinical disciplines closely related to it. Currently, the development of medical imaging represented by the development of CT MR technology is in such a stage. Among them, data mining technology plays an important role in medical imaging [5]. Nuclear magnetic resonance (NMR) refers to an atomic nucleus with a fixed magnetic moment, e.g., ^{1}H and ^{13}C. Under the action of constant magnetic field and alternating magnetic field, the phenomenon of energy exchange with alternating magnetic field is a quantitative effect of interenergy level transition, which is a new discipline that emerged in the late 19th century. Nuclear magnetic resonance phenomenon was first introduced by Hamdi and Benamira, independently observed by different methods in different laboratories at about the same time [6]. They made outstanding contributions to the research and development of nuclear magnetic resonance technology, for which they shared the Nobel Prize in Physics in 1952. From the beginning of these two classical nuclear magnetic resonance experiments, nuclear magnetic resonance technology soon received people's attention. With the progress of electrical technology and computer technology, NMR and MR1 technology also got rapid development [7, 8]. At present, nuclear magnetic resonance (NMR) technology is widely used in the study of hydrogen, and two important applied disciplines, NMR spectroscopy and NMR imaging, are generated on this basis. Figure 1 is the flow chart of data mining in NMR technology.

Based on this, through the analysis of injuries that occurred in sports training and prevention of them through medical imaging technology, this paper mainly focuses on

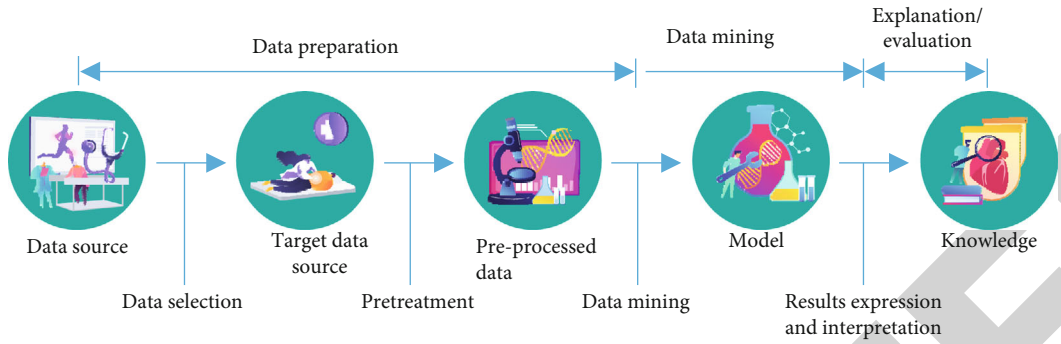

Figure 1: Data mining process.

MRI technology to discuss injury prevention, which can effectively prevent athletes from injury in the training process.

2. Literature Review

Sports injury refers to the occurrence of various traumatic sports injuries in the process of sports and sports events closely related to the technical movements, such as basketball and football which easily injured ankle joints and tennis, badminton, and table tennis that easily hurt the shoulder and elbow. Sports injury in severe life-threatening injury does not see more, a lot of damage to the skin, abrasions, and mild muscle and subcutaneous tissue contusion ligaments and tendons. Some sports injury prevention has more difficult projects, such as Sanda kickboxing and boxing, and some other body against fierce project sports injury is a minor injury or chronic injury; treatment with massage therapy is given priority [9, 10].

The physical condition of adolescent sprinters is an important factor of uneven sports injury degree. To be specific, there is a certain difference in the development of thigh muscle group and leg muscle strength of adolescent sprinters. The sprinters who have good coordination of thigh muscle group and can effectively balance the strength of leg flexor and extensor muscle will have a lower probability of sports injury. In addition, teenage sprinters also have their own exercise habits and muscle frequency in terms of pace adjustment and explosive performance. If the pace is unstable or the pace range is too large, the flexibility of the muscles cannot be reflected, and the strength borne by the tendon and the leg muscles is difficult to balance. The probability of muscle strain increases, and the athletes are more likely to suffer from sports injury [11]. Step by step, strengthen the physical performance of various functions, and do a good job of sprint sports competition before the preparation [12]. Strengthen the training of scientific development, in the process of game training teenager sprinter to their body function index to conduct a comprehensive evaluation, value of the power of their muscles and joints, and the stress range accurately, and then in view of the weak item for centralized training, strengthen the functional performance of the body, in order to better meet the requirements for sprint sports competition [13].

Nuclear magnetic resonance spectroscopy is a subject developed on the basis of magnetic resonance, which is mainly used in the study and analysis of the structure of various substances. It is also one of the most widely used fields of nuclear magnetic resonance technology at present [14]. Nuclear magnetic resonance (NMR) technology is divided into continuous wave NMR and pulsed NMR. The continuous wave NMR method uses the radio frequency field to continuously affect the nuclear system to observe and check the absorption of radio frequency energy or the resonance induction signal of the nuclear magnetization vector. Pulsed NMR method is used to observe the response signal of the nuclear system to the rf pulse in a narrow pulse mode, by induction attenuation signal (FID). From the advent of the first megahertz continuous wave commercial NMR spectrometer in 1953 to the widely used Fourier transform NMR imager, NMR technology has undergone a transformation from continuous wave to pulsed Fourier transform [15]. In particular, pulsed Fourier transform NMR spectroscopy was developed in 1966. This revolutionary leap enabled the development of high-resolution NMR spectrum and made the observation of the natural low abundance of nuclear become a reality, so that the solid NMR technology also developed [16].

In 1973, Stony Brook State University invented spatial coding with linear gradient magnetic field and obtained NMR images from experiment for the first time, thus generating another branch of nuclear magnetic resonance technology—nuclear magnetic resonance imaging (MRI). At present, MRI has developed into a powerful tool in medical diagnosis. In 1975, multidimensional NMR spectrum methodology theory was proposed, which also laid a new theoretical and experimental foundation for NMR imaging. NMR-CT was developed as "Fourier imaging," making NMR imaging different from CT and named as MRI [17].

Data mining is a process of extracting potentially useful information and knowledge hidden in a large amount of incomplete noisy fuzzy random actual application data, which is generally composed of data preparation stage, data mining stage, and result expression and interpretation stage. The data preparation stage can be further divided into data integration, data selection, and data preprocessing. The stage of mining operation includes determining the target of data mining and selecting appropriate tools to excavate knowledge and confirming the discovered knowledge. The task of the result expression and interpretation stage requires not only to express the result but also to filter the information. If the result is not satisfactory to the decision maker, the above data mining process should be repeated.

Based on the above research, MRI technology of injury prevention in athletes' sports training is deeply discussed and studied in this paper, and the occurrence of athletes' sports injuries can be further prevented by using data mining technology and MRI technology.

3. Research Method

3.1. The Specific Process of Data Mining Technology

3.1.1. The Association Rule Algorithm. Association rules are used to screen out the frequency relationship of data item sets in transaction database from a set of given data items and transaction database (each transaction is a collection of data items) and find the valuable correlation between data item sets in a large number of data. When mining association rules, various events in database data should be regarded as data items, and multiple data items constitute the item set of a particular thing. For example, in the medical image database, for the event of patient treatment, each examination item in the process of treatment constitutes its data item set. Microsoft association rule algorithm belongs to Apriori rule algorithm series, which can be divided into two steps: One is to find all frequent item sets whose support is greater than or equal to the predefined minimum support threshold; the other is to generate strong association rules satisfying the minimum confidence from frequent item sets.

3.1.2. Data Preparation. Due to the lack of necessary data verification during the migration of data use and maintenance for many years, as well as the gradual online of the functional modules of the image information system software, and the human error of the data input by the staff, repeated data loss, incompleteness, and error may result. Therefore, in order to ensure the quality of data, it is necessary to process the data. EISStudies and EISService of the RIS database of a hospital have recorded the information of examination items of hospital patients since 2005, from which the basic attributes of patients (number, name, gender, date of birth, etc.) are extracted. A new table was established for patient types (physical examination, outpatient, emergency, and hospitalization) and examination items (number, name, type, etc.). Due to the irregularities in the original entry of examination items, the same examination item has different numbers and names. For example, (X-ray (digital) chest radiography (orthographic)CR) and (X-ray (digital) chest radiography (orthographic)CR) are the same examination item. In order not to affect the analysis results, the examination items should be standardized and unified.

3.1.3. Frequent Item Sets and Association Rules. The primary task of the association rule algorithm is to mine frequent item sets. In order to obtain useful item sets and rules and reduce the model processing time due to the large number of patient examination items, the minimum-support parameter is set to 0.03; that is, only items with a frequency of no less than 3% are selected to generate association rules [18]. Figure 2 shows the generation process of frequent item sets.

According to the generation process of the above frequent item sets, the model generates association rules

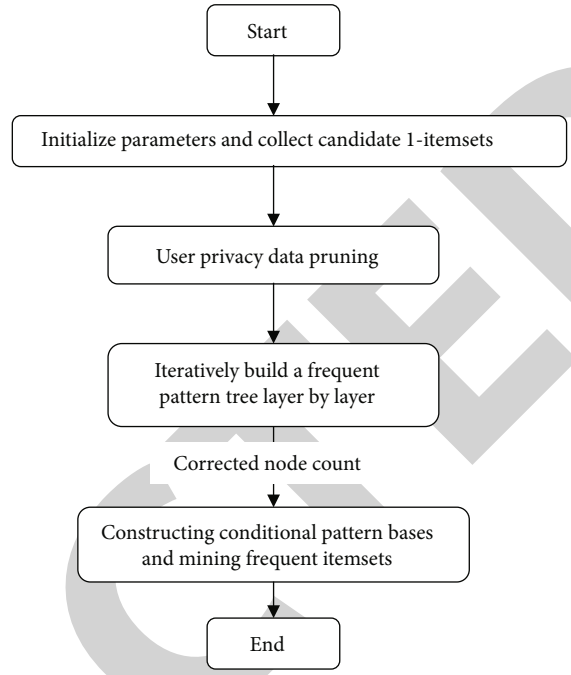

Figure 2: The generation process of frequent item sets.

(see Table 1), where the confidence refers to the probability of the occurrence of result B in the case of condition A. Importance refers to the logarithm of the proportion of the probability of outcome occurrence when the condition is established and when the condition is not established. The importance score is greater than zero, indicating that the rule is meaningful, and the larger the score is, the more significant the rule is. As can be seen from Table 1, in the physical examination items, the probability of patients receiving color ultrasound B (kidney, ureter, bladder, and prostate) and color ultrasound A (liver, gallbladder, spleen, and pancreas) was 98.2%, and the importance score of rules was 1.157. In hospitalized patients, the probability of simultaneous thoracotomy DR with the LEFT and right deep venous US was 73.1%, and the importance score of this rule was 2.867. It can be found that patients with physical examination have a high degree of confidence, which is consistent with the actual situation that patients with physical examination will do some examination item combination packages. However, for patients with door and emergency treatment, due to the uncertainty of examination items, the confidence degree of rules is generally not as high as that of physical examination.

Through association rule analysis, the correlation degree of examination items in patients' medical treatment can be found. If further combined with the disease type of patients, it can provide a basis for hospital clinical path management.

3.2. Equipment Inspection Quantity Forecast

3.2.1. Time Series Algorithm. The Microsoft sequential algorithm encapsulates two different computer learning algorithms. The first algorithm is the automatic regression tree (ART XP) using crossprediction, and the second algorithm

Table 1: Table of association rules.

Patients with type	Generated association rules	Confidence coefficient (%)	Importance
Physical examination	Color ultrasound B (kidney, ureter, bladder, prostate) color ultrasound A (liver, gallbladder, spleen, pancreas)	98.2	1.157
Be hospitalized	Deep vein US of left and right lower limbs→pereon DR	73.1	2.867
Emergency treatment	The four limb CR, plain scan of the liver, gallbladder, spleen, and pancreas→head CT plain scan	66.4	1.512
Outpatient service	Chest DR, arms, ureter, bladder, prostate→liver, spleen, and pancreas	73.2	1.101

is the automatic regression integrated with moving mean (ARIMA). By default, the Microsoft sequential algorithm combines the advantages of the two algorithms to achieve optimal prediction results [19].

3.2.2. Time Series Model Establishment and Verification. The modern imaging department has a large number of MRI digital imaging equipment, such as CT MR, CR, DR, and DF. Monthly inspection quantity of each equipment type is extracted and collected from an original item information table (EIS Service) of the RIS or PACS database, and the equipment monthly inspection scale is designed for the establishment of a timing model. Since the data in the new table has been processed without missing values and the data is summarized and recorded on a monthly basis, the sequence period is set to 12. Figure 3 is the flow chart of the timing model.

3.2.3. Comprehensive Prediction. In statistics, multiple index systems are generally used for comprehensive prediction to improve the accuracy of the check quantity forecast [20]. Here, comprehensive prediction of examination volume in 2012 is made according to the two index systems of patient type and equipment type. Since the time series algorithm is adopted for the examination volume prediction of the two index systems, it is assumed that the importance of the index system is the same, and the equal weight averaging method can be adopted to determine the weight of 0.5, as shown in Formulas (1), (2), and (3).

$$\begin{aligned} Q_1 = {} & Q(A\ \text{medical}) + Q(\text{in the hospital}) \\ & + Q(\text{the emergency department}) \\ & + Q(\text{outpatient service}), \end{aligned} \tag{1}$$

$$Q_2 = Q_{CT} + Q_{US} + Q_{CR} + \cdots + Q, \tag{2}$$

$$Q = 0.5Q_1 + 0.5Q_2. \tag{3}$$

Q is the total number of tests predicted by target, is the total number of tests predicted by patient type, and is the total number of tests predicted by device type. After obtaining the total inspection quantity according to Formula (3), the inspection quantity of each equipment type can be obtained according to the following formula:

$$Q'_{CT} = Q_{CT} * \frac{Q}{Q_2}. \tag{4}$$

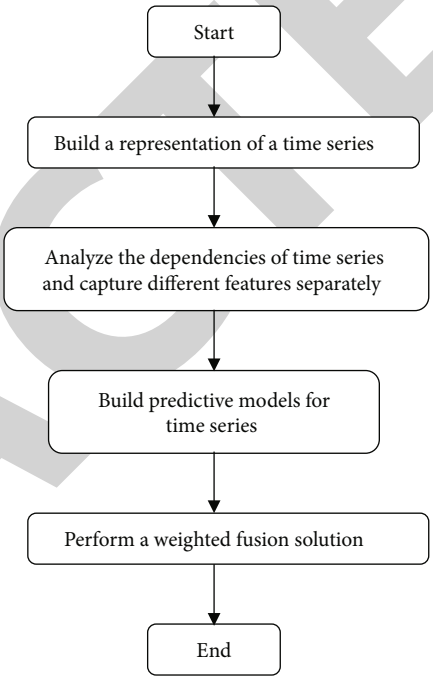

Figure 3: Sequence model flow chart.

3.3. MRI Technology and Principle. NMR signal detected by induction coil is an analog signal, which must be transformed into digital signal to reconstruct the image. Of course, the acquisition of magnetic resonance signal is not a simple digitalization of analog signal but also must conform to the sampling theorem and so on. Only by understanding the imaging method of NMR can we understand the arrangement of its original data and can we extract the data we need from the original data to calculate the distribution of T1 or T2.

There are many types of image reconstruction method; experiment using magnetic resonance imaging is a two-dimensional Fourier transform imaging. It is a special coding technique combined with inverse discrete Fourier transform and image reconstruction methods. Its characteristic is in the X, Y, and Z directions; add a gradient magnetic field to successive change corresponding direction of the spin of the proton precession phase, also known as phase encoding gradient. If the Z direction as a level will choose a gradient, with the excitation pulse function, imaging excitation level can be determined at the same time; then, in the X and Y direction applied within the excitation level on the proton gradient field space coding, acquisition of signal contains the characteristics of space information. By Fourier inverse

Table 2: Comparison table between the actual value and predicted value of inspection quantity of each equipment type in 2011.

	CT			US			MR		
	Actual value	Predicted value	Relative error	Actual value	Predicted value	Relative error	Actual value	Predicted value	Relative error
201101	4704	5020	0.0671	10946	12305	0.1239	1134	1189	0.0485
201102	4598	5112	0.1117	9732	11225	0.1534	1190	1043	0.1235
201103	5642	5518	0.0219	13757	14110	0.0256	1955	1424	0.2716
201104	5617	5678	0.0108	14338	14288	0.0034	1872	1388	0.2585
201105	5876	5772	0.0176	16591	15403	0.0716	1991	1365	0.3144
201106	5563	5782	0.0393	17100	15743	0.0793	2027	1436	0.2916
201107	5634	5748	0.0202	17409	17298	0.0063	2040	1427	0.3005
201108	5983	5864	0.0196	17314	16281	0.0596	2105	1155	0.4513
201109	5249	5897	0.1234	15988	14778	0.0756	1868	1335	0.2853
201110	5763	5991	0.0396	14772	14197	0.0389	2079	1336	0.3574
201111	5609	5841	0.0413	16180	15051	0.0697	2067	1252	0.3943
201112	5467	5972	0.0924	14400	14392	0.0005	1790	1276	0.2874
Average error	—	—	0.0504			0.0590			0.2820

transform reduction, spatial distribution of the signal can be rebuild magnetic resonance image beans.

The magnetic resonance signal is detected during the relaxation process after the rf excitation, so the strength of the magnetic resonance signal detected from a particular tissue depends not only on the relaxation time of that tissue but also on when the relaxation is measured and by what means that magnetic resonance imaging is a multiparameter imaging technique, right. The setting of various parameters involves a variety of sequences. Different sequences and parameters are required for different tissues to meet different requirements. Related technology has also developed into an independent MRI, which is also an important research area of MRI technology in medical application.

3.4. MRI T2 Measurement. Spin-spin relaxation is characterized by energy exchange between the same spin nuclei, so the relaxation efficiency is very high. After the nuclei are excited by an rf pulse in an external magnetic field, the time required for the process of reaching lateral thermal equilibrium within the spin system is called spin-white relaxation time, which is called T2.The rate of this energy transfer depends on the strength of the spin-spin interaction. T2 describes the decay of the transverse magnetization vector Mxy. In general, a 90 rf pulse shifts the equilibrium magnetization vector to the Y-axis, where Mxy = Mo. Subsequently, with the addition of 90 rf pulses, Mxy begins to decay in an exponential form. Since spin-spin relaxation is related to the inhomogeneity of the magnetic field, its result is represented by T2∗, which has a certain relationship with the true T2 of the system.

There are also various methods to measure T2. In this paper, CPMG pulse sequence is used in the actual measurement process, mainly to eliminate the influence of uneven magnetic field. If the magnetic field is not very uniform, the magnetization of the nucleus at different positions of

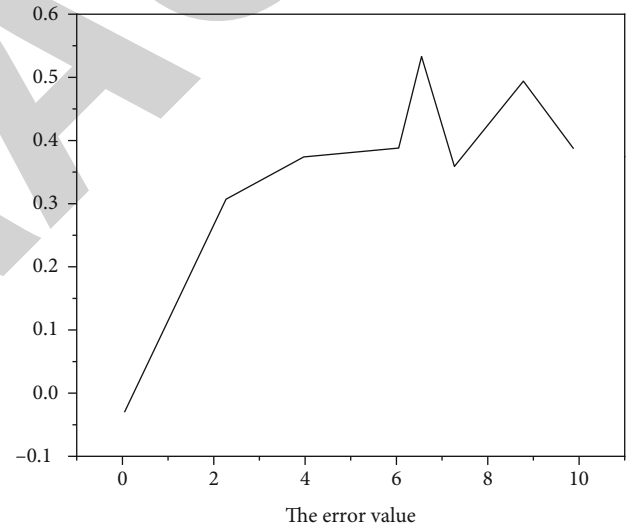

Figure 4: Statistical diagram of relative error broken line among CT, US, and MR.

the sample will be slightly different, resulting in the rotation of the nucleus at slightly different frequencies. When in uniform magnetic field, in any moment of relaxation process, all of the precession of the core of the same frequency rotation points to the same direction. In this case, all the precession nuclear in the same state or phase consistency and net magnetization of the spin system at any given time is equal to the system in any nuclear net magnetization precession, which can use the real T2 said. In contrast, in an inhomogeneous magnetic field, the precession core starts spinning at a different frequency. The spin points slightly differently, a phenomenon called spin precession phase dispersion. The spin core therefore loses phase consistency. Therefore, after the addition of the same pulse, the macroscopic magnetization

vector of the spin nucleon is smaller than that of the macroscopic magnetization vector engraved simultaneously in the homogeneous magnetic field system.

4. Results and Discussion

Table 2 lists the actual predicted values and relative errors of each equipment type in 2011. It can be seen from the table that the average prediction error of CT and US is about 5%, so it can be considered that the model can predict more accurately. The error of MR is as high as 28.2%, which is due to the mutation of examination quantity. Therefore, it is appropriate to use this time series to predict the amount of CT and US examination in MRI equipment, while MR examination quantity must be predicted by other methods. Figure 4 is the broken line statistics of CT, US, and MR relative error.

5. Conclusion

This paper studies the athlete's injury prevention of MRI techniques in the sports training study, through the correlation analysis of the research on data mining technology in the MRI algorithm of medical image information system and equipment and the principle of research, and analyzed the data mining technology in the role of MRI medical imaging information system, to solve the problem of injury prevention in the sports training. The experimental results show that the average prediction error of CT and US is about 5%. It can be considered that MRI technology can predict more accurately, indicating that this model can effectively prevent injuries in training.

Data Availability

The data used to support the findings of this study are available from the corresponding author upon request.

Conflicts of Interest

The author declares that there are no conflicts of interest.

References

[1] H. R. Song, Y. K. Yang, and J. S. Park, "The effect of exercising dance sports (tango variations routine) on the balance and muscle function of elderly people over 65 years," *Korean Journal of Sports Science*, vol. 29, no. 5, pp. 1015–1023, 2020.

[2] N. Hasani, F. Farhadi, M. A. Morris, M. Nikpanah, and B. Saboury, "Artificial intelligence in medical imaging and its impact on the rare disease community: threats, challenges and opportunities," *PET Clinics*, vol. 17, no. 1, pp. 13–29, 2022.

[3] Y. Mo, J. Liu, Q. Li, J. Ma, and H. Zhang, "Four-dimensional cone-beam CT reconstruction based on motion-compensated robust principal component analysis," *Journal of Southern Medical University*, vol. 41, no. 2, pp. 243–249, 2021.

[4] F. Susanto and H. S. Utami, "Variation of inversion delay for wrist joint MT imaging with SPAIR technique: which ID is optimal?," *Medisains*, vol. 19, no. 1, p. 9, 2021.

[5] R. A. Musa, M. E. Manaa, and G. Abdul-Majeed, "Predicting autism spectrum disorder (ASD) for toddlers and children using data mining techniques," *Journal of Physics: Conference Series*, vol. 1804, no. 1, article 012089, 2021.

[6] M. Hamdi and M. Benamira, "Crystallochemical characterizations, Raman spectroscopy and studies nuclear magnetic resonance (NMR) of Cu2Zn (Sn, Si) S4 compounds for photovoltaic applications," *Journal of Materials Science and Chemical Engineering*, vol. 10, no. 1, pp. 24–40, 2022.

[7] E. O. Ryan, Z. Jiang, H. Nguyen, and X. Wang, "Interactions of pleiotrophin with a structurally defined heparin hexasaccharide," *Biomolecules*, vol. 12, no. 1, p. 50, 2022.

[8] M. L. L. Watat, J. S. Chi, C. E. Asanji, and E. N. Nfor, "Synthesis, characterization, computational and antibacterial studies of novel dopamine-based derivatives," *International Journal of Organic Chemistry*, vol. 12, no. 1, pp. 40–52, 2022.

[9] S. H. Lhee, R. Jain, M. M. Sadasivam, S. Kim, and D. Y. Lee, "Sports injury and illness incidence among South Korean elite athletes in the 2018 Asian games: a single-physician prospective study of 782 athletes," *BMJ Open Sport & Exercise Medicine*, vol. 7, no. 1, article e000689, 2021.

[10] S. Mann and T. B. Grnlykke, "Does the Spraino low-friction shoe patch prevent lateral ankle sprain injury in indoor sports? A pilot randomised controlled trial with 510 participants with previous ankle injuries," *British Journal of Sports Medicine*, vol. 55, no. 2, pp. 92–98, 2021.

[11] K. Kim, S. Y. Yang, J. H. Park et al., "Torque-compensated bundle of artificial muscle to generate large forces," *Materials Research Express*, vol. 8, no. 11, article 115301, 2021.

[12] V. Haldane, S. Ratnapalan, N. Perera, Z. Zhang, and X. Wei, "Codevelopment of COVID-19 infection prevention and control guidelines in lower-middle-income countries: the 'SPRINT' principles," *British Medical Journal Global Health*, vol. 6, no. 8, article e006406, 2021.

[13] E. Y. Herawati, A. Darmawan, R. Valina, and R. I. Khasanah, "Abundance of phytoplankton and physical chemical parameters as indicators of water fertility in Lekok Coast, Pasuruan Regency, East Java Province, Indonesia," *IOP Conference Series: Earth and Environmental Science*, vol. 934, no. 1, article 012060, 2021.

[14] M. K. Ahmmed, A. Carne, S. Bunga, H. S. Tian, and E. Bekhit, "Lipidomic signature of Pacific lean fish species head and skin using gas chromatography and nuclear magnetic resonance spectroscopy," *Food*, vol. 365, article 130637, 2021.

[15] G. Zhou, L. Sun, C. Lu, and A. Lau, "Multi-symbol digital signal processing techniques for discrete eigenvalue transmissions based on nonlinear Fourier transform," *Journal of Lightwave Technology*, vol. 39, no. 17, pp. 5459–5467, 2021.

[16] G. Dhiman, V. Kumar, A. Kaur, and A. Sharma, "DON: deep learning and optimization-based framework for detection of novel coronavirus disease using X-ray images," *Interdisciplinary Sciences Computational Life Sciences*, vol. 13, no. 2, pp. 260–272, 2021.

[17] J. Jayakumar, S. Chacko, and P. Ajay, "Conceptual implementation of artificial intelligent based E-mobility controller in smart city environment," *Wireless Communications and Mobile Computing*, vol. 2021, Article ID 5325116, 8 pages, 2021.

[18] J. Chen, J. Liu, X. Liu, X. Xu, and F. Zhong, "Decomposition of toluene with a combined plasma photolysis (CPP) reactor: influence of UV irradiation and byproduct analysis," *Plasma*

Hindawi
Scanning
Volume 2023, Article ID 9801545, 1 page
https://doi.org/10.1155/2023/9801545

Retraction

Retracted: Diagnostic Value of Color Doppler Ultrasonography in Subacute Thyroiditis

Scanning

Received 12 December 2023; Accepted 12 December 2023; Published 13 December 2023

This article has been retracted by Hindawi, as publisher, following an investigation undertaken by the publisher [1]. This investigation has uncovered evidence of systematic manipulation of the publication and peer-review process. We cannot, therefore, vouch for the reliability or integrity of this article.

Please note that this notice is intended solely to alert readers that the peer-review process of this article has been compromised.

Wiley and Hindawi regret that the usual quality checks did not identify these issues before publication and have since put additional measures in place to safeguard research integrity.

We wish to credit our Research Integrity and Research Publishing teams and anonymous and named external researchers and research integrity experts for contributing to this investigation.

The corresponding author, as the representative of all authors, has been given the opportunity to register their agreement or disagreement to this retraction. We have kept a record of any response received.

References

[1] Y. Chen, S. Zhu, H. Chen et al., "Diagnostic Value of Color Doppler Ultrasonography in Subacute Thyroiditis," *Scanning*, vol. 2022, Article ID 7456622, 7 pages, 2022.

Hindawi
Scanning
Volume 2022, Article ID 7456622, 7 pages
https://doi.org/10.1155/2022/7456622

Research Article

Diagnostic Value of Color Doppler Ultrasonography in Subacute Thyroiditis

Yonggang Chen,[1] **Shulan Zhu**,[2] **Huabin Chen**,[3] **Liting Yao**,[1] **Jingmian Zhou**,[1] **Yi Xu**,[1] **Biqin Lin**,[1] **and Xiaoping Chen**[1]

[1]*Department of Ultrasound, Fujian Medical University Xiamen Humanity Hospital, Xiamen, Fujian 361006, China*
[2]*Department of Ultrasound, Zhongshan Hospital of Xiamen University, School of Medicine, Xiamen University, Xiamen, Fujian 361004, China*
[3]*National Demonstration Center for Experimental Electronic Information Education, Xiamen University, Xiamen, Fujian 361004, China*

Correspondence should be addressed to Shulan Zhu; 3100501048@caa.edu.cn

Received 20 July 2022; Revised 14 August 2022; Accepted 23 August 2022; Published 17 September 2022

Academic Editor: Danilo Pelusi

In order to explore the clinical effect of color Doppler ultrasonography in the diagnosis of subacute thyroiditis, a method for the diagnosis of subacute thyroiditis by color Doppler ultrasonography was proposed. From November 2019 to November 2020, 90 patients with subacute thyroiditis in our hospital were selected as the experimental group; 90 healthy people were selected as the control group during the same period. Both groups were diagnosed by color Doppler ultrasonography and compared. The experimental results showed that patients with subacute thyroiditis showed mild to moderate enlargement of the involved thyroid gland, and local or diffuse inhomogeneous hypoechoic areas may appear in bilateral or unilateral thyroid glands: irregular edges, unclear boundaries, no "ball feel," mottled changes, and accompanied by tenderness. The blood flow signal around the hypoechoic area is rich, and the internal blood flow signal is less. There was no significant increase in the blood flow velocity of the superior thyroid artery on the affected side. Color Doppler ultrasound not only is simple, economical, and non-invasive but also has a good diagnostic accuracy for subacute thyroiditis, which can provide an important basis for clinical diagnosis and treatment and is worthy of popularization and application.

1. Introduction

Thyroiditis is a series of clinical symptoms caused by pathological changes of thyroid tissue such as degeneration, exudation, necrosis, and hyperplasia. Among them, the incidence rate of Hashimoto's thyroiditis and subacute thyroiditis is relatively high. The course of thyroiditis is dynamic, which can be characterized by normal thyroid function, transient hyperthyroidism, or hypothyroidism, and a few patients will develop into permanent hypothyroidism [1]. The ultrasonic manifestations of thyroiditis in different stages will also be different. According to the different manifestations of ultrasonography, thyroiditis can be divided into diffuse type, focal type, and nodular type. Focal thyroiditis may be an early manifestation of thyroiditis or a chronic manifestation of thyroiditis. Compared with diffuse thyroiditis, it can be characterized by single or multiple nodular echoes on ultrasound. When the background of thyroid parenchyma is relatively normal, its sonogram can be diverse, which has many similarities with thyroid microcarcinoma. Subacute thyroiditis (SAT) is a common clinical thyroiditis. It is generally believed that SAT may be caused by thyroid injury caused by viral infection, and autoimmune response also plays a role in the occurrence and development of the disease. Subacute thyroiditis is a common clinical disease. There are many factors inducing the disease, and the condition is relatively complex. The health level of patients with the disease will decline, which will have a certain impact on their normal life. In the early stage of subacute thyroiditis, the disease starts rapidly, and patients

often have chills, fear of cold, loss of appetite, fatigue, and weakness. If they do not see a doctor in time, the disease is easy to develop, leading to more serious diseases. Therefore, it is very important to choose a scientific, reasonable, and accurate diagnostic method in clinic. Color Doppler ultrasound diagnosis is a common clinical diagnosis method. In recent years, with the continuous development of medical technology, color Doppler ultrasound diagnosis technology is also improving. In the diagnosis of subacute thyroiditis, color Doppler ultrasound can better observe the thyroid condition of patients, so as to diagnose the disease. The color ultrasound diagnostic images of patients with subacute thyroiditis are generally diffuse. After the focus of thyroiditis, there will be enlargement of one lobe and uneven echo. At the same time, when observing the patient's thyroid sonogram, there may also be single or multiple irregular hypoechoic areas. These echo areas have no clear boundary and contour, and the internal echo will also be uneven. The center to the periphery of the sonogram will gradually increase. Some patients will also have no echo due to physiological structure and other factors. In addition, the blood flow signal in the thyroid tissue of patients with subacute thyroiditis is usually not obvious in the low echo area, while the peripheral blood flow signal is gradually enriched, which can show star dot, ring, etc., when the blood vessels in the focus are compressed, the peak velocity of pulse Doppler will also increase. Therefore, the peak systolic velocity of human superior thyroid artery will increase to a certain extent in the presence of subacute thyroiditis. There is no obvious blood flow change in normal thyroid tissue, and there will be no blood flow signal or pressure bending. Therefore, in the diagnosis of subacute thyroiditis, color Doppler ultrasound diagnosis has significant clinical application value and is widely welcomed by doctors and patients [2].

With the clinical application and development of high-frequency ultrasound probe (Figure 1), it can clearly display the image characteristics of nodules with diameter less than 1.0 cm, which has become the first choice for thyroid diseases. The two-dimensional image can show the location, size, range, boundary, and internal echo of thyroid lesions. Combined with color Doppler ultrasound, important information such as blood flow distribution and blood flow velocity of thyroid parenchyma and lesions can be observed. Because the conventional ultrasound manifestations of focal thyroiditis and thyroid micropapillary carcinoma are very similar and the diagnosis is difficult, this paper reviews the color Doppler ultrasound manifestations of 90 patients with subacute thyroiditis, in order to further explore the value of color Doppler ultrasound in the diagnosis and differential diagnosis of subacute thyroiditis [3].

2. Literature Review

At present, scholars at home and abroad have done a lot of research on diffuse thyroid diseases such as SAT by using the ultrasonic elastography rating method: Villalba, Landry, and Brown believe that the diagnosis of typical SAT is not difficult. It usually occurs in winter and spring, with acute onset. At the initial stage of onset, it is characterized by pharyngeal pain, fatigue, general discomfort, fever of different degrees, and other symptoms of upper respiratory tract infection, including hoarseness and dysphagia. Thyroid mass and local pain are characteristic clinical manifestations [4]. Amaniampong et al. believe that SAT is multiple and has a good prognosis. Patients with mild symptoms do not need special treatment, can rest properly, and give non glucocorticoid anti-inflammatory and analgesic drugs. Patients with severe systemic symptoms, persistent high fever, goiter, and obvious tenderness can be treated with glucocorticoid. The main purpose of treatment is to reduce symptoms and prevent recurrence [5]. Hu et al. reported that normal thyroid parenchyma is composed of a large number of follicular cells filled with colloid. There are abundant capillaries between the follicles, so the hardness is small. The elastic diagram is mainly green and uniform [1]. Qi et al. reported that in the early stage of SAT, the pathological characteristics are a large number of inflammatory cells infiltrating in the thyroid stroma, destruction of follicles, formation of micro abscess, colloid overflow from microfollicles, surrounded by surrounding tissue cells, and multinuclear giant cells to form granuloma. These changes increase the number of cells per unit volume. In addition to tissue edema caused by inflammatory reaction, the hardness of the focus area will inevitably increase significantly. The elastic rendering of the focus is mainly blue. The research results of this group are also consistent with the literature report [6]. Ichou, Gauvin, and Faingold reported 2 cases of SAT diagnosed by puncture, of which 1 case showed only a small abnormal echo area on conventional ultrasound, but ultrasonic elastic imaging has obviously shown the increase of the hardness of the echo area. These studies suggest that SAT elastogram can display the lesion areas that cannot be displayed in two-dimensional ultrasound, which is of positive significance for accurately evaluating the lesion scope of SAT and finding potential lesions. This study shows that two-dimensional ultrasound was combined with ultrasound elastography [7]. Hua, Wang, and Zhang studied the clinical characteristics of 852 SAT patients before treatment and found that most of the laboratory test results were related to thyrotoxicosis and inflammation and liver dysfunction, and the abnormal peak level often appeared one week after the onset. The whole disease stage of typical SAT patients can be divided into three stages: acute stage with hyperthyroidism, remission stage with hypothyroidism (divided into transition stage and hypothyroidism stage), and recovery stage (normal thyroid function stage) [8]. Moreover, Svedin, Dillon, and Parker have found that when the volume of the lesion is too large and all the ROI contains the lesion tissue, but not the normal tissue for comparison, it is often difficult to obtain a satisfactory ultrasonic elastic image, and the results cannot reflect the real hardness of the lesion. Therefore, this study also introduces the SWV value measured by the ARFI elastic imaging vtq technology as a more objective quantitative index to judge SAT, ARFI compression, and transverse vibration. The transverse vibration propagates to the periphery in the form of shear wave. Vtq technology makes the tissue produce longitudinal. SWV can be calculated by using the time difference and wavelength of adjacent

Figure 1: High-frequency color Doppler ultrasound diagnosis.

peaks of shear wave, which can be used to reflect the hardness of tissue [9]. Tyurina et al. showed that the elastic strain rate ratio of the best diagnostic effect of benign and malignant thyroid nodules ranged from 2.96 to 4.22. The critical point of SR value in this study was 2.29, which was significantly lower than that in the above study. The reason was related to the small lesions in the malignant group. The change of microlesion hardness cannot be reflected on the elastic image, and the false negative result of elastic imaging is obtained [10].

3. Experimental Analysis

3.1. Subjects. From November 2019 to November 2020, 90 patients with subacute thyroiditis in our hospital were selected as the experimental group. The ratio of male to female patients was 47 : 43. The highest age of the patients was 69 years old, and the lowest was 21 years old, with an average of (40.37 ± 4.36) years old; the longest course of disease was 8 months and the shortest was 3 days, with an average of (45.38 ± 7.25) days [11]. In the same period, 90 healthy persons were selected as the control group, of which the male to female ratio was 55 : 45. The highest age of the patients was 68 years old, and the lowest was 22 years old, with an average of (41.31 ± 3.34) years old. Comparing the clinical data of the two groups, there was no significant statistical significance ($P > 0.05$), and the data were highly comparable [12].

Inclusion criteria: (1) The experimental group was confirmed as subacute thyroiditis by pathological diagnosis. (2) Before this study, the medical staff informed the subjects about the study and obtained the informed consent of the subjects. (3) All subjects were adults. Exclusion criteria: (1) Incomplete clinical data. (2) Combined with other serious diseases. (3) There are contraindications for color Doppler ultrasound diagnosis [13].

3.2. Experimental Method. Both groups were diagnosed by color Doppler ultrasound. The first experimental method is instrument selection. In this study, the color Doppler ultrasound diagnostic instrument with the model of LOGIQ E9 and its supporting related equipment are selected, and the probe is set as a wide range imaging linear array with the frequency of 7~14 MHz. The second method is position selection. All subjects shall be in a supine position. During the examination, a pillow shall be placed on the back shoulder of the subject, and the patient is required to stretch his neck and tilt back as much as possible to expose the thyroid area as much as possible [14]. The third method is scan diagnosis. The color Doppler ultrasound diagnostic instrument is used to scan the thyroid region of the subject in multiple sections; fully observe the shape, size, blood flow shape, capsule, and internal echo of the subject's thyroid; and measure the left and right diameter, anterior and posterior diameter, and long diameter of the thyroid, so as to fully understand the condition of the focus. At the same time, properly pressurize the probe, observe whether the subject has tenderness, and then focus on the acoustic image and blood flow characteristics of the focus, so as to further diagnose the disease. The ultrasonic images of all subjects were handed over to professionals for judgment, and the diagnostic results of the two groups were compared [15].

3.3. Observation Indicators. In this study, the anterior posterior diameter, left and right diameter, and blood flow characteristics of the thyroid gland in the affected and healthy sides of the two groups were used as observation indexes. Among them, the blood flow characteristics include the peak systolic velocity of the affected side superior thyroid artery and the peak systolic velocity of the healthy side superior thyroid artery.

3.4. Statistical Analysis. The final data of this study were processed by the spss22.0 data software. The measurement data such as the anterior posterior diameter, left and right diameter of the thyroid gland on the affected side and the healthy side, the peak systolic velocity of the superior thyroid artery on the affected side, and the peak systolic velocity of the superior thyroid artery on the healthy side were expressed by standard deviation ($x \pm s$). A t-test was used, and $P < 0.05$ indicated a statistically significant difference [16].

3.5. Experimental Analysis. The anterior and posterior diameters and left and right diameters of the affected lateral lobe thyroid in patients with subacute thyroiditis were significantly larger than those in healthy subjects, $t = 21.53$, 23.57, $P = 0.001$; the difference was statistically significant. There was no significant difference in the anterior and posterior diameter and left and right diameter of thyroid between the two groups, $t = 0.08$ and 0.04, $P = 0.97$ and 0.94. The difference was not statistically significant, as shown in Table 1.

The peak systolic velocity of superior lateral lobe artery in patients with subacute thyroiditis was significantly higher than that in healthy subjects, $t = 19.72$, $P = 0.001$. The difference was statistically significant [2]. There was no significant difference in systolic peak velocity between the two groups, $t = 1.85$, $P = 0.07$; the difference is statistically significant (see Table 2).

In the elastic group, there were 45 lesions, 43 were cured and 2 recurred. The cure rate was 95.6%, and the recurrence rate was 4.4%. In the clinical group, there were 40 lesions, 31 were cured and 9 recurred [3]. The cure rate was 77.5%, and the recurrence rate was 22.5%. There was significant difference between the two groups ($P < 0.05$) (see Table 3).

The area of lesions revealed by two-dimensional ultrasound ranged from 0.42 to 4.20 cm^2, with an average area of $1.35 + 0.90$ cm^2. The lesion area shown by elastogram ranged from 0.49 to 4.57 cm^2, with an average area of $1.77 + 0.91$ cm^2. The lesion area shown by elastogram was larger than that shown by two-dimensional ultrasound [4], and the difference was statistically significant ($t = 2.29$, $P < 0.05$) (see Table 4).

Compared with the pathological results, the SR of focal thyroiditis was 0.54–7.09, with an average of 1.760.92, and that of thyroid microcarcinoma was 1.21–9.84, with an average of $3.14 + 1.87$. The SR of thyroid microcarcinoma was significantly higher than that of focal thyroiditis. There was a significant difference between them by t-test ($P < 0.01$). The ROC curve is constructed with sensitivity as the ordinate and 1-specificity as the abscissa, as shown in Figure 2.

4. Discussion

Subacute thyroiditis is an autoimmune disease caused by viral infection. Patients often have a history of respiratory tract infection before onset. In the early stage of clinical onset, they often have pharyngeal pain, fever, and upper respiratory symptoms, which can be accompanied by increased erythrocyte sedimentation rate and abnormal thyroid function. The destruction and edema of thyroid follicles can lead to the increase of thyroid volume. The two-dimensional ultrasound image shows flake hypoechoic area, and some of them show nodular changes. Color Doppler ultrasound shows that the blood supply in the hypoechoic area is less than that in the normal tissue, and the blood supply around the nodular type is more abundant. This disease should be differentiated from the following diseases: (1) it should be differentiated from thyroid papillary carcinoma. Most of the lesions in the latter have clear boundaries and internal gravel calcification. Color Doppler flow imaging (CDFI): the blood flow in the lesions is rich. (2) Compared with chronic lymphocytic thyroiditis, the sonogram of the latter showed increased uniformity, obvious isthmus thickening, and CDFI: rich blood flow signals, mostly manifested as "Fire Sea sign.". (3) Compared with acute suppurative thyroiditis, the latter has a history of severe blood circulation infection such as hyperthermia and sepsis, and ultrasound showed irregular dark areas in the focus area. Two-dimensional ultrasound and color Doppler ultrasound can well show the focus and blood supply of subacute thyroiditis, with characteristic sonographic changes. Combined with clinical manifestations, ultrasound has high diagnostic accuracy and important diagnostic value for subacute thyroiditis.

Thyroiditis is not uncommon in clinic. Most patients are easy to diagnose because of their typical clinical manifestations, such as low fever, anterior cervical pain, goiter, and significantly accelerated ESR. However, some patients still have atypical symptoms in the initial stage of onset, which is difficult to distinguish from diseases such as upper respiratory tract infection, pharyngitis, thyroid nodule, or parenchymal hemorrhage [5]. The results show that the ultrasonic manifestations of subacute thyroiditis have certain characteristics: uneven echo reduction changes in varying degrees appear in the thyroid of all patients, most of which are one or more blurred echo reduction areas (limited type) in unilateral or bilateral thyroid, and a few are diffuse echo reduction changes (diffuse type) in unilateral or bilateral thyroid. There was significant tenderness in all hypoechoic sites, and the thickness of thyroid on the changed side of hypoechoic was significantly higher than that of normal ($P < 0.01$). The above results are consistent with the literature reports. The reason may be related to thyroid follicular destruction, inflammatory cell infiltration, and interstitial edema caused by inflammatory reaction. The more severe the inflammatory reaction is, the more obvious the echo reduction is. Some areas even show "cyst like" changes, but there is no later enhancement effect, so it can be distinguished from the real cystic lesions. In this paper, color ultrasound shows that the blood flow signal in the lesion is generally slightly higher than that in the surrounding normal tissues, but the distribution is uneven. Among them, the blood flow signal distribution in the area with significantly reduced echo is less. This study suggests that the part with more blood flow signal distribution may be the lesion in the early recovery state, while the area with significantly reduced echo has less blood flow distribution due to heavy inflammatory reaction and obvious interstitial edema. Doppler measurement shows that the arterial blood flow in the lesion is characterized by low resistance and low speed [17]. At the same time, although some patients will have increased thyroid hormone levels in the blood in the early stage of the disease, the increase is mild, which is reflected in the limited echo reduction type, and the speed of the superior thyroid artery on the lesion side is not significantly higher than that of normal. In diffuse hypoechoic type, the velocity of superior thyroid artery may be higher than normal due to the large range of lesions and severe condition. In differential diagnosis, diffuse hypoechoic subtype of thyroiditis is similar to Graves' disease and Hashimoto's disease

Table 1: Comparison of the anterior and posterior diameters and left and right diameters of thyroid gland in the affected and healthy sides of the two groups.

Group	Number of lateral leaves	Anterior posterior diameter of thyroid	Left and right thyroid diameter
Bilateral lobes in the control group	200	15.12 ± 1.76	21.13 ± 1.74
Experimental group affected lateral lobe	100	20.12 ± 2.17	26.11 ± 2.24
Contralateral lobe of experimental group	100	15.18 ± 1.78	20.23 ± 1.71
t (ratio of the affected side of the experimental group to the control group)		22.53	21.57
P (ratio of the affected side of the experimental group to the control group)		0.001	0.001
T (ratio of healthy side of experimental group to control group)		0.08	0.04
P (ratio of healthy side of experimental group to control group)		0.97	0.94

Table 2: Comparison of the peak systolic velocity of superior lobar artery on the affected side and healthy side between the two groups.

Group	Number of lateral leaves	Peak systolic velocity of superior artery
Bilateral lobes in the control group	200	22.44 ± 5.24
Experimental group affected lateral lobe	100	35.32 ± 5.33
Contralateral lobe of experimental group	100	21.71 ± 4.24
t (ratio of the affected side of the experimental group to the control group)		18.72
P (ratio of the affected side of the experimental group to the control group)		0.001
T (ratio of healthy side of experimental group to control group)		1.84
P (ratio of healthy side of experimental group to control group)		0.07

Table 3: Comparison of curative effect and course of treatment between the two groups.

Group	Number of lesions/piece	Course of treatment/D	Cure rate (%)	Recurrence rate (%)
Elastic group	45	93 ± 18	95.6	4.4
Clinical group	40	85 ± 21	77.5	22.5

Table 4: Comparison of elastogram grades between subacute thyroiditis disease group and healthy control group.

Elastic grading	SAT group	Control group	/P value
1	0	0	
I	0	31	
II	2	9	117.48 $P < 0.01$
III	55	0	
IV	28	0	

on sonogram, while limited hypoechoic type should be distinguished from papillary thyroid carcinoma and limited Hashimoto's disease. According to the author's experience, the vast majority of subacute thyroiditis show obvious tenderness during pressure scanning of its echo reduction area. This feature is rare in the above other thyroid diseases [18]. If combined with clinical manifestations at the same time, there is generally no great difficulty in differential diagnosis. For a small number of patients with atypical ultrasonic and clinical manifestations, ultrasound-guided puncture biopsy is needed for definite diagnosis.

100 patients were followed up by ultrasound after 1 ~ 6 months of treatment. Among them, 90 cases of hypoechoic areas completely disappeared or significantly narrowed, and 10 cases showed the increase of lesion scope or the change of "wandering shape" of lesions. After increasing the dosage or prolonging the medication time, the lesion areas significantly decreased or disappeared. The above results show that ultrasound can clearly distinguish the clinical treatment effect of subacute thyroiditis. Some authors reported that although most of the hypoechoic areas of subacute thyroiditis disappeared completely after treatment, a small number of patients still had small pieces of slightly

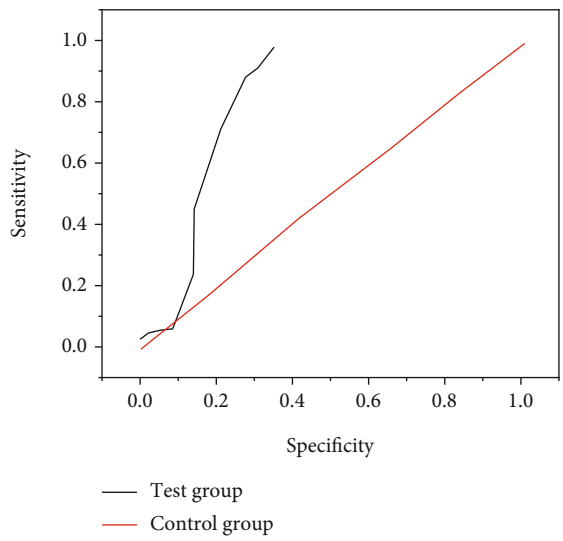

Figure 2: ROC curve of differential diagnosis between focal thyroiditis and thyroid microcarcinoma by elastic strain rate ratio method.

hypoechoic areas in their thyroid after long-term follow-up. Two cases were also seen in this paper (after 6 months of observation), but the distribution of blood flow signals in them was close to the surrounding normal thyroid tissue [10]. To sum up, the 2D and CDI manifestations of thyroiditis have certain characteristics, which can not only help the clinical diagnosis and differential diagnosis of the disease but also provide great help for the clinic in judging the treatment effect.

5. Conclusion

The thyroid lesions in the acute stage of SAT showed the internal punctate or abundant punctate blood flow distribution of the lesions, which was more concentrated without surrounding blood flow. Although the blood flow display distribution was not characteristic, it was different from the blood flow distribution around the lesions of adenoma and nodular goiter. The blood flow distribution of the focus in the acute phase of SAT reflects the inflammatory changes and blood flow changes of the focus in the acute phase. Observing the blood flow of the focus can better reflect the healing process and is a good index to guide the treatment. Two-dimensional ultrasound can show thyroiditis lesions in the acute stage of SAT, which has characteristic ultrasound images. Combined with clinical data, two-dimensional ultrasound has high diagnostic value in the acute stage of SAT. In conclusion, color Doppler ultrasound diagnosis in the diagnosis of subacute thyroiditis can better diagnose the disease and provide more reference data for follow-up treatment. It has high accuracy and safety and is worthy of clinical application.

Ultrasound can detect small lesions in the thyroid and can also vividly describe the blood supply and hemodynamic parameters inside and around the lesions. The purpose of applying combined ultrasound technology is to make a more accurate judgment on the nature of thyroid lesions through comprehensive analysis of multiple ultrasound indicators, so as to reduce unnecessary surgery, provide more accurate preoperative diagnosis for patients with thyroid cancer, and guide clinicians to develop more reasonable surgical methods for patients. In recent years, various new ultrasonic technologies have developed rapidly, such as ultrasonic elastic imaging technology, contrast-enhanced ultrasound, ultrasonic firefly technology, and two-dimensional ultrasonic imaging technology, which are constantly widely used in clinic. Interventional ultrasound technology will also develop safer and more advanced in the future, so as to improve the accuracy of puncture. With the further improvement and deepening of ultrasound technology research, ultrasound will have a broader application prospect in the diagnosis and characterization of small thyroid lesions.

Data Availability

The data used to support the findings of this study are available from the corresponding author upon request.

Conflicts of Interest

The authors declare that they have no conflicts of interest.

Acknowledgments

This study is funded by the 2021 Xiamen Medical and health Guidance Project, No. 3502Z20214ZD1101.

References

[1] Y. Hu, X. Wang, L. Jia, Y. Wang, and Y. Xin, "Diagnostic accuracy of high-frequency ultrasound in bleeding Meckel diverticulum in children," *Pediatric Radiology*, vol. 50, no. 6, pp. 833–839, 2020.

[2] J. Kim, H. M. Lew, J. H. Kim, S. Youn, and J. Y. Hwang, "Forward-looking multimodal endoscopic system based on optical multispectral and high-frequency ultrasound imaging techniques for tumor detection," *IEEE Transactions on Medical Imaging*, vol. 40, no. 2, pp. 594–606, 2020.

[3] M. Y. Wang, T. H. Yang, H. Huang, H. Y. Hsu, and C. C. Huang, "Evaluation of hand tendon movement by using high-frequency ultrasound vector doppler imaging," *IEEE Transactions on Biomedical Engineering*, vol. 67, no. 10, pp. 2945–2952, 2020.

[4] A. I. Villalba, T. Landry, and J. Brown, "Parallel computing using python-based software for a high-frequency ultrasound system," *The Journal of the Acoustical Society of America*, vol. 146, no. 4, pp. 3073–3073, 2019.

[5] P. N. Amaniampong, Q. T. Trinh, K. Vigier, D. Q. Dao, and F. J. Jérôme, "Synergistic effect of high-frequency ultrasound with cupric oxide catalyst resulting in a selectivity switch in glucose oxidation under argon," *Journal of the American Chemical Society*, vol. 141, no. 37, pp. 14772–14779, 2019.

[6] L. Qi, Q. Zhang, Y. Tan, K. H. Lam, H. Zheng, and M. Qian, "Non-contact high-frequency ultrasound microbeam stimulation: a novel finding and potential causes of cell responses,"

Hindawi
Scanning
Volume 2023, Article ID 9879863, 1 page
https://doi.org/10.1155/2023/9879863

Retraction

Retracted: Effect of Rehabilitation Physical Training on PE Teaching Sports Injury under Ultrasonic Examination

Scanning

Received 3 October 2023; Accepted 3 October 2023; Published 4 October 2023

This article has been retracted by Hindawi following an investigation undertaken by the publisher [1]. This investigation has uncovered evidence of one or more of the following indicators of systematic manipulation of the publication process:

(1) Discrepancies in scope

(2) Discrepancies in the description of the research reported

(3) Discrepancies between the availability of data and the research described

(4) Inappropriate citations

(5) Incoherent, meaningless and/or irrelevant content included in the article

(6) Peer-review manipulation

The presence of these indicators undermines our confidence in the integrity of the article's content and we cannot, therefore, vouch for its reliability. Please note that this notice is intended solely to alert readers that the content of this article is unreliable. We have not investigated whether authors were aware of or involved in the systematic manipulation of the publication process.

In addition, our investigation has also shown that one or more of the following human-subject reporting requirements has not been met in this article: ethical approval by an Institutional Review Board (IRB) committee or equivalent, patient/participant consent to participate, and/or agreement to publish patient/participant details (where relevant).

Wiley and Hindawi regrets that the usual quality checks did not identify these issues before publication and have since put additional measures in place to safeguard research integrity.

We wish to credit our own Research Integrity and Research Publishing teams and anonymous and named external researchers and research integrity experts for contributing to this investigation.

The corresponding author, as the representative of all authors, has been given the opportunity to register their agreement or disagreement to this retraction. We have kept a record of any response received.

References

[1] W. Li, "Effect of Rehabilitation Physical Training on PE Teaching Sports Injury under Ultrasonic Examination," *Scanning*, vol. 2022, Article ID 1470303, 6 pages, 2022.

Hindawi
Scanning
Volume 2022, Article ID 1470303, 6 pages
https://doi.org/10.1155/2022/1470303

Research Article

Effect of Rehabilitation Physical Training on PE Teaching Sports Injury under Ultrasonic Examination

Wangda Li

School of Physical Education, Ankang University, Ankang, Shaanxi 725099, China

Correspondence should be addressed to Wangda Li; 3100501001@caa.edu.cn

Received 5 August 2022; Revised 27 August 2022; Accepted 5 September 2022; Published 17 September 2022

Academic Editor: Danilo Pelusi

In order to solve the problem of the effect of rehabilitation physical training on physical education teaching injury, a method based on ultrasonic examination of rehabilitation physical training on physical education teaching injury effect observation method is proposed. In this method, the ISOMED isokinetic muscle strength test, the body shape test, the balance ability test, the lower limb explosive power test, and other methods are used to evaluate the knee joint of patients systematically, and the specific rehabilitation physical training plan is formulated to achieve the treatment purpose. The experimental results show that after the targeted training, a series of indicators on the affected side increase significantly: the power increases by 45.6%, the force increases by 8.3%, and the speed increases by 38.7%. It is concluded that the muscle strength, shape, balance ability, and lower limb explosive power of patients are significantly improved, which lays a solid foundation for athletes to recover smoothly and achieve good competition results.

1. Introduction

Physical training itself is a sport with strong sports intensity and high physical energy consumption. In the actual teaching process, when the training intensity required by teachers is too high, students' physical function is difficult to bear, so it is easy to cause injury. Of course, this is only one reason, and the other reason is that the balance between the exercise intensity and the training amount is not fully grasped. Before students' physical training activities, the first thing teachers should do is to lead students to complete the warm-up activities of sports, so that the muscles of the whole body are in a relaxed state, so as to effectively enhance students' muscle toughness [1]. But, in general, when part of the physical education teachers in colleges and universities lead the students to do exercises or a warm-up, they do not fully play the role of the warm-up activity, which consumes time, but the effect is not good. Because the students' understanding of the importance of a warm-up is not sufficient, in the process of preparing activities, they are perfunctory, eventually leading to the generation of sports injury. Unscientific and nonstandard technical movement is the main cause of sports injury. In the process of physical training activities, students, as the adaptable objects and subjects of training activities, have great individual differences and prominent differences in subjects. Each student's physical quality and learning ability will be different. Therefore, when teachers explain the essentials of technical movements, not all students can fully understand the essential skills taught by teachers, and not all students can use them proficiently and achieve standard movements [2]. For example, the football sport looks simple, but it tests the practitioner's body quality, participation attitude, strain capacity, and psychological state. At the same time, under the influence of external factors, it may also may prevent students from keeping a good state on the pitch, which can lead to a technical foul and collision conditions, thus sports injury problems. There is no absolute relationship between the occurrence of sports injuries and specific sports events, but there are some rules that can be used to refer to avoid more injuries. The main reason for the damage is that in the process of exercise, due to the confrontation between the two sides, there are many quick stops and rapid turns and so on, and these postures will inevitably affect the muscles in the waist and abdomen. Obviously, in

order to achieve the effect of fitness, we not only need to rely on exercise but also have the ability to analyze the rules of exercise and nursing knowledge [3]. Only in this way can we detect sports injuries in time and treat them quickly. Through the comparison and analysis of the damage area and the relationship between the sports events, it can be found that the damage area is mainly caused by some common action in the process of movement. As a result, there are some laws between the two factors, namely, certain key action and frequent action may cause damage to the corresponding part of the muscle [4]. For example, the most common injury part in football is the ankle and the related joints used in shooting. The shooting action in basketball, including jumping and running, will cause damage to the ankle and peripheral joints. At the same time, if the strength is too high during the passing, it is easy to tear ligaments and damage the meniscus. In addition, long-term confrontation sports can also cause tissue damage, such as muscle strain.

2. Literature Review

The characteristics of intense confrontation and high intensity of football determine that sports injuries will inevitably occur in college football training and competition. After the occurrence of sports injury, the conventional treatment is usually drug treatment or surgical treatment, reduction of training intensity, or suspension to promote the recovery of athletes, as shown in Figure 1 [5]. However, the above conventional treatment methods and treatment arrangements are mainly aimed at the treatment and rehabilitation strategies of the injury site, but they do not solve the root causes of the injury. In fact, in college football training, many acute injuries and chronic injuries are related to the athletes' own physical deficiency or physical decline, which is also an important reason why many sports injury accidents occur near the end of the training [6]. Injury treatment with medical means alone is helpful for the rehabilitation of injured parts, but it cannot solve the problem of athletes' lack of physical strength [7]. Even because of the reduction of training intensity or suspension during the treatment of rest, physical decline may appear in the athletes. In such a situation, coupled with the root causes of the injury of athletes which have not been solved, after the recovery of injury and reentry to normal training activities, athletes are often prone to recurrent injury problems, thus affecting the health level and sports level of athletes. Rehabilitation physical training is significantly different from the injury treatment by medical means alone [8]. Rehabilitation physical training is based on the support of rehabilitation medicine, which organically combines the athlete's rehabilitation and physical training. It not only helps in the treatment and rehabilitation of sports injuries but also can improve the physical reserves of athletes through long-term targeted application in athletes' daily training. This prevents the recurrence of sports injuries and achieves the "1 + 1 > 2" effect of rehabilitation and physical training, allowing athletes to better adapt to the needs of special football training and competitive competitions. Football players not only need sufficient strength qualities but also have higher requirements for qualities such as speed, agility, coordination, and endurance. At the same time, in football, the movements of the lower limbs account for a large proportion. The most common football injury is found to be the knee meniscus injury (prevalence 12.1%) [9]. Because the knee joint is located in the middle of the lower extremity, it needs to bear more stress and performs long-lasting three-dimensional movement, so the probability of injury is greater [10]. In the research, the concept and the method of rehabilitation physical training are applied to patients with knee joint injury, and the systematic and phased assessment is conducted through isokinetic muscle strength, lower limb circumference, and balance ability test methods [11]. According to the test results, the specific rehabilitation physical training can make their knee joints recover well, improve their physical quality and ability, and lay a solid foundation for good competition results.

3. Methods

3.1. Retrospective Research Subjects. The patient is female, 18 years old, a Chinese youth female football player, and a defender. During the training of the national team, there was discomfort in the right knee joint, with functional dysfunction and edema in the knee joint. Results of MRI film evaluation by a third-grade hospital are as follows: (1) anterior cruciate ligament (ACL) fracture of the right knee, (2) massive effusion of the right knee joint, and (3) rupture of the medial meniscus of the right knee and atrophy of the quadriceps muscle [12]. The medial meniscus of the right knee was removed, and the anterior cruciate ligament reconstruction of the right knee was performed. And then, physical training is carried out for rehabilitation.

3.2. Test Instrument and Method. The ISOMED isokinetic test system (including dynamic instrument, force measurement platform, and computer and various joint test accessories) is used to test isokinetic force. The system can set the movement speed of 0~500°/s. Four movements of knee flexion and extension, knee internal and external rotation, and ankle dorsiflexion/plantarflexion are selected. The slow peak torque is selected as the evaluation index reflecting the maximum muscle strength of the knee and ankle joints of athletes [13]. The body shape test includes body composition and lower limb muscle circumference test. The InBody 3.0 body composition analyzer is used for the comprehensive analysis of human composition. For lower limb circumference, thigh circumference and calf circumference are used to reflect the growth of muscle volume. The balance ability reflects the stability of lower limbs by standing on one foot with eyes closed. Lower limb explosive force is tested by the CMJ mode of a single-leg Counter Movement Jump, and the data are collected by the MYOTEST explosive force tester [14].

3.3. Rehabilitation Training Program. According to the patient's injury response and test results, a personalized training program is developed, which is divided into three stages for 5 weeks. The training program is optimized by

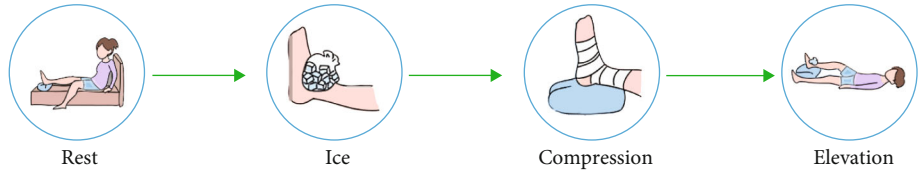

Figure 1: First aid method for sports injury.

Table 1: Rehabilitation training arrangement.

The training phase	Purpose of training	Training time and schedule	Training content and specific arrangements
Weeks 1-2	Restore knee joint function; improve the basic strength of the affected knee joint	Monday to Friday	(1) Functional training: it involves the movement patterns in the sagittal, coronal, and horizontal planes of the shoulder joint, mainly based on resistance training; the equipment is an elastic band, medicine ball, Swiss ball, etc., 3 sets. Practice moves such as ball squats, lunges, medicine ball standing, and more. (2) Basic strength training: resistance training based on single plane action mode, involving quadriceps femoris, biceps femoris, semimembranosus, triceps calf, etc.; the number of times is 8-12 times; and the number of sets is 3-4 sets.
Weeks 3-4	Knee muscle volume: knee muscle strength	Monday to Friday	Training to increase the volume and strength of the muscles around the knee joint: the resistance training is mainly based on the single-plane movement mode, involving the quadriceps femoris, biceps femoris, semimembranosus, and triceps calf. The equipment is barbell and dumbbell, kettlebell, MIHA, and Technogym multifunctional training equipment; the number of times is 4-8; and the number of groups is 4-6. Practice movements such as sitting knee extension and supine leg hook.
Week 5	Overall strength and endurance of lower body: explosive power of knee joint, special strength	Monday, Wednesday, Friday	(1) The overall strength and endurance of the knee joint: the resistance training is mainly based on the multiplane movement mode. The equipment is Technogym multifunctional training equipment, MIHA centrifugal training equipment, dumbbells, barbells, kettlebells, etc. The number of times is 10-15, and the number of sets is 3-4 groups. Practice movements such as weight-bearing half-squats, multidirectional lunges, and walking with bows and arrows. (2) Knee explosive power and special strength: focus on special movement, jumping, starting, and braking modes and choose elastic bands, medicine balls, etc. for equipment, 10-15 times, and 3-4 groups. Practice movements such as step jumps, court starting, and braking exercises.

Table 2: Isokinetic (60°/s) muscle strength test results of patients before rehabilitation training.

Test indicators		Knee flexion and extension			Internal and external rotation of the knee			Ankle dorsiflexion, plantar flexion		
		Flexion	Extension	Difference	Internal rotation	External rotation	Difference	Dorsiflexion	Plantar flexion	Difference
Peak torque (Nm)	Left	81	150	54.1	22	24	8.3	25	66	62.1
	Right (afflicted)	72	118	61.4	18	22	18.2	30	54	44.4
	Two-sided difference (%)	8.6	18.6	/	18.2	8.3	/	-20	18.2	/

Note: bilateral difference = (left − right)/left × 100%, difference in flexion and extension = (extension − flexion)/extension × 100%, difference in internal and external rotation = (external rotation − internal rotation)/external rotation × 100%, difference in dorsiflexion and plantarflexion = (plantar − dorsiflexion)/plantarflexion × 100%.

Table 3: Isokinetic (60°/s) muscle strength test results on the affected side of the patient after rehabilitation training.

Test indicators	Test time	Knee flexion and extension			Internal and external rotation of the knee			Ankle dorsiflexion, plantar flexion		
		Flexion	Extension	Difference	Internal rotation	External rotation	Difference	Dorsiflexion	Plantar flexion	Difference
Peak torque (Nm)	2012.9.24	72	118	61.4	18	22	18.2	30	54	44.4
	2012.10.31	85	142	60	19	24	20.8	28	81	65.4
	Change rate (%)	18.1	20.3	—	5.6	9.1	—	-6.7	50	—

Note: change rate = (poster − anterior)/anterior × 100%, difference in flexion and extension = (extension − flexion)/extension × 100%, difference in internal and external rotation = (external rotation − internal rotation)/external rotation × 100%, difference in dorsiflexion and plantarflexion = (plantar − dorsiflexion)/plantarflexion × 100%.

Table 4: Changes in body shape.

Test date	Body composition			Thigh and calf muscle circumference (cm)					
	Weight (kg)	Muscle weight (kg)	Body fat ratio	Thigh root		Knee edge		Calf circumference	
				Left	Right	Left	Right	Left	Right
9.24	52.3	40.3	18.2%	51.5	51.5	37.5	36.5	34.0	34.0
10.31	53.8	42.3	16.6%	51.8	51.6	38.0	37.5	34.3	34.2

evaluating the training effect of each stage, so as to ensure the quality of rehabilitation training for patients [15]. See Table 1 for specific training programs.

4. Results and Analysis

4.1. Isokinetic Muscle Force Test and Analysis. As can be seen from Table 2, the strength of the bilateral knee extensor muscle is significantly different, reaching 18.6%, indicating that the strength of the right quadriceps muscle is weaker than that of the left side. The strength of the bilateral internal pronator muscle group is lower than that of the external pronator muscle group, but the strength of the right internal pronator muscle group is significantly different from that of the left side, reaching 18.2%. The results show that the semitendinosus semimembrane muscle group on the right side of the patient is weaker than that on the left side, and the difference between pronation and supination is large, indicating that the semitendinosus semimembrane muscle on the right side is weaker than the biceps femoris muscle. Bilateral differences in dorsiflexion and plantar flexion are -20% and 18.2%, respectively, indicating that the right dorsiflexor muscle group is stronger than the left side, while the calf triceps is weaker than the left side [16]. Quadriceps atrophy and loss of strength of the medial rotator muscles are caused by the right knee that has undergone ACL reassignment and medial meniscectomy. Due to the lack of knee strength, ankle involvement is increased to maintain lower limb balance, resulting in the right dorsiflexor muscle group being stronger than the left.

As can be seen from Table 3, the increased range of knee flexion, extension, and ankle joint plantar flexion is obvious, which is directly related to the injury type, injury response, and rehabilitation training arrangement of patients. If the patient suffers from quadriceps atrophy and poor muscle strength, and the quadriceps muscle is the main extensor muscle group, the strength of the quadriceps muscle group can be increased by activating the quadriceps muscle and increasing the strength exercise of the knee extensor muscle group [17]. At the same time, the movement ability of football players on the field requires the plantar-flexion strength of the ankle joint, and the triceps muscle of the calf plays an important role in maintaining the balance of lower limbs and human body upright. In view of this situation, the plantar-flexion strength exercise of the ankle joint is added in training to increase the plantar-flexion strength [18]. Therefore, according to the situation of the muscle strength of the affected side of the athletes, the development of a highly targeted rehabilitation training plan has an obvious effect on the muscle strength recovery of the muscle group of the posterior shoulder joint.

4.2. Body Shape Test and Analysis. Table 4 shows that the patient's body weight and muscle weight are significantly changed, with an increase of 1.5 kg and 2.0 kg, respectively. Body weight and muscle weight are improved when the body fat ratio decreases, indicating that the muscle-building training program for patients has achieved certain results [19]. The combination component test shows that the lower limb muscle volume of patients increases, indicating that reasonable rehabilitation training plan has significant effect on the increase of lower limb muscle volume.

4.3. Test and Analysis of Balance Ability and Lower Limb Explosive Force. As can be seen from Table 5, the balance ability of the left and right sides has been strengthened, increasing by 35 s and 50s, respectively. Although the

Table 5: The test changes of balance ability and explosive force.

Test content	Balance ability		Explosive force								
			Power (w/kg)			Force (N/kg)			Speed (cm/s)		
	Left	Right	Left	Right	Difference	Left	Right	Difference	Left	Right	Difference
9.24	70	15	18.8	14.7	29.3	16.7	12.8	30.5	136	106	28.3
10. 31	105	65	19.2	21.4	-10.3	16.9	17.7	-4.5	137	147	-6.8
Change rate (%)	50	266.7	2.1	45.6	—	1.2	38.3	—	0.7	38.7	—

Note: change rate = (back − front)/front × 100%; bilateral difference (%) = (left − right)/right × 100%.

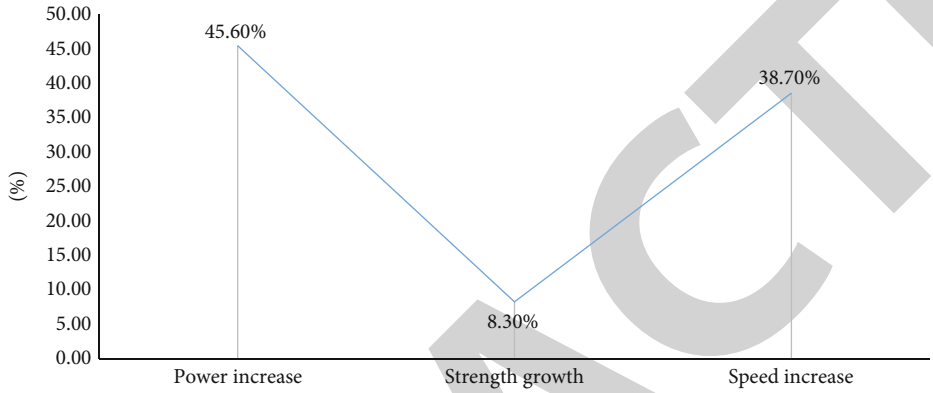

Figure 2: The increase of the affected side of the explosive power test index after the training.

improvement range is large, there is still a certain gap between the balance ability of the affected side and that of the healthy side, and the risk of injury of the affected side is still high in the process of stable support. Figure 2 shows that explosive power test indexes on the affected side increased significantly after training, with power increasing by 45.6%, force value increasing by 8.3%, and speed increasing by 38.7%, while the healthy side does not increase significantly [20]. At the same time, the explosive force index of the affected side is different from that of the healthy side, and all the data are higher than that of the left side.

5. Conclusions

In the research, the observation of the effect of rehabilitation physical training under ultrasonic examination on sports teaching injury is put forward. By using the concept of rehabilitation physical training, athletes' body shape, muscle strength level, explosive power, and balance ability can be improved effectively. By using the testing methods of body shape, function, and muscle strength, athletes can be effectively evaluated before training, monitored during training, and evaluated after training, which can ensure the systematic, effective, and scientific rehabilitation physical training. Rehabilitation physical training is of great significance in the prevention and treatment of sports injury in football projects. The understanding should be strengthened, and the rehabilitation thought centered on treatment should be changed, so as to establish the modern rehabilitation physical training concept of prevention first, treatment second, and prevention and treatment equally.

Data Availability

The data used to support the findings of this study are available from the corresponding author upon request.

Conflicts of Interest

The author declares that there are no conflicts of interest.

References

[1] M. Dreher, R. Liebscher, and A. Schwarting, "Erst rheuma, dann osteoporose–aktuelle empfehlungen aus sport- und bewegungstherapeutischer sicht," *B&G Bewegungstherapie und Gesundheitssport*, vol. 36, no. 1, pp. 3–11, 2020.

[2] C. J. D'Souza, H. Santhakumar, B. Bhandary, and A. Rokaya, "Immediate effect of stabilization exercises versus conventional exercises of the trunk on dynamic balance among trained soccer players," *Hong Kong Physiotherapy Journal*, vol. 42, no. 1, pp. 23–30, 2022.

[3] J. Dogra, S. Jain, A. Sharma, R. Kumar, and M. Sood, "Brain tumor detection from MR images employing fuzzy graph cut technique," *Recent Advances in Computer Science and Communications*, vol. 13, no. 3, pp. 362–369, 2020.

[4] L. Duan, "Empirical analysis on the reduction of sports injury by functional movement screening method under biological image data," *Revista Brasileira de Medicina do Esporte*, vol. 27, no. 4, pp. 400–404, 2021.

Hindawi
Scanning
Volume 2023, Article ID 9859036, 1 page
https://doi.org/10.1155/2023/9859036

Retraction

Retracted: Application of Low-Dose CT and MRI in the Evaluation of Soft Tissue Injury in Tibial Plateau Fractures

Scanning

Received 12 December 2023; Accepted 12 December 2023; Published 13 December 2023

This article has been retracted by Hindawi, as publisher, following an investigation undertaken by the publisher [1]. This investigation has uncovered evidence of systematic manipulation of the publication and peer-review process. We cannot, therefore, vouch for the reliability or integrity of this article.

Please note that this notice is intended solely to alert readers that the peer-review process of this article has been compromised.

Wiley and Hindawi regret that the usual quality checks did not identify these issues before publication and have since put additional measures in place to safeguard research integrity.

We wish to credit our Research Integrity and Research Publishing teams and anonymous and named external researchers and research integrity experts for contributing to this investigation.

The corresponding author, as the representative of all authors, has been given the opportunity to register their agreement or disagreement to this retraction. We have kept a record of any response received.

References

[1] Y. Qi, P. He, J. Zhu, Y. Wang, H. Zhao, and J. Chen, "Application of Low-Dose CT and MRI in the Evaluation of Soft Tissue Injury in Tibial Plateau Fractures," *Scanning*, vol. 2022, Article ID 7686485, 6 pages, 2022.

Hindawi
Scanning
Volume 2022, Article ID 7686485, 6 pages
https://doi.org/10.1155/2022/7686485

Research Article

Application of Low-Dose CT and MRI in the Evaluation of Soft Tissue Injury in Tibial Plateau Fractures

Yinping Qi, Peipei He, Jianping Zhu, Yanan Wang, Hong Zhao, and Junbo Chen

Department of Radiology, The Second Hospital of Yinzhou, Ningbo, Zhejiang 315100, China

Correspondence should be addressed to Jianping Zhu; 11231438@stu.wxic.edu.cn

Received 5 August 2022; Revised 31 August 2022; Accepted 5 September 2022; Published 16 September 2022

Academic Editor: Danilo Pelusi

Objective. To explore the application value of low-dose CT and MRI in the evaluation of soft tissue injury in tibial plateau fractures. *Methods*. This study included 89 patients with high suspicion of TPF and KI admitted to our hospital from July 2015 to May 2021. After arthroscopy, 81 patients were diagnosed with FTP combined with KI. The Schatzker classification based on X-ray and CT plain scan combined with three-dimensional reconstruction was recorded, and the soft tissue injury was recorded according to the MRI examination of the affected knee joint. *Results*. With the results of pathological examination and arthroscopic surgery as the gold standard, the results of MRI and pathological examination and arthroscopic examination were in good agreement (Kappa = 0.857, 0.844), and CT was moderately in agreement (Kappa = 0.697, 0.694). In KI examination, CT and MRI had no difference in the evaluation of ligament injury and bone injury ($P > 0.05$), but MRI had better diagnostic effect on meniscus injury ($P < 0.05$). Finally, the satisfaction survey showed that patients in the CT group were more satisfied with clinical services ($P < 0.05$). *Conclusion*. Both CT and MRI have certain diagnostic value for occult tibial plateau fractures, among which CT examination is more advantageous for trabecular bone fractures, MRI examination is more advantageous for cortical bone fractures, and MRI examination can improve occult tibial plateau fracture inspection accuracy.

1. Introduction

Tibial plateau fractures (TPF) refer to a continuous interruption of tibial plateau bone under the action of external forces, mostly commonly seen in motor vehicle accidents or sports injuries, with the symptoms of obvious local pain, swelling, deformity, and dyskinesia [1]. The tibial plateau is an important load structure of the knee joint. Generally, TPF is complicated with knee injuries (KI), which seriously affects patients' daily life. In addition, the rapid development of modern society and various means of transportation all increase the risk of accidents and consequently the incidence of TPF combined with KI [2, 3]. For such patients, timely diagnosis and effective intervention are critical in improving patient prognosis.

X-ray is commonly used in clinical imaging examinations of KI, but still, it has limitations. For example, the diagnosis effect is not comprehensive enough in the face of occult illness or complicated symptoms, and it has certain harm to the human body due to radiation. In addition, the anatomical resolution of X-ray is low due to the overlapping of the patient's bone structures [4]. Especially when the fracture plane is an inclined plane and the articular surface of the tibial plateau collapses, the tissue overlap will lead to the inability to accurately and effectively distinguish the joint injury [5]. Therefore, further arthroscopy is still needed to confirm KI in such patients, which will not only bring secondary trauma to patients with severe bone trauma but also increase the risk of fracture infection and thrombosis [6].

Low-dose CT is an imaging examination clinically advocated at present, which is to diagnose diseases with the minimum scanning range, the lowest dose, and the least X-ray, with less radiation and higher safety compared with traditional X-ray. MRI, another imaging approach, also has a

wide range of clinical applications [7]. Using magnetic resonance phenomenon to obtain electromagnetic signals from the human body, it can reconstruct human body information and obtain various physical characteristic parameters of substances and carry out multidirectional imaging. However, we found that there are few clinical reports on the evaluation effects of MRI and low-dose CT on TPF combined with KI [8]. Accordingly, we explored and observed the advantages and disadvantages of the two imaging examinations for the diagnosis of TPF combined with KI, to provide a more efficient and rapid diagnostic method for future clinical treatment.

2. Patient Data and Methods

2.1. Patient Data. This study enrolled 89 patients with high suspicion of TPF and KI admitted to our hospital from July 2015 to May 2021; after arthroscopy, 81 cases were confirmed to have FTP combined with KI. Inclusion criteria: (1) age 18-80; (2) presence of TPF; (3) MRI and CT examinations were accepted; (4) diagnosis of KI by arthroscopy; (5) surgical treatment in our hospital after admission; (6) time from injury to operation ≤ 1 week; (7) complete medical records. Exclusion criteria: (1) no clear history of trauma; (2) severe diseases of vital organs such as heart, lung, liver, and kidney; (3) coagulation dysfunction; (4) neurological dysfunction or mental disorders; (5) previous TPF history; (6) pregnant and lactating patients.

2.2. Inspection Methods. CT examination: a PHILIPS Brilliance 16-slice spiral CT scanner was used to scan patients in the supine position, and the scanning parameters were as follows: voltage 120 kV, current 90 mA, scanning slice thickness 3 mm, matrix 515 × 515, FOV 180 mm × 180 mm, and reconstruction interval 1.0-2.0 mm. After scanning, the original volume data were transferred to the workstation for multiplanar reconstruction (MPR), surface shaded display (SSD), volume rendering (VR), and other processing. MRI: scans were performed using a Kangda 1.5 T MR scanner. Patients were placed in the supine position, and the scanner was used to identify the cross-sectional spin echo (SE) pulse signal with the pulse sequence set as follows: T1WI (TE: 11 ms, TR: 540 ms); T2WI (TE: 80 ms, TR: 3200 ms); layer thickness 8-10 mm, layer spacing 1 mm, field of view 38 cm × 38 cm, and matrix 256 mm × 256 mm.

2.3. Evaluation of Image Results. The results of all imaging examinations were double-blindly read by 2 radiologists to evaluate the patient's KI condition. The test result was determined when physicians reached an agreement. And if there was a difference of opinion, a third physician would be consulted. FTP is classified according to the Schatzker classification criteria [9]: type I, split wedge of the lateral tibial plateau; type II, split wedge depression of the lateral tibial plateau; type III, pure depression of the lateral tibial plateau; type IV: split wedge of the medial tibial plateau; type V: bicondylar tibial plateau fracture, where there is continuity between the epiphysis and the diaphysis; type VI: bicondylar fracture with complete dissociation between the epiphysis and the diaphysis.

2.4. Outcome Measures. The diagnosis rate of TPF combined with KI by CT and MRI was evaluated, and the evaluation effects of the two inspection methods on the specific injury conditions of KI (including meniscus injury ligament injury and bone injury) were determined. Besides, a satisfaction survey (score range: 0-10) was conducted after surgery, with 10 being very satisfied, 7-9 being satisfied, 4-6 being in need of improvement, and 1-3 being dissatisfied. Overall satisfaction = (very satisfied + satisfied) cases/total cases × 100%.

2.5. Statistical Methods. SPSS22.0 software was used for statistical analysis. Quantitative and categorical data were given $\boxtimes\chi(\pm s)$ and by (%)/[n (%)] and compared using the independent samples t test and chi-square test, respectively, with $P < 0.05$ indicating statistically significant differences. The Kappa test examined the consistency of MRI and CT with arthroscopic surgery, with a Kappa value > 0.75, 0.4-0.75, and<0.4 indicating good, average, and poor consistency, respectively.

3. Results

3.1. FTP's Comparison of Inspection Accuracy. Pathological examination confirmed that 84 of 89 patients had FTP; using the results of pathological as the gold standard, the detection rates of KI by CT and MRI were found to be 72 and 82, respectively. MRI showed good consistency with pathological (Kappa = 0.857), while CT showed mediocre consistency (Kappa = 0.697) (Tables 1 and 2).

3.2. Types of FTP. Pathological examination results showed that 7 patients were type I, 14 were type II, 8 were type III, 30 were type IV, 16 were type V, and 9 were type VI. CT results showed that 3 patients were type I, 17 were type II, 6 were type III, 23 were type IV, 15 were type V, and 8 were type VI. MRI results showed that 8 patients were type I, 15 were type II, 8 were type III, 28 were type IV, 14 were type V, and 9 were type VI. Compared with pathological examination, both CT and MRI have excellent diagnostic performance for FTP typing ($P > 0.05$) (Tables 3 and 4).

3.3. KI's Comparison of Inspection Accuracy. Arthroscopic examination confirmed that 81 of 89 patients had FTP combined with KI; using the results of arthroscopy as the gold standard, the detection rates of KI by CT and MRI were found to be 63, and 77, respectively. MRI showed good consistency with arthroscopy (Kappa = 0.844), while CT showed mediocre consistency (Kappa = 0.694) (Tables 5 and 6).

3.4. CT and MRI Diagnosis of Meniscus Injury. Arthroscopy showed meniscus injury in 42 cases, while MRI diagnosis of meniscus injury in 41 cases showed high signal intensity on T2WI with elliptical, spherical, patchy, or linear distribution. CT examination diagnosed 37 cases of meniscus injury, with visible changes in meniscus morphology, loss of smooth edges, and visible bone fragments. After calculation, it was

Table 1: CT detection of FTP.

Arthroscopy	CT (+)	CT (-)	Total	Kappa	*P*
(+)	69	15	84		
(-)	3	2	5	0.697	0.034
Total	72	17	89		

Table 2: MRI detection of FTP.

Arthroscopy	CT (+)	CT (-)	Total	Kappa	*P*
(+)	82	2	84		
(-)	0	5	5	0.857	0.009
Total	82	7	89		

found that MRI had higher sensitivity, specificity, and accuracy in the diagnosis of meniscus injury than CT ($P < 0.05$) (Table 7).

3.5. Diagnostic Efficacy of CT and MRI for Ligament Injury. Arthroscopy showed 39 cases of ligament injury, including 17 of anterior cruciate ligament injury (3 of complete tear, 8 of partial tear, and 6 of rubbing); 10 of posterior cruciate ligament injury (2 of complete tear, 6 of partial tear, 2 of rubbing); 6 of medial collateral ligament injury; 4 of lateral collateral ligament injury; 2 of multiple ligamentous mixed injuries. MRI examination diagnosed 43 cases of ligament injury, and the main imaging manifestations were as follows: ligament contusions showed ligament thickening with undulating edges and high signal intensity on T1 and T2; partial tears of the ligament presented with uneven signals of the ligament accompanied by some abnormally high signals, but the ligament continuity was not interrupted; complete ligament tears were characterized by loss of ligament continuity, disappearance of ligament shadow, and irregular abnormally high signal intensity. 40 cases of ligament injury were diagnosed by CT. On CT scans, ligament contusions were manifested as thickened ligament, decreased density, and unclear surrounding adipose space; ligament tears were characterized by ligament contracture and swelling, as well as discontinuity and low density of the ligament. No statistical difference was determined in the sensitivity, specificity, and accuracy of MRI and CT in diagnosing ligament injury after calculation ($P > 0.05$) (Table 8).

3.6. Diagnostic Efficacy of CT and MRI for Bone Injury. Arthroscopy confirmed bone injury in 22 cases. 23 cases of bone injury were diagnosed by MRI, and the images showed low and isointensity on T1 while isointensity and high signal on T2. CT examination diagnosed bone injury in 25 cases, with obvious fracture lines found on images. After calculation, it can be seen that the sensitivity, specificity, and accuracy of MRI and CT in the diagnosis of ligament injury were not statistically different ($P > 0.05$) (Table 9).

4. Discussion

As we all know, the tibia, the most common fracture site in the human body, is also a key site that affects normal human walking and activities. The knee joint connected with the tibial plateau is one of the most important joint activity centers in the human body and also the most complex and frequently used flexion joint [10]. Although the occurrence of tibial fracture or KI can be diagnosed quickly and accurately by CT, MRI, X-ray, and other imaging methods at present, there is still a lack of reliable studies to provide reference for patients with TPF combined with KI. Therefore, a more secure and reliable means to evaluate TPF patients with KI is of great significance to ensure the rehabilitation and safety of patients.

MRI and CT, as the most classic and common imaging modalities, have a relatively stable evaluation effect for KI [11]. But their employment in TPF patients with KI is rarely reported, which warrants further investigation regarding their evaluation effects in such a patient population. Therefore, by comparing the merits and demerits of MRI and CT in evaluating TPF combined with KI, this study has profound reference significance for the future clinical diagnosis and treatment of such patients. In addition, the low-dose CT used in this study has higher safety for patients and can effectively reduce radiation injury during CT examination, which also enjoys wider clinical application potential.

Herein, we first compared the diagnostic accuracy of CT and MRI, and the results showed that MRI had a more ideal detection rate for TPF complicated with KI. At present, CT examination can only diagnose joint dislocation and fracture, but it is difficult to accurately diagnose cartilage fracture and meniscus injury [12]. MRI, on the other hand, has high resolution for blood vessels, soft tissue synovium, nerves, tendons, muscles, ligaments, and hyaline cartilage, which makes it feasible for clinical examination of hyaline cartilage degeneration and ischemic necrosis, cruciate ligament injury, knee meniscus, as well as osteomyelitis and neurologic complications of rheumatoid diseases [13, 14]. As we all know, the principle of MRI inspection is to place the human body in a special magnetic field, so that the radio frequency pulse reacts with the hydrogen nuclei in the human body to generate hydrogen nucleus resonance. After the radio frequency pulse stops, the hydrogen nuclei can emit radio signals according to their specific frequencies and form images through computer processing [15]. MRI, as a three-dimensional cross-sectional imaging, can obtain multidirectional examination images of patients without reconstruction, whereas the examination time and cost are high, and it is not suitable for patients with metal implants. Therefore, in the examination of fracture patients complicated with KI, MRI cannot be performed if the patient has undergone metal internal fixation. CT examination has no above limitations with higher clinical applicability, but its imaging results for body tissues are not as clear as MRI, which is also one of the main shortcomings [16]. In this paper, we found that MRI has excellent accuracy in diagnosing meniscus injury. This is due to the increase of hydrogen protons in fibrocartilage and the infiltration of synovial fluid

Table 3: CT results of FTP typing.

	Total	Type I	Type II	Type III	Type IV	Type V	Type VI
CT	72	3	17	6	23	15	8
Pathological examination	84	7	14	8	30	16	9
χ^2		1.122	1.174	0.067	0.246	0.078	0.006
P		0.290	0.279	0.795	0.620	0.781	0.937

Table 4: MRI results of FTP typing.

	Total	Type I	Type II	Type III	Type IV	Type V	Type VI
MRI	82	8	15	8	28	14	9
Pathological examination	84	7	14	8	30	16	9
χ^2		0.102	0.076	0.003	0.004	0.109	0.003
P		0.749	0.783	0.960	0.832	0.741	0.957

Table 5: CT detection of KI.

Arthroscopy	CT		Total	Kappa	P
	(+)	(-)			
(+)	57	24	81		
(-)	6	2	8	0.694	0.039
Total	63	26	89		

Table 6: MRI detection of KI.

Arthroscopy	MRI		Total	Kappa	P
	(+)	(-)			
(+)	75	6	81		
(-)	2	6	8	0.844	0.016
Total	77	12	89		

Table 7: Diagnostic efficacy of CT and MRI for meniscus injury.

	Sensitivity	Specificity	Accuracy
CT	72.97%	65.91%	69.14%
MRI	90.24%	87.50%	88.89%
χ^2	3.939	5.384	56.760
P	0.047	0.020	<0.001

Table 8: Diagnostic efficacy of CT and MRI for ligament injury.

	Sensitivity	Specificity	Accuracy
CT	87.50%	90.24%	88.89%
MRI	88.37%	97.37%	92.59%
χ^2	0.015	1.689	0.661
P	0.903	0.194	0.416

during meniscus damage, which turns the original low signal into high signal [17], so MRI can accurately identify meniscus injury, while CT relies on observation of meniscus morphological changes and edge smoothness for judgment [18], and it may not be able to present the full view of the meniscus from the same level when complicated with TPF, which may easily lead to missed diagnosis and misdiagnosis. Subsequently, in the assessment of ligament injury, we found no significant difference in the diagnostic performance between MRI and CT. Knee ligament injury often causes bleeding, edema, etc. MRI findings of the injured site may show obvious abnormal high signal intensity, as well as the loss of signal continuity of the ligament, showing irregular waves [19]. The imaging effect of CT for ligament injury is not as significant as that of MRI. However, with the rapid development of CT technology and the application of three-dimensional reconstruction technology in recent years, the definition of CT images has been improved, which can better present the structure and injury of the cruciate ligament and improve the accuracy of CT diagnosis of ligament injury through multilevel observation of bone and ligament [20]. In addition, in the evaluation of bone injury, the diagnostic performance of the two examination methods also shows obvious differences. MRI can effectively display bone injury and has different signal sensitivity to knee joint soft tissue of patients, with the characteristics of broad field of vision and multidirectional imaging, allowing for higher resolution and effective judgment of bone injury severity [21]. And although CT has a low resolution for soft tissue examination, it has an ideal evaluation effect for bone tissue [22]. In previous studies, we also found consistent performance of MRI and CT in evaluating bone injury in KI, which corroborated our results. Finally, the satisfaction survey results showed that patients in the CT group had a higher evaluation of clinical service quality, which we believe is also related to the longer examination time and higher cost of MRI. However, due to the reduction of voltage, current, and exposure time during CT examination, low-dose CT images are often considered to be not clear enough to meet

Table 9: Diagnostic efficacy of CT and MRI for bone injury.

	Sensitivity	Specificity	Accuracy
CT	80.00%	91.30%	91.30%
MRI	95.65%	98.28%	96.30%
χ^2	2.683	2.108	1.705
P	0.101	0.147	0.192

the needs of clinical evaluation, while this study showed that low-dose CT also had an excellent effect in FTP combined with KI, which is speculated to be due to the large difference in texture and density between knee bone and joint tissues and surrounding tissues. But in the examination of other human tissues, the quality of the image results of low-dose CT should be taken into consideration although it can effectively reduce radiation damage.

5. Conclusion

Both low-dose CT and MRI have excellent results in the evaluation of TPF combined with KI, of which the latter is more effective in diagnosing meniscus injury but with more complicated procedures and higher cost. In the actual clinical diagnosis, clinicians should choose the best diagnosis techniques for patients based on their specific conditions and family economic status. It is suggested that when evaluating patients with FTP complicated with KI, low-dose CT should be used for preliminary screening to identify the type of KI while ensuring less radiation damage, and MRI can be further applied to improve the diagnosis when low-dose CT cannot complete the evaluation.

Data Availability

The data used to support the findings of this study are available from the corresponding author upon request.

Conflicts of Interest

The authors declare that they have no conflicts of interest.

References

[1] B. Rudran, C. Little, A. Wiik, and K. Logishetty, "Tibial plateau fracture: anatomy, diagnosis and management," *British Journal of Hospital Medicine*, vol. 81, no. 10, pp. 1–9, 2020.

[2] J. Porrino, M. L. Richardson, K. Hovis, B. Twaddle, and A. Gee, "Association of tibial plateau fracture morphology with ligament disruption in the context of multiligament knee injury," *Current Problems in Diagnostic Radiology*, vol. 47, no. 6, pp. 410–416, 2018.

[3] J. Tomas-Hernandez, J. M. Monyart, J. T. Serra et al., "Large fracture of the anteromedial tibial plateau with isolated posterolateral knee corner injury: case series of an often missed unusual injury pattern," *Injury*, vol. 47, Supplement 3, pp. S35–S40, 2016.

[4] M. Avci and N. Kozaci, "Comparison of X-ray imaging and computed tomography scan in the evaluation of knee trauma," *Medicina (Kaunas)*, vol. 55, no. 10, 2019.

[5] K. Kolodziejczyk, K. Kulinski, K. Fedorowicz, M. Langner, J. Czubak, and S. Pomianowski, "Difficulties in treating complex knee injuries with fracture of posterior tibial plateau," *Ortopedia Traumatologia Rehabilitacja*, vol. 20, no. 4, pp. 293–300, 2018.

[6] J. W. Li, F. Ye, D. W. Bi, X. D. Zheng, and J. L. Chen, "Treatment of Schatzker IV tibial plateau fractures with arthroscopy combined with MIPPO technique," *Zhongguo Gu Shang*, vol. 31, no. 2, pp. 186–189, 2018.

[7] T. R. Moen, B. Chen, D. R. Holmes et al., "Low-dose CT image and projection dataset," *Medical Physics*, vol. 48, no. 2, pp. 902–911, 2021.

[8] T. Yousaf, G. Dervenoulas, and M. Politis, "Advances in MRI methodology," *International Review of Neurobiology*, vol. 141, pp. 31–76, 2018.

[9] B. Yan, W. Yin, X. Zhang et al., "Effectiveness analysis of surgical treatment of Schatzker type tibial plateau fractures," *Zhongguo Xiu Fu Chong Jian Wai Ke Za Zhi*, vol. 31, no. 11, pp. 1305–1310, 2017.

[10] L. Tan, Y. H. Li, Y. Li, T. Lin, D. Zhu, and D. H. Sun, "Tibial plateau fractures (AO type B3) combined with tibial tubercle fracture: case report and review of the literature," *Medicine (Baltimore)*, vol. 97, no. 36, article e12015, 2018.

[11] F. K. Ciliberti, L. Guerrini, A. E. Gunnarsson et al., "CT- and MRI-based 3D reconstruction of knee joint to assess cartilage and bone," *Diagnostics (Basel)*, vol. 12, no. 2, 2022.

[12] R. J. Kalke, G. A. Di Primio, and M. E. Schweitzer, "MR and CT arthrography of the knee," *Seminars in Musculoskeletal Radiology*, vol. 16, no. 1, pp. 57–68, 2012.

[13] T. Gorbachova, Y. Melenevsky, M. Cohen, and B. W. Cerniglia, "Osteochondral lesions of the knee: differentiating the most common entities at MRI," *Radiographics*, vol. 38, no. 5, pp. 1478–1495, 2018.

[14] A. P. Dold, S. Swensen, E. Strauss, and M. Alaia, "The posteromedial corner of the knee," *The Journal of the American Academy of Orthopaedic Surgeons*, vol. 25, no. 11, pp. 752–761, 2017.

[15] J. F. Griffith, "Five overlooked injuries on knee MRI," *AJR. American Journal of Roentgenology*, vol. 217, no. 5, pp. 1165–1174, 2021.

[16] A. G. Culvenor, B. E. Oiestad, H. F. Hart, J. J. Stefanik, A. Guermazi, and K. M. Crossley, "Prevalence of knee osteoarthritis features on magnetic resonance imaging in asymptomatic uninjured adults: a systematic review and meta-analysis," *British Journal of Sports Medicine*, vol. 53, no. 20, pp. 1268–1278, 2019.

[17] A. J. Krych, M. Hevesi, D. P. Leland, and M. J. Stuart, "Meniscal root injuries," *Journal of the American Academy of Orthopaedic Surgeons*, vol. 28, no. 12, pp. 491–499, 2020.

[18] J. Chen, J. Liu, X. Liu, X. Xiaoyi, and F. Zhong, "Decomposition of toluene with a combined plasma photolysis (CPP) reactor: influence of UV irradiation and byproduct analysis," *Plasma Chemistry and Plasma Processing*, vol. 41, no. 1, pp. 409–420, 2021.

[19] A. Sharma, R. Kumar, M. Talib, S. Srivastava, and R. Iqbal, "Network modelling and computation of quickest path for service-level agreements using bi-objective optimization," *International Journal of Distributed Sensor Networks*, vol. 15, Article ID 155014771988111, 2019.

Hindawi
Scanning
Volume 2023, Article ID 9784601, 1 page
https://doi.org/10.1155/2023/9784601

Retraction

Retracted: Optimal Modeling and Simulation of the Relationship between Athletes' High-Intensity Training and Sports Injuries

Scanning

Received 12 December 2023; Accepted 12 December 2023; Published 13 December 2023

This article has been retracted by Hindawi, as publisher, following an investigation undertaken by the publisher [1]. This investigation has uncovered evidence of systematic manipulation of the publication and peer-review process. We cannot, therefore, vouch for the reliability or integrity of this article.

Please note that this notice is intended solely to alert readers that the peer-review process of this article has been compromised.

Wiley and Hindawi regret that the usual quality checks did not identify these issues before publication and have since put additional measures in place to safeguard research integrity.

We wish to credit our Research Integrity and Research Publishing teams and anonymous and named external researchers and research integrity experts for contributing to this investigation.

The corresponding author, as the representative of all authors, has been given the opportunity to register their agreement or disagreement to this retraction. We have kept a record of any response received.

References

[1] Y. Zhang and Y. Chang, "Optimal Modeling and Simulation of the Relationship between Athletes' High-Intensity Training and Sports Injuries," *Scanning*, vol. 2022, Article ID 8447453, 7 pages, 2022.

Hindawi
Scanning
Volume 2022, Article ID 8447453, 7 pages
https://doi.org/10.1155/2022/8447453

Research Article

Optimal Modeling and Simulation of the Relationship between Athletes' High-Intensity Training and Sports Injuries

Youcheng Zhang and Yuanyuan Chang

College of Physical Education, Taiyuan University of Technology, Jinzhong, Shanxi 030600, China

Correspondence should be addressed to Yuanyuan Chang; 20160610@ayit.edu.cn

Received 21 July 2022; Revised 18 August 2022; Accepted 30 August 2022; Published 14 September 2022

Academic Editor: Danilo Pelusi

In order to take into account the physical health of athletes and the quality of sports training, an optimization modeling and simulation method for the relationship between high-intensity training and sports injuries of athletes is proposed. The research of the specific content of the method is based on the two-dimensional and three-dimensional registration principles. In the research process, the program is written strictly according to the registration principle, and the correctness of the method is effectively tested by means of experimental methods. Digital image reconstruction measures based on 3D models may be based on ray tracing methods. The experimental results show that the number of accurate cases of this method is 77, and the accuracy rate is 96.3%. The proposed method can formulate a scientific and effective injury prevention strategy for athletes during high-intensity training.

1. Introduction

With the development of sports, the industry is paying more and more attention to sports injuries. It is believed that sports injuries mainly refer to the results that occur in the process of training and competition, resulting in the reduction of the athlete's athletic ability, which can only be recovered through treatment, or the result of the athlete's poor social ability. It is believed that the research on sports injury should move from analysis to integration. Sports injury is an abnormal physical injury phenomenon that occurs in the process of sports training preparation activities or formally participating in sports [1]. The injury is affected by its own physiological condition, external environment, and sports characteristics. Sports injuries here are distinguished from accidental bodily injuries in daily life, which are highlighted by the inevitable relationship between the injury and the skills required to perform a certain sport.

The development of sports training can not only improve the physical quality of young athletes but also improve the psychological quality of young athletes. This means that physical training is of great significance to the development of young athletes. However, in the process of sports training, sports injuries are very likely to occur, and sports injuries not only affect the physical health of young athletes but also cause huge psychological pressure on young athletes and may even affect the students and living conditions of young athletes; at the same time, it has a certain degree of impact on teachers' teaching tasks and teaching plans. Therefore, it is very necessary to prevent sports injuries in sports training of young athletes [2].

Surveys show that more than 70% of the injuries suffered by athletes during training can be avoided. Prevention is fundamental to reducing physical harm. In the process of daily sports training, training teachers and athletes must learn the knowledge of scientific prevention of sports

injuries, strengthen the awareness of self-protection of athletes, so as to effectively reduce or avoid sports injuries, reduce the negative impact of sports injuries, and maintain the physical and mental health of athletes, healthy, and athletes can effectively engage in daily sports training.

2. Literature Review

The internal factors that cause sports injuries in the sports training of young athletes mainly include the following points: first, lack of ideological awareness. Sports injuries occur in young athletes in sports training, mainly because teachers and young athletes have insufficient ideological understanding of the meaning of sports injuries, and teachers lack the awareness of sports injury prevention for young athletes and blindly carry out sports in sports training, eager for success, often causing acute joint injuries in young athletes. Second, physical training preparation activities are unreasonable. The preparatory activities before sports training are to change the young athletes' bodies from quiet to active state, if the preparatory activities for sports training are insufficient, the chances of sports injuries for young athletes will be greatly increased, if the preparatory activities are excessive, it will cause young athletes to be in a state of fatigue and no longer suitable for sports training, thus increasing the occurrence of sports injuries in sports training for young athletes. Third, young athletes have low physical fitness. The low physical quality of young athletes is the fundamental cause of sports injuries in sports training. No matter what kind of sports, young athletes are required to have certain physical qualities, such as track and field requires speed and endurance, shot put requires strength, and gymnastics requires flexibility[3]. If young athletes do not have the corresponding physical fitness to carry out sports training, it will cause sports injuries, and even if young athletes carry out sports training when they lack special qualities, the probability of sports injuries for young athletes will be higher.

Based on the above problems, the author proposes a method for sports medicine image modeling and injury prevention in the process of sports training. The specific content of this method is that, according to the research situation of medical image 3D modeling and registration technology for precise radiotherapy devices, the functions of the medical image navigation system can be enriched to enhance the accuracy of the model [4]. In order to shorten the modeling time, the complexity of 3D modeling can also be appropriately reduced according to the actual situation of the research work. During the study period, a retrospective analysis was carried out according to the patient's diagnosis; during the period, the experimental verification platform included X-ray machines, graphic workstations, operating beds, and other equipment. According to the actual situation of the experimental research, the relevant personnel used CT equipment to complete the scanning of bone information and input the relevant image data into the workstation, processing to determine the closed contour of each image in the CT data. The method used in the construction of the 3D model is the volume mapping algorithm [5]. During the construction of the 3D model, the relevant personnel used image noise reduction measures, remove noise in CT image data, and improve image quality. Use the image segmentation tool for image segmentation algorithms during modeling. During the implementation of the three-dimensional reconstruction of CT data, relevant personnel use surface rendering and volume rendering to realize the three-dimensional image surface.

3. Method

3.1. Acquisition of Medical Images. Medical images are obtained by scanning the patient's lesions with various medical imaging equipment. With the development of science and technology, more and more new medical imaging devices are used in clinical practice. At present, the mainstream medical image acquisition methods are as follows: X-ray tomography (CT), magnetic resonance imaging (MRI), and positron emission tomography (PET) [6]. Each of these medical imaging devices has its own characteristics and advantages, but the principles of imaging are similar, and they all use Fourier transform or Radon inversion algorithms to infer three-dimensional space from ray projections in multiple directions, a certain physical property of an object in the system, and finally reconstruct the result to generate a tomographic image.

In order to unify the interface standards between equipment of different manufacturers and unify the image formats obtained by a variety of medical imaging equipment, the American College of Radiology (ACR) and the National Electrical Manufacturers Association (NEMA) formulated a unified standard in 1983, the standard storage format dedicated to medical images, the ACR-NEMA standard released in 1985. The Digital Imaging and Communications in Medicine (DICOM) 3.0 standard released in 1993 is the current international standard in the field of medical imaging informatics [7].

DICOM file consists of two parts: file header information (DICOMFileMeta Information) and DICOM data set (DICOMDataSet) [8]. The file header contains the identification information of the dataset (FilmMetaInformation), including the file identification prefix, dataset identification, storage format, and patient medical information. The DICOM data set uses the data element (DataElement) as the coding unit, and each data element stores the value of a certain attribute in the data set, including the following parts: Tag (Tag), data type (VR), data length (ValueLength), and data Field (ValueField). Multiple data elements are aggregated together to form a dataset. The format of the DICOM file and the encoding format of the data elements are shown in Figure 1.

According to the structure of the DICOM file, the program can read the image information in the DICOM file and convert it into a three-dimensional space data field.

3.2. VTK Class Library. Visualization Toolkit (VTK) is an open-source system visualization toolkit developed by Corporate R&D, it is mainly used for the writing of 3D computer graphics, image processing, and visualization programs, and

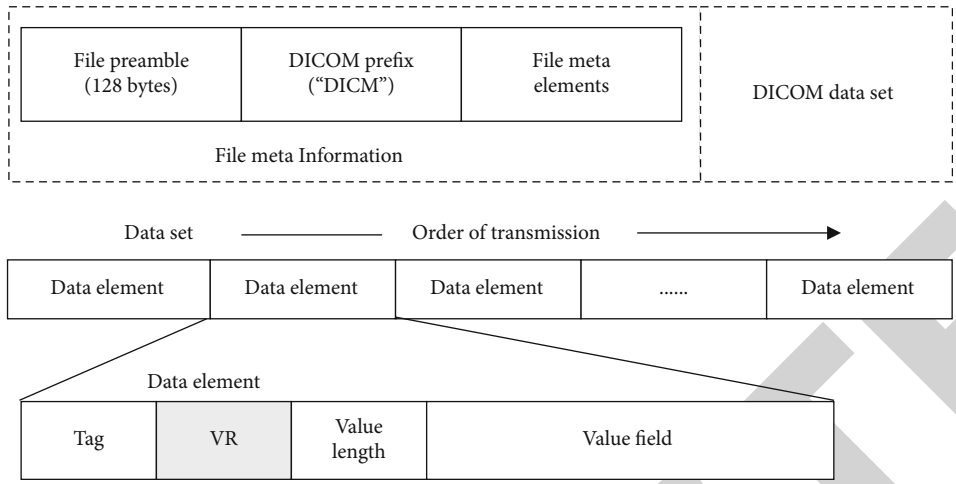

Figure 1: DICOM data set structure.

the field of application is quite extensive. Its core is built with C ++ and contains about 250,000 lines of code, more than 2000 classes, and several conversion interfaces; so, VTK can be freely used in Java, Python, and other languages. VTK uses object-oriented technology to encapsulate common algorithms in the field of image visualization into classes, which enables programmers to directly call algorithms through interfaces.

In order to manage the huge class library inside VTK simply and effectively, the classes included in VTK are divided into common base class (Common), graphics operation class (Imaging), graphics algorithm class (Graphics), data format conversion class (Filtering), and graphics rendering class (Rendering), etc. and generate the corresponding dynamic link library. Among them, the common base class is the parent class, and the other classes are the inheritance of the common base class and complete their own work according to specific requirements [9]. In addition to the C++ class library, VTK comes with an interpretation packaging layer system to wrap the C++ class library, which is convenient for the use of languages such as TCL and Java. The advantage of using this architecture is that programmers can use the C++ language to create efficient algorithms, and other scripting languages can be used for rapid development.

VTK uses data flow to convert source data into image data, this data exchange relationship is called Pipeline, which contains two basic objects: data object (vtkDataObject) and processing object (vtkProcessObject) [10]. The data object represents the data information such as the geometric structure, topological structure, and unit gray value of the image, and the processing object is also called the filter (Filter), which is used to manipulate and process the data object and generate new data. The processing object represents the algorithm by which the system processes the data. As shown in Figure 2 below, VTK connects data objects and processing objects through the data visualization pipeline to complete the data processing.

3.3. Image Preprocessing

3.3.1. Removing Image Noise. Noise is a collection of pixel distortions caused by various reasons in the image generation process. The existence of noise may affect the diagnosis of tiny lesions by doctors and may even lead to misdiagnosis and delay the treatment of patients. Therefore, sufficient attention must be paid to noise.

Since CT images are easily disturbed by noise during transmission and acquisition, in order to improve the quality of the images as much as possible, the images must be denoised and smoothed [11]. At present, many methods of image denoising have been proposed, such as neighborhood averaging method, median filtering method, and Gaussian filtering algorithm; according to some characteristics of medical images, we choose a method that can remove noise well and also a denoising method to protect image edge information.

Because precise radiotherapy requires real-time positioning, and the data scale of each set of CT is relatively large, it puts forward requirements for image processing time. Table 1 shows the processing time of three image filtering methods measured by computer for a single image.

It can be seen from Table 1 that the average neighborhood filtering method takes the least time and requires the least amount of computation, while the median filtering method takes the longest time and has the largest amount of computation [12]. The median filter method takes 2.29 times as long as it is the Gaussian low-pass filter method and 16 times as long as it is the average neighborhood method.

The denoising ability of median filtering and Gaussian low-pass filtering is weaker than that of average neighborhood filtering, but while removing noise, average neighborhood filtering will cause the image to deform locally at the boundary, which affects doctors' judgment of the disease [13]. Although the average neighborhood has the advantages of small calculation and short processing time, it cannot

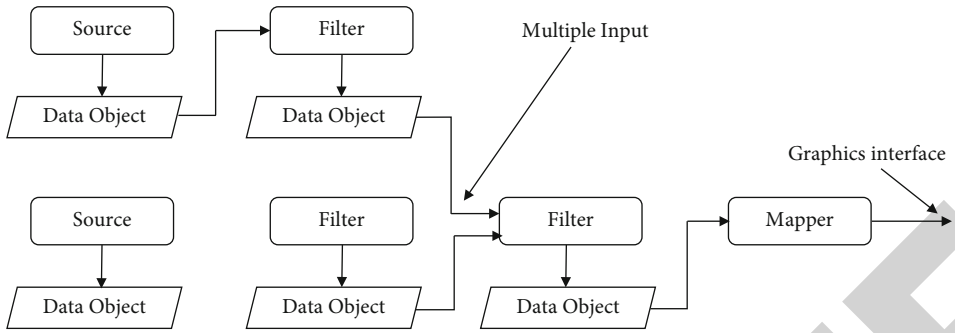

Figure 2: Schematic diagram of visualization pipeline.

Table 1: Time spent on a single image of each noise filtering method (unit: s).

Noise filtering method	Median filter	Average neighbor filtering	Gaussian low-pass filtering
Processing time	0.4992	0.0312	0.2184

meet the requirements of retaining feature points on the boundary; so, it is not suitable for the imaging system of radiotherapy. To sum up, this subject chooses Gaussian low-pass filtering as a method to remove image noise.

3.4. Establishment of 3D Model. Using the abovementioned methods of image denoising, threshold division, contour extraction, etc., the software system completed the preprocessing of CT images and obtained the closed contour of each image in the CT data set, which was carried out for the MC algorithm. 3D modeling is ready for work.

The 3D reconstruction technology extracts the corresponding data point set from the tomographic sequence image according to the set threshold to form the isosurface. According to the principle of triangulation, the isosurface is divided into several triangular patches, and the triangular patches are rendered by the graphics lighting model to form a three-dimensional image, so as to achieve the purpose of intuitive display of geometry. The program development kit of Visualization Toolkit (VTK) is widely used in the construction of 3D images. By calling the class library in VTK, the development of 3D software can be carried out quickly and efficiently, so that it has a powerful 3D graphics display function and can realize interactive 3D measurement.

Early three-dimensional modeling methods include Fourier transform and convolution back-projection. With the development of imagery, three-dimensional modeling methods such as multilevel reconstruction (MPR), maximum density projection (MIP), surface rendering, and volume rendering have been proposed [14]. The most widely used 3D modeling methods are surface fitting and Voxel-based volume rendering.

The basic steps to achieve 3D modeling with VTK are as follows:

(1) Preprocessing of CT slice data: image denoising method is used to remove noise in CT image data and improve image quality

(2) Segmentation of CT data: the CT image is segmented using an image segmentation algorithm, and the image edge dataset is searched

(3) 3D reconstruction of CT data: according to the image edge data set, the surface rendering and volume rendering methods are used to realize the three-dimensionalization of the image surface. In this subject, the MC algorithm is used to realize the three-dimensional reconstruction of medical images

3.4.1. Surface Reconstruction Algorithm and Volume Rendering Algorithm. The moving cube method (marching cubes, MC algorithm) is currently the most popular 3D reconstruction method [15]. The basic idea of the MC algorithm is as follows: according to the input tomographic image sequence, after segmentation and extraction, a three-dimensional data field is formed, the cubes intersecting with the isosurface are processed one by one, and then the intersection of the isosurface and the cube is calculated by the interpolation method. According to the relative position relationship between the intersection of the cube and the isosurface, connect the intersection of the isosurface and the cube in a certain way to form a new isosurface.

Voxel-based volume rendering methods can generally be classified into image-order methods, object-order methods, and hybrid-order methods. The algorithm based on the image space sequence method is represented by the ray casting method proposed in 1988 [16]. The algorithms based on the object space order method mainly include the footprint method (SplattingAlgorithm or FootprintAlgorithm), the sputtering algorithm (Splatting), and the shear warp algorithm (ShearWarp). The algorithm based on the hybrid order method has the shearwarp factorization algorithm. The advantage of the volume rendering algorithm is that there is no need for segmentation, and the volume data can be directly rendered through the set transformation function.

3.5. Digital Image Reconstruction

3.5.1. Principle of Digital Image Reconstruction. Digital image reconstruction (digitally reconstructed radiograph, DRR) is to generate a three-dimensional spatial data field from CT image data and observe the digital projection image

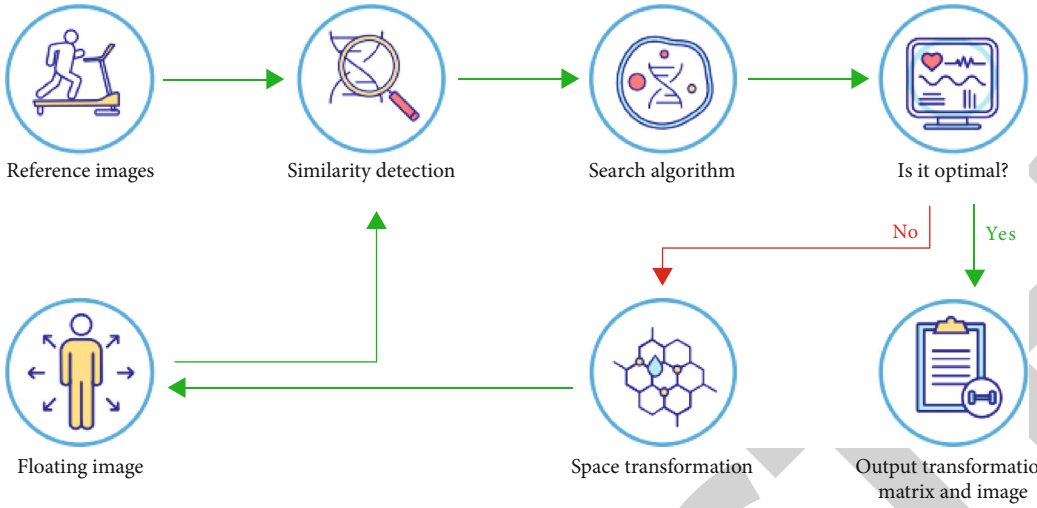

Figure 3: Schematic diagram of medical image registration process (high-end).

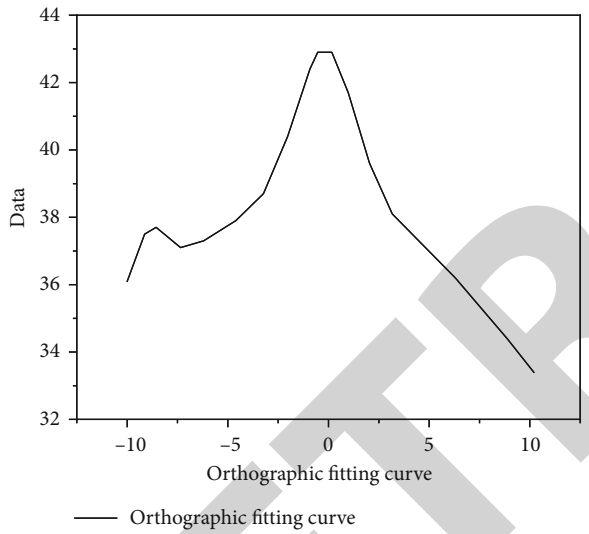

Figure 4: Positive fitting curve.

obtained from any direction in the spatial data field [17]. In order to simulate a real X-ray image, the information that DRR needs to simulate includes characteristics such as attenuation and scattering of X-rays as they pass through the 3D spatial data field. By calculating the attenuation of each ray through three-dimensional space, a simulated projected image is obtained on film.

There are two methods to obtain DRR images: projection method and ray tracing method. The projection method is to project each voxel on the film position, and the brightness of the pixel is proportional to the density of the projected voxel to obtain an analog image. The ray tracing method is to trace the intersection of each ray emitted from the light source and each pixel in the three-dimensional model and accumulate the density of the voxels that each ray passes through. The brightness value of the pixel is proportional to the accumulated value of the light. Of these two methods, the ray tracing method is more suitable for this subject. First, the performance requirements of the projection method grating system are very high; second, the accumulated value of the projection method is limited by the color depth of the shading system; so, it will affect the display accuracy; third, the projection method does not support forward display, while the ray tracing method supports forward display, which can take into account image quality and calculation speed. Through analysis and comparison, the author uses the method of ray tracing.

3.5.2. Ray Tracing Algorithms

(1) Principle of Ray Tracing Algorithm. Ray tracing is a multifunctional technique, which can use the same model to simulate the specular reflection and refraction of the light source and the ambient incident light on the surface and realize the scene blanking and generate shadows, etc. [18]. The ray tracing algorithm is an important algorithm for generating photorealistic graphics and can also be used as a basic technology for volume rendering.

The method of generating the DRR image is as follows: first, the ray tracing method needs to set up a light source, emit light from the light source to the 3D model, and set up a receiving plane at the same time. Then, watch the light coming from the light source, if the ray does not intersect the model, the ray will exit the frame and the trace will end. These rays are not the focus of the study. If the light intersects the scene in the scene, it must be divided into the following situations:

(1) The object where the intersection is located is an opaque object, the surface is an ideal diffuse reflection surface, and the ray tracing ends

(2) The object where the intersection is located is an opaque object, the surface is an ideal mirror reflection surface, and the light continues to trace along the direction of the mirror reflection

(3) The object where the intersection is located is a transparent or semitransparent object, and the light

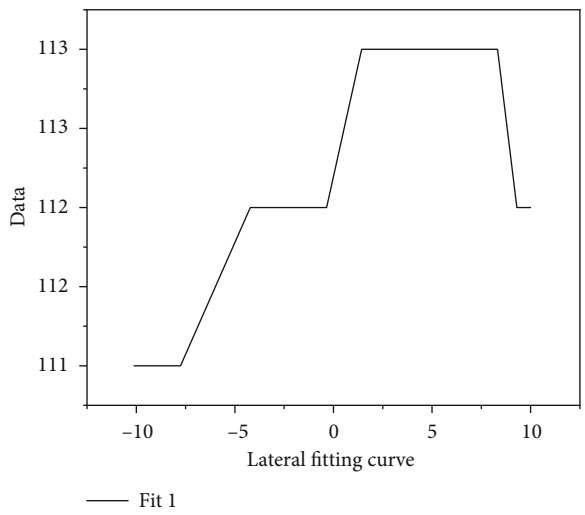

Figure 5: Lateral fitting curve.

continues to trace along its regular transmission direction according to the laws of reflection and refraction

Finally, when the ray intersects the receiving plane, the attenuation value of the ray is recorded to complete the tracing of the ray.

Since the ray tracing method needs to trace each ray from the viewpoint, it must involve a large number of intersection operations between the rays and the three-dimensional model. In order to make the ray tracing algorithm practical, it is necessary to improve the efficiency of the intersection operation and simplify the calculation.

(2) Implementation of Ray Tracing Algorithm. The implementation method of the simplified ray tracing algorithm is as follows: a virtual parallel X-ray is passed through the three-dimensional model established based on the CT image data, and the starting point of the ray is equivalent to the X light source. The attenuation of the ray is calculated from the CT value of the voxel that the ray intersects. The CT value is related to the density of the three-dimensional model; so, the attenuation value of the light can be calculated by using the CT value. Compute each voxel that intersects this ray, up to the 3D model. From these accumulated values, a pseudovisible optical density value for display can be calculated and then displayed on the screen like an X-ray image.

3.6. Overview of Image Registration

3.6.1. The Principle and Implementation of Image Registration. The registration of medical images is to use image registration technology to calculate the spatial transformation relationship between two images, so that the points in the floating image are spatially consistent with the corresponding points on the reference image after the transformation; that is, the same anatomical point on the human body has the same spatial position on the two medical images. Simply put, one of the images is selected as the reference image (ReferenceImage) to be fixed, and the floating image (FloatingImage) is spatially transformed so that the points on the same position of the two images correspond to the same anatomical position [19]. The ideal registration result is that all the medically valuable feature points in the two images can be in one-to-one correspondence [20].

The medical image registration method consists of four parts: feature space (FeatureSpace), search space (SearchSpace), search algorithm (searchalgorithm), and similarity measure (SimilarityMeasure). Feature space refers to the distribution of feature information in images to be registered. The search space refers to the range of spatial transformation of the floating image [21]. The search algorithm refers to the method of calculating the spatial transformation of the floating image, that is, the method of finding the optimal transformation matrix parameters [22]. Similarity measures refer to quantitative metrics used to measure the quality of image registration. The process of medical image registration is shown in Figure 3.

4. Results and Discussion

According to the change of the key parameter X value, the mutual information value in different situations can be obtained. Taking the X value as the X axis and the mutual information value as the Y axis, according to the corresponding relationship, the second-order curve fitting function can be used to fit the change curve of mutual information [23].

Positive mutual information value fitting curve: the positive mutual information value fitting curve obtained during the research period is shown in Figure 4; in this fitting curve, the mutual information curve has two extreme values [24].

Lateral fitting curve was as follows: the lateral fitting curve of the CT image processing results of the patient is shown in Figure 5; as explained in the figure, the lateral fitting curve only contains one extreme value [25].

Accuracy is as follows: the number of accurate cases in this research method is 77, with an accuracy rate of 96.3%.

5. Conclusion

The authors propose a method for sports medicine image modeling and injury prevention during sports training. The research of the specific content of this method is based on the principle of two-dimensional and three-dimensional registration; during the research, the program is written strictly according to the registration principle, and the correctness of this method is effectively tested by means of experimental methods. Digital image reconstruction measures based on 3D models can be based on ray tracing methods. The related parameter optimization method is the simulated annealing method. According to the research situation of medical image 3D modeling and registration technology for precision radiotherapy device, the functions of medical image navigation system can be enriched to enhance the accuracy of the model. In order to shorten the modeling time, the complexity of 3D modeling can also be appropriately reduced according to the actual situation of

Hindawi
Scanning
Volume 2023, Article ID 9869615, 1 page
https://doi.org/10.1155/2023/9869615

Retraction

Retracted: Intravoxel Incoherent Motion Diffusion-Weighted Imaging and 3D-ASL to Assess the Value of Ki-67 Labeling Index and Grade in Glioma

Scanning

Received 12 December 2023; Accepted 12 December 2023; Published 13 December 2023

This article has been retracted by Hindawi, as publisher, following an investigation undertaken by the publisher [1]. This investigation has uncovered evidence of systematic manipulation of the publication and peer-review process. We cannot, therefore, vouch for the reliability or integrity of this article.

Please note that this notice is intended solely to alert readers that the peer-review process of this article has been compromised.

Wiley and Hindawi regret that the usual quality checks did not identify these issues before publication and have since put additional measures in place to safeguard research integrity.

We wish to credit our Research Integrity and Research Publishing teams and anonymous and named external researchers and research integrity experts for contributing to this investigation.

The corresponding author, as the representative of all authors, has been given the opportunity to register their agreement or disagreement to this retraction. We have kept a record of any response received.

References

[1] J. Zhou, H. Li, X. Ma, M. Jin, X. Meng, and G. Zhang, "Intravoxel Incoherent Motion Diffusion-Weighted Imaging and 3D-ASL to Assess the Value of Ki-67 Labeling Index and Grade in Glioma," *Scanning*, vol. 2022, Article ID 8429659, 7 pages, 2022.

Hindawi
Scanning
Volume 2022, Article ID 8429659, 7 pages
https://doi.org/10.1155/2022/8429659

Research Article

Intravoxel Incoherent Motion Diffusion-Weighted Imaging and 3D-ASL to Assess the Value of Ki-67 Labeling Index and Grade in Glioma

Jian Zhou[1], **Huafeng Li**[2], **Xiaoming Ma**[3], **Miao Jin**[1], **Xin Meng**[1] and **Guangfeng Zhang**[1]

[1]*Department of MRI, The Third Affiliated Hospital of Qiqihar Medical University, Qiqihar, Heilongjiang 161000, China*
[2]*Department of Endocrinology (I), The Third Affiliated Hospital of Qiqihar Medical University, Qiqihar, Heilongjiang 161000, China*
[3]*Department of Ultrasound, The Third Affiliated Hospital of Qiqihar Medical University, Qiqihar, Heilongjiang 161000, China*

Correspondence should be addressed to Guangfeng Zhang; 11231412@stu.wxic.edu.cn

Received 6 July 2022; Revised 9 August 2022; Accepted 17 August 2022; Published 31 August 2022

Academic Editor: Danilo Pelusi

Objective. To determine the proportion of intravoxel incoherent motion diffusion-weighted images (IVIM-DWI) and three-dimensional arterial circulation markers (3D-ASL) in Ki-67 labeling index (Ki-67 LI) and glioma grading. *Methods*. According to the classification of diseases of the central nervous system dealt with by WHO in 2007, patients with stage II glioma were classified as low ($n = 20$) and patients with stages III-IV were divided into higher levels ($n = 22$). Prior to surgery, brain MRI, IVIM-DWI, and 3D-ASL were performed in all patients, and the actual water molecular diffusion coefficient (D), microcirculation coefficient ($D*$), blood flow fraction (f), and cerebral blood flow (CBF) were measured. A rank sum (Mann–Whitney U test) was used to compare the four upper and lower level Ki-67 LI measurements. Spearman's method is used to identify the relationship between 4 groups of quantification and Ki-67 LI. Reciprocal grafting (ROC) curves were used to measure the diagnosis of four groups of glioma grading defects. *Results*. There were significant differences in D, $D*$, f, and CBF between the solid region of the tumor and the normal white matter contralateral to it ($P < 0.05$). The significant differences of rD, $rD*$, rf, and rCBF were shown between patients with low-grade glioma and high-grade glioma ($P < 0.05$). Ki-67 LI was found to have negative correlation with rD ($r = 00.693$, $P < 0.001$) and rf ($r = 00.539$, $P < 0.001$), but similarly correlated with rCBF ($r = 0.665$, $P < 0.001$) in patients with glioma. Recipient efficacy for predicting advanced and secondary glioma from rD, rf, $rD*$, rCBF, and Ki-67 LI raises AUCs of 0.819, 0.747, 0.719, 0.836, and 0.907, respectively. *Conclusion*. IVIM-DWI has good application value for preoperative grading of glioma.

1. Introduction

Gliomas are tumors of the brain and are the most common type of cancer in young people, accounting for more than 70% of intracranial cancers [1]. Depending on the stage of leukemia, glioma is divided into stages I-IV. Type I includes pilocytic astrocytoma, pleomorphic xanthoastrocytoma, subependymal giant cell astrocytoma, type II oligodendroglioma, and astrocytoma. High-grade glioma is grade III and is represented by anaplastic oligodendroglioma, anaplastic astrocytoma, anaplastic oligoastrocytoma, anaplastic ependymoma, and grade IV glioblastoma [2]. The incidence rate of glioma is related to a series of factors, including histological type, age, gender, race, and country. It was reported that according to the standardized age, around 4.7 of 100,000 people suffered from glioma every year [3]. The annual age-adjusted incidence of grade IV glioblastoma ranged from 0.59 to 3.69 per 100,000 people, leading to high molarity [4].

In most cases, surgical resection is an important treatment for glioma. It contributed to reduced intracranial

pressure, relief of neurological symptoms, and prolongation of overall survival of the patients [5]. Accurate scoring of glioma before surgery is important in clinical selection and prognosis. Magnetic resonance imaging (MRI) procedures are often limited in their sensitivity to neurological changes. Diffusion-weighted magnetic resonance imaging (DWI), which dates back to 1985, has been successfully used to treat neurological disorders, particularly stroke [6]. Intravoxel incoherent motion (IVIM) is a method of seeing water in the 1988 study, which describes the movement of tissue through molecular diffusion and blood microcirculation, which affects the measurement of vision using the apparent diffusion coefficient (ADC) [7]. IVIM scores are critical for survival in glioma patients [8], as well as hyperacute brain stroke [9]. Arterial spin labeling (ASL) is a magnetic resonance perfusion assessment method based on water in the blood as an internal source to quantify the value of cerebral blood flow (CBF) [10]. This assessment method has been widely used in clinical area such as brain tumors [11] and cerebrovascular diseases [12]. The occurrence of glioma has proved to be associated with immune function disorder. Proliferative cancers can be diagnosed by Ki-67 immunohistochemistry, and the Ki-67 labeling index (Ki-67 LI) is widely used in cancer screening [13].

The method of IVIM and ASL is a noninvasive MRI technique without the use of contrast agents and has been applied to the study of glioma, but their diagnostic value remains unclear. So far, rare studies have found correlations between their parameters and Ki-67 LI and glioma score. The purpose of this study was to explore the correlation between IVIM-DWI and 3D-ASL quantitative parameters and Ki-67 LI of glioma and their value in glioma grading evaluation.

2. Materials and Methods

2.1. Study Design. 42 patients with glioma were included in the study between December 2016 and May 2019 at the Third Affiliated Hospital of Qiqihar Medical University. Patient's age ranged from 25 to 83 years, with average 53 ± 12 years. None received radiotherapy, chemotherapy, or steroid therapy prior to MRI examination. Each patient provided complete imaging data and underwent surgical resection within two weeks after MRI examination. Out of 42 patients, 20 patients with grade II, 12 patients with grade III, and 10 patients with grade IV were registered in 2007. The WHO modified the distribution of tumors in the central nervous system and the brain [14], and the classification was confirmed by their films read by two experienced pathologists. Patients with stage II glioma were included in the lower group, and patients with stages III-IV were included in the upper group. Written consent will be obtained from each patient. The curriculum is approved by the Legal Committee of the Third Affiliated Hospital of Qiqihar Medical University. This survey included 42 patients diagnosed with glioma.

2.2. Image Acquisition. Hom MR scan: cross-sectional fluid attenuation inversion recovery (FLAIR) sequence T1WI: TR 1850 ms, TE 24 ms, and TI 780 ms; fast spin echo (FSE) sequence T2WI: TR 6656 ms, TE 105 ms, field of view (FOV) 240 mm × 240 mm, matrix 352 × 256, slice thickness 5 mm, interslice spacing 0, and 34 scan layers.

IVIM-DWI: spin-echo single-shot echo-planar imaging (SS-EPI) DWI: TR 4500 ms; TE minimum value; set 13 b values of 0, 10, 20, 30, 50, 100, 150, 200, 400, 800, 1200, 2000, and 3000 s/mm^2; take 2, 1, 1, 1, 1, 1, 2, 2, 3, 3, 5, and 6 as the corresponding excitation times (NEX); and the scanning time is 378 s. FOV 240 mm × 240 mm, matrix 160 × 160 , layer thickness 5 mm, interlayer distance 0, and 34 scanning layer.

3D-ASL: FSE-based 3D spiral acquisition with combination of pulse and continuous manners: TR 4594.0 ms, TE 10.1 ms, points 512, arms 8, marking delay time 1525 ms, FOV 240 mm × 240 mm, layer thickness 4.0 mm, no interval, and 24 scanning layers.

Enhanced MR scan: cross-sectional T1WI-enhanced scan: TR 1850 ms, TE 24 ms, TI 780 ms, FOV 240 mm × 240 mm, matrix 352 × 256, slice thickness 0, slice spacing 0, and 34 scan layers.

2.3. Image Analysis. The images were transferred to the GE AW 4.5 Image Workstation (USA). The Functool MADC software was used to analyze IVIM-DWI, and 3D-ASL software was used to analyze and to obtain pseudocolor maps. Two neuroradiologists used different models to describe the region of interest (ROI) along the largest inner edge 3D-ASL uptake area of the tumor and then obtained CBF values on tumor and contralateral white matter using MR imaging at the cutoff cyst formation. An ROI (approximately 50 mm^2) was manually placed in the white matter area opposite the hemorrhagic or necrotic area in the same layer. Based on the ROI of the ASL image, the ROI of the IVIM-DWI image was defined, and the real molecular diffusion coefficient (D), microcirculation coefficient ($D*$), and vacuum (f) were doubled in exponential fashion. The ROI size and position of ASL and IVIM-DWI are consistent. Normal contralateral white matter was used for normalization. To obtain the correct molecular diffusion coefficient, the tumor volume was divided by the volume of the contralateral normal white matter (rD), relative microcirculation perfusion coefficient ($rD*$), relative perfusion fraction (rf), and relative cerebral blood flow (rCBF), so as to avoid individual differences between samples.

2.4. Ki-67 Labeling Index (Ki-67 LI). Immunohistochemical staining for Ki-67 was employing streptavidin-peroxidase- (SP-) based methods. The primary antibodies and dilutions were used for Ki-67 (MIB-1, 1 : 200, DakoCytomation, Glostrup, Denmark). Paraffin gland blocks were cut into 4-66 μm thick sections and placed on glass slides. Slides were deparaffinized twice in xylene every 20 min and diluted in 100% (10 min), 95% (5 min), 80% (5 min), and 70% (5 min) alcohol degree. Slides were incubated for 10 min in 3% H_2O_2 to block endogenous peroxidase, followed by heat-induced antigen retrieval. After incubation in 1% normal horse blood at room temperature for 30 min, the slides were incubated with the primary and secondary reactions. The slides were then dipped in a solution of polymerantibody-

Table 1: IVIM-DWI and 3D-ASL parameters between tumor and contralateral normal white matter in patients with gliomas.

ROI	D	$D*$	f	CBF
Tumor	0.83 (0.52-1.21)	4.46 (1.89-13.44)	0.34 (0.13-0.59)	81.59 (19.56-225.54)
Contralateral normal white matter	0.65 (0.41-0.95)	3.59 (1.70-20.06)	0.20 (0.09-0.33)	29.97 (10.56-78.29)
Z	-3.289	-2.232	-4.180	-4.620
P	0.001	0.026	<0.001	<0.001

Statistical analysis was performed using Wilcoxon test.

peroxidase complex and incubated at room temperature for 30 minutes. Using PBS, the slides were washed 3 times, each for 5 minutes, and reacted in DAB solution and hematoxylin. Finally, the slides were covered with a glass deck and observed by a light microscope. Ki-67-positive cells were counted by averaging 5 visual fields (×200) in each slide.

2.5. Statistical Analysis. SPSS 20.0 software was used for statistics. The classification of measurement data is always tested by Shapiro Wilk test. If the data do not fit into the conventional classification, they are presented as a mean (multiple) and analyzed using the Wilcoxon test or the Mann–Whitney U test. Correlation between rD, $rD*$, rf, rCBF, and Ki-67 LI was determined using the Pearson correlation coefficient. The receiver operating characteristic (ROC) and the area under the curve (AUC) were used to measure the diagnosis of rD, $rD*$, rf, and rCBF in differentiation between advanced and low-level gliomas. If the possibility (P) of difference was less than 0.05, the difference was considered statistically significant.

3. Results

3.1. IVIM-DWI and 3D-ASL Parameters between Tumor and Contralateral Normal White Matter in Patients with Gliomas. The D, $D*$, f, and CBF of the tumor solid area were 0.83 (0.52-1.21), 4.46 (1.89-13.44), 0.34 (0.13-0.59), and 81.59 (19.56-225.54), respectively. The D, $D*$, f, and CBF of the contralateral normal white matter were 0.65 (0.41-0.95), 3.59 (1.70-20.06), 0.20 (0.09-0.33), and 29.97 (10.56-78.29), respectively. Significant differences were observed between tumor and contralateral normal white matter for IVIM-DWI and 3D-ASL parameters ($P < 0.05$, Table 1, Figures 1 and 2).

3.2. IVIM-DWI, 3D-ASL Parameters, and Ki-67 LI between Low-Grade and High-Grade Glioma Patients. Next, we found differences between IVIM-DWI and 3D-ASL in patients with advanced glioma. Grade II glioma patients were included in the low group ($n = 20$), and patients with grades III-IV glioma were included in the high group ($n = 22$). The low-grade group was 52.15 ± 12.36 years, with 9 males and 11 females. The high-grade group was 53.23 ± 12.86 years, with 13 males and 9 females. There was no significant difference between the two age groups and gender distribution. To avoid individual variations among samples, the D, $D*$, f, and CBF of the tumor region were relative to those of the contralateral normal white matter for each patient, with rD, $rD*$, rf, and rCBF obtained. The rD, $rD*$, rf, and rCBF of low-grade glioma patients were 1.61 (0.88-2.41), 0.99 (0.41-2.64), 2.23 (0.43-4.83), and 1.65 (0.41-9.15), respectively. The rD, $rD*$, rf, and rCBF of high-grade glioma patients were 1.05 (0.63-1.73), 1.63 (0.33-5.89), 1.29 (0.54-4.27), and 3.49 (0.72-12.17), respectively. Remarkable differences were noted in the rD, $rD*$, rf, and rCBF between low-grade and high-grade glioma patients ($P < 0.05$, Table 2). The Ki-67 LI of low-grade glioma patients was 0.05 (0.02-0.17) and that of high-grade glioma patients was 0.26 (0.02-0.63), to show the significant differences between the two groups of the patients ($P < 0.001$, Table 2).

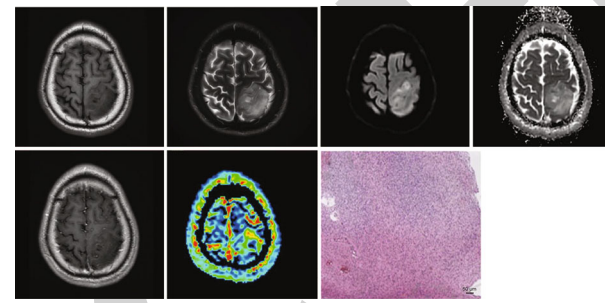

Figure 1: Representative images of the patient with gliomas. The patient was a 66-year-old man who developed a WHO grade II oligodendroglioma in his left frontal lobe.

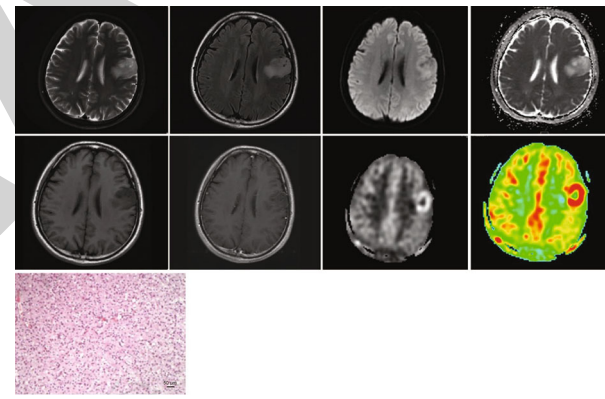

Figure 2: Representative images of the patient with gliomas. The patient was a 57-year-old man who developed a WHO grade III oligodendroglioma in his left frontal lobe.

3.3. Correlation between IVIM-DWI, 3D-ASL Parameters, and Ki-67 LI of Glioma Patients. In this part, we performed Pearson analysis to confirm the correlation between IVIM-DWI, 3D-ASL parameters, and Ki-67 LI of glioma patients, with r value ranging 0.71 to 1 as high correlation, 0.41 to

Table 2: IVIM-DWI, 3D-ASL parameters, and Ki-67 LI between low-grade and high-grade glioma patients.

Grade	*rD*	*rD* ∗	*rf*	*r*CBF	Ki-67 LI
Low grade	1.61 (0.88-2.41)	0.99 (0.41-2.64)	2.23 (0.43-4.83)	1.65 (0.41-9.15)	0.05 (0.02-0.17)
High grade	1.05 (0.63-1.73)	1.63 (0.33-5.89)	1.29 (0.54-4.27)	3.49 (0.72-12.17)	0.26 (0.02-0.63)
Z	-3.540	-2.430	-2.733	-2.166	-4.516
P	<0.001	0.015	0.006	0.030	<0.001

Statistical analysis was performed using Mann–Whitney *U* test.

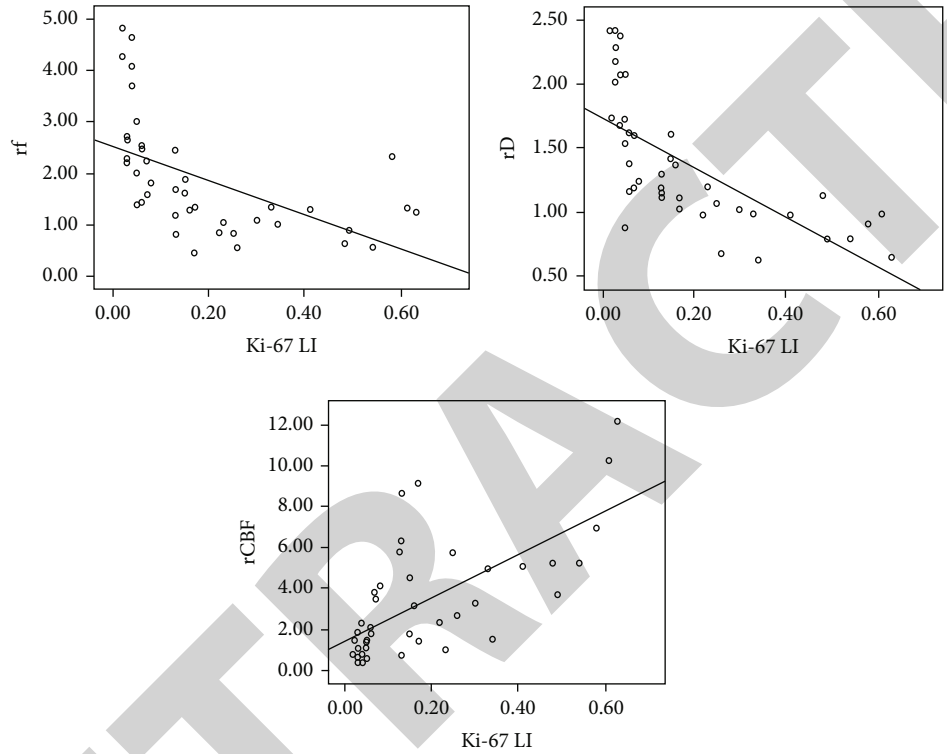

Figure 3: Correlation between *rD*, *rf*, *r*CBF, and Ki-67 LI in glioma patients.

0.70 as moderate correlation, and ≤0.40 as low correlation. Ki-67 LI was found to be negatively correlated with *rD* ($r = -0.693$, $P < 0.001$) and *rf* ($r = -0.539$, $P < 0.001$) but had no correlation with *r*CBF ($r = 0.665$, $P < 0.001$) in glioma patients (Figure 3). However, no significant correlation was noted between *rD* ∗ and Ki-67 LI of glioma patients.

3.4. Predictive Performance of IVIM-DWI, 3D-ASL Parameters, and Ki-67 LI for Different Grades of Glioma. The *rD*, *rD* ∗, *rf*, *r*CBF, and Ki-67 LI of glioma patients were used to predict high-grade glioma patients from low-grade glioma patients. The ROC (as shown in Figure 4) for prediction of high-grade glioma by *rD*, *rf*, *rD* ∗, *r*CBF, and Ki-67 LI yielded AUC of 0.819, 0.747, 0.719, 0.836, and 0.907, respectively. The sensitivity and specificity values are presented in Table 3.

4. Discussion

Glioma is the most common malignant neoplasm in adults and most commonly occurs in the brain and glial tissues. Currently, there is no unification of the histological classification of glioma, which is often named as similarity of glial cells. According to the WHO 2016 publication, the main gliomas include astrocytoma, oligodendroglioma, a combination of 2 cell types, ependymoma, neuroblastoma, and mixed glioma. Depending on the severity of the cancer, gliomas are classified into I-IV grades [15]. The incidence rate of glioma is 5.26/100,000 each year, and 17,000 cases are diagnosed annually. The patients with glioma are at risk of high mortality, especially for the population with grade IV represented by glioblastoma [16]. Therefore, accurate assessment of glioma level prior to treatment is important in treatment selection and evaluation.

On this study, IVIM and 3D-ASL were applied to the glioma patients with different grades to confirm their diagnostic evaluation. IVIM based on DWI is a contrast agent-free imaging technology, which randomly orients the blood flow of capillaries in tissues to simulate the pseudodiffusion process. It has been considered as an effective method applying to the field of tumor [17]. The approach of ASL is a method for imaging cerebral perfusion and cerebral angiography

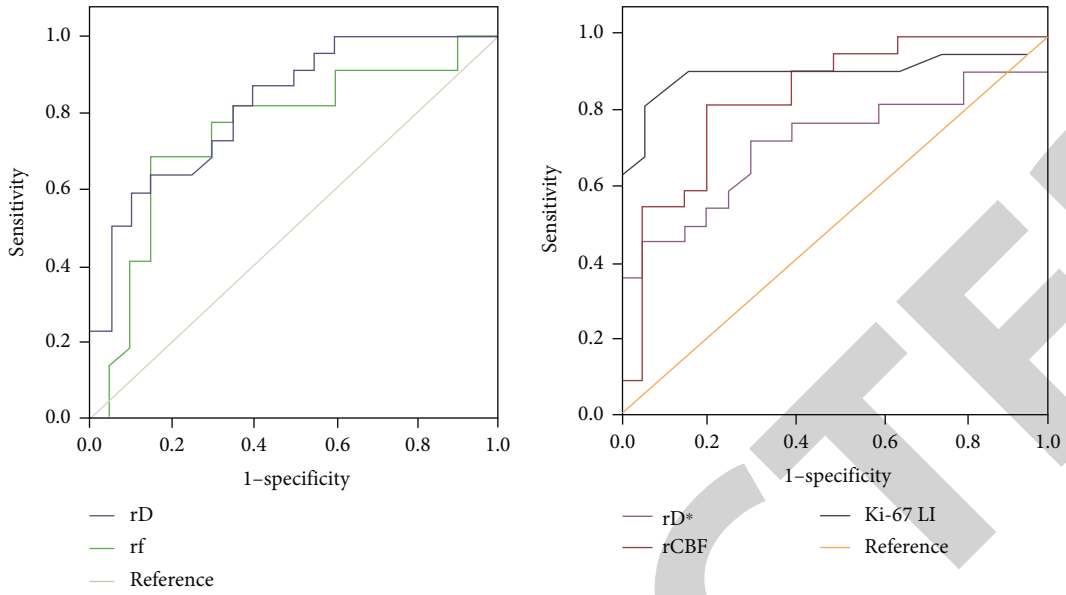

Figure 4: Predictive performance of IVIM-DWI, 3D-ASL parameters, and Ki-67 LI for different grades of glioma.

Table 3: Predictive performance of IVIM-DWI, 3D-ASL parameters, and Ki-67 LI for different grades of glioma.

	rD	*rD* ∗	*rf*	*r*CBF	Ki-67
AUC	0.819	0.719	0.747	0.836	0.907
P	<0.001	0.015	0.006	<0.001	<0.001
95% CI	0.694-0.945	0.560-0.878	0.589-0.904	0.712-0.961	0.777-1.000
Sensitivity (%)	84.93	73.77	76.23	86.20	90.03
Specificity (%)	83.23	67.58	69.43	85.11	88.84

[18]. The results presented in this study showed that significant difference was found in the median value of *D*, *D* ∗, *f*, and CBF between the healthy white matter and tumor solid. Higher median value of *D* in the glioma tissue indicated the diffusion movement of water molecules was remarkably stronger than that in healthy white matter. This might due to the increase of extracellular space caused by the destruction of normal cells. The severity of cancer infiltration was caused by *D* ∗, *f*, and CBF indices. Elevations in *D* ∗, *f*, and CBF did not directly indicate the presence of numerous microvessels in the glioma tissue [19]. A report by Bisdas et al. found significant differences in *D*, *D* ∗, and *f* levels of contralateral health problems white and advanced glioma. These results have been shown to be significantly different in patients with advanced glioma [20]. Togao et al. showed that the value of *D* in the advanced glioma group was lower in the lower group, while the value of *f* in the higher group was lower in the lower group, and there was no difference in *D* ∗ values of both groups [21]. These data were a little different from ours, indicating that, comparing to the low-grade group, lower *rf* value and higher value of *rD* ∗ were found in the high-grade group. However, our findings above were similar to the report represented by Lin et al. [22]. Chen et al. also showed that the high and low values of *f* on *D* ∗ were lower than the higher groups [23]. The differences in the *f* value between the two groups in studies might be related to various factors, such as difference in selected cases, tumor structural characteristics, the selection of *b* value, and setting in parameters of IVIM-DWI. In this study, the *rD* value of the upper group was lower than that of the lower group, which indirectly reflected tumor cells in high-grade glioma had stronger proliferation ability and higher cell density, resulting in limited diffusion of water molecules. Lin et al. demonstrated that higher CBF value was noted in the high-grade glioma, which was similar to our findings.

Ki-67 is a nuclear protein expressed at almost all stages of the cell cycle, and its expression is associated with tumor cell growth. A subset of Ki-67 LI is involved in disease therapy [24]. It was found that the high-grade glioma patients showed significant higher value of Ki-67 LI comparing to the patients with low-grade glioma, indicating the proliferative activity of tumor cells increased with its histological grade, which was proved by other studies [25, 26]. The Pearson analysis in this study revealed that Ki-67 LI expression was negatively correlated with *rD* and *rf*. A similar study indicated the level of *rD* and *rf* in high-grade and low-grade glioma were moderately negatively correlated with the Ki-67 LI [27]. The results indicated the level of *rD* and *rf* was related to changes in proliferative activity and cell density of tumor cells. In addition to this study, no remarkable correlation between *rD* ∗ and Ki-67 Li in patients with glioma was discovered, which suggested tumor proliferation

activity was not closely associated with blood perfusion. It was found that Ki-67 LI was positively correlated with *r*CBF of glioma patients, indicating the velocity of blood perfusion was related to the tumor proliferation activity. The ROC analysis showed that *rD*, *rf*, *rD* ∗, *r*CBF, and Ki-67 LI yielded AUC of 0.819, 0.747, 0.719, 0.836, and 0.907, respectively. The four parameters in IVIM-DWI and 3D-ASL, as well as the fraction of Ki-67 LI, can be used for assessment of grading in human glioma.

In conclusion, the parameters of IVIM-DWI and 3D-ASL are efficient in identifying glioma grade. The present study indicated that the value of *rD*, *rf*, and *r*CBF were closely associated with tumor proliferation activity, which can predict quantitatively the fraction of Ki-67 LI. These parameters contributed to the treatment scheme optimization and prognosis improvement in glioma. However, the data might not be completely reliable due to limited numbers of eligible patients involved in this study. Additionally, the detection of tumor solid area instead of the whole lesion may lead to data deviation. Further studies should be carried out to verify these results.

Data Availability

The data used to support the findings of this study are included in the sentence.

Conflicts of Interest

No conflict of interest is declared by the authors.

Acknowledgments

The research was supported by the "Kherkin State Colleges and Universities Basic Science Research Activity Research Fellowship (2019-KYYWF-1238)".

References

[1] O. Gusyatiner and M. E. Hegi, "Glioma epigenetics: from subclassification to novel treatment options," *Seminars in Cancer Biology*, vol. 51, pp. 50–58, 2018.

[2] R. Chen, M. Smith-Cohn, A. L. Cohen, and H. Colman, "Glioma subclassifications and their clinical significance," *Neurotherapeutics*, vol. 14, no. 2, pp. 284–297, 2017.

[3] S. Larjavaara, R. Mantyla, T. Salminen et al., "Incidence of gliomas by anatomic location," *Neuro-Oncology*, vol. 9, no. 3, pp. 319–325, 2007.

[4] Q. T. Ostrom, L. Bauchet, F. G. Davis et al., "The epidemiology of glioma in adults: a "state of the science" review," *Neuro-Oncology*, vol. 16, no. 7, pp. 896–913, 2014.

[5] R. S. D'Amico, Z. K. Englander, P. Canoll, and J. N. Bruce, "Extent of resection in glioma-a review of the cutting edge," *World Neurosurgery*, vol. 103, pp. 538–549, 2017.

[6] G. S. Chilla, C. H. Tan, C. Xu, and C. L. Poh, "Diffusion weighted magnetic resonance imaging and its recent trend-a survey," *Quantitative Imaging in Medicine and Surgery*, vol. 5, no. 3, pp. 407–422, 2015.

[7] D. Le Bihan, E. Breton, D. Lallemand, M. L. Aubin, J. Vignaud, and M. Laval-Jeantet, "Separation of diffusion and perfusion in intravoxel incoherent motion MR imaging," *Radiology*, vol. 168, no. 2, pp. 497–505, 1988.

[8] C. Federau, M. Cerny, M. Roux et al., "IVIM perfusion fraction is prognostic for survival in brain glioma," *Clinical Neuroradiology*, vol. 27, no. 4, pp. 485–492, 2017.

[9] C. Federau, M. Wintermark, S. Christensen et al., "Collateral blood flow measurement with intravoxel incoherent motion perfusion imaging in hyperacute brain stroke," *Neurology*, vol. 92, no. 21, pp. e2462–e2471, 2019.

[10] D. S. Williams, J. A. Detre, J. S. Leigh, and A. P. Koretsky, "Magnetic resonance imaging of perfusion using spin inversion of arterial water," *Proceedings of the National Academy of Sciences of the United States of America*, vol. 89, no. 1, pp. 212–216, 1992.

[11] A. A. K. Abdel Razek, M. Talaat, L. El-Serougy, G. Gaballa, and M. Abdelsalam, "Clinical applications of arterial spin labeling in brain tumors," *Journal of Computer Assisted Tomography*, vol. 43, no. 4, pp. 525–532, 2019.

[12] M. Helle, S. Rufer, M. J. van Osch et al., "Superselective arterial spin labeling applied for flow territory mapping in various cerebrovascular diseases," *Journal of Magnetic Resonance Imaging*, vol. 38, no. 2, pp. 496–503, 2013.

[13] J. Haapasalo, A. Mennander, P. Helen, H. Haapasalo, and J. Isola, "Ultrarapid Ki-67 immunostaining in frozen section interpretation of gliomas," *Journal of Clinical Pathology*, vol. 58, no. 3, pp. 263–268, 2005.

[14] D. N. Louis, H. Ohgaki, O. D. Wiestler et al., "The 2007 WHO classification of tumours of the central nervous system," *Acta Neuropathologica*, vol. 114, no. 2, pp. 97–109, 2007.

[15] D. N. Louis, A. Perry, G. Reifenberger et al., "The 2016 World Health Organization classification of tumors of the central nervous system: a summary," *Acta Neuropathologica*, vol. 131, no. 6, pp. 803–820, 2016.

[16] A. Omuro and L. M. DeAngelis, "Glioblastoma and other malignant gliomas," *JAMA*, vol. 310, no. 17, pp. 1842–1850, 2013.

[17] D. Le Bihan, "What can we see with IVIM MRI?," *NeuroImage*, vol. 187, pp. 56–67, 2019.

[18] P. Jezzard, M. A. Chappell, and T. W. Okell, "Arterial spin labeling for the measurement of cerebral perfusion and angiography," *Journal of Cerebral Blood Flow and Metabolism*, vol. 38, no. 4, pp. 603–626, 2018.

[19] Z. C. Liu, L. F. Yan, Y. C. Hu et al., "Combination of IVIM-DWI and 3D-ASL for differentiating true progression from pseudoprogression of glioblastoma multiforme after concurrent chemoradiotherapy: study protocol of a prospective diagnostic trial," *BMC Medical Imaging*, vol. 17, no. 1, p. 10, 2017.

[20] S. Bisdas, T. S. Koh, C. Roder et al., "Intravoxel incoherent motion diffusion-weighted MR imaging of gliomas: feasibility of the method and initial results," *Neuroradiology*, vol. 55, no. 10, pp. 1189–1196, 2013.

[21] O. Togao, A. Hiwatashi, K. Yamashita et al., "Differentiation of high-grade and low-grade diffuse gliomas by intravoxel incoherent motion MR imaging," *Neuro-Oncology*, vol. 18, no. 1, pp. 132–141, 2016.

[22] Y. Lin, J. Li, Z. Zhang et al., "Comparison of intravoxel incoherent motion diffusion-weighted MR imaging and arterial spin labeling MR imaging in gliomas," *BioMed Research International*, vol. 2015, Article ID 234245, 10 pages, 2015.

[23] J. Chen, J. Liu, X. Liu, X. Xiaoyi, and F. Zhong, "Decomposition of toluene with a combined plasma photolysis (CPP)

Hindawi
Scanning
Volume 2023, Article ID 9876203, 1 page
https://doi.org/10.1155/2023/9876203

Retraction

Retracted: Diagnostic Value of Specialist Systems in Sports Knee Injuries

Scanning

Received 12 December 2023; Accepted 12 December 2023; Published 13 December 2023

This article has been retracted by Hindawi, as publisher, following an investigation undertaken by the publisher [1]. This investigation has uncovered evidence of systematic manipulation of the publication and peer-review process. We cannot, therefore, vouch for the reliability or integrity of this article.

Please note that this notice is intended solely to alert readers that the peer-review process of this article has been compromised.

Wiley and Hindawi regret that the usual quality checks did not identify these issues before publication and have since put additional measures in place to safeguard research integrity.

We wish to credit our Research Integrity and Research Publishing teams and anonymous and named external researchers and research integrity experts for contributing to this investigation.

The corresponding author, as the representative of all authors, has been given the opportunity to register their agreement or disagreement to this retraction. We have kept a record of any response received.

References

[1] X. Chen, A. Yu, N. Cai, S. Wei, and Y. Tong, "Diagnostic Value of Specialist Systems in Sports Knee Injuries," *Scanning*, vol. 2022, Article ID 1892877, 7 pages, 2022.

Hindawi
Scanning
Volume 2022, Article ID 1892877, 7 pages
https://doi.org/10.1155/2022/1892877

Research Article

Diagnostic Value of Specialist Systems in Sports Knee Injuries

Xi Chen,[1] **Ao Yu**,[2] **Ning Cai**,[1] **Saite Wei**,[1] **and Yongqing Tong**[1]

[1]*College of Physical Education, Taiyuan University of Technology, Taiyuan, Shanxi 030000, China*
[2]*Woosuk University, Jeonju, Republic of Korea*

Correspondence should be addressed to Yongqing Tong; 20160625@ayit.edu.cn

Received 10 July 2022; Revised 29 July 2022; Accepted 4 August 2022; Published 31 August 2022

Academic Editor: Danilo Pelusi

In order to explore the diagnostic effect of the expert system in knee sports injury, a method of diagnostic value of expert system in sports knee sports injury is proposed. This paper mainly takes 200 professional football players in sports higher vocational colleges as the research object. There are 146 male athletes and 44 female athletes; we establish a football injury ontology knowledge base and use a reasoning engine to build an intelligent expert system diagnosis system, allowing users to quickly discover diseases, accurately diagnose injuries, and obtain the best means of rehabilitation. Through the investigation, it can be seen that the body parts caused by football injuries are more complex, and the types of injuries in each part are also different. Therefore, it is particularly important to establish an intelligent retrieval system with convenient query and clear diagnosis by the expert system. With the birth and development of computer and artificial intelligence technology, the development of artificial intelligence expert systems in the medical field has become a reality. The construction of this system will have theoretical and practical significance and application value.

1. Introduction

Expert system (ES), also known as knowledge-based system, is the most important and successful field of artificial intelligence research. The expert system came into being in the mid-1960s. After more than 30 years of research and development, it is becoming more and more mature in theory and technology. It has been widely used in all fields all over the world and has achieved great economic and social benefits [1]. At present, the main application fields of expert system are as follows: medical diagnosis, chemical engineering, speech recognition, image processing, financial decision-making, signal interpretation, geological exploration, commercial decision-making, crop field management, farm management, petroleum, military, and so on. The expert system has become one of the research focuses of countries all over the world. Japan, the United States, Britain, and other countries have listed it as a national key research project and invested a lot of manpower and funds. Japan regards the expert system as the core content of the fifth-generation computer research, and Britain has listed the expert system/intelligent database as one of the four key research directions of the country [2]. The expert system is mainly composed of three parts (Figure 1): man-machine interface, knowledge base, and inference engine.

(1) Man machine interface: the man machine interface, also known as man-machine interface, is the part where users communicate with expert system [3]. Through the man-machine interface, the user inputs the data and information required by the expert system. The system displays results and information through the man-machine interface. The media for users to communicate with the system can be text, sound, image, graphics, animation, audio-visual, etc. A friendly man-machine interface is one of the necessary conditions for a successful expert system, because it is the most direct part for users to communicate with the expert system. Its function and appearance are directly related to whether users can happily accept all the information transmitted by the system to them [4]

(2) Knowledge base: used to store the expertise provided by domain experts. These expertise include book knowledge related to the field, common sense knowledge,

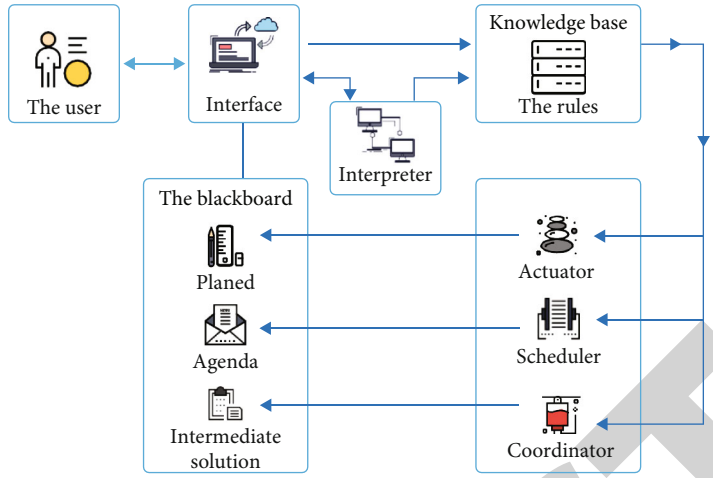

Figure 1: Structure of an ideal expert system.

and experience knowledge obtained by experts in practice. The problem solving of the expert system is carried out by using the special knowledge provided by experts to simulate the thinking mode of experts. Therefore, the quantity and quality of knowledge in the knowledge base have become the key factors of system performance and problem solving ability in an expert system. Therefore, the establishment of knowledge base is the central task of constructing expert system [5]

(3) Reasoning machine: a program used to memorize the rules and control strategies adopted by the inference engine, so that the whole expert system can work in a logical way. Inference engine can use knowledge to reason and draw conclusions, rather than simply searching ready-made answers [6]

(4) Interpretation facetyt: the interpreter can explain the behavior of the expert system to the user, including the correctness of the reasoning conclusion and the reason why the system outputs the candidate solution

(5) Global database: also known as global database or general database, it is used to store the initial data of the field or problem and the intermediate data (information) obtained in the reasoning process, that is, some current facts of the processed object [7]

2. Literature Review

He et al. believe that training without fatigue is ineffective and training without recovery is dangerous. However, it is also dangerous to exceed the maximum load of the knee joint. From the perspective of exercise physiology, after repeated overload stimulation of the knee joint for many times [8]. Chen et al. believe that the accumulation of fatigue and injury reduces the excitability of the nerve muscle contact, resulting in the disorder of the structure and metabolism of the internal dimension system of the joint, the fatigue of various tissues and cells, resulting in the abnormal energy metabolism and material metabolism of the whole knee joint, and the ability to maintain the movement of the knee joint can not be supplemented in time, resulting in the corresponding functional lesions of the knee joint [9]. Zhang believes that in the process of movement, the knee joint will produce corresponding compressive stress, tensile stress, shear stress, and hydrostatic pressure under various high-strength forces. In addition, there are reasons such as cartilage wear caused by mechanical stress imbalance or excessive load. The upper and lower bone levers of the knee joint are long, and the surrounding muscles are few. It is the most vulnerable joint in sports. The injury accounts for more than 50% in long jump. Athletes engaged in long jump have a history of acute or chronic injuries to varying degrees [10]. Meng et al. believe that in the standing long jump, consciousness dominates the body, and consciousness will be affected by psychological factors. In the long jump, psychological factors come from many aspects, which are mainly affected by the external environment and their own poor psychological quality. These two macrofactors are the main causes of sports injury to the knee joint [11]. Rudolph et al. believes that people's psychological development is slow and in the transition period from immature to mature, which will seriously affect the training process of athletes in the long jump and have a significant impact on the knee joint [12]. Li et al. believe that the knee joint is the link between the thigh and the lower leg. It is also the regulator that coordinates the up and down forces in the process of human movement and carries various internal and external factors such as gravity, self-generated gravity of the human body, and the supporting reaction force of the ground, so as to reduce the damage of human function in sports and play the role of dispersing pressure, transmitting weight, and reducing vibration. In this process, once the knee joint is overstimulated and the external force exceeds the maximum bearing capacity of the knee joint, violent injury will occur to the knee joint. At the same time, when excessive fatigue temporarily reduces the physical function, continuous long jump is also an important factor for acute injury [13]. Ren et al. believe that the repetitive injury of the knee joint is a closed cycle. Long-term single long jump exercise will make the knee repeatedly bear overload stimulation.

With the increase of time, the accumulation of overload stimulation on the knee will produce fatigue wear on the knee. In the interval standing long jump training, although there will be an interval for the recovery of physical function in each long jump, it is the same exercise in a few hours, a day, a few days, or a few weeks [14]. Liu et al. believe that the main part of the movement is for the knee joint, which constantly repeats the flexion and extension of the leg and the indirect and repeated overload stimulation of various forces on the knee joint, which will reduce the muscle strength around the knee joint, reduce the proprioception, and reduce the range of joint movement, and the long-term sports injury or pathological sports injury will lose the sports ability of the knee joint [15]. Zhang et al. believe that in sports, knee injuries are more acute injuries, and acute injuries will turn into chronic injuries if they are not treated [16].

Based on the current research, an expert system is proposed. This paper mainly takes 200 football professional athletes in sports vocational and technical college as the research object. There are 146 male athletes and 44 female athletes; we establish the ontology knowledge base of football injury and use the reasoning engine to build an intelligent expert system diagnosis system, so that users can quickly find the condition, accurately diagnose the injury, and get the best rehabilitation means.

3. Research Objects and Methods

3.1. Research Object. This paper mainly takes 200 football professional athletes in sports vocational and technical college as the research object. There are 146 male athletes and 44 female athletes.

3.2. Research Methods

(1) Literature review method

By consulting relevant literature such as CNKI, this paper summarizes the various parts of football players that are easy to be injured in sports, as well as the direct or indirect factors that lead to injury in training and competition [17].

(2) Expert interview method

Through discussion with experts and professors in general hospital, sports medicine experts, and football coaches, it mainly focuses on the characteristics, clinical manifestations, and formation methods of sports injury related to football. During the interview with experts, many problems were put forward and discussed in depth and detail. The views and suggestions of experts were incorporated into the conclusions as a research basis [18].

(3) Questionnaire survey method

The necessity of constructing this system is analyzed in the form of a questionnaire. The specific implementation process and results are as follows: the questionnaire is mainly aimed at players, coaches, team doctors, bone and joint experts, and football administrators. The topics of the questionnaire are divided into three categories: closed, semi-closed, and open. Problems include common parts of football acute injury, common parts of football chronic injury, and common rehabilitation methods and prevention methods. Taking the sports vocational and technical college, the football field of the Provincial Sports Bureau, the Football Association, the provincial physical fitness Museum, the provincial hospital, and the orthopedic ward of the First Affiliated Hospital of Medical University as the distribution places, a total of 127 questionnaires were distributed, and 100 questionnaires were actually effectively recovered, with a recovery rate of 78.74%. This result can be used as the basis for the research results [19].

(4) This expert system has the characteristics of distributed processing

Its main purpose is to decompose the functions of a Ge family system and distribute them to multiple processors for parallel processing, so as to improve the processing efficiency of the system as a whole. It can work in a tight multiprocessor working environment or a loose computer network environment, so its overall structure largely depends on its hardware environment. To design and implement a distributed expert system, the following problems need to be solved:

(1) Function distribution: that is, the functions or tasks of each part of the system decomposed are reasonably and evenly distributed to each processing node

(2) Knowledge distribution: according to the function distribution, the knowledge is reasonably divided and distributed to each processing node. On the one hand, the redundancy of knowledge should be reduced as much as possible; on the other hand, the inconsistency of knowledge should be avoided as much as possible [20]

(3) Interface design: the purpose of the interface design of each part is to make it easy for each part to communicate and synchronize with each other. On the premise of ensuring the completion of the overall task, it is necessary to make each part independent as far as possible, and the less the connection between parts, the better

(4) System structure: the design of the system structure depends on the environment and nature of the application on the one hand, and the hardware environment on the other hand

Distributed artificial intelligence mainly studies how multiple intelligent systems dispersed logically or physically solve problems in parallel and cooperate with each other. The cognitive model of distributed artificial intelligence research is that most of human activities involve social groups, and the solution of large and complex problems needs the cooperation of multiple professionals or

organizations. Distributed artificial intelligence theory has high application value in parallel programming, computer communication, network management, and control [21]. The main advantages of distributed expert system are as follows:

(i) It can effectively improve the problem-solving ability of the system. Firstly, the openness of the system is enhanced, and the problem-solving ability of the system can be improved by adding new logic processing nodes. In addition, due to the redundancy of communication path, processing node and knowledge, the system can still continue to operate in case of failure (allowing the reduction of response time or solution accuracy), and the reliability of the system is good

(ii) It can effectively improve the efficiency of problem solving. Each node in the system can work in parallel, so it can scientifically allocate the tasks of each node, so that each node can solve the problem in a coordinated, parallel and fast manner at the same time, that is, use the distributed structure for parallel and efficient reasoning and calculation [22]

(iii) It can effectively reduce the complexity of software. The system decomposes the solving task of the whole system into several relatively independent special subtasks, which reduces the complexity of the problem solving of each processing node

The research frontier of the distributed expert system is the research of distributed artificial intelligence based on multiagent structure, as well as the research of flexible and intelligent distributed software structure system, such as the research and construction of distributed computing architecture based on cD0M and CORBA technology.

4. Research Results and Analysis

4.1. Results. The following results are obtained after the research according to the above methods, and the data are sorted and analyzed:

It can be seen from Figure 2 that the common injured parts of football sports include the knee, ankle, head, and foot, mainly ankle and knee joint injuries. Especially in high-intensity professional football matches, players are often very focused in the game, which is very easy to cause injury in physical confrontation. If the nonball player tackles the ball player, it will cause injury to the ankle and knee joint [23].

It can be seen from Figure 3 that among the common injuries in football sports, the main injury diseases of knee joint injury are cruciate ligament injury, medial ligament injury, lateral ligament injury, and meniscus injury. There are many ligaments in the knee joint, so there is a great possibility of strain and long recovery time. Therefore, offsite preparation activities should be sufficient and physical training should be scientific. In knee ligament strain, the most common cause of avulsion is that the knee joint is impacted by external force during torsion, and it is easy to cause osteoarthritis due to the knee joint with imperfect function of anterior cruciate ligament [24].

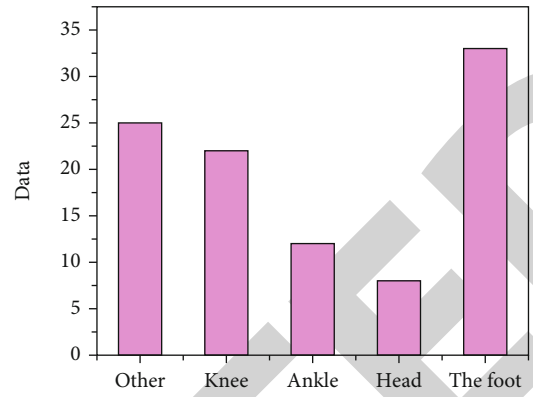

Figure 2: Proportion of common injury sites in football events ($n = 200$).

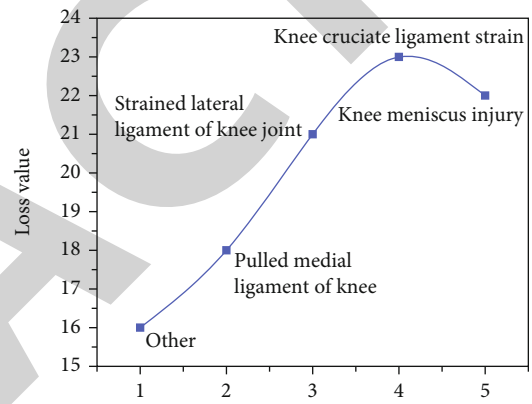

Figure 3: Proportion of knee joint injury diseases in football events ($n = 200$).

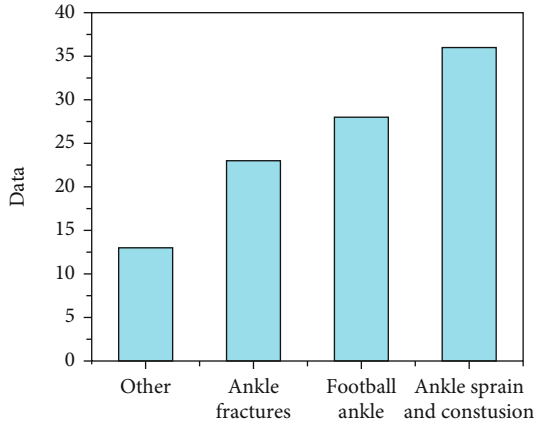

Figure 4: Proportion of knee joint injury diseases in football events ($n = 200$).

It can be seen from Figure 4 that among the common injuries in football, the injury rate of ankle sprain and contusion is the highest, followed by football ankle and ankle fracture. Because football players often jump to compete for the

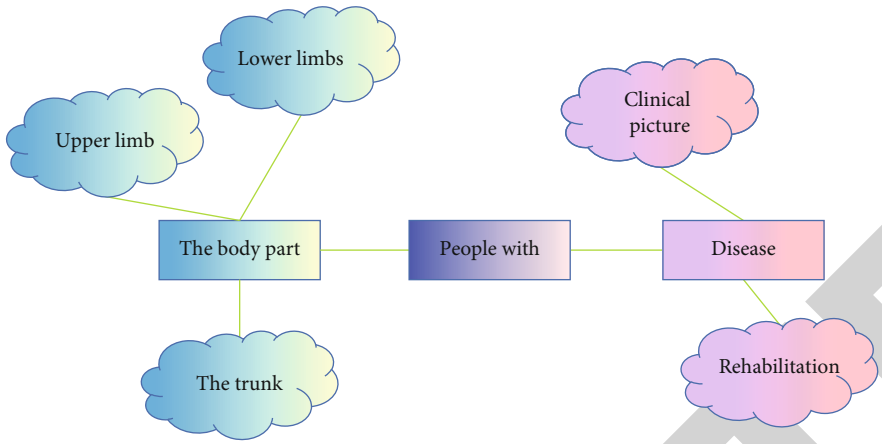

Figure 5: ER diagram of information management inquiry module of football injury.

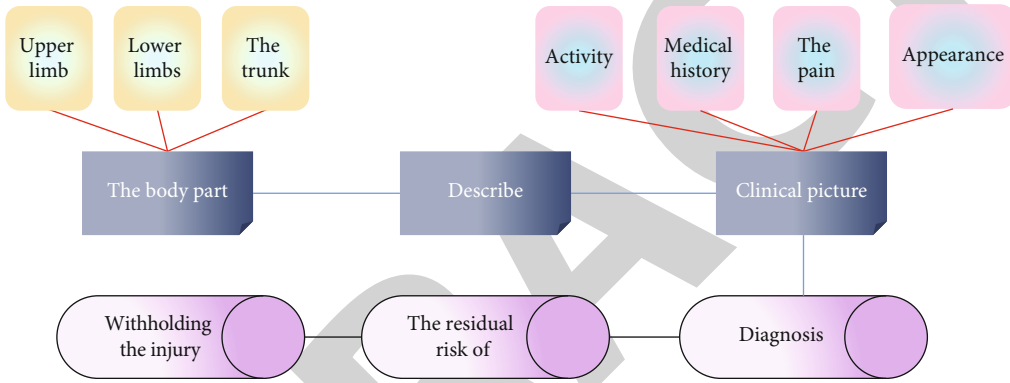

Figure 6: ER diagram of football injury diagnosis module.

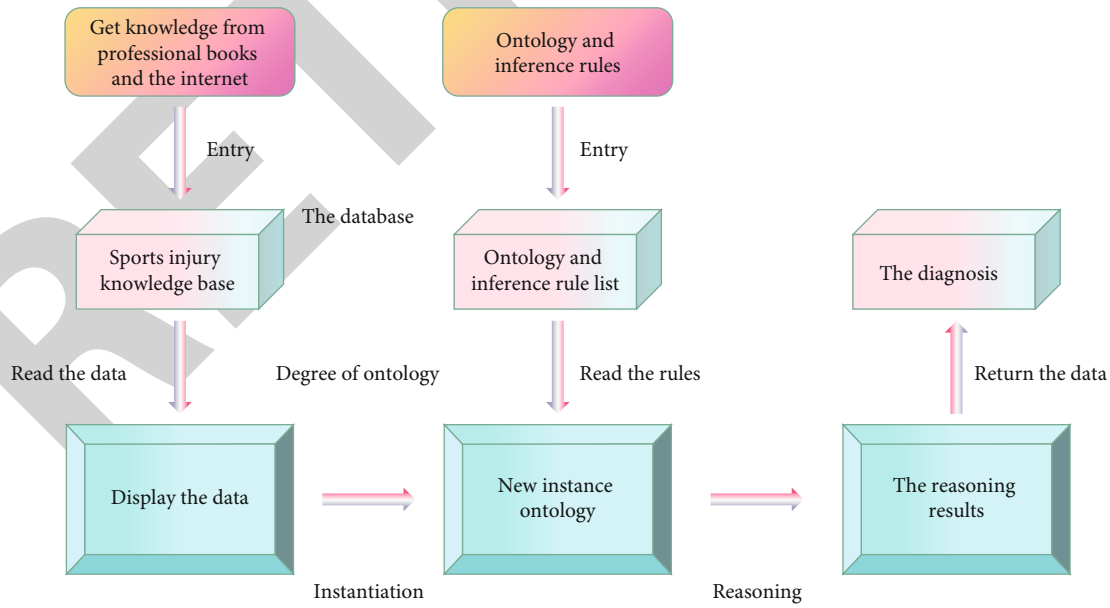

Figure 7: System framework diagram.

header, it is easy for two players to lose their center of gravity and land unsteadily due to fierce collision when taking off, which is very easy to cause ankle fracture. Through the investigation, we can see that the body parts caused by football injury are more complex, and the types of injuries in each part are also different. Therefore, it is particularly

important to establish an intelligent retrieval system with convenient query and clear expert system diagnosis [25].

4.2. Establish Expert System Diagnosis Intelligent Retrieval System

(1) Football injury information management query module

The system extracts keywords according to the damage location name or fuzzy representation selected by the user and retrieves the damage instance and corresponding attributes in the damage ontology database. The ER relationship diagram of this module is shown in Figure 5.

(2) Diagnosis module of football injury expert system

The system can judge through the user's selection or fuzzy input of the damaged part of the human body, and then through the selection of clinical manifestations, the system finally makes reasoning and judgment and feeds back the damage results diagnosed by the expert system to the user. The ER relationship diagram of this module is shown in Figure 6.

(3) Injury and rehabilitation means module

According to the injury inquired by the user, the system matches the reasonable rehabilitation treatment means mainly through the acute and chronic injury and feeds back to the user [26].

(4) The overall structure of the system is designed, and the specific expert system diagnosis flow chart is shown in Figure 7.

5. Conclusion

This paper chooses football injury as the research object. By extracting the field knowledge of football injury, constructing the ontology database, using the reasoning mechanism to realize the reasoning expert system diagnosis, and establishing the intelligent expert system diagnosis system, the system not only provides a useful exploration for the expert system diagnosis of football injury but also makes a contribution to the intelligent digital medical treatment. The main work is as follows:

(1) The professional knowledge of football injury was extracted and discussed and verified with human experts. Then, the formal language is used to describe the knowledge and construct the ontology knowledge base

(2) Add constraints to related classes in ontology knowledge base and realize internal retrieval through the built-in inference engine of Protégé tool

(3) Jena inference engine is selected as the inference engine of the system, and its inference mechanism is used to complete the diagnosis of the inference expert system. The research results promote the innovation of the accuracy of knowledge expression in the field of football injury, the scientificity of organization construction, and the integrity of hierarchical structure and lay a solid foundation for improving the level of sports injury intelligent expert system diagnosis and establishing football injury disease database. It also lays a foundation for establishing a richer sports injury knowledge base and medical expert system diagnosis system in the future

Data Availability

The data used to support the findings of this study are available from the corresponding author upon request.

Conflicts of Interest

The authors declare that they have no conflicts of interest.

References

[1] A. Prabhu, B. Abaid, S. Fathima, S. Naik, and S. Lippmann, "Sports-injury encephalopathy," *Southern Medical Journal*, vol. 112, no. 10, pp. 547–550, 2019.

[2] M. E. Varkiani, M. H. Alizadeh, R. Rajabi, and H. Minoonejad, "The design and implementation of sport injury surveillance system," *British Journal of Sports Medicine*, vol. 55, no. Suppl 1, p. A134, 2021.

[3] D. Musu, G. Bardini, F. Ideo, S. Mezzena, and E. Cotti, "Management of the sequelae of a sport-related traumatic dental injury using ultrasound examination in the diagnosis and follow-up," *Dentistry Journal*, vol. 9, no. 3, p. 27, 2021.

[4] H. V. Eetvelde, L. D. Mendona, C. Ley, R. Seil, and T. Tischer, "Machine learning methods in sport injury prediction and prevention: a systematic review," *Journal of Experimental Orthopaedics*, vol. 8, no. 1, p. 27, 2021.

[5] D. M. Jones, K. E. Webster, K. M. Crossley et al., "Psychometric properties of the hip–return to sport after injury scale (short form) for evaluating psychological readiness to return to sports after arthroscopic hip surgery," *The American Journal of Sports Medicine*, vol. 48, no. 2, pp. 376–384, 2019.

[6] L. Huang and G. Liu, "Functional motion detection based on artificial intelligence," *The Journal of Supercomputing*, vol. 78, no. 3, pp. 4290–4329, 2022.

[7] Y. K. Yi, "Establishment of preliminary evaluation system of the convergence design education program by type, for which expert verification was implemented," *The Korean Society of Science & Art*, vol. 37, no. 2, pp. 61–73, 2019.

[8] Q. He, Y. Gao, B. Cui, and H. Han, "A preliminary study on establishment of AI-assisted remote imaging diagnosis system for major infectious diseases," *Chinese Journal of Medical Science Research Management*, vol. 33, pp. E010–E010, 2020.

[9] G. Chen, B. Jiang, and L. Yang, "Research on the establishment of society-university security system in the new era," *International Journal of Social Science and Education Research*, vol. 3, no. 4, pp. 9–11, 2020.

[10] T. Zhang, "Research on the establishment of robot workpiece coordinate system and its approximation method," in *IOP Conference Series: Earth and Environmental Science*, vol. 714, Beijing city of China, 2021.

Hindawi
Scanning
Volume 2023, Article ID 9847959, 1 page
https://doi.org/10.1155/2023/9847959

Retraction

Retracted: Application of Moving Target Information Perception Technology in Intelligent Supervision System

Scanning

Received 12 December 2023; Accepted 12 December 2023; Published 13 December 2023

This article has been retracted by Hindawi, as publisher, following an investigation undertaken by the publisher [1]. This investigation has uncovered evidence of systematic manipulation of the publication and peer-review process. We cannot, therefore, vouch for the reliability or integrity of this article.

Please note that this notice is intended solely to alert readers that the peer-review process of this article has been compromised.

Wiley and Hindawi regret that the usual quality checks did not identify these issues before publication and have since put additional measures in place to safeguard research integrity.

We wish to credit our Research Integrity and Research Publishing teams and anonymous and named external researchers and research integrity experts for contributing to this investigation.

The corresponding author, as the representative of all authors, has been given the opportunity to register their agreement or disagreement to this retraction. We have kept a record of any response received.

References

[1] M. Zhu, "Application of Moving Target Information Perception Technology in Intelligent Supervision System," *Scanning*, vol. 2022, Article ID 5192601, 7 pages, 2022.

Hindawi
Scanning
Volume 2022, Article ID 5192601, 7 pages
https://doi.org/10.1155/2022/5192601

Research Article

Application of Moving Target Information Perception Technology in Intelligent Supervision System

Mingjiang Zhu

Department of Physical Education, North China University of Water Resources and Electric Power, Zhengzhou, Henan 450046, China

Correspondence should be addressed to Mingjiang Zhu; 201903519@stu.ncwu.edu.cn

Received 10 July 2022; Revised 25 July 2022; Accepted 29 July 2022; Published 31 August 2022

Academic Editor: Danilo Pelusi

In order to solve the problems of inaccurate information collection, incomplete information collection, and inconsistency of collected images in traditional sports injury collection methods, an application method of moving target information perception technology in intelligent supervision system is proposed. By judging and analyzing the potential motion damage posture of the motion posture intelligent tracking images, the collected motion intelligence tracking images are judged. The intelligent tracking image matrix can make up for the shortcomings of traditional images that are not connected, complete the identification, detect potential damage in time, and take targeted preventive measures and means. Finally, according to the target detection algorithm and target tracking algorithm, combined with OpenCV computer vision library and QT image library, an intelligent video surveillance target tracking simulation system is developed. The algorithm studied in this paper is to realize the target tracking function of the intelligent video surveillance system. Through the comparison of experimental results, the design method can accurately collect damage attitude information, without calculating continuous values, and the use of three-dimensional images in the positioning process can analyze the damage attitude from multiple angles.

1. Introduction

Athletes' mistakes during daily competitions and training can ultimately lead to injuries. In addition to introducing modern science and technology to sports, some research and technology has been used to identify and document the specifics of sports in order to avoid injuries to athletes in the sports process [1]. Procedures typically record the physical data of a sports injury process by limiting physical exercise, imaging, and image counting systems. Data obtained from known fault locations by differential and data outputs are error data and offset data, including method modeling, some errors, and data limits. The accurate analysis and prediction of human motion posture can provide effective data support for sports training. By obtaining the relevant data of human movement and correcting the details of athletes' actions in combination with the standard database data, we can improve the athletes' sports level [2]. An intelligent multiple-object tracking system adopts advanced image detection, recognition, and tracking technology and cooperates with a precision motion control system to realize continuous and rapid tracking and capture of multiple moving targets in large scenes, as shown in Figure 1. It integrates the multitarget tracking and detection and video analysis functions in a large scene into an independent system. Through the intelligent analysis of the video information collected by the front-end camera, it automatically collects and classifies the abnormal behavior and events and linkage alarm. At the same time, the background can see the analysis data and record videos in real time, and video extraction and forensics can be carried out through event retrieval [3]. One of the biggest advantages of the system is that it can identify and monitor different behavior patterns of multiple targets in the same scene at the same time. It can be widely used in various large public places, including airports, stations, prisons, ports, mines, oil fields, nursing homes, streets, communities, shopping malls, and other important places, which are used to detect, classify, track, and record passing pedestrians, vehicles, and other suspicious objects, to judge whether there is abnormal behavior and give an alarm.

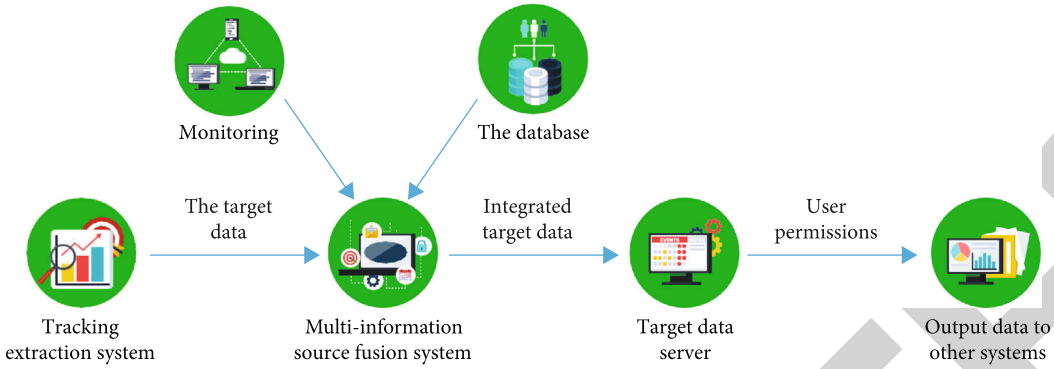

Figure 1: Intelligent multitarget tracking system.

2. Literature Review

Son and others now believe that all personal activities are active and rapidly evolving, that human health is gradually expanding, and that athletes' feelings of injury are becoming more common. As the importance of concealing the dangers of sports grows, so does the demand for sports to prevent injuries [4]. Kadupitiya and others have suggested that this paper consider the relationship between mental health factors such as risk and decision-making in terms of mental sports. Kadupitiya et al. indicated that from the perspective of sports psychology, the correlation between psychological predictors such as risk cognition, risk taking, exercise ability, sports injury experience, and sports injury in the mass fitness population was explored. The above cases of sports injuries and their gender differences with real physical effort are studied in order to establish a theoretical basis for the reduction and prevention of sports injuries [5]. Studies by Xu and others on the sports injury location platform at this stage have shown to some extent the impact of sports injuries, and athletes believe that they protect themselves and their coaches from injury and other professionals [6]. Rohei and others believe that sports injury prevention courses are only for professionals in the field of sports. As each sport differs in stats and defenses, athletes cannot identify injuries, causing problems for defenses, protection of athletes, resulting in recovery, wasted resources, and reduced efficiency [7]. Assaqty and others argue that the ability to prevent sports injuries is widely used in major sports. Based on the new prevention strategy, prevention strategies are developed for all injuries on the sports field, examining and implementing complex procedures and interventions involving injuries and injury data. The complex and closely related damage data information can be analyzed and processed efficiently and conveniently [8]. Moradi and Ehsanian believed that the risk factors for sports injuries at this stage are the wrists, hips, and knees. Most of them are incarcerated, usually chronic, which poses a serious risk to the health of athletes [9]. Prasad et al. stated that the biggest problem in physical examination may be the injury of athletes' daily energy and two-dimensional imaging technology, such as wrists, hips, and knees and other parts which cannot be guaranteed, and changes in injury cannot be observed intuitively. Internal distribution of internal information on the importance of movement cannot be distributed efficiently. As a result, the errors and distortions in the fine posture analysis of these parts are large and cannot be combined with clinical practice [10]. Kwak and others said that with the rapid development of computer vision, the intelligent technology of video surveillance system has also made some progress, and the research on target tracking method for intelligent video surveillance system has become a hot spot in computer vision-related professional research [11]. Pathak and others believe that target tracking is the core function of the intelligent video surveillance system and the basis of intelligent target surveillance system for target recognition, behavior analysis, and other work, which has important research value [12].

3. Method

3.1. Image Denoising. Noise refers to the factors that cause adverse effects in the processing or analysis of images. In most cases, the noise is a random signal and unpredictable, but it can be mathematically described by the method of probability and statistics. Noise comes from image acquisition, transmission, compression, and other links, in which the acquisition stage is the most serious link. When the noise is too large, it will affect the results of image processing and analysis and produce large errors [13]. Therefore, the first step of image analysis is to denoise the image, suppress the influence of noise, and improve the processing accuracy. With the continuous in-depth study of image noise, image noise is classified, which is mainly composed of salt-and-pepper noise and Gaussian noise. Gray image is the simplest kind of image, and the brightness exists in the image in the form of two-dimensional distribution. The noise $n(x, y)$ of a gray-scale image can be regarded as the interference to image brightness. The description of noise is completed by the average value and variance of probability statistics [14].

The average value of noise is generally used to describe the global intensity of noise, as shown in the following equation:

$$\bar{n} = E[n(x,y)] = \frac{1}{M \times N} \sum_{x=1}^{M} \sum_{y=1}^{N} n(x,y). \quad (1)$$

The variance of noise is used to express the density of noise distribution on the image, as shown in the following equation:

$$D(n) = E[n(x,y) - \bar{n}]^2 = \frac{1}{M \times N} \sum_{x=1}^{M} \sum_{y=1}^{N} [n(x,y) - \bar{n}]^2. \quad (2)$$

3.1.1. Common Image Noise. According to probability, image noise can be divided into Gaussian noise and impulse noise. These noises are briefly introduced below.

(1) Gaussian Noise. Gaussian noise is a common noise, and its mathematical expression is relatively simple, as shown in the following equation:

$$p(z) = \frac{1}{\sqrt{2\pi}\sigma} \exp\left[-\frac{(z-u)^2}{2\sigma^2}\right]. \quad (3)$$

In Formula (3), z is the gray level of pixels, u is the mean value of z, σ is the standard deviation, and z exists in the form of normal distribution.

(2) Impulse Noise (Salt-and-Pepper Noise). In image segmentation, the noise occurs frequently, which is specifically manifested as light noise in dark areas. The distribution function of dark noise in light areas can be given by the following equation:

$$p(z) = \begin{cases} P_a, & z = a, \\ P_b, & z = b, \\ 0, & \text{other}. \end{cases} \quad (4)$$

3.1.2. Common Image Denoising Algorithms

(1) Median Filter. This is an effective noise reduction method using sorting statistics. Its core algorithm is to calculate the average gray value of the neighborhood of a single point and characterize the gray value of a single point, and the isolated noise points are filtered out to filter out the interference of the pixels at this position. After Fourier change, the gray gradient of the high-frequency component is large. This method can smooth the image effect, but it can partially destroy the low-frequency component [15]. The mathematical expression of this method is shown in the following equation:

$$g(x,y) = \text{Med}\{f(x-k, y-l), (k,l) \in W\}. \quad (5)$$

$f(x,y)$ and $g(x,y)$ are the input and output, respectively. W is the neighborhood size of filtering, mostly 3×3 or 7×7 square, or linear or circular shaped which can be used as the neighborhood range of median filtering.

By processing an image with salt-and-pepper noise, it can be found that the median filter has good filtering effect for the image with salt-and-pepper noise, with high restoration degree and very obvious image contour [16]. This is because the salt-and-pepper noises are discrete points. The average value of the gray value of the salt-and-pepper noise section is used to replace the original pixel value in order to filter the salt-and-pepper interference in the image. However, after filtering, the sharpness of the image decreases, and there will be slight sawtooth at the boundary.

(2) Gaussian Filtering. Gaussian filtering belongs to the category of linear filtering, which can better filter the Gaussian noise in the image, and is widely used in the field of image denoising. The essence of Gaussian filtering is to remove noise through weighted average calculation. The pixel value of any point on the image is obtained by weighted averaging the initial value of the point and the values of other points in the neighborhood of the set size. Gaussian filtering can obtain filtering results in two ways: the first is Fourier transform and the second is convolution calculation with setting the neighborhood as the discretization window [17]. The second method is more common, but when setting a large neighborhood, the amount of calculation is very large. This is the first method that can be used. In Gaussian filtering, the weight of each pixel is determined by the adopted Gaussian function. The commonly used Gaussian function is shown in the following equation:

$$g(x) = \exp\left(-\frac{x^2}{2\sigma^2}\right). \quad (6)$$

In formula (6), σ is the mean square deviation, and the width of the Gaussian function changes with the size of this parameter.

In the field of noise removal, Gaussian filtering often uses the discrete two-dimensional zero mean Gaussian function, as shown in the following equation:

$$g(x) = \exp\left(-\frac{x^2 + y^2}{2\sigma^2}\right). \quad (7)$$

The Gaussian filter performs the weighted average operation on the gray value of any point in the selected neighborhood and uses the operation result to replace the pixel value in the center of the neighborhood.

3.2. Improved Algorithm. The above algorithms are continuous algorithms based on the characteristics of target detection initialization. The tracking effect is not particularly ideal when the target characteristics change. This paper proposes an online learning target tracking algorithm. The biggest difference between it and the traditional tracking algorithm is the combination of detection algorithm and tracking algorithm. It uses the semisupervised learning mechanism to continuously update the tracking target. It has good tracking performance for target changes and partial occlusion, can adapt to more complex tracking environment, and has higher robustness [18]. The improved

algorithm consists of three modules: detection, tracking, and learning, as shown in Figure 2.

The tracking module is the basis of the whole system. It estimates the position of the target in the next frame image through the position of the target in the previous frame image. In the improved algorithm, the tracking module can enter the working mode only when the detection module determines that the target exists. During the working process of the tracking module, the tracking track generated by it is added to the positive sample training set of the learning module.

The main function of the detection module is to estimate the error of the results of the tracking module. When the error is greater than the given threshold, intervene in the tracking results and correct the results. Its main working principle is to traverse the image pixels in the way of a sliding window, marking the positions similar to the target to be tracked as positive samples and the rest as negative samples. Pass the classification results to the learning module, and select a positive sample with the greatest confidence from the results as the initial position of the current tracking target to track the target in the next frame.

The learning module mainly uses the positive and negative samples transmitted from the initial training set and the detection module to continuously improve the classifier through iterative methods to improve its classification accuracy.

Before tracking, it is necessary to mark the position of the tracking target on the initial image manually, then input the position into the tracking module, track it through the mean hit tracking method, and transfer it to the learning module after obtaining the tracking results. In the learning module, the initialization target is selected as the positive sample input to the training set, and a part of the background area is selected as the negative sample training set to train the detection module. After such an initialization process, the detection module has the ability to judge, and then, the subsequent images can be inputted into the tracker. When the tracker obtains the detection results, it uses the detector to judge and correct, outputs the corrected results, and inputs the results into the learning module to improve the performance of the detector and ensure the accuracy of its detection. An online model will be established in the learning module to judge the results of the tracking module and determine that the target exists in the image. The model will also be updated online.

In the improved algorithm, the tracking and detection results are transmitted to the learning module as samples, and the updated online model updates the tracking and detection module to ensure stable tracking when the tracking target is deformed [19].

3.3. Realize Sports Injury Posture Acquisition. This paper uses intelligent tracking to identify the athlete's injury data. Firstly, it needs to confirm the injury mark of intelligent tracking. It is not possible to determine the extent of the injury because the expert's guidance was used to determine the path to the above procedure. Assuming that the loss of intelligent trace image data is in $n(a,t)$, its damage action is expressed by duplicate data $c+y$. The structure of the trauma matrix is shown in the following equation:

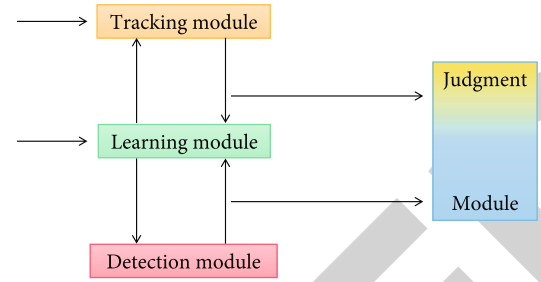

Figure 2: Improved mean shift composition framework.

$$\mu_{cy} = \sum_{a}\sum_{t}(a-\bar{a})^{c}(t-\bar{t})^{y}n(a,t), \tag{8}$$

where a and t represent the symbolic meaning of a sports injury and $y=(c+y)/2+1$. Through simultaneous normalization, equation (9) is obtained:

$$\eta_{cy} = \frac{\mu_{cy}}{\mu_{00}}. \tag{9}$$

Explain the time difference in the sports injury decision matrix, as shown in the following equation:

$$\phi = \mu_{cy} + \eta_{cy}. \tag{10}$$

Because different intelligent tracking images have different shooting angles, it will affect the image definition. The state of the data is changed as shown in equation (11) to avoid image distortion and data loss:

$$W_{cy} = \mu_{cy}\left(\mu_{c}^{2} - \mu_{y}^{2}\right) - \mu\left(\mu_{y}^{c}\mu_{c} - \mu_{y}^{c}\mu_{y}\right), \tag{11}$$

where μ_{c}^{2} is the athlete's injury calibration data through the change of injury matrix and injury image display of intelligent tracking and μ_{y}^{2} is the correlation parameter of damage. In order to realize the data positioning of the attitude, μ_{y}^{2} is used as the judgment data, and μ_{c} and μ_{y} are the parameters of the motion attitude matrix.

Damaged data can be obtained by determining the constraints on the model matrix and calculating the variance. If the difference is less than the required theoretical value, it can be used to subtract the theoretical value [20]. The implementation process of the motion injury attitude acquisition method based on intelligent tracking image analysis designed in this paper is shown in Figure 3.

4. Results and Analysis

The software for the Arduino is designed to receive a DMP signal from an InvenSense MPU-6050 IMU to transmit a signal to a computer via an XBee-PRO wireless serial connection. The inserted DMP is in the IMU and can be used by the host processor to change the calculation of the operating algorithm. The DMP receives data from acceleration meters and gyroscopes and provides an integrated melting output. To display and retrieve data received from XBee, a

computer program was developed that developed data-readable text using a communication port. The subjects were placed between four Kinect cameras, and the torso movement of the subjects was recorded with customized software [21]. Using the transformation matrix from the calibration step, stitching the images of each frame of the four cameras together can obtain a set of 3D point cloud information. By comparing the point clouds at each frame, the movement changes of the tested person can be accurately deduced. In order to deduce the changes of personnel actions, Geomagic Studio 2012 is used to calculate the set macrodata created. To sum up, the recording and deduction steps of the experimental data are as follows: load each point cloud exported from the customized software, build a 3D mesh, fill the mesh, and smooth the mesh with the mesh diagnosis tool. In order to ensure the accurate analysis of body motion, it is necessary to limit the analysis range, that is, place a boundary around the initial image and limit the volume calculation to the field of the human trunk. The database obtained by the experiment contains 2235 records of 144 different subjects, which perform a variety of complex actions. Since many records were sampled at 120 Hz while others were sampled at 60 Hz, the previous test sampling was reduced to 60 Hz. For evaluation, the preprocessed H3.6M data set is used to train the current model with 100 frames and 1660 ms time window. In this paper, the whole motion sequence is classified instead of a single motion sequence. The prediction ability of three models (S-TE, C-TE, and H-TE) is compared with the recently proposed ERD classification prediction algorithm. These models have been trained by recording the H3.6M data set. Reduce the sampling frequency to 25 Hz and convert the joint angle into an exponential graph. When the time window covers about 1660 Ms, the cyclic network will be initialized to 40 frames, equivalent to 1600 Ms. For each action, a separate pretraining recursive model is used. Although LSTM3l performs better than some models in the initial prediction, the time encoder C-TE shows better performance in the prediction of 160 ms or more. Because human action is a complex nonstationary action, it is difficult for the cyclic network to make a short-term prediction, but the model can infer the future prediction framework. In most predictions, the symmetric time encoder S-TE and convolutional time encoder C-TE are better than the layered time encoder H-TE, which shows that the structure a priori is beneficial to motion prediction. The hybrid coding method reduces the prediction error of fine-tuning specific actions and can effectively classify and predict the actions not included in the original training data. Movement processes in a simulation environment are obtained using computer simulations that mimic the damage of various processes. The measurement criteria are shown in Table 1.

Modeling a smart tracking image detection method based on the direction of the environment penetrates a potentially harmful operating system. Taking advantage of sports performance, a moving environment is created and image control skills detect discrepancies. Simulation of posture judgment of potential sports injuries is based on intelligent tracking image analysis.

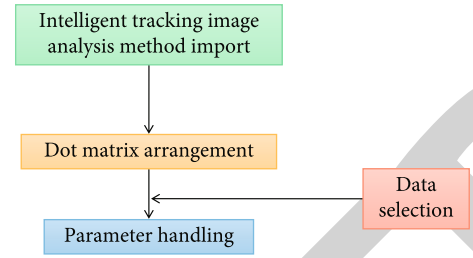

Figure 3: Implementation of motion injury posture acquisition method based on intelligent tracking image analysis.

Table 1: Simulation parameter setting.

Simulation parameters	Set value
Transportation damage degree	Below level 3 damage
Relative muscle exercise	More than 40%
Simulation image floating parameters	[-10, 50]
Data fixed point quantity (GB)	6
Exercise interval (s)	[8, 15]
Simulation times	760
Simulation duration (min)	20

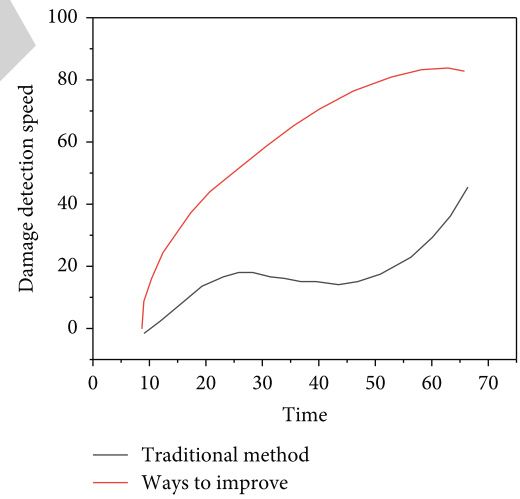

Figure 4: Damage detection speed of traditional method and new method.

Destruction of existing and new processes is done on various examples in the sports field, as shown in Figure 4.

The x-axis in Figure 4 represents the time in minutes. The y-axis represents the speed of the sports injury. In different perspectives, traditional detection speeds are slower and less efficient. The actual damage to the traditional and new process sequences in the game environment was examined using multiple point examples, as shown in Figure 5.

In Figure 5, the x-axis represents the sequence of magnitudes. The y-axis represents the accuracy of sports decisions. Many finds are similar, but the results are often less accurate.

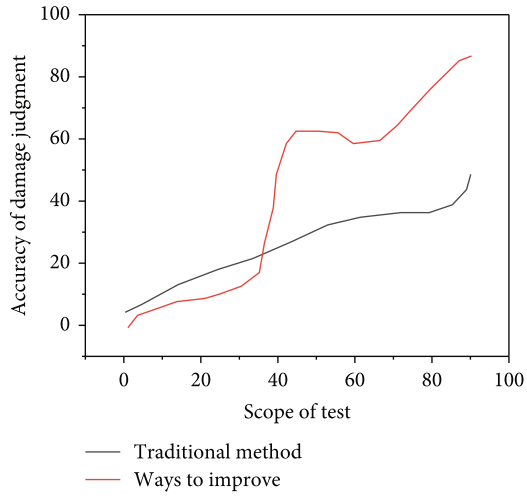

Figure 5: Accuracy of damage judgment of traditional method and new method.

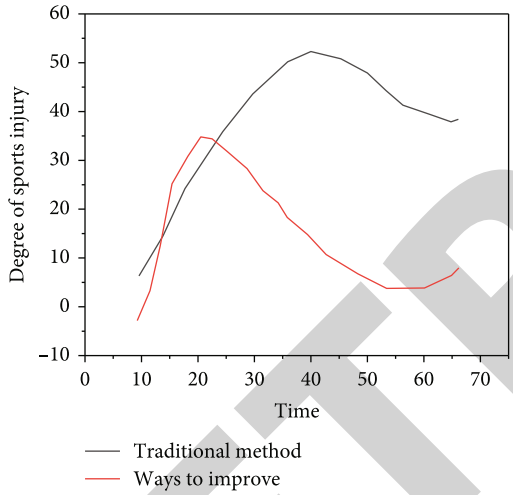

Figure 6: Sports injury degree of traditional method and new method.

In an athletics environment, the degree of injury to the athlete shall be checked with normal and new techniques as shown in Figure 6.

In Figure 6, the x-axis represents time. The y-axis indicates the degree of physical injury. The simulation time is the same, but the damage in technical sports is always high. From the simulation results, the modeling of physical fitness based on triangular analysis improves the incompleteness of the initial fitness information, which is limited only by the characteristics that can prevent injury according to the instructions. With the participation of experts, the continuity of movement from the site of injury will be improved, the evolution of injuries will be more clearly understood, and the average of athletes will be correctly distributed [22]. It reduces the risk of injury to athletes, improves the speed and accuracy of injury decisions, reduces the incidence of injuries to athletes, and improves performance. This reduces the incidence of blindness in athletes and prevents waste of resources.

5. Conclusion

This paper provides a way to get an injury of movement based on intelligent image analysis skills. The introduction of intelligent imaging analysis techniques to monitor the location of sports injuries, the use of intelligent simulation control techniques to count the procedures to correct movement restrictions, and the use of counting procedures instead of the traditional selection process can be avoided to avoid multiple procedures to change the quantity and finally understand the collection information at the site of the sports injury. At this stage, the analysis and research to determine the location of potential sports injuries revealed that there are insufficient rules for locating sports injuries in a self-limiting environment to prevent sports injuries. We offer an intelligent control imaging analysis based on a model that can be used to make decisions about physical harm. Using the calculation process instead of the traditional selection process can effectively avoid the selection of process quantity and variation quantity and finally realize the information acquisition of motion injury posture. The simulations try to prove the accuracy of the received, to adopt a method of observing sharp images in moving space, and to solve the problem of injuries of existing athletes. It is impossible to make a correct and timely conclusion. This meets the unsustainable need for intelligent tracking images found in heavy work environments. It can accurately and quickly record tracking images of smart athletes to identify the body of an injured athlete. It effectively improves the ability to prevent sports injuries and ensures the safety and health of athletes.

Data Availability

The data used to support the findings of this study are available from the corresponding author upon request.

Conflicts of Interest

The author declares that they have no conflicts of interest.

References

[1] H. Jiang, M. Wang, D. Liu, and S. Zhou, "Ctrack: acoustic device-free and collaborative hands motion tracking on smartphones," *IEEE Internet of Things Journal*, vol. 8, pp. 14658–14671, 2021.

[2] S. Park, M. Constantinides, L. M. Aiello, D. Quercia, and P. V. Gent, "Wellbeat: a framework for tracking daily well-being using smartwatches," *IEEE Internet Computing*, vol. 24, pp. 10–17, 2020.

[3] S. Andrade, G. O. Contente, L. B. Rodrigues, L. X. Lima, N. L. Vijaykumar, and C. R. L. Francês, "Smart home tracking: a smart home architecture for smart energy consumption in a residence with multiple users," *Wireless Personal Communications*, vol. 123, no. 4, pp. 3241–3262, 2022.

Hindawi
Scanning
Volume 2023, Article ID 9795735, 1 page
https://doi.org/10.1155/2023/9795735

Retraction

Retracted: Management Strategies and Imaging Observation of Early and Delayed Intelligent Treatment of Meniscus Sports Injury under Knee Osteoarthroscopy

Scanning

Received 12 December 2023; Accepted 12 December 2023; Published 13 December 2023

This article has been retracted by Hindawi, as publisher, following an investigation undertaken by the publisher [1]. This investigation has uncovered evidence of systematic manipulation of the publication and peer-review process. We cannot, therefore, vouch for the reliability or integrity of this article.

Please note that this notice is intended solely to alert readers that the peer-review process of this article has been compromised.

Wiley and Hindawi regret that the usual quality checks did not identify these issues before publication and have since put additional measures in place to safeguard research integrity.

We wish to credit our Research Integrity and Research Publishing teams and anonymous and named external researchers and research integrity experts for contributing to this investigation.

The corresponding author, as the representative of all authors, has been given the opportunity to register their agreement or disagreement to this retraction. We have kept a record of any response received.

References

[1] T. Deng, X. Li, Z. Guo et al., "Management Strategies and Imaging Observation of Early and Delayed Intelligent Treatment of Meniscus Sports Injury under Knee Osteoarthroscopy," *Scanning*, vol. 2022, Article ID 8716823, 6 pages, 2022.

Hindawi
Scanning
Volume 2022, Article ID 8716823, 6 pages
https://doi.org/10.1155/2022/8716823

Research Article

Management Strategies and Imaging Observation of Early and Delayed Intelligent Treatment of Meniscus Sports Injury under Knee Osteoarthroscopy

Tong Deng,[1] **Xu Li**,[2] **Zhe Guo**,[2] **Shuang Guo**,[2] **Yan Zhou**,[2] **Wei Zhang**,[2] **and Ying Zhang**[2]

[1]*Department of Radiology, Beijing Jishuitan Hospital, Beijing 100035, China*
[2]*Beijing Jishuitan Hospital, Beijing 100035, China*

Correspondence should be addressed to Xu Li; 201804201@stu.ncwu.edu.cn

Received 6 July 2022; Revised 5 August 2022; Accepted 17 August 2022; Published 30 August 2022

Academic Editor: Danilo Pelusi

Objective. To investigate the meniscus characteristics of knee osteoarthritis and its guiding significance for minimally invasive surgery. *Methods*. A total of 100 patients with knee meniscus sports injuries who were treated in our hospital from January 2019 to January 2022 were selected as the research subjects and were grouped according to the interval between injury and surgery, with an interval of 2 months: the early group (53 cases) within 2 months and the delayed group (47 cases) with an interval of more than 2 months. The distribution of intraoperative complications in the two groups was observed and recorded, and the changes in pain degree, joint range of motion, knee joint function, and quality of life scores before and after operation were compared between the two groups. *Results*. The postoperative VAS score, range of motion, Lysholm score, IKDC knee subjective function score, and quality of life score were significantly improved in both groups ($P < 0.05$). The incidence of intra-articular cartilage injury in the delayed group was significantly higher than that in the early group ($P < 0.05$). The patellofemoral cartilage injury was the main part of intra-articular cartilage injury in the two groups, and the incidence of patellofemoral cartilage injury in the delayed group was significantly higher than that in the early group ($P < 0.05$). The cartilage damage was mainly cartilage damage, and the grades I-II and III-IV cartilage damages were significantly increased in the extension group. *Conclusion*. Meniscal injury in knee osteoarthritis has certain microscopic characteristics. In this paper, the microscopic classification of meniscus injury in knee osteoarthritis is helpful to guide microscopic surgery and improve the minimally invasive knee osteoarthritis effect of surgical treatment.

1. Introduction

With social progress, economic development, the improvement of residents' living standards, and the rise of national sports, people are paying more and more attention to their physical fitness and health, which makes more people join sports. In the process of exercising, due to the lack of understanding of the exercise load, exercise time, and correct exercise posture that oneself can bear, it is bound to cause sports injuries in some parts of the body [1, 2]. The meniscus is the cartilage between the tibia and the femur, one on each side. The iliac crest is C-shaped, with the anterior aspect of the tibial muscle connected to the posterior tibial ligament and the posterior tibial ligament entering the lateral tibial and posterior tibial ligament. Before the river [3], and there are fibers connected to the semimembranosus [4]. Its main functions are (1) bearing gravity, absorbing oscillations, and transmitting loads; (2) cooperating with knee extension, flexion, and rotation to prevent knee hyperextension, hyperflexion, and overrotation; and (3) dispersing stress and regulating synovial fluid [5, 6]. It plays an important role in maintaining the stability and flexibility of the knee joint.

Meniscus injuries are one of the most common sports injuries of the knee, occurring mostly in older age groups and those who actively participate in sports. Abrams et al.

[7, 8] reported that between 2005 and 2011, there were approximately 55,000 half-moon wrench operations in the United States each year, with more men than women. Swenson et al. [9] reported that among middle school athletes in the United States, there were 25,700 knee injuries, of which 9.3% were meniscal injuries, and the ratio of men and women was almost the same. In Poehling et al.'s [10] study, the age of meniscus injury was 31-40 years old in men and 11-20 years old in women. This may be related to the multiple lateral discoid cartilage in our country. After the meniscus injury, the knee joint function of patients will be greatly affected, and the posterior and rotational stability of the knee joint will be destroyed. In the long run, it will lead to complications such as knee cartilage destruction. According to domestic and foreign reports, it can be seen that the knee joint cartilage injury rate of joint patients exceeds 50%, and in most young people, meniscus injury is the most common primary disease in cartilage injury [11–13]. There are about 43 million patients with cartilage injury in the United States every year. Foreign literature studies show that the incidence of articular cartilage injury is 5%, while the incidence of specific groups such as athletes is as high as 22%.

At present, surgery is often used in clinical treatment of knee meniscus injury, but the anatomical position of the meniscus is complex, the operation is difficult, and the technical requirements of the surgeon are high. Minimally invasive surgery has the characteristics of less trauma and is conducive to local functional recovery of patients after surgery. According to research, the degree of articular cartilage damage is positively correlated with the time of meniscus damage [14, 15]. In acute injury, the cartilage is rarely damaged immediately, but the meniscus is generally damaged. If it is not treated in time, it will further lead to cartilage damage. Therefore, in this study, the incidence of intra-articular complications and postoperative efficacy of arthroscopic treatment in the early (acute phase ≤2 months) and delayed (>2 months) arthroscopic treatment were summarized and compared in this study, to provide a reference for the selection of surgical timing for patients with knee meniscus sports injury. The report is as follows [16–18].

2. Materials and Methods

2.1. General Information. From January 2019 to January 2022, 100 patients with meniscus knee injury were included in the study, including time reported by Keene et al. [19]. For cohort, patients with a duration of 2 months or less were included in the first group (53 patients), and patients with a duration of more than 2 months were included in the first group (53 patients) and slow group (47 patients). In the first group, there were 27 males and 26 females aged 29-442, middle age (36.49 ± 2.58). 20 cases of left knee meniscus damage and 33 right knee pad injuries were closed. The next group consisted of 25 men and 22 women, 33-42 years, mean age (36.57 ± 2.01), 18 patients of left knee, and 29 right knee pad fractures. There were no significant differences in the overall data of the two groups ($P > 0.05$) and the comparison. Diagnostic criteria are as follows: (1) unilateral knee meniscus injury was diagnosed by MRI or arthroscopy, with different degrees of meniscus injury and local tenderness on the affected side; clinical and imaging data were complete [20]. Inclusion criteria are as follows: (1) those who complied with rehabilitation training; (2) all who underwent arthroscopic meniscus; (3) all meniscus injuries that were caused by exercise; and (4) all family members and patients who can participate in this study and who sign a consent form, and the study was approved by the Justice Department of our network hospital. Exclusion procedures are as follows: (1) patients who do not comply; (2) mentally ill patients who are unable to communicate; (3) patients with previous surgical treatment; (4) patients with other vital organ dysfunction; and (5) patients with malignant tumors and diseases that cause myotonia.

2.2. Treatment Methods. The two groups were placed in the supine position, epidural anesthesia was performed before operation, and routine operations such as disinfection and draping and tourniquet inflation were perfected. An entrance with a length of about 0.5 cm was made on both sides of the anterior patellar ligament of the knee joint, and then an arthroscope was placed, and 0.9% sodium chloride injection was injected to observe the shape of the meniscus, the specific location, and the extent of the injury. Arthroscopic meniscus plasty pays attention to retain the meniscus tissue (width 6~8 mm) and repair the residual meniscus to make it similar to the normal state and uses the radiofrequency knife to smoothen the edge of the residual meniscus. Group 2 received ice compress on the affected knee and anti-infective treatment after operation and postoperative functional exercise (straight leg raising exercise 1 day after operation, knee flexion exercise 2-3 days after operation, and getting out of bed with crutches 3 days after operation) activity.

2.3. Observation Indicators. (1) In the evaluation of pain degree and knee joint range of motion, visual analogue score (VAS) was used to evaluate the pain degree of the two groups before and after operation. Total VAS scores were 10 points, with 0 indicating no pain, 10 indicating severe pain, and higher scores indicating additional pain [21]. Before and after the evaluation, when the patient's muscles were completely relaxed and when there was no dynamic support of the Lokomat system, L-ROM was used to evaluate the range of motion of the affected knee joint by measuring the arc of motion through which the joint was moved by external force [22]. (2) In the observation of knee function, Lysholm scores and the International Knee Documentation Committee (IKDC) scores of knees were used to measure knee reoperation before and 6 months after labor. (3) To determine quality of life, the World Health Organization Quality of Life Scale-Short Form Questionnaire (WHOQOL-BREF) was used to determine quality of life in two groups before and after surgery: WHOQOL-BREF included social work and life support and included physical and mental activity [23]. The higher the score, the better the quality of life. (4) In the preoperative and postoperative complications, the iliac crest was recorded at the patellofemoral joint surface and the medial and lateral tibial joint at the affected

knee during surgery. Bone marrow damage according to the Outerbridge measurement is as follows [24]: grade 0 indicates normal articular cartilage; grade 1 indicates softened and swollen cartilage; grade 2 indicates early fissure but does not reach subchondral bone, diameter< 0•5 inches (1•27 cm); grade 3 indicates fissure reaching subchondral bone, but not exposed, > 0•5 inches (1•27 cm) in diameter; grade 4 is bare subchondral bone of various diameters. Patients followed up 6 months after surgery, and problems occurred upon return from both groups.

2.4. Statistical Analysis. SPSS 27.0 was used for statistical analysis; measurement and enumeration data were expressed as ($\bar{x} \pm s$), (n, %), and t, and 2 tests were used between groups; $P < 0.05$ indicated a statistically significant difference.

3. Results

3.1. Image Observation under Arthroscopy. According to the intraoperative conditions, meniscus injuries are divided into (1) non-torn (including normal MRI diagnosis, grade I injury signal, part of the meniscus with grade II injury, and degenerative meniscus), (2) ciliated (grade II meniscus diagnosed by MRI injury signal), and (3) tear (MRI diagnosis of grade III meniscus injury signal). After arthroscopic exploration, meniscus tears can be roughly divided into the following types, and the tear methods are different, and the relationship with the articular surface is different: (1) vertical tear: longitudinal tear, barrel tear, radial tear, and oblique tear (parrot beak tear); (2) horizontal tear; and (3) compound tear. It is especially worth noting that for the meniscus with grade II degenerative damage signal on MRI, the probe hook is used to touch and pull the meniscus and feel and observe the quality of the meniscus, and it can be seen that the meniscus activity increases, and the flexibility and elasticity decrease. Do plasty, subtotal resection, or total resection of the injured meniscus, and suture and fix the meniscus tear with blood supply. Degenerative grade I injury and grade II injury were treated with joint cavity debridement. For traumatic grade I injuries, such as meniscus contusion, only external fixation of the knee joint is performed, and no arthroscopic exploration is performed, and regular review is required.

3.2. Comparison of Knee Range of Motion and VAS Score of Patients in Each Group. Prior to treatment in all groups, knee joint mobility and VAS scores in the early group were significantly better than in the slow group ($P < 0.05$). See Table 1.

3.3. Comparison of Knee Joint Function in Each Group. Prior to treatment in all groups, the Lysholm score and IKDC knee function on the control group were significantly better than in the late group ($P < 0.05$). After treatment, the scores of each group were significantly improved compared with those before treatment, and the scores of the early group were better than those of the late group ($P < 0.05$). See Table 2.

Table 1: Comparison of knee range of motion and VAS score of patients in each group ($\bar{x} \pm s$).

Group	VAS score(score)	Range of motion(°)
Early group ($n = 53$)		
Before treatment	$4.81 \pm 1.44^{\#}$	$120.58 \pm 9.29^{\#}$
After treatment	$3.89 \pm 1.00^{*\#}$	$130.57 \pm 9.00^{*\#}$
Delayed group ($n = 47$)		
Before treatment	5.55 ± 1.38	109.51 ± 8.00
After treatment	$4.43 \pm 1.16^{*}$	$119.38 \pm 9.04^{*}$

Note: Compared with before treatment, $^{*}P < 0.05$; compared with advanced group, $^{\#}P < 0.05$.

Table 2: Comparison of knee joint function in each group ($\bar{x} \pm s$, 分).

Group	Lysholm score	IKDC score
Early group ($n = 53$)		
Before treatment	$68.43 \pm 9.51^{\#}$	$63.53 \pm 4.73^{\#}$
After treatment	$90.11 \pm 4.37^{*\#}$	$93.42 \pm 4.35^{*\#}$
Delayed group ($n = 47$)		
Before treatment	62.02 ± 8.94	53.91 ± 4.64
After treatment	$80.49 \pm 9.74^{*}$	$87.40 \pm 4.28^{*}$

Note: Compared with before treatment, $^{*}P < 0.05$; compared with advanced group, $^{\#}P < 0.05$.

3.4. Comparison of Quality of Life in Each Group. Before treatment in each group, the scores of four domains of quality of life in the early group were better than those in the delayed group ($P < 0.05$). After treatment, the quality of life scores in each group were significantly improved, and group B was significantly higher than group A ($P < 0.05$). See Table 3.

3.5. Comparison of the Incidence of Preoperative Complications in Each Group. Before surgery, the incidence of intra-articular cartilage injury in the delayed group was significantly higher than that in the early group ($P < 0.05$). The patellofemoral articular cartilage injury was the main site of intra-articular cartilage injury in both groups, and the incidence of patellofemoral bone marrow damage in the late group was higher than in the early group ($P < 0.05$). Bone loss was significant, and there was an increase in grades I-II and III-IV cartilage in the stretching group. See Table 4.

3.6. Comparison of Postoperative Complications in each Group. The two groups were followed up for 6 months in the form of outpatient reexamination, and the follow-up deadline was January 2022. During the follow-up period, there were no obvious complications in both groups.

4. Discussion

The meniscus is one of the important structures of the knee joint. It is located on the medial and lateral articular surfaces

Table 3: Comparison of quality of life in each group ($\bar{x} \pm s$, score).

Group	Social function	Physical function	Material life	Psychological function
Early group ($n = 53$)				
Before treatment	$41.36 \pm 2.77^{\#}$	$42.34 \pm 3.51^{\#}$	$43.40 \pm 4.00^{\#}$	$46.58 \pm 4.02^{\#}$
After treatment	$58.00 \pm 3.29^{*\#}$	$55.64 \pm 3.66^{*\#}$	$59.94 \pm 3.50^{*\#}$	$64.92 \pm 3.42^{*\#}$
Delayed group ($n = 47$)				
Before treatment	35.96 ± 3.62	37.11 ± 4.11	38.13 ± 3.89	39.47 ± 5.09
After treatment	$49.60 \pm 4.49^{*}$	$50.13 \pm 4.12^{*}$	$49.87 \pm 1.06^{*}$	$56.94 \pm 5.09^{*}$

Note: Compared with before treatment, $^{*}P < 0.05$; compared with advanced group, $^{\#}P < 0.05$.

Table 4: Comparison of preoperative complication rates in each group (n (%)).

Group	Cartilage injury	Patellofemoral joint	Medial tibiofemoral joint	Lateral tibiofemoral joint	Total incidence
Early group ($n = 53$)	I-II	13 (24.53)	3 (5.66)	1 (1.89)	24 (45.28)$^{\#}$
	III-IV	2 (3.77)	4 (7.55)	1 (1.89)	
Delayed group ($n = 47$)	I-II	18 (38.30)	5 (10.64)	3 (6.38)	44 (93.62)
	III-IV	9 (19.15)	5 (10.64)	4 (8.51)	

Note: Compared with advanced group, $^{\#}P < 0.05$.

of the tibial plateau. It restricts excessive flexion of the hip, improves stability of the femoral ankle and tibial relationship, provides some flexibility and flexibility, plays a buffer role, and helps to avoid knee injury. Most of the patients with meniscus injury have a history of knee sprain, and they feel severe pain after the injury and cannot straighten automatically [25]. Conservative treatment will aggravate the degree of meniscus wear, which is not conducive to alleviating clinical symptoms such as knee joint swelling and pain. With the development of arthroscopy technology, its application frequency in patients with meniscus injury has increased year by year. Arthroscopic surgery is minimally invasive and effective, with few postoperative complications and high safety, and can promote postoperative recovery of patients [26]. The results of this study showed that there was a significant improvement in scores after VAS; joint movement, Lysholm scored, IKDC knee function scored, and the scores were good in both groups, and the results were similar to those reported by Rongen et al. [27]. Angioplasty has a good effect on patients with joint injury and can effectively improve the clinical symptoms of patients.

Biomechanical studies have found that the meniscus plays a very important role in maintaining the function of the knee joint, mainly including conducting loads to increase the stability of the knee joint and absorbing and buffering shocks and other functions [28], but the meniscus injury is very common in clinical practice. The broken meniscus causes the movement of the joint out of the groove, which often leads to the disorder of the knee joint function. In addition, because only part of the blood supply to the meniscus has poor self-repair ability, if the treatment is not timely, the damage will be aggravated during repeated exercise, thereby increasing the difficulty of repair. According to studies, it is found that the inflammatory reaction of the joint is caused by the meniscus injury, which secretes enzymes that soften the torn meniscus, degrades its fibers and collagen, and further reduces its healing ability [29]. According to DeHaven et al. [30], the time from injury to meniscal repair has been found to have a positive correlation with the cost of failure. In this study, 100 meniscal sports injury patients treated in our hospital were divided into two groups: time from meniscal injury to recovery, early (pain stage ≤2); months) and extended (>2 months). Knee function, knee range of motion, pain level, and quality of life in the pre- and postsurgery groups were better than those in the slow group, and it was reported that menisci patients can be treated if authorized and treated in the first stage. The function of the knee joint can be restored to the greatest extent, and the results are consistent with previous studies.

The most common cause of meniscal injury is cartilage, and bone marrow damage has been reported to have a positive impact with the duration of meniscal injury. Therefore, compared with the early group, there was a significant difference in the recovery of knee joint function in the delayed group. The results showed that the incidence of bone loss and bone injury in the delayed group was 93.62%, higher than that in the early group (45.28%). Grades I-II and III-IV bone marrow transplants increased in the next group, and previous studies also pointed out that the normal meniscus has the functions of nourishing, lubricating, and protecting cartilage. The average pressure and the uniform distribution of the skin force are affected, and the broken tissue wears down the cartilage and the mutual compression and wear of the cartilage, resulting in the degeneration and death of the chondrocytes; on the other hand, the injury of the meniscus changes the knee joint. Changes in the properties of the synovial fluid and endocrine conditions in the internal environment lead to changes in its microstructure and lead to cartilage lesions. Moreover, due to the lack of blood vessels and other poor self-repairing ability

of cartilage, good recovery cannot be obtained even after intraoperative ablation, and there are still sequelae such as osteoarthritis and pain, which affects the recovery of patients' postoperative function [31]. In addition, no problems occurred after surgery in a group on recovery, which may be due to the inadequacy of the study. Therefore, in the next phase, the study will expand the sample size and further examine the meniscus under arthroscopy. The long-term effect of angioplasty on patients with early and delayed knee meniscus injury provides new ideas and new solutions for clinical treatment of knee meniscus injury.

5. Conclusions

In conclusion, meniscus sports injuries should be treated surgically as soon as possible to reduce the incidence of complications, maximize the recovery of knee joint function, and improve the quality of life of patients.

Data Availability

The data used to support the findings of this study are available from the corresponding author upon request.

Conflicts of Interest

The authors declare that they have no conflicts of interest.

References

[1] A. J. Fox, F. Wanivenhaus, A. J. Burge, R. F. Warren, and S. A. Rodeo, "The human meniscus: a review of anatomy, function, injury, and advances in treatment," *Clinical Anatomy*, vol. 28, no. 2, pp. 269–287, 2015.

[2] W. Wang, "Artificial intelligence in repairing meniscus injury in football sports with perovskite nanobiomaterials," *Journal of Healthcare Engineering*, vol. 2021, Article ID 4324138, 11 pages, 2021.

[3] S. M. Gee and M. Posner, "Meniscus anatomy and basic science," *Sports Medicine and Arthroscopy Review*, vol. 29, no. 3, pp. e18–e23, 2021.

[4] F. Flandry and G. Hommel, "Normal anatomy and biomechanics of the knee," *Sports Medicine and Arthroscopy Review*, vol. 19, no. 2, pp. 82–92, 2011.

[5] A. R. Markes, J. D. Hodax, and C. B. Ma, "Meniscus form and function," *Clinics in Sports Medicine*, vol. 39, no. 1, pp. 1–12, 2020.

[6] E. A. Makris, P. Hadidi, and K. A. Athanasiou, "The knee meniscus: Structure-function, pathophysiology, current repair techniques, and prospects for regeneration," *Biomaterials*, vol. 32, no. 30, pp. 7411–7431, 2011.

[7] P. R. Kurzweil, W. D. Cannon, and K. E. DeHaven, "Meniscus repair and replacement," *Sports Medicine and Arthroscopy Review*, vol. 26, no. 4, pp. 160–164, 2018.

[8] G. D. Abrams, R. M. Frank, A. K. Gupta, J. D. Harris, F. M. Mccormick, and B. J. Cole, "Trends in meniscus repair and meniscectomy in the United States, 2005-2011," *American Journal of Sports Medicine*, vol. 41, no. 10, pp. 2333–2339, 2013.

[9] D. M. Swenson, C. L. Collins, T. M. Best, D. C. Flanigan, S. K. Fields, and R. D. Comstock, "Epidemiology of knee injuries among U.S. high school athletes, 2005/2006-2010/2011," *Medicine & Science in Sports & Exercise*, vol. 45, no. 3, pp. 462–469, 2013.

[10] G. G. Poehling, D. S. Ruch, and S. J. Chabon, "The landscape of meniscal injuries," *Clinics in Sports Medicine*, vol. 9, no. 3, pp. 539–549, 1990.

[11] J. R. Slauterbeck, P. Kousa, B. C. Clifton et al., "Geographic mapping of meniscus and cartilage lesions associated with anterior cruciate ligament injuries," *The Journal of Bone and Joint Surgery. American Volume*, vol. 91, no. 9, pp. 2094–2103, 2009.

[12] C. C. A. Haley, C. M. Posner, and M. M. Donohue, "Meniscus review," *Sports Medicine and Arthroscopy Review*, vol. 29, no. 3, p. 153, 2021.

[13] H. Moksnes, L. Engebretsen, and M. A. Risberg, "Prevalence and incidence of new meniscus and cartilage injuries after a nonoperative treatment algorithm for ACL tears in skeletally immature children: a prospective MRI study," *The American Journal of Sports Medicine*, vol. 41, no. 8, pp. 1771–1779, 2013.

[14] D. P. Piasecki, K. P. Spindler, T. A. Warren, J. T. Andrish, and R. D. Parker, "Intraarticular injuries associated with anterior cruciate ligament tear: findings at ligament reconstruction in high school and recreational athletes. An analysis of sex-based differences," *The American Journal of Sports Medicine*, vol. 31, no. 4, pp. 601–605, 2003.

[15] Y. Shi, Z. Tian, L. Zhu, J. Zeng, R. Liu, and J. Zhou, "Clinical efficacy of meniscus plasty under arthroscopy in middle-aged and elderly patients with meniscus injury," *Experimental and Therapeutic Medicine*, vol. 16, no. 4, pp. 3089–3093, 2018.

[16] W. Wilson, B. van Rietbergen, C. C. van Donkelaar, and R. Huiskes, "Pathways of load-induced cartilage damage causing cartilage degeneration in the knee after meniscectomy," *Journal of Biomechanics*, vol. 36, no. 6, pp. 845–851, 2003.

[17] M. Nishida, H. Higuchi, Y. Kobayashi, and K. Takagishi, "Histological and biochemical changes of experimental meniscus tear in the dog knee," *Journal of Orthopaedic Science*, vol. 10, no. 4, pp. 406–413, 2005.

[18] E. Peña, B. Calvo, M. A. Martínez, D. Palanca, and M. Doblaré, "Finite element analysis of the effect of meniscal tears and meniscectomies on human knee biomechanics," *Clinical Biomechanics*, vol. 20, no. 5, pp. 498–507, 2005.

[19] G. C. Keene, D. Bickerstaff, P. J. Rae, and R. S. Paterson, "The natural history of meniscal tears in anterior cruciate ligament insufficiency," *The American Journal of Sports Medicine*, vol. 21, no. 5, pp. 672–679, 1993.

[20] D. W. Stoller, C. Martin, J. V. Crues, L. Kaplan, and J. H. Mink, "Meniscal tears: pathologic correlation with MR imaging," *Radiology*, vol. 163, no. 3, pp. 731–735, 1987.

[21] S. V. Nemade and K. J. Shinde, "Clinical efficacy of tinnitus retraining therapy based on tinnitus questionnaire score and visual analogue scale score in patients with subjective tinnitus," *Turkish Archives Of Otorhinolaryngology*, vol. 57, no. 1, pp. 34–38, 2019.

[22] R. Stefanescu, A. Moosavi, and A. Sandu, "Parametric domain decomposition for accurate reduced order models: applications of MP-LROM methodology," *Journal of Computational and Applied Mathematics*, vol. 340, pp. 629–644, 2018.

[23] H. H. Wang, M. C. Ho, K. Y. Hung, and H. T. Cheng, "A single question regarding mobility in the World Health Organization quality of life questionnaire predicts 3-year mortality in

Hindawi
Scanning
Volume 2023, Article ID 9894170, 1 page
https://doi.org/10.1155/2023/9894170

Retraction

Retracted: Diagnostic Value of Endoscopic Narrow-Band Imaging Technique in Early Gastric Cancer and Precancerous Lesions

Scanning

Received 17 October 2023; Accepted 17 October 2023; Published 18 October 2023

This article has been retracted by Hindawi following an investigation undertaken by the publisher [1]. This investigation has uncovered evidence of one or more of the following indicators of systematic manipulation of the publication process:

(1) Discrepancies in scope

(2) Discrepancies in the description of the research reported

(3) Discrepancies between the availability of data and the research described

(4) Inappropriate citations

(5) Incoherent, meaningless and/or irrelevant content included in the article

(6) Peer-review manipulation

The presence of these indicators undermines our confidence in the integrity of the article's content and we cannot, therefore, vouch for its reliability. Please note that this notice is intended solely to alert readers that the content of this article is unreliable. We have not investigated whether authors were aware of or involved in the systematic manipulation of the publication process.

In addition, our investigation has also shown that one or more of the following human-subject reporting requirements has not been met in this article: ethical approval by an Institutional Review Board (IRB) committee or equivalent, patient/participant consent to participate, and/or agreement to publish patient/participant details (where relevant).

Wiley and Hindawi regrets that the usual quality checks did not identify these issues before publication and have since put additional measures in place to safeguard research integrity.

We wish to credit our own Research Integrity and Research Publishing teams and anonymous and named external researchers and research integrity experts for contributing to this investigation.

The corresponding author, as the representative of all authors, has been given the opportunity to register their agreement or disagreement to this retraction. We have kept a record of any response received.

References

[1] X. Huang, R. Chen, and L. Zhao, "Diagnostic Value of Endoscopic Narrow-Band Imaging Technique in Early Gastric Cancer and Precancerous Lesions," *Scanning*, vol. 2022, Article ID 9205150, 6 pages, 2022.

Hindawi
Scanning
Volume 2022, Article ID 9205150, 6 pages
https://doi.org/10.1155/2022/9205150

Research Article

Diagnostic Value of Endoscopic Narrow-Band Imaging Technique in Early Gastric Cancer and Precancerous Lesions

Xianxin Huang, Rong Chen, and Liang Zhao

Dongdong Medical Group Downtown Hospital, Huangshi, Hubei 435000, China

Correspondence should be addressed to Liang Zhao; 202005000136@hceb.edu.cn

Received 6 July 2022; Revised 5 August 2022; Accepted 17 August 2022; Published 30 August 2022

Academic Editor: Danilo Pelusi

Objective. To investigate the diagnostic value of endoscopic narrow-band imaging technique in early gastric cancer and precancerous lesions. *Methods*. A total of 100 patients with recurrent upper gastrointestinal symptoms in our hospital from January 2017 to January 2022 were selected and divided into group A and group B according to the random number table method, with 50 cases in each group. Group A received white light endoscopy, and group B received narrow-band imaging technology combined with endoscopy. Narrow-band imaging combined with magnifying endoscopy was used to stain the area with suspicious mucosal lesions with indigo carmine and magnified observation. *Results*. The endoscopic image clarity of group B was significantly better than that of group A in terms of lesion outline, gastric pit, and microvascular morphology ($P < 0.05$). There were 10 cases of early gastric cancer, 18 cases of benign lesions, and 9 cases of gastric cancer (nonearly stage); 17 cases of precancerous lesions, 12 cases of early gastric cancer, 13 cases of benign lesions, and 6 cases of gastric cancer (nonearly stage) were diagnosed by ordinary white light endoscopy. Pathological results confirmed that among the 50 patients in group B, there were 15 cases of precancerous lesions, 11 cases of early gastric cancer, 17 cases of benign lesions, and 7 cases of gastric cancer (nonearly stage). Among the 50 patients in group A, 16 were precancerous lesions, 11 were early gastric cancer, 15 were benign lesions, and 8 were gastric cancer (non early stage). In the diagnosis of precancerous lesions and early gastric cancer, the diagnostic consistency, sensitivity, and specificity of group B were better than those of group A ($P < 0.05$); NBI combined with endoscopy in the diagnosis of precancerous lesions and early gastric cancer (kappa = 0.860, kappa = 0.883) was more consistent with pathological diagnosis than common white light endoscopy (kappa = 0.433, kappa = 0.535). *Conclusion*. The value of narrow-band imaging technology combined with endoscopy in the diagnosis of precancerous lesions and early gastric cancer is better than that of ordinary white light endoscopy, and it can be widely used in clinical practice.

1. Introduction

Due to the influence of changes in modern lifestyles, dietary habits, and other factors, gastric cancer has become a very common malignant tumor in the case of a high infection rate of Helicobacter pylori. According to incomplete data from the National Cancer Registry, in 2015, there were 679,000 gastric cancer cases and 498,000 deaths in my country. Gastric cancer has become a serious threat to national health. At present, due to Helicobacter pylori, the cure rate, environmental improvement, and quality of life have improved, leading to a reduction in the risk factors of gastric cancer. The current morbidity and mortality in my country are decreasing year by year [1–3], but the prevention and treatment of gastric cancer should not be overlooked.

Early endocrine dissection (EGC) presents with multiple endoscopic features, and its clinical manifestations are not significantly different from other gastric diseases, and it is not specific and difficult to detect. It is generally believed that the canceration of the gastric mucosa develops from chronic superficial gastritis to atrophic gastritis. Under the influence of adverse factors, it will develop into intestinal metaplasia, then form atypical hyperplasia, and finally lead to canceration, for a long time [4, 5]. Therefore, it is especially important to monitor changes in the microstructure of the gastric mucosa. At this stage in our country, the

diagnosis of gastric cancer and precancerous disease is low. Multiple metastases to peripheral lymph nodes and in severe cases to distant organs bring great difficulties to the treatment, and the prognosis of gastric cancer is closely related to the stage. Relevant studies have shown that most gastric malignancies can be resectioned and radically assisted by endoscopy in the early stage, and more than 90% of the patients who have undergone this partial resection and radical resection have a survival period of more than 5 years [6]. At present, the diagnosis and treatment strategy of gastric malignant tumor in my country has shifted from the treatment of advanced gastric malignant tumor to the level of early prevention, early detection, and early intervention.

In recent years, leukemia treatment, especially early leukemia, has been followed by minimal endoscopic treatment. Early diagnosis and early treatment of intestinal obstruction are essential to improve patient well-being [7]. Currently, endoscopy technology is recognized as an important method for the diagnosis of lymphoma and precancerous disease, but with the development of endoscopy technology at home and abroad, narrow-band imaging (NBI) has been widely used for diagnosis of gastrointestinal diseases; it not only improves the contrast of endoscopic imaging but also can clearly display the superficial microvascular morphology and surface microstructure of the mucosa [8, 9]. Combined with magnification technology, the observation effect can be further improved. In this study, 100 patients with symptoms of organ dysfunction in our hospital from January 2017 to January 2022 were examined for NBI treatment costs combined with endoscopy in early leukemia and precancerous lesions were involved in this study. The recipe is as follows.

2. Materials and Methods

2.1. General Data. From January 2017 to January 2022, 100 patients with recurrent symptoms of indigestion (acid insufficiency, belching, bloating, and abdominal pain) for 3 years or more were selected from the random number table and divided into groups A and B, with 50 patients in each group. In group A, there were 27 males and 23 females aged 40-66, middle age (54.66 ± 6.36); in group B, there were 28 males and 22 females aged 41-771, middle age (54.86 ± 7.09). There were no significant differences in the overall data of the two groups ($P > 0.05$) and the comparison. Diagnostic procedures were as follows: (1) biopsies and NBI endoscopic examination of the gastrointestinal tract were performed in accordance with the "WHO Classification of Tumors of Digestive System 2019." Inclusion criteria were as follows: (1) under the microscope, the gastric cells were enlarged in strips, arranged in fish scales, and distributed diffusely or in strips; (2) the gastric mucosa was found to be granular, dark in color, exposed blood vessels, and small in folds; (3) single or multiple pale yellow nodules appeared during the examination; the surface of the nodules was fine granular or villiform, flat, and prominent, with a diameter of about 2 to 3 mm; (4) the gastric mucosa was found to be granular and dark in color, blood vessels are revealed, there were small folds or local mucosal depression, microprotrusion or congestion and erosion, and abnormal color during examination; and (5) family members and patients can participate in the study and sign an informed consent form. This study was approved by our hospital practice team. Exclusion criteria were as follows: (1) patients with contraindications to gastroscopy; (2) patients with mental disorders who cannot communicate; (3) patients with advanced gastric cancer, gastric submucosal lesions, and a history of gastric surgery; (4) combined with other patients with vital organ dysfunction; and (5) people who have been taking nonsteroidal anti-inflammatory medications in the last 2 weeks.

2.2. Methods. All patients in group A underwent common white light endoscopy (Olympus GIF-H260Z electronic gastroscope). Fifteen minutes before the examination, 6 mL of dimethicone defoaming agent, 20,000 U of pronase, and 1 g of sodium bicarbonate were dissolved in 50 mL of warm water, and the subjects were instructed to take it. In order to enable the operating physician to make careful and in-place observations calmly, necessary sedatives and narcotic analgesics can be given reasonably as appropriate, which will help reduce the patient's uncomfortable symptoms and create good examination conditions. During the examination, it is necessary to carefully observe the changes in the local color of the gastric mucosa (such as redness, fading pale, and mixed red and white) and slight changes in the morphology of the gastric mucosa (such as bulge, depression, or unevenness) and observe whether there are lesions, clear lesion outline, mucosal surface structure, microvascular conditions, etc. In group B, on the basis of ordinary white light endoscopy, narrow-band imaging technology combined with magnification function was used to further observe the lesion site in detail, marginal epithelium, crypt opening, white opaque material, intercrypt, etc. and also need to observe the characteristics of local microvessels, whether there are irregular arrangement, uneven shape, asymmetric distribution, and other phenomena. Next, the diagnosis was made according to the VS classification method proposed by the Japanese Yao Jianshi expert: lesions with a clear demarcation line combined with irregular surface microstructure (IMSP) or combined with irregular microvessels (IMVP) were judged as early cancer. A precise biopsy is performed on the site of the most visible lesion. The "gold standard" for diagnosis in this study was histopathological results, which were used to analyze and evaluate the diagnostic accuracy of ordinary white light endoscopy and narrow-band imaging technology combined with endoscopy.

2.3. Observation Indicators. (1) Referring to the relevant endoscopic image scoring standards, assess the image clarity of the patient's gastric mucosal lesion contour and gastric mucosal microstructure, with a score of 1 to 4. The endoscopic image is blurred, and the gastric mucosal lesion contour and microstructure can be distinguished. Difficulty is scored as 1 point, the endoscopic image is blurred, but the outline and microstructure of gastric mucosal lesions can be basically distinguished, and the endoscopic image is clearly displayed. Clearly, the outline and microstructure of

gastric mucosal lesions can be accurately identified and scored 4 points. For patients included in the group A study, the endoscopic classification of suspicious lesions was recorded [10]. For type I (raised type), the lesion protrudes into the gastric cavity; type II (flat type): the bulge and depression of the lesion are not conspicuous, including type IIA (superficial raised type, the lesions are slightly raised), type IIB (superficial flat type, the depression and elevation of the lesions are not significant), and type IIC (superficial depression type, the lesions are slightly depressed, equivalent to erosion); type III (deep depression) type): the concave lesions are more prominent. The endoscopic light sources in group B were all CLV-290SL, and the endoscopic diagnosis of suspicious lesions (cancer and noncancer) and the diagnosis time (the time from the entrance of the gastroscope to the end of the observation) were recorded. The diagnostic criteria are based on the VS classification system [11]: irregular MV structure and demarcation line and irregular MS structure and demarcation line; the presence of any one or both of the above can be diagnosed as cancer. (2) Based on the "gold standard" for histopathological diagnosis, the coincidence, sensitivity, and specificity of narrow-band imaging technology combined with endoscopic diagnosis and common white light endoscopic diagnosis were calculated. Histological typing is based on the Vienna classification of gastrointestinal epithelial tumors [12]: type I: no tumor cells and dysplasia, including inflammatory response, regeneration, hypertrophy, atrophy, and atypia of normal epithelium; type II: suspicious dysplasia; type III: low-grade dysplasia without invasion; type IV: severe dysplasia without invasion, further divided into severe dysplasia, carcinoma in situ, intramucosal carcinoma, and suspected invasive carcinoma; types IV to V are cancerous; and types I to III are noncancerous

2.4. Statistical Analysis. SPSS27.0 was used for statistical analysis. To measure and count data ($x \pm s$), (n, %), t, 2 tests of groups, Mann–Whitney test to compare test data of groups, expressed as $P < 0.05$, have identified the values.

3. Results

3.1. Comparison of Endoscopic Image Clarity of Patients in Each Group. The endoscopic image clarity of group B was significantly better than that of group A in terms of lesion outline, gastric pit, and microvascular morphology ($P < 0.05$) (see Table 1).

3.2. Comparison of Results of Group A with Pathological Results. Pathological results confirmed that among the 50 patients in group A, there were 13 patients with precancerous lesions, 10 patients with early gastric cancer, 18 patients with benign lesions, and 9 patients with gastric cancer (nonearly stage); 17 patients with precancerous lesions were diagnosed by ordinary white light endoscopy, 12 patients with early gastric cancer, 13 patients with benign lesions, and 8 patients with gastric cancer (nonearly stage). The detection results are shown in Tables 2 and 3.

3.3. Comparison of Group B Results with Pathological Results. According to the pathological outcomes, out of 50 patients in group B, there were 15 patients with precancerous disease, 11 patients with early leukemia, 17 patients with benign disease, and 7 patients with leukemia (not early). Among the 50 patients in group A, 16 were precancerous lesions, 11 were early gastric cancer, 15 were benign lesions, and 8 were gastric cancer (non early stage). Findings are shown in Table 4 and Table 5.

3.4. Comparison of the Diagnostic Efficacy of the Two Groups of Inspection Methods. In the diagnosis of precancerous lesions and early gastric cancer, the diagnostic consistency, sensitivity, and specificity of group B were better than those of group A ($P < 0.05$); and combined NBI endoscopy in early detection of premalignant and malignant tumors (kappa = 0.860, kappa = 0.883) was better than free light endoscopy (kappa = 0.433, kappa = 0.535) in diagnosis of pathology. The comparison is shown in Table 6.

4. Discussion

Gastric cancer (GC) is a fairly common malignant tumor worldwide, and the prognosis of gastric cancer is poor compared with other malignant tumors. According to the relevant tumor data officially released by the World Cancer Research Agency, it can be found that in 2012, 951,000 people worldwide suffered from gastric cancer, and 723,000 people died from gastric cancer (5th and 3rd in mortality rate) [13]. Precancerous lesions of the stomach refer to a type of histopathological changes in the gastric mucosa that are prone to cancer, namely, intraepithelial neoplasia of the gastric mucosa. Early gastric cancer refers to cancerous growths that live in the mucosa, even if they have metastasized to the lymph nodes. When 5-year survival after treatment for early leukemia is more than 90% [14], 5-year survival on leukemia is around 30%, but now, the early gastric cancer detected by gastroscopy in my country only accounts for about 10% of all gastric cancers [15], and most gastric cancers have reached the advanced stage at the time of diagnosis. Therefore, accurate identification of gastric precancerous lesions and early gastric cancer is of great significance for early intervention and improvement of prognosis.

Yoshida et al. [16] first proposed that the development of intestinal-type gastric cancer (accounting for more than 80% of all gastric cancers) went through superficial gastritis and then developed into atrophic gastritis. Under the continuous action of harmful factors, it developed into intestinal metaplasia. Then, there is atypical hyperplasia, which eventually develops into gastric cancer, known as the Correa pattern. When normal gastric mucosal epithelium becomes cancerous, the microsurface gland openings and microvascular morphology of gastric mucosal epithelium will also change accordingly. Therefore, observing the subtle changes in gastric mucosal epithelium can help us identify malignant lesions. Traditionally, ordinary white light endoscopy (WLE) is commonly used to observe the lesions. WLE can observe the color tone and morphological changes of the lesions, such as redness, whiteness, and

Table 1: Comparison of endoscopic image clarity in each group of patients.

	Group	1 score	2 score	3 score	4 score
Gastric pit shape	B group ($n = 50$)	1	6	18	25*
	A group ($n = 50$)	2	24	20	4
Microvascular morphology	B group ($n = 50$)	0	9	19	21*
	A group ($n = 50$)	1	17	21	11
Lesion outline	B group ($n = 50$)	0	6	17	27*
	A group ($n = 50$)	1	18	21	10

Note: compared with group A, $^*P < 0.05$.

Table 2: Comparison of precancerous lesion detection results and pathological results in group A.

Diagnostic method	Type	Precancerous lesions	Non-precancerous lesions	Total
Ordinary white light endoscopy	Precancerous lesions	9	8	17
	Non-precancerous lesions	4	29	33

Table 3: Comparison of early gastric cancer detection results and pathological results in group A.

Diagnostic method	Type	Precancerous lesions	Non-precancerous lesions	Total
Ordinary white light endoscopy	Precancerous lesions	7	5	12
	Non-precancerous lesions	3	35	38

Table 4: Comparison of the detection results of precancerous lesions and the pathological results in group B.

Diagnostic method	Type	Precancerous lesions	Non-precancerous lesions	Total
NBI combined with endoscopy	Precancerous lesions	14	2	16
	Non-precancerous lesions	1	33	34

Table 5: Comparison of early gastric cancer detection results and pathological results in group B.

Diagnostic method	Type	Precancerous lesions	Non-precancerous lesions	Total
NBI combined with endoscopy	Precancerous lesions	10	1	11
	Non-precancerous lesions	1	38	39

Table 6: Comparison of the diagnostic efficacy of the two groups of inspection methods.

	Precancerous lesions				Early gastric cancer			
Measurement site	Accuracy (%)	Sensitivity (%)	Specificity (%)	Kappa value	Accuracy (%)	Sensitivity (%)	Specificity (%)	Kappa value
B group ($n = 50$)	94.00*	93.33*	94.29*	0.860	96.00*	90.90*	97.43*	0.883
A group ($n = 50$)	76.00	69.23	78.38	0.433	84.00	70.00	87.50	0.535

Note: compared with group A, $^*P < 0.05$.

uneven lesions, but the observation of the microscopic morphology of the mucosa is not effective, so it is not suitable for early detection. The diagnostic accuracy of cancer is low, and it is prone to misdiagnosis and misdiagnosis [17, 18]. A cross-sectional study [19] found that the high-resolution white light has an accuracy of 88%, a sensitivity of 75%, and a specificity of 94% for diagnosis of intestinal metaplasia. In a multicenter prospective study [20], high-resolution free light endoscopy had an accuracy of 83% and a specificity of 98%, but a sensitivity of 53% for diagnosis of intestinal metaplasia. In recent years, many advances have been made in endoscopic procedures. NBI is a new optical technique that allows the determination of mucosal changes [21]. In the NBI mode, the illumination can be changed from wide-

band blue, green, and red to narrow-band blue (415 nm) and green (540 nm) [22]. As a result, the blood vessels of the superficial mucosa are brown. Since 540 nm images are transmitted to the red channel, deep veins can be seen with green-blue light. The narrow capillary network at the base of the mucosa is brown, and the thick veins are blue. Blood vessels are clearly shown because hemoglobin is the chromophore that determines the color of the mucosa. The two narrow-band illuminations (415 nm and 540 nm) used in the NBI system are consistent with the two absorption peaks of hemoglobin. Therefore, blue narrow-band illumination has strong scattering and absorption properties, which can enhance the visualization of blood vessels [23, 24]. The results of this study showed that the endoscopic image clarity of group B was significantly better than that of group A in terms of lesion contour, microvascular morphology, and gastric pit morphology ($P < 0.05$), indicating that NBI combined with endoscopy can clearly display the lesion contour, gastric. The fovea morphology and microvascular morphological structure can improve the definition of endoscopic images to avoid affecting the diagnostic accuracy due to individual differences. The results are similar to those of Kanesaka et al. [25]. In addition, the results of this study suggest that the observation of the three indicators of lesion outline, gastric pit shape, and microvascular structure is helpful to distinguish benign lesions from precancerous lesions and early gastric cancer.

The VS classification system proposed by Chen et al. [26] has been accepted by digestive endoscopists in many countries. Using VS classification to diagnose early gastric cancer has high sensitivity and specificity [27]. Judging the nature of the lesions according to the VS diagnostic criteria also helps the endoscopist to carry out precise biopsy in a targeted manner, which greatly improves the diagnostic efficiency. Previous literature pointed out that NBI is helpful for the judgment of benign and malignant lesions under endoscopy [28] and can be further classified according to NBI images to predict the different degrees of differentiation of early tumors [29, 30]. This study shows that NBI combined with endoscopy is the best light white endoscopy based on the true, sensitive, unique, and consistent pathologic results ($P < 0.05$) in the diagnosis of premalignant and early leukemia. The method can significantly improve the coincidence rate of lesion examination and the diagnosis rate of gastric mucosal neoplastic lesions.

5. Conclusions

In conclusion, narrow-band imaging technology has good diagnostic value in gastric precancerous lesions and early gastric cancer and can provide a reliable treatment base for future health plans, which are necessary for supporting the treatment. In conclusion, NBI has higher resolution than ordinary endoscopy and chromoendoscopy in the diagnosis of early gastric cancer and precancerous lesions and has higher sensitivity, specificity, and accuracy, which is of great significance for the detection and diagnosis of early gastric cancer and precancerous lesions.

Data Availability

The data used to support the findings of this study are available from the corresponding author upon request.

Conflicts of Interest

The authors declare that they have no conflicts of interest.

References

[1] W. Q. Chen, R. S. Zheng, P. D. Baade et al., "Cancer statistics in China, 2015," *CA: a Cancer Journal for Clinicians*, vol. 66, no. 2, pp. 115–132, 2016.

[2] C. Fitzmaurice, D. Dicker, A. Pain et al., "The global burden of cancer 2013," *JAMA Oncology*, vol. 1, no. 4, pp. 505–527, 2015.

[3] P. Pimentel-Nunes, D. Libânio, R. Marcos-Pinto et al., "Management of epithelial precancerousconditions and lesions in the stomach (MAPS II):European Society of Gastrointestinal Endoscopy (ESGE), European Helicobacter and Microbiota Study Group(EHMSG), European Society of Pathology (ESP), and Sociedade Portuguesa de Endoscopia Digestiva (SPED) guideline update 2019," *Endoscopy*, vol. 51, no. 4, pp. 365–388, 2019.

[4] WHO Classification of Tumours Editorial Board, *WHO Classification of Tumours of Digestive System [M]*, IARC Press, Lyon, 2019.

[5] S. R. Hamilton and L. A. Aaltonen, *World Health Organization classification of tumours. Pathology and Genetics of Tumours of Digestive System*, IARC Press, Lyon, 2000.

[6] H. Osawa, H. Yamamoto, Y. Miura et al., "Blue laser imaging provides excellent endoscopic images of upper gastrointestinal lesions," *Video Journal and Encyclopedia of GI Endoscopy*, vol. 1, no. 3-4, pp. 607–610, 2014.

[7] X. Liu, C. T. Guan, L. Y. Xue et al., "Effect of premedication on lesion detection rate and visualization of the mucosa during upper gastrointestinal endoscopy: a multicenter large sample randomized controlled double-blind study," *Surgical Endoscopy*, vol. 32, no. 8, pp. 3548–3556, 2018.

[8] J.-H. Cho, S. R. Jeon, and S.-Y. Jin, "Clinical applicability of gastroscopy with narrow-band imaging for the diagnosis ofHelicobacter pylorigastritis, precancerous gastric lesion, and neoplasia," *World Journal of Clinical Cases*, vol. 8, no. 14, pp. 2902–2916, 2020.

[9] Y. Zhang, H. Y. Chen, X. L. Zhou, W. S. Pan, X. X. Zhou, and H. H. Pan, "Diagnostic efficacy of the Japan Narrow-band-imaging Expert Team and Pit pattern classifications for colorectal lesions: a meta-analysis," *World Journal of Gastroenterology*, vol. 26, no. 40, pp. 6279–6294, 2020.

[10] N. Li, Y. Wang, W. Deng, and S. H. Lin, "Poly (ADP-ribose) polymerases (PARPs) and PARP inhibitor-targeted therapeutics," *Anti-Cancer Agents in Medicinal Chemistry*, vol. 19, no. 2, pp. 206–212, 2019.

[11] M. Robson, S. A. Im, E. Senkus et al., "Olaparib for metastatic breast cancer in patients with a germlineBRCAmutation," *The New England Journal of Medicine*, vol. 377, no. 6, pp. 523–533, 2017.

[12] N. M. Tung, S. A. Im, E. Senkus-Konefka et al., "Olaparib versus chemotherapy treatment of physician's choice in patients with a germline *BRCA* mutation and HER2-negative metastatic breast cancer (OlympiAD): efficacy in patients with visceral

Hindawi
Scanning
Volume 2023, Article ID 9897839, 1 page
https://doi.org/10.1155/2023/9897839

Retraction

Retracted: Clinical Analysis of Echocardiography and Serum IL-6 and TNF-α Changes in Pregnant Women with Hypertension

Scanning

Received 10 October 2023; Accepted 10 October 2023; Published 11 October 2023

This article has been retracted by Hindawi following an investigation undertaken by the publisher [1]. This investigation has uncovered evidence of one or more of the following indicators of systematic manipulation of the publication process:

(1) Discrepancies in scope

(2) Discrepancies in the description of the research reported

(3) Discrepancies between the availability of data and the research described

(4) Inappropriate citations

(5) Incoherent, meaningless and/or irrelevant content included in the article

(6) Peer-review manipulation

The presence of these indicators undermines our confidence in the integrity of the article's content and we cannot, therefore, vouch for its reliability. Please note that this notice is intended solely to alert readers that the content of this article is unreliable. We have not investigated whether authors were aware of or involved in the systematic manipulation of the publication process.

In addition, our investigation has also shown that one or more of the following human-subject reporting requirements has not been met in this article: ethical approval by an Institutional Review Board (IRB) committee or equivalent, patient/participant consent to participate, and/or agreement to publish patient/participant details (where relevant).

Wiley and Hindawi regrets that the usual quality checks did not identify these issues before publication and have since put additional measures in place to safeguard research integrity.

We wish to credit our own Research Integrity and Research Publishing teams and anonymous and named external researchers and research integrity experts for contributing to this investigation.

The corresponding author, as the representative of all authors, has been given the opportunity to register their agreement or disagreement to this retraction. We have kept a record of any response received.

References

[1] Y. Liu, X. Hou, M. Yu, and J. Zhou, "Clinical Analysis of Echocardiography and Serum IL-6 and TNF-α Changes in Pregnant Women with Hypertension," *Scanning*, vol. 2022, Article ID 9299746, 7 pages, 2022.

Hindawi
Scanning
Volume 2022, Article ID 9299746, 7 pages
https://doi.org/10.1155/2022/9299746

Research Article

Clinical Analysis of Echocardiography and Serum IL-6 and TNF-α Changes in Pregnant Women with Hypertension

Ying Liu,[1] **Xiaolin Hou**,[2] **Mei Yu**,[2] **and Jin Zhou**[3]

[1]*Obstetrical Department VIII, The Fourth Hospital of Shijiazhuang (The Obstetrics and Gynecology Hospital of Hebei Medical University), Shijiazhuang, Hebei 050000, China*
[2]*Prenatal Diagnosis Center, The Fourth Hospital of Shijiazhuang (The Obstetrics and Gynecology Hospital of Hebei Medical University), Shijiazhuang, Hebei 050000, China*
[3]*Health Care Center, The First Hospital of Hebei Medical University, Shijiazhuang, Hebei 050000, China*

Correspondence should be addressed to Mei Yu; 11231508@stu.wxic.edu.cn

Received 9 July 2022; Revised 9 August 2022; Accepted 17 August 2022; Published 30 August 2022

Academic Editor: Danilo Pelusi

In order to explore the changes and clinical significance of serum TNF-α and IL-6 and ET levels in the pathogenesis of hypertensive disorders of pregnancy (HDIP), echocardiography, and serum IL-6 and TNF-α changes in pregnant women with a hypertensive disorder, a clinical analysis method was proposed. A retrospective analysis of 59 pregnant women who visited the obstetrics department of a provincial hospital was divided into 2 groups. The normal control group consisted of 32 normal, uncomplicated pregnant women; the preeclampsia group included 27 patients with systolic blood pressure > 140 mmHg and/or diastolic blood pressure > 90 mmHg who developed proteinuria after 20 weeks of gestation. The levels of TNF-α and IL-6 in serum of normal pregnant women and pregnant women with preeclampsia were detected by enzyme-linked immunosorbent assay (ELISA). The results showed that compared with normal pregnant women, the serum levels of TNF-α and IL-6 in the early pregnant women of Zizhi were significantly increased, and the trend of increased TNF-α and IL-6 levels was related to the severity of complications. With the mean pulmonary arterypressure > 50 mmHg, the serum TNF-α level of pregnant women was significantly higher than that of pregnant women with mean pulmonary arterypressure < 50 mmHg. The analysis found that the serum levels of TNF-α and IL-6 in patients with hypoxic gestational hypertension were significantly increased, and the results of lung tissue immunohistochemistry also showed that serum TNF-α and IL-6 levels in patients with hypoxic gestational hypertension were significantly increased. And serum TNF-α and IL-6 levels were positively correlated with right ventricular systolic blood pressure (RVSP). *Conclusion*. This study revealed that the elevated levels of serum TNF-α and IL-6 are closely related to the pathophysiological process of gestational hypertension. Serum levels of TNF-α and IL-6 and ET were significantly increased, and the changes of serum TNF-α and IL-6 and ET levels had important clinical value for closely monitoring the severity of the disease and the development of the disease.

1. Introduction

Pregnancy is a special physiological period for women, and various physiological indicators of the body will change, in order to facilitate the growth of the fetus in the mother and the later delivery. During pregnancy, the levels of progesterone and estrogen in pregnant women change significantly, and their serum levels reach their peaks in the third trimester; these hormones affect the synthesis, metabolism, and secretion functions of the liver and kidney. Pregnancy hypertension is a group of diseases associated with gestational hypertension, preeclampsia, and eclampsia; chronic hypertension is associated with complications of preeclampsia; pregnancy with complications of hypertension will increase with gestational age. Damage to pregnant women is shown in Figure 1; the effect can be reversible [1]. Hypertensive disease during pregnancy has always been a disease of great concern to obstetric workers, and it is a major risk factor for maternal and perinatal life and death. The incidence rate in China is 9.4%, and the reported incidence rate

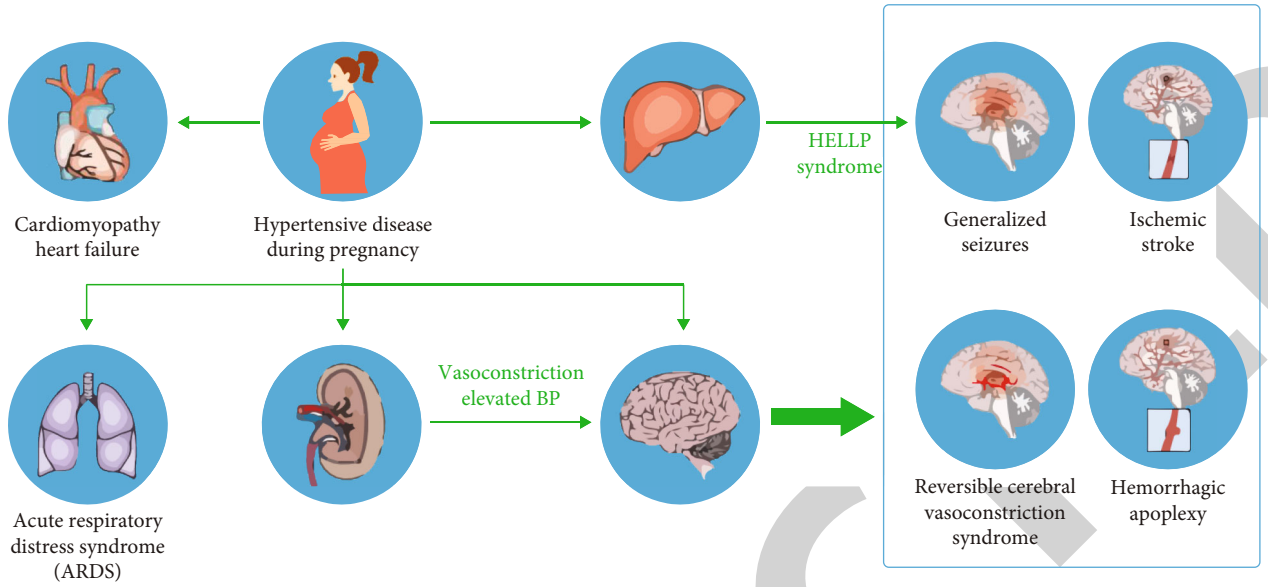

Figure 1: Effects of gestational hypertension.

in foreign countries is 7%-12%, and the death caused by it accounts for 12% of maternal deaths; it is one of the main reasons that threatens the safety of mothers and babies and causes maternal death. In recent years, although researches on hypertensive disorders of pregnancy have emerged in an endless stream, so far, the pathogenesis of the disease has not been elucidated [2]. The main clinical manifestations of gestational hypertension are high blood pressure, heart and kidney failure, edema, proteinuria, convulsions, etc.; with the gradual development of the disease, some patients may have serious complications such as renal failure, premature birth, coma, and even death; among these complications, acute kidney injury (AKI) is the main complication and the leading cause of maternal miscarriage, preterm birth, fetal growth retardation, and maternal death [3]. Because the damage of renal function can be reversed in time through treatment in the early stage, and the renal function can be restored to normal, so early diagnosis and early treatment are recommended in clinical treatment.

2. Literature Review

Gabbay-Benziv et al. cultured trophoblast cells in vitro and detected inhibin A, indicating that there is mRNA encoding inhibin A in trophoblast cells [4]. Contro et al. showed that the expression of inhibin A was different in the trophoblast cells of normal pregnant women and women with preeclampsia, and the latter was higher than the former [5]. The results of a case-control study by Wang et al. showed that inhibin A was 295pg/L, with a sensitivity of 85.7%, a specificity of 98.5%, and an accuracy of 0.954, suggesting that inhibin A can be used as an indicator factor for early prediction of preeclampsia [6]. Fisher found that in women who developed hypertensive disorders of pregnancy in the second trimester, serum inhibin A levels were not different from those of normal pregnant women [7]. Yi et al. suggested that the serum inhibin A concentration of pregnant women in the second trimester was not associated with the occurrence of preeclampsia [8]. Kumar et al. showed that activin A can be used as an independent risk factor for predicting early-onset preeclampsia, and it is associated with cell-free fetal DNA, both of which are higher in the serum of pregnant women with preeclampsia [9]. Roukoz compared 50 cases of preeclampsia and 250 normal cases at 11-13 weeks of gestation and 30-33 weeks of gestation. It was found that there was no significant difference in serum activin A levels between the two groups at 11-13 weeks of gestation, but it was significant at 30-33 weeks of gestation, and combined with serum activin A levels at 30-33 weeks of gestation and the general clinical data of pregnant women, it was possible to detect 50% of patients with preeclampsia [10]. Combined with PP13, PAPP-A, ADAM12, activin A, inhibin A, and uterine artery Doppler hemodynamics in the second trimester, the sensitivity for predicting preeclampsia can reach 60%-80%, and the specificity can reach 60%-80%; when the specificity of activin A combined with PI value in predicting preeclampsia was 90%, the sensitivity was only 57%. Iwahasi et al. took the serum of pregnant women with early-onset preeclampsia and normal pregnant women and detected PAPP-A in serum; using median comparison, they found that pregnant women with early-onset preeclampsia were lower than normal pregnant women (0.80 MoMs vs. 1.05 MoMs, $P = 0.005$), combined with RBP4, predicting a 34% increase in DR in early-onset preeclampsia, and PAPP-A can be used as a useful indicator for predicting early-onset and severe preeclampsia [11].

3. Research Methods

3.1. Echocardiographic Assessment of Pain in Gestational Hypertension. Echocardiography was performed by an echocardiographer with more than 10 years of clinical experience. The following points should be noted during the examination: the echocardiographic image grade should

not be lower than grade C. The calculated value of pulmonary artery pressure is uniformly plus 5 mmHg (mild) on the basis of the tricuspid transvalvular pressure difference. The report should include tricuspid regurgitation velocity, transvalvular pressure gradient, and estimated pulmonary systolic pressure. If the pulmonary artery pressure is above 50 mmHg, it should be regarded as pathological and should not be treated as a normal pregnant woman.

The main evaluation indicators included the following echocardiographic indicators:

(1) Longitudinal axis of left ventricle: aortic main diameter, left atrium diameter, interventricular septum thickness, left ventricular end diastolic diameter, left ventricular systolic end diameter, and left ventricular posterior wall thickness

(2) Long-axis view of the pulmonary trunk: pulmonary trunk

(3) Right heart measurements (apical four-chamber view): right ventricular base diameter, right atrium diameter, left ventricular mass index (LVMI), and tricuspid annular presystolic amplitude (TAPSE)

(4) Measurement of left ventricular systolic function: left ventricular ejection fraction (EF), left ventricular short-term shortening (FS), stroke rate (SV), and minute output (cardiac output, CO)

(5) Measurement of left ventricular diastolic function: spectral diagram of mitral valve blood flow: E peak, A peak, E/A, and E peak time delay (EDT); Doppler imaging TDI: early systolic peak velocity (S), early diastolic peak velocity (e'), and late diastolic peak velocity (a')

(6) Pulmonary arterial pressure measurement: tricuspid regurgitation velocity, tricuspid transvalvular pressure gradient, and estimated pulmonary artery systolic pressure

At the same time, this study also recorded the subjects' age, heart rate, height, and weight and asked the patients their prepregnancy weight as their standard weight [12].

The inside diameter of the left ventricle and its walls are measured against the longitudinal axis of the left ventricle. When measuring, select an area perpendicular to the longitudinal axis and measure at or near the apex of the mitral valve. An electrical cursor is placed at the junction of the myocardial wall and the heart chamber, between the ventricular wall and the pericardium. The inner diameter of the chamber can be obtained with 2D ultrasound guided M-mode, but a better method is to obtain it directly with 2D ultrasound images, which avoids the bevel of the ventricle and makes it more accurate.

Fractional shortening can be obtained from a 2D guided M-mode image, but it is best to measure radial lines directly on the 2D image. In the case of segmental wall motion abnormalities caused by coronary heart disease or conduction abnormalities, the overall function of the left ventricle based on diameter measurements is very problematic. In patients with uncomplicated hypertension, obesity, or valvular disease, such as without clinically confirmed myocardial infarction, such segmental differences are rare, so fractional shortening can provide clinically useful information. In patients with basal LV but increased medial and left venous volume, the LV value was higher than that of the basal LV.

Calculate the fraction (EF) that differs from the mean values of the left ventricular systolic volume (EDV) and the left ventricular diastolic volume (ESV), and its formula is as follows:

$$EF = \frac{(EDV - ESV)}{EDV}. \quad (1)$$

Left heart measurement should be done in 2D or 3D. The interface between the thick myocardium and the left ventricular cavity is closed, and the entire contour is closed with a straight line to the mitral annulus. Longer lines were selected in apical two-chamber view and four-chamber view. Left ventricular volume should be measured at apical four-chamber and two-chamber views. Select the largest left ventricular area of the left ventricle, and try not to shorten the left ventricle and underestimation of the left ventricular volume [13]. When examining, reduce the depth of the image to focus on the left ventricular cavity, which reduces the chance of left ventricular shortening; it also minimizes errors in tracing the endocardium.

In the left heart, M type, 2D, and 3D are valid methods for counting left heart. All measurements should be made at the end of the diastole (the frame before the mitral valve closes, or the frame with the largest central chamber diameter or volume during the cardiac cycle). Left ventricular diastolic diameter and wall thickness measured with M type or 2D both rely on geometric models to calculate the left ventricular diameter, while 3D ultrasound can measure LV volume directly, all the way to change the volume to size by taking the volume of myocardial by myocardial density. At the same time, the study also recorded age, heart rate, height, and weight and asked patients their weight before pregnancy based on their weight.

3.2. Correlation between Serum Markers TNF-a and IL-6 Levels and Gestational Hypertension

3.2.1. Study Population. The subjects of the analysis were the records of pregnant women who delivered inpatients in the obstetrics department of a provincial hospital between May 2021 and May 2022. The study included 59 participants who were divided into two groups. One of the groups was 27 pregnant women who suffered from prepain and gave birth in our hospital and was designated as the prepain group. Significant symptoms are two or more wet measurements of pregnant woman blood pressure after 20 weeks of gestation, systolic blood pressure > 140 mmHg, and/or diastolic pressure > 90 mmHg, and the measurement time was at least 4 hours, proteinuria. In another group, 32 pregnant women who gave birth without problems during pregnancy were identified as the normal control group. The gestational

age and maternal age of pregnant women in pre-Ziton and control groups were always similar. All pregnant women had one pregnancy, and this study did not include women with high blood pressure, heart disease, kidney disease, or type 1 or type 2 diabetes.

3.2.2. Methods. The analysis groups were set up as follows: (1) normoxia control pregnancy group, (2) pregnancy-induced hypertension group, and (3) treprostinil treatment group [14]. Blood samples for TNF-α and IL-6 were collected from the heart and stored at -80°C.

(1) Right Ventricular Systolic Blood Pressure Detection. Pentohexidine was administered intravenously (30 mg/kg) was injected intravenously, and the trachea was intubated and placed in a well-ventilated environment. The thoracic cavity was opened, a PE-50 polyethylene tube was inserted into the right ventricle, and the right ventricular systolic pressure was collected by energy-Lab data collection.

(2) Extraction of Total RNA. Use TRIzol to extract total RNA from lung tissue, and the specific operation steps are as follows:

(a) 50 mg of lung tissue was added to 1 ml of TRIzol, placed in liquid nitrogen, and homogenized by a homogenizer

(b) The homogenized samples were placed at room temperature for 5 min to completely separate nucleic acid and protein

(c) Add 200 μl chloroform, shake for 15 s, and allow to stand at room temperature for 1 min

(d) Centrifuge at 10,000 × g for 15 min at 4° C. After centrifugation, the sample was divided into three layers: the lower layer (red organic phenol-chloroform phase), the middle layer, and the upper colorless aqueous phase. RNA in the upper colorless aqueous phase

(e) Transfer the colorless water-free phase to a new EP tube, add 500 isopropanol, and allow to stand at room temperature for 10 minutes

(f) Centrifuge at 10,000 × g for 15 min at 4° C to remove the top layer

(g) To wash the RNA pellets, add 1 ml of precooled 75% ethyl alcohol, centrifuge at 7500 × g at 40° C for 5 min, and remove the top layer

(h) Dry the RNA pellets at room temperature, adding about 50 (depending on the size of the pellets) RNase-free water, and store at 80° C to dissolve the RNA pellets

(3) Reverse Transcription of RNA. cDNA was synthesized in vitro by Moloney's leukemia virus reverse transcriptase (M-MLV RT), and the operation steps were as follows:

Table 1: Nuclease-free microcentrifuge tube components.

Reagent	Volume
Random primer	150 ng
Total RNA	500 ng
Nuclease-free water replenishes the total volume	14 μl

Table 2: Components added after brief centrifugation.

Reagent	Volume
M-MLV RT 5 × reaction buffer	5 μl
dATP, 10 mM	1.25 μl
dCTP, 10 mM	1.25 μl
dGTT, 10 mM	1.25 μl
dTTP, 10 mM	1.25 μl
M-MLV RT (H-) point mutant	1 μl (50–100 units)
Nuclease-free water replenishes the total volume	25 μl

(a) Add the following components in Table 1 to a nuclease-free microcentrifuge tube

(b) After the mixture was heated at 70°C for 5 minutes, it was quickly cooled on ice for 5 minutes

(c) After a brief centrifugation, the following components were added as shown in Table 2

(d) The components were mixed gently and reacted at room temperature for 10 minutes and then heated at 45°C for 50 minutes

(e) Heat at 70°C for 15 minutes to stop the reaction

(4) Real-Time Quantitative PCR (Real-Time Quantitative PCR). The SYBR∗ Pemix Ex Tag™ kit was used for the real-time fluorescent quantitative PCR reaction. The specific steps are as follows:

(a) Prepare the reaction system according to the components in Table 3 (the preparation should be carried out on ice)

(b) Run the RT-PCR reaction. The reaction process is shown in Table 4

(5) Immunohistochemistry.

(i) Dewaxing

Table 3: Components of the distribution reaction system.

Reagent	Volume
SYBR∗ Premix Ex Tag™ (2×)	12.5 μl
PCR forward primer (10 μM)	1 μl
PCR reverse primer (10 μM)	1 μl
DNA template	2 μl
ddH_2O	8.5 μl
Total	25 μl

Table 4: RT-PCR reaction process.

Cycle	Temperature	Duration
Loop 1 (2×)	95°C	10s
Loop 2 (40×)	95°C	10s
	60°C	30s
	90 °C	10s
Cycle 3 (dissolution curve)	60°C	1 min
	95°C	10s

(a) Paraffin sections of 4 thickness were sequentially placed in 100% xylene (a) and 100% xylene (b) at 37°C for 15 min each

(b) The slices were sequentially placed in 100% ethanol-100% ethanol-95% ethanol-80% ethanol-70% ethanol-plus % ethanol for 2 minutes each

(c) The slices were soaked in double-distilled water for 2 minutes and repeated 3 times [15]

(ii) Antigen Retrieval

(a) After dewaxing, the samples were placed in 3% H_2O, treated at room temperature for 15 minutes, and then soaked in double-distilled water for 2 minutes, repeating 3 times

(b) Preheat the 0.1 m citric acid solution in the microwave for 3 minutes, quickly put the slices into the sodium citrate solution, and continue to boil for 15 to 20 minutes

(iii) Serum Blocking

(a) The samples were cooled for 30 minutes and then soaked in double-distilled water for 2 minutes, repeating 3 times

(b) After the double-distilled water on the tissue evaporated, immediately add serum-containing peroxidase blocking agent to block, and incubate at 37°C for 30 minutes

(iv) Antibody Incubation

(a) Incubate with primary antibody, incubate at 37°C for 30 minutes, discard the blocking solution, add TNF-α or IL-6 antibody, and incubate at 4°C overnight

(b) After incubation with the secondary antibody, after recovering the primary antibody, the samples were washed three times with PBS for 5 minutes each time. After washing, biotinylated rabbit anti-goat secondary antibody was added and incubated at room temperature for 15 minutes

(v) Color Rendering

After adding the chromogenic substrate 3,3-diaminobenzidine (3,3-diaminobenzidine DAB), the sample reacts with horseradish peroxidase-labeled streptavidin, and the color is observed under a microscope. Rinse with clean water after sufficient color development.

(vi) Counterstaining

The slides were washed in double-distilled water for 3 minutes and then counterstained with hematoxylin for 30 seconds after repeated 3 times. Rinse twice with tap water for 6 minutes each time.

(vii) Dehydration

The slides were washed in double-distilled water for 3 minutes, repeated 3 times and then placed in 70% ethanol-80% ethanol-90% ethanol-95% ethanol-100% ethanol-100% ethanol-xylene-xylene for 2 minutes, and finally soaked in xylene [16].

(viii) Cover Sheet

Drop the neutral gum next to the tissue, cover with a coverslip, and lay down one side first and then the other to avoid air bubbles. Dry the sealed slides in a 65°C oven overnight.

3.2.3. Data Analysis. Unless otherwise specified, all data are indicated as average ± SD. Tukey's post hoc tests were performed using Prism version 5 software to determine whether there was a discrepancy between the control panel and the test group using *t*-test or unilateral ANOVA. The correlation of the differences was evaluated by Pearson's

Table 5: Summary of clinical information of 59 pregnant women.

Basic features	Gestational hypertension group ($n = 27$)	Control group ($n = 32$)
Mean age of mother (years)	27.3	28.2
Prepregnancy body mass index BMI (kg/m^2)	25.2	17.8
Anemia	9/27 (33.3%)	1/32 (3.1%)
Asian ethnic group	27/27 (100.0%)	32/32 (100.0%)
Reproductive history		
History of spontaneous abortion (>3)	3/27 (11.1%)	4/32 (12.5%)
Number of pregnancies (>3)	7/27 (25.9%)	9/32 (28.1%)

correlation coefficient [17]. $P < 0.5$ was considered statistically significant.

4. Analysis of Results

4.1. Clinical Characteristics of Participants. The clinical characteristics of all participants in the concept of pregnancy are shown in Table 5. There were no significant differences in marital, birth history, ethnicity, or education level of control group and antenatal hypertension group [18]. However, in pregnant women in the gestational hypertension group with the same gestational and maternal age, compared with the control group, their prepregnancy body mass index was higher, and they had a higher incidence of anemia.

4.2. The Serum Levels of TNF-α and IL-6 Increased in the Serum of Pregnant Women in the Early Stage of Zitong. Blood levels of TNF-α and IL-6 were detected by ELISA assay, and blood levels of TNF-α in pregnant women were detected at an earlier stage than in the control group. The Ziji group has grown. In addition, we found plasma levels of TNF-α and IL-6 in the blood, due to which pregnancy causes patients with pulmonary arterial hypertension, and pathophysiological changes in pulmonary arterial hypertension increase morbidity and mortality for pregnant women. Hypertension during pregnancy is determined by the average value of pulmonary arterial pressure [19]. We retrospectively analyzed the hemodynamic data of 27 pregnant women with preeclampsia and serum TNF-α levels of pregnant women with mean pulmonary arterypressure ≥ 50 mmHg, significantly higher than the average pulmonary arterypressure < 50 mmHgin pregnant women (Figure 2).

Plasma TNF-α levels in pregnant women mean pulmonary arterial pressure ≥ 50 mmHg is higher than in pregnant women who mean pulmonary arterial pressure less than 50 mmHg. In the meandata + standarddeviation,$P < 0.01$ means the significant difference compared to the control group. Levels of IL-6 in pregnant women, which means pulmonary arterial pressure ≥ 50 mmHg and pulmonary arterial pressure less than 50 mmHg, meet TNF-α levels. Based on the above results, serum levels of TNF-α and IL-6 were significantly elevated in pregnant women with gestational hypertension and were associated with the severity of complications.

4.3. Drug Therapy Can Reduce Serum TNF-α and IL-6 Levels in Hypoxia-Induced Gestational Hypertension. To determine which plasma TNF-α and IL-6 levels can be used as biomarkers in prenatal hypertension, we examined blood TNF-α and IL-6 levels in pregnancy samples treated with treprostinil [20]. Treprostinil is a group of vasodilators used to treat pulmonary arterial hypertension. Three recent studies have shown that treprostinil is effective in treating pulmonary hypertension in pregnant women with hypoxia-induced hypertension. Compared with normoxic administration, the right ventricular systolic blood pressure was increased during hypoxia, and treprostinil treatment reduced the right ventricular systolic blood pressure during hypoxia-induced gestational hypertension. Treprostinil treatment has been shown to significantly reduce the incidence of gestational hypertension due to hypoxia.

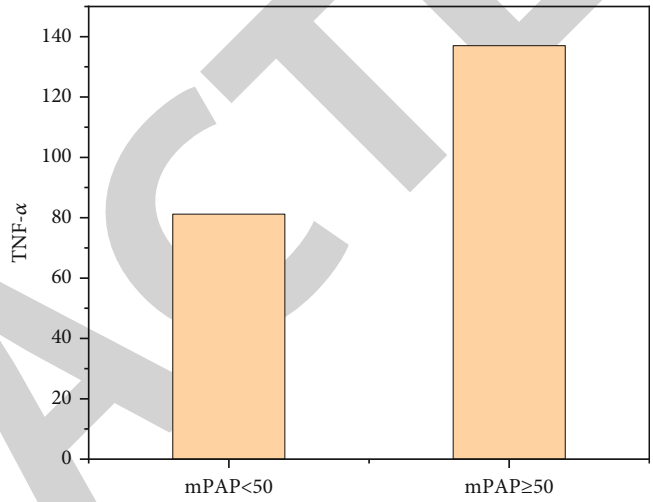

Figure 2: Relationship between mean pulmonary arterial pressure and serum TNF-α level in pregnant women with gestational hypertension.

5. Conclusion

Studies have shown that blood TNF-α and IL-6 levels are higher in pregnant women with higher blood pressure than in pregnant women, indicating that TNF-α and IL-6 levels are higher, associated with high blood pressure. Right ventricular systolic blood pressure was significantly higher in patients exposed to hypoxia than in normoxic controls. When treated with treprostinil, right ventricular systolic blood pressure in hypoxic-induced hypertensive depression of pregnancy was decreased. Plasma levels of TNF-α and

Hindawi
Scanning
Volume 2023, Article ID 9869713, 1 page
https://doi.org/10.1155/2023/9869713

Retraction

Retracted: Image Effect Observation of Acanthopanax senticosus on Antifatigue Activity after Exercise

Scanning

Received 20 June 2023; Accepted 20 June 2023; Published 21 June 2023

This article has been retracted by Hindawi following an investigation undertaken by the publisher [1]. This investigation has uncovered evidence of one or more of the following indicators of systematic manipulation of the publication process:

(1) Discrepancies in scope

(2) Discrepancies in the description of the research reported

(3) Discrepancies between the availability of data and the research described

(4) Inappropriate citations

(5) Incoherent, meaningless and/or irrelevant content included in the article

(6) Peer-review manipulation

The presence of these indicators undermines our confidence in the integrity of the article's content and we cannot, therefore, vouch for its reliability. Please note that this notice is intended solely to alert readers that the content of this article is unreliable. We have not investigated whether authors were aware of or involved in the systematic manipulation of the publication process.

Wiley and Hindawi regrets that the usual quality checks did not identify these issues before publication and have since put additional measures in place to safeguard research integrity.

We wish to credit our own Research Integrity and Research Publishing teams and anonymous and named external researchers and research integrity experts for contributing to this investigation.

The corresponding author, as the representative of all authors, has been given the opportunity to register their agreement or disagreement to this retraction. We have kept a record of any response received.

References

[1] X. Zhang and W. Zhu, "Image Effect Observation of Acanthopanax senticosus on Antifatigue Activity after Exercise," *Scanning*, vol. 2022, Article ID 7588680, 7 pages, 2022.

Hindawi
Scanning
Volume 2022, Article ID 7588680, 7 pages
https://doi.org/10.1155/2022/7588680

Research Article

Image Effect Observation of Acanthopanax senticosus on Antifatigue Activity after Exercise

Xiangdong Zhang[1] **and Wanning Zhu**[2]

[1]*Beijing Normal University at Zhuhai, Zhuhai, Guangdong 519087, China*
[2]*Sports Institute of Chengdu University of Technology, Chengdu, Sichuan 610059, China*

Correspondence should be addressed to Wanning Zhu; 202007000161@hceb.edu.cn

Received 10 July 2022; Revised 7 August 2022; Accepted 17 August 2022; Published 27 August 2022

Academic Editor: Danilo Pelusi

In order to explore the effect of Acanthopanax senticosus on antifatigue activity after exercise, this paper proposes an image effect observation based on the effect of Acanthopanax senticosus on antifatigue activity after exercise. This method recommends key technical problems and solutions based on the information represented by image effect observation and explores the influence of Acanthopanax senticosus on antifatigue after exercise. Through the retrospective analysis of certain personnel, it is shown that the image effect observation based on the influence of Acanthopanax senticosus on the antifatigue activity after exercise is about 25% more accurate than the traditional method. Most of the active ingredients of Acanthopanax senticosus have phenolic hydroxyl groups, which can resist oxidation, fatigue, focus attention, and reduce work mistakes. This experiment shows that after sleep deprivation, the antioxidant capacity of the body decreases with time. Acanthopanax senticosus extract can significantly improve the above symptoms and fight fatigue.

1. Introduction

Fatigue is a comprehensive response to many physiological and biochemical changes in the body caused by multiple factors [1]. In 1982, the Fifth International Conference on exercise biochemistry defined it as follows: the physiological process of the body cannot maintain its function at a specific level or each organ cannot maintain its predetermined exercise intensity [2]. Fatigue is divided into physical fatigue and psychological fatigue. Physical fatigue is mainly manifested in the decline of sports ability, and psychological fatigue is mainly manifested in the negative changes of behavior and will. The process and mechanism of fatigue are very complex, and there are many theories to explain the mechanism of fatigue, such as the theory of energy exhaustion, the theory of metabolite accumulation, the theory of free radical increase, the theory of internal environment disorder, the theory of nerve fatigue, and the theory of body mutation [3]. These theories provide a theoretical basis for the prevention and treatment of fatigue and the study of its mechanism. However, due to the complexity of the fatigue process, various theories cannot fully explain the exact mechanism of fatigue, and different drugs have different mechanisms of alleviating fatigue, so in-depth research is needed.

With the increasing pressure of life, it has become a common phenomenon in contemporary society. Long-term sleep deprivation will have a significant impact on the central nervous system, accelerate the oxidative aging of the body, and aggravate fatigue. Sleep deprivation (SD) refers to a series of clinical symptoms caused by sleep loss in various pathological or physiological states [4]. With the gradual deepening of the global research on sleep deprivation, the phenomenon of sleep deprivation has gradually attracted attention, but at present, there are few reports on the effect of Acanthopanax senticosus on sleep-deprived human body.

Fatigue is a normal physiological phenomenon in a certain range [5]. With the development of society, the use of high technology has greatly improved the efficiency of work and life, and then, the pace of life has become faster and faster. The pressure from work, family, housing, medical treatment, interpersonal relations, and so on makes people in a

state of tension for a long time, which is easy to cause physical fatigue and psychological fatigue. If it cannot be alleviated for a long time, it will turn into pathological fatigue, which will endanger people's physical and mental health and seriously degrade the quality of life. Therefore, looking for effective and safe antifatigue drugs has become a research focus of modern medicine. At the same time, the research on the mechanism of fatigue and the search for effective antifatigue drugs have also attracted extensive attention in sports medicine and military medicine. In the field of sports, athletes need to carry out long-term high-intensity training of physical strength, endurance, and strength in order to improve their performance in competitive sports. During the training process, a large amount of energy and materials are consumed, muscles continue to contract, and metabolites are accumulated, making the body in a state of fatigue, so it is difficult to achieve ideal sports performance. In the military field, military operations often need to be carried out in special environments, such as natural environments such as plateau hypoxic areas, cold areas, and hot areas, and special environments such as closed cabins and underground shelter projects. Most of the environment is bad, and affected by many composite factors such as high temperature, high humidity, noise, vibration, ionizing radiation, and harmful gases, the physical consumption and mental burden of officers and soldiers are increased. Long-term exposure to this environment will do harm to the physical and mental health of operators and may show fatigue symptoms such as inattention, anxiety, fatigue, endocrine disorders, and decreased immunity. This state will seriously affects the operational efficiency and combat effectiveness of military personnel. Therefore, the research of antifatigue drugs is also of great significance to military medicine [6].

At present, most of the antifatigue drugs on the market are chemical drugs, which not only play a good therapeutic effect but also bring great side effects. Traditional Chinese medicine has the characteristics of many active ingredients, mild effects, and small side effects. As an antifatigue drug, the research and development of traditional Chinese medicine has broad prospects [7]. Acanthopanax senticosus is the dry root and rhizome or stem of Acanthopanax senticosus, a plant belonging to Acanthopanax senticosus family. Its main pharmacodynamic components are saponins, lignans, and Echinacea polyphenols (eugenin and Acanthopanax senticosus glycoside E). Pharmacological experiments have verified that Acanthopanax senticosus has the effects of compression resistance, antiulcer, antitumor, anti-inflammatory, antiradiation, and liver protection.

Human internal psychological processes cannot be directly observed, and researchers can only infer the process in the brain based on the observed stimulus response. The research on the process of memory in the brain can only measure the coding form, storage capacity, retention time, and the conditions they depend on by measuring their performance or reaction time at a certain interval after human learning or performing a task. The foundation of learning and memory experimental methodology is conditioned reflex, from which various methods are derived, as shown in Figure 1.

2. Literature Review

Kkj et al. said that somatic fatigue can be divided into two types: peripheral fatigue and central fatigue [8]. Peripheral fatigue mainly refers to the fatigue of sports organ muscles, which is reflected in the decline of energy and material output power and muscle strength, that is, the decline of sports endurance. Bokp et al. said that exercise endurance is the most direct, objective, and powerful index to evaluate body fatigue [9]. Human models used to measure exercise endurance include treadmill model, swimming model, and pole climbing model. The running platform model equipment is expensive, which has great mechanical damage to human feet, and few people can measure it at the same time, which is not convenient for popularization. The climbing pole model device is simple, but some often jump down because they are unwilling to climb the pole, and uncontrollable factors such as the smoothness and scratch degree of the climbing pole will also affect the experimental results. Therefore, at present, swimming experiment with simple experimental device, no mechanical injury, mandatory, and good reliability of experimental results is the most extensive choice for sports endurance experiment.

Boehncke et al. showed through the experimental results that people have poor memory in the spatial resolution learning task of the rotating platform and found that their LTP effect is poor [10]. At the same time, they found that even among the same group, there was a significant correlation between people's memory ability and their LTP response intensity. Phillips et al. reported that the training process of conditioned reflex was accompanied by the change of LTP. They carried out ¥ maze learning training on people and found that the amplitude of group spike evoked by perforin fibers 4 hours and 24 hours after training was significantly higher than that before training. Among them, the LTP effect of people with good memory increased significantly, while the LTP effect of people with poor memory did not increase significantly [11]. Conversely, studies have shown that factors or drugs that affect LTP can also affect learning and memory processes. In conclusion, these data suggest that LTP may be the neural basis of learning and memory.

O'Neill et al. found that NE concentration increased and metabolism accelerated during REM sleep deprivation, and its transporter NE transporter located on the postsynaptic membrane also appeared in large numbers. It has the function of reingesting NE to maintain the relative reserves of NE in synapses and improve the efficiency of synaptic transmission [12]. The results showed that the concentration of NE in human hippocampus increased significantly after 48 hours of sleep deprivation and decreased significantly when sleep deprivation reached more than 96 hours, accompanied by a significant reduction in human learning ability.

There is excessive production of oxygen free radicals in brain tissue. Free radicals can cause degenerative changes in tissues and cells of the body and can cause abnormal lipid metabolism and produce excessive lipofuscin and MDA, thereby damaging the functions of cell membranes, organelles, and enzymes. SOD is a specific enzyme for the body

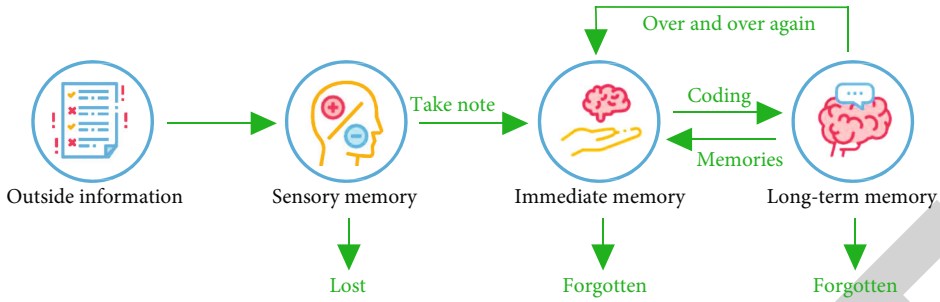

Figure 1: Basic principle of research method for memory process in brain.

to eliminate oxygen free radicals. The level of SOD can reflect the level of oxygen free radicals. The increase of SOD activity in brain tissue after sleep deprivation suggests that the content of oxygen free radicals in brain increases. Therefore, it is speculated that the increase of oxygen free radicals and the decrease of their scavenging ability may be one of the important reasons for the impairment of brain function and the decline of learning and memory ability after sleep deprivation.

Lee et al. believe that dopamine in the brain is related to maintaining muscle movement balance, affecting the secretion of some hormones in the pituitary gland and participating in mental activities. Brain dopamine plays an important role in controlling the process of exercise. With the emergence of exercise-induced fatigue, the content of pivot tends to decrease [13]. The concentration and activity of dopamine in the brain decrease, which reduces the coordination ability of muscle activities, leading to fatigue. Zhao et al. found in the experiment that the increase of brain 5-htida ratio can lead to exercise-induced fatigue by weakening the level of promotion and the loss of motor nerve coordination [14].

3. Method

3.1. Evaluation Index. In order to fairly compare different algorithms in the field of image segmentation, there must be standard and widely recognized indicators for evaluation. The commonly used evaluation criteria for medical image segmentation algorithms are accuracy, recall, specificity, Dice coefficient, and Jaccard index. A is the true annotation of a medical image, and B is the prediction result of the segmentation model. Then, the accuracy AC, recall SE, specificity SP, Dice coefficient DSC, and Jaccard index JAC are expressed, respectively, as shown in the following formulas:

$$\mathrm{AC} = \frac{\mathrm{TP} + \mathrm{TN}}{\mathrm{TP} + \mathrm{TN} + \mathrm{FP} + \mathrm{FN}}, \tag{1}$$

$$\mathrm{SE} = \frac{\mathrm{TP}}{\mathrm{TP} + \mathrm{FN}}, \tag{2}$$

$$\mathrm{SP} = \frac{\mathrm{TN}}{\mathrm{TN} + \mathrm{FP}}, \tag{3}$$

$$\mathrm{DSC} = \frac{2(A \cap B)}{A + B}, \tag{4}$$

$$\mathrm{JAC} = \frac{A \cap B}{A \cup B}, \tag{5}$$

Accuracy refers to the percentage of correctly predicted pixels in the total pixels. In the case of unbalanced categories, it cannot be used as a good indicator to measure the segmentation results [15, 16]. Recall rate, also known as sensitivity, only focuses on the proportion of true labels correctly predicted, while the focus on specificity is just the opposite. These two indicators are relatively sensitive to the size of segmentation targets [17]. Dice coefficient is the most commonly used evaluation index in the task of medical image segmentation, which can better avoid the problem of category imbalance in the field of medical image. Jaccard index is also called intersection union ratio (IoU), and its relationship with Dice coefficient is shown in the following formula:

$$\mathrm{DSC} = \frac{2\mathrm{JAC}}{1 + \mathrm{JAC}}. \tag{6}$$

In practical applications, we often choose the above evaluation indicators according to the needs and prove the accuracy and stability of the segmentation algorithm from multiple dimensions.

3.2. Uniform Design. The commonly used uniform design table is that n is an odd number table. According to the literature, when n is an even number, the uniform design table is an odd number uniform design table with $n + 1$ removed from the last row [18]. Therefore, the experimental design table of 3 factors and 8 levels is obtained by crossing out the last row on the basis of the uniform design table and selecting columns 1, 3, and 5 at the same time, as shown in Tables 1 and 2.

According to the experimental arrangement in Tables 1 and 2, weigh different amounts of Acanthopanax senticosus, Astragalus membranaceus, and Codonopsis pilosula, and get 8 compounds with different proportions. Eight different compounds were soaked in 8 times the amount of water for 0.5 h and extracted three times with a condensing reflux device for 2 h each time. The extracts were combined, reduced with pressure, and concentrated with a rotary evaporator, and the concentrated solution was dried to obtain the extract [13, 19].

Table 1: Level of uniform design factors.

Level/factor	1	2	3	4	5	6	7	8
(A) Acanthopanax senticosus (g)	9	12	15	18	21	24	27	30
(B) Astragalus (g)	9	12	15	18	21	24	27	30
(C) Dangshen (g)	6	7	8	9	10	11	12	13

Table 2: Three-factor eight-level uniform design.

Experiment No.	Acanthopanax senticosus	Astragalus membranaceus	Dangshen of Ming Dynasty
1	1 (9)	4 (18)	7 (12)
2	2 (12)	8 (30)	5 (10)
3	3 (15)	3 (15)	3 (8)
4	4 (18)	7 (27)	1 (6)
5	5 (21)	2 (12)	8 (13)
6	6 (24)	6 (24)	6 (11)
7	7 (27)	1 (9)	4 (9)
8	8 (30)	5 (21)	2 (7)

The results of uniform design experiment were statistically processed by uniform design u 3.00 software, and regression analysis was carried out by full regression method. The significance level was $\alpha = 0.05$. The results of human weight-bearing swimming experiment were statistically processed by the SPSS 18.0 software. All data were expressed in XTS. The time of exhausted swimming was analyzed by one-way ANOVA. The differences between groups were compared by LSD-t method, and the significance level was $\alpha = 0.05$.

In the retrospective analysis, the personnel in each group were in good condition without any adverse reactions. There was no significant difference between the body weight at the beginning of the analysis and the body weight at the end of the experiment, as well as the weight increased during the experiment, indicating that the compound with different proportions had no significant effect on the growth of body weight.

The compatibility of Acanthopanax senticosus, Astragalus membranaceus, and Codonopsis pilosula has a good antifatigue effect by harmonizing the five internal organs and warming and cooling. In this section of the experiment, the uniform design method was used to arrange the experiment, and the best dose ratio relationship of the compound was investigated with the exhaustion swimming time in the endurance experiment as the evaluation index. Through visual analysis of the experimental results, it was found that the exhaustion swimming time of the two groups with the ratio of 30 : 21 : 7 and 3 : 1 : 1 was the longest [20, 21]. From the regression equation $Y = 8.46 + 0.184X\,; +0.739Xz - 0.194X$, it can be seen that the coefficients of X and X are positive, indicating that the exhausted swimming time increases with the increase of the dosage ratio of Acanthopanax senticosus and astragalus, while the coefficient of $X3$ is negative, indicating that the exhausted swimming time decreases with the increase of the dosage ratio of Radix Codonopsis. The absolute value of partial regression coefficient $x2 > x3 > x1$ shows that the primary and secondary order of the influence of the three drugs on swimming time is Astragalus membranaceus>Acanthopanax senticosus>Codonopsis pilosula. Therefore, when determining the optimal experimental scheme, within the specified dose range, the dosage ratio of Acanthopanax senticosus and Astragalus should be higher than the upper limit, and the dosage ratio of Codonopsis pilosula should be lower than the lower limit, that is, Acanthopanax senticosus 30 g, Astragalus 30 g, and Codonopsis pilosula 6 g, which is basically consistent with the trend of intuitive analysis. At the same time, the optimization results of uniform design also showed that when Acanthopanax senticosus 30 g, Astragalus 30 g, and mingdangshen 6G, that is, when the ratio is 5 : 5 : 1, the effect of delaying fatigue is the best. The original formula of the compound 3 : 2 : 1 also has a better effect of alleviating fatigue. Whether the optimized formula has a better effect of alleviating fatigue than the original formula needs to be verified in the next step.

At present, Morris water maze has been widely used in the study of neurobiological mechanism of learning and memory and neuropharmacology because of its reasonable design. It is mainly used to study the measurement of spatial learning and memory ability and working memory of experimental human body. The classic water maze experiment includes location navigation experiment and spatial search experiment. The former measures adult learning ability, and the latter measures adult memory ability. Compared with platform jumping, avoiding darkness, and other detection tools, its main advantages include the following: it can provide more experimental parameters, systematically and comprehensively investigate the process of spatial cognitive processing of experimental human body, and objectively reflect its cognitive level. The learning and memory disorders of the experimental human body are separated from sensory and motor defects, so as to reduce their interference to the detection of learning and memory process; the operation is simple, and the data error is small. It has reliable sensitivity to age-related spatial memory impairment and is a particularly useful tool for judging people's spatial learning ability. The disadvantage is that there are many factors to be considered in the design of the experimental procedure, which requires the experimenter to have a certain knowledge of neurobiology, cognitive psychology, and mathematical statistics. Its statistical analysis is more complex: it is insensitive to the slight decline of learning and memory ability; immersing the human body in water may cause endocrine or other stress reactions. Due to too much physical exertion, it is difficult for people who lose too much body temperature to complete the task; there are high requirements for

experimental conditions, so it is necessary to keep the spatial clues provided by the objects around the maze fixed, the water temperature should be kept constant, and it is also important to keep quiet and consistent light during the experiment [22, 23].

The hexagonal maze box experimental device has been proved to be an effective learning and memory test tool through a large number of experiments. The maze combines the advantages of the above experimental methods: for example, it can quantify human behavior, provide more experimental parameters, and systematically and comprehensively investigate human cognitive process. Objectively reflect the cognitive level of the human body. Active avoidance and passive avoidance can be observed at the same time. It can detect both spatial reference memory and spatial working memory. It can record the search route of human body and reflect its search strategy. It will not consume too much physical strength.

The above behavioral methods can evaluate the learning and memory of the subjects as a whole. With the continuous deepening of the study of learning and memory and the emergence of various new theories of learning and memory, new experimental models and advanced experimental technology are applied to the research, which also poses new challenges to the study of learning and memory. Therefore, how to combine the traditional behavioral methods with the latest technical means to provide more scientific, accurate, and intuitive data for the study of learning and memory has become a problem that must be solved in the field of behavioral research in the future. The results of human hexagonal maze are shown in Figure 2.

The results showed that compared with the large platform control group, the search frequency of each group after sleep deprivation was significantly increased, and the search time was shortened. Among them, each dose group of Acanthopanax senticosus was shorter than that of the sleep deprivation group. Compared with the large platform control group, the number of errors in the sleep deprivation group was significantly increased and the cognitive rate was reduced ($p < 0.01$). Compared with the sleep deprivation group, the cognitive rate was increased in each dose group of Acanthopanax senticosus, and the difference between the high- and medium-dose groups was extremely significant ($p < 0.01$), and the difference between the low-dose group was significant ($p < 0.05$).

Neurophysiological methods can record electrophysiological signals of the central nervous system at different levels by using a variety of techniques, such as detection of electrical signals of the nervous system, induction of electrical signals of synaptic circuits of neurons, microelectrode recording, and patch clamp, for example, the electrical signals of cerebral cortex, the potential signals of neuronal groups in various brain tissues, the membrane potential signals of single nerve cells, and the current signals of ion channels on the membrane of nerve cells. Analyze the changes of these electrophysiological signals under the action of drugs, so as to study the effect and mechanism of drugs [24].

Neurophysiological research (from whole to ion channel) has multiple levels of methods, but it can be roughly

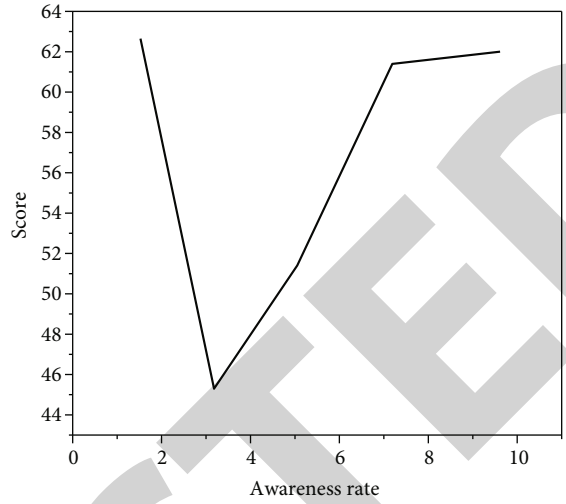

Figure 2: Human hexagonal maze performance.

divided into two categories: in vitro and in vivo. Among them, brain tissue slice in vitro incubation method and patch clamp ion channel method belong to in vitro research methods. The advantages of these methods are as follows: there is no blood-brain barrier, the components of perfusate can be changed flexibly, the speed of drug application and elution is fast, it is easy to control the concentration of perfusate drugs to establish a dose-response relationship, and it can clearly observe the morphology of nerve tissue or nerve cells, and correctly grasp the drug action site and signal detection site. We can observe the response of the single synaptic circuit cell population of the nervous system to the single ion channel of the nerve cell membrane at different levels. However, in vitro research methods, cut off the normal synaptic connection between brain slices and surrounding tissues and affect various regulatory factors, which may change some response characteristics of neurons. Moreover, in vitro research methods require the use of relatively single drug components, which is especially suitable for the study of the action mechanism of agonists and antagonists of various nerve receptors. For the crude extract or Decoction of traditional Chinese medicine, it will interfere with the evaluation of in vitro experimental results due to the influence of impurities and physical and chemical properties (impurity particles, pH of drugs, etc.).

4. Results and Analysis

A certain number of personnel were selected for retrospective analysis. During the analysis, all groups were in good condition without any adverse reactions. The weight changes of people in different groups are shown in Table 3. It can be seen from the table that there is no significant difference between the weight of people at the beginning of the experiment and the weight at the end of the experiment, as well as the weight increased during the experiment, indicating that different drugs have no significant impact on the growth of human weight [25].

Table 3: Effects of different proportions of compound Acanthopanax senticosus on human body weight ($n = 10$).

Group	Initial weight (g)	Final weight (g)	Increased weight (g)
Control	22.37 ± 1.20	31.19 ± 1.28	8.82 ± 0.57
Red ginseng	22.22 ± 0.96	31.21 ± 1.06	8.99 ± 0.60
3 : 2 : 1	22.19 ± 1.08	31.86 ± 1.52	9.67 ± 0.77
5 : 5 : 1	22.41 ± 0.71	31.41 ± 1.85	9.00 ± 1.21

Table 4: Effects of different proportions of compound Acanthopanax senticosus on human exhaustion swimming time ($n = 10$).

Group	Dose (mg/kg)	Swimming time (min)
Control	-	9.17 ± 2.45
Red ginseng	200	12.95 ± 4.21*
3 : 2 : 1	500	14.03 ± 5.25*
5 : 5 : 1	500	14.75 ± 5.43*

According to the results of human weight-bearing swimming experiment in Table 4, compared with the blank group, the positive drug group, the ratio of 3 : 2 : 1 group, and the ratio of 5 : 5 : 1 group all prolonged the exhaustion swimming time of people to varying degrees, with significant difference ($p < 0.05$), as shown in Table 4.

Exhaustive swimming time is the simplest and most intuitive index in sports endurance experiment. In the validation experiment, the compound extract with the ratio of 3 : 2 : 1 and the compound extract with the ratio of 5 : 5 : 1 showed better antifatigue effect, and there was a significant difference between the two groups. However, there is no significant difference in the effect of alleviating fatigue between the two proportions. Because the original prescription ratio of 3 : 2 : 1 is the clinical experience prescription of the hospital, its effectiveness and safety are good, and the proportion of Astragalus in this ratio is small, and the cost is relatively low.

Fatigue is the result of multiple factors. The most direct and objective performance is the reduction of muscle contractility, the decline of exercise endurance, and the emergence of exhaustion. The length of exhaustive swimming is the most direct behavioral indicator of exercise endurance in human weight-bearing swimming experiments. The analysis of exhaustion swimming time shows that the total extract HD group, 40% ethanol and 75% ethanol elution site HD group, has a longer exhaustion swimming time, which has a significant difference compared with the blank group. Among them, the total extract HD group has the best effect, indicating that the compound total extract has a better antifatigue effect.

The process of fatigue is complex, and the specific mechanism is not clear. At present, the more recognized mechanisms are energy exhaustion theory, metabolite accumulation theory, internal environment disorder theory P, etc. According to the above different theories, four representative biochemical indicators, TG, bun, LDH, and CK, are selected for detection. If two or more indicators are positive, it indicates that the tested drug has antifatigue effect.

5. Conclusion

Due to the influence of various social factors such as high work pressure, fast pace of life, high consumption level, and special working environment such as high temperature, high humidity, noise, harmful gases, and ionizing radiation, fatigue in various fields is becoming more and more serious, and more and more people are tired. Therefore, fatigue has become the research focus of social medicine, sports medicine, military medicine, preventive medicine, and other disciplines. Acanthopanax senticosus replenishes Qi, invigorates the spleen, invigorates the kidney, and calms the nerves. Astragalus membranaceus can not only tonify the spleen but also elevate the middle Qi, brighten Codonopsis pilosula, nourish yin and stomach, and calm the liver and detoxify. The three prescriptions are warm and cool, regulate and tonify the liver and kidney, and take into account the spleen and stomach, which is consistent with the understanding of traditional Chinese medicine on the pathogenesis of fatigue, and this prescription has been used in hospitals as a hospital preparation to treat fatigue. Therefore, this study is guided by pharmacological activity to find an effective part against fatigue caused by continuous exercise, further study the effect of this part on fatigue in special environment, and preliminarily analyze its antifatigue material basis.

In the experiment of optimizing the proportion of compound Acanthopanax senticosus, the compounds with different proportions were obtained through uniform design. Through the human weight-bearing swimming experiment, the optimal proportion of antifatigue effect was found with the exhaustion swimming time as the evaluation index. The results showed that the extracts with the ratio of 30 : 21 : 7 and 3 : 1 : 1 significantly prolonged the exhaustion time. The regression equation $Y = 8.46 + 0.184X_1 + 0.739X_2 - 0.194X_3$ was obtained by using the uniform design software. The equation was significant. On this basis, the optimal ratio was optimized to be 5 : 5 : 1. The original formula of compound Acanthopanax senticosus is 3 : 2 : 1. Comparing it with the effect of the extract with the optimal ratio on people's swimming time, it is found that there is no significant difference in the antifatigue effect of the two formulas. As an empirical formula, the original formula of 3 : 2 : 1 has better effectiveness and safety, and the cost is relatively low, so it is the optimal compatibility ratio after comprehensive consideration. The best proportion of antifatigue effect of compound Acanthopanax senticosus was confirmed, the best extraction method was determined, and the effective parts for resisting fatigue caused by continuous exercise and alleviating fatigue in special environment were screened through in vivo experiments. The main pharmacodynamic components of the effective parts were determined based on liquid chromatography-mass spectrometry, and the safety of the effective parts was evaluated, and no obvious acute toxicity was found.

Hindawi
Scanning
Volume 2023, Article ID 9839032, 1 page
https://doi.org/10.1155/2023/9839032

Retraction

Retracted: Intelligent Scanning Detection System of Muscle Exercise Fatigue Based on Surface Electromyography

Scanning

Received 12 December 2023; Accepted 12 December 2023; Published 13 December 2023

This article has been retracted by Hindawi, as publisher, following an investigation undertaken by the publisher [1]. This investigation has uncovered evidence of systematic manipulation of the publication and peer-review process. We cannot, therefore, vouch for the reliability or integrity of this article.

Please note that this notice is intended solely to alert readers that the peer-review process of this article has been compromised.

Wiley and Hindawi regret that the usual quality checks did not identify these issues before publication and have since put additional measures in place to safeguard research integrity.

We wish to credit our Research Integrity and Research Publishing teams and anonymous and named external researchers and research integrity experts for contributing to this investigation.

The corresponding author, as the representative of all authors, has been given the opportunity to register their agreement or disagreement to this retraction. We have kept a record of any response received.

References

[1] W. Wang, "Intelligent Scanning Detection System of Muscle Exercise Fatigue Based on Surface Electromyography," *Scanning*, vol. 2022, Article ID 9163978, 7 pages, 2022.

Hindawi
Scanning
Volume 2022, Article ID 9163978, 7 pages
https://doi.org/10.1155/2022/9163978

Research Article

Intelligent Scanning Detection System of Muscle Exercise Fatigue Based on Surface Electromyography

Weiqi Wang

Fuyang Normal University, Fuyang, Anhui 236037, China

Correspondence should be addressed to Weiqi Wang; 11231437@stu.wxic.edu.cn

Received 5 July 2022; Revised 6 August 2022; Accepted 17 August 2022; Published 27 August 2022

Academic Editor: Danilo Pelusi

In order to use the surface EMG signal to *automatically* detect the muscle fatigue state, a research method of the muscle exercise fatigue intelligent scanning detection system based on surface EMG was proposed, and the sEMG signal features of 10 subjects before and after fatigue were extracted. A time-varying parameter autoregressive model is established. By introducing the Legendre basis function, the parameter identification of the linear nonstationary process is transformed into the parameter identification of the linear time-invariant system. Combined with the correlation index, the optimal Legendre base function dimension of the time-varying system parameter estimation can be obtained, then the best model fitting effect can be obtained, and the time-invariant parameters are solved by the least square method. Using the rate of change of the first time-varying parameter (ARC1) of the autoregressive model before and after fatigue as an index to detect muscle fatigue sensitivity, a two-tailed t test was used to compare the mean power frequency (MPF) and the median frequency (MF) with the rate of change. The results showed that the change rates of ARC1, MPF, and MF before and after fatigue were34.33% ± 2.5%, 68% + 2.03%, and 22.80% + 2.19%, which were 41% and 25%, respectively. The rate of change of ACR1 was significantly higher than that of MPF and MF ($P < 0.05$). When detecting muscle fatigue by sEMG signal, it has the advantages of short time and high sensitivity. It can be used for online real-time analysis of muscle fatigue, providing a potential analysis tool for limb muscle strain, rehabilitation, and ergonomics assessment.

1. Introduction

Exercise-induced muscle fatigue refers to the physiological phenomenon that exercise causes the muscle to produce the maximum random contraction force or the temporary decline of output power [1]. Its mechanism is extremely complex, involving a variety of physiological processes, such as central motor drive, neuromuscular junction excitation contraction coupling, and muscle energy metabolism. In recent years, with the development of electromyography technology, using EMG to record and study muscle fatigue has become a more and more common method in physiology, as shown in Figure 1. EMG technology has the advantages of noninvasive, real-time, and multitarget measurement [2]. The study of EMG can reveal the mechanism of muscle fatigue, for example, to judge fatigue in sports practice and guide training. It is especially suitable for measuring changes in EMG during exercise, and EMG will gradually be used in many aspects of sports science research. The analysis of EMG signal mainly includes time domain and frequency domain analysis. The time domain analysis of EMG can provide us with the discharge time, total discharge amount, discharge frequency, and discharge amplitude of various muscle fibers under the electrode, especially in the analysis of movement technology. The EMG frequency domain analysis can provide us with the following information: we can know the concentration trend of discharge energy at a certain frequency, the mobilization of different types of muscle fibers, and the relationship between the change of neuromuscular function and the change of discharge frequency. For clarifying the working mechanism and functional state of nerve and muscle, the best way is to apply time domain and frequency domain analysis at the same time, especially the latter. In the static working state, the more consistent conclusion is that the amplitude value of iEMG from initial state to fatigue state increases with

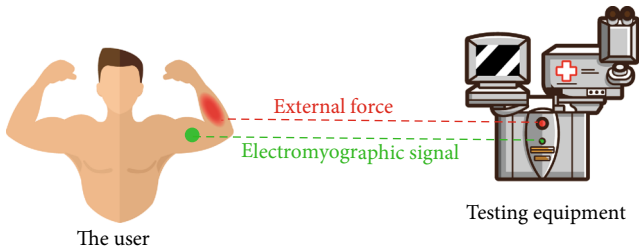

Figure 1: Detection of muscle exercise fatigue.

the deepening of fatigue degree, and the power spectrum of frequency domain value shifts to low frequency. In addition, the specific range of frequency reduction was clearly obtained. They concluded that the left shift value of the corresponding frequency of the maximum spectral peak was (9-18 Hz). In addition to the change in the recruitment form of fast and slow muscle fiber components during skeletal muscle contraction, i5s may also be caused by the hyperpolarization of muscle cell membrane potential caused by the increase of pH value in muscle tissue, resulting in the outflow of K+ in cells. K + outflow will block the hyperpolarization of cell membrane potential and reduce the excitability of muscle cells and the conduction velocity of muscle fibers, resulting in the transfer of muscle discharge frequency to low frequency band [3]. However, we do not rule out this possibility: according to the current research, muscle tissue has the function of low-pass filtering. During muscle contraction, the length of the muscle is shortened, the thickness is increased, and the distance between the recording electrode and the moving unit is increased, resulting in the filtering of some high-frequency signals and the increase of the proportion of low-frequency signals and resulting in the low shift of the spectrum.

2. Literature Review

Er and Erk found that muscle activity is a complex exercise under the control of the central nervous system. Muscle fatigue usually refers to the temporary decline of the maximum work capacity or maximum contraction capacity of the system [4]. Fan and others have shown that there have been different opinions on the mechanism of exercise-induced muscle fatigue for a long time [5]. In fact, Ben et al. have found that the human body is a complex organism, and various systems and organs are not isolated, but interconnected and restricted under the regulation of the nervous system [6]. The essence of fatigue is the weakening of the function of the transverse bridge of muscle fibers and matrix network, resulting in the weakening of muscle filament sliding. Shaoting and others found that ADP/ATP increased in the triple tube structure, resulting in the decrease of calcium uptake by the matrix network. The surface EMG signal is the bioelectric signal recorded during the activity of the neuromuscular system guided by the electrode from the skin surface. It has different degrees of correlation with the activity state and function of the muscle, so it can reflect the activity of the neuromuscular system to a certain extent [7]. Lindinger and Cairns found that electromyography measurement generally uses three electrodes, two electrodes are placed at the part where the action potential can be measured and amplified, and the third electrode is the grounding electrode. Before placing the electrode, the body hair of the measurement part should be scraped off, the skin should be cleaned with fine sand and absolute ethanol, and conductive paste should be used to reduce the impact of skin resistance on electromyography signal [8]. Most scholars believe that the position of the surface electrode should be as close to the abdominal center as possible to obtain the maximum EMG signal from the rhomboid muscle. Dong and others believe that by sticking the electrode to the geometric center of muscle contraction and the electrode direction along the longitudinal axis of muscle fiber, the measured EMG signal is the most reliable, the two electrodes gather for 2-3 cm, and the ground wire is connected to a relatively stable place when moving close to the electrode, so the collected EMG signal is the most stable [9]. Greco and others found that the surface electrode can comprehensively reflect the activity of this part of the muscle. Surface electromyography collects one-dimensional time series signals [10]. It is the superposition of electrode changes in time and space when the surface guide electrode touches multiple moving units. From a physiological point of view, Tang and others are related to the fiber composition and anatomical structure of muscle, the number of motor units participating in activities under different functional and active states, the discharge frequency of different motor units, the degree of synchronization of motor unit activities, and the recruitment mode of motor units [11]. The influence of adipose tissue on the test results is greater when muscle is relaxed than when muscle is moving, but it does not affect the symmetry of both sides. EMG signals can be derived from random contraction and electrical induction. Random contraction EMG signals are the sum of action potentials of many motor units. During electrical induction, Sunayana and others found that due to external stimulation, motor unit action potential synchronization produced an exact evoked response, namely, M wave. This recording method can help us confirm the most superficial motor unit, which is more rapid than muscle fatigue caused by random contraction, and the obtained EMG signal has less change and more stable [12]. Grabowski and others found that in recent years, with the rapid development of computer, the quantitative analysis of electromyography has become possible. SEMG signal analysis includes time domain analysis and frequency domain analysis [13]. Kou and Zhang believe that its detection has the advantages of noninvasive, real-time, and multitarget measurement [14]. SEMG signal analysis is a means and method to find the change law and characteristics of sEMG signal by using the theory and method of signal analysis. Time domain analysis can provide us with the discharge time, total discharge amount, discharge frequency, discharge amplitude, etc. of muscle fibers, especially in the motion analysis of sports technology. Frequency domain analysis can provide us with the following information: The mobilization of different types of muscle fibers, the energy supply state of neuromuscles, and the concentration trend of discharge are at a certain frequency. For practical application, time domain and frequency domain analysis should be used at the same time.

3. Method

The subjects were 10 healthy men, who had no history of upper limb muscle strain, normal body mass index, and did not participate in any violent activities within 24 hours before the experiment. Before the experiment, each subject received the experiment notice, signed the informed consent, and conducted the experiment action training. The experiment was conducted in a key laboratory of medical engineering. Before the experiment, the laboratory adjusted the temperature to 279°C, removed the jewelry of the subject, and put the electrode piece in the middle of the biceps brachii of the right upper limb. The right hand of each group of subjects is upward, the upper arm is parallel to the body, and the angle between the forearm and the upper arm elbow is 90°. Hold 1.5 kg dumbbell and start isometric contraction until the subjects subjectively feel that muscle fatigue cannot continue. Collect and record the data of the early and late stage of biceps brachii fatigue of the right upper limb. Due to the large differences in age and individual among each subject, it is required that the dumbbell weight and electrode placement position must be consistent [15]. Experimental equipment and materials: before the experiment, prepare the experimental equipment and materials, including computer, wireless surface EMG acquisition system (including 1 DTS EMG sensor, 1 DTS desktop receiving box, 1 double electrode clamp, 5 V DC charging line, mini USB data line, and 1 elastic fixing belt), 2 electrode pieces, alcohol, cotton swab, and subject information. The brand is Noraxon, the model is sEMG sensor signal acquisition system, and the version is mr3 6 software. The wireless surface electromyography signal sensor is used. The disposable Ag/AgCl electrode sheet is used. The time constant is set to 0.05 s, and the sampling frequency is 1500 Hz. The disposable electrode sheet is pasted according to the muscle model, and the spacing between the electrode sheets is 20 mm. Because the sEMG signal is relatively weak, the useful signal is distributed in the frequency range of 0 ~500 Hz, and the main energy part is distributed in the frequency range of 50~150 Hz. Surface EMG signals detected by body surface electrodes mainly include power frequency interference (50 Hz), baseline drift, and ECG interference (5 ~ 20 Hz). These noises will seriously affect the quality of surface EMG signals [16]. In order to enhance the effective components of sEMG signal and suppress noise and artifacts, the effective elimination of noise is very important for the subsequent processing of sEMG signal. Butterworth 20~500 Hz band-pass filter is used to eliminate baseline drift and ECG interference, and Butterworth band stop filter is used to eliminate 50 Hz power frequency interference. There are differences in muscle activity among different subjects. In order to uniformly compare the effects of different parameter eigenvalues on fatigue characterization, it is necessary to normalize the surface EMG signal [17].

In this experiment, the autoregressive model (AR) describes a "short-term stable" random process. The observed value x_n of the random process at this time is correlated with the observed value x_{n-1} before that time. The calculation formula of autoregressive model with p-order parameters is shown in the following formula:

$$x_n = -\sum_{i=1}^{p} a_i(n)x_{n-i} + e_n, \tag{1}$$

where $a_i(n)$ is the autoregressive coefficient and also the parameter of AR (P) model; $n = 1, 2, \cdots, N$, N is the length of sampling data; e_n is a stationary white noise process; x_n is the observation value, and x_{n-i} is the observation sequence value.

Since the sampling frequency of the EMG acquisition equipment is 1500 Hz, the time-varying system parameters change too fast, and the convergence of the adaptive algorithm is defective. Therefore, the basis function expansion method is used [18]. The basis function expansion method is used to identify the time-varying system. Is the time-varying coefficient $a_i(n)$ expressed as a linear combination of a set of basis functions? See the following equation:

$$ai(n) = \sum_{j=1}^{m} a_{ij}(n)f_i(n), \tag{2}$$

where a_{i_j} is the time invariant coefficient of the expansion, $f_j(n)$ is the basis function, and M is the extended dimension of the basis function.

Then, equation (2) can be rewritten as

$$X = BA + e. \tag{3}$$

Using the basis function expansion, the identification problem of P time-varying coefficients in the time-varying model formula (1) is transformed into the identification of $P \times M$ constant parameters, that is, the parameter identification of the original nonstationary process is transformed into the identification of a linear time invariant system [19]. After the model is expressed in matrix form, the estimated value $\widehat{A}$ of time invariant parameter a is solved by the least square method, as shown in the following formula:

$$\widehat{A} = \left(B^T B\right)^1 B^T + e \tag{4}$$

Substitute equation (4) into equation (2) to obtain the estimated value $\widehat{a_i}(n)$ of time-varying parameter $a_i(n)$.

Frequency domain analysis is to analyze the characteristics of sEMG signal from the perspective of frequency. The method is to obtain the spectrum or power spectrum of sEMG signal after short-time Fourier transform. The common analysis parameters of frequency domain analysis are MPF and MF. Because MPF and MF are based on short-time Fourier analysis, their time and resolution are fixed. However, for surface myoelectric signals, when the spectrum distribution range is wide, it is difficult to find a suitable time window for analysis, that is, their time and frequency resolution are low.

By comparing and analyzing the change rate (CR) of the fatigue index before and after fatigue of the three methods, we can determine which characteristic parameter value

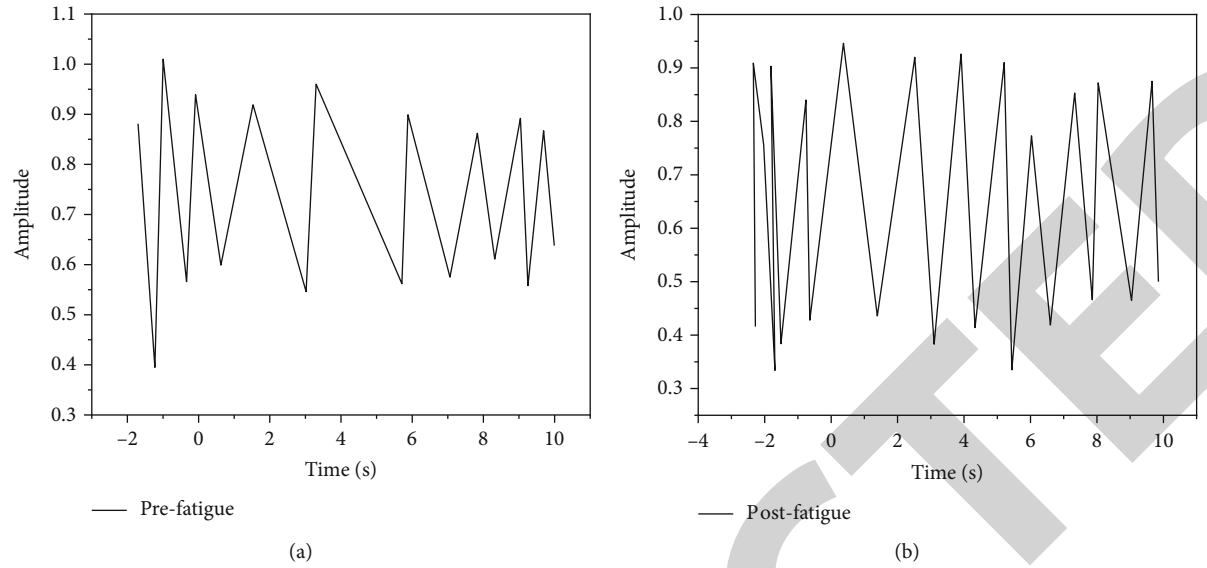

Figure 2: (a) Surface electromyography prefatigue. (b) Surface electromyography late fatigue.

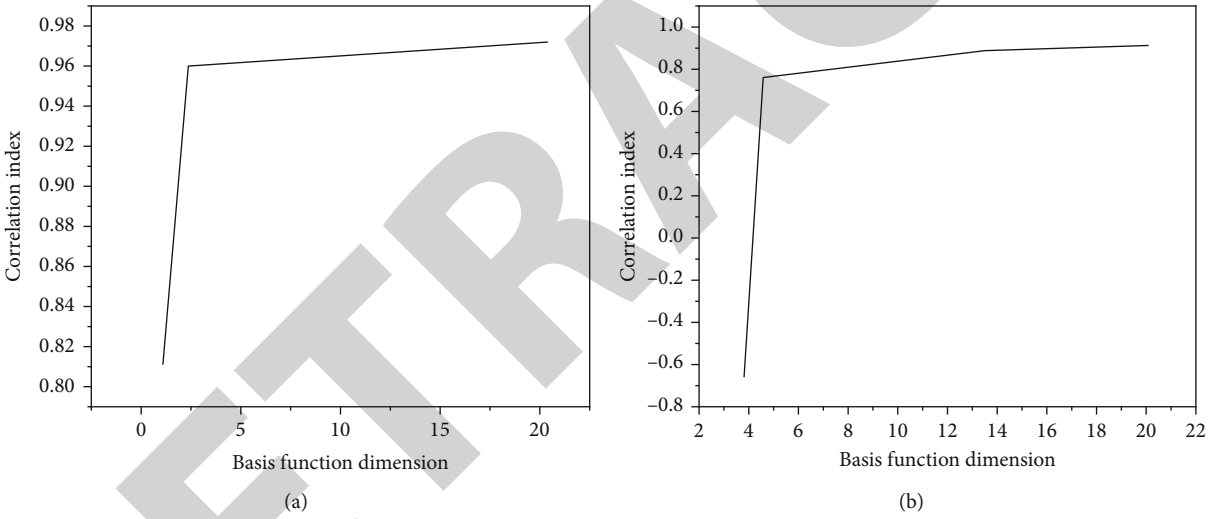

Figure 3: (a) Correlation index changes with the dimension of basis function before fatigue. (b) Correlation index changes with the dimension of basis function after fatigue.

index has higher sensitivity to muscle fatigue response, and further explain which method is suitable to characterize muscle fatigue. The change rate of relevant characteristic parameter values before and after fatigue is defined in the following formula:

$$\mathrm{CR} = \frac{(\mathrm{y}_{i+M} - \mathrm{y}_i)}{y_i \times 100\%}, \tag{5}$$

where$y$ andy_i are the value before fatigue, and y_{i+m} is the value after fatigue.

After calculation, the MPF of surface EMG signals before and after fatigue is 208.34 and 149.35 Hz, respectively, and the MF is 132.98 and 104.75 Hz, respectively. The MPF change rate obtained from equation (5) is -28.68%, and the MF change rate is -21.66%. Because MPF and MF are based on the principle of short-time Fourier, they have long sampling time, poor real-time performance and resolution. In order to compare the sensitivity of the three methods to muscle fatigue, the following MPF and MF eigenvalues are calculated based on the data length of $n = 15000$ points ($t = 10$ s). Based on the characteristics of time-varying AR model, such as short sampling time and rapid response to time, the corresponding time-varying parameters can be obtained by using time-varying parameter AR model to process the first $n = 150$ point ($t = 0.1$ s) data before and after fatigue. After calculation, the ARC1 of surface EMG signals before and after fatigue is -2.35 and -3.79, respectively. The change rate of ARC1 obtained from equation (5) is 37.39%. The time-varying autoregressive model method analyzes the surface EMG signal from the perspective of least

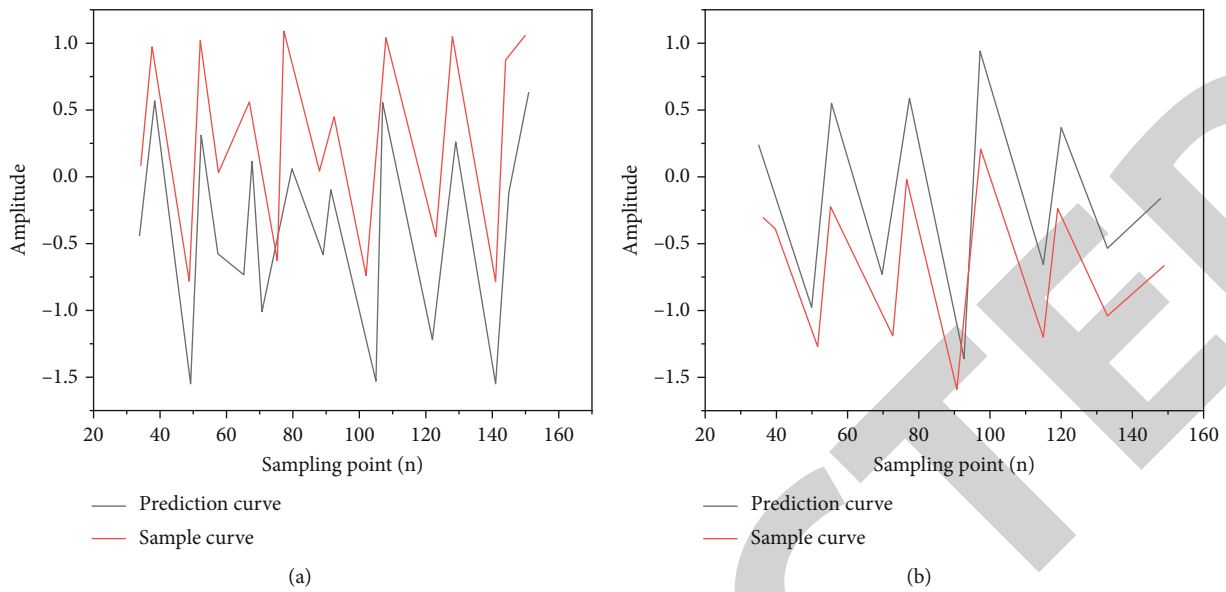

Figure 4: (a) Time-varying parameter identification results based on Legendre expansion method before fatigue. (b) Time varying parameter identification results based on Legendre expansion method after fatigue.

Table 1: Fatigue characteristic value and its change rate of each subject (before and after fatigue).

Subject	Average power frequency/MPF			First parameter of AR model/ARCI			Median frequency/MF		
	Before fatigue/Hz	After fatigue/Hz	Change rate/%	Before fatigue	After fatigue	Change rate/%	Before fatigue/Hz	After fatigue/Hz	Change rate/%
1	209.33	149.30	26.86	-2.25	-3.09	37.39	132.95	104.15	21.66
2	171.83	128.63	25.21	-2.12	-2.75	34.95	123.19	96.28	21.85
3	199.56	143.22	25.14	-2.41	-3.17	29.77	126.82	100.48	20.77
4	161.30	125.44	28.23	-1.89	-2.50	31.74	122.61	90.69	26.03
5	190.10	137.63	22.23	-2.18	-2.92	32.18	128.78	101.28	21.36
6	193.21	148.57	27.60	-2.42	-3.30	33.92	145.59	109.47	24.81
7	148.49	112.36	23.10	-2.26	-3.05	36.14	96.09	76.74	20.13
8	190.69	137.96	24.33	-2.72	-3.44	35.12	126.38	99.26	21.46
9	174.80	130.73	27.65	-2.00	-2.71	36.47	128.08	97.38	23.97
10	207.28	152.47	26.44	-2.09	-2.84	35.66	165.79	122.76	25.95
Mean ± SD		25.68 ± 2.03			34.33 ± 2.41			22.80 ± 2.19	

mean square error fitting, which overcomes the shortcomings of low frequency resolution and poor variance performance of classical spectrum estimation. Compared with the short-time Fourier transform analysis, it overcomes the problem that the sampling time of sEMG signal is long enough for the traditional extraction of frequency-domain parameters. Taking the sampling frequency of 1500 Hz and 512 points of time window as an example, the shortest data also needs $512/1500 \approx 0.34\,s > 0.1\,s$ when calculating MPF and MF parameters.

The data analysis module of Excel 2013 software is adopted. The two tailed t-test analysis method is used to analyze the statistical difference of the sensitivity effect of each parameter eigenvalue on fatigue response, that is, to analyze the statistical difference of each parameter eigenvalue on the characterization effect of muscle fatigue degree. Statistical steps of change rate data: F test shall be conducted first, which is also called variance homogeneity test. F-test is used in the two sample t-test. The purpose of F-test is to determine whether to use the two sample equal variance t-test or the two sample heteroscedasticity t-test. If the two times of one tailed P value of F test is greater than 0.05, it indicates that there is no significant difference between the two variances, then double sample equal variance t test is used. Otherwise, a two sample heteroscedasticity t-test is selected.

4. Experiment and Discussion

Figure 2 shows the surface EMG signal diagram of biceps brachii of a typical subject. It can be seen that the amplitude of surface EMG signal of muscle before and after fatigue

tends to increase, which reflects the increase in the number of exercise units participating in activities from muscle contraction to fatigue, which is reflected in the increase in the amplitude of surface EMG signal during muscle fatigue [20].

Figure 3 shows that the correlation index l obtained by estimating the 6th order AR model based on the basis function expansion method of a typical subject changes with the dimension of the basis function, and the optimal dimension of Legendre basis function is obtained from equation (10) [21]. As can be seen from Figure 3, when the dimension of the basis function $m \geq 4$, the parameter identification effect fluctuates little and tends to be stable. A large number of experiments show that the parameter identification effect is the best when $P = 6$ and $M = 7$.

Figure 4 shows the time-varying parameter identification results of a typical subject based on Legendre expansion method. It can be seen that the Legendre expansion method can better track the signal because of its good local characteristics, and the identification result is relatively smooth, especially there is no sudden change of parameter position at the peak and trough [22]. Therefore, Legendre expansion method has ideal identification effect.

Table 1 shows the fatigue characteristic values of subjects before and after fatigue. The experimental results show that 10 groups of time-varying parameters are obtained. The first parameter of each group of AR model (ARC1) is the most important. It directly reflects the relationship between the current time and the previous time. It is the most direct quantity of the change of muscle state with time. Each order of AR parameters changes with time point. ARC1 in the estimated signal 0.1 s time period is calculated as the index to evaluate muscle fatigue state. MPPF and MF within 10 s of the estimated signal are calculated as indicators for evaluating muscle fatigue [23].

From the change trend of characteristic parameters before and after fatigue, ARC1, MPF, and MF show a decreasing trend. From the change rate of characteristic parameters before and after fatigue, the change rate of ARC1 is high. AR model is adopted to overcome the problem that MF and MPF require long enough sampling time of sEMG signal [24]. The change rates of MPF, MF, and ARC1 of 10 subjects before and after fatigue were taken as fatigue indicators. The change rates were statistically analyzed. The mean value and standard deviation of the change rates were 25.68% + 2.03%, 22.80% + 2.19%, and 34.33% + 2.41%, respectively. Because there are significant differences between ARC1 and MPF and between ARC1 and MF, which are significantly higher than MPF and MF, respectively, it shows that using ARC1 parameter index to track muscle fatigue has high resolution sensitivity [25].

Legendre basis function is used to expand the parameters of linear time-varying system under white noise excitation, and the correlation index is used to select the best dimension of Legendre basis function. Through the experimental study of muscle fatigue, the characteristic parameters analyze the characterization effect of muscle fatigue. Through experiments, ARC1 is compared with traditional frequency domain parameters MPF and MF to prove the feasibility and effectiveness of ARC1 in the field of evaluating muscle fatigue [26].

5. Conclusion

The Legendre basis function expansion method is used to transform the identification problem of linear nonstationary process into the identification problem of linear time invariant system. The surface EMG signals of 10 subjects were extracted. The change rate of ARC1 in a short time was used as the index to evaluate the sensitivity of muscle fatigue. The experiment proved that it was more sensitive to fatigue response than MPF and MF, so it had the effect of amplifying the subtle feature information and making the unobvious feature information obvious.

The detection of muscle fatigue by sEMG signal can not only better characterize the change degree of muscle fatigue but also has the advantages of short time and high sensitivity. It can be applied to online and real-time detection of muscle fatigue and provide a reliable analysis tool for upper limb muscle strain assessment, rehabilitation treatment, and ergonomics research. The problem of time-varying parameter identification has always been a research difficulty in academic circles. It can be seen from the fact that the sensitivity of ARC1 in 10 subjects is higher than that of MPF and MF. This research method has applicability. In order to further verify and consolidate the correctness and practicability of the above results, in addition to a large number of simulations to verify that the experiment has the advantages of short time and high sensitivity, a large number of experiments still need to be carried out in the later stage of the next research, so as to further improve its practical value in the fields of muscle fatigue judgment.

Data Availability

The data used to support the findings of this study are available from the corresponding author upon request.

Conflicts of Interest

The authors declare that they have no conflicts of interest.

Acknowledgments

The study was supported by 2020 Humanities and Social Sciences in Anhui University: Research on the Revision and Improvement of Physical Education Professional Evaluation Index System under the Scope of Core Literacy (2020jyxm1989).

References

[1] S. Salagare, P. S. Adarakatti, and Y. Venkataramanappa, "Designing and construction of carboxyl functionalised mwcnts/co-mofs-based electrochemical sensor for the sensitive detection of nitrite," *International Journal of Environmental Analytical Chemistry*, vol. 2, pp. 1–20, 2020.

[2] S. Katila, P. M. Laine, and P. Parkkari, "Sociomateriality and affect in institutional work: constructing the identity of start-up entrepreneurs," *Journal of Management Inquiry*, vol. 28, no. 3, pp. 381–394, 2019.

Hindawi
Scanning
Volume 2023, Article ID 9826840, 1 page
https://doi.org/10.1155/2023/9826840

Retraction

Retracted: Discuss the Application of Data Services in Data Health Management of High-Risk Pregnant and Lying-In Women in Smart Medical Care

Scanning

Received 3 October 2023; Accepted 3 October 2023; Published 4 October 2023

This article has been retracted by Hindawi following an investigation undertaken by the publisher [1]. This investigation has uncovered evidence of one or more of the following indicators of systematic manipulation of the publication process:

(1) Discrepancies in scope

(2) Discrepancies in the description of the research reported

(3) Discrepancies between the availability of data and the research described

(4) Inappropriate citations

(5) Incoherent, meaningless and/or irrelevant content included in the article

(6) Peer-review manipulation

The presence of these indicators undermines our confidence in the integrity of the article's content and we cannot, therefore, vouch for its reliability. Please note that this notice is intended solely to alert readers that the content of this article is unreliable. We have not investigated whether authors were aware of or involved in the systematic manipulation of the publication process.

In addition, our investigation has also shown that one or more of the following human-subject reporting requirements has not been met in this article: ethical approval by an Institutional Review Board (IRB) committee or equivalent, patient/participant consent to participate, and/or agreement to publish patient/participant details (where relevant).

Wiley and Hindawi regrets that the usual quality checks did not identify these issues before publication and have since put additional measures in place to safeguard research integrity.

We wish to credit our own Research Integrity and Research Publishing teams and anonymous and named external researchers and research integrity experts for contributing to this investigation.

The corresponding author, as the representative of all authors, has been given the opportunity to register their agreement or disagreement to this retraction. We have kept a record of any response received.

References

[1] L. Shen, W. Shi, L. Cai, J. An, and Q. Ling, "Discuss the Application of Data Services in Data Health Management of High-Risk Pregnant and Lying-In Women in Smart Medical Care," *Scanning*, vol. 2022, Article ID 5957697, 7 pages, 2022.

Hindawi
Scanning
Volume 2022, Article ID 5957697, 7 pages
https://doi.org/10.1155/2022/5957697

Research Article

Discuss the Application of Data Services in Data Health Management of High-Risk Pregnant and Lying-In Women in Smart Medical Care

Leifen Shen,[1] **Weiqin Shi**,[2] **Liwen Cai**,[1] **Jing An**,[3] **and Qian Ling**[4]

[1]*Maternity Group Healthcare Department, Huzhou Maternity & Child Health Care Hospital, Huzhou, Zhejiang 313000, China*
[2]*Healthcare Department, Huzhou Maternity & Child Health Care Hospital, Huzhou, Zhejiang 313000, China*
[3]*Child Group Health Department, Huzhou Maternity & Child Health Care Hospital, Huzhou, Zhejiang 313000, China*
[4]*Obstetrics and Gynecology Department, Huzhou Maternity & Child Health Care Hospital, Huzhou, Zhejiang 313000, China*

Correspondence should be addressed to Weiqin Shi; 1811121108@hbut.edu.cn

Received 5 July 2022; Revised 6 August 2022; Accepted 16 August 2022; Published 25 August 2022

Academic Editor: Danilo Pelusi

Objective. In order to improve the refined management of hospitals, promote the scientific development of smart hospitals in medical institutions, and solve the problem of data filling and reporting that is increasing year by year in the country, province, and city. *Methods*. A total of 84 high-risk pregnant women admitted to our hospital from January 2020 to October 2021 were selected and screened for high-risk pregnant women. Risk pregnant women were divided into a routine intervention group and a DS medical group, with 42 cases in each group. High-risk pregnant women in the routine intervention group received routine intervention, and the DS medical group applied data to serve smart medical services on the basis of routine intervention. The scores of self-care, anxiety, and depression were compared between the two groups, the coping styles were analyzed, the satisfaction rate and incidence of adverse conditions of the high-risk puerperae were recorded, and the delivery methods of the two groups were compared. *Results*. After the intervention, the activities of daily living, follow-up, fetal monitoring, and self-protection behaviors in the DS medical group were higher than those in the routine intervention group, and the difference was statistically significant ($P < 0.05$). The scores of anxiety and depression in the group were lower, with statistical significance ($P < 0.05$); after the intervention, the scores of negative coping styles in the DS medical group were lower than those in the conventional intervention group, while the scores for positive coping styles were higher than those in the conventional intervention group; the DS medical group had higher risk. The satisfaction of pregnant women was significantly higher than that of the routine intervention group, and the difference was statistically significant ($P < 0.05$); the overall incidence of adverse maternal outcomes among high-risk pregnant women in the DS medical group was lower than that of the routine intervention group, and the difference was not statistically significant ($P > 0.05$). Compared with the routine group, the DS medical group had a higher number of vaginal deliveries and a lower number of cesarean deliveries, and the difference was statistically significant ($P < 0.05$). *Conclusion*. The application of data services in a smart medical high-risk maternity-related data management platform enables the promotion of high-risk pregnant women's self-care behaviors and improves negative emotions, enables them to cooperate in delivery with positive behaviors, and reduces the number of cases of cesarean delivery.

1. Introduction

High-risk pregnant women have a high risk of dystocia and preterm delivery, which may lead to a series of postpartum complications in serious cases [1, 2]. Effective nursing intervention is conducive to reducing maternal mortality, which makes it of great significance to grasp the health status of high-risk pregnant women [3]. With the progress of medical technology, data services have been effectively and widely applied [4]. In the context of the rapid formation of smart medical services, it is necessary to pay timely attention to high-risk pregnant women through data analysis in order to strengthen the protection of themselves and their fetuses [5]. Data services: data extraction based on smart medicine,

referred to as DS system platform, provides support for hospital management capabilities through the application of data technology and intelligent means [6]. In order to provide basis for the construction of high-level intelligent hospitals with data-driven core, this paper chooses to explore the application of data services in the intelligent medical data management platform for high-risk pregnant women, so as to provide support for strengthening the core competitiveness of hospitals.

2. Materials and Methods

2.1. Material. A total of 84 high-risk pregnant women treated in our hospital from January 2020 to October 2021 were selected. High-risk pregnant women were divided into the routine intervention group and the DS medical group, 42 cases in each group. The age of the conventional intervention group was 22 to 42 years old, with an average age of 31.95 ± 9.84 years and an average gestational age of 38.99 ± 1.26 weeks. There were 39 primiparas and 3 multiparas. The age of the DS group ranged from 23 to 44 years old, with an average age of 32.56 years (10.74 years) and an average gestational age of 38.93 weeks (1.22 weeks). There were 40 primiparas and 2 multiparas. There was no statistical difference in the general data of high-risk pregnant women between the two groups ($P > 0.05$), indicating comparability.

Inclusion criteria are as follows: ① the data were complete, all were single pregnancy, ② including bleeding during pregnancy, pregnancy complications, and abnormal pregnancy history.

Exclusion criteria are as follows: ① heart, lung, and liver dysfunction; ② diabetes history; ③ people with mental illness; ④ data not complete; (5) multiple children; ⑥ poor compliance; and ⑦ the existence of immune diseases.

2.2. Methods

2.2.1. Intervention Methods. In the routine intervention group, high-risk pregnant women were treated with traditional management mode and examined before delivery. Medical staff for pregnancy guidance and psychological intervention pay close attention to maternal blood pressure, blood sugar, and other levels. The medical staff observed the progress of puerpera's labor and assisted puerpera's delivery.

On the basis of the routine intervention group, the DS medical group applied data services to intelligent medical services. First, the DS medical team was established, consisting of doctors, midwives, and obstetric nurses. Develop manuals on integrated medical, nursing, and patient services. And train team members to master work procedures and standards. Quasidiagnostic services were as follows: examination and evaluation, health education, health education files, physiological status nutrition, weight management, healthcare of physiological status, skull defect screening, common discomfort treatment, skull education, and skull observation. The data were recorded, and the risk of pregnancy was assessed. Data extracted from data services is used to establish background database on the basis of intelligent medical treatment, so as to facilitate the guidance of nursing intervention for high-risk pregnant women by medical staff. The medical team collected data on the conditions of pregnant women during the nursing process. After the data is uploaded to the platform through DS, it will be analyzed by doctors and then medical intervention will be carried out. Through data service intelligent medical data analysis of high-risk maternal psychological status, psychological care is given. In particular, for older pregnant women, nursing staff should timely communicate with pregnant women and give them psychological comfort to promote their elimination of psychological barriers and build confidence in treatment. Throughout the labor: once the woman is in labor, the team achievement collects data and provides ongoing psychological, physical, secular, and physical support and care according to the delivery schedule. Members of the team should work closely to understand the mix of medical treatment and medical assistance. Based on data services, data support to perceive dynamic changes in maternity and analyze treatment plans and events at medical assistance points and implement them. After the establishment of high-risk maternal archives, high-risk maternal risk screening and scoring were performed. Dynamic pregnancy of pregnant women with higher scores was followed; high scores of late pregnant women, for many visits, carefully recorded, ready for delivery at any time. Establish a reasonable plan. At the same time, for high-risk pregnant women, a daily diet and exercise plan should be made. Provide pregnant women with affordable nutrition and acceptable exercise based on relevant risk factors, and specify the amount of exercise.

2.2.2. Self-Care Management Score. The maternal self-care management level questionnaire independently developed by our hospital was used to evaluate and compare the self-care management level of the two groups after intervention and before intervention. Cronbach's O coefficient was L 0.852, and the retest validity was 0.862, covering daily life (8 items). Compliance behavior (4 items), fetal monitoring behavior (5 items), and self-protection behavior were divided into 4 dimensions, with 2 items for each. Each item was graded from 1 to 5 with a score of 25 to 125. There was a positive correlation between the level of self-care management behavior and the evaluation score.

2.2.3. SAS and SDS Scores. In this study, SAS and SDS scores were used to compare the anxiety and depression of high-risk pregnant women. SAS is an anxiety scale with a total score of 100 and 20 items. According to the 4-point scoring method, the higher the score, the more serious the disease. SDS is a scale commonly used in clinical evaluation of inhibition [7]. The total score was 100 points, and there were 20 items. The higher the score, the more serious the disease.

2.2.4. Scoring Coping Style. Summary coping style questionnaire (SCSQ) was used to evaluate coping style of high-risk pregnant women before and after intervention, including 12 items of positive coping style and 8 items of negative coping style. Grades are given on a 4-point scale. When the positive coping score is high, the corresponding negative score is low, indicating that high-risk pregnant women have a positive coping style [8].

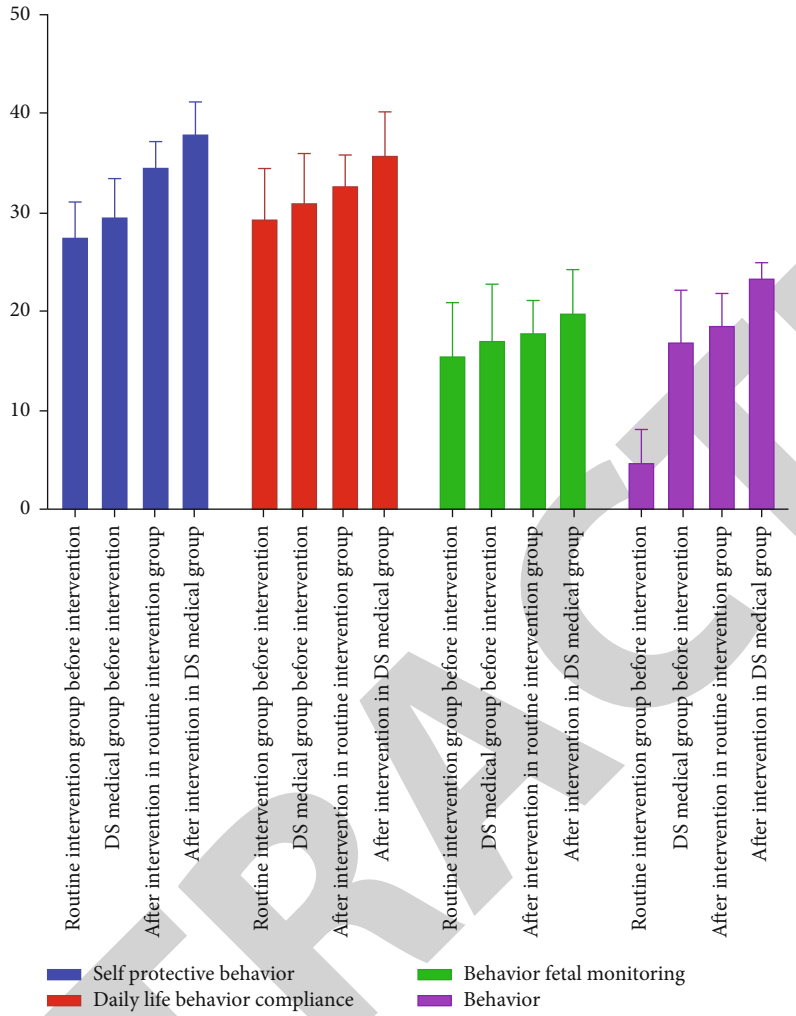

Figure 1: Comparison of maternal self-care levels between the two groups.

2.2.5. Satisfaction, Adverse Conditions, and Delivery Methods. The two groups of high-risk pregnant women were followed up by senior physicians in our hospital, and the satisfaction of the two groups was evaluated, which was divided into relatively satisfied, satisfied, and dissatisfied, satisfaction = relatively satisfied + satisfied/%. At the same time, the adverse conditions of pregnant women in the intervention process were recorded, including neonatal asphyxia, postpartum hemorrhage, and premature delivery, and the delivery methods of the two groups were recorded by the above-mentioned physicians.

2.3. Statistical Treatment. Make use of software general SPSS 20.0 statistical data analysis using software operation mode which can sample statistical data analysis and data processing. () was used to compare the measurement error between sample groups, and t-difference was used to compare the calculation error of frequency comparison between groups. Measurement data line % inspection. The intergroup mean error: X^2 test was used for the calculation error of intergroup frequency comparison, and $P < 0.05$ indicated statistically significant difference.

3. Results

3.1. Self-Healthcare Analysis. As shown in Figure 1, the comparison of daily life, compliance with doctors, fetal monitoring, and self-protection behaviors between the two groups before intervention was not statistically significant ($P > 0.05$). After intervention, the daily life, compliance, fetal monitoring, and self-protection behaviors of the DS medical group were higher than those of the conventional intervention group, with statistical significance ($P < 0.05$).

3.2. Comparison of Anxiety and Depression Scores. As shown in Figure 2, before intervention, the anxiety scores and depression scores of the two groups were not statistically significant ($P > 0.05$). After intervention, the scores of anxiety and depression in the DS medical group were lower than those in the conventional intervention group, which was statistically significant ($P < 0.05$).

3.3. Comparison of Coping Style Scores. As shown in Figure 3, before intervention, there was no statistical significance in the scores of coping styles between the two groups

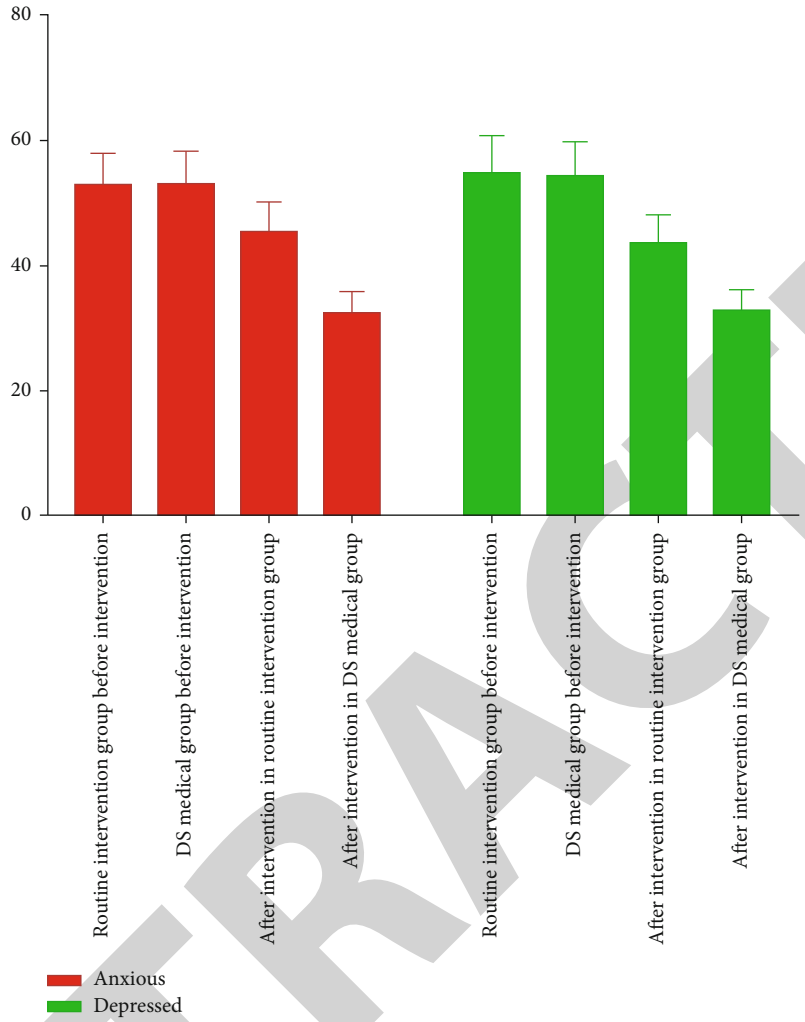

Figure 2: Comparison of anxiety and depression scores between the two groups.

compared with the conventional intervention group ($P > 0.05$). After intervention, the DS group scored lower on negative coping style. The positive coping score was significantly higher than that of the conventional intervention group ($P < 0.05$).

3.4. Satisfaction Analysis of the Two Groups. As shown in Table 1, the satisfaction degree of high-risk pregnant women in the DS medical group was significantly higher than that in the routine intervention group, which was statistically significant ($P < 0.05$).

3.5. Comparison of Adverse Events. As shown in Table 2, the total incidence of adverse events in high-risk pregnant women in the DS group was lower than that in the routine intervention group, and the comparison between the two groups was not statistically significant ($P > 0.05$).

3.6. Comparison of Delivery Methods between the Two Groups of High-Risk Pregnant Women. As shown in Table 3, compared with the conventional group, there were more cases of vaginal delivery and fewer cases of cesarean delivery in the DS medical group, which was statistically significant ($P < 0.05$).

4. Discussion

High-risk pregnancy refers to certain complications or pathogenic factors during pregnancy, which may harm pregnant women, fetuses, and newborns or lead to dystocia. Pregnant women with high-risk pregnancy factors are called high-risk pregnant women [9]. Management of high-risk pregnant women is an important link in improving obstetric quality. Timely intervention and screening enable pregnant women to receive corresponding medical services in time according to the situation, which helps reduce the complications of high-risk pregnant women [10, 11]. Healthcare information management is widely used in Europe and America and has achieved remarkable results in clinical application. Therefore, the information management system has been established in most countries [12, 13]. Recording individual medical information in the computer reduces the incidence of medical errors, thus improving the overall level of medical treatment and providing better medical services for patients

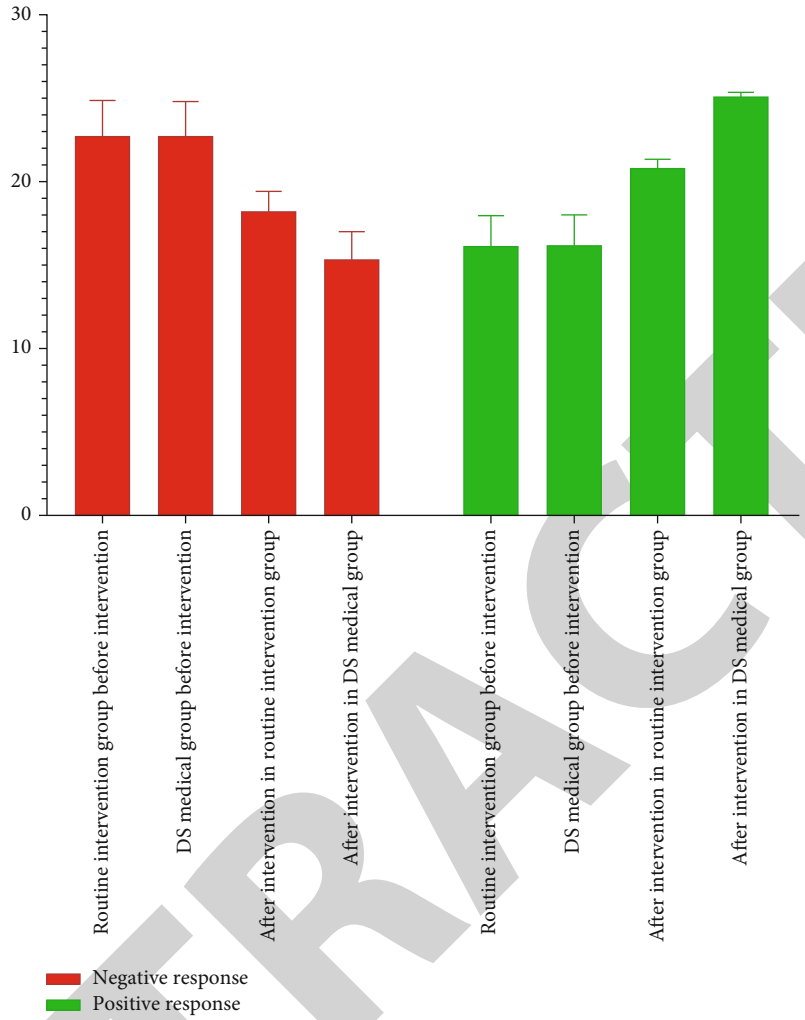

Figure 3: Comparison of coping style scores between the two groups.

[14, 15]. The method of DS data extraction is parallelism between system instances and serial extraction of tables between system instances [16]. Compared with other data processing systems, DS has the characteristics of high speed and efficiency in processing big data [17].

Clinical studies have found that high-risk pregnancy will seriously threaten the life and health of the fetus and pregnant women and even cause dystocia and neonatal asphyxia. The main factor leading to the increase in the rate of neonatal defects is that pregnant women do not have regular prenatal checkups. In strengthening the management of high-risk pregnant women, we should consider from various aspects. The mother needs to be protected and the newborn needs to be considered. Strengthen the relevant health knowledge and safety education, and strengthen the awareness of maternal self-protection. Through the support of medical data, pregnant women should be arranged for maternity checkup in a timely manner. In addition, prenatal education should be strengthened to enable pregnant women to have a comprehensive understanding and understanding of themselves and their importance, which can help reduce the occurrence of neonatal defects [18].

The results of this study showed that the application of data services in intelligent medical data management platform combined with routine intervention resulted in higher daily life, compliance with doctors, fetal monitoring, and self-protection behaviors of high-risk pregnant women, indicating that the application of data service intelligent medical data management platform can help promote the self-care of high-risk pregnant women. The reason may be the analysis of high-risk pregnant women based on the data service intelligent medical data management platform, which enables medical staff to guide and intervene high-risk pregnant women in a timely manner, thus promoting the self-care behavior of high-risk pregnant women.

At present, most cities in our country's medical institutions also established medical information management system; the application of this management system is to strengthen and improve the management ability and level of pregnant women themselves, and at the same time, the hospital in-patient department accordingly lowers the danger in pregnant women throughout the pregnancy, thereby reducing the labor cost management of pregnant women [19]. In high-risk pregnant women, timely analysis of

Table 1: Comparison of satisfaction between two groups [n, %].

Group	Number of cases (n)	Very satisfied	Satisfied	Dissatisfied	Satisfaction (%)
Conventional intervention group	42	21 (50.00)	12 (28.57)	9 (21.43)	33 (78.57)
DS medical group	42	24 (57.14)	16 (30.09)	2 (4.76)	40 (95.24)
x^2					5.126
P					0.024

Table 2: Comparison of adverse events between the two groups [n, %].

Group	Number of cases (n)	Neonatal asphyxia	Postpartum hemorrhage	Premature delivery	Overall incidence (%)
Conventional intervention group	42	2 (4.76)	2 (4.76)	3 (7.14)	7 (16.67)
DS medical group	42	1 (2.38)	2 (4.76)	2 (4.76)	5 (11.90)
x^2					0.389
P					0.533

Table 3: Comparison of delivery modes between the two groups of high-risk pregnant women [n, %].

Group	Number of cases (n)	Mode of vaginal delivery		Mode of cesarean delivery
Conventional intervention group	42	25 (4.76)		17 (4.76)
DS medical group	42	34 (2.38)		8 (4.76)
x^2			6.523	
P			0.011	

maternal status and effective guidance can enable high-risk pregnant women to actively face difficulties [20]. Positive attitude towards the disease and effective cooperation with doctors' guidance can help reduce the risk of high-risk pregnant women [21]. The research results of this paper show that the application of data services in the intelligent medical data management platform for high-risk pregnant women can improve their anxiety, depression, and other negative emotions.

Childbirth is a persistent and intense stress source for puerpera, especially for high-risk pregnant women, which inevitably leads to fear, anxiety, depression, and other negative psychological states of high-risk pregnant women [22]. The relationship between psychological factors and human health and disease rehabilitation has attracted more and more attention [23]. In maternal status, anxiety and depression are psychological problems—kinds of expression form; the mood changes in pregnant women have now been confirmed to cause uterine hypoxia, thus reducing uteroplacental blood flow, and fetal blood anoxia happens, such as during cesarean delivery operation, reducing the degree of tolerance of pregnant women more, the incidence of fetal blood anoxic increases more [24]. The research results of this paper show that the application of data services in the intelligent medical-related data management platform for high-risk pregnant women has a higher positive response score. The application of the data services in data management platform enables high-risk pregnant women to give birth actively.

The risk of maternal death during the perinatal period is strongly linked to maternal age, chronic diseases, pregnancy complications, and bad behavior, which in severe cases can have a significant impact on pregnancy outcomes. Based on this, the level of opportunity for adverse pregnant women was comprehensively assessed. Through different levels of early warning and tracking, effective nursing management is implemented to achieve dynamic health management. It is helpful for timely detection of adverse events and has good application value for the development of puerpera and newborn. The research results of this paper show that the application of data services in the intelligent medical-related data management platform for high-risk pregnant women has a high degree of satisfaction. The number of cases of vaginal delivery was more than that of cesarean section.

In conclusion, the application of data services can promote the self-care behavior of high-risk pregnant women, enable them to cooperate with delivery with positive behavior, and reduce the number of cesarean section cases [25].

Data Availability

The data used to support the findings of this study are available from the corresponding author upon request.

Conflicts of Interest

The authors declare that they have no conflicts of interest.

Hindawi
Scanning
Volume 2023, Article ID 9814192, 1 page
https://doi.org/10.1155/2023/9814192

Retraction

Retracted: Changes of Volume Parameters in the Treatment of Graves Ophthalmopathy by Endoscopic Transethmoidal Decompression of the Orbital Inner Wall Combined with Fat Decompression

Scanning

Received 12 December 2023; Accepted 12 December 2023; Published 13 December 2023

This article has been retracted by Hindawi, as publisher, following an investigation undertaken by the publisher [1]. This investigation has uncovered evidence of systematic manipulation of the publication and peer-review process. We cannot, therefore, vouch for the reliability or integrity of this article.

Please note that this notice is intended solely to alert readers that the peer-review process of this article has been compromised.

Wiley and Hindawi regret that the usual quality checks did not identify these issues before publication and have since put additional measures in place to safeguard research integrity.

We wish to credit our Research Integrity and Research Publishing teams and anonymous and named external researchers and research integrity experts for contributing to this investigation.

The corresponding author, as the representative of all authors, has been given the opportunity to register their agreement or disagreement to this retraction. We have kept a record of any response received.

References

[1] W. Fu, "Changes of Volume Parameters in the Treatment of Graves Ophthalmopathy by Endoscopic Transethmoidal Decompression of the Orbital Inner Wall Combined with Fat Decompression," *Scanning*, vol. 2022, Article ID 8149247, 6 pages, 2022.

Hindawi
Scanning
Volume 2022, Article ID 8149247, 6 pages
https://doi.org/10.1155/2022/8149247

Research Article

Changes of Volume Parameters in the Treatment of Graves Ophthalmopathy by Endoscopic Transethmoidal Decompression of the Orbital Inner Wall Combined with Fat Decompression

Weina Fu

Department of Ophthalmology, Ningbo Medical Center Lihuili Hospital, Ningbo, Zhejiang 315040, China

Correspondence should be addressed to Weina Fu; 201804125@stu.ncwu.edu.cn

Received 5 July 2022; Revised 5 August 2022; Accepted 16 August 2022; Published 24 August 2022

Academic Editor: Danilo Pelusi

Objective. To observe the orbital volume changes and the analysis of surgical effect of Graves orbitopathy (GO) after endoscopic medial wall decompression combined with muscle cone fat. *Methods*. Twenty-two patients (30 eyes) with Graves orbital disease who visited the Department of Ophthalmology of Ningbo Medical Center from December 2019 to September 2021 were retrospectively collected. All patients were diagnosed as nonorganic active stage before operation, and all of them received endoscopic transethmoidal decompression of the medial orbital wall combined with intramuscular orbital fat decompression due to decreased vision, visual field defect or color vision disorder, and concomitant proptosis. Regular follow-up after operation. The curative effect is judged according to the degree of improvement of visual acuity, color vision, degree of correction of exophthalmos, diplopia, and other complications at 9 months after operation. Orbital CT combined with computer aided measurement software (Mimics 21) was used to measure the changes of orbital volume before and after exophthalmos surgery. The relationship between the value and eyeball regression is analyzed. *Results*. Preoperative exophthalmos ranged from 17.4 mm to 27.6 mm, with an average of (22.08 ± 2.86) mm. The postoperative exophthalmos was 14-25 mm, with an average of (19.52 ± 3.10) mm. Among them, 7 eyes (23.3%) had exophthalmos regression less than 1 mm, 6 eyes (20%) had a regression of 1-2 mm, 7 eyes (23.3%) had a regression of 2-3 mm, 5 eyes (16.7%) had a regression of 3-4 mm, and 5 eyes (16.7%) had a regression of 4-5.3 mm. The exophthalmos after operation was significantly lower than that before operation, and the difference was statistically significant ($t = 9.909$, $P < 0.05$). The preoperative orbital volume was 18.6 cm^3-25.3 cm^3 with an average of (22.39 ± 1.91) cm^3. The postoperative orbital volume was 19.8 cm^3-26.6 cm^3, with an average of (23.89 ± 1.90) cm^3.The orbital volume change range is 0.1 cm^3-3.8 cm^3, and the average orbital volume change is (1.51 ± 1.00) cm^3. Compared with preoperative orbital volume, the difference was statistically significant ($t = -8.074$, $P < 0.05$). *Conclusion*. Endoscopic decompression of the medial orbital wall through the ethmoid approach combined with decompression of the orbital fat within the muscle cone can effectively correct the exophthalmos while decompressing the orbital apex, and it is minimally invasive and has no facial scars. It has the advantages of extremely low incidence of postoperative diplopia and eye shift. There is a significant correlation between orbital volume changes and the regression of exophthalmos, which can provide reference for clinical guidance of surgical methods and prediction of surgical results.

1. Introduction

Graves' orbital disease (GO) is the most common extrathyroid manifestation of Graves' disease, which is found in about 25-50% of patients [1, 2]. GO is a common clinical disease and requires multidisciplinary treatment. A high incidence of orbital diseases has occurred in recent years. The incidence rate of eye diseases has been increasing year by year. The increase of orbital muscle contents and orbital pressure increase the incidence of ocular protrusion, the incidence of

eye closure, corneal keratopathy, and diplopia and oppressive optic neuropathy may result in decreased vision or even blindness in [3, 4]. Orbital decompression surgery releases more orbital space by removing part of the bony orbital wall, so as to increase the orbital volume, reduce the pressure of orbital contents, and retract the eyeball [5, 6]. The operation can achieve two main purposes: one is to improve the decline of visual function caused by great orbital pressure, and the other is to improve exophthalmos and repair facial appearance. The traditional orbital decompression is carried out under direct vision through the external orbital approach, which has obvious disadvantages, narrow operation field, inaccurate positioning, and large tissue trauma. In recent years, our hospital has carried out transnasal endoscopic orbital decompression in the treatment of graves orbital disease. It is a minimally invasive operation with small trauma, definite curative effect, and rapid recovery. At present, this operation is the best treatment for severe go and mild go eager to improve facial appearance.

2. General Information

Twenty two patients (30 eyes) diagnosed as Graves orbital disease and treated with orbital decompression surgery in the ophthalmology department of Li Huili Hospital of Ningbo medical center from December 2019 to September 2021 were collected retrospectively. Among them, 11 cases (15 eyes) were female and 11 cases (15 eyes) were male. The age ranged from 26 to 60 years, with an average of $(43.17.00 \pm 10.11)$ years. 3 cases were monocular and were followed up for more than 3 months. It was approved by the hospital ethics committee (ky2022pj009). The inclusion criteria are as follows: (1) meet the diagnosis of go; (2) no history of orbital decompression and ocular radiotherapy in the past; (3) available preoperative and postoperative ophthalmic examinations; (4) over 20 years old; (5) all patients were in the period of nonorganized activity for at least 6 months; (7) all patients failed to improve their visual acuity or were eager to improve their appearance due to the decline of visual acuity caused by exophthalmos, exposed corneal ulcer, diplopia, and optic neuropathy after conservative treatment. In all cases, as in the seventh case, patient informed consent can be obtained.

Meanwhile, the exclusion criteria were as follows: indications for orbital surgery other than go. The follow-up period was less than 3 months. Paitens who are under 18 years and patients in the fourth category will lack of informed consent for the study.

All patients underwent transnasal endoscopic medial orbital wall combined with muscle cone fat decompression. The operation was completed by the same operator. Methylprednisolone 500 mg was used for 3 days after operation. All patients underwent orbital CT before and 3 months after operation.

3. Inspection Indicators and Methods

3.1. Routine Inspection. Routine examinations include best corrected visual acuity, intraocular pressure, slit lamp examination, fundus visual field, ocular motion, diplopia, nasal endoscopy.

3.2. Measurement of Exophthalmos. Select the layer with the fullest lens as the measurement layer, connect the front edge of the lateral bone wall of both eyes, and measure the vertical distance from the corneal apex to the line. All results were measured by the same doctor for 3 times, and the average value was obtained.

3.3. CT Examination. The examination was performed with brillce 16 row spiral CT scanner (Philips, USA). The examinee was in supine position, the cross section was infraorbital line, and the coronal plane was perpendicular to the hard palate. The setting voltage is 120 kv, the current is 250 mA, the layer thickness is 1 mm, the layer spacing is 0.5 mm, the pitch is 0.69, and the matrix is 512×512. The window width is 300 hu, and the window level is 35 7hu. Keep the hard palate parallel to the baseline.

3.4. Data Transmission and Processing. The orbital CT examination results are output in DICOM format and transferred to eword image integration platform (Ningbo Quanwangyun Medical Technology Co., Ltd.). During measurement, the DICOM file was imported into mimics (materials interactive medical image control system) 21.0 software for three-dimensional reconstruction of orbital bone.

3.5. Orbital Volume Measurement. The anatomical marker points are (1) anterior orbital marker points: outer edge of orbit (the junction of zygomatic frontal suture and orbital arch surface), (2) dacryon point (the junction of lacrimal bone, frontal bone, and maxillary frontal tubercle), (3) supraorbital notch and infraorbital notch, and (4) posterior orbital marker points: lateral wall of optic canal. Using Mimics 21.0 measurement software, first create a mask, manually draw the orbital volume image from the horizontal level with a multislice edit brush (the description method is similar to the magnetic lasso tool of Photoshop software layer), and use the interpolate function to obtain the continuous level of orbital volume. At this time, the measurer can verify the description in the horizontal, coronal, and sagittal positions to make the corrected contour consistent with the actual contour. Finally, the orbital volume model is established by using the three-dimensional reconstruction function of the measurement software mimics 21.0, and the orbital volume is automatically calculated by the mask properties function system, see Figure 1.

4. Operation Method and Postoperative Treatment

The operative method was endonasal endoscopic orbital wall decompression + muscle cone fat decompression. Operated by the same ophthalmologist, the nasal mucosa convergence and surface anesthesia were completed through air tube intubation, intravenous compound anesthesia, routine disinfection, and towel laying. The operation steps were as follows: excision of sulcus process and medial wall of maxillary sinus under nasal endoscope and expansion of natural

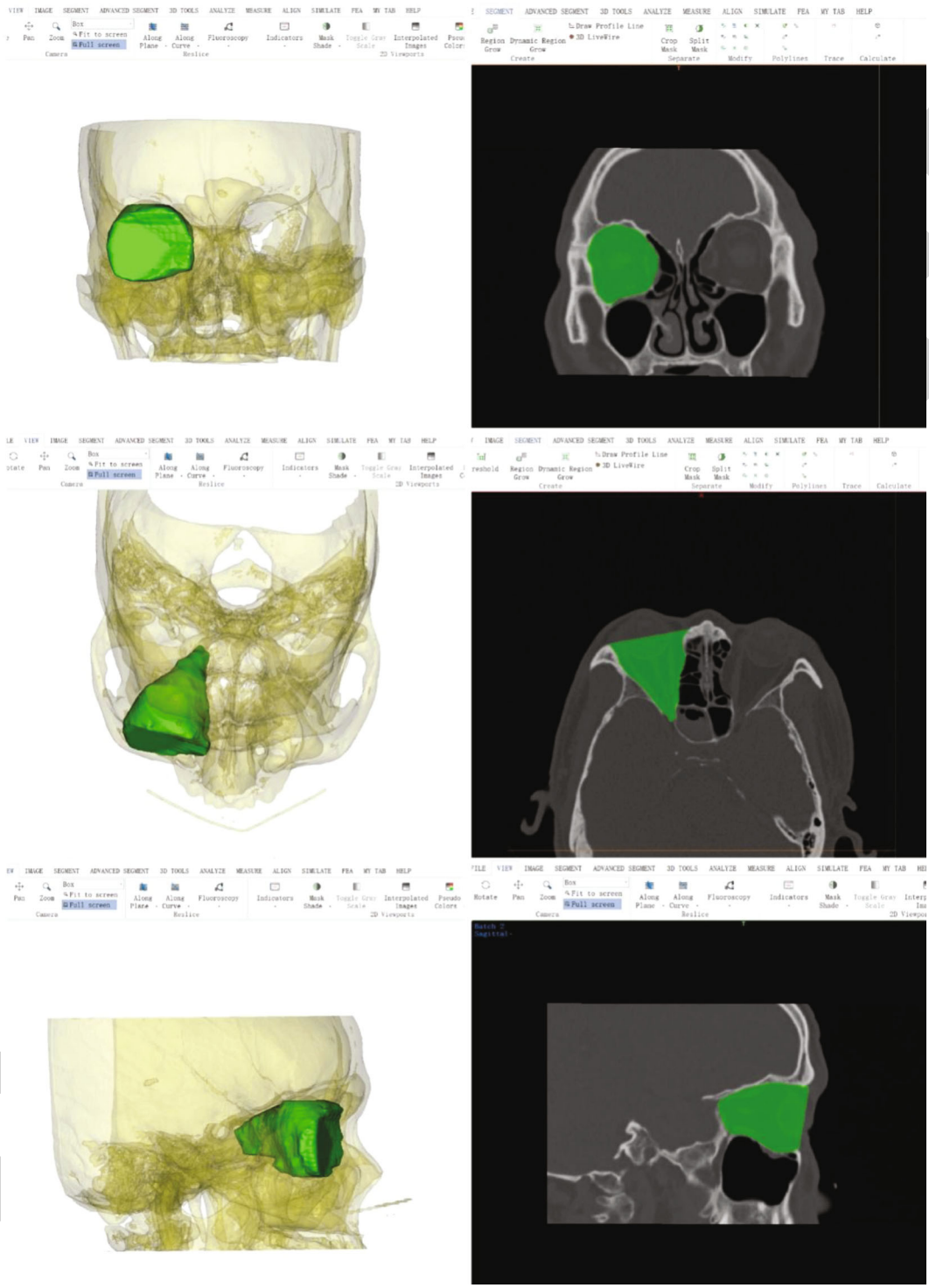

Figure 1: 3D image model of orbit reconstructed by mimics 21 software.

opening of maxillary sinus; remove the bone at the root of the middle turbinate, enter the upper nasal tract, remove the upper turbinate, and expand the natural mouth of the sphenoid sinus; grind the drill and thin the bone of the optic nerve spine, completely expose the paper template of the ethmoid bone, the orbital apex, and the front end of the optic nerve canal; remove the ethmoid paperboard, the bone of the medial part of the orbital floor, the bone of the lower part of the orbit, the bone of the orbital apex, and the anterior optic nerve canal; cut the orbital fascia to the orbital apex vertically; and cut the general health ring to decompress the orbital apex. The fat outside the medial muscle cone and part of the fat inside the muscle cone were removed by forceps. The operation cavity was filled after

Table 1: Preoperative and postoperative visual acuity distribution of GO patients.

Corrected vision	Preoperative cases	Number of postoperative cases	Intraocular pressure mmHg	Preoperative cases	Number of postoperative cases
0.2	1	1	12-21	26	28
0.5	2	2	22-23	1	1
0.7-0.8	3	4	25-30	3	1
1.0-1.2	21	20			
1.5	3	3			

no active bleeding was observed. After operation, broad-spectrum antibiotics were used routinely, and the packing in ethmoid sinus and nasal cavity was removed within 24-48 hours to prevent intraoperative and orbital infection. The patients were followed up for 3 months to 1 year.

5. Statistical Methods

IBM SPSS statistics 26 software is used for data analysis, and the measurement data are expressed as mean ± standard deviation ($x \pm s$). Paired sample t-test was used to compare the parameters (visual acuity, intraocular pressure, exophthalmos, and orbital volume) before and after operation. The correlation between the changes of each measured volume parameter before and after operation and ocular regression was analyzed by linear correlation. The difference was statistically significant ($P < 0.05$).

6. Results

6.1. Vision and Intraocular Pressure. The postoperative visual acuity of 1 eye (3.3%) in 30 eyes decreased by 0.5, 4 eyes (13.3%) improved by 0.1-0.3, and the other 25 eyes (83.3%) had no change before and after operation. Intraocular pressure decreased by 0.2-15 mmHg (1 mmh = 0.133 kPa) in 10 eyes (33.3%), including 2 eyes (6.7%) with a decrease of more than 10 mmHg and 5 eyes (16.7%) with a decrease of less than 5 mmHg. The intraocular pressure of the other 20 eyes (66.7%) was in the normal range before and after operation, see Table 1.

6.2. Exophthalmos. Preoperative exophthalmos was 17.4-27.6 mm, with an average of (22.08 ± 2.86) mm. The postoperative exophthalmos was 14-25 mm, with an average of (19.52 ± 3.10) mm. Among them, 7 eyes (23.3%) had a postoperative proptosis retreat of ≤1 mm, 6 eyes (20%) had a postoperative proptosis retreat of 1-2 mm, 7 eyes (23.3%) had a postoperative proptosis retreat of 2-3 mm, 5 eyes (16.7%) had a postoperative proptosis retreat of 3-4 mm, and 5 eyes (16.7%) had a postoperative proptosis retreat of 4-5.3 mm. The degree of exophthalmos after operation was significantly lower than that before operation ($t = 9.909$, $P < 0.05$), see Table 2.

6.3. Orbital Volume. The preoperative orbital volume was 18.6-25.3 cm^3, with an average of (22.39 ± 1.91) cm^3. The postoperative orbital volume was 19.8-26.6 cm3, with an average of (23.89 ± 1.90) cm^3. The change range of orbital volume was 0.1-3.8 cm^3, and the average change of orbital volume was (1.51 ± 1.00) cm^3. There was significant difference in orbital volume before and after operation ($t = -8.074$, $P < 0.05$), see Table 3.

Table 2: Changes of intraocular protrusion in GO patients before and after operation ($x \pm s$).

Observation time	Exophthalmos (mm, $X \pm s$)	Min-max
Preoperative	22.08 ± 2.86	17.4-27.6
After operation	19.52 ± 3.10	14-25
Change a value	2.56 ± 1.41	0.4-5.3
t value	9.909	
P value	0.000	

6.4. Correlation Analysis between Absolute Value of Eyeball Retraction and Orbital Volume Change. The changes of orbital volume before and after operation were positively correlated with the retraction of eyeball ($r = 0.805$, $P = 0.000$), and the difference was statistically significant ($P < 0.05$).

6.5. Complications. 15 eyes (50%) had no diplopia before and after operation, 10 eyes (33.3%) had no improvement in diplopia after operation, and 5 eyes (16.7%) had new diplopia after operation. In 2 eyes (6.7%), the entropion of the lower eyelid was aggravated.

7. Discussion

The pathological changes of GO are mainly manifested in extraocular muscle fibrosis and fat production. Lymphocytes participate in the autoimmune process of the disease and can secrete specific cytokines, which play an important role in the process of tissue changes and fibrosis in go patients [7]. In addition, fibroblasts participate in the occurrence and progress of go and can differentiate into different subtypes. On the one hand, they can produce hydrophilic substances such as hyaluronic acid and mucopolysaccharide to cause edema. On the other hand, they can differentiate into preadipocytes and adipocytes under certain conditions. Finally, the volume of orbital tissue increases, resulting in eyelid edema, eyelid retraction, exophthalmos, limitation of extraocular muscle function, and even exposure keratitis and thyroid optic neuropathy [8].

Because the research on the pathogenesis has not been clear, and there is no specific etiological treatment, the

Table 3: Changes of orbital volume before and after operation in GO patients ($x \pm s$).

Observation time	Orbital volume	Min-max
Preoperative	22.39 ± 1.91	18.6-25.3
After operation	23.89 ± 1.90	19.8-26.6
Change a value	1.51 ± 1.00	0.1-3.8
t value	-8.074	
P value	0.000	

current treatment is only symptomatic. The treatment of GO is carried out according to the stage and degree of the disease. Nonsurgical treatment of orbital decompression in active phase includes glucocorticoid therapy (GC) or other immunosuppressive drug therapy (such as rituximab) and orbital radiotherapy (RTH) [9, 10]. The above methods may shorten the course of the disease. The surgical treatment of orbital decompression in active stage [11, 12] is only used for the manifestations of poor curative effect of nonsurgical treatment but specific destructive visual impairment, such as thyroid related optical neuropathy (Don), which aims to relieve the compression of the optic nerve caused by the increase of orbital pressure by reducing the volume of orbital soft tissue (fat decompression) or expanding orbital volume (bone orbital decompression). However, surgery has limitations (including increased risk and unpredictable postoperative outcomes), and surgery usually does not shorten the course of orbital disease. When the condition of go is inactive, surgical treatment can be carried out as rehabilitation ophthalmic surgery [13]. The order of rehabilitation surgery includes orbital decompression, strabismus surgery, and finally, eyelid surgery as needed. Orbital decompression includes removing one or more orbital bone walls to strive for more accommodation space for overgrown muscle and adipose tissue, so as to reduce intraorbital pressure and retract the eyeball. In principle, each of the four orbital bone walls can be decompressed, but the most commonly used type of orbital decompression is endoscopic medial wall decompression and its expansion or medial wall combined with inferior wall decompression. Orbital decompression surgery is required when no improvement is observed after conservative treatment. The main advantages of transnasal endoscopic orbital decompression are as follows: (1) the anatomical structure and operation field can be well observed; (2) intraoperative evaluation of orbital tissue can accurately control the movement of fat into the nasal cavity and preserve the physiological drainage path of paranasal sinus; (3) the wound is small, the postoperative recovery is fast, and the hospital stay of patients is shortened.

The development of computed tomography (CT) and various computer-aided measurement software has achieved today's "era of surgical refinement." Researchers and surgeons can measure the volume of each orbital structure in a three-dimensional way [14]. In addition to the "emergency medical decompression" in the active phase, in the inactive phase, they can customize the expected and clear operation plan according to the patient's individual anatomical structure, give full play to the advantages of Science and technology, and minimize the surgical complications. In this study, the orbital volume was measured by three-dimensional CT combined with mimics (materials interactive medical image control system) 21.0 software. The results showed that the orbital volume increased significantly after endoscopic medial wall decompression combined with muscle cone fat decompression in go patients, which was positively correlated with the degree of eyeball retraction. Previous studies have shown that the eyeball regression value of go patients after medial orbital decompression combined with fat decompression is 4 ~ 9 mm [15, 16], which is similar to the results of this study. Endoscopic medial wall decompression has been one of the classic decompression methods of go. Endoscopic operation under direct vision has less damage and definite curative effect. However, the degree of exophthalmos corrected by medial wall decompression alone is very limited. Therefore, in order to achieve better decompression effect, this study combined to suck out the fat in the muscle cone during the operation. Previous studies have shown that there may be other factors unrelated to the operation that play an important role in eyeball retraction, such as individual orbital shape, the ratio of eyeball to orbital volume, and the hardness of eyeball soft tissue. The latter may affect the herniation of orbital soft tissue into the newly formed orbital space. This study focused on the changes of orbital volume before and after operation. The results showed that there was a positive correlation between the changes of orbital volume before and after operation and the retraction of eyeball ($r = 0.805$, $P = 0.000$), and the difference was statistically significant ($P < 0.05$). The results showed that 5 eyes (16.7%) had new diplopia, and 2 eyes (6.7%) had entropion and aggravation of eyelashes. It is reported that the incidence of new diplopia after endoscopic decompression is still 19-45% [17–19]. This huge difference in reported results may reflect the difference of surgical technology. The possible causes of new diplopia after operation are as follows: after decompression of the medial wall, the internal rectus muscle moves into the nasal cavity; surgical trauma will destroy the stability of adipose tissue, and adipose tissue may regenerate after operation. At present, there are three main methods that can avoid or reduce the occurrence of postoperative diplopia: balanced orbital decompression of inner and outer wall; the orbital sling is a periorbital band that retains about 1 cm along the medial rectus muscle to support the medial rectus muscle and prevent its excessive displacement, which can reduce the occurrence of diplopia and eyeball sinking; retain the orbital strut structure, which is the bone at the bone connection between ethmoid bone and maxilla. Diplopia is easy to occur after removing the strut structure in the decompression of inner inferior wall. Some patients show temporary diplopia, which can be improved by conservative treatment. Adequate orbital decompression may be at the cost of increasing the risk of postoperative diplopia. Reasonably measure the balance between the removal of fat and bone wall, the degree of eyeball regression, and the risk of postoperative strabismus. Therefore, the purpose of this study is to expand the sample size for further research and to clarify the best benefit point

Hindawi
Scanning
Volume 2023, Article ID 9781403, 1 page
https://doi.org/10.1155/2023/9781403

Retraction

Retracted: The Effect of CT Imaging Technology in the Diagnosis of Thoracic and Cardiac Surgery Diseases

Scanning

Received 3 October 2023; Accepted 3 October 2023; Published 4 October 2023

This article has been retracted by Hindawi following an investigation undertaken by the publisher [1]. This investigation has uncovered evidence of one or more of the following indicators of systematic manipulation of the publication process:

(1) Discrepancies in scope

(2) Discrepancies in the description of the research reported

(3) Discrepancies between the availability of data and the research described

(4) Inappropriate citations

(5) Incoherent, meaningless and/or irrelevant content included in the article

(6) Peer-review manipulation

The presence of these indicators undermines our confidence in the integrity of the article's content and we cannot, therefore, vouch for its reliability. Please note that this notice is intended solely to alert readers that the content of this article is unreliable. We have not investigated whether authors were aware of or involved in the systematic manipulation of the publication process.

In addition, our investigation has also shown that one or more of the following human-subject reporting requirements has not been met in this article: ethical approval by an Institutional Review Board (IRB) committee or equivalent, patient/participant consent to participate, and/or agreement to publish patient/participant details (where relevant).

Wiley and Hindawi regrets that the usual quality checks did not identify these issues before publication and have since put additional measures in place to safeguard research integrity.

We wish to credit our own Research Integrity and Research Publishing teams and anonymous and named external researchers and research integrity experts for contributing to this investigation.

The corresponding author, as the representative of all authors, has been given the opportunity to register their agreement or disagreement to this retraction. We have kept a record of any response received.

References

[1] M. Yang, H. Qian, D. Zhang, and Y. Gui, "The Effect of CT Imaging Technology in the Diagnosis of Thoracic and Cardiac Surgery Diseases," *Scanning*, vol. 2022, Article ID 9385451, 7 pages, 2022.

Hindawi
Scanning
Volume 2022, Article ID 9385451, 7 pages
https://doi.org/10.1155/2022/9385451

Research Article

The Effect of CT Imaging Technology in the Diagnosis of Thoracic and Cardiac Surgery Diseases

Min Yang, Hongbo Qian, Dafa Zhang, and Yingjing Gui

Cardiothoracic Surgery, The First Affiliated Hospital of Wannan Medical College (Yijishan Hospital), Wuhu, Anhui 241000, China

Correspondence should be addressed to Yingjing Gui; 202000000096@hceb.edu.cn

Received 22 June 2022; Revised 29 July 2022; Accepted 5 August 2022; Published 24 August 2022

Academic Editor: Danilo Pelusi

In order to increase doctors' cognition of the three-dimensional anatomical structure of cardiothoracic and cardiothoracic surgery and increase the diagnosis rate and cure rate of cardiothoracic surgery diseases, the authors propose a method of CT imaging technology for diagnosing cardiothoracic surgery diseases. Through the joint Hookwire positioning of 3D-CTBA, application in thoracoscopic segmentectomy and CT energy spectrum curve, retrospective analysis of diagnosis of intrathoracic lymph node metastasis in non-small-cell lung cancer, 3D-CTBA and CT-guided Hookwire localization, and preoperative CT-enhanced scanning were performed using two methods. The experimental results showed that the chest tube placement time, postoperative thoracic drainage volume, and postoperative hospital stay after the first operation all showed a good trend. The diagnostic sensitivity was 87.1%. The specificity was 92.6%. The correct index was 79.7%. The accuracy was 91.3%. The positive predictive value was 79.4%. And the negative predictive value was 95.7%. These data prove that CT imaging technology has high diagnostic value for thoracic and cardiac surgery diseases and can effectively help the formulation and implementation of thoracic and cardiac surgery diseases.

1. Introduction

Cardiothoracic surgery (Figure 1) is a highly specialized clinical discipline, involving many types of diseases, and new theories and technologies are updated rapidly; during the diagnosis and treatment process, doctors are required to be proficient in imaging and anatomy knowledge. Traditional (multimedia) clinical teaching methods are mainly based on lecture-style theoretical knowledge teaching and learning; although the teaching effect is relatively stable, it is difficult to stimulate students' enthusiasm and interest in learning. In addition, it lags behind the rapid development of diagnosis and treatment technologies (endoscopy, intervention, robot-assisted surgery, etc.), making it difficult for students to understand the three-dimensional anatomy of the cardiothoracic structure for clinical applications [1]. In recent years, CT imaging technology has been gradually applied in clinical teaching of orthopedics, neurosurgery, general surgery, and stomatology and achieved good results because of its immersion, interactivity, and conception effect. More importantly, the application of CT imaging-related technology in thoracic and cardiac surgery has achieved initial results, and many operations have achieved great success with the assistance of CT imaging technology [2]. Clinically, chest CT examination is the main examination method for the diagnosis of lung cancer; conventional CT can distinguish the size and texture of the tumor through iodine contrast, thereby judging the nature of the tumor. With the advancement of science and technology, the imaging resolution of CT has become higher and higher, and high-definition imaging has been achieved. Compared with other imaging methods, CT spectral imaging has higher spatial and temporal resolution. At the same time, it can avoid hardening artifacts and volume effects and can provide single-energy images and iodine-based images with the best contrast-to-noise ratio to enhance the display of iodine contrast agents, thereby avoiding omission and misdiagnosis of small lesions and improving the detection rate of small lesions and multiple lesions. The energy spectrum curve is the curve of the attenuation (CT value) of a substance or structure changing with the X-ray energy; from the energy spectrum curve, the average CT value and standard deviation of each energy

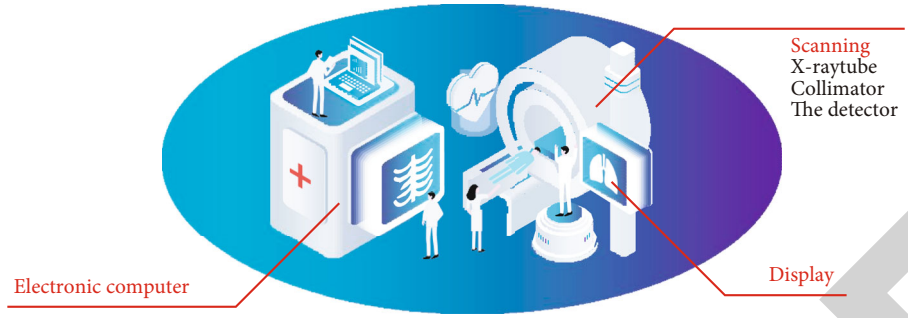

Figure 1: Principle of CT imaging.

point between 40 and 140 keV can be obtained [3]. The energy spectrum curve (CT value decay curve) is determined by the chemical molecular structure of the constituent substances; tissues with different chemical compositions have different CT value decay curves; the difference in CT value decay curves can be used to distinguish different chemical components in the human body. Therefore, in such a large environment, the authors propose to discuss the effect of CT imaging technology in diagnosing thoracic and cardiac surgery diseases. Objective analysis of CT imaging technology can reduce the time for finding and identifying lesions during surgery, minimize surgical damage, and preserve effective human tissue, so as to achieve anatomical, precise, and individualized treatment.

2. Literature Review

Visbal et al. found that 38.7% of severely calcified plaques on coronary CT scans were undiagnosed due to calcification artifacts [4, 5]. Coronary subtraction technology is to register the enhanced coronary CTA with the unenhanced calcification integral data, perform the overall deformable alignment based on the pixel grid model and the rigid alignment algorithm of local calcification, and then subtract it, which is a postprocessing technique. Calcified plaques and artifacts in the enhancement phase were eliminated by subtracting the data from two scans, followed by curved surface reconstruction for a more precise assessment of calcified stenosis. Liu et al. found that the 320-slice CT coronary subtraction technique can effectively overcome such calcification/sclerosis artifacts and improve the accuracy of diagnosis [6]. In order to obtain high-quality subtraction images, accurate alignment and registration of coronary CTA in the enhanced phase and calcium integral data in the plain scan phase are the key. Therefore, Fang et al. place the coronary unenhanced scan after the enhanced scan; the overall scanning time is shortened, and the patient can be scanned with one breath hold; however, the disadvantage of this method is that the residual iodine contrast agent cannot accurately calculate the calcification score during the plain scan [7]. Han et al. used the low-dose test method to shorten the two scan times within 20 s, and the patient completed one breath-holding scan. But the low-dose test method increases the amount of contrast injected. Therefore, the traditional "twice-holding" scanning method greatly reduces the requirement for long-term breath-holding scanning of patients and has the maximum application value. Due to individual differences, the quality of coronary subtraction images obtained from "two breath hold" scans is affected by many factors [8]. Cardillo and Emi found that the quality of CT pulmonary vein imaging depends on the best enhancement of the left atrium and proximal pulmonary vein, while the enhancement of the pulmonary artery is not obvious; that is, there is a significant difference in enhancement between the pulmonary vein and the pulmonary artery, which is helpful to distinguish the pulmonary artery from the pulmonary vein [9]. Because it is not easy to show the intersection of pulmonary artery branches and pulmonary veins at the hilar level, especially the main pulmonary artery and bilateral inferior pulmonary arteries, whether the pulmonary artery branches can be successfully removed during postprocessing, it is of great significance to determine whether there is variation in the bilateral upper pulmonary veins. The peak CT value of the pulmonary vein alone cannot guarantee the removal of the overlap of the pulmonary artery, which requires accurate estimation of the time when the contrast agent reaches the peak value and optimization of the injection plan; that is, the CT value of pulmonary artery and pulmonary vein and the difference between the two are used to quantitatively evaluate the effect of pulmonary vein imaging. Although there are different literatures at home and abroad concerning the enhancement scheme of MSCT pulmonary vein imaging, there is no unified opinion [10].

On the basis of current research, based on the application of 3D-CTBA combined with Hookwire localization in thoracoscopic segmentectomy and the CT energy spectrum curve, retrospective analysis of the diagnosis of intrathoracic lymph node metastases in non-small-cell lung cancer, by observing the surgical pathology and surgical process, the diagnostic value of CT imaging-related techniques was judged.

3. Methods

3.1. Scanning Trajectory Design. Common CT scan trajectories include circular trajectory, spiral trajectory, circular plus straight line, and double circle plus straight line. Since the circular trajectory does not meet the data completeness condition, it is not considered here [11]. Since the rotational

motion of the object does not cause the overall movement of the two-axis electric object carrier, the motion range of the two-axis electric object carrier is completely determined by the translation stroke of the object. The following is an investigation of the translation travel required by the object in the latter three trajectories, and the trajectory with the shortest travel is selected as the scanning trajectory of the CT scanning system. It is assumed that the scanning radii of the above three trajectories are all R. The object support is a cylinder of radius r and height H. Let $\mu = r/R$.

For a circle plus a straight line, point out that its translation stroke T_1 (i.e., the length of the straight line) is at least

$$T_1 = \frac{2H}{1-\mu}. \tag{1}$$

That is, its translation stroke is more than twice the length of the phantom.

For the double circle plus straight line trajectory, point out that its translation stroke T_2 (that is, the length of the straight line trajectory) is at least

$$T_2 = H. \tag{2}$$

That is, its translation stroke is equivalent to the length of the phantom.

For the helical trajectory, its translation travel T_3 is at least

$$T_3 = H + \left(1 - \frac{\arccos \mu}{\pi}\right)(1+\mu)h, \tag{3}$$

where h is the pitch of the helical trajectory, and its translation stroke is greater than the length of the phantom; the three trajectories are shown in Figures 2 and 3.

Comparing the three equations (1), (2), and (3), it can be seen that the translation stroke required by the double circle plus the linear trajectory is the smallest, and it is only related to the length of the phantom, and the width of the phantom and the parameters of the scanning trajectory are all related; it does not matter. In order to compare the three trajectories more intuitively, an example is given below. Assume that the scanning radius is $R = 450$ mm, the size of the phantom is $r = 30$ mm, and $H = 100$ mm. In order to make the rotation degree of the spiral track similar to the double circle plus straight line track, the pitch of the spiral track is selected as $h = 50$ mm. According to the above three formulas, there are $T_1 = 214.3$ mm, $T_2 = 100.0$ mm. It can also be seen that T_2 is significantly smaller than T_1. According to the above discussion, in the application of medical CT scanning, the double circle plus straight line trajectory is selected as the scanning trajectory [12].

3.2. Application of 3D-CTBA Combined with Hookwire Localization in Thoracoscopic Segmentectomy

3.2.1. General Information. A retrospective analysis was performed on 48 patients with VATS segmentectomy in the Department of Thoracic and Cardiovascular Surgery of a hospital in a city, including 22 males and 26 females, with

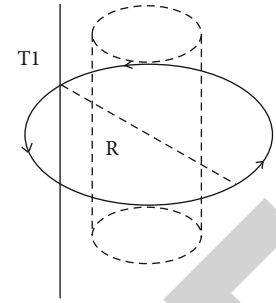

Figure 2: Circle plus straight line trajectory.

an average age of 59.75 ± 9.46 years. All patients had no obvious symptoms and signs such as cough, sputum, and blood in sputum, and the presence of pulmonary nodules was confirmed by chest thin-section CT. There were 56 small pulmonary nodules in 48 patients, including 48 GGN, 6 solid nodules, and 2 partially solid nodules. Among them, 2 nodules were <8 mm in diameter, 24 were 8-10 mm in diameter, and 30 were 11-20 mm in diameter, with an average diameter of 12.08 ± 3.48 mm. All patients underwent three-dimensional reconstruction with Mimics Medical 20.0 software before operation and were positioned with Hookwire under CT guidance and then sent to the operating room for surgical treatment, with preoperative routine improvement of three routines, chest enhanced CT, head MRA, abdominal color Doppler ultrasound, bone ECT scan, and cardiopulmonary function examinations [13].

(1) *Inclusion Criteria*. (1) Unable to tolerate lobectomy; (2) nodules located in 1/3 around the lung field, with a diameter of ≤2 cm; (3) if it is a malignant tumor, it should be non-small-cell carcinoma, and the tumor stage is T1N0M0; (4) CT shows that the ground glass component is ≥50%, and the doubling time is ≥400 days; (5) lymph node biopsy excludes distant metastasis; (6) no previous thoracotomy or previous diseases that cause pleural adhesions; (7) Indications for VATS surgery; and (8) voluntary participation in this study and signed informed consent [14].

(2) *Exclusion Criteria*. (1) Patients with severe heart and lung dysfunction, unable to tolerate surgery, with abnormal coagulation function, and unable to tolerate one-lung ventilation tuberculosis; (2) mental disorders; (3) refusal of the study or resistance of the operation.

3.2.2. Specific Method

(1) *3D-CTBA and CT-Guided Hookwire Localization.* All patients underwent chest enhanced CT examination before surgery, and the imaging data were imported into Mimics Medical 20.0 software in DICOM format, and the surgeon and an assistant jointly constructed a three-dimensional reconstructed image [15]. Identify the lung segment where the nodule is located, analyze the course of the arterial (venous)

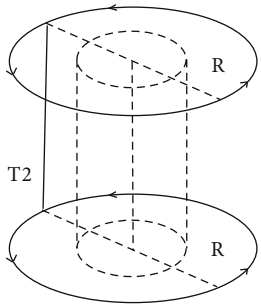

Figure 3: Double circle plus straight line trajectory.

artery and bronchi and the anatomical structure relationship of the target segment, observe whether there is variation, and mark it with different colors. The surgical team discussed the surgical plan, planned the best surgical path, and performed simulated surgery.

(2) *Preoperative Preparation*. All patients were intramuscularly injected with pethidine 50 mg before positioning, and appropriate body positions were taken according to the position of the nodule after three-dimensional reconstruction and the surgical approach, and the patients were instructed to keep a relatively static state and a relatively stable breathing range as much as possible [16]. CT scan is performed to display the location of the target lesion. The radiologist and the surgeon will negotiate to determine the optimal intercostal and angle of needle insertion, measure the distance between the lesion and the chest wall, and determine the depth of needle insertion. Then use the CT laser positioning line to establish the body surface positioning mark, and place a metal positioning mark ruler at the body surface positioning line. Perform routine disinfection, drape, local infiltration anesthesia, and insertion into the parietal pleura according to the planned puncture route. CT scan was performed again to determine whether the direction of the puncture needle was facing the lesion, and if there was a deviation, a small angle was adjusted. Then, insert the needle into the lesion, withdraw the needle core, rapidly expand and release the Hookwire positioning needle, repeat the CT scan, and confirm that the positioning needle is located in the lesion or not more than 5 mm away from the lesion. The skin was flushed, and the metal wire was cut, bandaged with gauze and fixed with tape, and sent to the operating room for surgical treatment [17]. According to imaging manifestations, clinical symptoms, and intraoperative exploration, determine whether the patient has pneumothorax or hemothorax due to localization, and record the time of localization.

(3) *Surgical Method*. After the double-lumen endotracheal intubation was stabilized under general anesthesia, the patient was placed in a lateral decubitus position, the surgical field was routinely disinfected, and a sterile drape was laid. Usually, a 1.5 cm incision is made at the posterior axillary line of the seventh intercostal space, the thoracic cavity is separated layer by layer, one-lung ventilation is performed, and a 1.2 cm Trocar is inserted into the thoracoscope, exploring whether there is pleural effusion and adhesion and observing the development of lung surface and hilar lymph nodes. Under the guidance of a thoracoscope, make a 5.0 cm incision on the anterior axillary line of the fourth intercostal space, introduce instruments, find the positioning needle, and determine the target segment based on preoperative 3D-CTBA images. According to the surgical path planned before operation, dissect the target bronchus, arteries, and veins and try to dissociate along the vascular sheath to the distal end during the dissection, carefully identify and operate with caution, preserve the intersegmental veins, reveal the plane of the lung segment by the inflation and collapse method and mark for separation, use a straight cut suture to completely resect the lung segment, and send for rapid pathological examination. If the pathological result is a benign nodule, atypical adenomatous hyperplasia, adenocarcinoma in situ, or minimally invasive adenocarcinoma, the operation is over. If the pathological result is invasive adenocarcinoma, routinely sample and dissect N1 and N2 lymph nodes, and send for rapid pathological examination; lobectomy+systemic lymph node dissection was performed instead (lymph node metastasis was excluded in this study).

(4) *Observation Indicators*. According to imaging manifestations, clinical symptoms, and intraoperative exploration, determine whether the patient has pneumothorax or hemothorax due to positioning, and record the positioning time. The operation time and intraoperative blood loss were statistically analyzed according to the anesthesia records, and the postoperative chest tube intubation time, postoperative chest drainage volume, and postoperative hospital stay were statistically analyzed according to the postoperative nursing records; postoperative complications were recorded according to patient symptoms and imaging data, and pathological data were recorded according to intraoperative rapid pathology and postoperative routine pathology [18].

3.2.3. Statistical Analysis. All data were entered and analyzed using SPSS 22.0, and the data in this study were expressed as the mean ± standard deviation.

3.2.4. The Diagnosis of Intrathoracic Lymph Node Metastasis in Non-Small-Cell Lung Cancer by CT Energy Spectrum Curve

(1) General Information. 53 patients with non-small-cell lung cancer who were diagnosed and treated in a hospital

Table 1: General information/case of 53 patients with non-small-cell lung cancer.

Project	Number of cases	Project	Number of cases	Project	Number of cases
Gender		Tumor location		TNM staging	
Male	27	Upper right lobe	14	IA	7
Female	26	Right middle lobe	6	IB	10
Age		Lower right lobe	12	IA	11
<50	5	Upper left lobe	9	IB	13
50-60	13	Lower left lobe	12	IMA	7
60-70	28			IMB	5
>70	7			V	0

Table 2: Types/cases of 53 patients with non-small-cell lung cancer.

Project	Number of cases
Types of non-small-cell lung cancer	13
Squamous cell carcinoma	17
Adenocarcinoma	36

in a certain year and month were selected; all patients underwent radical surgery for lung cancer and were confirmed by pathology. Among them, 27 were male and 26 were female; 17 were squamous cell carcinoma, 36 were adenocarcinoma, 41 were peripheral lung cancer, and 12 were central lung cancer. The general information of the patients is shown in Tables 1 and 2.

(2) Specific Methods. All patients underwent enhanced CT scans before surgery. Spectral imaging was performed using a GE HealthCare discovery CT 750 HD; the tube voltage was switched instantaneously between 80 kVp and 140 kVp, the tube current was 600 mA, the layer thickness was 5.0 mm, the interval was 5.0 mm, the matrix was 512 × 512, the pitch was 1.375 : 1, and the rotational speed was 0.6 s/cycle or 0.8 s/cycle. The enhanced scan was performed using a German Orrich double-barrel high-pressure syringe, and 370 mgI/ml of Univitamin was injected through the median cubital vein at a dose of 70 ml, followed by 30 ml of normal saline at a rate of 4.0 ml/s, the arterial phase, and the venous phase. The delay period starts scanning at 25, 55, and 140 s, respectively. The primary lesions and CT-visible lymph nodes were analyzed by energy spectrum. The original data was reconstructed into an image set with a slice thickness of 0.625 mm under the single-energy reconstruction algorithm and transferred to the postprocessing workstation GEAw 4.5 (GE HealthCare, USA); all data were analyzed and processed using GSIViewer software. Select the homogeneous part of the lesion as the region of interest; try to avoid necrotic tissue, cavities, calcifications and blood vessels, etc.; measure the energy spectrum curve of the region of interest and calculate the slope of the curve; according to the slope of the energy spectrum curve between 40 and 140 keV, diagnosis was made and divided into the metastatic and nonmetastatic groups [19].

(3) Related Standards. Diagnostic criteria: when the difference between the energy spectrum slopes of the primary tumor and the lymph node is less than 0.2, the two curves are considered to be consistent [20]. If the primary tumor is homologous to the lymph node, the lymph node is considered a metastatic lymph node; otherwise, there is no metastasis. *Gold standard*: the gold standard is surgical dissection and marking of intrathoracic lymph nodes and pathological diagnosis to determine whether metastatic lymph nodes are present. Create a matching four-table, using pathological diagnosis as the gold standard, the diagnostic results of spectral CT were evaluated.

(4) Evaluation Indicators. Calculate accuracy, sensitivity, specificity, misdiagnosis rate, missed diagnosis rate, positive predictive value, negative predictive value, and correct index, in order to evaluate the diagnostic value of the CT energy spectrum curve for intrathoracic lymph node metastasis of non-small-cell carcinoma.

4. Results and Discussion

Hookwire positioning under CT guidance was successfully performed, and the average positioning time was 19.71 ± 3.94 min; intraoperative exploration clearly showed the complete Hookwire, no positioning needle displacement and falling off, and no residue. Combined with the patient's imaging data, symptoms, and lung surface exploration, 5 cases of pneumothorax occurred, but no hemothorax; after timely symptomatic treatment such as oxygen inhalation and puncture, the implementation of VATS was not affected. All patients successfully completed VATS according to the preoperative plan; there was no conversion to thoracotomy. The intraoperative anatomy was basically the same as the preoperative 3D reconstruction image, the nodule was located accurately, and the resection margin met the oncological requirements; the specific lung segment statistics are shown in Figure 4. The average operation time was 109.67 ± 17.21 min, intraoperative blood loss was 65.42 ± 21.62 ml, postoperative chest tube placement time was 4.13 ± 1.26 d, postoperative chest drainage volume was 548.33 ± 228.78 ml, and the postoperative hospital stay was 6.25 ± 1.48 d. Postoperative complications occurred in 6 cases, including 1 case of chylothorax, 1 case of pulmonary

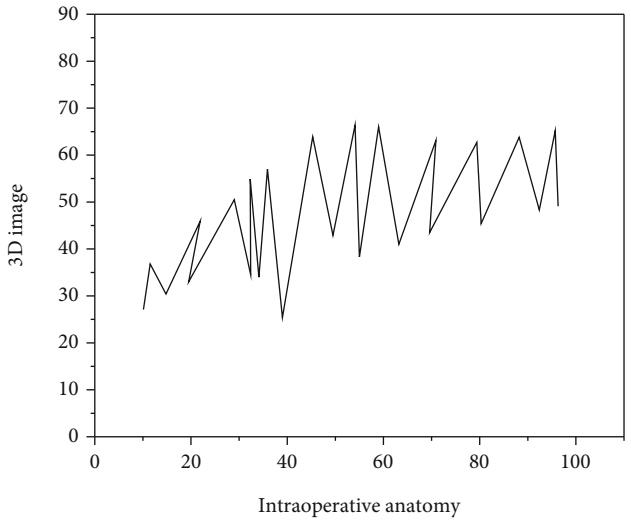

Figure 4: Intraoperative anatomy and preoperative 3D reconstructed images.

infection, 2 cases of arrhythmia, and 2 cases of pulmonary air leakage; all patients were discharged after active symptomatic treatment, and there were no deaths [21].

Pathological data: there were 2 cases of inflammatory granuloma, 2 cases of bronchiolar adenoma, and 3 cases of inflammatory nodules. There were 1 case of squamous cell carcinoma, 2 cases of atypical adenomatous hyperplasia, 3 cases of adenocarcinoma in situ, 14 cases of invasive adenocarcinoma, and 29 cases of minimally invasive adenocarcinoma, all without lymph node metastasis.

The patients in this group underwent radical surgery for lung cancer from Table 3, the pathological diagnosis was non-small-cell lung cancer, and 126 groups of lymph nodes were analyzed by the energy spectrum curve. Among them, GSI diagnosed metastatic lymph nodes in 31 groups (slope 1.19 ± 0.14) and nonmetastatic lymph nodes in 95 groups (slope 1.87 ± 0.23). There were 115 groups that were consistent with the pathological results and 11 groups that were not. Among them, the pathological results were metastatic lymph nodes, while the energy spectrum analysis showed that there were 4 groups of nonmetastatic lymph nodes, with a missed diagnosis rate of 12.9% (among them, R4 lymph node group 1, L10 lymph node group 1, R11 lymph node group 1, and L11 lymph node group 1). The pathological results were nonmetastatic lymph nodes, while the energy spectrum analysis showed that there were 7 groups of metastatic lymph nodes, with a misdiagnosis rate of 7.4% (among them, group 7 lymph node group 3, R10 lymph node group 2, R4 lymph node group 1, and L4 lymph node group 1). The sensitivity was 87.1%. The specificity was 92.6%. The correct index was 79.7%.. The accuracy was 91.3%. The positive predictive value was 79.4%. And the negative predictive value was 95.7%.

Clinically, chest CT examination is the main examination method for the diagnosis of lung cancer; conventional CT can distinguish the size and texture of the tumor through iodine contrast, thereby judging the nature of the tumor [22]. With the advancement of science and technology, the

Table 3: Parts of lung segments resected in 48 patients with thoracoscopic segmentectomy (cases).

Lung segment	Right lung	Left lung
S1	4	1
S2	5	0
S3	8	0
S1 + 2	0	5
S1 + 2 + 3	0	7
S4 + 5	0	2
S6	5	7
S7 + 8	1	1
S8	1	1
S9	I	0
S10	2	1
S9 + 10	1	0

imaging resolution of CT is getting higher and higher, and high-definition imaging has been realized. Compared with other imaging methods, CT spectral imaging has higher spatial and temporal resolution. At the same time, it can also avoid hardening artifacts and volume effects and can provide single-energy images and iodine-based images with the best contrast-to-noise ratio to enhance the display of iodine contrast agents, thereby avoiding omission and misdiagnosis of small lesions and improving small lesions and multiple lesions and detection rate [23]. Spectral CT uses the instantaneous switching of high and low dual energy (80 kVp and 140 kVp) of a single tube (<0.5 ms energy time resolution) to generate dual energy data, realize data space energy spectrum analysis, and provide material density images and single-energy image; material separation can be achieved, and the characteristic energy spectrum curve of material can be obtained [24]. The energy spectrum curve is the curve of the attenuation (CT value) of a substance or structure with the X-ray energy. From the energy spectrum curve, the average CT value and standard deviation of each energy point between 40 and 140 keV can be obtained. The energy spectrum curve (CT value attenuation curve) is determined by the chemical molecular structure of the constituent substances, different chemically composed tissues have different CT value attenuation curves, and the difference in the CT value attenuation curve can be used to distinguish different chemical components in the human body. Substances with different components have different slopes of decay curves, but the slopes are similar, indicating that there is homology between the two. By comparing the energy spectrum slopes of mediastinal and intrapulmonary lymph nodes with the primary lesion, it was judged whether it was a metastatic lymph node.

5. Conclusion

Through the joint Hookwire positioning of 3D-CTBA, application in thoracoscopic segmentectomy and CT energy spectrum curve, a retrospective analysis of the diagnosis of intrathoracic lymph node metastases in non-small-cell lung

Hindawi
Scanning
Volume 2023, Article ID 9757214, 1 page
https://doi.org/10.1155/2023/9757214

Retraction

Retracted: Influence of Comprehensive Nursing Intervention Combined with WeChat Platform Propaganda and Education of ERAS Concept on Postoperative Functional Recovery of Patients with Gallbladder Polyps

Scanning

Received 3 October 2023; Accepted 3 October 2023; Published 4 October 2023

This article has been retracted by Hindawi following an investigation undertaken by the publisher [1]. This investigation has uncovered evidence of one or more of the following indicators of systematic manipulation of the publication process:

(1) Discrepancies in scope

(2) Discrepancies in the description of the research reported

(3) Discrepancies between the availability of data and the research described

(4) Inappropriate citations

(5) Incoherent, meaningless and/or irrelevant content included in the article

(6) Peer-review manipulation

The presence of these indicators undermines our confidence in the integrity of the article's content and we cannot, therefore, vouch for its reliability. Please note that this notice is intended solely to alert readers that the content of this article is unreliable. We have not investigated whether authors were aware of or involved in the systematic manipulation of the publication process.

Wiley and Hindawi regrets that the usual quality checks did not identify these issues before publication and have since put additional measures in place to safeguard research integrity.

We wish to credit our own Research Integrity and Research Publishing teams and anonymous and named external researchers and research integrity experts for contributing to this investigation.

The corresponding author, as the representative of all authors, has been given the opportunity to register their agreement or disagreement to this retraction. We have kept a record of any response received.

References

[1] Y. Zhang, D. Guo, X. Yang et al., "Influence of Comprehensive Nursing Intervention Combined with WeChat Platform Propaganda and Education of ERAS Concept on Postoperative Functional Recovery of Patients with Gallbladder Polyps," *Scanning*, vol. 2022, Article ID 6919130, 7 pages, 2022.

Hindawi
Scanning
Volume 2022, Article ID 6919130, 7 pages
https://doi.org/10.1155/2022/6919130

Research Article

Influence of Comprehensive Nursing Intervention Combined with WeChat Platform Propaganda and Education of ERAS Concept on Postoperative Functional Recovery of Patients with Gallbladder Polyps

Yan Zhang, Dongmei Guo, Xiaocui Yang, Xiaojing Sun, Yajuan Dong, Jun Zhang, Yujiao Gao, Zhanhua Guo, Haikun Zhou, and Quanfu Li

Department of Hepatobiliary Surgery, Second Hospital of Baoding, Baoding, Hebei 071051, China

Correspondence should be addressed to Quanfu Li; 201804110@stu.ncwu.edu.cn

Received 5 July 2022; Revised 21 July 2022; Accepted 29 July 2022; Published 10 August 2022

Academic Editor: Danilo Pelusi

To analyze the effect of comprehensive nursing intervention based on ERAS's concept in laparoscopic gallbladder polyp (GP) surgery on patients' postoperative quality of life and nursing job satisfaction. Ninety patients with polyps were included in this article until October 2021. In this format, the 45 cases are divided into governing bodies and committees according to their processing time. As recommended by the ERAS committee, the committee provides daily and patient care, as well as training on the WeChat platform. The pain level (visual analogue scale (VAS) score), the quality of life (life quality index (GLQI) score), and the incidence of complications were compared between the two groups before and after the intervention. The VAS score of the control group at 2 h after operation was lower than that of the control group, and the difference was statistically significant ($P < 0.05$). After the intervention, the GLQI scores of the two groups were higher than those before the intervention, and the GLQI scores of the control group were higher than those of the control group, with significant differences (all $P < 0.05$). Studies have shown that comprehensive nursing intervention applied to patients with gallbladder polyps can reduce postoperative pain with less complications and can also improve nursing satisfaction, which is worthy of clinical promotion.

1. Introduction

ERAS, minimally invasive surgery, and artificial intelligence are three important development directions of modern surgical technology in the twenty-first century. ERAS is not a new surgical technique, but a new concept of perioperative management, which is an important supplement to traditional surgery. ERAS's core principle is to reduce the risk of complications through a multimodal approach to surgical stress response. ERAS operating mode is multidisciplinary collaboration (MDT). This includes disciplines such as surgical anesthesia care, surgical care, nutrition, psychological rehabilitation, and cooperation between patients and their relatives, which are the prerequisites for ERAS. The importance of active participation of patients and their relatives must be emphasized here; otherwise, the effects of ERAS cannot be fully realized [1]. The interdisciplinary optimized perioperative management measures and operation of the MDT process reengineering commonly used measures include preoperative education, preoperative assessment, prevention of complications, shortening the time of fasting before operation, encouragement of the use of minimally invasive surgery, short-acting general anesthesia, local anesthesia multimode analgesia, trying not to place drainage, early postoperative oral feeding, early ambulation, and early catheter removal. Each optimization measure should be supported by evidence-based medical evidence, and perioperative MDT combination should be applied to the same patient in preoperative, intraoperative, and postoperative management. Close collaboration is maintained throughout

to achieve the best results, to reduce pain and risk, and to achieve rapid recovery, as shown in Figure 1. ERAS can reduce the stress response, reduce the incidence of surgical complications, and reduce the risk of surgery by improving the conventional treatment process effectively and reasonably. In this way, the postoperative recovery of patients can be accelerated, the postoperative hospital stay can be shortened, the cost of hospitalization can be reduced, the quality of life of patients can be improved, the surgical experience can be improved, and satisfaction can be improved [2]. ERAS's core is to minimize the stress response of the body during the operation and block the conduction of afferent nerve to the stress signal, so as to reduce the psychological and physical damage of patients. Anesthesia management is an important part of ERAS, and the Postanesthesia Care Unit (PACU) is an important part of ERAS anesthesia management. It is aimed at providing regular care to the patient after anesthesia, reducing the incidence of postoperative complications, and improving the quality of anesthesia healing, which is important for the rapid recovery of postoperative patients. Gallbladder polyp, also known as cystic mucosal eminence, is a growth in the gallbladder, including cholesterol polyps, inflammatory polyps, and gallbladder adenomatous polyps, which will increase the risk of cancer if not treated in a timely and effective manner [3]. Clinical surgery is often used to treat gallbladder polyps, but, if the postoperative lack of corresponding nursing guidance, will cause slow recovery of patients and reduced quality of life. Now, for young adults in interpersonal communication more dependent on the online world, WeChat platform is a powerful interactive information communication platform and not only has the function of text; you can also add images, voice, and video, through health preach. WeChat platform could give patients and their families more directly and more rapid and effective nursing knowledge of disease. It not only saves human resources but also enables patients to continue to obtain relevant knowledge after discharge and communicate with medical staff anytime and anywhere, which is an efficient way of working.

2. Literature Review

Erman et al. said that in their clinical work, we often see patients with adhesive ileus after abdominal surgery. This has a certain impact on the recovery of patients, to our nursing work caused a certain degree of difficulty [4]. Teo et al. believe that among the many causes of adhesive ileus, the probability of surgical causes is higher. For surgical nursing managers, how to improve perioperative patient management and prevent complications is the key problem that we need to solve and think about [5]. Khojamli et al. believe that the concept of accelerated rehabilitation surgery (ERAS) is a set of optimized interventions based on evidence-based medicine for perioperative management to achieve rapid recovery [6]. Thompson and Haddad said that in order to prevent and reduce postoperative complications in patients undergoing abdominal surgery, promote the early recovery of gastrointestinal function, and achieve rapid recovery of patients, ERAS concept and comprehensive nursing interventions were adopted in the study, which significantly improved the recovery effect of intestinal peristalsis, reduced the incidence of complications, and improved patient satisfaction [7]. Gleadhill et al. said that gallbladder polyp is a common clinical disease. Although it is a benign disease, if not treated in time, it has a certain risk of deterioration. Therefore, surgery should be taken as soon as possible after diagnosis to remove polyps to ensure patient safety [8]. Zer and Kurt believed that in the past, due to the underdeveloped medical technology, gallbladder polyp surgery often brought great trauma and pain to patients, but in recent years, with the continuous development of minimally invasive technology, its application in gallbladder polyp surgery has effectively improved many defects of traditional surgery [9]. Yin et al. believe that, now, more and more patients with gallbladder polyp choose minimally invasive gallbladder polyp removal for treatment, which not only has less trauma, less pain, and lower risk but also has faster postoperative recovery and fewer complications [10]. Gautam et al. thought that surgical treatment alone is not enough to guarantee the prognosis of patients, and the role of nursing intervention is equally important. Only effective nursing intervention in perioperative period can ensure the smooth implementation of surgery and postoperative rehabilitation effect of patients [11]. Boz et al. thought that in the past, routine nursing intervention was generally carried out for patients in the perioperative period, but there are shortcomings of routine nursing intervention, such as the content of nursing is not comprehensive enough, the details of nursing, and the lack of pertinence, which can no longer meet the actual needs of modern clinical nursing work [12]. Wennmacker et al. thought that ERAS's concept combined with comprehensive nursing intervention can change the traditional concept of medical staff and provide comprehensive, systematic, meticulous, and patient nursing services for patients, enabling remarkable recovery effects of intestinal peristalsis. The time to get out of bed and exhaust was shortened significantly, the incidence of adhesive ileus was significantly reduced, and the patients fully mastered the health

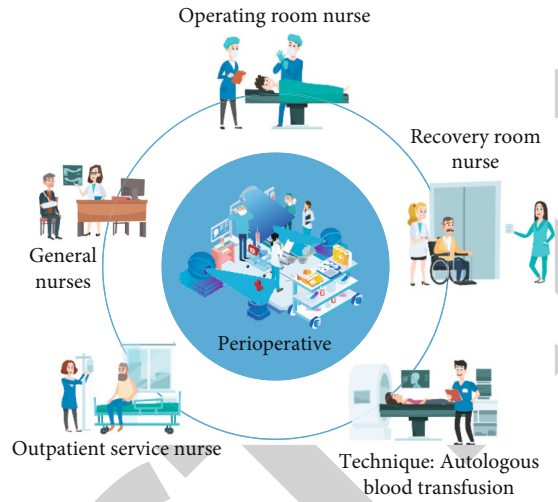

Figure 1: ERAS concept map.

education content, so that the satisfaction of nursing work will be significantly improved, which is worthy of continuous promotion and application in clinical work [13].

3. Method

3.1. Research Data. A total of 90 patients with gallbladder polyps who underwent surgery in Chinese medicine between October 2019 and October 2021 were selected and divided into a board and a monitoring team, followed by admission time, and 45 patients in each group. There are 21 men and 24 women on the board. Their age is 29-65, the average age (47.12-4.36). Disease classification is 0.8~4 a, mean (2.12 ± 0.54) a. The study involved 27 men and 18 women. The mean age is 30–60 years, and the mean age is (45.35 ± 6.21). Bacteria range from 1 to 4 a, with an average of (2.36 ± 0.62) a. There were no significant differences in the general data between the two groups (total $P > 0.05$). Patients can participate in this study and sign a consent form. The study was approved by the Medical Health Committee [14]. Inclusion criteria: diagnosis of gallbladder polyp requiring surgical treatment. Exclusion criteria: accompanied by severe cognitive impairment or mental illness; with other serious organic diseases of the whole body.

3.2. Nursing Methods

3.2.1. Control Group. Routine care was taken to keep the ward clean and tidy, disinfection was performed once a day, humidity was 50%-60%, and temperature was 24-36°C. Instruct patients to take medicine on time and give routine psychological nursing and diet intervention. Health education was given to patients and their families, including common knowledge of diseases and possible complications, and discharge manuals were issued before discharge [15].

3.2.2. Observation Group. Comprehensive nursing intervention combined with ERAS concept is implemented as follows:

(1) Training and testing

Due to the influence of traditional beliefs among health care professionals, there is insufficient awareness of the best evidence for early activity. The department strengthened training and assessment, including abdominal nursing content, the effect of early activities, specific methods, and patient communication skills. The assessment results were included in the department performance assessment, and the training rate and awareness rate reached 100%.

(2) Psychological counseling intervention

Patients and their families think that patients need to recuperate after surgery; nurses should be patient psychological counseling, so that patients will fully remove ideological concerns and active with sports rehabilitation nursing. In ordinary work, we should learn to listen to patients' ideas and perspective-taking, respect patients, to establish a good nurse-patient relationship, and use their own professional knowledge to provide help for patients, so that patients can actively realize the necessity and importance of early postoperative activities.

(3) Dietary intervention

① Eat a soft and digestible diet for lunch before surgery; have a semiliquid diet for dinner, fasting after 00:00, and no drinking after 04:00; ② postoperative dietary intervention according to the site and method of operation to formulate the feeding plan.

(4) Oral intervention

After the operation, prepare a transparent lipstick to apply lips or cucumber slices to apply lips, remember not to use cotton swabs with water to apply lips, air evaporation is easy to dry lips. Prepare a bottle of sugar-free gum (such as patients without dentures under the supervision of family members, the first day after the operation, chew a piece of gum for 10 minutes in the morning and afternoon and spit it out for 7 consecutive days), promote the recovery of intestinal peristalsis, stimulate the increase of saliva secretion, and reduce dry mouth and bad breath.

(5) Abdominal massage

The first day after the operation began to massage along the umbilical circumference, the technique is standard, light, and moderate, two times a day alternately counterclockwise massage, 20 minutes each time, last for a week.

(6) Exercise intervention

After the patient wakes up from anesthesia, raise the head of the bed 30-45 to help the patient turn over. The patient was instructed to exercise in bed on the first postoperative day: ① ankle pump movement: instruct client to lie flat or half-lying→legs straight and together→press the instep so that the toe is as straight as possible (hold 5 s)→return your feet to their original position and swing them to the left (hold 5 seconds)→swing your feet to the right (hold 5 seconds)→return your feet to their original position and rotate clockwise for the maximum possible time→rotate your feet counterclockwise as much as possible→repeat 10 times; this can promote lower limb blood circulation and prevent lower limb venous thrombosis. ② Carry buttock movement: instruct client to lie flat on the bed→apply pressure to the wound from both sides of the waist to prevent pain→step on the bed with your legs bent→lift hips with leg strength (hold 5 s)→gently put your hips back on the bed→repeat the procedure 10 times to promote gastrointestinal motility and help ventilation. ③ Cough movement: instruct client to be in semilying or sitting position→apply pressure to the wound from both sides of the waist to prevent pain→take several deep and slow breaths, then take a deep breath through your nose and hold your breath for 3 seconds→2-3 short, strong deep coughs from the chest, and when sputum is present, cough up the sputum→repeat the procedure 10 more times to help your lungs expand and prevent infection. On the second day after

the operation, on the basis of completing the activity goals of the first day, the patients were instructed to sit, sit, stand, and go to the toilet in the ward three times a day for 20-30 minutes each time. Gradually increase the amount and time of activity each day according to the patient's physical fitness and self-perception. In the process of exercise to observe the patient's situation, such as the patient self-feeling palpitation, complexion change sweating, immediately stop the activity, and standardized disposal [16].

(7) Progress of activity

Nursing staff should carefully observe the patient's activity and keep relevant records. For the first time, all activities are encouraged by a nurse at the bedside. Based on the concept of integrated nursing intervention combined with ERAS ERAS, health education via WeChat is established to enable patients and their families to follow the WeChat platform by scanning the QR code, and the nurses in charge will introduce the use of the WeChat platform to patients and their families. The content of WeChat platform mainly includes basic knowledge of diseases (manifestations and treatment process of diseases, etc.), hospital examination (examination items and cost-related to diseases), nursing knowledge (key points of continuing care of diseases, manifestation, and treatment of common complications), and discharge propaganda and education (matters needing attention after discharge, etc.). For patients with gallbladder polyp, postoperative nursing knowledge should be regularly pushed in the continuing care, including the intake of protein and the amount of oxalate-rich food. Pictures and videos of routine gallbladder disease prevention were sent, and a special person was responsible for answering patients' questions on WeChat platform, and a total of 1 month of nursing intervention [17].

3.3. Observation Target. Performance-related measures and positive life scores before and after the intervention were evaluated and compared between the two groups.

3.4. Statistical Analysis. Statistical software SPSS21.0 was used for data analysis. Measurement data were represented by mean ± standard deviation, $\bar{x} \pm s$, and comparison between the two groups was performed by t test. Data collection x^2 was used to compare the groups, and $P < 0.05$ was considered significant.

4. Results and Discussion

4.1. Operation-Related Indicators. Comparison of surgery-related indicators between the two groups showed that the observation group was significantly better ($P < 0.05$), as shown in Table 1.

4.2. Quality of Life Scores before and after Intervention. There was no significant difference in mean life expectancy scores between the two groups prior to the intervention ($P > 0.05$). After the intervention, the control group was as high as shown in Table 2 ($P < 0.05$).

4.3. The Degree of Pain 2 H after Surgery. 2 h after surgery, VAS score of the observation group (2.96 1.02) was lower than that of the control group (4.88 1.36); the difference was statistically significant ($P < 0.05$).

4.4. Incidence of Complications. In the control group, there were 1 case of abdominal bleeding, 3 cases of incision infection, 2 cases of biliary leakage, and 2 cases of biliary duct injury. The complication rate was 19.05%. There was 1 case of biliary duct injury in the observation group, and the complication rate was 2.38%. The control group problems were smaller than those in the control group and differed significantly ($P < 0.05$).

4.5. Living Quality. Prior to the intervention, there was no significant difference in GLQI scores between the two groups ($P > 0.05$). After the intervention, the CLQI scores of the two groups were significantly higher than before the intervention, and the control group's GLQI scores were significantly different from those of the control group (both $P < 0.05$), as shown in Table 3.

The interest rates in both groups were 97.23% higher in the control group than in the control group ($P < 0.05$), as shown in Table 4 and Figure 2.

4.6. Discussion. ERAS is an important development and revolution in surgery in this century. It is not a single measure, but the integration of a series of optimized measures with the best evidence. The ERAS concept and ERAS care has been widely recognized by the medical community today, and its clinical implementation has been effectively verified [18]. ERAS is also known as accelerated rehabilitation surgery. Traditionally, recovery begins after surgery, so there are many literatures on postoperative care under ERAS's concept, while less attention has been paid to accelerated rehabilitation care during surgery. Surgical patients need a holistic and continuous nursing process, and many factors in the surgical process have been proven to affect patient prognosis. Therefore, nursing management to accelerate the recovery of patients should be advanced to the preoperative and cover the whole operation process. Clinical perioperative management under the current ERAS concept needs to be optimized from the preoperative, intraoperative, and postoperative stages to minimize emergency response and promote recovery. It requires the cooperation of surgeons, anesthesiologists, operating room specialists, nurses, and ward nurses. The development of the ERAS concept to today is no longer to discuss whether it is better than the traditional model, but the implementation and implementation of the concept and strategy. In particular, the application of accelerated intraoperative rehabilitation nursing in patients with gallbladder polyps under ERAS's concept is still in its infancy, requiring a group led by operating room nurses to explore and study the implementation methods of relevant strategies [19]. Through improving the preoperative visit model, scientific management of the preoperative fasting time, optimization of intraoperative temperature management, prevention of intraoperative thrombosis, and improvement of postoperative resuscitation care, ERAS

Table 1: Comparison table of operation-related indicators between the two groups.

Group	Time to get out of bed (h)	Anus exhausting time (h)	Length of stay (d)
Observation group ($n = 45$)	8.85 ± 1.61	15.32 ± 3.40	4.51 ± 0.88
Control group ($n = 45$)	12.24 ± 1.98	20.33 ± 4.14	6.21 ± 1.02
t	8.351	5.928	8.705
P	<0.05	<0.05	<0.05

Table 2: Comparison of quality scores of the two groups before and after the intervention.

Group	Physical function		Mental functioning	
	Before the intervention	After the intervention	Before the intervention	After the intervention
Observation group ($n = 29$)	56.58 ± 6.99	78.24 ± 6.25	55.15 ± 5.95	8123 ± 6.78
Control group ($n = 29$)	56.43 ± 5.14	66.85 ± 7.21	54.98 ± 5.28	70.27 ± 6.98
t	0.026	7.182	0.028	8.147
P	> 0.05	<0.05	>0.05	<0.05

Table 3: Comparison of GLQI scores between the two groups before and after intervention.

Group	Number of cases	GLQI score	
		Preoperative	Postoperation
Control group	45	81.65 ± 14.95	94.51 ± 17.95
Observation group	45	80.35 ± 15.24	108.26 ± 20.65

concepts are combined with clinical practice. Starting from the three stages of preoperative, intraoperative, and postoperative surgery, the adverse reactions caused by surgical stress should be minimized, and the tolerance and coping level of surgical patients should be improved as a whole, to improve prognosis and promote rehabilitation. Therefore, the application of accelerated rehabilitation nursing interventions in surgery under ERAS's concept should be studied. It not only enables continuous perioperative holistic nursing concept of ERAS but also has urgent practical significance for further optimizing and standardizing the implementation of relevant strategies of ERAS and also provides scientific theoretical and practical basis for specialized nurses in the operating room to effectively carry out intraoperative accelerated rehabilitation nursing intervention under ERAS concept. Under this ERAS concept, accelerate rehabilitation nursing to reduce operation and stress as the core goal, from optimization of preoperative supervision mode, to ban the scientific management of fasting time, intraoperative blood clots to intraoperative temperature management of prevention, and management optimization to improve postoperative recovery nursing way; notting is not to reduce the operation as the core of the best stress cycle on the basis of clinical practice. Integrated visits to operating rooms and wards reduced preoperative anxiety levels. Stable core body temperature can promote drug metabolism, shorten the recovery time, reduce the incidence of postoperative SSI, and promote postoperative ALT AST recovery. The family arousal pattern reduced the occurrence of EA, improved the quality of resuscitation, and reduced the use of muscle relaxation antagonists for resuscitation and symptomatic treatment of EA. Reduce PACU stay and monitoring time, so that the drug expenditure and PACU monitoring costs will greatly reduce. The reduction of postoperative complications also greatly reduces the cost of subsequent treatment. The relative stability of the patient's internal environment and the improvement of the overall tolerance to surgery can promote rehabilitation without compromising the safety of the patient's treatment, thus shortening the length of hospitalization and reducing hospitalization costs [20]. This makes intraoperative care under the ERAS concept cost-effective in many aspects of clinical practice. Traditional health knowledge propaganda adopts oral education or paper version of the propaganda, one is not wide enough, and two is lack of vitality; the content is monotonous and boring. The health promotion on WeChat, the most widely used social network platform, is making up for these shortcomings. You can receive text, pictures, voice, and video messages with your mobile phone. Compared with traditional health education, WeChat platform is more specific, more convenient, and vivid. Not only patients but also the public can learn relevant knowledge about diseases anytime and anywhere. Meanwhile, it can also stimulate the public's initiative to explore more medical health knowledge, which effectively improves the effect of health education [21]. WeChat platform use is not restricted by time and space, can arrange one or more according to the needs of clinical medical personnel to handle, not only save human resources, and improve the patient's satisfaction, to improve the quality of life of patients after discharge and the lack of medical

Table 4: Nursing job satisfaction was compared between the two groups.

Group	Number of cases	Great satisfaction	Satisfaction	Dissatisfaction	Nursing job satisfaction
Observation group	45	29	16	0	45 (100%)
Control group	45	27	11	7	38 (84.44%)
x^2					8.347
P					0.004

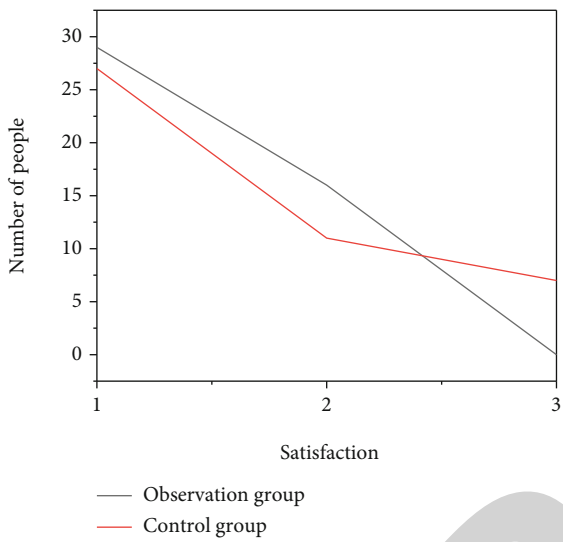

Figure 2: The line chart of nursing job satisfaction was compared between the two groups.

professional knowledge of patients, and their families do not have to bother to identify the authenticity of information. Through WeChat platform, the hospital can receive timely feedback from patients and urge patients to come to the hospital for regular review. Medical staff can help discharged patients deal with problems in a timely manner, which not only makes patients feel relieved but also enables medical staff to accumulate more relevant knowledge and experience [22]. In addition, the results of this study showed that after different propaganda and education methods in continuous care, patients in the observation group had a deeper understanding of the disease than those in the control group and were more satisfied with the health propaganda and education methods on WeChat platform.

5. Conclusion

Gallbladder polyp is a common gallbladder disease. The common symptoms are abdominal bloating, nausea, and vomiting. If not treated in time and effectively, it can be developed into gallbladder cancer. Common surgical treatment has many risks such as improper surgical stress response and nursing, leading to a high incidence of postoperative complications and delaying the rehabilitation process. Therefore, should be in the treatment at the same time should cooperate with scientific and effective nursing intervention measures; comprehensive nursing intervention emphasizes in the preoperative, intraoperative, and postoperative stages according to the patient's physiological, psychological, cultural, and spiritual needs in many aspects, to provide the best way of nursing. Before surgery, health education and psychological counseling were carried out to prepare for surgery, relieve tension and anxiety, improve patient compliance, and enhance confidence. During the operation, we strictly followed the operation procedures, paid close attention to the changes of patients' vital signs, and timely dealt with the abnormal conditions. After surgery, we conducted intervention on patients' postural activities, abdominal drainage, lifestyle, diet, etc. The results of this study showed that VAS score and complication rate of the observation group were lower than those of the control group after intervention, indicating that this nursing mode can relieve pain and reduce complications. In this study, through preaching during hospitalization, patients were improved to be familiar with the knowledge of disease etiology care and treatment, to enhance their confidence in recovery, to guide reasonable diet, regular life, appropriate exercise, work, and rest, and to avoid mental tension or overwork. GLQI scores in both groups after intervention were higher than before intervention, and GLQI scores in the control group were higher in the control group, indicating that health care can improve the quality of care, improving postoperative well-being of patients with gallbladder polyps. In conclusion, good health care reduces pain and discomfort in patients with gallbladder polyps and improves quality of life. They were divided into control groups and controlled groups using a sequential distribution procedure, with 45 patients in each group. The board provided regular caregivers and the care team provided health information on WeChat as part of routine care. To sum up, WeChat integrates functions such as text, voice, pictures, and video, which makes it easier for the public to accept and understand and has the advantages of economy, simplicity, and effectiveness. Health education based on WeChat platform can significantly improve patients' satisfaction and awareness of the disease and is more conducive to patients' health recovery in continuous care. Health education on WeChat platform has improved patients' and their families' understanding of disease-related knowledge and stimulated the public's initiative to learn medical knowledge in daily life, which is worthy of further promotion in clinical practice.

Data Availability

The data used to support the findings of this study are available from the corresponding author upon request.

Hindawi
Scanning
Volume 2023, Article ID 9821689, 1 page
https://doi.org/10.1155/2023/9821689

Retraction

Retracted: High-Intensity Injury Recognition Pattern of Sports Athletes Based on the Deep Neural Network

Scanning

Received 20 June 2023; Accepted 20 June 2023; Published 21 June 2023

This article has been retracted by Hindawi following an investigation undertaken by the publisher [1]. This investigation has uncovered evidence of one or more of the following indicators of systematic manipulation of the publication process:

(1) Discrepancies in scope

(2) Discrepancies in the description of the research reported

(3) Discrepancies between the availability of data and the research described

(4) Inappropriate citations

(5) Incoherent, meaningless and/or irrelevant content included in the article

(6) Peer-review manipulation

The presence of these indicators undermines our confidence in the integrity of the article's content and we cannot, therefore, vouch for its reliability. Please note that this notice is intended solely to alert readers that the content of this article is unreliable. We have not investigated whether authors were aware of or involved in the systematic manipulation of the publication process.

In addition, our investigation has also shown that one or more of the following human-subject reporting requirements has not been met in this article: ethical approval by an Institutional Review Board (IRB) committee or equivalent, patient/participant consent to participate, and/or agreement to publish patient/participant details (where relevant).

Wiley and Hindawi regrets that the usual quality checks did not identify these issues before publication and have since put additional measures in place to safeguard research integrity.

We wish to credit our own Research Integrity and Research Publishing teams and anonymous and named external researchers and research integrity experts for contributing to this investigation.

The corresponding author, as the representative of all authors, has been given the opportunity to register their agreement or disagreement to this retraction. We have kept a record of any response received.

References

[1] N. Chen and Y. Zhang, "High-Intensity Injury Recognition Pattern of Sports Athletes Based on the Deep Neural Network," *Scanning*, vol. 2022, Article ID 2794225, 6 pages, 2022.

Hindawi
Scanning
Volume 2022, Article ID 2794225, 6 pages
https://doi.org/10.1155/2022/2794225

Research Article

High-Intensity Injury Recognition Pattern of Sports Athletes Based on the Deep Neural Network

Nan Chen [1] **and Yang Zhang** [2]

[1]*Anyang Institute of Technology, Anyang, Henan 455000, China*
[2]*Department of Physical Education, Shandong Jianzhu University, Jinan Shandong 250101, China*

Correspondence should be addressed to Yang Zhang; 201804311@stu.ncwu.edu.cn

Received 12 June 2022; Revised 16 July 2022; Accepted 22 July 2022; Published 10 August 2022

Academic Editor: Danilo Pelusi

In order to solve the problem of low efficiency and accuracy of injury image recognition for sports athletes in high-intensity injury treatment, this paper proposes an injury recognition mode based on the deep neural network. In this paper, the image of sports injury is converted to gray level, and the contour of the injury part in the image is extracted according to the combination of adaptive thresholding and mathematical morphology. In this model, the seed points are selected, the active contour is used to approximate the initial contour, and the curve fitting method is used to fit the obtained discrete points to obtain the final damaged contour. The digital matrix is constructed by using the extracted number of pixels at the damaged position and relevant information. The images are arranged into feature vectors with a length of 64 according to the mode of column concatenation. The overall mean vector of the image is calculated. The calculation results, training samples, and image samples to be recognized are substituted into the Euclidean distance to obtain the preliminary recognition results of the damaged position of the image of sports injury. Then, the image segmentation is realized by clustering. The clustering segmentation results are used to color describe the pixel categories of the original image, calculate the relative damage proportion area in the sports injury image, and identify the damage parts of the high-intensity sports injury image. The experimental results show that the recognition rate of the neural network is 80%-100%, and the recognition time of this method is 0-0.6/s. The above method can improve the accuracy of the recognition of the damaged part of the sports injury image and shorten the recognition time and has certain feasibility in determining the sports injury part.

1. Introduction

After high-intensity training, athletes will inevitably suffer a certain degree of body damage, and athletes will continue to repeat a certain action, which will also cause wear and tear of body joints or skin [1]. For example, a competitive diver can be kept for a short period of time. The diver jumps from a high table, causing heavy movement in the air and eventually falling into the water. Throughout the procedure, all parts of the diver's body are injured [2].

Not only the diving athletes but also the winter ice and snow athletes are seriously injured. Athletes often have injuries in relevant parts in winter sports, such as waist and back sports injuries, knee and ankle injuries, and large and small leg muscle injuries. Winter sports have higher technical requirements for athletes. In the day-to-day single training, athletes are easy to cause excessive load on the sports parts, resulting in lumbar muscle strain, ankle injury, and knee injury (Figure 1). The analysis of the survey results shows that the muscle and ligament injuries of winter sports athletes during exercise are consistent with the sports injuries of the patients included in this study. In this study, the patients' waist, back, knee, and ankle injuries had the highest probability, followed by shoulder, wrist, and leg injuries. In the process of daily training or competition, athletes' bodies are often kept at low temperature, and their muscles are easy to stiffen rapidly. When they do strenuous exercises to contract their muscles, they may cause muscle strain due to

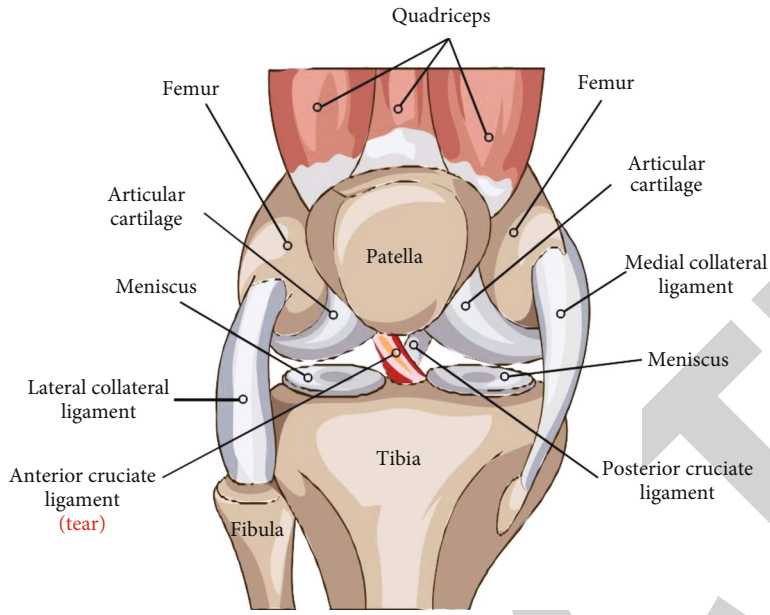

Figure 1: Sports injury.

excessive strength and may also cause damage to the auxiliary tissues around the muscles. Because the distribution of blood vessels and muscles in the knee and ankle joints is less, they are prone to fatigue and slow recovery, so athletes are prone to sports injury in these two parts. The injury rate of athletes in daily training was 55.2%, and that in event competition was 36.8%. In addition, different sports and different injuries of athletes also have correlation. The sports injuries of ice athletes mainly occur in the waist, back, and limb joints. Therefore, in the process of sports, athletes' psychological pressure is greater, and the speed and impact are more intense than ordinary sports. Further analysis found that the main injury type of athletes was joint sprain, followed by muscle strain, which was consistent with other research results at home and abroad. The probability of sprain in winter sports is the highest, followed by abrasions, falls, and bumps. The characteristics of winter sports are related to the types of injury. Ice athletes have high technical requirements, high speed, and great difficulty and are prone to fall, impact, and fall or crash. Snow athletes are prone to crash or fall when they encounter road obstacles in training or competition. In addition, due to the low temperature in winter, if winter athletes do not keep warm or for other reasons, the blood flow in the body is not smooth, and they are prone to frostbite on the face, hands, and feet.

Many athletic events during athletic training involve high performance, and due to the repetition of training, some injuries are often eroded [3]. Injury must be treated. Determining the location of a wound in a wound image can help improve the outcome of treatment [4].

In conclusion, it is necessary to identify the damage of the image of the athlete with the injury, to repair the injury, and to suggest ways to treat the injury. Research and analysis of wounds have been the focus of research in many areas [5]. Therefore, this paper provides a model for identifying injuries based on the deep neural network.

2. Literature Review

Based on the success of big data analysis, the deep neural network and its training algorithms have become well known in education and industry. Compared with traditional processes, in-depth studies are based on data and can extract objects (knowledge) from data. They have the advantage of analyzing large files of nonexistent, unambiguous, modified patterns, and names. The deep neural network currently used in big data analysis is usually a neural communication network, which is the advantage of creating static data and suitable for distributed according to application options. However, due to its limited structure, its ability to decompose temporary data is limited. An infinitely deep neural network is a type of frequency neural network with feedback connection. Basically, it is a dynamic system. Changes in the state of the network over time are important to this network. This is combined with "time loss," which is necessary for extracting data over time series products and estimating large data. The conceptual model of this network expands over time. With the operation of time, this network can be "infinite depth," so it is called an infinite depth neural network. In recent years, the infinite depth neural network computing method based on the restorative network structure has attracted more and more attention and has quickly become a research hotspot. It can be seen that the infinite depth neural network has great potential in processing time series data, and its powerful computing power in big data analysis and prediction tasks is increasingly apparent. As "big data analysis combined with intelligent computing" has become a research hotspot in the big data era, more new theories and methods in the field of infinite depth neural network computing will be proposed, and its application effect will be constantly refreshed, promoting the development and innovation of big data analysis technology.

Di and others have devised a method of examining wounds based on the characteristics of isolation and ultrasound. The results of the removal of the negative characteristics are achieved by analyzing the separation, and the completion process can be combined with LIBSVM to determine the damage [6]. Experimental results show that this method is effective, but the overall validity is low. Zhang and others devised a treatment based on the spectral improvement group [7]. Parida and others use multidimensional gray entropy based on similar characteristics to obtain a sample point spectrogram based on the analysis of the characteristics of the adjacent space and achieve the reduction in the weight of the spectrogram [8]. Beer and others argue that weight matching to the first lowest point in the statistical group is essential for the team to succeed. In order to reduce the loss of data to determine the damage, the process of calculating the value of self in spectral aggregation and obtaining better self-vectors was carried out [9]. Experimental results show that the level of data loss during error analysis is low, but the accuracy of the findings is not high. Hanteh and Rezaifar have proposed disaster management based on the wave coefficient Hu. HIFU is used to irradiate biological tissue, take B-ultrasound images before and after radiation, and take negative images [10]. A supporting vector technology is used to study and classify the structure of tissues by obtaining the results of wave coefficients and three percent values of the current subwave coefficients. Experimental results show that this method has some numerical accuracy, but the guarantee time is longer. Awareness of advanced trauma-based deep neural networks is recommended for athletes who use deep neural network devices to solve the problem of low accuracy and cognitive impairment.

3. Method

3.1. Damage Image Processing. First, there must be a conversion on the sports map. For color images, the pixels can be represented by 3 bytes, and their corresponding bytes for lighting are made up of 3 elements, of which 3 elements are represented by R, G, and B. If the three components are the same, it is gray; otherwise, it is a color image. The formula for changing the grayscale value is as follows:

$$\mathrm{Gray}(i,j) = 0.299 \cdot R(i,j) + 0.587 \cdot G(i,j) + 0.114 \cdot B(i,j). \tag{1}$$

A 24-bit image does not change after conversion. An important role of replacing gray matter is to improve visual acuity [11].

3.2. Contour Extraction and Preliminary Recognition of Image Damage Location. In order to improve the accuracy of the defect detection, it is necessary to draw its contours. In this paper, mathematical morphology and adaptive thresholding methods will be used to create contours, and curves will be used to obtain broken contours [12]. The heavy injury contour design is a snake pattern that can receive the contour of the injured area. When the snake

Table 1: Details of subjects.

Project	Remarks
Male/person	55
Female/person	45
Height range (cm)	162 ~ 183
Weight range (kg)	44 ~ 75
Training program	Weightlifting, sprinting, long-distance running, long jump, high jump, shot put, basketball
	Football, table tennis, javelin, etc.

points in equilibrium, the energy is very small and the resulting contour coincides with the edge of the damaged area. Therefore, the contour strength must be reduced to a minimum in order to identify the damage. The two models for the contour movement expression are as follows:

$$E(C) = [\alpha E_{\mathrm{in}}(C) + \beta E_{\mathrm{ex}}(C)]\mathrm{Gray}(i,j), \tag{2}$$

where α and β represent weighted values and $E_{\mathrm{ex}}(C)$ and $E_{\mathrm{in}}(C)$ represent external energy and internal energy, respectively. Once the wound contour has been obtained, the site can be estimated using the K-L exchange method [13]. Once the contour has been removed, the number of pixels damaged and other important information can be obtained, so use this information to determine the digital matrix. In order to improve the accuracy of determining the location of the damage, it is necessary to place the images in 64 characteristic vectors that are arranged in a linear fashion. So there are m images, $X = \{x_1, x_2, \cdots, x_m\}$, so formula (3) is for calculating the overall mean vector of images:

$$\mu = \frac{1}{m}\sum_{i=1}^{m} x_i \cdot E(C). \tag{3}$$

Arrange the eigenvalues A in a decreasing manner. After the arrangement is completed, select the first j eigenvalues λ_i that are not zero, and then, extract their corresponding vector v_i. Therefore, the covariance matrix eigenvector μ_i can be calculated according to formula (4). Select the first 60% of the eigenvalues, so that most of the damage images can be retained. In formula (4), $A = [x_1 - \mu, x_2 - \mu, \cdots, x_m - \mu]$.

$$u_i = A\frac{1}{\sqrt{\lambda_i}} X \cdot v_i \cdot \mu. \tag{4}$$

Then, all the design drawings and training models that need to be decided are prepared in private space U, and the projection coefficient is calculated by

$$y_i = U^T \cdot u_i. \tag{5}$$

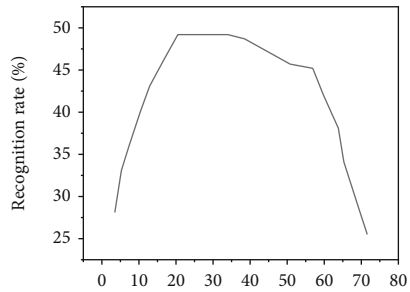

(a) Levels of discrimination and screening procedures based on ultrasound diagnosis

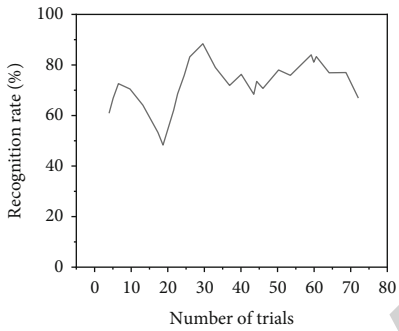

(b) Speed to determine the process of damage treatment based on improved spectral agglomeration

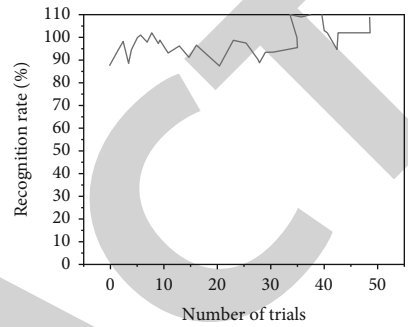

(c) Recognition rate of damage extraction method based on the neural network

Figure 2: Recognition rate results of different methods.

Then, compare all the drawing models and training models to determine using equation (6). The model with the lowest spacing is the result of a preliminary analysis of the model [14].

$$d(x,y) = \left[\sum_{i=1}^{n} (x_i - y_i)^2\right]^{1/2}. \quad (6)$$

Here, n is the number of training patterns and $d(x,y)$ is the Euclidean distance.

3.3. Pixel Calculation of Damaged Image Based on the Neural Network. Through the above analysis, the damage location can be preliminarily identified, but the accurate location cannot be obtained. Therefore, the paper will further identify the damaged part by using the neural network, so as to obtain a more accurate damaged part and calculate the area of the damaged area [15].

Using the neural network in image damage recognition is to treat each solution as a fish, and then, all solutions form a solution set. There are two ways to find the final solution in the solution set: taking the cluster center as the solution and the cluster result as the solution. In order to improve the accuracy of the analysis, subgroups were used as a solution in this sentence [16, 17]. Therefore, the average vectors of each group are calculated for each fish, and the position of the fish can be used to represent one pixel in the image. Therefore, the target function of the fish can be indicated by the following model:

$$j_g = \sum_{i=1}^{g} V_i - x_k{}^2 \cdot d(x,y), \quad (7)$$

where g represents the number of cluster centers, x_h represents the cluster object, and V_i represents the pixel cluster centers. When j_g is the minimum value in the formula, it is set as the best clustering point, which is helpful to achieve the purpose of damage image segmentation [18].

After clustering, the gray pixel value of the image will reach the corresponding effect with the original pixel. After clustering results, the color rendering of pixels is realized, so different colors in the image will represent different representations. Thus, the RGB representation value of pixels can be calculated by accumulating the GRB flux of each type of pixel value and dividing it by the total number of pixels [19].

After the above analysis, the relative proportional area of the damage image can be expressed by

$$\text{Area}_{\text{ital}} = \left(\frac{W'}{D'}\right) \cdot 2.54 \cdot \left(\frac{H'}{D'}\right) \cdot 2.54, \quad (8)$$

where D' represents the image resolution and H' and W' represent the number of pixels in different directions, with

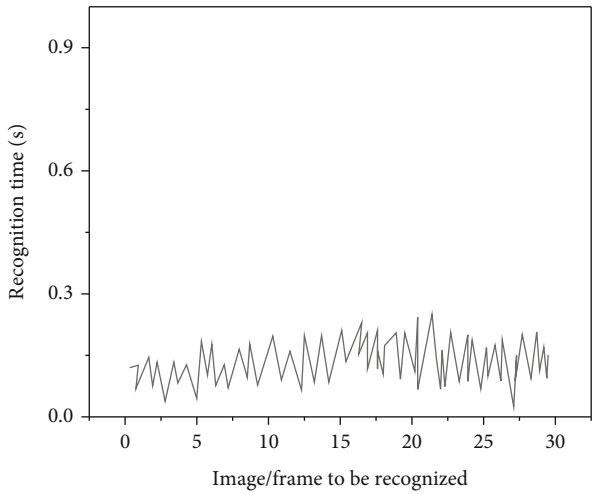

Figure 3: Time-consuming results of different methods.

H' representing the vertical direction and W' representing the horizontal direction [20–22].

After clustering and segmentation of the original image, the area of the damaged area can be calculated through the correlation ratio, which is the ratio of the total number of damaged pixels P to the total number of image pixels P', so formula (9) for the area of damaged pixels is as follows:

$$\text{Area}_i = \frac{P}{P'} \cdot \text{Area}_{\text{inal}} \cdot \min J_g. \tag{9}$$

In the process of sports, athletes may have injuries at various positions of the human body, such as shoulder joint injuries, back injuries, and eye injuries. Through the above research based on the neural network, it can accurately identify the athletes' injury location and can improve the recognition efficiency. In order to further illustrate the accuracy and efficiency of this method, an experimental study will be carried out to verify its application effect.

4. Results and Discussion

100 athletes were selected as subjects, and the relevant information of athletes is shown in Table 1.

The instrument is used to check the injury of each athlete in order to collect relevant data. Relevant data are obtained after the experiment, and then, the effect of damage image recognition based on the neural network is tested by using the recognition rate and recognition time.

(1) Benefits of advanced research: to determine the effectiveness of self-assessment studied in this article, other assessments were selected as comparisons. Figure 2 shows a comparison of the approvals of the different processes. Figure 2(a) shows that the level of intelligence tends to change, first increases and then decreases, and its overall level decreases [23]. It can be explained that the research on the effectiveness of this method is flawed and it is not possible to determine the location of the loss, because the change in the rating level as can be seen in Figures 2(b) and 2(c) is also high. The level of acceptance of the assessment process studied in this sentence is better than that of the two methods, and the pattern of its changes is also similar. Recognition of sports images with serious injuries as neural connections allows athletes to first receive images of the injured area and then first identify the injury. The injury area is identified using K-L conversion analysis. Therefore, in order to verify authenticity, neural networks are used to divide the images and ultimately to obtain diagnostics with greater accuracy [24]. Therefore, the assessment process learned in this article is more feasible and robust than other methods

(2) Recognition time-consuming analysis results: Figure 3 shows the time-consuming results of different recognition methods. It can be seen from the figure that when the number of images to be recognized is different, the recognition method based on the neural network takes the shortest time among the three methods. Therefore, it can be concluded that the method studied in this paper has faster recognition efficiency than the other two methods. Because the method has undergone image gray conversion before recognition, this step is conducive to improving the recognition efficiency [25]

The experiments shown in Figures 2 and 3 show that the plan has the advantages of both speed assurance and acceptance, and it can provide the basis strength and support for research in this area.

5. Conclusion

This phrase provides a way to determine the severity of injuries in athletes based on deep neural networks. Athletes may be injured during sports. Determining their injury profile can help improve an athlete's performance in medical care. In this article, the damage of the image will be identified according to the neural network. Compared with the two methods of identification, the process in this document will help to improve the accuracy and authenticity of the analysis. Athletes can easily get injured during sports. In order to minimize injuries to athletes, we must adhere to strict operating standards to avoid serious injuries during training.

Data Availability

The data used to support the findings of this study are available from the corresponding author upon request.

Conflicts of Interest

The authors declare that they have no conflicts of interest.

Hindawi
Scanning
Volume 2023, Article ID 9853105, 1 page
https://doi.org/10.1155/2023/9853105

Retraction

Retracted: Sports Medical Image Modeling of Injury Prevention in Wushu Training

Scanning

Received 3 October 2023; Accepted 3 October 2023; Published 4 October 2023

This article has been retracted by Hindawi following an investigation undertaken by the publisher [1]. This investigation has uncovered evidence of one or more of the following indicators of systematic manipulation of the publication process:

(1) Discrepancies in scope

(2) Discrepancies in the description of the research reported

(3) Discrepancies between the availability of data and the research described

(4) Inappropriate citations

(5) Incoherent, meaningless and/or irrelevant content included in the article

(6) Peer-review manipulation

The presence of these indicators undermines our confidence in the integrity of the article's content and we cannot, therefore, vouch for its reliability. Please note that this notice is intended solely to alert readers that the content of this article is unreliable. We have not investigated whether authors were aware of or involved in the systematic manipulation of the publication process.

Wiley and Hindawi regrets that the usual quality checks did not identify these issues before publication and have since put additional measures in place to safeguard research integrity.

We wish to credit our own Research Integrity and Research Publishing teams and anonymous and named external researchers and research integrity experts for contributing to this investigation.

The corresponding author, as the representative of all authors, has been given the opportunity to register their agreement or disagreement to this retraction. We have kept a record of any response received.

References

[1] Y. Feng, "Sports Medical Image Modeling of Injury Prevention in Wushu Training," *Scanning*, vol. 2022, Article ID 5201952, 6 pages, 2022.

Hindawi
Scanning
Volume 2022, Article ID 5201952, 6 pages
https://doi.org/10.1155/2022/5201952

Research Article

Sports Medical Image Modeling of Injury Prevention in Wushu Training

Yuanyuan Feng [1,2]

[1]*Faculty of History and Culture, Chengdu Sport University, Chengdu, Sichuan 610041, China*
[2]*College of Physical Education, Sichuan Agricultural University, Ya'an, Sichuan 625014, China*

Correspondence should be addressed to Yuanyuan Feng; 201804313@stu.ncwu.edu.cn

Received 13 June 2022; Revised 15 July 2022; Accepted 22 July 2022; Published 9 August 2022

Academic Editor: Danilo Pelusi

In order to solve the problem of injury prevention in Wushu training, this paper proposes a research on modeling using sports medical images. The main content of this technology research is to drive the muscle strength modeling method based on the sports medical image data. According to the acquisition of MRI/CT images, through the research and application of DFIS, it is concluded that the research on sports medical image modeling has a high accuracy for injury prevention in Wushu training. The experimental results show that translation accuracy ≤ 0.03~0.27, rotation accuracy ≤ 0.24~0.63, flexion and extension accuracy ≤ 0.1, translation retest error ≤ 0.2~1.2, rotation retest error ≤ 0.5~3.4, rotation retest accuracy ≤ 0.4~1.04, and sports medical images have a high accuracy for injury prevention in Wushu training. It is proved that the research on sports medical image modeling is effective and accurate for the problem of injury prevention in Wushu training.

1. Introduction

In the process of the steady development of China's sports cause, the social and economic developments are striding forward, the development of Wushu is also moving forward, and its movement difficulty is also gradually increasing, resulting in many Wushu Athletes' increasing injuries in training [1]. Athletes' injuries will not only make their bodies bear some degree of pain but also affect their future training and even affect the psychology of Wushu athletes. Therefore, in the development process of Wushu events, we should constantly summarize and summarize various influencing factors of athletes' sports injury, record various morbidity laws, and take effective measures to prevent according to specific reasons, so as to effectively reduce the probability of athletes' injury and improve the efficiency of Wushu events, so as to promote the orderly development of Wushu.

Compared with other sports, Wushu is more confrontational. Athletes must master the corresponding movement skills before they can complete the confrontational training more easily and freely. In the teaching and training of Wushu, sports personnel will be free from sports injuries of different degrees, which will also have an impact on the physical and mental health of sports personnel. Therefore, in Wushu teaching and training, teachers must take scientific measures to prevent and deal with injury accidents in combination with the actual situation, so that athletes can learn Taekwondo knowledge and skills more happily. Sports injury refers to the injury occurring in the process of sports. It is closely related to sports events, sports technical actions, physical conditions of exercisers, venues, and equipment. If the method of engaging in sports activities is improper, it may cause unnecessary harm and bring adverse effects on everyone's physical health, study, life, and psychology. Sports injuries are common among athletes, who need to regularly carry out various sports, and require high technical difficulty, high intensity, and strong antagonism, so the incidence of sports injuries is higher [2].

In recent years, Wushu has developed rapidly in various provinces and cities, is popular widely, and is welcomed and loved by the masses. However, at the same time of sports,

because people have not yet fully mastered and understood Wushu, there are hidden dangers in the training process, and injuries often occur [3]. Therefore, corresponding preventive measures should be put forward in time and effectively to effectively ensure the performance and physical health in Wushu training.

2. Literature Review

With the vigorous development of physical education in the country, under the current background, physical education has gradually developed to lifelong physical education. Lifelong physical education pursues the continuous physical exercise and the improvement of physical learning ability in people's life. It is a new concept accompanied by the importance of lifelong learning. The implementation of lifelong physical education in sports will bring about great changes in the concept of physical education teaching and training [4]. As an important part of physical exercise theory, the prevention mechanism of sports injury is closely related to people's physical health, the effective implementation of physical education teaching and training, and the improvement of lifelong exercise ability. Therefore, the content of the research on the prevention mechanism of sports injury itself is also an important part of lifelong physical education, which may be closely connected with the teaching content of its related courses. Therefore, considering the particularity of sports and the requirements of lifelong physical education, the research on the prevention mechanism of sports injury has high practical value. We should strengthen the monitoring of exercise load, reasonably arrange teaching and training, take preventive measures, reasonably arrange teaching and training, formulate training plans in line with scientific principles, and scientifically and reasonably arrange preparatory activities. The purpose of preparatory activities is to improve the excitability of the central nervous system through a variety of exercises, enhance the coordination ability of various organ systems, overcome the inertia of human body functions, and enable the human body to be prepared from a relatively static state to a tense active state, so as to shorten the adaptation process of the human body to movement. Generally speaking, the injuries caused in the process of Wushu training are caused by the ideological neglect of athletes and Wushu coaches. In particular, they attach great importance to the training results but neglect the safety education. Therefore, they do not give relevant reminders to athletes and do not use useful measures to carry out corresponding prevention. Some athletes do not pay attention to their own safety issues in the process of Wushu training, and their attitude is not correct, which greatly increases the probability of physical injury. In a word, it is very important to pay attention to the prevention and treatment of athletes' sports injuries in Wushu training. Therefore, in practice, we must fully understand the common injuries in Wushu training, grasp the causes of injuries, and take scientific measures to prevent sports injuries on this basis, so as to promote the quality of Wushu training.

In view of the above problems, this paper proposes a research on sports medical image modeling to improve injury prevention in Wushu training [5]. The main content of this technology research is to drive the muscle strength modeling method based on the sports medical image data. According to the acquisition of MRI/CT images, through the research and application of DFIS, it is concluded that the research on sports medical image modeling has a high accuracy for injury prevention in Wushu training. So as to provide more accurate data, more advanced technology and more reliable methods [6].

3. Research Methods

3.1. Data Driven Muscle Strength Modeling Method for Sports Medical Images

3.1.1. Modeling Method and Process. The data-driven modeling process of sports medical images includes the following steps, as shown in Figure 1: the first is the acquisition of medical image data, usually including CT or MRI. The second is the registration, fusion, and segmentation of the acquired medical image data. Then, the three-dimensional reconstruction of the target area is carried out, and the physical parameters such as the volume and moment of inertia of the current area are calculated. Then, the joint system is modeled. Mechanical modeling of skeletal muscle was based on hill theory. Then, the kinematics data and inverse dynamics data are used for multibody dynamics modeling and analysis [7]. Finally, the static optimization method is used to estimate the muscle force, and the fusion analysis of the model is carried out.

3.1.2. Acquisition of MRI/CT Images. Both MRI and CT are indispensable medical imaging techniques in clinic. Because of the difference between MRI and CT images, the fusion of MRI and CT images becomes very meaningful. The first step of image fusion is registration. Segmentation is to generate pixel set (pixel block) from the image containing the target tissue part and separate it from the whole image. In medical images, segmentation is usually related to the specific structure described. The segmentation algorithm of medical images combines the data structure and medical information and achieves the purpose of target tissue segmentation through the combination of the two. Fusion is to extract the information of interest from the image data from different sources and then combine it into a new image that can reflect the characteristics of a variety of image data [8].

The three-dimensional reconstruction of the target area and the complete three-dimensional curve and surface geometric model are the basis of the human biomedical simulation model and subsequent dynamic analysis and calculation [9]. In this paper, the cubic rational periodic B-spline curve approximation method is used to segment the fused image directly and output the spline curve model of bone tissue contour directly. This algorithm has the following advantages: firstly, with the help of anatomists, accurate segmentation results can be obtained; Secondly, by using the local property of cubic rational periodic B-spline curve, the curve shape can be easily adjusted, and at the same time, a very accurate approximation curve can be obtained with only a

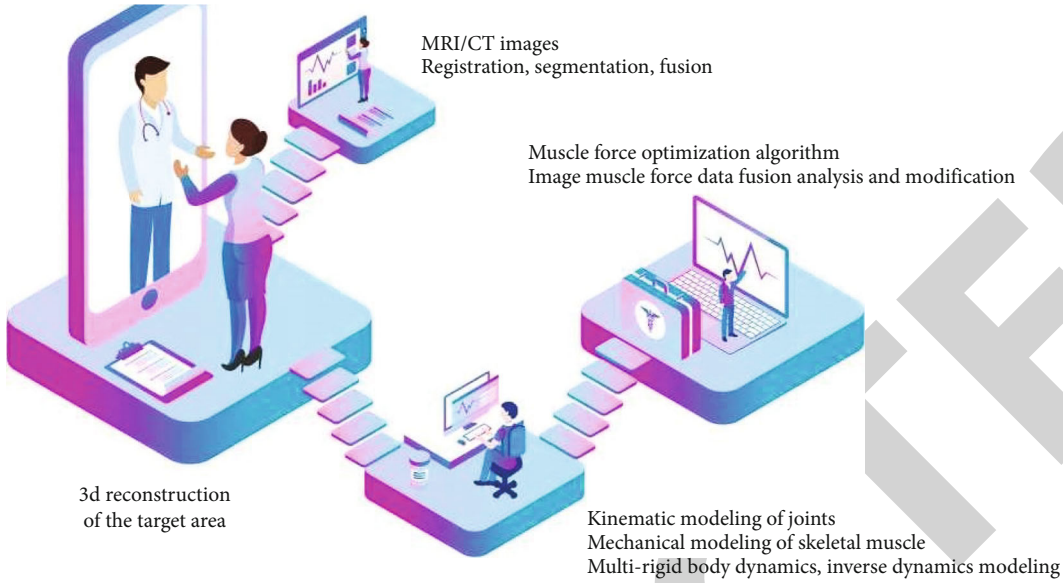

Figure 1: Flow chart of muscle strength modeling driven by medical image data.

small number of feature points. The final data can be written in IGES format, which is a standard three-dimensional model data file for subsequent skeletal muscle force calculation and analysis.

3.1.3. Medical Imaging Technology. The rapid development of medical imaging technology, computer image processing technology, and network technology has promoted the continuous upgrading of radiotherapy equipment used in clinical treatment [10]. After the arrival of the era of precision radiotherapy, three-dimensional conformal radiotherapy, spiral tomography, and X-ray real-time imaging technology have been applied in the field of clinical treatment. In terms of the current development of clinical treatment, medical image 3D reconstruction technology plays an important role in the treatment planning system. Registration between two-dimensional images and three-dimensional models is inseparable from the support of three-dimensional reconstruction of medical images. CT diagnosis is a common technique in clinical treatment. It is a reference factor for medical staff to judge the condition and determine the treatment plan. At this stage, China has entered the digital imaging era. The accuracy of diagnostic basis is the focus of clinical treatment [11].

During the study, retrospective analysis was conducted according to the diagnosis of patients. During the study, the test verification platform included X-ray machine, graphic workstation, operating table, and other equipment. According to the actual situation of the experimental study, the relevant personnel used CT equipment to complete the bone information scanning and input the relevant image data into the workstation. In the three-dimensional model and processing stage, the researchers used image noise reduction, threshold division, and isoline extraction to carry out image preprocessing and determine the closed isoline of each image in the CT data. The method used in the construction of the 3D model is volume rendering algorithm [12].

In the process of 3D model construction, relevant personnel used image noise reduction measures to remove the noise in CT image data and improve image quality. During modeling, image segmentation tools are used as image segmentation algorithms. During the implementation of 3D reconstruction of CT data, relevant personnel realized 3D image surface by means of surface rendering and volume rendering [13]. The fitting curve of positive-position mutual information value is shown in Figure 2. In this fitting curve, there are two extreme values in the mutual information curve.

The lateral fitting curve of the patient's CT image processing results is shown in Figure 3. According to the contents of the figure, the lateral fitting curve only contains an extreme value. Researchers can obtain complete 2D-3D registration parameters according to the research methods applied to this study [14].

3.2. Research and Application of DFIS

3.2.1. DFIS Study. DFIS originated from the fluoroscopy imaging technology invented in 1895 [15]. Since its invention, fluoroscopy imaging technology has been widely used in medical imaging detection because of its penetrability and noninvasiveness. However, medical imaging detection is mainly based on static image analysis, which has great limitations in the field of human motion. Therefore, researchers have combined fluoroscopy imaging technology with image shooting technology to invent a single plane fluoroscopy analysis system, which has been widely used in the field of medicine and human low-speed movement. Its limitation is that it is unable to quantify the 6DOF movement of joint bone structure and accurately analyze the relationship between the movement of bone structure and injury. Combining fluoroscopy imaging technology, 2D/3D registration technology, and 3D motion analysis technology, a low-speed DFIS (sampling frequency ≤ 30 Hz) is developed to realize dynamic 3D tracking and analysis of bone and joint

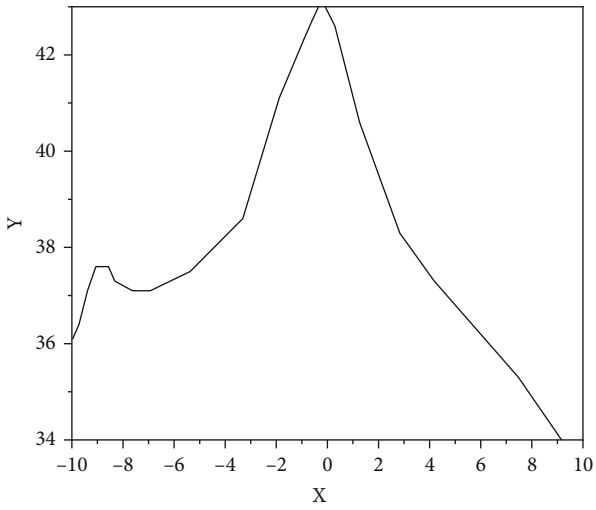

Figure 2: Positive fitting curve.

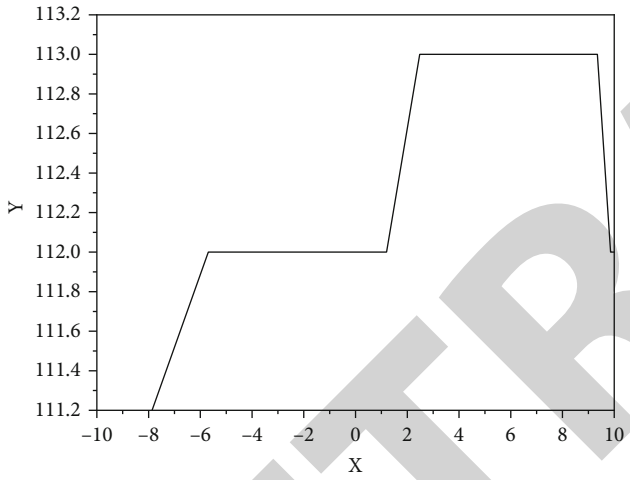

Figure 3: Lateral fitting curve.

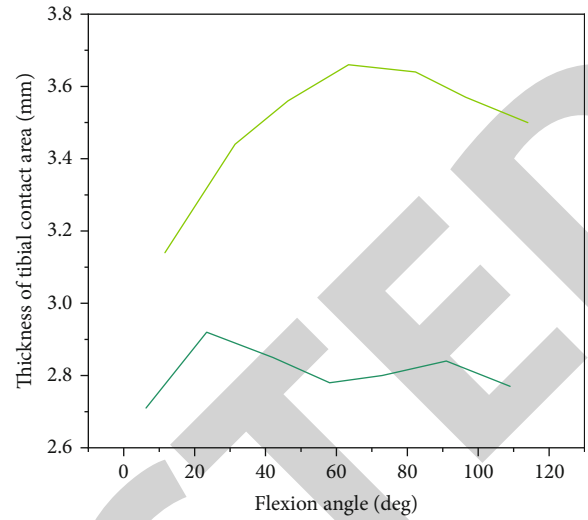

Figure 4: Contact area and track of femur and tibial cartilage.

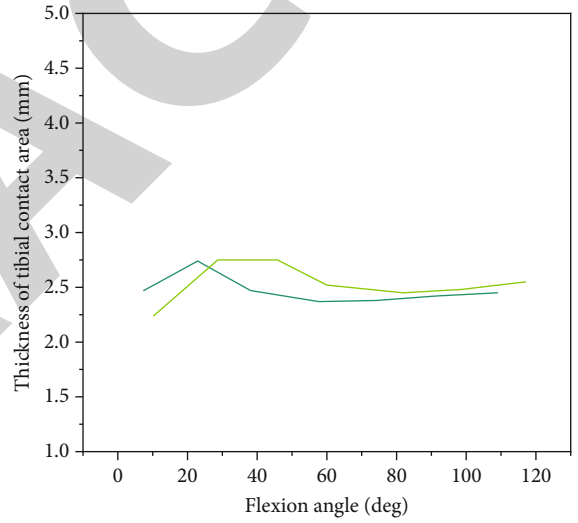

Figure 5: Contact area and track between tibia and medial and lateral femoral condyle cartilage.

motion in vivo 2-25. The biplane orthogonal fluorescence imaging system is improved to expand the shooting range and increase the shooting frequency (sampling frequency ≥ 100 Hz, shutter speed ≥ 1/500 s). At present, these systems have been successfully applied in the fields of cardiac/cerebral angiography imaging, joint surgery positioning, personalized 3D joint prosthesis replacement, and the movement of human bone structure in the body weight-bearing functional position.

Human movement takes the bone as lever, the joint as fulcrum, and the skeletal muscle contraction as power. The mechanism of joint injury (usually caused by irregular movement or high impact) has always been a research hotspot [16]. The commonly used traditional motion capture system indirectly measured the rotation angle error of subtalar joint more than 10°. The tibial movement distance during knee flexion is greater than the real movement distance. Due to the error of the skin and soft tissue, there is a defect in indirect inference when discussing the mechanism of joint injury. DFIS can dynamically track the position relationship and deformation of joint bone structure, ligament, and cartilage in vivo during human movement and, more intuitively, truly and accurately explore the mechanism of joint injury. Researchers have successfully used DFIS to explore some sports injury mechanisms of shoulder joint, lumbar spine, knee joint, and ankle joint (the knee joint is the most concerned), and there are still many sports injury mechanisms that have not been explored [17].

3.2.2. Application of DFIS in the Mechanism of Knee Joint Sports Injury. Some studies have used DFIS to explore the mechanism of anterior cruciate ligament (ACL) injury caused by weight-bearing knee bending and landing. The results showed that the peak value of relative elongation of posterior lateral bundle (PL) of ACL was 5.9% when the subjects bent the knee 15° with load, and the peak value of relative elongation of anterior medial bundle (AM) of ACL was 4.4% when the subjects bent the knee 30° with load,

Table 1: Reliability, validity, and accuracy of DFIS in evaluating human joint motion.

	Translation accuracy (mm)	Rotation accuracy (°)	Flexion and extension accuracy (°)	Translation retest error (mm)	Rotation retest error (°)	Rotation remeasurement accuracy (°)
Meng brachial joint	≤0.13~0.39	≤0.47~0.7	—	≤0.2~1.2	—	—
Acromioclavicular joint	—	—	—	—	≤0.5~3.4	≤0.4~1.04
Lumbar vertebra	≤0.35~0.43	≤0.65~0.7	—	≤0.36	—	—
Brittle joint	≤0.2	≤0.45~0.59	—	—	—	—
Knee joint	≤0.15	—	≤0.1	—	—	—
Ankle joint	≤0.03~0.27	≤0.24~0.63	—	—	—	—

indicating that the pl of ACL was easy to break when the subjects bent the knee 15° with load. The AM of the ACL is prone to fracture at 30 flexion. The study also found that the peak distance of tibial displacement at 40 cm landing was 5.6 mm, which was greater than 3.1 mm when walking (90 steps/min) and 2.6 mm when stretching the knee without load. There was no difference in the peak value of tibial internal rotation at 40 cm landing, maximum isometric knee extension (flexion 70°), and no load extension (14.5°~19.4°), which was greater than 3.907 when walking. It indicates that the increase of applied load will increase the distance of tibial femoral forward movement and then increase the risk of ACL fracture. This situation is related to the increase of exercise height and intensity and the increase of muscle and soft tissue load. When the healthy subjects landed with straight knee and bent knee, there was no significant difference in the peak value of tibial femoral forward movement distance, but the ground reaction force and knee extension torque on the straight knee landing were greater than those on the bent knee landing. The passive relaxation of the knee joint forward was related to the peak value of tibial forward movement distance at the landing time. The tibial anteroposterior movement distance of healthy subjects was not related to knee extension torque or anteroposterior shear force 3.51, indicating that joint relaxation may increase the risk of ACL injury when landing. When the subject lands, the knee valgus angle has a direct relationship with the tibial forward displacement distance and lateral displacement distance. It indirectly indicates that the increase of knee valgus may increase the risk of ACL injury [18].

Some studies have used DFIS to discuss the mechanism of knee medial cartilage injury caused by weight-bearing flexion, walking, and stepping on steps. The results show that the probability of knee osteoarthritis is twice that of ordinary people, and the pressure behind the knee joint is 58.3% higher than that of daily walking. From full extension to 90° flexion, the contact point of the tibia and femur is at the medial side of tibial plateau and femoral condyle. The contact point between tibia and femur platform was more medial and lateral in large-scale flexion. The minimum deformation of knee joint cartilage occurs when the knee is bent by 30°, and the maximum deformation occurs when the knee is bent by 120°, and the contact area and deformation of the medial side (see Figure 4) are greater than that of the lateral side (see Figure 5) indicating that the posterior pressure in the tibial plateau is large during the large-scale flexion of the knee joint. If the knee is bent by more than 120° for a long time, the incidence of medial cartilage damage increases. The study found that when the subjects were treading on the ground at a slow pace (knee extension), the horizontal range of motion of the medial femoral condyle was greater than that of the lateral femoral condyle. When stepping on the steps to extend the knee, the contact point between the femur and the medial tibial plateau moved backward. The contact radius of the medial tibial plateau in the sagittal plane is larger than that of the lateral tibial plateau, indicating that the pedaling and stretching exercise will increase the injury rate of the medial femoral cartilage and the medial tibial plateau of the knee joint. Therefore, repeated large-scale flexion and pedaling and stretching of the knee joint may cause damage to the medial cartilage of the knee joint [19].

4. Result Analysis

The application of DFIS in sports medicine depends on the reliability, validity, and accuracy of the system in analyzing 6DOF motion of human joint internal structure [20]. Tantalum beads were implanted into human humerus, scapula, clavicle, and lumbar vertebrae. Steel balls were implanted into human lumbar vertebrae and medullary joints. Balls of different materials were implanted into the knee joint specimens. The specimens of the tibia, talus, and calcaneus were embedded with copper beads [21]. The foot model and gait are used to simulate the robot, and the model is used to calculate. It is confirmed that the system can be used to analyze the 6DOF constant and high-speed movements of the internal bone structures of shoulder, lumbar spine, medullary joint, knee, and ankle and has certain effectiveness, repeatability, and accuracy, as shown in Table 1. It is concluded that the translation accuracy is ≤0.03~0.27, the rotation accuracy is ≤0.24~0.63, the flexion and extension accuracy is ≤0.1, the translation retest error is ≤0.2~1.2, the rotation retest error is ≤0.5~3.4, and the rotation retest accuracy is ≤0.4~1.04.

5. Conclusion

In order to solve the problem of injury prevention in Wushu training, this paper presents a research on modeling using sports medical images. The main content of this technology

Hindawi
Scanning
Volume 2023, Article ID 9857053, 1 page
https://doi.org/10.1155/2023/9857053

Retraction

Retracted: Observation on the Effect of Rehabilitative Physical Training on Ice and Snow Sports Injury under Ultrasound Examination

Scanning

Received 20 June 2023; Accepted 20 June 2023; Published 21 June 2023

This article has been retracted by Hindawi following an investigation undertaken by the publisher [1]. This investigation has uncovered evidence of one or more of the following indicators of systematic manipulation of the publication process:

(1) Discrepancies in scope

(2) Discrepancies in the description of the research reported

(3) Discrepancies between the availability of data and the research described

(4) Inappropriate citations

(5) Incoherent, meaningless and/or irrelevant content included in the article

(6) Peer-review manipulation

The presence of these indicators undermines our confidence in the integrity of the article's content and we cannot, therefore, vouch for its reliability. Please note that this notice is intended solely to alert readers that the content of this article is unreliable. We have not investigated whether authors were aware of or involved in the systematic manipulation of the publication process.

In addition, our investigation has also shown that one or more of the following human-subject reporting requirements has not been met in this article: ethical approval by an Institutional Review Board (IRB) committee or equivalent, patient/participant consent to participate, and/or agreement to publish patient/participant details (where relevant).

Wiley and Hindawi regrets that the usual quality checks did not identify these issues before publication and have since put additional measures in place to safeguard research integrity.

We wish to credit our own Research Integrity and Research Publishing teams and anonymous and named external researchers and research integrity experts for contributing to this investigation.

The corresponding author, as the representative of all authors, has been given the opportunity to register their agreement or disagreement to this retraction. We have kept a record of any response received.

References

[1] Y. Wang and Y. Zhou, "Observation on the Effect of Rehabilitative Physical Training on Ice and Snow Sports Injury under Ultrasound Examination," *Scanning*, vol. 2022, Article ID 2931686, 7 pages, 2022.

Hindawi
Scanning
Volume 2022, Article ID 2931686, 7 pages
https://doi.org/10.1155/2022/2931686

Research Article

Observation on the Effect of Rehabilitative Physical Training on Ice and Snow Sports Injury under Ultrasound Examination

Yang Wang and Yongzhi Zhou

Physical Culture Institute, Jilin Normal University, Siping, Jilin 136000, China

Correspondence should be addressed to Yongzhi Zhou; 31115404@njau.edu.cn

Received 12 June 2022; Revised 14 July 2022; Accepted 22 July 2022; Published 8 August 2022

Academic Editor: Danilo Pelusi

In order to solve the problem of rehabilitative physical training on ice and snow sports injuries, the author proposed an observation method using ultrasonography to be proposed. This method selects patients with anterior talofibular ligament injury treated in a hospital, forty-nine patients who did not undergo conventional rehabilitation under the surveillance of sports medicine ultrasound were set as the control group, a total of 49 patients with anterior talofibular ligament injury who underwent rehabilitation treatment under the monitoring of sports medicine ultrasound were selected as the experimental group, and the clinical efficacy of the two groups of patients was retrospectively analyzed, in order to discuss the application value of sports medicine ultrasound in the rehabilitation of anterior talofibular ligament injury. The results showed that comparing the rehabilitation effect, ankle function score, and daily living ability of the two groups of patients, the experimental group was better than the control group. Comparing the thickness of ligament and effusion between the two groups, the experimental group was also better than the control group, and the difference was statistically significant ($P < 0.05$). Ultrasound medical examination can help doctors to effectively judge the degree of injury and recovery of patients, and doctors can adjust the treatment plan in time according to the examination results and formulate an effective rehabilitation plan, which can greatly shorten the recovery time of patients, improve the treatment effect, promote the functional recovery of the ankle joint, and reduce the occurrence of complications.

1. Introduction

Competitive sports are often accompanied by sports injuries, which are one of the biggest obstacles for athletes to create good results and have a negative impact on athletes' normal training, competitive competition, and life psychology and even affect their sports career [1]. Years of training, coupled with the strict technical and movement requirements of ice and snow events, have resulted in common injuries to the lower back, knees, ankles, and other parts of the athletes; this type of injury has the characteristics of inconspicuous pathogenesis, lack of targeted treatment, poor efficacy, and difficult to cure, which seriously affects the career and physical and mental health of athletes in winter sports [2]. Chinese scholars have done a lot of research on winter sports injuries, but there are few data on the application of personalized rehabilitation therapy for sports injuries, and it is mainly based on conventional treatment after the injury occurs and lacks specificity [3]. How to minimize the pain and injury of athletes, create better competitive performance, and specific treatment plan, this is a topic that many scholars at home and abroad pay great attention to.

The vast majority of sports injuries are soft tissue injuries, and the corresponding diagnostic methods rely on clinical examinations, such as palpation, percussion, and functional tests, which depend to a certain extent on the experience of clinicians, ultrasound examination can provide a direct and objective diagnostic basis of sonographic images [4]. The application of ultrasound to the musculoskeletal system has been tried by scholars in various historical periods, but it was really applied in the field of orthopedics, especially the diagnosis of muscle, ligament, and soft tissue injuries after the 1980s. In the past five years, there have been more and more researches on this aspect, covering all

countries in the world. In my country, there have also been reports on the application of ultrasound to bone and soft tissue injuries, but no systematic report on the use of ultrasound in sports injuries has been found, the author introduces the diagnosis and treatment of nearly 49 cases of sports injuries by using ultrasonography, and through clinical and related diagnostic techniques, according to the experimental data, the effect of rehabilitative physical training on ice and snow sports injury under ultrasound examination was observed [5].

2. Literature Review

Winter sports have higher technical requirements for athletes, and athletes are likely to overload their sports parts during day-to-day single-event training, resulting in lumbar muscle strain, ankle injury, knee joint injury, etc. [6]. In winter sports athletes, muscle strains and ligament strains occur during exercise, and the patients have the highest probability of injury to the lower back, knees, and ankles, followed by shoulders, wrists, and legs [7]. During daily training or competition of athletes, the body is often kept at a low temperature, and the muscles are easily stiffened rapidly, when doing strenuous exercise to contract the muscles, the muscles are strained due to excessive force, and the auxiliary tissues around the muscles may also be damaged [8]. Because of the less blood vessels and muscles in the knee and ankle joints, easy fatigue, and slow recovery, athletes are prone to sports injuries in these two parts [9]. Bullen et al. found that the injury rate of athletes was 55.2% in daily training and 36.8% in event competition [10]. In addition, different sports and different injuries of athletes are also related. Majumder and Deen believed that sports injuries of athletes in ice sports mainly occurred in the lower back and limb joints [11]. Therefore, in the process of exercising, athletes have greater psychological pressure, and the speed and impact force are more intense than general exercise [12]. Further analysis found that joint sprains accounted for the highest proportion of major injuries in athletes, followed by muscle strains [13]. Winter sports have the highest rate of sprains, followed by abrasions, falls, and bruises. Winter sports characteristics are related to the type of injury that occurs. Ice athletes have high technical requirements, high speed, and great difficulty and are prone to falls and collisions, resulting in falls or bruises [14]. Snow athletes are prone to bumps or falls when they encounter road obstacles during training or competition. In addition, due to the low temperature in winter, if athletes in winter sports do not keep warm or other reasons, the blood flow in the body is not smooth, and frostbite on the face, hands, and feet is prone to occur [15].

Taking patients who visited the orthopedics department of a hospital from January 2020 to January 2021 as an example, there was no statistical difference in the general population data between the two groups ($P > 0.05$) (Table 1).

By comparing the main sports injury parts of the two groups of patients, it was found that the lower back, knee, and ankle joints had the highest incidence of injury, followed by the shoulder, wrist, and leg, and the chest and abdomen had the lowest injury probability. There was no significant difference in the main sports injury sites between the two groups ($P > 0.05$) (Table 2).

The statistics and comparison results of the main injury types of the two groups of patients are shown in Table 3. Among the injury types, joint sprains accounted for the highest proportion, followed by muscle strains, ligament strains and myofasciitis injuries were also more common, with the lowest rates of abrasions and frostbite. There was no significant difference in the main types of sports injuries between the two groups ($P > 0.05$).

Ultrasound technology has shown many advantages in the diagnosis and treatment of athletes' rehabilitation physical training (Figure 1), mainly because it is noninvasive, economical, and real-time, it is popular with athletes and coaches, because this technology can solve problems quickly without affecting training [16], no preparation is required before the examination, and the examination results are immediately available; during the examination, the coaches can directly participate in the understanding of the situation, and there is no need to rest after the examination, therefore, it is meaningful to add ultrasound equipment as a sports injury research department and a front-line training base.

3. Methods

3.1. General Information. Select the anterior talofibular ligament injury treated in a hospital from January to December 2020, forty-nine patients who did not undergo conventional rehabilitation under the surveillance of sports medicine ultrasound were set as the control group, and a total of 49 patients with anterior talofibular ligament injury who underwent rehabilitation treatment under the surveillance of sports medicine ultrasound from January to December 2020 were selected as the experimental group for retrospective analysis [17]. Among them, there were 31 males and 18 females in the experimental group, with an average age of (30.97 ± 5.16) years. Among them, there were 32 patients with right ligament injury, 21 males and 11 females, and 17 left ligament injuries, 10 males and 7 females. In the control group, there were 30 males and 19 females with an average age of (31.01 ± 5.39) years. Among them, there were 34 patients with right ligament injury, 22 males and 12 females, and 15 left ligament injuries, and 8 male cases and 7 females. The comparison of general data showed that the difference was not statistically significant ($P > 0.05$), which was comparable.

3.2. Inclusion and Exclusion Criteria

(1) Inclusion criteria

(1) Approved by the ethics committee of the hospital. (2) All patients and their families signed the informed consent. (3) All patients underwent stress imaging X-ray films before treatment, and the posterior opening of the ankle joint was ≥6 mm, which was in line with the clinical criteria for anterior talofibular ligament injury. The fracture site of the patients is often associated with other medical conditions.

Table 1: Comparison of general data of the two groups of patients.

Project	Personalization group ($n = 40$)	Regular group ($n = 40$)	t/x^2	P value
Gender: male female	14/26	12/28	1.747	0.533
Age	17.7 ± 2.1	17.2 ± 1.9	0.825	0.876
Average training time/year	4.3 ± 2.0	4.8 ± 2.5	1.443	0.452

Table 2: Comparison of main injury sites in the two groups of patients.

Injury site	Personalization group ($n = 40$)		Regular group ($n = 40$)		P value
	Number of cases/cases	Rate/%	Number of cases/cases	Rate/%	
Lower back	11	27.5	12	30.0	0.468
Knee and hip joints	13	32.5	15	37.5	0.332
Shoulder and wrist joints	6	15.0	4	10.0	0.317
Head and face	2	5.0	1	2.5	0.462
Chest and abdomen	1	2.5	0	0.0	–
Legs	5	12.5	4	10.0	0.428
Other	2	5.0	4	10.0	0.347

Table 3: Comparison of main injury types between the two groups of patients.

Damage type	Personalization group ($n = 40$)		Regular group ($n = 40$)		P value
	Number of cases/cases	Rate/%	Number of cases/cases	Rate/%	
Joint sprain	12	30.0	12	30.0	1.000
Muscle strain	8	20.0	10	25.0	0.419
Myofasciitis	4	10.0	3	7.5	0.283
Joint contusion	3	7.5	4	10.0	0.507
Belt strain	7	17.5	7	17.5	0.462
Bruises	2	5.0	1	2.5	0.404
Bruise	3	7.5	2	5.0	0.393
Frozen	1	2.5	1	2.5	1.000

(2) Exclusion criteria

(1) Patients are with mental illness. (2) Patients are with disorders of consciousness and communication. (3) Patients are with coagulation disorders. (4) Patients are with major diseases of other organs. (5) Patients are with contraindications to related drugs and treatment. (6) Fracture location patients are with other severe diseases [18]

3.3. Experimental Method

(1) Control group

The patients were treated with conventional rehabilitation therapy: (1) ankle mobilization was performed for the patient, 30 min/time, 1 time/d; continuous treatment for 30 times was a course of treatment; according to the specific conditions of the patients, 2 to 3 courses of treatment were performed, and the manipulation was grade 3 to 4. (2) If the patient undergoes surgical treatment, the patient should be elevated after surgery, and an ice pack should be used to cool the ankle joint, 2 times a day, for 3 to 5 days, and 1 day after the operation, the patient should be helped to perform ankle pump exercise through the protection of the ankle joint brace, and the exercise content includes straight leg raises and stepping on a bottle of wine on the affected foot. 2 days after the operation, the patients were instructed to perform ankle dorsiflexion, rotation, and active plantar flexion, 10 min/time, 3-7 times/d, so that the patient could reach the maximum range of motion of the ankle within 2 weeks. On the 7th day after operation, incomplete weight-bearing training with crutches was used to gradually increase the intensity of foot resistance exercises, followed by weight-bearing walking training; after 3 weeks of operation, the patient could walk without crutches; 3 months after surgery, you can basically return to normal exercise capacity [19]. Passive exercise can be added if necessary, but the intensity of exercise should be well controlled, and the exercise should be done gradually to avoid re-injury. If there is fluid accumulation in the ankle joint of the patient, the exercise

Figure 1: Rehabilitation physical training.

Table 4: Comparison of rehabilitation effects between the two groups of patients (cases (%)).

Group	Recover completely	General recovery	Not fully recovered
Test group ($n = 49$)	46 (93.88)	10 (51.23)	3 (6.12)
Control group ($n = 49$)	39 (79.59)	9 (12.34)	10 (20.41)
χ^2 value		4.3460	
P value		0.0371	

intensity of the patient should be appropriately reduced, and timely treatment should be performed; if necessary, puncture and fluid extraction can be performed. (3) Perform computer intermediate frequency therapy, 2 times/d, mainly for the function of the patient's tibialis anterior muscle and gastrocnemius muscle. In addition, high-power short-wave and pulsed magnetic therapy and electric weight loss gait therapy and air pressure therapy are used, 1-2 times/d. Continue treatment for 1 month.

(2) Test group

The patients were supplemented with sports medicine ultrasound examination on the basis of the control group: (1) the high-frequency ultrasound diagnosis grading of ligament injury was analyzed by ultrasonography, 25 cases (51.02%) of grade I injury (contusion) occurred, the ligament was thickened, with good continuity, and the echo was reduced and uneven. In 17 cases (34.69%) of grade II injury (partial laceration), part of the ligament was interrupted and thinned, the echo was reduced, and there was a fissure-like or sheet-like hypoechoic area, with or without effusion in the joint cavity. In 7 cases (14.29%) of grade III injury (complete laceration), the continuity of the ligament was completely interrupted, the broken end was separated, the echo was reduced, the surrounding echo was disordered, and dynamic scanning showed that the ligament tension disappeared [20]. (2) The doctor adjusts the patient's rehabilitation training intensity and methods according to the examination results, formulates a targeted rehabilitation training plan, and conducts the rehabilitation training before and after the patient's treatment. Ultrasonography was performed at 1 month, 2 months, and 3 months, respectively, to observe the swelling, exudation, and repair of the patient's ligament and adjust the treatment plan according to the results.

3.4. Observation Indicators. (1) Comparing the rehabilitation effects of the two groups of patients after 6 months of treatment, the echoes of the fully recovered ligaments were uniform, and the structure was flat and smooth. The pain and swelling of the ankle joint disappeared completely, the patient walked normally, and the range of motion of the joint was normal. Ultrasound examination of incompletely recovered ligaments showed bilateral contrast thickening, incomplete structure, abnormal joint mobility, and pain when walking. (2) The thickness of the anterior talofibular ligament and the thickness of the effusion were compared between the two groups of patients before and after treatment. (3) The ankle function scores of the two groups of patients after 3 months of treatment were compared, the Biard-Jackson scale was used to evaluate the ankle joint function, the excellent ankle function was 96-100 points, the good was 91-95 points, the average was 81-90 points, and the poor was 81 points or less. (4) The daily living ability of the two groups before and 3 months after treatment was compared, and the activity of daily living scale (ADL) was used to evaluate the daily living ability, the full score was 100 points, the higher the score, the better the living ability, the stronger.

3.5. Statistical Processing. The article uses SPSS 22.0 statistical software to process and analyze, the count data is expressed by $(n, \%)$, the χ^2 test is carried out, the measurement data is described by $(\bar{x} \pm s)$, and the t test is used. $P < 0.05$ indicates that the difference is statistically significant.

3.5.1. t-Test. t-test is a hypothesis test method established by British statistician W.S. Gosset in 1908 based on the principle of t-distribution, and it is often used to compare the means of two small samples in measurement data. Theoretically, the application condition of the t test is that the samples are from a normally distributed population, and the variance of the two populations is equal when the means of the two samples are compared. But in actual work, it deviates slightly from the above conditions, as long as its distribution is unimodal and approximately normal distribution, it can also be applied.

Table 5: Comparison of the thickness of the anterior talofibular ligament and the thickness of the effusion between the two groups of patients before and after treatment (mm, $\bar{x} \pm s$).

Group	Ligament thickness		Effusion thickness	
	Before therapy	After treatment	Before therapy	After treatment
Test group ($n = 49$)	4.37 ± 0.59	3.67 ± 0.57	7.54 ± 2.17	2.82 ± 0.67
Control group ($n = 49$)	4.61 ± 0.63	4.03 ± 0.65	7.49 ± 2.13	5.20 ± 1.78
t value	1.8444	2.7622	0.1091	8.3006
P value	0.0686	0.0070	0.9134	0.0000

There are three types of commonly used t-tests: (1) single-sample t-test: it is used to infer whether the overall mean represented by the sample mean and the known overall mean are statistically significant. When the number of samples is small ($n < 60$) and the overall standard deviation is unknown, the t-test is used; conversely, when the number of samples is large or the number of samples is small and the overall standard deviation is known, the u test can be used. (2) Paired specimen t-test: it is suitable for the comparison of the means of the two specimens in the paired design, and attention should be paid to whether the two specimens are paired design data when selecting [21]. The commonly used paired design data mainly have the following three situations: two homogeneous subjects receive two different treatments. The same subject or two parts of the same specimen received different treatments, respectively. The results of the same subject before and after treatment were compared. (3) Two independent samples t-test: also known as grouped t-test, it is suitable for the comparison of the means of two samples in a completely random design. Unlike the paired t-test, before performing the two-independent t-test, the homogeneity of variance test must also be performed on the two groups of data. If the sample is small and the variance is homogeneous, the t-test is used; otherwise, if the variance is unequal, the corrected t-test (t-test) is used or use data transformation methods (such as logarithm, square root, and reciprocal) to make the two groups of data have homogeneity of variance and then carry out t-test or use nonparametric test. In addition, when the number of samples in the two groups is large ($n1$, $n2 > 50$), the calculation of the t-test is cumbersome, and the u test can be used.

4. Results and Discussion

4.1. Comparison of Rehabilitation Effects between the Two Groups of Patients. The rehabilitation effect of the patients in the experimental group was better than that of the patients in the control group, and the difference was statistically significant ($P < 0.05$), as shown in Table 4.

4.2. Comparison of the Thickness of the Anterior Talofibular Ligament and the Thickness of the Effusion between the Two Groups of Patients before and after Treatment. The values of the experimental group were better than those of the control group, and the difference was statistically significant ($P < 0.05$), see Table 5.

Table 6: Comparison of ankle function scores between two groups of patients (points, $\bar{x} \pm s$).

Group	Biard-Jackson score	
	Before therapy	After treatment
Test group ($n = 49$)	62.35 ± 6.71	89.71 ± 2.17
Control group ($n = 49$)	62.76 ± 6.05	80.45 ± 1.98
t value	0.3010	20.9098
P value	0.7641	0.0000

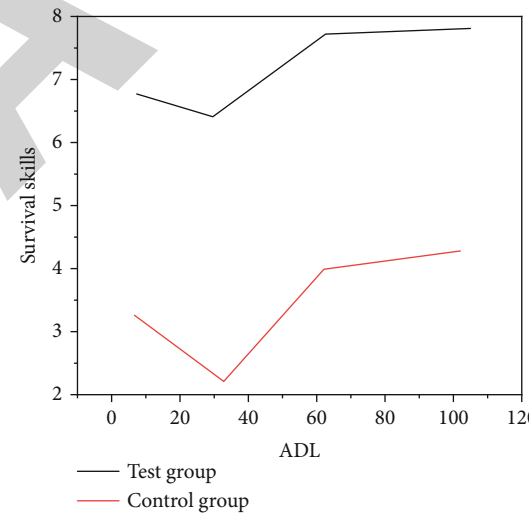

Figure 2: Comparison of daily living ability between the two groups of patients (score, $\bar{x} \pm s$).

4.3. Comparison of Ankle Function Scores between the Two Groups of Patients. The ankle joint score of the experimental group was higher than that of the control group, and the difference was statistically significant ($P < 0.05$), as shown in Table 6.

4.4. Comparison of Daily Living Ability between the Two Groups of Patients. The living ability of the patients in the experimental group was better than that in the control group, and the difference was statistically significant ($P < 0.05$), as shown in Figure 2.

4.5. Discussion. With the continuous development of ultrasound technology, it has been at a high level, especially the

sports medicine ultrasound technology has made great progress, its application in the examination and evaluation of soft tissue injuries has higher value, and doctors can obtain more objective data and indicators through this examination to improve their evaluation level [22]. When a patient has ligament injury, sports medicine ultrasonography can be used to determine the degree of tear of the patient's anterior talofibular ligament, and the treatment plan can be formulated according to the examination results. This examination method is used as an auxiliary means during the treatment and rehabilitation of patients, which can monitor the rehabilitation status of patients, which is of great significance for the timely adjustment of rehabilitation methods. Doctors can provide effective rehabilitation guidance in the process of patient recovery, shorten the patient's recovery time, and speed up the patient's recovery. The author compared the rehabilitation effect, ankle function score, and daily living ability of the two groups of patients; and the experimental group was better than the control group. Comparing the thickness of ligament and effusion between the two groups, the experimental group was also better than the control group, and the difference was statistically significant ($P < 0.05$). In summary, in the treatment of patients with anterior talofibular ligament injury, the use of sports ultrasound medical examination can help doctors to effectively judge the degree of injury and recovery of patients, and doctors can adjust the treatment plan in time according to the examination results and formulate an effective rehabilitation plan, which can greatly shorten the patient's rehabilitation time, improve the treatment effect, promote the functional recovery of the ankle joint, and reduce the occurrence of complications.

5. Conclusion

The author proposes to use ultrasound examination to observe the effects of rehabilitative physical training on ice and snow sports injuries, by dividing the patients into experimental group and control group for experimental data analysis, and it is concluded that the experimental group is superior to the control group. With the continuous development of ultrasound technology, it has been at a high level, especially the sports medicine ultrasound technology has made great progress, its application in the examination and evaluation of soft tissue injuries has higher value, and doctors can obtain more objective data and indicators through this examination and improve their evaluation level. Therefore, it can be determined that this method can effectively improve the treatment effect of patients, reduce pain, relieve psychological pressure, and be applied to the rehabilitation of winter sports system injuries.

Data Availability

The data used to support the findings of this study are available from the corresponding author upon request.

Conflicts of Interest

The authors declare that they have no conflicts of interest.

References

[1] L. Ye and P. Di, "Optimizing the regulation and control of sports injury and fatigue of winter olympic ice and snow athletes based on injury prevention," *Revista Brasileira de Medicina do Esporte*, vol. 27, no. spe2, pp. 79–82, 2021.

[2] E. Burrows and S. Mcardle, "Psychoeducation through digital video for olympic and paralympic athletic career transition," *Health Education Journal*, vol. 79, no. 5, pp. 516–528, 2020.

[3] P. Zhang, X. Yang, Y. Yin, Z. Zhang, and Y. Yao, "Effects of multidisciplinary model of damage control on acute cervical spinal cord injury in winter olympic sports," *American Journal of Translational Research*, vol. 13, no. 5, pp. 5051–5058, 2021.

[4] M. Maschke, "Ultrasound device," *Ultrasound in Medicine & Biology*, vol. 47, no. 4, pp. 982–997, 2021.

[5] M. I. Chushkin, L. A. Popova, S. Y. Mandrykin, and N. L. Kaprina, "Use of exercise tests and physical training in pulmonary rehabilitation," *Voprosy Kurortologii, Fizioterapii, i Lechebnoi Fizicheskoi Kultury*, vol. 98, no. 1, p. 64, 2021.

[6] A. Jp, A. Aw, B. Kk, C. Cyk, and C. Ag, "Preoperative mri for the multiligament knee injury: what the surgeon needs to know," *Current Problems in Diagnostic Radiology*, vol. 49, no. 3, pp. 188–198, 2020.

[7] J. Bailey, R. Irving, P. Dawson, D. R. Brown, and E. Campbell, "Influence of training-induced testosterone and cortisol changes on skeletal muscle and performance in elite junior athletes," *American Journal of Sports Science and Medicine*, vol. 9, no. 1, pp. 13–23, 2021.

[8] T. Akbulut, V. Inar, S. Ner, and R. Erdoan, "Strength development, muscle and tissue damage in different training models," *Journal of Pharmaceutical Research International*, vol. 33, no. 19B, pp. 1–6, 2021.

[9] X. Xi, W. Jiang, X. Hua, H. Wang, and Z. Luo, "Simultaneous and continuous estimation of joint angles based on surface electromyography state-space model," *IEEE Sensors Journal*, vol. 21, no. 6, pp. 8089–8099, 2021.

[10] A. L. Bullen, W. Cashion, L. Webster, P. M. Palevsky, S. D. Weisbord, and J. H. Ix, "Estimated urinary flow rate and contrast-associated acute kidney injury risk: the preserve (prevention of serious adverse events following angiography) trial," *Kidney Medicine*, vol. 3, no. 3, pp. 461–463, 2021.

[11] S. Majumder and M. J. Deen, "Wearable imu-based system for real-time monitoring of lower-limb joints," *IEEE sensors journal*, vol. 99, 2021.

[12] J. W. Agnew, A. L. Roy, S. B. Hammer, and F. F. Strale, "Pain sensitivity increases more in younger runners during an ultra-marathon," *Scandinavian Journal of Pain*, vol. 21, no. 2, pp. 364–371, 2021.

[13] Y. Liu, Y. Sun, W. Zhu, and J. Yu, "Comments to "Mechanism of hamstring muscle strain injury in sprinting" by Yu et al.," *Journal of Sport and Health Science*, vol. 6, no. 2, pp. 139-140, 2017.

[14] J. Lai and S. Issa, "A bump on the head…," *Emergency Medicine Journal*, vol. 38, no. 5, pp. 348–370, 2021.

[15] A. L. Valentyukevich, V. D. Melamed, and N. I. Prokopchik, "Experimental modeling of frostbites of varying severity in laboratory animals. Part 2. Morphological assessment of the

Hindawi
Scanning
Volume 2023, Article ID 9782180, 1 page
https://doi.org/10.1155/2023/9782180

Retraction

Retracted: Effect of Running Exercise on Brain Functional Magnetic Resonance Characteristics of College Students with Depression

Scanning

Received 12 December 2023; Accepted 12 December 2023; Published 13 December 2023

This article has been retracted by Hindawi, as publisher, following an investigation undertaken by the publisher [1]. This investigation has uncovered evidence of systematic manipulation of the publication and peer-review process. We cannot, therefore, vouch for the reliability or integrity of this article.

Please note that this notice is intended solely to alert readers that the peer-review process of this article has been compromised.

Wiley and Hindawi regret that the usual quality checks did not identify these issues before publication and have since put additional measures in place to safeguard research integrity.

We wish to credit our Research Integrity and Research Publishing teams and anonymous and named external researchers and research integrity experts for contributing to this investigation.

The corresponding author, as the representative of all authors, has been given the opportunity to register their agreement or disagreement to this retraction. We have kept a record of any response received.

References

[1] W. Li and J. Yang, "Effect of Running Exercise on Brain Functional Magnetic Resonance Characteristics of College Students with Depression," *Scanning*, vol. 2022, Article ID 7558807, 8 pages, 2022.

Hindawi
Scanning
Volume 2022, Article ID 7558807, 8 pages
https://doi.org/10.1155/2022/7558807

Research Article

Effect of Running Exercise on Brain Functional Magnetic Resonance Characteristics of College Students with Depression

Wangda Li and Jun Yang

School of Physical Education, Ankang University, Ankang, Shaanxi 725099, China

Correspondence should be addressed to Jun Yang; 11231124@stu.wxic.edu.cn

Received 14 June 2022; Revised 14 July 2022; Accepted 22 July 2022; Published 5 August 2022

Academic Editor: Danilo Pelusi

In order to effectively reduce the incidence of depression in college students, the author proposes a method to influence brain functional magnetic resonance through running exercise. Aiming at the effect of running exercise on the brain functional magnetic resonance characteristics of depression in college students, through the comparison experiment between the MDD group and the HC group and the retrospective analysis of the sugar water preference experiment in rats, explore it in depth. Experimental results show that under the running exercise for six consecutive weeks, the average body weight of the rats in the depression model group was significantly lower than that in the blank control group, and the health status was significantly better than that in the blank group. Running exercise can effectively affect and reduce the incidence of depression in college students.

1. Introduction

Depression (Figure 1) is a common clinical mood disorder, mainly manifested as persistent sadness, anhedonia, loss of interest, lack of energy and physical strength, and decreased self-confidence. Most of the patients were also accompanied by unexplained somatization symptoms, varying degrees of cognitive impairment, and obvious retardation of thinking and action. They are always dissatisfied with the surrounding environment and quality of life, and they cannot experience the happiness they want, in severe cases, suicidal ideation and suicidal behavior occur. With the increase of life pressure, the prevalence of depression is increasing year by year, and it is getting younger. A survey in the United States showed that among 10,000 young people aged 13-18, about 15.9% of young men and 15.9% of young women had experienced a depressive episode, and most of the young people's symptoms became chronic into adulthood or even aggravated [1]. According to the World Health Organization, about 100% of people will experience a depressive episode in their lifetime, and it is predicted that by 2020, depression may become the second most common disease after heart disease, which damages personal mental health and social function and also affects families, and society brings an unbearable burden [2]. Therefore, depression is a major problem that threatens public health and needs to be solved urgently.

Running is defined by the American College of Sports Medicine as one of the organized and planned repetitive physical movements [3]. In recent years, it has received extensive attention as a nondrug antidepressant treatment. Studies have shown that running exercise 3 times a week for at least 8 weeks can achieve a therapeutic effect on patients with severe depression, and the intensity of the effect is about moderate to high; it was also found in animal experiments that running exercise can effectively improve the depression-like or anxiety-like behavior of experimental animals [4]. However, some people have put forward the opposite conclusion, they believe that running exercise has no antidepressant effect, and in the follow-up study of patients with depression, there is no significant improvement in the quality of life and disease severity of patients with depression [5]. If running can improve symptoms of depression or depressive-like behaviors, what is the mechanism by which running can improve depression?

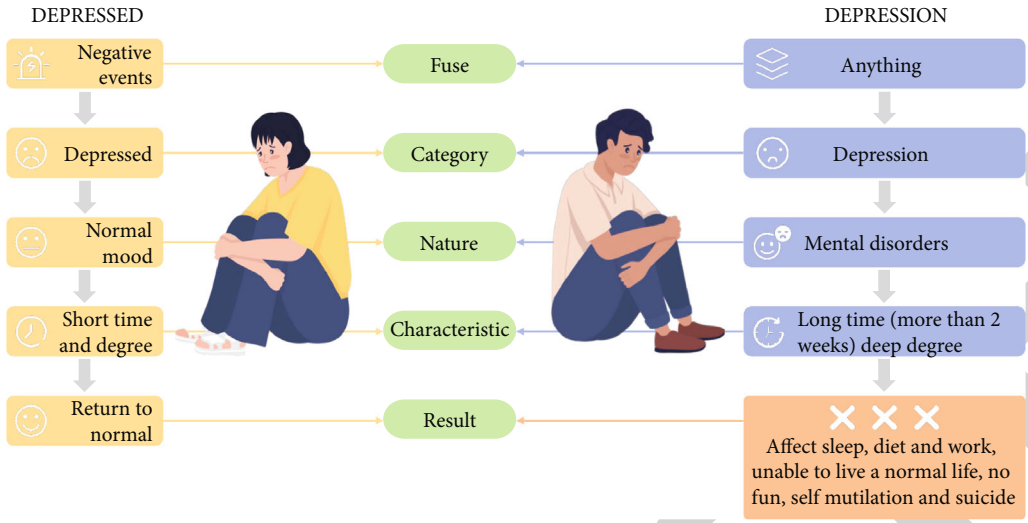

Figure 1: Depression.

In order to further study the effect of running exercise on patients with depression, therefore, from the perspective of brain functional magnetic resonance characteristics, we can quickly and effectively draw conclusions and provide a therapeutic method for the treatment of depression.

2. Literature Review

Depression is a common mental disorder; its main clinical manifestations are low mood, decreased interest, and decreased energy; these symptoms have a high rate of disability and recurrence; in severe cases, suicidal behavior occurs. According to statistics from the World Health Organization, there are currently more than 350 million MDD patients in the world; a large epidemiological study in my country shows that the lifetime prevalence of MDD has reached, and the incidence is increasing year by year; at the same time, more people have depression, calculated in terms of disability-adjusted life years; the disability rate of depression ranks second and shows an upward trend [6]. If the incidence of MDD continues to rise and is not effectively controlled, it will become a significant contributor to the global burden of disease and disability. If MDD is not properly treated, not only is it easy to relapse, but with the increase of the number of relapses, the patient's social function and cognitive function will gradually decline. At present, MDD has become an urgent worldwide public health problem [7].

In recent years, with the gradual deepening of research on MDD, it has been found that it has a trend of younger age, so adolescent MDD has gradually received attention. Unlike adult MDD, adolescent MDD usually has a slow, long-term course. Studies have shown that after entering adolescence, the incidence of depression in adolescents increases sharply. Compared with adults, the risk of MDD in adolescence is doubled, and the detection rate of depressive symptoms in adolescents is between 60.7%; the total value is higher than the detection rate of adults and the elderly in my country; the recurrence rate of depressive symptoms is high [8]. At the same time, the depressive symptoms of adolescents also have atypical characteristics; the onset is insidious and may manifest as emotional problems such as emotional instability and irritability or behavioral problems such as truancy, substance abuse, fighting, and suicide. Adolescents not only face tremendous physical changes, but also are under enormous psychological pressure; if depression is not well regulated, it may lead to a series of long-term negative outcomes, including declining academic performance, interpersonal tension, substance abuse, dropping out of school, and health problems. Therefore, early identification of adolescents with MDD, and providing timely, evidence-based treatment, is important to reduce disability and suffering.

At the same time, an fMRI study of adolescent depression found that the limbic system-pallidal-thalamic circuit has abnormal brain functional activity [9, 10]. However, it has not been found that NLE can cause abnormal brain function in adolescents with MDD [11]. Therefore, whether NLE is an influencing factor of abnormal brain activity in adolescent MDD patients, the result is unknown and needs to be further explored.

According to literature records, Grońska-Pski et al. proposed in that running exercise can significantly increase the number of precursor cells in the hippocampal dentate gyrus of C57BL/6 mice and promote the survival of new neurons [12]. Botterill et al. pointed out that running exercise can significantly increase the number of new neurons in the hippocampal dentate gyrus of aged rats and reduce dentate gyrus apoptosis [13]. A large number of studies have shown that the antidepressant effect of exercise depends on the changes in the new ability of hippocampal neurons, but the fluorescent semiquantitative $BRDU^{+}$ cells obtained in previous studies cannot fully reflect the changes of new neurons, precise quantitative study on the effect of running exercise on new hippocampal neurons in improving depression symptoms; related reports have not been seen [14].

On the other hand, previous studies have shown that running exercise can effectively improve depression symptoms and promote the regeneration of neurons in the dentate gyrus of the hippocampus, so does the new generation of neurons mean the renewal of the neural signaling system? And are the changes in the proliferation and differentiation of oligodendrocytes and their oligodendrocyte precursor cells, which are closely related to neural signal transduction, also involved?

Based on the above research, the author conducted a related study on the effect of running exercise on the brain functional magnetic resonance characteristics of college students' depression. The authors retrospectively analyzed the relationship between NLE and brain region function in first-episode adolescent MDD patients based on fMRI. The first-episode adolescent patients with depression who were not treated with drugs were selected as the research objects, and the correlation between NLE and the functional activity of brain regions in the first-episode adolescent MDD patients was investigated based on fMRI, and the effect of running exercise on it was further explored and provides a treatment plan for depression treatment.

3. Methods

Experiment 1: In order to explore the correlation between NLE and brain region function in first-episode adolescent MDD patients based on functional magnetic resonance imaging.

3.1. Selection of Research Objects. In order to exclude related confounding factors such as drugs and disease duration, the authors selected the data of the first-episode, untreated adolescent MDD patients in a certain experiment for a retrospective analysis [15].

3.1.1. First-Episode Adolescent Depression Group (MDD Group) (1) Inclusion Criteria.

(i) According to the diagnostic criteria of DSM-5, patients diagnosed with depression by two or more attending psychiatric clinicians have five manic episodes, which are the first depressive episodes

(ii) Age 18-22

(iii) HAMD-24≧18 points

(iv) Have never received antidepressant treatment in various ways such as psychotropic drugs, psychotherapy, and electroconvulsive therapy

(v) Han nationality, right-handed

(vi) Able to cooperate with the completion of the scale assessment

(2) Exclusion Criteria.

(i) A previous definite episode of mania or hypomania

(ii) Those with a previous diagnosis of bipolar disorder, schizophrenia or other mental disorders

(iii) Patients with a history of substance abuse and acute poisoning

(iv) Head trauma, loss of consciousness or serious physical illness

(v) Contraindications for MRI scanning, such as artificial heart valves, metal foreign bodies, etc.

3.1.2. Healthy Controls (HC Group). Inclusion criteria:

(i) Age 18-22 years old

(ii) HAMD-24≦7 points

(iii) Han nationality, right-handed

(iv) No serious physical or mental illness

(v) Have not taken sleeping, anesthesia, analgesic, and other drugs in the past month before enrollment

(1) Able to cooperate with the completion of the scale assessment

Exclusion criteria:

(i) Those with a previous diagnosis of depression, bipolar disorder, schizophrenia, or other mental disorders associated with other diseases

(ii) Patients with a history of substance dependence and acute poisoning in the past

(iii) Head trauma, loss of consciousness or serious physical illness

(iv) Contraindications for MRI scanning, such as artificial heart valves and metal foreign bodies, etc.

3.2. Research Tools

3.2.1. General Population Information Collection. A self-made questionnaire was used to collect the demographic information of all subjects, including name, age, gender, right-handedness, ethnicity, years of education, family history, past history, and personal history, as well as the time of the onset and the last MDD medical history information such as monthly drug use [16].

3.2.2. Hamilton Depression Scale (HAMD-24). Developed in 1960, this scale is one of the scales commonly used clinically to assess the severity of depression and depressive symptoms, and the assessment time range is the most recent week. The HAMD-24 has 24 items covering the following 7 categories of factors: anxiety/somatization, blockade, cognitive impairment, sense of hopelessness, weight changes, sleep disturbances, and circadian variability, of which 10 items are on a 3 scale from 0 to 2 For scoring, 14 items were scored on a 5-

point scale from 0 to 4. The total score indicates that there are no depressive symptoms; the score that may have mild or moderate depression may indicate severe depression [17].

3.2.3. Hamilton Anxiety Scale (HAMA). The scale was developed in 1959; HAMA is one of the commonly used clinical scales to evaluate anxiety symptoms, and the assessment time range is the situation of the most recent week. There are 14 items in HAMA, which can be classified into two factors: mental anxiety and somatic anxiety. A 5-point scale from 0 to 4 was used. The total score of <7 points has no anxiety symptoms; ⩾7 points may have anxiety; ⩾14 points must have anxiety; ⩾21 points must have obvious anxiety; ⩾29 points may indicate severe anxiety [18].

3.2.4. Adolescent Life Events Self-Rating Scale (ASLES). The scale is a combination of domestic and foreign literatures by many domestic experts, based on the actual situation in my country; it was compiled in 1987; the scale measures the influence of negative life events in adolescents in the past 12 months, currently widely used. ASLEC has a total of 27 items with a 5-level score [19]. It can be divided into the following six categories of factors: learning stress factor, interpersonal relationship factor, loss factor, punishment factor, health adaptation factor, and others (including school fatigue, relationship dissatisfaction or breakdown, quarrel with others, parental beating, and scolding 4 items); the higher the score, the more negative sexual events have a greater impact. The scale has good reliability and validity. It applies to adolescents to assess stress intensity and frequency of life events.

3.3. Research Methods

3.3.1. Clinical Data and Scale Data Collection. According to the inclusion criteria, the demographic data collection was completed on the same day as outpatient visits or hospitalizations by trained researchers in the adolescent MDD group; at the same time, all subjects were asked to complete the scale assessment in a mental health center psychological testing center. The HC group was under the guidance of trained researchers to collect general demographic data and evaluate the scale; after completing the above steps, the resting state brain function MRI data of the research subjects were collected.

3.3.2. Resting-State Functional Brain MRI Data Acquisition. Magnetic resonance data acquisition of study subjects was completed in a mental health center. The data of three modalities of structural image, BOLD, and diffusion tensor imaging were collected for all subjects. During the acquisition process, the head position of the research subject was fixed, and active and passive movements of the head and other parts were avoided, and the subjects were in a quiet supine position; during the scanning process, anti-irritability headphones were worn to reduce the interference caused by noise. The patient was asked to stay awake, still, eyes closed, and try to avoid moving and thinking during the entire MRI scan. Echo-planar imaging (EPI) sequence was used for scanning, and the parameters were scanned by resting state functional image: Repetition Time = 2000ms, acquisition matrix = 64×64, flip angle = 90°, Rield of View = 240 × 240mm, Echo Time = 30ms, depth of stratum: 4.0mm, no layer spacing, a total of 35 layers [20].

3.3.3. Image Processing

(1) Preprocessing. Firstly, the MRI conversion software was used to convert the DICOM format images into NIfTI format for data processing. The images were then preprocessed using DPARSF software. Specific steps are as follows:

(1) Remove time points: considering that the uneven magnetic field may affect the image, the first 10 time points of the image are removed, in order to stabilize the MRI signal, and the research subjects need to adapt to the scanning environment noise

(2) Time series correction: correct the image acquisition time, in order to eliminate the influence of the time difference of the brain due to the different scanning time on the image time series of each layer

(3) Correction of head movement: the rotation on the x, y, and z axes is greater than 3° or culling images with a maximum head movement translation exceeding 3 mm; head movement parameters, cerebrospinal fluid, and white matter were used as covariates

(4) Normalization: the authors registered the T1 structural and functional images, and then matched them with the Montreal Neurological Institute template for $3 \times 3 \times 3$ mm voxel resampling

(5) Smoothing: convolve and smooth the normalized image using an isotropic Gaussian kernel (maximum width at half maximum = 8 mm) to reduce spatial noise

(6) Delinear drift and filter processing: in order to reduce low-frequency drift and eliminate physiological noise, the filter signal with frequency in the range of 0.01-0.08 Hz is extracted

(2) ALFF, fALFF analysis. ALFF is the Fourier transform of the time series for each voxel throughout the brain, and convert to domain power spectrum. The area under the power spectrum can be regarded as the signal energy intensity, and then the area under the peak is squared, and the result is the change intensity of the BOLD signal, which represents the amplitude of the signal oscillation. The ALFF value for each voxel was divided by the whole-brain average ALFF value as the normalized ALFF value for each voxel. ALFF can be used to reflect the strength of spontaneous activity of voxels in the resting state, thereby reflecting the strength of local neuronal activity. ALFF is a modified ALFF that can effectively suppress nonspecific hyperintensity from the cisternal region and improve the sensitivity and specificity of spontaneous neuron detection.

(3) REHO Analysis. REHO reflects the synchronization of local neuronal activity in brain regions. Perform local consistency analysis on the unsmoothed data, calculate and

compare the time series synchronization of each voxel in the whole brain with its adjacent 26 voxels, obtain the Kendall harmony coefficient, that is, the REHO value, and then divide by the whole brain REHO mean, and then smoothed with an 8-mm FWHM Gaussian kernel.

3.4. Statistical Analysis. Data entry and statistical analysis were performed in SPSS software. On SPSS 24.0 software, the general data of the two groups were compared by x^2 test and t -test. The t-test and nonparametric test were used to compare the scores of HAMD-24, HAMA, and ASLEC between the two groups. The measurement data were expressed with mean ± standard deviation$(x \pm s)$. Inspection level $\alpha = 0.05$. Using SPM software, t-test was performed on the ALFF value, fALFF value, and REHO value of the two groups. The xjview plug-in and BrainNet software were used to calculate and display brain areas with statistically significant differences (Alphasim correction, the areas of $P < 0.01$ and voxel >20 are defined as statistically significant differences). Pearson correlation analysis was used to analyze the correlation between ASLEC and HAMD-24 score in MDD group. The correlation between the different brain regions in MDD group and HAMD-24 was analyzed. Partial correlation analysis was performed between different brain regions in MDD group and ASLEC.

3.5. Quality Control

(1) When the research subjects were enrolled, two or more attending physicians conducted structured interviews with the patients, in order to ensure the accuracy of diagnosis

(2) The other scale assessments (HAMD-24, HAMA) were completed by two uniformly trained researchers, respectively, in order to ensure the authenticity of the test results

(3) For Self-Assessment Scale Filling (ASLEC), before filling in, the researcher will introduce the purpose and filling method of the scale and inform that if you have any questions, please raise your hand, and the researcher will give a neutral explanation

Experiment 2: Establishment of depression model rats and research on the behavioral effect of running exercise.

3.5.1. Experimental Animals and Groups. Sprague-Dawley rats in a certain experimental experiment were selected as the research objects for retrospective analysis; about one rat was in a cage (room temperature, with a day-night cycle between 7 : 00 and 19 : 00); food and water supplies are adequate. One week later, SD rats were randomly divided into blank control group (UCG) and depression model group (DMG). The sugar water preference test and open field test were used to evaluate the sugar water preference and autonomous activity ability of experimental rats, so as to avoid the influence of individual rat individual differences on the establishment of chronic unpredictable stress model. During the subsequent establishment of the depression model, a sugar water preference experiment was conducted every weekend to evaluate the establishment of the depression model; after the depression model was established, the rats in the depression model group were further divided into the depression model control group (MCG) and the depression running model group (RMG).

3.5.2. Establishment of a Chronic Unpredictable Stress-Depression Model. Rats were randomly divided into blank control group and depression model group. Rats in the blank control group were given one cage per cage and were normally provided with food and water (room temperature, with a day-night cycle between 7 : 00 and 19 : 00), and the cleaning bedding was changed regularly every week. The depression model group established a rat model of chronic unpredictable stress-induced depression according to the method, as follows: All the rats in the depression model group were kept in single cages, randomly arranged stimuli each day; the various stressful stimuli required for model establishment include food deprivation, water deprivation, continuous noise (80 dB), continuous horizontal vibration, damp litter, 3 confinement, continuous tilted cage (45 degrees tilt), cold and hot bath day and night reversed, continuous clamping tail, overnight lighting, and foot shock (current intensity). The above stimuli lasted for 7 weeks, and each stress appeared several times during the modeling process, and the reappearance of the same stimuli required an interval of 5 days or more. After the stress, according to the behavioral test results, the successfully modeled depression model rats were randomly divided into a model control group and a depression running exercise group. During the modeling period, the rats in the blank control group did not receive any intervention.

3.5.3. Running Workouts. After the model was established, the rats in the depression running exercise group were given a 6-week running exercise intervention; in the experiment, a horizontal treadmill was selected as the exercise equipment for the rats; in order to ensure that the rats in the depression running exercise group can receive regular running exercise, the initial speed of running exercise was 10 m/min in the first week and then accelerated to 20 m/min every day. In the second week, the running exercise continued at the speed of 20 m/min. Run 5 days a week with 2 days off. The blank control group and the model control group were given running intervention at the end.

3.6. Weight. The body weight of the experimental rats was recorded every week during the whole experiment.

3.7. Behavioral Tests

3.7.1. Sugar Preference Experiment (SPT). The authors conducted a retrospective analysis of the sugar water preference experiment; in the experiment, the sugar water preference laboratory was the gold index for evaluating the anhedonia characteristics of depressed animal models. In the training stage before the experiment, rats were given 200 ml/bottle of 1% sucrose water and pure water, respectively; it is used to avoid the fear response of new things in experimental rats and affect the later formal test. In the formal experiment of sugar water preference, experimental rats can freely ingest 1% sucrose water or pure water for 24 hours and record the weight of sucrose water and pure water before and after the test, respectively, so as to obtain the respective consumption

Table 1: The areas where the ALFF value increased in the MDD group compared with the HC group.

Brain area	MNI coordinates			t value	Bulk voxels
	x	y	z		
Bilateral thalamus	15	-12	3	4.11	285
Left parahippocampal gyrus	-24	-33	-18	3.79	253
Right fusiform gyrus, parahippocampal gyrus	36	-51	-12	4.05	338

Table 2: The areas where the fALFF value of the MDD group increased compared with the HC group.

Brain area	MNI coordinates			t value	Bulk voxels
	x	y	z		
Wedge leaf	15	-69	24	3.82	242
Medial prefrontal lobe	-15	63	-3	4.26	191
Cerebellum	-39	-72	-30	5.44	110

Table 3: Areas of increased REHO value in MDD group compared with HC group.

Brain area	MNI coordinates			t value	Bulk voxels
	x	y	z		
Calcaroid gyrus	0	-87	-3	3.95	43
Right cerebellum	18	-57	-39	3.83	46

of sucrose water and pure water; the percentage of preference for sugar water for each rat was then calculated according to the formula (% sugar water preference = sugar water consumption/total fluid consumption × 100%); during the period, all the experimental rats were kept in single cages and fed normally, and the sugar water preference experiment was conducted once a week.

4. Results and Discussion

Experiment 1: In order to explore the correlation between NLE and brain region function in first-episode adolescent MDD patients based on functional magnetic resonance imaging.

4.1. Comparison of Brain Function Activity between the Two Groups

4.1.1. Comparison of ALFF Values between MDD Group and HC Group. Compared with the HC group, the ALFF values of the bilateral thalamus, right fusiform gyrus, and bilateral parahippocampal gyrus increased in the MDD group, and the difference was statistically significant (see Table 1); there were no brain regions with lower ALFF values in the MDD group than in the HC group, and the difference was not statistically significant ($P > 0.005$).

4.1.2. Comparison of fALFF Values between MDD Group and HC Group. Compared with the HC group, the fALFF values in the cuneiform, medial prefrontal cortex, and cerebellum regions of the MDD group were increased, and the difference was statistically significant (see Table 2).

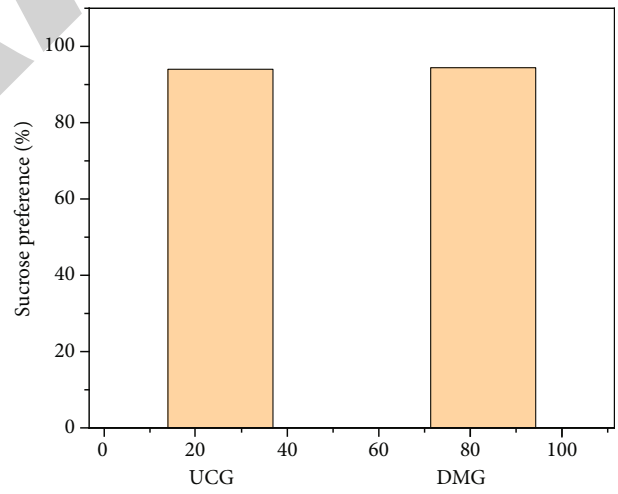

Figure 2: Comparison of sugar water preference between blank control group and depression model group.

4.1.3. Comparison of REHO Values between MDD Group and HC Group. Compared with the HC group, the MDD group had higher REHO values in the talar gyrus and right cerebellum, and the difference was statistically significant (see Table 3); no brain regions with lower REHO values were found in the MDD group than in the HC group. There was no statistical difference ($P > 0.005$).

Experiment 2: Establishment of depression model rats and research on the behavioral effect of running exercise.

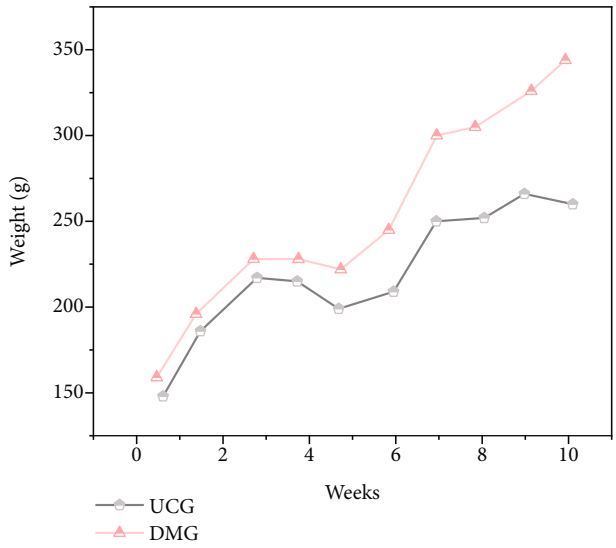

Figure 3: Statistics of body weight of rats in depression model group and blank control group.

4.2. Screening before Modeling. Before the establishment of the chronic unpredictable stress depression model, the sugar water preference test was used to screen the initial sugar water preference of the rats; the results showed that in the sugar water test [21], there was no significant difference in the sugar water preference between the blank control group and the depression model group (Figure 2).

4.3. Weight. Before the establishment of the chronic unpredictable stress depression model, the body weight of the blank control group and the depression model group showed a steady upward trend, and there was no significant difference in body weight between the two groups in Figure 3.

5. Conclusion

The author studies the effect of running exercise on the brain functional magnetic resonance characteristics of college students' depression; through the comparison experiment between MDD group and HC group and the retrospective analysis of the rats' sugar water preference experiment, the in-depth discussion was carried out. The results showed that under the running exercise for six consecutive weeks, the average body weight of the rats in the depression model group was significantly lower than that in the blank control group 22.5%; it shows that running exercise has a relieving effect on college students' depression.

Data Availability

The data used to support the findings of this study are available from the corresponding author upon request.

Conflicts of Interest

The authors declare that they have no conflicts of interest.

References

[1] F. Abo-Rass, P. Werner, and S. Shinan-Altman, "Cognitive illness representations among Israeli Arabs diagnosed with depression and their relationship with health-related quality of life," *International Journal of Social Psychiatry*, vol. 68, no. 3, pp. 582–588, 2022.

[2] W. C. Drevets, G. M. Wittenberg, E. T. Bullmore, and H. K. Manji, "Immune targets for therapeutic development in depression: towards precision medicine," *Nature Reviews Drug Discovery*, vol. 21, no. 3, pp. 224–244, 2022.

[3] S. Aryanti and E. Pangestu, "Uphill running exercise of speed on futsal extracurricular high schools," *Journal of Physics Conference Series*, vol. 1832, no. 1, p. 012057, 2021.

[4] S. Bonnaerens, P. Fiers, S. Galle, R. Derie, and V. Segers, "Relationship between duty factor and external forces in slow recreational runners," *BMJ Open Sport & Exercise Medicine*, vol. 7, no. 1, article e000996, 2021.

[5] M. Ishikawa, "Long working hours, depression and suicidality among OB/GYNS in Japan," *Occupational Medicine*, vol. 72, no. 3, pp. 200–206, 2022.

[6] M. Ogawa, M. Fujikawa, K. Jin, Y. Kakisaka, and N. Nakasato, "Acceptance of disability predicts quality of life in patients with epilepsy," *Epilepsy & Behavior*, vol. 120, Suppl 2, p. 107979, 2021.

[7] S. Pridmore, M. Rybak, R. Morey, and T. May, "The impact of transcranial magnetic stimulation (TMS) on irritability occurring with acute major depressive disorder (MDD)," *Australasian Psychiatry*, vol. 29, no. 2, pp. 218–221, 2021.

[8] R. Hrynyschyn and C. Dockweiler, "Effectiveness of smartphone-based cognitive behavioral therapy among patients with major depression: systematic review of health implications," *JMIR mHealth and uHealth*, vol. 9, no. 2, article e24703, 2021.

[9] M. C. Ho, H. A. Shen, Y. Chang, and J. C. Weng, "A CNN-based autoencoder and machine learning model for identifying betel-quid chewers using functional MRI features," *Brain Sciences*, vol. 11, no. 6, p. 809, 2021.

[10] M. Jafarian, S. Mousavi, S. Rahimi, F. G. Pakdel, and A. Gorji, "The effect of gabaergic neurotransmission on the seizure-related activity of the laterodorsal thalamic nuclei and the somatosensory cortex in a genetic model of absence epilepsy," *Brain Research*, vol. 1757, p. 147304, 2021.

[11] U. Gke, B. E. Drtkardeler, and A. Aslan, "Demographic, epidemiologic and clinical analyses of paediatric patients hospitalized with henoch-schonlein purpura: a retrospective study," *The Journal of Pediatric Research*, vol. 8, no. 1, pp. 35–40, 2021.

[12] M. Grońska-Pski, J. T. Gonalves, and J. M. Hébert, "Enriched environment promotes adult hippocampal neurogenesis through FGFRS," *The Journal of Neuroscience*, vol. 41, no. 13, pp. 2899–2910, 2021.

[13] J. J. Botterill, K. Y. Vinod, K. J. Gerencer, C. M. Teixeira, and H. E. Scharfman, "Bidirectional regulation of cognitive and anxiety-like behaviors by dentate gyrus mossy cells in male and female mice," *The Journal of Neuroscience*, vol. 41, no. 11, pp. 2475–2495, 2021.

[14] R. Guo, W. S. Qin, S. Y. Zhang, and S. L. Zhang, "Effects of ganmai dazao tang on synaptic structure of hippocampal neurons in depression model rats," *Zhongguo ying yong sheng li xue za zhi = Zhongguo yingyong shenglixue zazhi = Chinese journal of applied physiology*, vol. 36, no. 5, pp. 444–448, 2020.

Hindawi
Scanning
Volume 2023, Article ID 9829873, 1 page
https://doi.org/10.1155/2023/9829873

Retraction

Retracted: Effect of Foot and Hand Massage on Abdominal Pain of Cesarean Section Incision under Ultrasound Guidance

Scanning

Received 3 October 2023; Accepted 3 October 2023; Published 4 October 2023

This article has been retracted by Hindawi following an investigation undertaken by the publisher [1]. This investigation has uncovered evidence of one or more of the following indicators of systematic manipulation of the publication process:

(1) Discrepancies in scope

(2) Discrepancies in the description of the research reported

(3) Discrepancies between the availability of data and the research described

(4) Inappropriate citations

(5) Incoherent, meaningless and/or irrelevant content included in the article

(6) Peer-review manipulation

The presence of these indicators undermines our confidence in the integrity of the article's content and we cannot, therefore, vouch for its reliability. Please note that this notice is intended solely to alert readers that the content of this article is unreliable. We have not investigated whether authors were aware of or involved in the systematic manipulation of the publication process.

In addition, our investigation has also shown that one or more of the following human-subject reporting requirements has not been met in this article: ethical approval by an Institutional Review Board (IRB) committee or equivalent, patient/participant consent to participate, and/or agreement to publish patient/participant details (where relevant).

Wiley and Hindawi regrets that the usual quality checks did not identify these issues before publication and have since put additional measures in place to safeguard research integrity.

We wish to credit our own Research Integrity and Research Publishing teams and anonymous and named external researchers and research integrity experts for contributing to this investigation.

The corresponding author, as the representative of all authors, has been given the opportunity to register their agreement or disagreement to this retraction. We have kept a record of any response received.

References

[1] Y. Q. Wang, R. Jiang, and J. Pan, "Effect of Foot and Hand Massage on Abdominal Pain of Cesarean Section Incision under Ultrasound Guidance," *Scanning*, vol. 2022, Article ID 8356256, 7 pages, 2022.

Hindawi
Scanning
Volume 2022, Article ID 8356256, 7 pages
https://doi.org/10.1155/2022/8356256

Research Article

Effect of Foot and Hand Massage on Abdominal Pain of Cesarean Section Incision under Ultrasound Guidance

Yu Qing Wang,[1] **Rongrong Jiang**,[2] **and Jianmin Pan**[2]

[1]*Pregnant Women School, Changyi People's Hospital, Weifang, Shandong 261300, China*
[2]*Delivery Room, Changyi People's Hospital, Weifang, Shandong 261300, China*

Correspondence should be addressed to Yu Qing Wang; 20160599@ayit.edu.cn

Received 16 June 2022; Revised 4 July 2022; Accepted 14 July 2022; Published 27 July 2022

Academic Editor: Danilo Pelusi

In order to relieve the pain of incision after cesarean section, a method of foot and hand massage for abdominal pain of cesarean section incision under ultrasound guidance was proposed in this paper. In this paper, the experimental control method and retrospective analysis were used to relax the patients through massage, so that the pregnant women could focus on the reaction caused by hand and foot massage, distract their attention, and reduce the pain. The results showed that 60 cases of puerpera after cesarean section were divided into two groups with 30 cases in each group. The control group was only given routine care. The intervention group received 20 min hand and foot massage on the basis of routine care. The visual analog scale (VAS) of pain before, immediately after, 30 min after, and 60 min after massage in the intervention group was evaluated and recorded, and the VAS scores of the control group at the corresponding time points were recorded. The VAS score of the intervention group at each time point after massage was significantly lower than that before massage ($P < 0.05$), and the VAS score of the intervention group at each time point was significantly lower than that of the control group ($P < 0.01$). Hand and foot massage can effectively relieve incision pain after cesarean section.

1. Introduction

Pregnancy and childbirth are normal physiological processes of human reproduction. Most women can naturally give birth to healthy babies. Cesarean section refers to the obstetric operation to remove the fetus and its appendages by cutting the abdominal wall and uterine wall after 28 weeks of pregnancy. Cesarean section is an important means to solve dystocia and some high-risk pregnancies and save the lives of mothers and infants.

With the development of society, cesarean section has become one of the important ways for parturients to deliver. It is an important means to solve many obstetric conditions, such as cephalopelvic disproportion, fetal malposition, and fetal distress, and reduce the maternal and neonatal mortality [1]. As well as the improvement of pregnant women's requirements for delivery, the cesarean section rate remains at a high level. In the number of deliveries, 1593425 cases had cesarean section, and the cesarean section rate was 50.67%. From 2019 to 2021, the age standardized cesarean section rates were 52.37%, 49.90%, 49.75%, 51.13%, and 50.66%, respectively, showing a downward trend first and then an upward trend (Figure 1). The average age of cesarean section delivery was 28.23 years, and the average age of noncesarean section delivery was 26.49 years.

It is necessary to further clarify the relevant factors that affect the choice of cesarean section for pregnant women, so as to provide corresponding basic support for this study. The analysis results of this study show that the independent factors affecting cesarean section include age, education level, registered residence, type of delivery hospital, prepregnancy BMI, maternal type, mode of pregnancy, adverse pregnancy and childbirth history, pregnancy complications or complications, and the number of pregnancy examinations. The cesarean section rate of pregnant women in area B is still high, as shown in Table 1.

After cesarean section, the anesthetic effect gradually subsides, and the pain sensation of lower abdominal incision begins to recover. Generally, it is most obvious within 24 h after the operation, which not only brings discomfort to

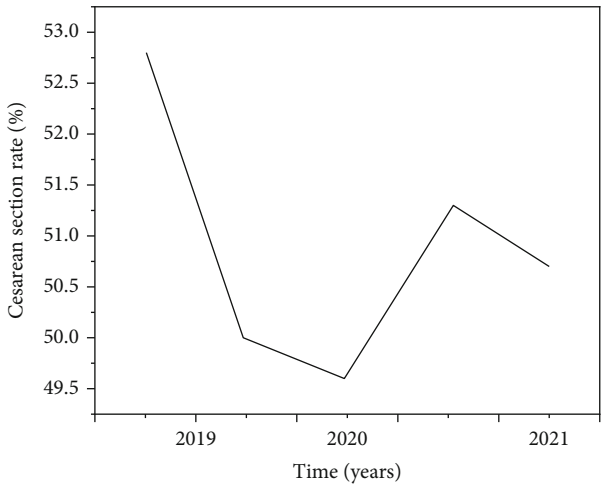

Figure 1: Time trend of cesarean section rate from 2019 to 2021.

the body but also psychological damage [2]. Pain is defined as the fifth vital sign after the four vital signs of body temperature, pulse, respiration, and blood pressure [3]. Therefore, relieving the incision pain after cesarean section has become one of the important tasks of nursing staff [4]. Pain after cesarean section is an important factor affecting the postoperative recovery and lactation of parturients. Good analgesia can reduce pain response and promote rapid postoperative recovery and postoperative lactation. The traditional methods of clinical analgesia are mainly epidural analgesia and intravenous analgesia. The effect of epidural analgesia is good, but it needs to retain epidural catheter (Figure 2). It is difficult to manage after operation. Maternal activities are easy to lead to catheter prolapse, motor block, urinary retention, and other adverse reactions. Intravenous analgesia is easy to use and manage, but opioid analgesics are prone to respiratory depression, excessive sedation, nausea, vomiting, and other adverse reactions. Multimodal analgesia is increasingly used in clinic to improve the analgesic effect and reduce adverse reactions. However, at present, there are still deficiencies in pain control after routine analgesia [5]. Ultrasound-guided foot and hand massage is effective in relieving postoperative incision pain [6]. The purpose of this study is to explore the intervention effect of foot and hand massage guided by ultrasound on incision pain of patients after cesarean section, to seek intervention methods to relieve their pain to the greatest extent, and to provide scientific basis for clinical practice [7].

2. Literature Review

There are many reasons for the postoperative pain of parturients. The most important ones are the pain of incision and the uterine contraction pain caused by the recovery of uterus, and the uterine contraction pain is more obvious after operation. With the disappearance of anesthetics after cesarean section, pregnant women will feel pain. The pain is not only limited to incision pain but also accompanied by contractile pain caused by intravenous oxytocin. If postoperative analgesia is not used, the degree of pain is mostly severe (VAS > 7 points) [8]. It can be seen from Table 2 that compared with cesarean section, the estimated value, real value, and recall value of pain in natural delivery were slightly higher, but the difference was not statistically significant ($P > 0.05$). There was no significant difference in the predicted value, the true value, and the recall value of pain among the parturients who gave birth naturally ($P > 0.05$). The estimated value of pain in cesarean section women was significantly lower than the real value, and the difference was statistically significant ($P < 0.05$). It can be seen from Table 3 that the estimated pain value of the parturients who choose cesarean section actively or passively is far lower than the real value, and the difference is statistically significant ($P < 0.05$).

The expectation of cesarean section women on delivery pain is far lower than the real experience value, while the estimated pain value of active cesarean section women is lower than the real value, indicating that the expectation of active cesarean section women on reducing production pain through surgical delivery is too high. Especially for the parturients who strongly expressed that they could not bear the pain of natural delivery and chose cesarean section, even after giving postoperative analgesia, they still had a deeper memory of the pain during delivery than the parturients who gave birth naturally. However, the estimated value of pain during delivery of the women who passively choose cesarean section is higher than the postpartum recall value. The reason for analysis may be that the women have a certain understanding of cesarean section and postoperative pain, so that they have a better psychological preparation. On the other hand, it is related to the fact that they pay more attention to the safety of mother and baby than to the pain.

In the past, continuous patient-controlled epidural analgesia and patient-controlled intravenous analgesia were used [9]. Patient controlled epidural analgesia (PCEA) has a definite effect, but it has some disadvantages, such as urinary retention, numbness of both lower limbs, inability to get out of bed early, and easy to fall off of epidural catheter due to turning over, which affect its clinical application. In the simple patient-controlled intravenous analgesia mode, individual sensitivity to drugs may easily lead to large individual differences in medication effects. Some people use large amounts of drugs, and the incidence of adverse reactions such as dizziness, nausea, and vomiting is high [10].

Massage can promote qi and blood circulation, dredge meridians, and achieve the purpose of pain relief [11]. Moreover, pain receptors are generally located in the skin and subcutaneous tissue, and the most dense places are the hands and feet. After mechanical stimulation, the receptors on the body surface are transmitted to the brain along the spinal cord, and then, the brain sends information to excite the vagus nerve to act on the hypothalamus, which promotes the increase of enkephalin and dynorphin, the content of pain causing substances in the body, and affects the secretion and metabolism of pain-related neurotransmitters, hormones, and the evolution and release of chemical substances in the body, thus playing the role of analgesia. Therefore, the use of hand and foot joint massage to relieve postoperative pain is a valuable intervention [12].

Table 1: Results of multifactor analysis on influencing factors of cesarean section among parturients in area B.

Influence factor	Classification	β	SE	Wald χ^2 value	P value	OR (95% CI)
Age (years)	20 ~ 24 = 1, 25 ~ 34 = 2, and >35 = 3	1.456	0.612	5.660	0.017	4.289 (1.292~1.4232)
Degree of education	Junior high school and below = 1, high school = 2, and college degree or above = 3	0.451	0.101	19.939	<0.001	1.570 (1.288~1.914)
Registered residence (rural as reference)	City	0.734	0.277	7.022	0.008	2.083 (1211~3.586)
Type of delivery hospital (township/town level as reference)	District/county level	0.342	0.215	2.530	0.065	1.408 (0.924~2.146)
	Municipal level and above	1.158	0.329	12.389	<0.001	3.184 (1.677~6.067)
Prepregnancy BMI (kg/m^2, 18.5~23.9 as reference)	<18.5	0.734	0.465	2.492	0.065	2.083 (0.837~5.183)
	24.0~	0.158	0.219	0.521	0.853	1.171 (0.762~1.799)
	>28.0	0.685	0.165	17.235	<0.001	1.984 (1.436~2.741)
Maternal type (primipara as reference)	Parturient women	-1.347	0.224	36.161	<0.001	0.260 (0.168~0.403)
Fertility formula (multiple photos for natural pregnancy)	Assisted reproduction	0.403	0.078	26.694	<0.001	1.496 (1.284~1.743)
Adverse pregnancy and childbirth history (no as reference)	Yes	0.902	0.450	4.018	0.045	2.465 (1.020~5.954)
Complications or complications during pregnancy (no as reference)	Yes	2.426	0.545	19.815	<0.001	11.314 (3.888~32.924)
Times of antenatal examination (<5 as reference)	5~7	0.333	0.171	3.792	0.052	1.395 (0.998~1.951)
	≥8	0.790	0.379	4.345	0.047	2.203 (1.048~4.631)

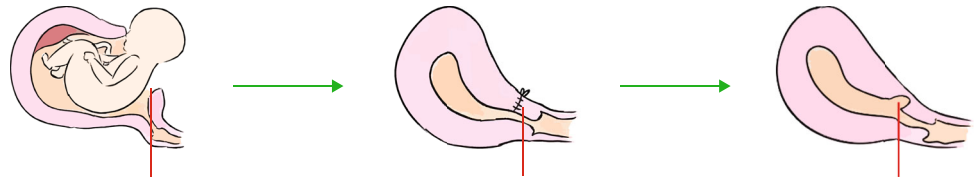

Figure 2: Cesarean section incision.

Table 2: Comparison of maternal pain scores in different delivery modes ($\bar{x}$±s, points).

Mode of delivery	Estimated value	True value	Recall value	F	P
Spontaneous childbirth	3.80 ± 0.84	4.63 ± 0.554	4.42 ± 0.894	1.444	0.274
Cesarean section	3.01 ± 0.71	4.60 ± 0.54a	4.04 ± 0.960	5.442	0.021
t	1.372	-0.343	1.177		
P	0.242	0.749	0.305		

a: estimated value comparison, $P < 0.05$.

Table 3: Comparison of pain scores of cesarean section women with different selection methods ($\bar{x}$±s, points).

Selection method	Estimated value	True value	Recall value	F	P
Active selection	2.86 ± 0.44	4.40 ± 0.53[a]	3.82 ± 0.84	5.360	0.022
Passive selection	3.44 ± 1.14	4.80 ± 0.45[a]	3.03 ± 0.97	8.167	0.006
t	0.885	1.002	−2.138		
P	0.426	0.374	0.099		

a: estimated value comparison, $P < 0.05$.

3. Method

3.1. Object Selection. 60 cases of cesarean section in hospital B were selected as data samples, of which the main age was 18-40 years (27.3 ± 4.8 years). They were randomly divided into control group and intervention group, with 30 cases in each group. Inclusion criteria are as follows: those with normal cognition; volunteer to participate in the study; it conforms to grades I and II of the American Society of Anesthesiologists' disease classification standard; and those who have undergone cesarean section [13]. Exclusion criteria are as follows: patients with consciousness disorder and psychosis; postoperative patient-controlled analgesia; damaged tissue and skin of hand or foot, phlebitis, arthritis, burn wound, inflammation, eczema, etc.; and pregnant women with heart disease, high blood pressure, and excessive intraoperative bleeding. There was no significant difference between the two groups in educational level, age, place of residence, gestational weeks, and anesthesia methods ($P > 0.05$).

3.2. Massage Method

3.2.1. Intervention Methods. This study adopts the clinical trial research method [14]. The control group was given routine nursing, and the intervention group was given 20 min hand and foot massage on the basis of routine nursing. On the first day before operation, explain the use of visual analogue scale (VAS) for pain to the pregnant women who volunteered to participate in the study. On the first day after operation, provide a comfortable place for pregnant women. The room temperature is controlled at 18°C~22°C, keep the environment quiet, and the bed is clean, dry, and free of debris [15]. Before intervention, the operator washed his hands, cut his nails, did not wear jewelry, rubbed his hands to keep them warm, and asked the patient to lie flat. On the basis of consulting relevant experts and consulting literatures, the massage steps were formulated: put the thumbs of both hands in the middle of the back of the patient's hands and the other four fingers close to the palm of the hand to do the action of grasping and sliding. Turn the patient's hand over, place the two thumbs of the operator in the middle of the patient's palm, and stick the other four fingers on the back of the hand. The two thumbs slide from the center of the hand to the left and right sides and then return to the origin, so as to massage the thenar, 2 or 3 times for each hand. After the hand massage, one hand holds the foot, the other half clenches the fist, the index finger bends, and apply force to the vertex of the first finger joint of the index finger. During the pressing, keep the index finger bones in line with the palm, forearm, and big arm, and the force should be appropriate and uniform. According to the patient's sensitivity to pain, grasp the massage force properly, press the corresponding part of the foot reflection area as a

Table 4: Repeated measurement ANOVA results.

Source of variation	Sum of squares of deviation from mean	Freedom	Mean square	F	P
Treatment factors	23.361	1	23.361	79.340	<0.001
Time factor	24.389	2	12.194	30.276	<0.001
Processing factor ∗ time factor	17.056	2	8.528	21.172	<0.001
Individual error	2.944	10	0.294		
Repeated measurement error	8.056	20	0.403		

Table 5: Comparison of VAS scores of the two groups at different time points ($\bar{x}$±s).

Group	Number of cases	Before massage	Immediately after massage	30 min after massage	60 min after massage	F value	P
Control group	30	5.50 ± 0.57	5.63 ± 0.72	5.93 ± 0.74	5.70 ± 0.70	2.301	>0.05
Intervention group	30	5.53 ± 0.86	3.10 ± 0.80[1)]	2.67 ± 0.71[1)2)]	3.60 ± 1.00[1)2)3)]	110.220	<0.01
t value		-0.18	12.88	17.437	9.391		
P		>0.05	<0.01	<0.01	<0.01		

1): compared with before massage, $P < 0.05$; 2): compared with immediately after massage, $P < 0.05$; 3): compared with 30 min after massage, $P < 0.05$.

whole, and then fix the patient's foot and ankle, with the palm facing the patient's foot bottom, help them flex and extend their toes for 10~15 times, and do the opposite side with the same method.

3.2.2. Measuring Tools. In this study, general information questionnaire and VAS were used as data collection tools. Measure and record the pain intensity of the intervention group before massage, immediately after massage, 30 min after massage, and 60 min after massage, and record the pain of the control group at the corresponding time point [16]. The general information questionnaire is designed by the researcher according to the research needs and perfected under the guidance of relevant experts, including age, occupation, education level, and residence. VAS is to draw a straight line on the paper, with 0 and 10 marked on both ends, respectively. 0 represents no pain, and 10 represents the most severe pain. Let the puerpera mark the number on the straight line according to the degree of incision pain they feel; that is, score the pain intensity of the puerpera. VAS is an effective tool commonly used in scientific research and clinical practice. Its reliability and validity in pain assessment have been proved.

3.2.3. Statistical Methods. Medical statistics is an important tool for medical research. It is widely used in experimental design, data collection, and data analysis. The correct application of statistical methods has an extremely important significance and role in effectively carrying out scientific research and improving the academic quality of medical scientific papers. The basic methods of statistics are generally not difficult to master, but whether they can be correctly used is still a common problem.

SPSS19.0 software will be used for statistical analysis of the data in this paper. The main statistical methods include t-test and repeated measurement analysis of variance [17].

(1) Repeated Measurement Method. Repeated measurement method is widely used in medical research, such as clinical research on the short-term and long-term efficacy of a certain treatment method, blood drug concentration of different doses of the same drug at various time points after use, etc. The repeated measurement design is used to analyze the change trend of observation indicators and related influencing factors, and the repeated measurement data are arranged in time. The randomized block design is mainly to control the influence of other factors other than the treatment factors on the test results, so that the treatment groups can be balanced and comparable as far as possible. Therefore, the data between the treatment groups are independent. According to the output results of SPSS19.0, we can sort out the results as shown in Table 4.

(2) t-Test. t-test is a hypothesis test method established by the British statistician W.S. Gosset based on the t-distribution principle in 1908. It is often used to compare the mean of two small samples in the measurement data. In theory, the application condition of t-test is that the sample is from the population with normal distribution. When comparing the mean of two samples, it also requires that the variance of the two populations be equal. However, in practice, it deviates slightly from the above conditions. As long as its distribution is unimodal and approximate normal distribution, it can also be applied.

There are three types of t-tests commonly used: (1) t-test of single sample: it is used to infer whether the population mean represented by the sample mean and the known population mean has statistical significance. When the number of samples is small ($n < 60$) and the overall standard deviation is unknown, t-test is used. On the contrary, when the number of samples is large or small, and the overall standard deviation is known, U-test can be used. (2) Paired specimen t-test: it is applicable to the comparison of the mean number

of two specimens in the paired design. When selecting, attention should be paid to whether the two specimens are paired design data. The commonly used paired design data mainly include the following three cases: two homogeneous subjects receive two different treatments, respectively. The same subject or two parts of the same specimen were treated differently. Compare the results of the same subject before and after treatment. (3) t-test of two independent samples: also known as group t-test, it is applicable to the comparison of the mean of two samples with completely random design. Different from the paired t-test, before the t-test of two independent samples, the homogeneity of variance test must be carried out for the two groups of data. If it is a small sample with homogeneous variance, t-test is used. On the contrary, if the variance is not uniform, the corrected t-test (t-test) is used, or the data transformation method (such as logarithm, square root, and reciprocal) is used to make the two groups of data have the homogeneity of variance before the t-test, or the nonparametric test is used. In addition, when the number of samples in the two groups is large ($N1$, $n2 > 50$), the calculation of t-test is cumbersome, and U-test can be used.

4. Results and Discussion

4.1. Result Analysis. There was significant difference in VAS scores at each time point in the intervention group ($P < 0.01$). There were significant differences in VAS scores between two groups at different time points in the intervention group ($P < 0.05$). There was no significant difference in VAS score of the control group at each time point ($P > 0.05$). The VAS scores of the intervention group at each time point after massage were significantly lower than those of the control group ($P < 0.01$) (see Table 5).

4.2. Result Discussion

4.2.1. Role of Hand and Foot Massage. The results of this study show that after the analgesic effect of anesthetics disappears after cesarean section, routine nursing has no significant effect on postoperative incision pain of parturients [18]. However, the VAS at 30 min after massage intervention was the lowest (2.67 ± 0.71), which was significantly lower than that before massage. Although the VAS at 60 min after massage rose again, it was still lower than that before massage [19]. The comparison between the two groups showed that the VAS score of the intervention group after massage was lower than that of the control group, suggesting that hand and foot massage can reduce the intensity of incision pain of pregnant women after cesarean section. The results of this study are similar to those of foreign scholars. The joint massage of hands and feet for 20 min can effectively relieve the postoperative pain of dissecting uterus parturients, and the effect of massage lasted until 60 min after massage, and the degree of pain increased slightly 90 min after massage.

4.2.2. Principle of Hand and Foot Massage for Relieving Incision Pain after Cesarean Section. Massage is a natural health care method that integrates the meridian theory, modern pathophysiology, bioholographic embryo theory, reflection theory, etc. [20]. Traditional Chinese medicine believes that "if there is no obstruction, there will be pain, and if there is general, there will be no pain." After the operation, the blood of the meridians overflows outside the veins and remains in the skin, resulting in qi stagnation and blood stasis, and blocked channels. Massage can promote qi and blood circulation, dredge meridians, and achieve the purpose of pain relief. Moreover, pain receptors are generally located in the skin and subcutaneous tissue, and the most dense places are the hands and feet [21]. The receptors on the body surface are mechanically stimulated and transmitted to the brain along the spinal cord, and then, the brain sends information to excite the vagus nerve to act on the hypothalamus, which promotes the increase of enkephalins and dynorphins and the decrease of the content of pain causing substances in the body. It affects the secretion and metabolism of neurotransmitters and hormones related to pain and the evolution and release of chemicals in the body, thus playing an analgesic role. In addition, massage brings relaxation to the patient, which makes the pregnant woman focus on the reaction caused by hand and foot massage, distracting her attention, thus reducing the pain.

5. Conclusion

This paper presents a method of foot and hand massage for abdominal pain in cesarean section incision under ultrasound guidance. Massage can promote qi and blood circulation, dredge meridians, and achieve the purpose of pain relief. Pain receptors are generally located in the skin and subcutaneous tissue, and the most dense places are the hands and feet. The receptors on the body surface are mechanically stimulated and transmitted to the brain along the spinal cord, and then, the brain sends information to excite the vagus nerve to act on the hypothalamus, which promotes the increase of enkephalin and dynorphin and the decrease of the content of pain causing substances in the body. It affects the secretion and metabolism of neurotransmitters and hormones related to pain and the evolution and release of chemicals in the body, thus playing an analgesic role. In addition, massage brings relaxation to the patient, which makes the pregnant woman focus on the reaction caused by hand and foot massage, distracting her attention, thus reducing the pain. In the high-cost medical care environment, using hand and foot joint massage to relieve postoperative pain is a valuable intervention, which improves the nursing level of nurses for postoperative pain.

Data Availability

The data used to support the findings of this study are available from the corresponding author upon request.

Conflicts of Interest

The authors declare that they have no conflicts of interest.

References

[1] Y. Athiel, A. Girault, C. L. Ray, and F. Goffinet, "Association between hospitals' cesarean delivery rates for breech presentation and their success rates for external cephalic version,"

Hindawi
Scanning
Volume 2023, Article ID 9792567, 1 page
https://doi.org/10.1155/2023/9792567

Retraction

Retracted: Sports Medical Image Modeling of Injury Prevention in Dance Learning and Sports Training

Scanning

Received 20 June 2023; Accepted 20 June 2023; Published 21 June 2023

This article has been retracted by Hindawi following an investigation undertaken by the publisher [1]. This investigation has uncovered evidence of one or more of the following indicators of systematic manipulation of the publication process:

(1) Discrepancies in scope

(2) Discrepancies in the description of the research reported

(3) Discrepancies between the availability of data and the research described

(4) Inappropriate citations

(5) Incoherent, meaningless and/or irrelevant content included in the article

(6) Peer-review manipulation

The presence of these indicators undermines our confidence in the integrity of the article's content and we cannot, therefore, vouch for its reliability. Please note that this notice is intended solely to alert readers that the content of this article is unreliable. We have not investigated whether authors were aware of or involved in the systematic manipulation of the publication process.

Wiley and Hindawi regrets that the usual quality checks did not identify these issues before publication and have since put additional measures in place to safeguard research integrity.

We wish to credit our own Research Integrity and Research Publishing teams and anonymous and named external researchers and research integrity experts for contributing to this investigation.

The corresponding author, as the representative of all authors, has been given the opportunity to register their agreement or disagreement to this retraction. We have kept a record of any response received.

References

[1] R. Fei, "Sports Medical Image Modeling of Injury Prevention in Dance Learning and Sports Training," *Scanning*, vol. 2022, Article ID 7027007, 7 pages, 2022.

Hindawi
Scanning
Volume 2022, Article ID 7027007, 7 pages
https://doi.org/10.1155/2022/7027007

Research Article

Sports Medical Image Modeling of Injury Prevention in Dance Learning and Sports Training

Renying Fei

Liupanshui Normal University, Liupanshui, Guizhou 553004, China

Correspondence should be addressed to Renying Fei; 1710221628@hbut.edu.cn

Received 16 June 2022; Revised 9 July 2022; Accepted 16 July 2022; Published 27 July 2022

Academic Editor: Danilo Pelusi

In order to effectively prevent injuries in dance learning and sports training, this paper proposes a method based on sports medical image modeling. This method solves the problem of injury prevention in dance learning by studying the association analysis algorithm, medical image information system, and CT technology and analyzing the role of data mining technology in the medical image information system. The experimental results show that the average prediction error of CT and US is about 5%, which can be considered that the model can predict accurately. The error of MR is as high as 28.2%, and the prediction is relatively inaccurate. *Conclusion*. the model can effectively prevent the injury in training.

1. Introduction

In order to interpret the dance performance perfectly during the training process, dancers often need to do some difficult movements, which will cause dance sports injuries. The sports injury caused by dance training is often complex; such sports injuries are usually associated with dance training. Dance sports injuries may require rehabilitation at least or may lead to the end of dance sports career [1]. Many excellent dancers and dancers have to say goodbye to their dance career and give up their favorite dance career because of sports injury. It can be said that dance sports injury has become a problem that many dancers have to face. Therefore, it is very important to prevent injuries in the process of dance learning.

Medical imaging is an equipment-dependent discipline. Medical imaging equipment, especially CT and MR equipment, is driven by the most rapidly developing cutting-edge technology in natural science and is developing at a veritable speed [2–4]. At each stage of the development of medical imaging, it will have an important and sometimes epoch-making impact on other clinical disciplines closely related to it. At present, the development of medical imaging represented by the development of CT and MR technology is at such a stage. Among them, data mining technology plays an important role in medical imaging [5]. Data mining technology is a process of extracting hidden, unknown, but potentially useful information and knowledge from a large number of incomplete, noisy, fuzzy, and random practical application data. This process generally consists of the data preparation stage, data mining stage, and result expression and interpretation stage (see Figure 1). The data preparation stage can be further divided into data integration, data selection, and data preprocessing; The mining operation stage includes determining the goal of data mining, selecting appropriate tools, mining knowledge, and verifying the discovered knowledge. The task of the result expression and interpretation stage requires not only expressing the results but also filtering the information. If the results cannot satisfy the decision-maker, the above data mining process should be repeated.

Based on this, through the analysis of the injuries in dance training, and through the prevention of medical imaging technology, we can effectively prevent the injuries of dancers in the training process.

2. Literature Review

Dance sports injury refers to the emergency changes and changes in physiological and biochemical indicators of the dancer's body tissues or body structures and organs caused by multiple factors in the process of dance performance or

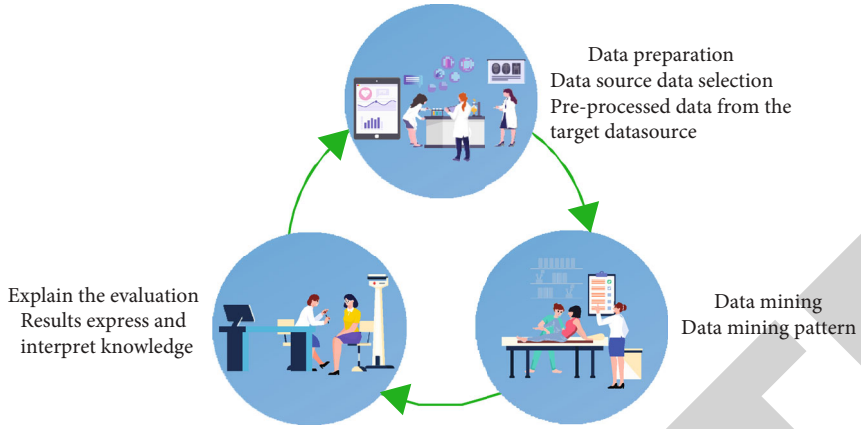

Figure 1: Data mining process.

dance training. These changes mainly occur in the basic motor system of dancers and also have adverse effects on the nervous system and vascular system. In order to present the most perfect side to the audience, dancers often carry out arduous training "day after day, year after year." Such training often exceeds the physical limit, and long-term high-intensity training causes sports injuries to dancers. According to the research and analysis, the training injuries of dancers are usually caused by the following three reasons:

(1) Insufficient preparation activities

(2) Lack of tacit cooperation when two people cooperate

(3) Low physical and psychological quality

In view of the reasons, it can effectively prevent serious injuries caused by dancers in the training process.

1998 is another epoch-making mark in the development of CT technology [6]. In this year, several major CT equipment manufacturers simultaneously launched four layer acquisition spiral CT (multislice spiral CT), and its principle has been introduced in other literatures [7]. Taking this as a starting point, the 8-layer spiral CT was launched in 2000. In 2001, the 16-slice spiral CT was introduced, and 2-slice, 6-slice, and 10-slice spiral CT with similar principle were also developed. Improved electron beam CT was introduced in 2002 [8].

The key breakthrough of multislice spiral CT is the use of a multirow wide body detector instead of single-row detector of the single-slice spiral CT [9]. By controlling the switch of the information channel of each detector column, the reconstructed images with 4 as the cardinal number and different layer thicknesses can be obtained. The detector width of the thinnest column in the multicolumn detector determines the thinnest acquisition layer thickness, i.e., z -axis resolution. For example, in the current detector design, the width of the thinnest column detector is 0.5 mm (Toshiba), 0.625 mm (GE), and 0.75 mm (Siemens and Philips), which is the thinnest layer thickness that can be collected by each equipment. The setting of the thinnest layer thickness is not random. It is closely related to several main performance parameters, namely, cone-shaped X-ray harness reconstruction mathematics, scanning speed, X-ray dose, computer performance, and voxel isotropy, which is highly valued in clinical applications [10–12].

Data mining technology is a process of extracting hidden, unknown, but potentially useful information and knowledge from a large number of incomplete, noisy, fuzzy, and random practical application data. This process generally consists of the data preparation stage, data mining stage, and result expression and interpretation stage. The data preparation stage can be further divided into data integration, data selection, and data preprocessing. The mining operation stage includes determining the goal of data mining, selecting appropriate tools, mining knowledge, and verifying the discovered knowledge. The task of the result expression and interpretation stage requires not only expressing the results but also filtering the information. If the results cannot satisfy the decision-maker, the above data mining process should be repeated. Data mining generally relies on professional tools. Common data mining technologies mainly include association rule analysis, artificial neural network, decision tree analysis, time series analysis, cluster analysis, etc. [13]. Focus on the application of association rule analysis and time series analysis in the medical image information system. With the development of medical informatization, more and more hospitals begin to popularize the application of the medical image information system, which is mainly composed of the medical image information system (RIS) and medical image archiving and transmission system (PACS) [14]. RIS is mainly responsible for examination registration, examination photography, report editing, review and follow-up, department management, and other functions, while PACS is mainly responsible for the acquisition, transmission, storage, display, and management of medical images. Over the years since the implementation of RIS/PACS in a class III hospital, the inspection records have reached more than 1 million, and the image records have reached more than 5 million. The massive data accumulated in the database provides a good foundation for data mining and utilization.

Based on the above research, this paper makes an in-depth discussion and research on the sports medical impact modeling of injury prevention in dance learning and sports training. Through the research of the association analysis

algorithm, medical impact information system, and CT technology, data mining technology is applied to medical imaging technology, and finally, an effective prevention of dance training injury is achieved.

3. Research Methods

3.1. Correlation Analysis of Inspection Items

3.1.1. Association Rule Algorithm. Association rules are used to filter out the frequency relationship of data item sets in the transaction database from a given set of data items and the transaction database (each transaction is a collection of data items) and to find valuable correlation between data item sets in a large amount of data. When mining association rules, various events in the database data must be taken as data items, and multiple data items form an itemset of a specific thing [15]. For example, in the medical image database, for the event of patient visit, each examination item in the process of visit constitutes its data item set. Microsoft association rule algorithm belongs to the Apriori rule algorithm series, which can be divided into two steps: one is to find all frequent itemsets whose support is greater than or equal to the predefined minimum support threshold; the other is to generate strong association rules that meet the minimum confidence from the frequent itemsets.

3.1.2. Data Preparation. Due to the lack of necessary data verification during the use, maintenance, and migration of data for many years, coupled with the gradual launch of the software function module of the image information system, and the human error of the staff when entering the data, the data may be repeated, missing, incomplete, and wrong. Therefore, in order to ensure the quality of data, it is necessary to process the data.

The EISStudies (check information table) and EISService (item information sheet) in the RIS database of a hospital record the information about the examination items of patients in the hospital since 2005, from which the basic attributes of patients (number, name, gender, date of birth, etc.), patient types (physical examination, outpatient, emergency, inpatient), and examination items (number, name, type, etc.) are extracted to establish a new table. Because the original entry of inspection items is not standardized, the same inspection item has different numbers and names [16]. For example, (X-ray (digital) chest film (positive position) CR) and (X-ray (digital) chest film Cr (positive position)) are the same inspection item. In order not to affect the analysis results, the inspection items need to be uniformly standardized.

3.1.3. Frequent Itemsets and Association Rules. The primary task of the association rule algorithm is to mine frequent itemsets. Due to the large number of patient examination items, in order to obtain useful itemsets and rules and reduce model processing time, the minimum support parameter is set to 0.03; that is, only itemsets with a frequency of not less than 3% are selected to generate association rules [17, 18]. Figure 2 shows the generation process of frequent itemsets.

According to the generation process of the above frequent itemsets, the model generates association rules (see Table 1), where confidence refers to the probability of the occurrence of result B when condition A occurs, importance refers to the logarithm of the ratio of the occurrence probability of the result when the condition is true to the occurrence probability of the result when the condition is not true, and the importance score is greater than zero, indicating that the rule is meaningful, and the greater the score, the more significant the rule is. It can be seen from Table 1 that in the physical examination items, the probability of color ultrasound B (kidney, ureter, bladder, prostate) and color ultrasound A (liver, gallbladder, spleen, pancreas) is 98.2%, and the importance score of the rule is 1.157. Among inpatients, the probability of taking chest DR at the same time of US project of the left and right lower limb deep vein was 73.1%, and the importance score of this rule was 2.867. It can be found that the patients whose type is physical examination have high confidence, which is consistent with the fact that the physical examination patients will do some combination packages of examination items. Because of the uncertainty of the examination items of outpatient and emergency patients, the confidence of the rules is generally not as high as that of the physical examination.

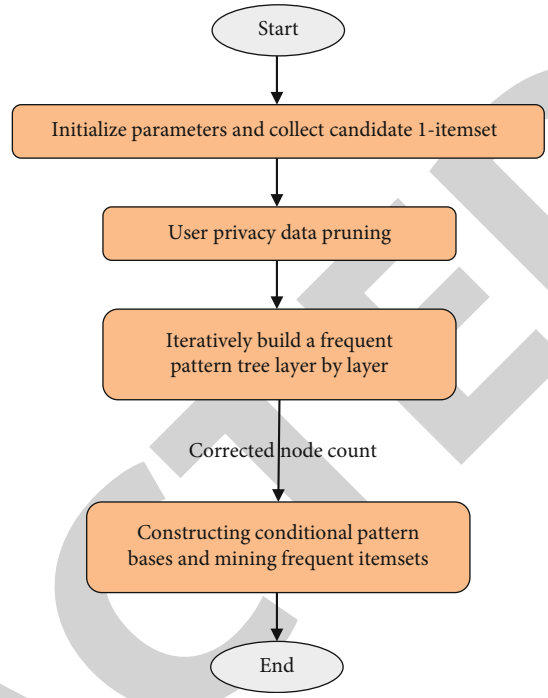

Figure 2: Generation process of frequent itemsets.

Through association rule analysis, we can find the association degree of the inspection items during the patient's visit. If we further combine the patient's disease type, it can provide a basis for the hospital's clinical path management.

3.2. Forecast of Equipment Inspection Quantity

3.2.1. Timing Algorithm. The Microsoft time series algorithm encapsulates two different computer learning algorithms. The first algorithm is the automatic regression tree (ARTxp) using cross-prediction, and the second algorithm

Table 1: Association rules.

Patient type	Generated association rules	Confidence (%)	Importance
Physical examination	Color ultrasound B (kidney, ureter, bladder, prostate)→color ultrasound A (liver, gallbladder, spleen, pancreas)	98.2	1.157
Hospitalization	Left and right lower limb deep vein US→chest DR	73.1	2.867
Emergency treatment	CR of limbs, plain scan of liver, gallbladder, spleen and pancreas→plain scan of head CT	66.4	1.512
Outpatient department	Chest DR, double arm ureter bladder prostate→liver, gallbladder, spleen, and pancreas	73.2	1.101

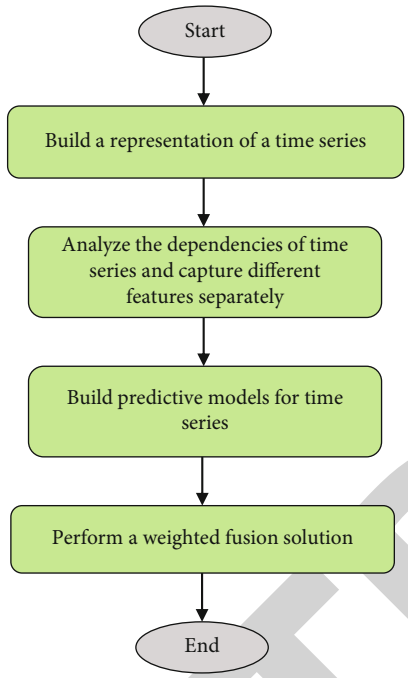

Figure 3: Flow chart of time series model.

is automatic regression (ARIMA) integrated with moving average. The Microsoft time series algorithm combines the advantages of the two algorithms by default to achieve the optimal prediction results [19].

3.2.2. Establishment and Verification of Time Series Model. The modern imaging department has a large number of digital imaging equipment, such as CT, MR, CR, DR, and DF. It extracts and collects the monthly inspection quantity of each equipment type from the original eisservice in the RIS/PACS database and designs the monthly inspection quantity of equipment to establish the time series model. Since the data in the new table has been processed, there is no missing value, the data is summarized and recorded on a monthly basis, and the sequence cycle is set to 12. Figure 3 is the flow chart of the timing model.

3.2.3. Comprehensive Forecast. In statistics, multiple index systems are generally used for comprehensive prediction to improve the prediction accuracy of inspection volume [20]. Here, the examination volume in 2021 is comprehensively predicted according to the two index systems of the patient type and equipment type. Since the inspection volume prediction of the two indicator systems adopts the time series algorithm, now assuming that the importance of the indicator system is the same, the equal weight average method can be used to determine that the weight is 0.5.

Table 2: Forecast of inspection volume of each equipment type in 2021.

	2018	2019	2020	2021	Forecast growth rate in 2021
CT	49391	60161	65705	71822	8.52%
US	157132	166843	178529	186691	4.37%
CR	26624	21708	22358	23429	4.57%
DR	44505	55208	55854	58588	4.67%
MR	15590	15831	22118	28852	4.00%

$$Q_1 = Q(\text{physical examination}) + Q(\text{hospitalization}) + Q(\text{emergency treatment}) + Q(\text{outpatient Department}), \quad (1)$$

$$Q_2 = Q_{CT} + Q_{US} + Q_{CR} + \cdots + Q, \quad (2)$$

$$Q = 0.5Q_1 + 0.5Q_2, \quad (3)$$

where Q is the target predicted total examination volume, is the predicted total examination volume by patient type, and is the predicted total examination measurement by device type. After the total inspection quantity is obtained according to equation (3), the inspection quantity of each equipment type can be obtained according to the following equation:

$$Q'_{CT} = Q_{CT} * \frac{Q}{Q_2}. \quad (4)$$

After the comprehensive prediction model is determined, the time series model is used to predict the monthly examination volume of the imaging department in 2021 according to the patient type and equipment type index system. Due to the abrupt change of the MR examination volume in 2020, the direct prediction error according to the time series is large. Now, according to the historical data, the average growth rate of MR in recent years is calculated to be about 3.5%, and the growth rate has a trend of increasing year by year. After comprehensive consideration, 4% is added to the actual value in 2020 as the prediction result of the MR examination type in 2021.

Table 3: Comparison of actual and predicted values of inspection quantities of various equipment types in 2020.

	CT			US			MR		
	Actual value	Estimate	Relative error	Actual value	Estimate	Relative error	Actual value	Estimate	Relative error
202001	4704	5020	0.0671	10946	12305	0.1239	1134	1189	0.0485
202002	4598	5112	0.1117	9732	11225	0.1534	1190	1043	0.1235
202003	5642	5518	0.0219	13757	14110	0.0256	1955	1424	0.2716
202004	5617	5678	0.0108	14338	14288	0.0034	1872	1388	0.2585
202005	5876	5772	0.0176	16591	15403	0.0716	1991	1365	0.3144
202006	5563	5782	0.0393	17100	15743	0.0793	2027	1436	0.2916
202007	5634	5748	0.0202	17409	17298	0.0063	2040	1427	0.3005
202008	5983	5864	0.0196	17314	16281	0.0596	2105	1155	0.4513
202009	5249	5897	0.1234	15988	14778	0.0756	1868	1335	0.2853
202010	5763	5991	0.0396	14772	14197	0.0389	2079	1336	0.3574
202011	5609	5841	0.0413	16180	15051	0.0697	2067	1252	0.3943
202012	5467	5972	0.0924	14400	14392	0.0005	1790	1276	0.2874
Average error	—	—	0.0504	—	—	0.0590	—	—	0.2820

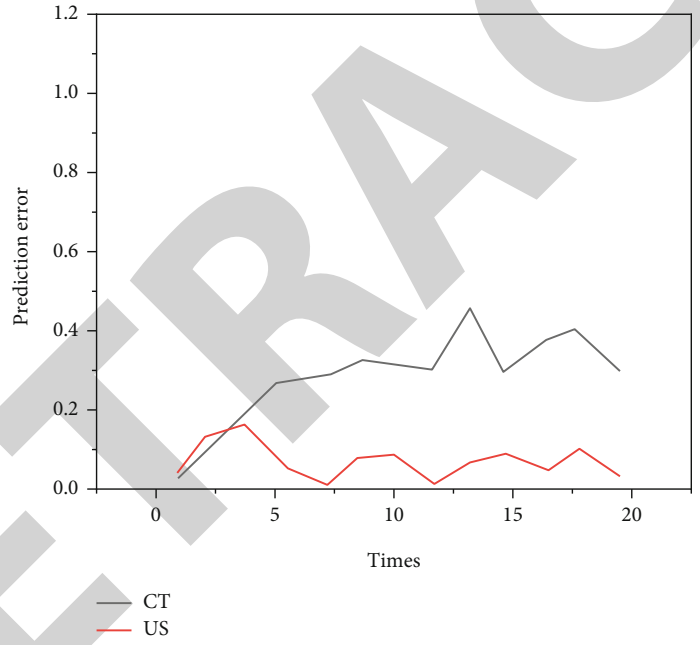

Figure 4: Broken line statistics of relative errors of CT and US.

After the total inspection amount of each equipment type is obtained, the total inspection amount in 2021 can be obtained according to equation (3), and then, the inspection amount of each equipment inspection type can be calculated according to equation (4). Table 2 shows the predicted values of the inspection volume of each equipment type in 2021, the historical data from 2018 to 2020, and the growth of various inspection volumes in 2021. Based on this prediction result, the decision-makers can know the department equipment inspection volume in 2021 in advance, make the allocation of equipment and personnel in advance, and improve the decision-making management level. For example, in view of the high growth rate of CT in 2021, new CT equipment has been considered to actively respond to the growth of examination business to improve the quality of medical services [21].

3.3. CT Detector. The design of CT detector can specify the size of the pixel and matrix. When the earliest layer acquisition and display method is applied, the layer thickness only involves the distortion caused by "partial volume effect." When using multislice spiral CT to display reconstructed images, it involves not only the concept of pixel and matrix but also the concept of voxel. The concept that pixels are "areas" is two-dimensional. "Voxel" is the concept of "volume," which is three-dimensional, that is, length, width, and height. Where "length" and "width" are two-dimensional parameters of "pixels," "height" is determined by the acquisition layer thickness. When the acquisition layer thickness is the same as "length" and "width," the voxel is "isotropic"; otherwise, it is "anisotropic." When using isotropic voxel data for reconstruction, the reconstructed image

will not be distorted. If voxel data is anisotropic, the reconstructed image will be distorted to varying degrees.

In fact, in order to achieve isotropic voxel acquisition, it is necessary to select an appropriate field of view (FOV). When the data is collected with the quadratic matrix of 512, the design of a company needs to use 32 cm FOV to obtain 0.625 cubic mm isotropic voxels. The design of a company needs to adopt 38 cm FOV to obtain 0.75-cubic-millimeter isotropic voxels. The design of a company needs to select 25 cm FOV to obtain 0.5-cubic-millimeter isotropic voxels.

In addition to the acquisition method, this type of design also involves problems such as the high scanning dose, the need for new reconstruction algorithms, the need to greatly improve the computer capacity due to the large increase in the amount of data, and the cost and design of the flat panel detector itself (for example, the flat panel detector can only be placed horizontally, not in an arc) which need to be further solved.

4. Results and Discussion

Table 3 lists the actual value, predicted value, and relative error of each equipment type in 2020. It can be seen from the table that the average prediction error of CT and US is about 5%, so it can be considered that the model can predict more accurately. The error of MR is as high as 28.2%. The reason is that there is a sudden change in the inspection volume of MR from February to March 2020, which is much larger than in previous years. After in-depth understanding, it is the newly added inspection items in the hospital MR room after external training which lead to a significant increase in business volume and a large error in the time series prediction results. Therefore, it is appropriate to use this time series to predict CT and US volume, while other methods must be used to predict MR volume. Figure 4 shows the line chart of relative error of each equipment.

It can be seen from Table 3 that the average prediction error of CT and US is about 5%, so it can be considered that the model can predict more accurately. The error of MR is as high as 28.2%, and the data mining technology is used to process the massive data accumulated in the application of the medical imaging information system (RIS/PACS) in a hospital for several years [22]. The association rule algorithm is mainly used to conduct association analysis on patient examination items, which provides a reference for hospital clinical path management, provides a certain technical basis for injury prediction in dance training, and effectively improves the prediction rate.

5. Conclusion

This paper studies the research of sports medical image modeling for injury prevention in dance learning and sports training, through the research of association analysis algorithm, medical image information system, and CT technology. This paper also analyzes the role of data mining technology in the medical image information system to solve the problem of injury prevention in dance learning. The experimental results show that the average prediction error of CT and US is about 5%, which can be considered that the model can predict accurately.

Data Availability

The data used to support the findings of this study are available from the corresponding author upon request.

Conflicts of Interest

The author declares that they have no conflicts of interest.

References

[1] H. R. Song, Y. K. Yang, and J. S. Park, "The effect of exercising dance sports (tango variations routine) on the balance and muscle function of elderly people over 65 years," *Korean Journal of Sports Science*, vol. 29, no. 5, pp. 1015–1023, 2020.

[2] N. Hasani, F. Farhadi, M. A. Morris, M. Nikpanah, and B. Saboury, "Artificial intelligence in medical imaging and its impact on the rare disease community: threats, challenges and opportunities," *PET Clinics*, vol. 17, no. 1, article S155685982100078X, pp. 13–29, 2022.

[3] Y. Mo, J. Liu, Q. Li, J. Ma, and H. Zhang, "Four-dimensional cone-beam ct reconstruction based on motion-compensated robust principal component analysis," *Nan fang yi ke da xue xue bao = Journal of Southern Medical University*, vol. 41, no. 2, pp. 243–249, 2021.

[4] F. Susanto and H. S. Utami, "Variation of inversion delay for wrist joint MR imaging with SPAIR technique: which ID is optimal?," *MEDISAINS*, vol. 19, no. 1, p. 9, 2021.

[5] R. A. Musa, M. E. Manaa, and G. Abdul-Majeed, "Predicting autism spectrum disorder (ASD) for toddlers and children using data mining techniques," in *Journal of Physics: Conference Series, 1804 (1), 012089*, IOP Publishing, 2021.

[6] N. H. Smallwood, "The potential role for CT in the diagnosis of coronavirus disease 2019," *Chest*, vol. 159, no. 3, article S0012369220355008, pp. 906-907, 2021.

[7] M. Toguchi, T. Takagi, Y. Ogawa, S. Morita, and K. Tanabe, "Detection of a peritumoral pseudocapsule in patients with renal cell carcinoma undergoing robot-assisted partial nephrectomy using enhanced MDCT," *Scientific Reports*, vol. 11, no. 1, article 81922, p. 2245, 2021.

[8] R. Malinowski, A. Raszkowska-Kaczor, K. Moraczewski, W. Guszewski, and L. Wedderburn, "The structure and mechanical properties of hemp fibers-reinforced poly(ε-caprolactone) composites modified by electron beam irradiation," *Applied Sciences*, vol. 11, no. 12, article app11125317, p. 5317, 2021.

[9] X. Q. Lu, Y. X. Li, J. P. Ding, and K. L. Deng, "CT characteristics of consolidation type of pulmonary cryptococcosis in immunocompetent patients," *Acta Academiae Medicinae Sinicae*, vol. 43, no. 2, pp. 216–221, 2021.

[10] J. G. Sanctorum, S. V. Wassenbergh, V. Nguyen, J. D. Beenhouwer, J. Sijbers, and J. J. J. Dirckx, "Extended imaging volume in cone-beam x-ray tomography using the weighted simultaneous iterative reconstruction technique," *Physics in Medicine & Biology*, vol. 66, no. 16, p. 165008, 2021.

[11] H. Yoshitani, T. Fujibuchi, and C. Anam, "Basic study on evaluation of x-ray dose distribution using plastic scintillator plate and digital cmos camera," *Journal of Physics: Conference Series*, vol. 2021, no. 1, article 012058, 1943.

Hindawi
Scanning
Volume 2023, Article ID 9765484, 1 page
https://doi.org/10.1155/2023/9765484

Retraction

Retracted: Research and Implementation of Robot Vision Scanning Tracking Algorithm Based on Deep Learning

Scanning

Received 20 June 2023; Accepted 20 June 2023; Published 21 June 2023

This article has been retracted by Hindawi following an investigation undertaken by the publisher [1]. This investigation has uncovered evidence of one or more of the following indicators of systematic manipulation of the publication process:

(1) Discrepancies in scope

(2) Discrepancies in the description of the research reported

(3) Discrepancies between the availability of data and the research described

(4) Inappropriate citations

(5) Incoherent, meaningless and/or irrelevant content included in the article

(6) Peer-review manipulation

The presence of these indicators undermines our confidence in the integrity of the article's content and we cannot, therefore, vouch for its reliability. Please note that this notice is intended solely to alert readers that the content of this article is unreliable. We have not investigated whether authors were aware of or involved in the systematic manipulation of the publication process.

Wiley and Hindawi regrets that the usual quality checks did not identify these issues before publication and have since put additional measures in place to safeguard research integrity.

We wish to credit our own Research Integrity and Research Publishing teams and anonymous and named external researchers and research integrity experts for contributing to this investigation.

The corresponding author, as the representative of all authors, has been given the opportunity to register their agreement or disagreement to this retraction. We have kept a record of any response received.

References

[1] H. Guo, W. Li, N. Zhou, H. Sun, and Z. Han, "Research and Implementation of Robot Vision Scanning Tracking Algorithm Based on Deep Learning," *Scanning*, vol. 2022, Article ID 3330427, 8 pages, 2022.

Hindawi
Scanning
Volume 2022, Article ID 3330427, 8 pages
https://doi.org/10.1155/2022/3330427

Research Article

Research and Implementation of Robot Vision Scanning Tracking Algorithm Based on Deep Learning

Haifeng Guo, Wenyi Li, Na Zhou, He Sun, and Zhao Han

College of Electrical and Information Engineering, Liaoning Institute of Science and Technology, Benxi, Liaoning 117004, China

Correspondence should be addressed to Haifeng Guo; 31115311@njau.edu.cn

Received 30 May 2022; Revised 28 June 2022; Accepted 8 July 2022; Published 26 July 2022

Academic Editor: Danilo Pelusi

In order to solve the difficult problem of deep learning-based robot vision tracking algorithm research and implementation, a deep learning-based target tracking algorithm and a classical tracking algorithm were proposed. It mainly uses the combination of traditional TLD algorithm and GOTURN algorithm to benefit from a large number of offline training data and updates the learner online, so that the whole system has better performance in real-time and accuracy. The results show that the performance of the TLD algorithm is poor regardless of the accuracy curve or the accuracy curve, and the performance of GOTURN-LD is significantly improved when the illumination changes. In the face of occlusion problem, the TLD algorithm shows strong robustness. Although GOTURN-LD is not very stable, its performance is better than GOTURN on the whole.

1. Introduction

In recent years, with the rapid development of science and technology, the application of robot technology has become the most promising field. As the computing power of graphics processor has been greatly improved, the speed of computer processing massive data has been significantly accelerated. Robot technology has been widely used in navigation and positioning, disaster rescue, unmanned driving, and other fields. In addition, China's aging population is becoming increasingly serious; so, the service robots are increasingly needed to solve the problem of labor shortages, and the basic function of the service robot is to follow the designated pedestrians and provide corresponding services at the same time [1].

The research of the robot target tracking system involves many disciplines, including computer vision, robot motion control, sensor fusion, and deep learning. The application of target tracking technology can be seen in intelligent monitoring, virtual reality, advanced human-computer interaction, motion analysis, autonomous navigation, and robot vision. For machine vision researchers, target tracking technology arouses their high research enthusiasm because it is one of the core problems in computer vision, and there are still a lot of problems to be solved [2]. Although researchers continue to try to combine the theoretical research results of mathematics, image processing, pattern recognition, artificial intelligence, machine learning, and other aspects, it is still very difficult to achieve the complete replacement of human eyes by machines.

Deep learning leads the scientific community to open the door to big data training artificial intelligence systems, leading scientists into a new era. Since 2013, deep learning has begun to show its edge in the field of target tracking and gradually shows its superiority in tracking effect [3]. Object tracking based on deep learning has two advantages. First, outperform used by the deep learning training network model is better than the traditional artificial convolutional feature representation, and as an input, it is directly used in correlation filtering or tracking framework; so, its tracking results are also better. Another advantage is it achieves end-to-end output, as long as the original image data input, the target tracking image, can be obtained.

Compared with traditional computer vision algorithms, deep learning algorithms can often provide better results because they can obtain more accurate feature expression by training a large amount of data. Therefore, deep learning

technology is the mainstream solution to target tracking at present. The existing tracking algorithm based on convolutional neural network can reach the processing speed of 100 fps in video processing, which fully meets the requirements of real-time performance and has high tracking accuracy [4]. Therefore, applying deep learning to robots will be a new direction for future development of robots, and applying object tracking algorithm based on deep learning to robots will be a new direction for future development of service robots.

2. Literature Review

Liu et al. proposed a target tracking algorithm, which uses the Meanshift as the core, and the feature representation method of the two-digit histogram is selected by using the color and gray information of the target image to represent the target model. At the same time, combined with the motion detection module, the key information is provided for the path planning, navigation, and other high-level decisions of the autonomous mobile robot in the indoor environment [5]. Mayandi et al. built a robot sorting experimental system based on machine vision; in this system, the targets continuously enter the operation area the system controls the robot to achieve the object sorting, the system continuously and automatically obtains the image of the object through the camera, and the software analyzes the collected images, transforms the coordinates of target objects, identifies the classification information of target objects, and maintains the movement traces of sorting targets [6]. Prateek and Arya proposed a navigation method of reconnaissance robot based on visual target tracking, in which a binary robust independent element feature extraction (BRIEF) method was used to detect and describe the local invariant feature points of the visual target to be tracked, and the target localization was carried out from coarse to fine based on fast feature matching calculation. Experiments verify that this method can make the reconnaissance robot guide the target accurately in real time and accomplish the autonomous navigation task of moving to the target reliably in the complex obstacle environment [7]. Ramirez et al. proposed a mobile robot tracking system based on Kinect [8]. The skeleton tracking function of Kinect is used to identify a specific person in the depth image, and then the ranging data obtained from the Kinect sensor is used to obtain the position of the identified target in the local coordinates of the robot, and according to the law of keeping a fixed distance between human and mobile robot in depth image, a regular control law is designed to control robot movement. The experiment was done in the office corridor and showed good stability but slow response. Lvet al. proposed a DSST algorithm to study the tracking of pedestrian target by robot using monocular camera [9], which was a combination of DSST and TLD algorithm, because the DSST algorithm has no tracking failure detection mechanism, and it cannot deal with the problem of target complete occlusion. On the contrary, the TLD algorithm has tracking failure detection mechanism and can also deal with target complete occlusion. So, the advantages and disadvantages of the two algorithms are complementary, and the experimental results showed a good tracking effect. Lv et al. proposed a human visual tracking algorithm based on deep learning and probability model in order to solve the problem of service robot visual tracking for astronauts, which used deep convolutional neural network to detect the stability of the human body with various clothing and arbitrary posture, combined with the human body detection results, and the motion prediction probability model was designed to achieve accurate and continuous tracking of the designated person. The experimental results show that the proposed algorithm can track the human body stably with various clothing and arbitrary posture, and this algorithm provides an effective solution for the visual tracking of astronauts by the in-cabin following service robot in space station [10]. While the research on robot vision tracking started relatively early in foreign countries, since the 20th century, target following robots have been widely studied and applied. Creisméas et al. developed a mobile robot to locate the head position of pedestrians through skin color detection [11]. Dong et al. proposed that two panoramic stereo cameras should be vertically distributed on the top of the robot to achieve robot following [12]. Sami et al., who based on the SuperScout platform, assembled a horizontal laser scanner and then configured it on a mobile robot to sense the environment, and then go track another mobile robot [13]. In the case of low speed, the scheme can basically ensure the tracking target is not lost. Mourad et al. developed a robot which could do target tracking, and the robot could obtain the information of the tracker's back and shoulder through the camera to achieve target tracking. The powerful pattern detection and recognition system is used to solve the tracking problem in the complex background image, which makes the tracking more stable. The experimental results show that it is feasible and effective to select clothing texture and human shoulder image as the template of detection and recognition, and the tracking effect is good [14]. In the early 2000s, Segway RMP, a mobile robot tracking platform, was designed, and that robot tracking platform used LTK (Lukas-Tomasi-Kanande) feature tracking algorithm to compensate the motion of each image and calculate the difference between frames. Finally, the EM clustering algorithm was used to calculate the motion distribution of particle swarm. However, the tracking accuracy of this algorithm decreases obviously when the target moving speed increases. Li et al. developed a medical robot to assist nurses on the Kinect platform, which also had its own obstacle avoidance function and could constantly adjust the direction to avoid obstacles by judging the position of pedestrians [15] .Gao et al. proposed the tracking method of detector based on laser and RGB-D and detector that can integrate multiple associated data and Kalman filter, wanting to be implemented on a mobile robot operation system (ROS), so that in a target-dense environment, the robot can not only avoid obstacles but also intelligently detect and track specific targets [16].

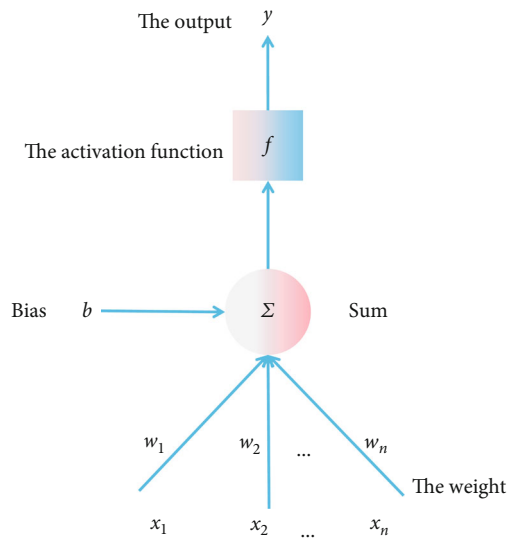

Figure 1: Diagram of a single neuron model.

3. Methods

3.1. Convolutional Layer Neural Network. The predecessor of convolutional neural network is artificial neural network, which is a unique and very important branch direction in machine learning, and a large number of studies on it contributed to the birth of convolutional neural network. Artificial neural network is a hierarchical network formed by widely connecting many simple computing units, which mimics the structure of biological neural networks and mimics the characteristics of biological neurons that can excite and inhibit, learn, and forget, providing a new solution for solving highly nonlinear and complex problems in machine learning. Firstly, the structure of artificial neural network will be briefly introduced [17].

The model of neural network can represent a very complex nonlinear function, which can express the function relation between the output signal and the input signal by the connection of multiple neurons and their hierarchical relations. Therefore, one of the characteristics of artificial neural networks is the description of nonlinear functions. The basic units of an artificial neural network are called neurons, and each neuron is shown in Figure 1.

Among them, the x1, x2, …, xn represent the input signal received by a single neuron. For each input signal, there is a weight multiplied by w1,w2, …, wn, then you take the weighted sum, and you add the offset b of +1 to get the sum y, and then y passes through the nonlinear and differentiable activation function F to obtain the output function $f(x)$ of the weight and bias signal. The sum result y is abstracted by mathematical formula, as shown in Formula (1):

$$y = f\left(\sum_{i=1}^{n} w_i x_i + b\right). \tag{1}$$

If there is no activation function to transform the sum y, then the single neuron model can only deal with the antecedent problem, if activation function is added, nonlinear transformation will be realized, so that neurons can deal with complex problems. The above activation function f usually uses sigmoid function and ReLU function. Here, we use the sigmoid function as an example, sigmoid function expression, which maps the weighted sum to (0, 1), and derivative, $\sigma'(z) = \sigma(z)(1-\sigma(z))$, has good mathematical properties [18], as shown in Formula (2):

$$\sigma(z) = \frac{1}{1+e^{-z}}. \tag{2}$$

Then, the final output result expression of the single neuron model is shown in Formula (3):

$$y = f_{w,b}(x) = \frac{1}{1+\exp\left(-\sum_i w_i x_i - b\right)}. \tag{3}$$

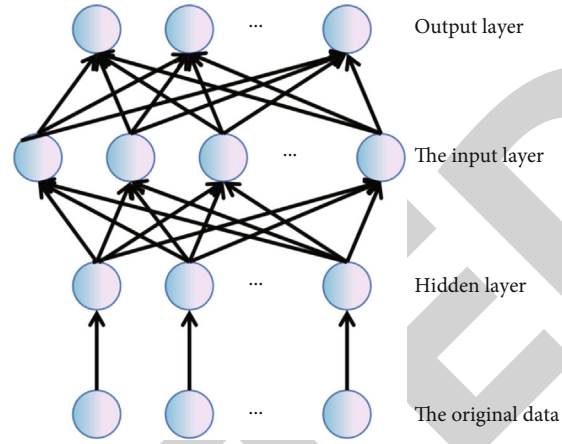

Figure 2: Simple neural network.

Multiple simple neurons are connected in parallel and combined hierarchically to form a neural network model, as shown in Figure 2. God network is divided into three parts: input layer, hidden layer, and output layer. Layer L1 is the input layer, layer L2 and layer Ln-1 are the hidden layer, and layer Ln is the output layer. The number of hidden layers and the number of neurons in each layer are set artificially, while the number of nodes in input and output layers is fixed and related to tasks. Each layer of neurons is fully connected to the next layer, but there is no connection between the neurons of this layer; in the figure, except the node with the value of+1 represents the bias term b, each of the remaining connecting lines represents a weight w, and the arrow direction indicates the direction of data flow during forward network operation.

In Figure 2, the neural network has N layers, and suppose the activation functions are sigmoid functions, called $\sigma_l (l = 2, \cdots, n)$, w_{ij}^l is used to represent the connection weight value of the j-th neuron at layer l-1 and the i-th neuron at layer l, and weights and bias items will be constantly modified to minimize the error of the model during training, if u_i^l and y_i^l are used to represent the input and output values

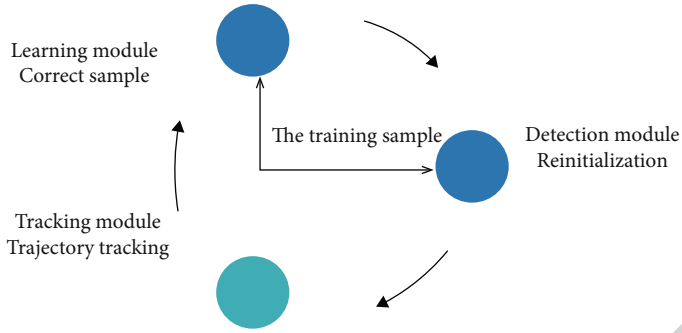

Figure 3: TLD algorithm framework.

of the i-th neuron in layer l, respectively; so, the relationship of each value in the forward operation of the network will be as follows:

$$\begin{cases} y_i' = \sigma\left(u_i'\right) \\ u_i' = \sum_j w_{ij}^{l-1} y_j^{l-1} \end{cases} \quad l = 1, 2, \cdots, n \tag{4}$$

The advantages of the convolutional neural network model lie in three core aspects. The first is local perception, also known as local connection. Each neuron only connects with small local regions in the previous layer. By taking advantage of the characteristics of strong correlation between regions with close distances in the image and weak distance, then local information is integrated at a higher level to obtain global information, thus to reduce the number of parameter training. The second is shared weight, which on the basis of local connection to further reduce the number of parameters. Since some features in the image will appear repeatedly in other positions, the same weight can be used to carry out convolution calculation for different regions of the image, independent of the local position of the image. And the last is multiconvolution kernels, and the weights and offsets are called the convolution kernel or filter [19]. A convolution kernel represents a feature. In order to obtain different feature sets, the convolution layer has multiple convolution kernels to generate different features.

3.2. GOTURN-LD Algorithm Design

3.2.1. Advantages and Disadvantages of TLD Algorithm. Tracking-Learning-Detection (TLD) is a new tracking framework proposed in 2012, which can effectively decompose complex tracking tasks into three parts. The tracker retrieves two frames of data, and then the forward trajectory of the target feature point from the previous frame to the target feature point in the current frame is calculated by using pyramid LK optical flow method and next calculate the reverse trajectory, and finally, based on the results, the target position information of the current frame is predicted. The detector is responsible for collecting target characteristics and background information and marks the target as a positive sample and the background as a negative sample, and then the scanned samples are sent to the learner through three cascade classifiers to distinguish positive and negative samples. The learner updates the target model by adjusting parameters, mainly according to the results of the detector, so as to prevent the occurrence of wrong sample values in the future. TLD developed a new learning method, P-N learning, which estimates the sample error by a pair of P-N experts [20]. The learning process is modeled as a discrete dynamic system, and the learning module is improved in the dynamic adjustment. After extensive quantitative evaluation analysis, it shows a significant improvement over the traditional tracking algorithm. The whole structure is shown in Figure 3.

The advantage of the TLD algorithm lies in the tracking failure detection mechanism, which enables TLD to complete the long-term tracking task, but most algorithms lack this mechanism; so, it can only be tracked for a short time. Since the algorithm has a global detection module, that is, detection capability, when the target deformation is too large or is completely blocked, leading to tracking failure, the algorithm will detect the target in each subsequent frame of the image, and the tracking will resume as soon as the target is detected[21]. The disadvantage of the TLD algorithm lies in the tracking module. The tracking algorithm used by the module is the pyramid LK optical flow tracking method. The tracking algorithm is greatly affected by lighting, and it is easy to lead to the tracking failure of the LK algorithm when the target moves fast or the target has nonrigid deformation. Therefore, the TLD algorithm is suitable for tracking small targets with stable illumination, significant illumination, no background, and no violent movement.

3.2.2. Advantages and Disadvantages of GOTURN Algorithm. The advantage of the GOTURN algorithm lies in its fast tracking speed, up to 100 fps, which is better than most algorithms based on deep learning, which generates a Generic Object Tracking during the training phase. In the test phase, no tuning is required, tracing is performed directly, computation is reduced, and the speed is increased. At the same time, the influence of illumination on target tracking is reduced by using convolutional neural network to extract features.

The disadvantage of the GOTURN algorithm is that the effect is poor with occlusion, since the algorithm uses logistic regression, and the assumption of this regression method is

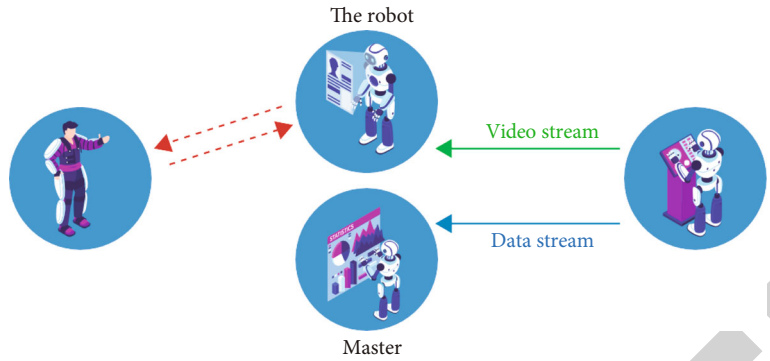

Figure 4: Actual development environment diagram.

that the target moves slowly, and there is no occlusion. The algorithm is suitable for short time tracking and has no tracking failure detection mechanism. If the target is occluded and tracking drift occurs, it cannot be retrieved due to the lack of detection module. After the above analysis, the advantages and disadvantages of TLD algorithm and GOTURN algorithm are summarized, and GOTURN-LD considering the combination of the advantages of the two algorithms, an improved tracking algorithm GOTURN-LD is proposed based on the redesigned tracking module and detection module [22].

3.2.3. GOTURN-LD Algorithm Design. The improvement of the GOTURN-LD algorithm is mainly based on TLD framework, using track-detection framework. The improvement not only overcomes the defect of TLD algorithm tracking module but also changes GOTURN, which can only track for a short time, into a long time tracking. In addition, the detection module of GOTURN-LD is improved, which reduces time-consuming calculation and affect the sample size of target model; so, it not only speeds up the retrieval speed after occlusion or loss but also improves the detection accuracy and makes the algorithm more reliable [23].

The tracking module of the TLD algorithm uses the pyramid LK optical flow tracking method, which is a fast tracking algorithm with the image as the input and the target box as the output, and GOTURN is also an end-to-end algorithm. Therefore, the tracking module of TLD algorithm can be replaced by GOTURN algorithm, while other modules remain unchanged, so that GOTURN algorithm can be combined with TLD algorithm to form a new GOTURN-LD algorithm.

In the tracking module, since the input and output of GOTURN and TLD algorithms are consistent, therefore, the tracking algorithm is regarded as a black box, and the GOTURN algorithm can be directly used to replace the LK optical flow tracking method. However, the TLD trace module has a trace failure detection mechanism; so again, a failure detection method suitable for the GOTURN algorithm needs to be designed [24]. We know that the GOTURN trace will receive two inputs; after clipping, the similarity of the two images will be calculated. If the similarity is too small, it means the tracing fails; so, the detection module is required to scan the image. So the target model needs to be updated, and the trace module needs to be reinitialized. Referring to the TLD tracking module, the error square and D as measuring standards are chosen, and the calculation formula is shown in Formula (5):

$$D(i,j) = \sum_{(i,j)\in w} (I_1(i,j) - I_2(i,j))^2. \tag{5}$$

Here, i and j represent pixel points, I1 and I2 represent the corresponding gray values of the clipping graph of the previous frame and the current frame, respectively. After the test, it is found that when D is greater than 0.7, the error is large, and the similarity is small, which is judged as tracking failure.

And then we use the strategy of hierarchical grouping, in which way we calculate the similarity and next merge these subregions are which are used as candidate images. The similarity is expressed as formula (6):

$$s(r_i, r_j) = a_1 s_{\text{color}}(r_i, r_j) + a_2 s_{\text{size}}(r_i, r_j) \tag{6}$$

Colors represent the color similarity, and the expression is shown in formula (7):

$$s_{\text{color}}(r_i, r_j) = \sum_{k=1}^{n} \min\left(c_i^k, c_j^k\right). \tag{7}$$

Size represents the scale similarity, and im represents the merged region, as shown in Formula (8):

$$S_{\text{size}}(r_i, r_j) = 1 - \frac{\text{size}(r_i) + \text{size}(r_j)}{\text{size}(im)}. \tag{8}$$

An image block P and a target model M are given arbitrarily and then use the correlation similarity index to determine the target area, and the correlation similarity ranges from 0 to 1. The larger the value, the more similar it is, and the more likely it is to be the target region. The calculation formula of correlation similarity is shown in Formula (9):

$$S^r = \frac{S^+}{S^+ + S^-}. \tag{9}$$

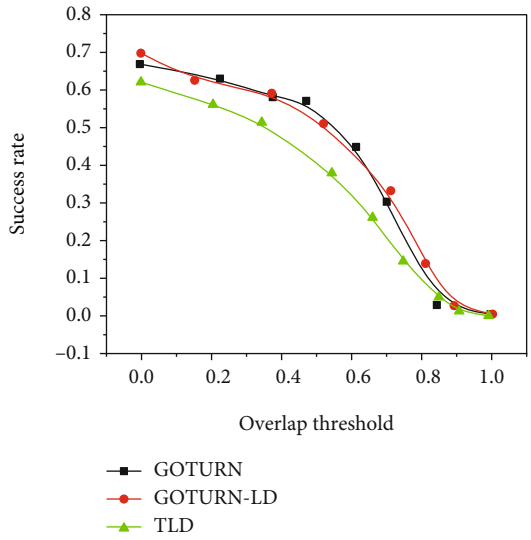

Figure 5: SRE success rate curves for illumination and occlusion problems.

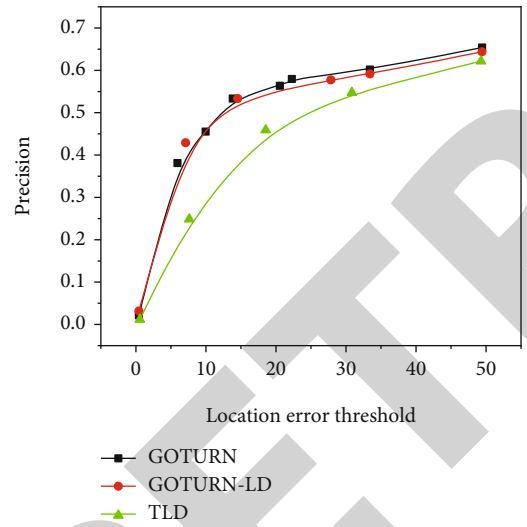

Figure 6: SRE accuracy curves for illumination and occlusion problems.

The definition of image similarity is shown in Formula (10), and NCC is the normalized crossrelation number.

$$S\left(p_i, p_j\right) = 0.5\left(\mathrm{NCC}\left(p_i, p_j\right) + 1\right). \quad (10)$$

With the target model, the image blocks output in the previous step can be detected and classified. The final image block is output by judging whether its correlation similarity is greater than the given threshold value. The image block that passes through the three cascaded classifiers is the final output of the detection module, that is, the positive sample [25].

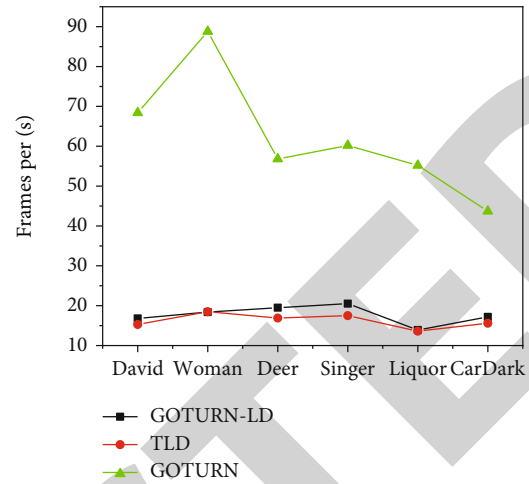

Figure 7: Tracking speed comparison (frames/s) of GOTURN-LD, TLD, and GOTURN.

4. Experimental Results and Discussion

In the actual verification, the effect is not good because of the delay of network video transmission. So, a laptop instead of a server to deal with computing problems is chosen, a camera instead of a webcam to deal with video streaming is chosen, and through USB to connect the camera to the laptop is chosen. The tracking system framework of the test is shown in Figure 4.

In order to evaluate the performance of the algorithm in more detail, OTB50, a traditional data set in the field of target tracking, was chosen to carry out specific experiments. OTB50 provides video sequences with 11 target variation challenges and 51 video sequences with real target locations. There are usually three quantitative evaluation indexes of OTB50, which are OPE, TRE, and SRE. OPE refers to the tracking evaluation by initializing the tracker through the artificially calibrated initialization box of the first frame; TRE refers to the evaluation of the robustness of a tracking algorithm over time; SRE refers to the evaluation of the robustness of tracking algorithms from space. For each metric, there are precision plot and success plot plots to show performance.

Since only illumination and occlusion are considered, six representative video sequences such as David and woman are selected to test and compare the performance of TLD, GOTURN, and GOTURN-LD algorithms. We choose SRE index to analyze the algorithm from the success rate and accuracy rate, respectively, see Figures 5 and 6.

When the illumination changes, the performance of the TLD algorithm is poor, whether the accuracy curve or the accuracy curve, and the performance of GOTURN-LD is significantly improved. When faced with occlusion problem, The TLD algorithm shows strong robustness. However, GOTURN-LD is not very stable, and its overall performance is better than GOTURN. These two points also verify the performance of the proposed improved algorithm, and it does combine the advantages of the two algorithms. The overall performance is good. The real-time analysis of the

algorithm usually uses the tracking speed as the evaluation index, and the tracking speed is expressed by frame/s. Similarly, six videos such as David and woman in OTB50 were selected as test sequences. After testing and comparing the tracking speeds of GOTURN-LD, TLD, and GOTURN algorithms, the results are shown in Figure 7.

According to the results, the GOTURN-LD algorithm failed to show the high speed of the GOTURN algorithm because of the detection mechanism, but compared with the TLD algorithm, it has some advantages. In general, it can basically meet the real-time requirements.

5. Results

The difficult problem of research and implementation of the robot vision tracking algorithm based on deep learning are solved. By analyzing the target tracking algorithm based on deep learning and classical tracking algorithm, their advantages and disadvantages are analyzed, and some suggestions for improvement are put forward. The traditional TLD algorithm combined with the GOTURN algorithm is mainly adopted, benefits from a large amount of offline training data are gained, and the learner online is updated, so that the whole system has a better performance in real-time and accuracy. As for the improved algorithm, the robot vision tracking system based on deep learning is mainly composed of two parts: a server that integrates high-performance GPU and a multifunctional intelligent robot with depth camera. The experimental process of the designed system in the test environment is as follows: first, the server takes visual information from the network and processes it with core deep learning algorithms by using monocular cameras to collect visual information to obtain information about the location of the target to be tracked; then, the location information is sent to the intelligent robot. The intelligent robot completes the machine movement according to the obtained position information to achieve the effect of target tracking. And it turns out, for single target tracking, the system designed in this paper has a good performance on the problems of illumination change, target occlusion, and reappearance after disappearance.

Data Availability

The data used to support the findings of this study are available from the corresponding author upon request.

Conflicts of Interest

The authors declare that they have no conflicts of interest.

Acknowledgments

This work was supported by Basic Scientific Research Project of Liaoning Provincial Department of Education, "research on key technologies of health assessment of high safety equipment based on deep learning (Project No. LJKZ1061)."

References

[1] S. Cao, R. Li, Y. Shi, and Y. Song, "A low-cost estimator for target localization and circumnavigation using bearing measurements," *Journal of the Franklin Institute*, vol. 357, no. 14, pp. 9654–9672, 2020.

[2] X. Zhou, Y. Li, and W. Liang, "CNN-RNN based intelligent recommendation for online medical pre-diagnosis support," *IEEE/ACM Transactions on Computational Biology and Bioinformatics*, vol. 18, no. 3, pp. 912–921, 2021.

[3] B. Yang, B. Wu, Y. You, C. Guo, L. Qiao, and Z. Lv, "Edge Intelligence Based Digital Twins for Internet of Autonomous Unmanned Vehicles," *Software: Practice and Experience*, vol. 2, 2022.

[4] Z. Wan, Y. Dong, Z. Yu, H. Lv, and Z. Lv, "Semi-supervised support vector machine for digital twins based brain image fusion," *Frontiers in Neuroscience*, vol. 15, p. 802, 2021.

[5] A. J. Liu, J. B. Lusk, J. Ervin, J. Burke, R. O'Brien, and S. H. J. Wang, "Tuberous sclerosis complex is a novel, amyloid-independent tauopathy associated with elevated phosphorylated 3r/4r tau aggregation," *Acta Neuropathologica Communications*, vol. 10, no. 1, pp. 1–8, 2022.

[6] J. Mayandi, T. G. Finstad, M. Stange et al., "Controlling the electrical properties of reactively sputtered high entropy alloy crfenicocu films," *Journal of Electronic Materials*, vol. 51, no. 2, pp. 803–812, 2022.

[7] R. A. Prateek, "An underwater localization scheme for sparse sensing acoustic positioning in stratified and perturbed uasns," *Wireless Networks*, vol. 28, no. 1, pp. 241–256, 2022.

[8] D. H. Ramirez, B. Yang, A. K. D'Souza, D. Shen, and C. M. Woo, "Truncation of the tpr domain of ogt alters substrate and glycosite selection," *Analytical and Bioanalytical Chemistry*, vol. 413, no. 30, pp. 7385–7399, 2021.

[9] Z. Lv, Y. Han, A. K. Singh, G. Manogaran, and H. Lv, "Trustworthiness in industrial IoT systems based on artificial intelligence," *IEEE Transactions on Industrial Informatics*, vol. 17, no. 2, pp. 1496–1504, 2021.

[10] Z. Lv, W. Kong, X. Zhang, D. Jiang, H. Lv, and X. Lu, "Intelligent security planning for regional distributed energy internet," *IEEE Transactions on Industrial Informatics*, vol. 16, no. 5, pp. 3540–3547, 2020.

[11] A. Creisméas, C. Gazaille, A. Bourdon et al., "Trpc 3, but not trpc 1, as a good therapeutic target for standalone or complementary treatment of dmd," *Journal of Translational Medicine*, vol. 19, no. 1, pp. 1–17, 2021.

[12] K. Dong, S. Gao, S. Xin, and Y. Zhou, "Probability driven approach for point cloud registration of indoor scene," *The Visual Computer*, vol. 38, no. 1, pp. 51–63, 2022.

[13] H. Sami, A. Mourad, and W. El Haj, "Vehicular-OBUs-as-on-demand-fogs: resource and context aware deployment of containerized micro-services," *IEEE/ACM Transactions on Networking*, vol. 28, no. 2, pp. 778–790, 2020.

[14] A. Mourad, A. Srour, H. Harmanani, C. Jenainati, and M. Arafeh, "Critical impact of social networks Infodemic on defeating coronavirus COVID-19 pandemic: twitter-based study and research directions," *IEEE Transactions on Network and Service Management*, vol. 17, no. 4, pp. 2145–2155, 2020.

[15] Z. Li, Z. Jiang, X. Chen, K. Cao, and Q. Gu, "Laprob: a label propagation-based software bug localization method," *Information and Software Technology*, vol. 130, no. 4, article 106410, 2020.

Hindawi
Scanning
Volume 2023, Article ID 9816104, 1 page
https://doi.org/10.1155/2023/9816104

Retraction

Retracted: Image Observation Study on Improving the Effectiveness of Muscle Strength Training for Sprinters

Scanning

Received 20 June 2023; Accepted 20 June 2023; Published 21 June 2023

This article has been retracted by Hindawi following an investigation undertaken by the publisher [1]. This investigation has uncovered evidence of one or more of the following indicators of systematic manipulation of the publication process:

(1) Discrepancies in scope

(2) Discrepancies in the description of the research reported

(3) Discrepancies between the availability of data and the research described

(4) Inappropriate citations

(5) Incoherent, meaningless and/or irrelevant content included in the article

(6) Peer-review manipulation

The presence of these indicators undermines our confidence in the integrity of the article's content and we cannot, therefore, vouch for its reliability. Please note that this notice is intended solely to alert readers that the content of this article is unreliable. We have not investigated whether authors were aware of or involved in the systematic manipulation of the publication process.

In addition, our investigation has also shown that one or more of the following human-subject reporting requirements has not been met in this article: ethical approval by an Institutional Review Board (IRB) committee or equivalent, patient/participant consent to participate, and/or agreement to publish patient/participant details (where relevant).

Wiley and Hindawi regrets that the usual quality checks did not identify these issues before publication and have since put additional measures in place to safeguard research integrity.

We wish to credit our own Research Integrity and Research Publishing teams and anonymous and named external researchers and research integrity experts for contributing to this investigation.

The corresponding author, as the representative of all authors, has been given the opportunity to register their agreement or disagreement to this retraction. We have kept a record of any response received.

References

[1] Y. Zou and L. Han, "Image Observation Study on Improving the Effectiveness of Muscle Strength Training for Sprinters," *Scanning*, vol. 2022, Article ID 4987782, 7 pages, 2022.

Hindawi
Scanning
Volume 2022, Article ID 4987782, 7 pages
https://doi.org/10.1155/2022/4987782

Research Article

Image Observation Study on Improving the Effectiveness of Muscle Strength Training for Sprinters

Yimin Zou[1] **and Liming Han**[2]

[1]*Ministry of Culture, Sports and Labour, Gannan Healthcare Vocational College, Ganzhou, Jiangxi 341000, China*
[2]*College of Physical Education, Xingtai University, Xingtai, Hebei 054001, China*

Correspondence should be addressed to Liming Han; 202007000041@hceb.edu.cn

Received 13 June 2022; Revised 5 July 2022; Accepted 13 July 2022; Published 25 July 2022

Academic Editor: Danilo Pelusi

In order to solve the problem of improving the effectiveness of muscle strength training for sprinters, this paper presents a study using image observation technology. The main content of this technology research is to determine the experimental object and method according to the image observation and muscle characteristics. Through the data processing and other processes, it is concluded that the image observation technology has a high accuracy in the observation of muscle movement patterns. The experimental results show that when the relationship number $r = 0.99$, the average error of prediction is 0.09, and the image observation technology has a high accuracy in the observation of muscle movement. *Conclusion*. It is proved that the technical research of image observation is effective and accurate for improving the training of sports muscle strength of sprinters.

1. Introduction

In the process of the steady development of China's sports cause, the emphasis on training has gradually increased, as has the sprint team. When carrying out the special strength training of the sprint team (Figure 1), it is necessary to adjust the traditional training methods, so that the special strength of the sprint can play a role together with the general strength training, improve the performance of the sprinters, and hope to have some help for the development of China's sports school athletes [1]. For a long time, traditional strength training has played a key role in enhancing the strength of athletes' upper and lower limbs, and the sprint performance has been continuously improved, but our elite athletes have hardly achieved good results in sprint events [2]. In recent years, scholars have strengthened the theoretical research of strength training, especially carried out a series of experiments on the shortcomings of traditional strength training, and formed a corresponding comparison between the new strength training methods and traditional strength training. Strength training refers to the ability of human neuromuscular system to overcome or resist resistance during work.

Traditional strength training has been playing an important role in improving sprint performance. It is mainly based on the principle of excess recovery to do incremental resistance strength training to improve muscle strength. In the process of exercise, the ability of human neuromuscular system to overcome and resist resistance at work is simply based on increasing load to enhance strength. Traditional strength training pays attention to the development of a single muscle. When muscle strength is enhanced, muscle volume is also increasing. Its basic methods mainly include dynamic isometric contraction training, static isometric contraction training, isometric contraction training, super isometric contraction training, and circular training, which are widely used in sprint strength training [3].

Scientifically and reasonably designing strength training, developing the strength ratio of the flexor and extensor muscles in the medulla, the coordinated and balanced

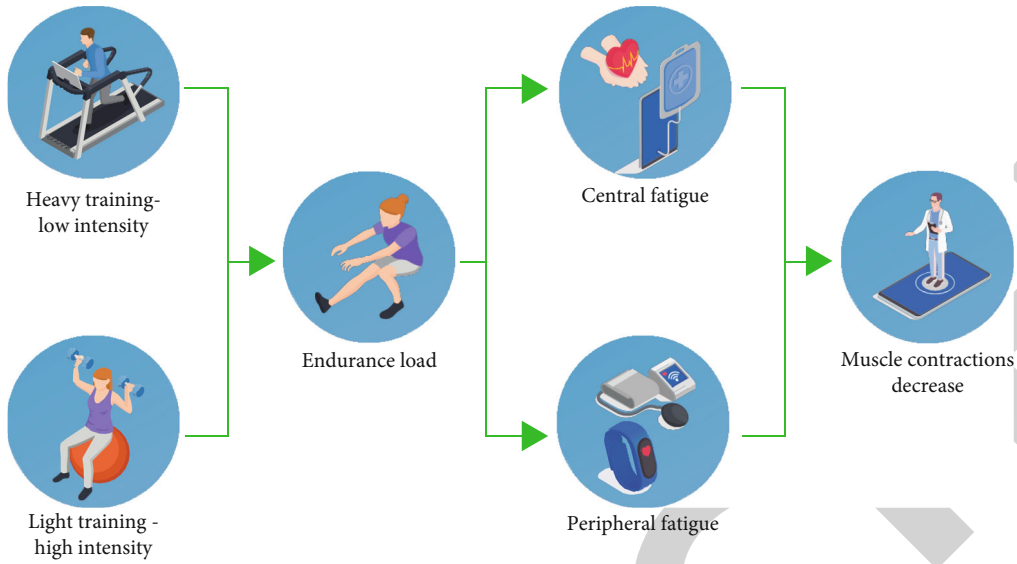

Figure 1: Weight training.

development of the strength of the upper and lower limbs, and the contraction ability of the muscles of the metacarpophalangeal and ankle joints are the most important to improve the performance of sprint. In the traditional strength training, the general strength training and special strength training are applied repeatedly, which enhances the muscle strength of athletes and lays a certain foundation for the improvement of performance. We should pay more attention to the strength training of the extensor group instead of the flexor group and from the training of maximum strength to the training of fast strength and strength endurance. This training guiding ideology is more in line with the characteristics of modern sprint sports and provides more pertinence and scientificity for better improving sprint performance [4].

2. Literature Review

With the country's vigorous sports undertakings, under the current background, strength training has an important impact on the improvement of sprint performance; the world record of 100 m performance especially has been broken repeatedly. We should strengthen strength training and combine it with sprint technology. In strength training, it is necessary to design strength training methods and means suitable for project characteristics and sports biomechanics characteristics according to the working forms and force characteristics of sprint technical movements. Traditional strength training has always played an important role in improving sprint performance, but there are also some shortcomings in traditional strength training. We should make up for them. It is the all-round development of Chinese athletes' muscle strength to improve their sprint performance. Strength training can effectively enhance the contractility of muscles, improve the resistance of human neuromuscles to external activities, and effectively exercise the human skeletal system [5]. High school physical education teachers should constantly guide students to carry out strength training, ensure the explosive power of muscle groups through the training of outburst, reaction, and starting strength, emphasize the integrity and continuity, and establish a perfect evaluation and monitoring system to timely point out the lack of training of students and improve the sprint training effect, so as to enable students to develop a good physique and promote physical health. The development level of athletes' muscle strength quality and the good coaxiality and coordination among active muscle, antagonistic muscle, and synergetic muscle in sports are one of the main factors to measure sprint technology and determine sports performance. The ultimate purpose of selecting strength training methods is to effectively develop the strength of the muscles and muscle groups participating in special sports, make them work in line with the characteristics of special technology, and form a strength quality system with special projects as the core, so as to enhance the special ability of athletes and further improve their special performance. Strength training is the source of all kinds of sports. Sprint is a periodic speed strength event. Muscle strength and speed are directly related to running speed. Double the running speed and quadruple the resistance; that is to say, the faster the speed is, the greater the muscle strength is required. Therefore, if you want to improve the speed, you must enhance the muscle strength, so strength is very important to improve the sprint performance.

In view of the above problems, this paper proposes an image observation study to improve the effectiveness of muscle strength training for sprint athletes [6]. The main content of this study is to determine the experimental objects and methods based on image observation and muscle characteristics, and through data processing, it is concluded that the image observation technology has a high accuracy in the observation of muscle movement patterns. Accurate observation of the impact of strength training on the athletes' muscles helps in formulating a targeted way of strength training for athletes and providing a scientific basis for improving sprint performance.

3. Research Methods

3.1. Image Observation and Muscle Characteristics. Muscle (especially skeletal muscle) contraction is the driving force for human body to generate movement. In order to understand human movement and reveal the mechanical law of movement, it is necessary to study the structure, function, and characteristics of human muscle [7]. Due to the complexity and diversity of the movement process, the study of muscle function and characteristics in the movement process is a complex and arduous task, especially how to simultaneously obtain a variety of information from a single muscle in the human body and carry out multilevel comprehensive processing is still a difficult problem to be solved.

Surface electromyographic signal (SEMG, hereinafter referred to as SEMG) is an electrophysiological signal obtained from the skin surface. It is a common method to study the activities of the neuromuscular system and is widely used in biomechanics, rehabilitation medicine, and other fields [8]. EMG signal is the superposition of action potentials generated by many motor units in muscle fibers during contraction. Its time-frequency characteristics can quantitatively reflect the characteristics and laws of muscle function, muscle strength level, multimuscle group coordination, etc. However, EMG signal is vulnerable to various potential factors, such as electrode position, muscle type, and adjacent muscle interference, which restrict the application of EMG signal in muscle evaluation.

Different from EMG signals, muscle tone signals (MMG, also translated into muscle motion signals) are signals generated by the lateral vibration of muscle fibers during muscle contraction and also contain the functional state information of muscles [9]. EMG reflects the electrical activity of the moving unit, while MMG reflects the mechanical activity of the moving unit. MMG can be collected by a variety of sensors, including piezoelectric sensors, micro microphones, and acceleration sensors. Many studies have compared EMG with MMG, and the results show that MMG has different time-frequency characteristics from EMG. MMG combined with EMG can provide complementary information about muscle movement.

Muscle contraction will cause changes in muscle morphology, so changes in muscle morphology can directly reflect the state of muscle activity. Various clinical imaging methods, including CT, MRI, and ultrasound, have been used to study muscle morphological changes. Among them, ultrasonic imaging (US) has the characteristics of nondestructive, real time, and easy to use, which has been more applied [10]. Since the 1990s, researchers have tried to use morphological parameters extracted from ultrasound images to reflect the changes of muscle function. These parameters include muscle thickness, cross-sectional area, muscle fiber length, and feather angle, which are closely related to muscle function. Due to the real-time nature of US, it can be applied to various forms of muscle movement, including isometric movement, standing, walking, and muscle contraction caused by electrical stimulation [11]. All these studies show that US, that is, simple, nondestructive, and real time, can measure muscle contraction, which is difficult to achieve by other existing technologies. Compared with EMG, US has the advantage that it is not affected by adjacent muscles and can measure deep muscles. In some cases, it is more sensitive to changes in muscle contraction. Among the muscle morphological parameters, cross-sectional area (CSA) is of special significance, which determines the strength of muscle. However, most studies focus on the influence of age, training, and other factors on CSA. Few studies have studied the changes of CSA during muscle dynamic contraction. The main reason is that it is a difficult problem to automatically obtain CSA from continuous ultrasound images.

EMG, MMG, and US, respectively, reflect the electrical, mechanical, and morphological changes of muscle movement and can provide complementary information for the study of muscle movement. Previous studies mostly combined EMG with ultrasonic MMG. But so far, few studies have combined the three to further reveal the internal physiological mechanism of muscle continuous movement. Based on the above considerations, the author developed a multichannel motion signal acquisition system, which can synchronously collect US, EMG, MMG, joint angle, and torque signals. In addition, in order to track the continuous change of CSA, the author also developed a new image tracking algorithm to achieve the automatic acquisition of CSA. Using this system, this study studied the isometric contraction of rectus femoris (RF) during knee extension, analyzed the characteristics of various signals collected, and preliminarily established a new method for multimodal study of muscle motion characteristics [12].

3.2. Experimental Process

3.2.1. Test Object and Method. A total of 9 subjects participated in the experiment, including 6 males and 3 females. During the experiment, the subjects sit on the experimental chair of the isokinetic muscle strength test system and fix the body with safety belts. The hip and knee joints are kept at 90°, and the lower leg is fixed on the rotating shaft through the fixing belt, so the isometric contraction movement of knee joint extension can be carried out [13].

Before the beginning of the experiment, a rectus femoris image was collected as a reference when the subjects were relaxed. Then, the subjects completed two isometric knee extension movements lasting for 6 s to determine the maximum arbitrary contraction (MVC) of the muscle and defined MVC as the maximum amplitude of isometric contraction of the muscle [14]. Then, the subjects did several warm-up exercises to familiarize themselves with the experimental rules. After 5 min of rest, the subjects will complete isometric muscle contraction under continuous increasing load, and the torque requirements will increase linearly from 0%MVC to 90%MVC for 6 s. In the experiment, the knee joint extension torque generated by the subjects will be detected by the system, and its time-varying waveform will be displayed on the display screen in front of the subjects in real time. The standard torque waveform (from 0%MVC to 90%MVC within 6 s) will also be displayed at the same time. The subjects will adjust their actions to make the torque waveform generated by themselves match the

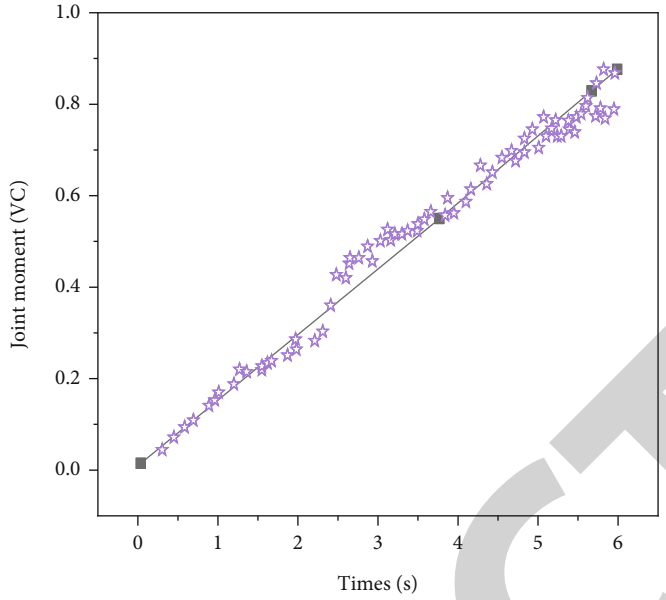

Figure 2: Waveform of joint torque with time during muscle contraction.

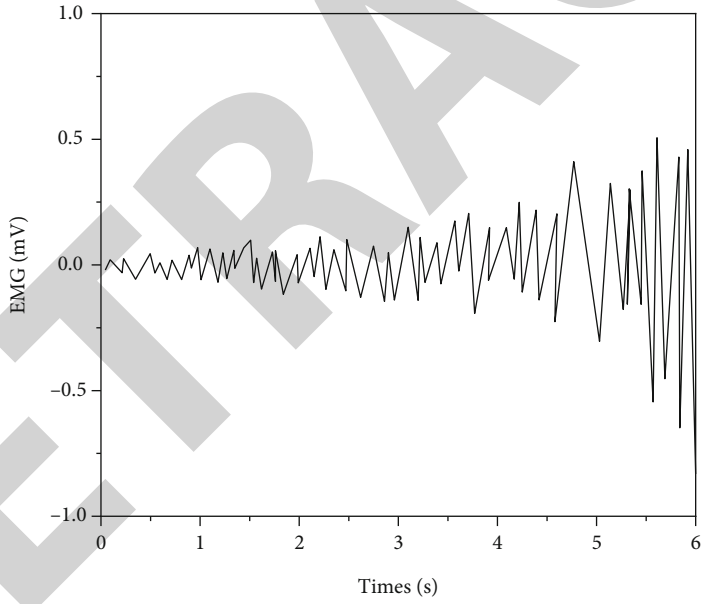

Figure 3: EMG waveform.

standard waveform as much as possible. The subjects will repeat the experiment for 3 times and rest for 5 min between every two adjacent experiments [15].

During the experiment, ultrasound images of rectus femoris muscle were obtained by ultrasound scanner. The ultrasonic probe is fixed above the thigh through a self-made multiangle bracket, and its long axis is perpendicular to the direction of the thigh. The video output of the ultrasonic equipment is captured by the video acquisition card, and the sampling frequency is 25 frames/s. Two surface EMG electrodes are attached to the rectus femoris muscle abdomen, along the muscle fiber direction, at the positions on both sides of the probe, and the reference electrode is attached to the knee. The acceleration sensor is pasted on the muscle surface near the ultrasonic probe with double-sided tape to collect MMG signals. EMG and MMG are amplified by a self-made amplifier with a gain of 2000, and then, bandpass filtering of 10~400 Hz and 5~100 Hz is performed, respectively, and finally digitized by a data acquisition card with a sampling frequency of 1 kHz. The torque signal output by the isokinetic muscle strength tester is also sampled by the data acquisition card, and the display, synchronous acquisition, and storage of all signals are completed by the self-developed software, and the saved data will be further analyzed and processed [16].

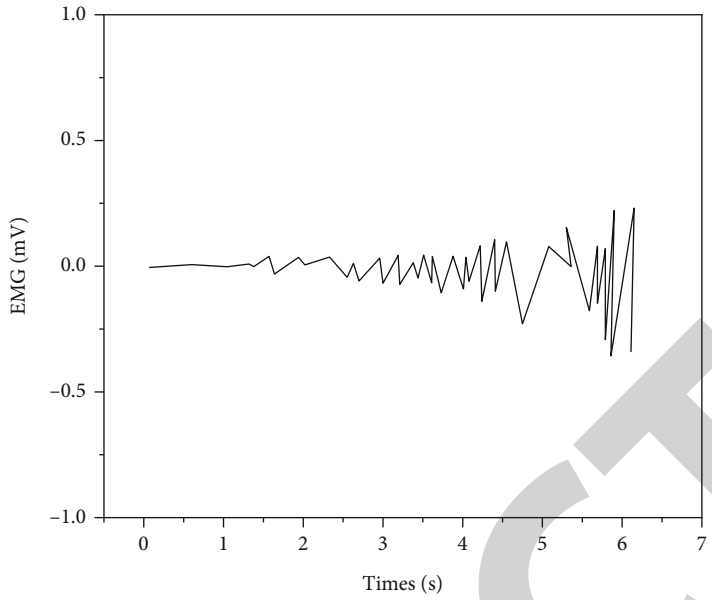

Figure 4: MMG waveform.

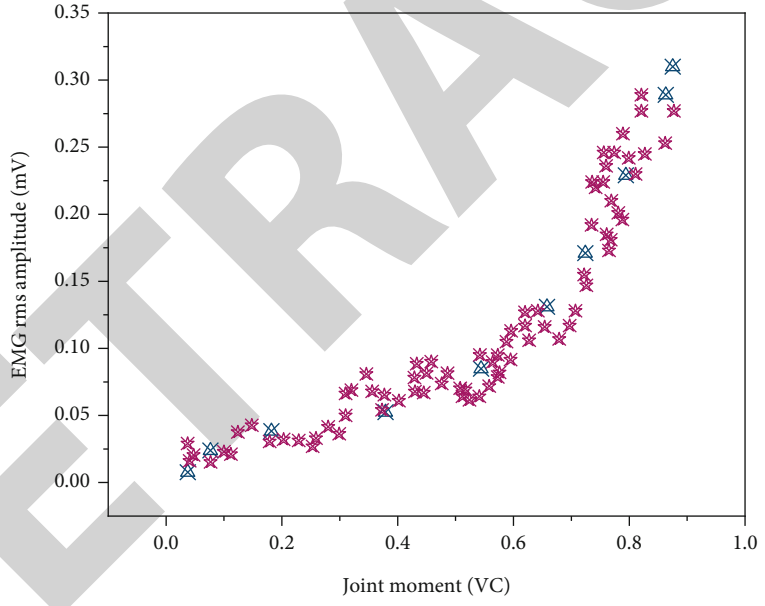

Figure 5: Relationship between EMG root mean square amplitude and joint torque.

Table 1: Fitting results.

Project	Numerical value
Slope	1
Correlation coefficient	0.99
Forecast average error	0.09

3.2.2. Data Processing. EMG and MMG signals of each subject were processed offline by software. The EMG and MMG are divided into 256 MS segments according to time, and the time center of each segment is aligned with the corresponding ultrasonic image acquisition time [17]. Since the sampling frequency of the image is 25 frames/s, there is a certain coincidence between the two adjacent segments of EMG and MMG. Then, the root mean square value of each segment is calculated as the time domain characteristic index of EMG and MMG. By definition, RMS is calculated as follows.

$$\mathrm{RMS} = \sqrt{\frac{1}{N}\sum_{i=1}^{N} x_i^2} \quad (1)$$

In the global transformation, the transformation parameters are composed of the global scale, translation, and rotation

transformations of two images, and the global affine transformation function $T = \psi[x, y, 1]T$, where x and y are image coordinates and ψ is an affine transformation matrix of 3×3. If a and B are the images to be matched, the global mutual information is calculated as follows.

$$\begin{aligned} \mathrm{MI} &= I(A; T(B)) = H(p_A(i_A)) + H\left(p_{T(B)}(i_B)\right) \\ &\quad - H\left(p_{A,T(B)}(i_A, i_B)\right) \\ &= \iint_{I(A),I(B)} p_{A,T(B)}(i_A, i_B) \lg\left(\frac{p_{A,T(B)}(i_A, i_B)}{p_A(i_A)p_{T(B)}(i_B)}\right) \mathrm{d}i_A i_B. \end{aligned} \tag{2}$$

Continue to perform local transformation on the results after global transformation, and use 2D spline function TL (B') to describe the local transformation [18]. M and N are the number of horizontal and vertical control points, respectively. In the third-order neighborhood of the control point, the transformation function can perform third-order spline interpolation based on the transformation result of the control point, and formula (3) is calculated.

$$P(i, j) = \sum_{\mu=0}^{3} \sum_{\gamma=0}^{3} \beta_\mu(u)\beta_\gamma(v)P_c(m + \mu, n + \gamma). \tag{3}$$

Leave one test is used to test the accuracy of multiparameter linear estimation. Each time, the data of one subject is left for test, and the data of other subjects are used as the linear regression coefficient to calculate the coefficient. Then, the fitting coefficient is used to predict the torque of the left subject, and the error with the real torque is calculated. This is repeated many times, so that each subject is left alone for a test, and finally calculate the average prediction error [19].

4. Result Analysis

During muscle contraction, typical joint torque signals are shown in Figure 2. The circle in the figure represents the joint torque generated by the subject, and the solid line represents the standard torque signal used to guide the subject [20]. These two signals will be displayed in front of the subject in real time in the experiment.

The original waveform and RMS amplitude of EMG and MMG are shown in Figures 3 and 4. In order to study the relationship between RMSEMG, RMSMMG, and joint torque, curves are drawn in the same coordinates, as shown in Figure 5 [21].

100 ultrasound images were processed manually and by image algorithm. The results of ICC analysis were 0.987 ($P < 0.0001$). The results show that the image algorithm can accurately track the muscle boundary and basically achieve the same effect as manual processing. The relationship between the overall average value of different parameters and joint torque is composed of the upper and lower limits of the data average standard error se, and the solid line is a cubic polynomial fitting curve [22]. Image tracking algorithm can automatically extract the boundaries of rectus femoris muscle in all images and calculate the corresponding CSA. The relationship between CSA and joint torque in this experiment changes. The cubic polynomial curve is used for fitting, and the fitting results are also displayed.

EMG is a traditional method to study muscle activity. A large number of researchers have deeply discussed the relationship between EMG and muscle strength. At present, it is generally believed that the relationship between the two is nonlinear and affected by many factors. It is difficult to accurately estimate the muscle force only from the EMG of a single channel. MMG is a signal produced by the lateral vibration of muscle fibers during muscle contraction, which is different from EMG in nature.

Combining the three parameters of RMSEMG, RMSMMG, and CSA, carry out multiparameter linear fitting for the joint torque. The fitting results are compared with the actual measurement. The abscissa is the actual measured torque, the ordinate is the fitted torque, the circle is the fitting data point, and the solid line is the reference line with a slope of 1. The correlation coefficient $R = 0.99$ is obtained, and the average error of prediction is 0.09 through the leave one test, as shown in Table 1.

5. Conclusion

In order to solve the problem of improving the effectiveness of muscle strength training for sprinters, this paper presents a study using image observation technology. The main content of this technology research is to determine the experimental object and method according to the image observation and muscle characteristics. Through the data processing and other processes, it is concluded that the image observation technology has a high accuracy in the observation of muscle movement patterns. Accurately observe the impact of strength training on Athletes' muscles, so as to formulate a targeted way of strength training for athletes and form a strength quality system with special projects as the core, so as to enhance athletes' special ability and further improve their special performance, which provides a scientific basis for improving sprint performance and is very important for improving sprint performance.

Data Availability

The data used to support the findings of this study are available from the corresponding author upon request.

Conflicts of Interest

The authors declare that they have no conflicts of interest.

References

[1] T. Ohya, K. Kusanagi, J. Koizumi, R. Ando, and Y. Suzuki, "Effect of moderate- or high-intensity inspiratory muscle strength training on maximal inspiratory mouth pressure and swimming performance in highly trained competitive

Hindawi
Scanning
Volume 2023, Article ID 9859421, 1 page
https://doi.org/10.1155/2023/9859421

Retraction

Retracted: Application of Ultrasound Combined with Magnetic Resonance Imaging in the Diagnosis and Grading of Patients with Prenatal Placenta Accreta

Scanning

Received 20 June 2023; Accepted 20 June 2023; Published 21 June 2023

This article has been retracted by Hindawi following an investigation undertaken by the publisher [1]. This investigation has uncovered evidence of one or more of the following indicators of systematic manipulation of the publication process:

(1) Discrepancies in scope

(2) Discrepancies in the description of the research reported

(3) Discrepancies between the availability of data and the research described

(4) Inappropriate citations

(5) Incoherent, meaningless and/or irrelevant content included in the article

(6) Peer-review manipulation

The presence of these indicators undermines our confidence in the integrity of the article's content and we cannot, therefore, vouch for its reliability. Please note that this notice is intended solely to alert readers that the content of this article is unreliable. We have not investigated whether authors were aware of or involved in the systematic manipulation of the publication process.

In addition, our investigation has also shown that one or more of the following human-subject reporting requirements has not been met in this article: ethical approval by an Institutional Review Board (IRB) committee or equivalent, patient/participant consent to participate, and/or agreement to publish patient/participant details (where relevant).

Wiley and Hindawi regrets that the usual quality checks did not identify these issues before publication and have since put additional measures in place to safeguard research integrity.

We wish to credit our own Research Integrity and Research Publishing teams and anonymous and named external researchers and research integrity experts for contributing to this investigation.

The corresponding author, as the representative of all authors, has been given the opportunity to register their agreement or disagreement to this retraction. We have kept a record of any response received.

References

[1] X. Zhang, F. Liu, and X. Wang, "Application of Ultrasound Combined with Magnetic Resonance Imaging in the Diagnosis and Grading of Patients with Prenatal Placenta Accreta," *Scanning*, vol. 2022, Article ID 1199210, 7 pages, 2022.

Hindawi
Scanning
Volume 2022, Article ID 1199210, 7 pages
https://doi.org/10.1155/2022/1199210

Research Article

Application of Ultrasound Combined with Magnetic Resonance Imaging in the Diagnosis and Grading of Patients with Prenatal Placenta Accreta

Xiaoyan Zhang, Fengfeng Liu, and Xiaoyan Wang

Department of Obstetrics and Gynecology Women and Children's Hospital of Chongqing Medical University, China

Correspondence should be addressed to Xiaoyan Wang; 201804325@stu.ncwu.edu.cn

Received 5 June 2022; Revised 29 June 2022; Accepted 7 July 2022; Published 22 July 2022

Academic Editor: Danilo Pelusi

In order to study the clinical application value of placenta accreta (PIA) diagnosis and grading, the authors propose a method based on ultrasound combined with magnetic resonance imaging in the diagnosis and grading of prenatal placenta accreta patients. This method is adopted in materials and methods: a retrospective analysis of hospital patients with high suspicion of placenta accreta by clinical or ultrasonography between October 2019 and October 2021, the imaging and clinical data of 312 patients who underwent placental MRI examination. The MRI imaging data of all patients were jointly analyzed, and the main observation indicators are as follows: (1) dark zone in the placenta, (2) disruption of the border of the myometrium, (3) disruption of the myometrium, (4) abnormal blood vessels in the placenta, (5) enlargement of the lower part of the uterus, and (6) local bulge of the bladder/or invasion of the adjacent tissues of the uterus. The results show the following: in MRI combined with ultrasonography ($P < 0.05$), there was no statistical significance in the specificity and accuracy of MRI combined with ultrasound to diagnose PIA ($P > 0.05$). The comparison of graded diagnostic accuracy showed that in ultrasound alone < MRI alone < MRI combined with ultrasound, the differences were statistically significant ($P < 0.05$). Ultrasound combined with MRI in the diagnosis of placenta accreta is in good agreement with the clinical and surgical pathological results; MRI examination can be used as an important method for prenatal placenta accreta screening. MRI can classify placenta accreta to some extent.

1. Introduction

Placenta accreta (PIA) is due to uterine hypoplasia or injury(Figure 1), resulting in partial loss of decidua basalis, and placental chorionic trophoblasts invade the myometrium through the missing part and even break through the serosa, involving parametrial tissues and organs, an abnormal placental implantation. Depending on the depth of implantation of the placental villi into the myometrium, divide it into three types: (1) placenta accreta (placenta accreta) refers to the placental villi attached or adhered to the superficial muscle layer, but does not invade the deep muscle layer, (2) placenta accreta (placenta accreta) refers to the implantation of the placenta into the deep muscle layer and does not reach the serosa layer, and (3) placenta accreta (placenta percreta) is when placental villi penetrate the muscularis layer and involve the serosal layer; it even involves adjacent tissues and organs, which is the most serious type [1]. Risk factors for placenta accreta are often related to endometrial trauma and endometrial dysplasia. A previous history of cesarean section (LUSC), placenta previa (PP), history of multiple miscarriages or multiple hysterectomy, and previous history of other uterine surgery are the main risk factors for placenta accreta; among them, placenta previa and the history of previous cesarean section are the most important; if the two exist together, the incidence of placenta accreta will be significantly increased. Therefore, some scholars believe that caesarean section is the most important risk factor for PIA, and the risk of placenta accreta increases with the increase in the number of caesarean sections. Because

the cause of placenta accreta may be endometrial damage, in addition to cesarean section, the history of repeated uterine removal, other intrauterine surgical operations, and intrauterine infection are also risk factors for placenta accreta. Another scholar's research has shown that advanced pregnancy (age>35 years) is also one of the independent risk factors for placenta accreta. Some scholars have shown that assisted reproductive technology is another independent risk factor for placenta accreta [2].

The clinical importance of PIA arises from increased maternal morbidity and mortality and massive postpartum and sometimes intrapartum or antepartum hemorrhage. When there is placenta accreta, it is difficult to separate the placenta from the uterus, sometimes requiring instrumental forceps, which can lead to massive bleeding before, during and after the operation, and the bleeding is difficult to control and can cause shock in severe cases; it can also be complicated by disseminated intravascular coagulation (DIC), uterine perforation, and subsequent severe intrauterine infection, which increases the probability of hysterectomy and even endangers the lives of mothers and babies. In recent years, the incidence of placenta accreta has increased significantly, reaching 1/533, which is 20 times higher than before. It has become an important cause of postpartum hemorrhage, perinatal emergency hysterectomy, and maternal death. According to a WHO survey on caesarean section rates in 2007-2008, among the nine Asian countries surveyed, China has the highest rate of caesarean section at 46.2%. With changes in social concepts and population policy adjustments, the age of childbearing has been delayed, and the number of "second children" has increased; many people with "second children" are advanced mothers, which may increase the incidence of placenta accreta and clinical issues that must be faced by an obstetrician [3]. Accurate prenatal diagnosis, planned cesarean section, and hysterectomy can reduce complications and mortality in pregnancy with placenta accreta. Magnetic resonance imaging (MRI), on the other hand, with its higher soft tissue resolution, comprehensive imaging information is provided before birth. Based on this, the authors intend to explore the diagnostic efficacy of MRI combined with ultrasound (US) in the diagnosis and grading of PIA, the results are reported as follows.

2. Literature Review

Jiao and others believed that clinical symptoms, signs, and laboratory examinations of placenta accreta were of limited value, and imaging examinations became an important auxiliary diagnosis. Currently, the first-line test for obstetricians to screen for and diagnose antenatal placenta accreta is transabdominal or transvaginal color Doppler ultrasonography [4]. Ha et al., in a systematic evaluation of the value of ultrasound in the diagnosis of prenatal placenta accreta, concluded that the sensitivity of ultrasonography in the diagnosis of prenatal placenta accreta was 77%-88% and the specificity was 93%-96% [5]. Zhang et al. believe that the biggest advantage of ultrasonography is the convenience of examination, the blood flow signals of the placenta and

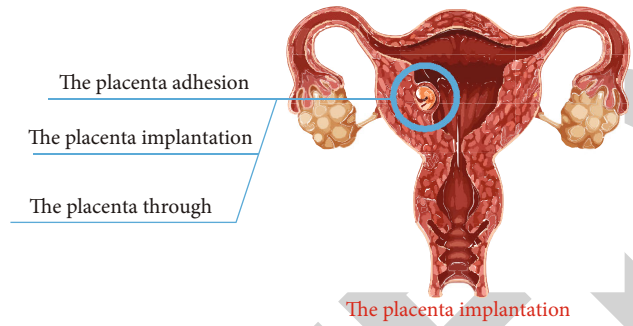

Figure 1: Placenta implantation.

uterus can be observed, but ultrasound also has shortcomings; for example, the soft tissue resolution and spatial resolution are relatively low, and the field of view (FOV) is small; in addition, the imaging quality of pregnant women is poor, such as obesity, oligohydramnios, and more intestinal gas in the imaging area, and the placenta is located in the posterior wall of the uterus; these factors will affect the image quality and diagnostic results to varying degrees [6]. Mcdannold et al. believe that MRI has high soft tissue resolution, no ionizing radiation, can scan in any orientation, and has a large scanning field of view, and it is not interfered by factors such as the body shape of the pregnant woman, intestinal gas, and placenta position; in the past, conventional spin echo sequence scanning was used for magnetic resonance imaging, which took a long time, and it was difficult to overcome the respiratory motion artifacts and fetal movement artifacts, which limited the application of MRI in obstetrics [7]. In the past ten years, with the development of MRI hardware and software and the application of fast scanning technology, the impact of physiological motion artifacts on image quality has been reduced, and its application advantages in prenatal examinations have become prominent, when the diagnosis of placenta accreta is not clear by ultrasonography, especially when evaluating the depth of placenta accreta and the infiltration of parametrial tissues and organs, MRI can be used as a supplementary imaging method [8]. US is the preferred auxiliary examination for obstetricians, and it is recognized as a relatively safe and effective imaging examination. For the application of MRI in prenatal examination, most researchers generally believe that it is relatively safe. However, considering the special physiological characteristics of fetal development, the embryonic development has not been completed in the first 3 months of pregnancy and is easily affected by various physical factors [9]. The SAR value of fetal magnetic resonance examination should be lower than 3 W/kg, SAR value is proportional to the square of the static magnetic field strength, 1.5T magnetic resonance SAR value is significantly lower than 3.0 T magnetic resonance, and therefore, 1.5T magnetic resonance imaging is often used in prenatal examinations. Since the body heat production caused by radio frequency pulse is mainly located on the surface of the body and is weakest in the center of the body and the amniotic fluid has a certain protective effect on the fetus, there has been no report on fetal injury [10].

3. Methods

3.1. Analysis Objects. From October 2019 to October 2021, 312 pregnant women who gave birth in our hospital and were diagnosed with placenta accreta by intraoperative clinical diagnosis and postoperative pathological diagnosis were selected as the research objects, the age ranged from 22 to 38 years, with an average of 26.98 ± 5.85 years old, the gestational age was 30 to 38 weeks, with an average of 35.69 ± 2.58 weeks, and the pregnancy was 1 to 5 times, with an average of 2.69 ± 2.69 ± 2.58 weeks. The parity was 1 to 4 times, with an average of 2.08 ± 0.87 times, 280 cases had a history of cesarean section, 20 cases had a history of myomectomy, and 12 cases had a history of other uterine cavity operations; all pregnant women were clearly conscious, without serious cardiovascular and cerebrovascular diseases, abnormal liver and kidney functions, coagulation disorders, and mental disorders [11].

3.2. Analysis Method

3.2.1. US Examination and Graded Diagnosis. Using Philips iU22 color US diagnostic system, with a probe frequency of 3.5 Hz, two US professional deputy chief physicians performed US images to assess whether there was placenta accreta, and the cases diagnosed with placenta accreta were classified according to the previous literature: In Grade I, the retroplacental space disappears and is occupied by placental tissue, the strong echo lines of the decidua disappear, and the myometrium becomes thin (<2 mm). In Grade II, in addition to the manifestations of Grade I, the myometrium disappears, and there are venous pools of different sizes in the placenta, which are the same as the abnormally dilated blood vessels on the uterine wall after the placenta [12]. In Grade III, in addition to grade II manifestations, the uterine serosa layer is interrupted, local blood vessels and solid mass shadows protrude to the bladder, the posterior wall of the bladder is not smooth or uneven, and at the same time, the authors classified cases where US failed to diagnose placenta accreta as Grade 0. If the evaluations are consistent, the consistency evaluation results will be accepted [13]. If there are differences in the evaluation results, the two evaluating physicians will reach a consensus after consultation as the evaluation result.

3.2.2. MRI Examination and Graded Diagnosis. Philips Achieva 1.5t dual gradient superconducting magnetic resonance equipment (maximum gradient field intensity 66 mm/Tm, maximum gradient switching rate 180 T/m/s, and climbing time 0.18 ms, AchievaNovalDual) and 16-channel body phase controlled front ring were adopted. T1-weighted imaging (T1WI) was performed using a gradient echo sequence [repetition time (TR): 500 ms, echo time (TE): 14 ms]. T2-weighted imaging (T2WI) was performed using a single excited fast spin echo sequence (TR: 1800 ms, TE:12 ms) and a short reversal time reversal recovery (STIR) sequence (TR: 1600 ms, TE: 70 ms) [14]. Imaging parameters are as follows: matrix of 256 × 256, acquisition times of 2~3 times, slice thickness of 3~5 mm, and slice spacing of 0.5~1.0 mm. The pregnant woman is in a supine position, her feet are advanced, and her bladder is moderately full; combined with the previous literature, the coronal orientation of the pelvic cavity of pregnant women is upward, and the pelvic sagittal, coronal, and axial scans are performed. 312 cases underwent contrast-enhanced scanning, magnetic resonance contrast agent (Gd-DTPA), dose 0.1 mmol/kg, injected through cubital vein, firstly underwent T1WI cross-sectional dynamic enhanced scanning, and then underwent sagittal and coronal scanning. The scan parameters are the same as the TIWI scan sequence above [15], the scanning range is from about 2 cm above the uterine fundus to the pubic symphysis. Diagnosis was made by two senior radiologists who were unaware of surgical and pathological results, and the placenta morphology, location, signal intensity, implantation site, uterine wall, and adjacent organs were observed in MRI. Combined with a previous literature, placenta accreta was divided into three grades according to MRI findings: in Grade I: MRI sees that the placenta is still in a regular shape, clearly demarcated with the uterine wall, and the bladder wall is smooth. In Grade II, MRI shows abnormal placenta signal, low signal in the placenta on T2WI, the placenta implantation is located in the uterine wall, and the bladder wall is smooth [16]. In Dish grade, MRI shows placenta accreta, and the placenta implantation invades the pelvic organs, such as the bladder. Invasion, local nodular changes in the bladder wall. At the same time, the authors classified cases where MRI failed to diagnose placenta accreta as grade 0.

3.2.3. MRI Combined with US Diagnosis and Grading Diagnosis. Prenatal MRI was combined with US diagnostic grading results, determined by discussion and consultation between 1 radiologist and 1 US physician. If the diagnostic grades of the two physicians are the same, this grade is used as the combined diagnostic grade; if the US and MRI physicians have different diagnostic grades [17], the US shall prevail for Grades 0 and I, and the MRI grades shall prevail for Grades II and III.

3.2.4. Pathological Examination. First, the tissue was grossly observed, then HE stained smears and microscopic observation. Histopathologically, it is confirmed whether there is placenta accreta [18]. If there is, according to the degree of placental villi invading the myometrium, it is divided into 3 types: adhesion, accreta, and penetrating placenta. At the same time, they were, respectively, defined as follows: placenta accreta was Grade I, placenta accreta was Grade II, and placenta penetratus was Grade III.

3.2.5. Image Processing and Evaluation Criteria. Under the condition of not knowing the results of pathological examination, the single-blind method was used to read the films, and the MRI images focused on analyzing the signal in the placenta, the relationship between the placenta and the myometrium, the localized swelling or thinning of the uterus, the swelling of the lower segment of the uterus, the relationship between the placenta and the cervix [19], and the tortuosity in the placenta, dilated vascular shadow, comprehensive consideration, and interpretation. The diagnosis of PIA is based on the Masselli pathological classification: (1) adhesion—the placental villi are attached to the myometrium

without infiltration; (2) implantation—the placental villi invade the myometrium without reaching the serosa; and penetrating—the placental villi went through the muscularis to reach or penetrate the serosa.

3.3. Statistical Analysis. Statistical method SPSS16.0 software was used for statistical analysis of the data, and the measurement data was represented by xts; Prenatal MRI, US diagnosis and MRI combined with US diagnosis were performed by chi-square test, respectively [20]; The Kappa test was used to test the consistency of prenatal USMRI diagnostic grading, MRI combined with US diagnosis and postoperative pathological grading, and the Kappa coefficient was used to test the consistency of the two evaluation results, good agreement, Kappa ≥0.7 indicates strong agreement.

3.4. Analysis of Results. There was no statistical significance in the comparison of the sensitivity of the three examination schemes for diagnosing PIA, however, the specificity and accuracy of ultrasound alone in diagnosing PIA were significantly lower than those of MRI alone, MRI combined with ultrasound examination, and the differences were statistically significant ($P < 0.05$), there was no statistical significance in the specificity and accuracy of MRI combined with ultrasound to diagnose PIA ($P > 0.05$), as shown in Table 1.

The comparison of the grading diagnostic accuracy showed that the difference was statistically significant between ultrasound alone < MRI alone < MRI combined with ultrasound ($P < 0.05$), as shown in Table 2.

As can be seen from Table 3, among the 312 patients with placenta accreta, 187 were diagnosed with placenta accreta by prenatal MRI combined with US [21], with a diagnostic rate of 86.27%, which was higher than the diagnostic coincidence rate of placenta accreta by prenatal MRI alone (76.47%), and the difference was statistically significant ($X^2 = 53.536$, $P = 0.00$). The degree of agreement between the combined diagnostic grading and postoperative pathological grading was strong (kappa = 0.842, $P = 0.000$).

After comparing the gold standard data of surgical or pathological diagnosis, it was found that the index of magnetic resonance imaging in the diagnosis of placenta accreta was 74%, which was slightly higher than that of color Doppler diagnostic index of 60.5%; there was no significant difference in the diagnostic index between the two groups ($P > 0.05$) [22]. The kappa value of magnetic resonance imaging was 0.739, and the kappa value of acoustic Doppler was 0.610, both > 0.4, which were consistent with the gold standard, as shown in Table 4.

Ultrasound features with high sensitivity and specificity are as follows: placental lacuna and partial or complete disappearance of the retroplacental space, with a sensitivity of 92.1% and 79.4% and a specificity of 73.9% and 65.2%, respectively. The features with high sensitivity and specificity in MRI were irregular enlargement and deformation of uterine volume; the sensitivity and specificity were 87.3% and 87.0%; the second was the thinning or disappearance of the dark zone in the placenta and the myometrium on T2-weighted images; the sensitivity and specificity were 79.4%, 79.4%, and 69.6%, 78.3%, respectively. See Figure 2.

4. Discussion

Placenta accreta refers to the invasion of placental villi into the myometrium due to primary decidual hypoplasia or traumatic endometrial defect, which can lead to severe postpartum hemorrhage, uterine perforation, and secondary infection and is a common emergency in obstetrics [23]. Pathologically, it is divided into 3 types according to the severity of placental villi invading the muscularis: placenta accreta, placenta accreta, and placenta penetra. Different degrees of placenta accreta have completely different treatment methods. Placenta accreta and placenta penetrance are often the main culprits that lead to postpartum hemorrhage, uterine perforation, and coinfection; therefore, early, noninvasive, and accurate diagnosis and grading of placenta accreta have very important clinical guiding value.

Ultrasound is an imaging method represented by noninvasive, simple, nonradiation, and low-cost characteristics and has become an indispensable examination link during pregnancy. Relevant studies suggest that after the occurrence of PIA, the placenta can show abnormal thickening echo signs under ultrasound, and the hypoechoic zone of the myometrium at the attachment site becomes thin or even disappears, and due to the formation of venous blood pool, there are often multiple anechoes of different sizes and shapes in the placenta. In the recessed area, for pregnant women with placenta previa, the increase in gestational age was not accompanied by an upward shift in the echogenicity of the lower edge of the placenta. In this study, there was little difference in the sensitivity of the three examination schemes for the diagnosis of PIA, and the specificity and accuracy of the ultrasound examination scheme were significantly lower than those of MRI alone and MRI combined with ultrasound examination, which indicated that MRI was more suitable for the diagnosis of PAI, although the PIA placental parenchyma is usually accompanied by focal lacunar blood flow under color Doppler ultrasound, and the basal facial venous plexus is rich in signal; the acoustic signal is easily disturbed by the abdominal fat layer [24], amniotic fluid, and fetal bone, and even the position of the placenta, the beam attenuation, and absorption are significant, so the resolution of soft tissue is far inferior to that of MRI, which hinders accurate preoperative diagnosis. Relevant experts suggested that for pregnant women with suspected PIA diagnosed by ultrasound, MRI should be used as a routine examination, which can guide the rational choice of delivery mode after early diagnosis and provide direct anatomical evidence for the design of cesarean section.

MRI is more expensive and takes longer to scan; it is far less widely used in prenatal examination than ultrasound, but because of its high resolution of soft tissue, large imaging range, and more flexible orientation, it has positive significance for the diagnosis of PIA and the evaluation of implantation depth. According to relevant literature reports, the T2WI sequence of MRI can fully demonstrate the thinning and interruption of the myometrium and the nodular

Table 1: Results of MRI, ultrasound, and their combined examination to confirm the diagnosis of PIA (cases).

Check the scheme		Postpartum pathological detection			Sensitivity (%)	Specificity (%)	Accuracy (%)
		Negative	Negative	Negative			
Simple MRI	Negative	64	45	79	62.79	87.76	81.99
	Positive	43	251	283			
	Total	79	271	372			
Simple ultrasound	Negative	60	71	141	69.77	71.68	71.24
	Positive	25	205	201			
	Total	76	217	317			
The MRI was combined with the ultrasound procedure	Negative	53	26	88	72.09	90.91	86.56
	Positive	23	260	284			
	Total	76	286	372			

Table 2: The results of MRI, ultrasound, and their combined examinations for grading diagnosis of PIA [cases (%)].

Check the scheme		Postpartum pathological detection				Accuracy (%)
		Adhesive	Implantable	Penetrability	Total	
Simple MRI	Negative	33	9	0	33	52.16%
	Adhesive	26	5	0	23	
	Implantable	3	19	5	34	
	Penetrability	0	0	9	9	
	Total	62	33	11	86	
Simple ultrasound	Negative	32	4	0	26	35.05%
	Adhesive	8	10	1	21	
	Implantable	7	13	2	32	
	Penetrability	3	6	8	27	
	Total	52	33	21	76	
The MRI was combined with the ultrasound procedure	Negative	31	4	0	22	65.28%
	Adhesive	41	2	0	23	
	Implantable	1	32	1	38	
	Penetrability	0	1	10	11	
	Total	42	33	11	86	

Table 3: The graded diagnosis and pathological comparison of placenta accreta by prenatal MRI.US and combined diagnosis.

	Placental implantation grade n			
	Level 0	Level I	Level II	Level III
Pathologic diagnosis	0	21	43	20
MRI diagnose	33	34	24	16
US diagnose	20	15	35	23
MRI in combination with US diagnosis	7	15	32	9

Table 4: Evaluation of ultrasound and MRI in the diagnosis of placenta accreta (%).

Group	False yang rate	False yin rate	Positive predictive value	Negative predictive value
Ultrasound group	7.2	31.2	78	83.5
The US was combined with the MR group	7.8	32.2	81	90.5

hyperintensity sign in the hypointense myometrium, and the serrated degeneration of the interface is more common in adhesive PIA; the placenta can be peeled off with bare hands, which can cause the placental surface to be rough and associated with a lot of blood oozing. Implantable PIA can find that the myometrium and placental tissue are fused with each other, and a large resistance can be felt when peeling off with bare hands; if the peeling is unsuccessful or the

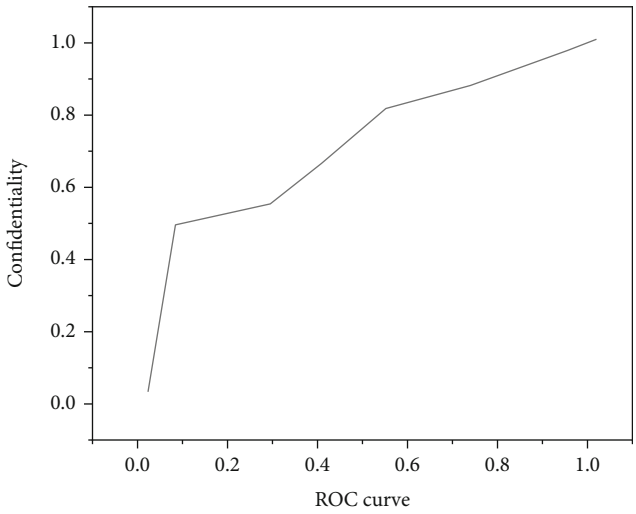

Figure 2: Sensitivity of ultrasound- and MRI-related features.

bleeding is excessive, hysterectomy should be planned. Penetrating PIA shows that the uterus and bladder wall are not intact, and it is impossible to dissect the uterus by hand; it is necessary to be careful to avoid uterine rupture and properly formulate a hysterectomy operation plan. This study found that prenatal application of MRI combined with ultrasound can obtain a more prominent PIA grading diagnosis effect, suggesting that the combined diagnosis can carry out multifaceted analysis of the PIA implantation depth, and objective selection of consistent diagnostic information can more accurately reflect the actual situation. And the degree of disturbance is not strongly correlated with the depth of placenta accreta; the diagnostic efficiency of color Doppler ultrasound in grading PIA is insufficient; although MRI has higher resolution, with the increase of gestational age, the difference of T2WI signal between placental stroma and placental lobule becomes more and more prominent, resulting in uneven internal signal, which may increase some false negative cases; therefore, the combined application of multiple imaging methods is more necessary [25].

5. Conclusion

Prenatal MRI combined with US examination can better detect patients with placenta accreta, can reflect the basic pathological features of placenta accreta, and can better show the site of placenta accreta, the depth of invasion, and the involvement of adjacent organs. Prenatal MRI combined with US examination may play an important role in the graded diagnosis of placenta accreta, the setting of treatment plans, and the evaluation of efficacy; at the same time, it can provide an accurate imaging basis for the formulation of clinical surgical plans. In conclusion, both prenatal magnetic resonance imaging examination and ultrasonography have high diagnostic value for placenta accreta, and magnetic resonance imaging examination has a slight advantage, which can play a supplementary role in the diagnosis of placenta accreta by ultrasonography.

Data Availability

The data used to support the findings of this study are available from the corresponding author upon request.

Conflicts of Interest

The authors declare that they have no conflicts of interest.

References

[1] O. Solomon, R. Cohen, Y. Zhang et al., "Deep unfolded robust PCA with application to clutter suppression in ultrasound," *IEEE transactions on medical imaging*, vol. 39, no. 4, pp. 1051–1063, 2020.

[2] H. Waqar, R. Riaz, N. M. Ahmed, A. I. Majeed, and S. R. Abbas, "Monodisperse magnetic lecithin-pfp submicron bubbles as dual imaging contrast agents for ultrasound (us) and mri," *RSC Advances*, vol. 12, no. 17, pp. 10504–10513, 2022.

[3] M. H. Raj, J. N. Mullins, J. M. Chi, A. H. Choy, G. M. Grimaldi, and B. Friedman, "The utility of abdominopelvic CT in pregnant patients with abdominal pain and a negative or inconclusive abdominal MRI," *Clinical Imaging*, vol. 59, no. 1, pp. 88–94, 2020.

[4] J. Jiao, A. I. Namburete, A. T. Papageorghiou, and J. A. Noble, "Self-supervised ultrasound to MRI fetal brain image synthesis," *IEEE Transactions on Medical Imaging*, vol. 39, no. 12, pp. 4413–4424, 2020.

[5] I. Y. Ha, M. Wilms, H. Handels, and M. P. Heinrich, "Model-based sparse-to-dense image registration for realtime respiratory motion estimation in image-guided interventions," *IEEE Transactions on Biomedical Engineering*, vol. 66, no. 2, pp. 302–310, 2019.

[6] Y. Zhang, Y. Dong, H. Fu, H. Huang, and Y. Sun, "Multifunctional tumor-targeted PLGA nanoparticles delivering Pt(IV)/sibirc5 for US/MRI imaging and overcoming ovarian cancer resistance," *Biomaterials*, vol. 269, no. 1, p. 1204786, 2020.

[7] N. McDannold, P. J. White, and G. R. Cosgrove, "Using phase data from MR temperature imaging to visualize anatomy during MRI-guided focused ultrasound neurosurgery," *IEEE transactions on medical imaging*, vol. 39, no. 12, pp. 3821–3830, 2020.

[8] B. Luijten, R. Cohen, F. Bruijn, H. Schmeitz, and R. Sloun, "Adaptive ultrasound beamforming using deep learning," *IEEE Transactions on Medical Imaging*, vol. 39, no. 12, pp. 3967–3978, 2020.

[9] Y. Wang, Y. Liu, H. Wu, J. Zhang, Q. Tian, and S. Yang, "Functionalized holmium-doped hollow silica nanospheres for combined sonodynamic and hypoxia-activated therapy," *Advanced Functional Materials*, vol. 29, no. 3, pp. 1805764.1–1805764.17, 2019.

[10] T. Bekoulis, A. P. Apostolopoulos, A. Papatheodorou, E. Lakiotaki, and A. Papanikolaou, "Primary extranodal skeletal-muscle non-Hodgkin b cell lymphoma: clinical presentation and diagnostic approach," *Journal of Long-Term Effects of Medical Implants*, vol. 31, no. 1, pp. 43–47, 2021.

[11] Q. Dong, C. Wan, H. Yang et al., "Targeted gold nanoshelled hybrid nanocapsules encapsulating doxorubicin for bimodal imaging and near-infrared triggered synergistic therapy of Her2-positve breast cancer," *Journal of Biomaterials Applications*, vol. 35, no. 3, pp. 430–445, 2020.

Hindawi
Scanning
Volume 2023, Article ID 9765894, 1 page
https://doi.org/10.1155/2023/9765894

Retraction

Retracted: 3D Convolutional Neural Network Framework with Deep Learning for Nuclear Medicine

Scanning

Received 12 December 2023; Accepted 12 December 2023; Published 13 December 2023

This article has been retracted by Hindawi, as publisher, following an investigation undertaken by the publisher [1]. This investigation has uncovered evidence of systematic manipulation of the publication and peer-review process. We cannot, therefore, vouch for the reliability or integrity of this article.

Please note that this notice is intended solely to alert readers that the peer-review process of this article has been compromised.

Wiley and Hindawi regret that the usual quality checks did not identify these issues before publication and have since put additional measures in place to safeguard research integrity.

We wish to credit our Research Integrity and Research Publishing teams and anonymous and named external researchers and research integrity experts for contributing to this investigation.

The corresponding author, as the representative of all authors, has been given the opportunity to register their agreement or disagreement to this retraction. We have kept a record of any response received.

References

[1] P. Manimegalai, R. Suresh Kumar, P. Valsalan, R. Dhanagopal, P. T. Vasanth Raj, and J. Christhudass, "3D Convolutional Neural Network Framework with Deep Learning for Nuclear Medicine," *Scanning*, vol. 2022, Article ID 9640177, 9 pages, 2022.

Hindawi
Scanning
Volume 2022, Article ID 9640177, 9 pages
https://doi.org/10.1155/2022/9640177

Review Article

3D Convolutional Neural Network Framework with Deep Learning for Nuclear Medicine

P. Manimegalai,[1] **R. Suresh Kumar**,[2] **Prajoona Valsalan**,[3] **R. Dhanagopal**,[2] **P. T. Vasanth Raj**,[2] **and Jerome Christhudass**[1]

[1]*Department of Biomedical Engineering, Karunya Institute of Technology and Sciences, Coimbatore, India*
[2]*Center for System Design, Chennai Institute of Technology, Chennai, India*
[3]*Department of Electrical and Computer Engineering, Dhofar University, Salalah, Oman*

Correspondence should be addressed to P. Manimegalai; manimegalai@karunya.edu

Received 14 April 2022; Accepted 27 June 2022; Published 16 July 2022

Academic Editor: Danilo Pelusi

Though artificial intelligence (AI) has been used in nuclear medicine for more than 50 years, more progress has been made in deep learning (DL) and machine learning (ML), which have driven the development of new AI abilities in the field. ANNs are used in both deep learning and machine learning in nuclear medicine. Alternatively, if 3D convolutional neural network (CNN) is used, the inputs may be the actual images that are being analyzed, rather than a set of inputs. In nuclear medicine, artificial intelligence reimagines and reengineers the field's therapeutic and scientific capabilities. Understanding the concepts of 3D CNN and U-Net in the context of nuclear medicine provides for a deeper engagement with clinical and research applications, as well as the ability to troubleshoot problems when they emerge. Business analytics, risk assessment, quality assurance, and basic classifications are all examples of simple ML applications. General nuclear medicine, SPECT, PET, MRI, and CT may benefit from more advanced DL applications for classification, detection, localization, segmentation, quantification, and radiomic feature extraction utilizing 3D CNNs. An ANN may be used to analyze a small dataset at the same time as traditional statistical methods, as well as bigger datasets. Nuclear medicine's clinical and research practices have been largely unaffected by the introduction of artificial intelligence (AI). Clinical and research landscapes have been fundamentally altered by the advent of 3D CNN and U-Net applications. Nuclear medicine professionals must now have at least an elementary understanding of AI principles such as neural networks (ANNs) and convolutional neural networks (CNNs).

1. Introduction

The use of artificial intelligence (AI) in molecular imaging and nuclear medicine has gained considerable momentum and promises to be a disruptive, yet inventive, technology. Nuclear medicine has been using AI for many years, and the excitement surrounding AI in radiology obscures this fact (e.g., cardiac quantitative software packages). Artificial neural networks (ANN), DL, and ML have all recently seen significant advances, which has reignited interest in AI while also sparking controversy about the ethical and legal issues that come with using AI in health and medicine. In the midst of this conversation, a crucial aspect is often overlooked: As with any tool, the best way to use AI is up to the user.

In nuclear medicine and radiology, a wide array of machine learning and deep learning capabilities are available. At one end of the spectrum, for example, there may be a straightforward use of machine learning for quality assurance, business analytics, risk assessment, and basic classifications. Detected, localized, and classified images may be found in a wide range of deep learning applications. Another extreme is the large and complex CT, PET, and MRI data put into convolutional neural networks (CNNs) to get insight into segmentation, detection, localization, classification, quantification, and radiomic feature extraction using

deep learning (DL). Certain CNN and deep learning applications may go beyond the extreme (ultra-zone) when used in conjunction with hybrid technologies that need picture registration across several modalities, equipment, and sample lengths. At the low end of the spectrum (dubbed the "infra zone"), the use of artificial neural networks (ANNs) and machine learning (ML) enables the study of both small and big datasets concurrently.

Clinical and scientific skills may be improved as well as workflow and productivity in nuclear medicine by using AI in molecular imaging and nuclear medicine. Innovation comes with a sense of duty to one's profession and to one's patients. Social, legal, and ethical duties all fall under this umbrella. Ethical, social, and legal concerns with AI in molecular imaging and nuclear medicine center on the data utilized, the algorithms employed, and the practical application of those algorithms.

As a result of technological advancements such as multimodality imaging equipment being deployed in the 2000s [1] and rapid detector technologies being developed [1, 2], nuclear medicine and radiology have seen significant progress in the previous two decades. Software advancements have also resulted in significant increases in signal-to-noise ratio and reconstructed picture spatial resolution, for example, by including information from the time of flight (ToF) and point-spread function into PET image reconstruction [3]. Nuclear medicine images are employed in a relatively restricted manner in the majority of clinical articles, clinical research, and, most importantly, in daily clinical practice (i.e., analyzed mostly visually or semiquantitatively). Medical image analysis is becoming increasingly automated, and many characteristics, some of which may not be visible to the untrained eye, are being extracted [4, 5]. When it comes to precision medicine, the most important goal of this paradigm shift is to effectively use the information offered by imaging investigations to influence patient treatment workflow. Medical imaging should play a larger and more essential role in this new paradigm than just diagnosing. It should also play a bigger and more important role in treatment planning, monitoring, and evaluation, as well as predictive modeling and stratification, to become an important part of the future clinical decision-making process.

The ANN is essential to MR and DL in nuclear medicine. An ANN is a node-based analytic technique that consists of many layers of nodes. Radiomic characteristics derived from the picture files or the photos themselves may be used as inputs to a CNN. Clinical and research capacities in nuclear medicine are being reengineered and reimagined by AI. An ANN is made up of nodes arranged in a hierarchical structure (depth). Inputs from other nodes are weighted (Figure 1). By modifying the node weightings, the ANN aims to maximize accurate outputs as assessed against a grounded truth [6, 7]. Iterations (epochs) of the answer get it closer to the truth.

The study of algorithms that learn and develop over the course of time is known as machine learning, and it is an essential concept in artificial intelligence. Unsupervised or (semi-) supervised learning is the most common classification. Unsupervised learning involves discovering patterns in unlabeled data, while supervised learning relies on labels to make inferences about categorization or regression, and semisupervised learning involves a small quantity of labeled data and a big amount of unlabeled data. When it comes to medical imaging, the typical procedure or the deep learning pipeline is often applied directly to the majority of tasks.

It is often believed that the advent of AI in medicine would lead to "superhuman" capabilities and more precise treatment. Conversely, it is easy to overlook the fact that a significant portion of a physician's daily work consists of routine tasks, and that delegating these tasks to AI would free up human resources to focus on higher value activities that typically necessitate human attributes like cognitive insight, creativity, empathy, or meaning.

1.1. Artificial Intelligence and Deep Learning Used in Nuclear Medicine Imaging. Artificial Intelligence (AI) has a broad range of potential applications in nuclear medicine [8]. Data processing at the detector level is the initial stage in using AI for picture reconstruction, including adjustments for the many physical processes involved in the detection process (e.g., attenuation and scatter). AI may be used for a variety of image processing tasks, including denoising, segmentation, and fusion, in addition to reconstruction. To wrap things up, artificial intelligence (AI) may be used to build models based on information gleaned from photos that can be utilized for predictive, tailored therapy.

The software used to make PET images has also improved a lot over the years. For example, time of flight (ToF) information and point spread function can now be used to make PET images look better. Some of the most important medical papers use nuclear medicine images very carefully. This is true for both clinical studies and "normal" medical care (i.e., analyzed mostly visually or semiquantitatively).

PET scanners with lots of crystal pixelation could use a computer network to improve picture resolution and noise quality, as well as to figure out the time of flight from two digitized detector waveforms that are both digitized at the same time [9, 10]. When it comes to iterative picture reconstruction, the use of a deep neural network may increase the final product's quality [11, 12]. For attenuation adjustment and registration in PET/MR and PET/CT, deep learning approaches have already been presented [13–17]. These methods can create attenuation maps with excellent accuracy. Deep learning, like the MLAA, has been used to enhance the maximum likelihood reconstruction of activity and attenuation in ToF PET data (MLAA) [18]. It is one of the most common ways to use deep learning to process images. Full-dose PET pictures are one example of how this technique may be employed [19] or how it can filter reconstructed PET images directly [20].

Images may be segmented and counted using an automated system. This can be used for diagnosis and treatment planning, among other things. Older, shaky machine learning frameworks could not attain the degree of automation and precision required for clinical practice or swiftly handle hundreds of radiomics patients simultaneously. A rising number of companies are depending on deep learning approaches to improve both automation and performance,

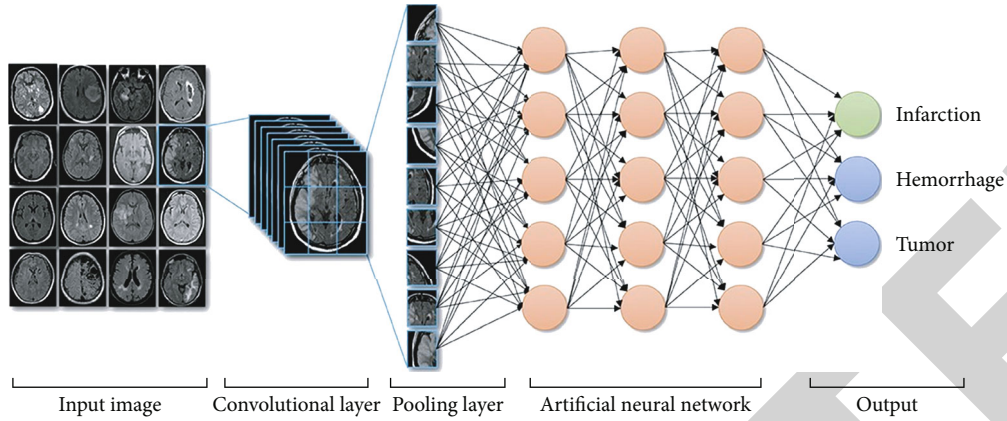

Figure 1: Convolutional and pooling layer neural network.

although others are still using "older" techniques. Medical picture segmentation is an excellent use case for CNNs [21]. This may be explained by the fact that segmentation learning happens at the voxel level, as opposed to classification tasks (one label per picture) (one label per voxel). As a result, the network parameters may be trained more effectively. According to a recent PET functional volume segmentation MICCAI competition, a strategy using an already-trained CNN was the best (although not much higher than the results for some of the more traditional methods) [22]. Multiple PET/CT cosegmentation has been tackled using CNNs [23–25]. The radiomics pipeline is anticipated to give completely automated solutions for this stage, which will eliminate this key bottleneck, based on pipelines for tumor identification and segmentation that use a deep learning framework [26–28]. Planning, picture acquisition, analysis, and reporting are the four stages that make up a typical medical imaging workflow (Figure 2). The entrance and payment processes might also be incorporated. We have zeroed down on the steps of the process in which the doctor plays a pivotal role.

The fundamental concept that underpins the Mask R-CNN approach [29, 30] is to specialize an image classifier model by equipping it with a large number of trainable modules in order to extract features of varying sizes, bounding boxes, object classes, and individual masks.

Some of the datasets used for the analysis of nuclear imaging are as follows: MoNuSeg–Grand Challenge, Mitos-Atypia-14–Grand Challenge, Kaggle Data Science Bowl, dataset from immunohistochemistry, neurosphere dataset, and electron microscopy dataset.

2. Convolutional Neural Network

CNN uses convolution and pooling layers to extract features from pictures, but ANNs need particular data (features) to be fed into the system (Figure 3). A convolution approach employs a variety of kernels (often three by three) to apply to a subset array of pixels in an image in order to extract radiomic features, and the output of these kernels is summed together to generate a single integer value across all of the extracted features [31–35]. Before taking a sample from further in the convolution layers, activation functions form feature maps. Several layers of data are flattened as a consequence of several convolution, kernel, and pooling stages occurring in succession [32–34].

In order to extract radiomic information from photographs and offer an output as some sort of classification, convolutional and pooling levels are used in conjunction with a fully connected network in a CNN. Linear convolution is used to extract visual information from an input tensor by applying an appropriate kernel (often 3×3). Kernel elements are overlaid on input tensor elements, and the stride determines how often the kernel is moved. The kernel is applied to the input tensor one at a time, with a stride of 1. A stride of 2 is utilized when the kernel is applied to each and every second element of the input tensor. Downsampling may be best saved for the pooling function if a stride bigger than 1 is used. One numerical value (and corresponding coordinate values) is generated by summating the product of the individual components of each input tensor and the kernel (output tensor). With the use of different kernels, each convolution layer may be created. However, the Z dimension is not compressed, despite the fact that it has been reduced in size.

Pooling is a technique for reducing the number of samples taken. There were two main ways to do this: global average pooling and max pooling. This is called "max pooling down." It samples the components to get an output that is the same as the largest value in a certain area of data on the feature map. In order to do this, we down sample each group of four components until we get a single value for each that is the same as the maximum value. Global pooling makes the feature map into a 1×1 array with a single value for each element in this case. This makes the feature map easier to read. Mean value: The sum of the values of each element is equal to the sum of all the values of all of them. A single direction array of vectors is made from data that has been convolution and pooled (numbers).

The selection loss is a measure of the generalizability of the artificial neural network (ANN), also known as its agility. Using these loss functions, one is able to optimize both the

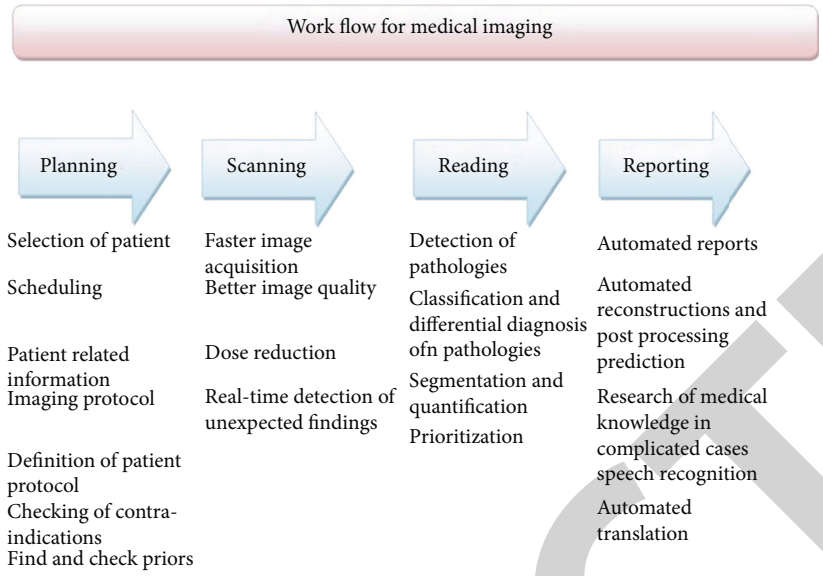

Figure 2: Division of typical medical imaging workflow.

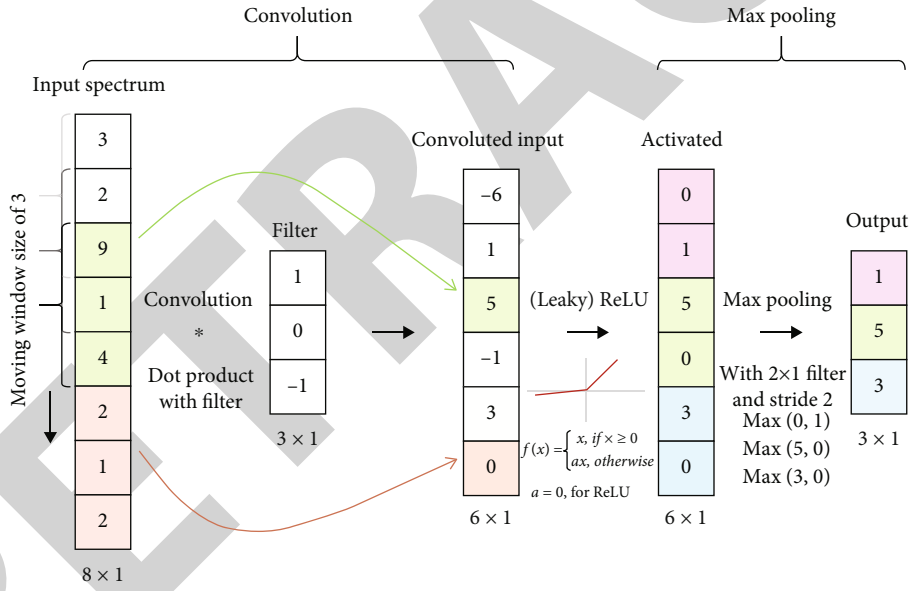

Figure 3: A schematic diagram of convolution and max pooling layer.

number of neurons in each hidden layer of repetitions used in the final design. In the final design of the artificial neural network (ANN) or model selection process, choose loss, also known as the error associated with the sequence and range of data, has to be taken into consideration. The output of the ANN as well as the accuracy of the output are both impacted by the amount of nodes present in the hidden layers; hence, order selection is tied to the ANN's depth. To prevent an over or underfit, it is critical to strike a balance between order selection and data complexity. The complexity of an ANN is determined by the number of hidden units as well as the node included inside those hidden layers. Using very few nodes and layers results in a higher rate of selection mistakes. In contrast, an overly complicated ANN with an excessive number of nodes or layers leads to overfitting, which raises the selection error.

It is possible to reduce the number of node and levels, and hence the complexity, of the ANN by taking steps to reduce the selection error. An ANN's selection error assesses how well it performs with fresh data when compared to its training error (generalizability). Optimizing the ANN structure needs a delicate balancing act between training and selection errors (Figure 4). In order to increase the ANN complexity, each mistake may be computed (order).

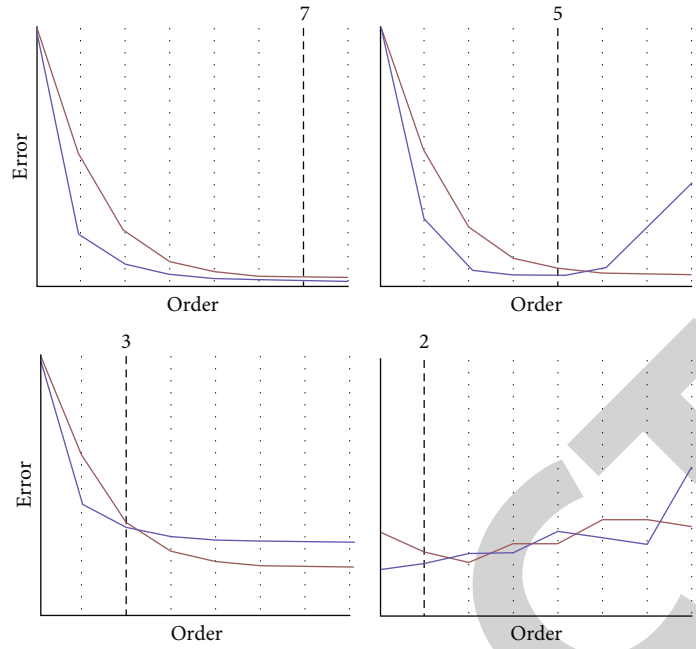

Figure 4: A picture of the trade-off between training and selection error.

3. 3D CNN

The 3D CNN is a three-dimensional array of the conventional neural network, and it uses a multifiber unit like the one shown in Figure 5 and dilated weighted convolutions to extract feature attributes at different scales for volumetric segmentation.

Preprocessing: Data is preprocessed using a number of techniques before being input into the network during training (mirroring, rotation, and cropping).

Training: In order to train the model, we employed a patch size of 128 × 128, as well as a new loss function that merged the focused loss with the generalized loss.

Inference: In order for the network to properly partition the MRI data, it was zero-padded such that the original 240 × 240 × 155 voxels became 240 × 240 × 160 voxels. Once the network is ready for inference, we feed the data through it and generate probability maps. After creating these maps, the ensemble uses them to generate its given level of output.

4. 3D U-Net

The U-Net architecture for biomedical image segmentation was suggested in 2015 [36]. Segmenting neural structures in electron microscopy stacks or cells in light microscopy pictures proved to be a breeze for the scientists, who used the design in a number of other problems.

Convolutional layers of the U-Net design further extend this upsampling channel, enabling context information to be propagated to higher-resolution layers [36]. This creates a symmetrical U-shaped structure with a condensing and expanding route (see Figure 6). An encoder–decoder network is another name for this sort of design. For better localization, we have introduced skip links between the encoder path's high-resolution features and the decoder path's upsampled feature maps. Although U-Nets have advanced in recent years, they are still the best option for many segmentation tasks.

CNNs were often used to assign a single class label to a whole picture. However, localization is essential in many computer vision applications, where each pixel is tagged with the class of item to which it belongs. CNN classification architectures were often used for these so-called semantic segmentation problems. The classification network classifies each pixel individually by supplying a local area (also known as a patch) surrounding it. A sliding-window method is used to classify every pixel in a picture. Because so many patches can be retrieved from a single picture, this method has the added benefit of generating more training data. The restricted quantity of training data in biomedical jobs makes this particularly valuable. Although this method has its advantages, there are a few downsides. Because multiple overlapping patches need to be broadcast via the network, segmentation of a picture is a waste of time and resources. A trade-off between bigger patches providing more information and smaller ones for better localization makes it challenging to discover the ideal patch size.

The fully convolutional network [37] was proposed to incorporate context with high localization accuracy. Alternately, upsampling layers might be added after the normal expanding categorization network in order to get the output resolution of the picture back to where it was originally. There are no completely linked layers utilized to retain spatial data. Simple bilinear upsampling may be used to improve the output resolution. It is also possible to employ

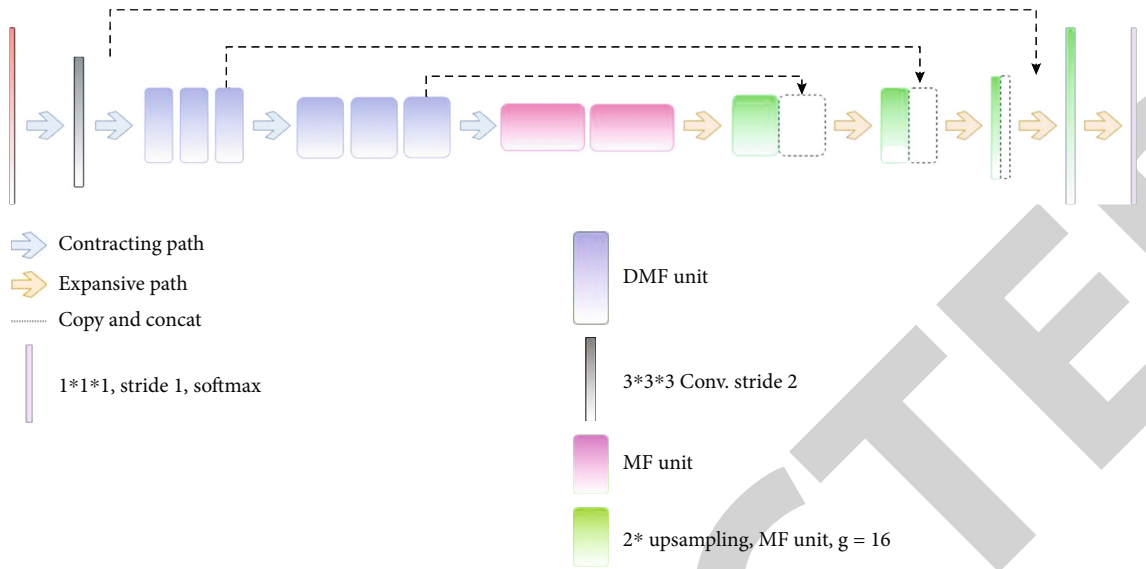

Figure 5: Architecture of 3D CNN.

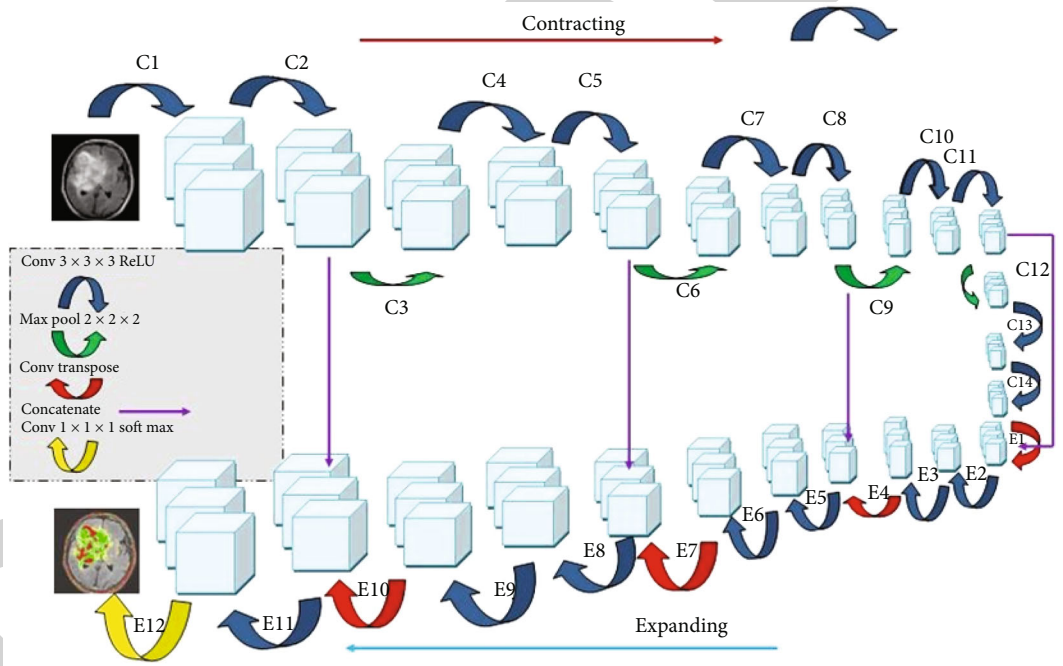

Figure 6: Architecture of 3D U-Net.

transposed convolutions, which are sometimes known as up- or deconvolutions. The transposed convolution layer's output size is determined on the kernel size and stride used.

5. Deep Learning's Challenges in Neuroimaging Techniques

Finally, deep learning is a kind of machine learning that employs artificial neural networks (ANN) and may be used to almost any type of learning. As a consequence, the application of deep learning to neuroimaging is still in its infancy, and various difficulties have to be addressed.

Overfitting is the one of them. Overfitting is always a problem when training a complicated classifier on a limited dataset. In general, deep learning models perform an excellent job of fitting the data, but this does not guarantee that they can be used to generalize problems. Overfitting has been reduced in several experiments by a variety of methods, including regularization [38], early halting [39], and dropping out [40]. For example, an algorithm's performance on a separate test dataset may be used to assess overfitting,

but it may not perform well on comparable pictures taken at other locations, on various scanners, or with different patient demographics. In general, larger datasets from various locations are obtained utilizing various scanners and protocols with subtle differences in picture attributes, resulting in poor performance [41]. Data augmentation without standard criteria, on the other hand, cannot deal with the problems that come up when working with tiny datasets. If these technologies are to be broadly used, they must overcome a challenge known as "brittle AI." As a result, deep learning is a data-intensive technique. In order to accomplish precise classification and confirm its performance for clinical use, a large number of well-labeled instances is needed. As opposed to classification algorithms, upstream applications like as picture quality enhancement learn from numerous predictions in a single image instead of just one (where only one learning data point is available per person). Nevertheless, the creation of large, publicly accessible medical picture datasets with labeled images is critical, notwithstanding the challenges posed by privacy issues, costs, assessing ground truth, and label accuracy [42]. Because the high dose or completely sampled pictures act as labels in the classification process, image collection applications provide an advantage over other methods because the data is already labeled. Deep learning presents a number of ethical and legal issues, as well as a problem in understanding the findings physically or mechanically. Data is fed into a "black box" and an output prediction, such as an image or classification, is generated [43]. The "Mythos of Model Interpretability" has been defined to describe the operation of all deep learning algorithms at dimensions higher than what the human mind can directly see [44]. It would be nice to get some estimates of the network's uncertainty in prediction to better understand the pictures generated.

It is important to realize the limitations of AI applications in the medical field, despite the fact that these applications have tremendous promise. It is well knowledge that there are challenges associated with the interpretability of models. Understanding symbolic artificial intelligence or simple convolutional neural networks, including such as regression analysis or decision trees, is still possible for humans, but it becomes extremely difficult with more advanced techniques and is now incredibly difficult with many machine learning techniques, resulting in unpredictable outcomes and nondeterministic behavior. Symbolic artificial intelligence and conventional deep learning include decision trees and linear regression. It is still unclear whether predictive AI can and should be used to make significant and important decisions when the exact mode of action is unknown, despite the fact that this problem also applies to other medical treatments (such as pharmacology in which the specific modes of action are often rarely discussed).

6. Conclusion

As AI has become more and more common in nuclear medicine over the last few decades, there has not been a lot of fuss or disruption. The rise of 3D CNN and U-Net applications has caused a huge shift in the landscape. From the infrazone (data and analytics) to the ultrazone (imaging), AI is being used in nuclear medicine in a wide range of ways (true synthetic intelligence). It will be easier for nuclear medicine professionals to get used to 3D CNN and U-Net for better assimilation. As a result, we think that 3D CNN and U-Net will become more and more widespread in clinical practice over the next several decades as a result of the development of explainable AI and bigger, more standardized datasets.

Data Availability

No data were used for this study.

Conflicts of Interest

The authors declared that they have no conflicts of interest regarding this work.

Acknowledgments

This work is funded by Centre for System Design, Chennai Institute of Technology, Chennai, vide funding number is CIT/CSD/2022/006.

References

[1] T. Beyer, D. W. Townsend, T. Brun et al., "A combined PET/CT scanner for clinical oncology," *Journal of Nuclear Medicine*, vol. 41, no. 8, pp. 1369–1379, 2000.

[2] P. Lecoq, "Pushing the limits in time-of-flight PET imaging," *IEEE Trans Radiat Plasma Med Sci.*, vol. 1, no. 6, pp. 473–485, 2017.

[3] E. Berg and S. R. Cherry, "Innovations in instrumentation for positron emission tomography," *Seminars in Nuclear Medicine*, vol. 48, no. 4, pp. 311–331, 2018.

[4] H. Aerts, "Radiomics: there is more than meets the eye in medical imaging," *Plenary presentation from SPIE Medical Imaging 2016: computer-aided diagnosis*, vol. 9785, p. 97850O, 2016.

[5] M. Hatt, F. Tixier, D. Visvikis, and C. Cheze le Rest, "Radiomics in PET/CT: more than meets the eye?," *Journal of Nuclear Medicine*, vol. 58, no. 3, pp. 365-366, 2017.

[6] M. P. McBee, O. A. Awan, A. T. Colucci et al., "Deep learning in radiology," *Academic Radiology*, vol. 25, no. 11, pp. 1472–1480, 2018.

[7] A. Tang, R. Tam, A. Cadrin-Chênevert et al., "Canadian Association of Radiologists white paper on artificial intelligence in radiology," *Canadian Association of Radiologists Journal*, vol. 69, no. 2, pp. 120–135, 2018.

[8] M. Hatt, C. Parmar, J. Qi, and I. E. Naqa, "Machine (deep) learning methods for image processing and radiomics," *IEEE Trans Radiat Plasma Med Sci.*, vol. 3, no. 2, pp. 104–108, 2019.

[9] X. Hong, Y. Zan, F. Weng, W. Tao, Q. Peng, and Q. Huang, "Enhancing the image quality via transferred deep residual learning of coarse PET sinograms," *IEEE Transactions on Medical Imaging*, vol. 37, no. 10, pp. 2322–2332, 2018.

[10] E. Berg and S. R. Cherry, "Using convolutional neural networks to estimate time-of-flight from PET detector waveforms," *Physics in Medicine and Biology*, vol. 63, no. 2, p. 02LT01, 2018.

[11] K. Gong, J. Guan, K. Kim et al., "Iterative PET image reconstruction using convolutional neural network representation," *IEEE Transactions on Medical Imaging*, vol. 38, no. 3, pp. 675–685, 2019.

[12] K. Kim, D. Wu, K. Gong et al., "Penalized PET reconstruction using deep learning prior and local linear fitting," *IEEE Transactions on Medical Imaging*, vol. 37, no. 6, pp. 1478–1487, 2018.

[13] D. Nie, X. Cao, Y. Gao, L. Wang, and D. Shen, "Estimating CT image from MRI data using 3D fully convolutional networks," in *Deep Learning and Data Labeling for Medical Applications–First International Workshop, LABELS 2016, and Second International Workshop, DLMIA 2016, held in conjunction with MICCAI 2016*, pp. 170–178, Athens, Greece, 2016.

[14] A. Torrado-Carvajal, J. Vera-Olmos, D. Izquierdo-Garcia et al., "Dixon-VIBE deep learning (DIVIDE) pseudo-CT synthesis for pelvis PET/MR attenuation correction," *Journal of Nuclear Medicine*, vol. 60, no. 3, pp. 429–435, 2019.

[15] D. Hwang, K. Y. Kim, S. K. Kang et al., "Improving the accuracy of simultaneously reconstructed activity and attenuation maps using deep learning," *Journal of Nuclear Medicine*, vol. 59, no. 10, pp. 1624–1629, 2018.

[16] S. Kaplan and Y.-M. Zhu, "Full-dose PET image estimation from lowdose PET image using deep learning: a pilot study," *Journal of Digital Imaging*, vol. 32, no. 5, pp. 773–778, 2019.

[17] K. Gong, J. Guan, C. Liu, and J. Qi, "PET image denoising using a deep neural network through fine tuning," *IEEE Trans Radiat Plasma Med Sci.*, vol. 3, no. 2, pp. 153–161, 2019.

[18] G. Litjens, T. Kooi, B. E. Bejnordi et al., "A survey on deep learning in medical image analysis," *Medical Image Analysis*, vol. 42, pp. 60–88, 2017.

[19] X. Zhao, L. Li, W. Lu, and S. Tan, "Tumor co-segmentation in PET/CT using multi-modality fully convolutional neural network," *Physics in Medicine and Biology*, vol. 64, no. 1, article 015011, 2019.

[20] Z. Zhong, Y. Kim, K. Plichta et al., "Simultaneous cosegmentation of tumors in PET-CT images using deep fully convolutional networks," *Medical Physics*, vol. 46, no. 2, pp. 619–633, 2019.

[21] D. Visvikis, C. Cheze Le Rest, V. Jaouen, and M. Hatt, "Artificial intelligence, machine (deep) learning and radio(geno)mics: definitions and nuclear medicine imaging applications," *European Journal of Nuclear Medicine and Molecular Imaging*, vol. 46, pp. 2630–2637, 2019.

[22] M. Hatt, B. Laurent, A. Ouahabi et al., "The first MICCAI challenge on PET tumor segmentation," *Medical Image Analysis*, vol. 44, pp. 177–195, 2018.

[23] H. Choi, "Deep Learning in Nuclear Medicine and Molecular Imaging: Current Perspectives and Future Directions," *Nuclear Medicine and Molecular Imaging*, vol. 52, pp. 109–118, 2018.

[24] M. Kirienko, M. Biroli, F. Gelardi, E. Seregni, A. Chiti, and M. Sollini M, "Deep learning in Nuclear Medicine—focus on CNN-based approaches for PET/CT and PET/MR: where do we stand?," *Clinical and Translational Imaging*, vol. 9, pp. 37–55, 2021.

[25] Z. Guo, X. Li, H. Huang, N. Guo, and Q. Li, "Deep learning-based image segmentation on multi-modal medical imaging," *IEEE Trans Radiat Plasma Med Sci.*, vol. 3, no. 2, pp. 162–169, 2019.

[26] P. Blanc-Durand, A. Van Der Gucht, N. Schaefer, E. Itti, and J. O. Prior, "Automatic lesion detection and segmentation of 18F-FET PET in gliomas: a full 3D U-net convolutional neural network study," *PLoS One*, vol. 13, no. 4, article e0195798, 2018.

[27] A. Akhavanallaf, I. Shiri, H. Arabi, and H. Zaidi, "Whole-body voxel-based internal dosimetry using deep learning," *European Journal of Nuclear Medicine and Molecular Imaging*, vol. 48, pp. 670–682, 2021.

[28] M. Schwyzer, D. A. Ferraro, U. J. Muehlematter et al., "Automated detection of lung cancer at ultralow dose PET/CT by deep neural networks—initial results," *Lung Cancer*, vol. 126, pp. 170–173, 2018.

[29] A. S. Goncharova, A. Honigmann, F. Jug, and A. Krull, "Improving blind spot denoising for microscopy," *Computer vision – ECCV 2020 Workshops (Lecture Notes in Computer Science), Vol. 12535 (ed. A. Bartoli and A. Fusiello)*, pp. 380–393, 2020.

[30] K. He, G. Gkioxari, P. Dollár, and R. Girshick, "Mask R-CNN," *IEEE Transactions on Pattern Analysis and Machine Intelligence*, vol. 42, no. 2, pp. 386–397, 2020.

[31] G. Currie, "Intelligent imaging: Artificial intelligence augmented nuclear medicine," *Journal of Nuclear Medicine Technology*, vol. 47, no. 3, pp. 217–222, 2019.

[32] R. Yamashita, M. Nishio, R. K. G. Do, and K. Togashi, "Convolutional neural networks: an overview and application in radiology," *Insights Into Imaging*, vol. 9, pp. 611–629, 2018.

[33] A. S. Lundervold and A. Lundervold, "An overview of deep learning in medical imaging focusing on MRI," *Zeitschrift für Medizinische Physik*, vol. 29, no. 2, pp. 102–127, 2019.

[34] A. Maier, C. Syben, T. Lasser, and C. Riess, "A gentle introduction to deep learning in medical imaging processing," *Zeitschrift für Medizinische Physik*, vol. 29, pp. 86–101, 2019.

[35] D. Shen, G. Wu, and H. Suk, "Deep learning in medical image analysis," *Annual Review of Biomedical Engineering*, vol. 19, no. 1, pp. 221–248, 2017.

[36] O. Ronneberger, P. Fischer, and T. Brox, "U-net: convolutional networks for biomedical image segmentation," *Lecture Notes in Computer Science (including subseries Lecture Notes in Artifcial Intelligence and Lecture Notes in Bioinformatics)*, vol. 9351, pp. 234–241, 2015.

[37] J. Long, E. Shelhamer, and T. Darrell, "Fully convolutional networks for semantic segmentation," *Proceedings of the IEEE conference on computer vision and pattern recognition (CVPR)*, pp. 3431–3440, 2015.

[38] M. Kolbak, K. Lauria, I. Lee, S. Mohan, H. P. Phan, and J. Salisbury, "Regularization for deep learning," in *Deep Learning*, pp. 221–265, MIT Press, Cambridge, 2016.

[39] L. Prechelt, "Early stopping—but when?," in *Neural Networks: Tricks of the Trade*, pp. 53–67, Springer, 2012.

[40] N. Srivastava, G. Hinton, A. Krizhevsky, I. Sutskever, and R. Salakhutdinov, "Dropout: a simple way to prevent neural networks from overfitting," *Journal of Machine Learning Research*, vol. 15, pp. 1929–1958, 2014.

[41] F. Pesapane, C. Volonté, M. Codari, and F. Sardanelli, "Artificial intelligence as a medical device in radiology: ethical and regulatory issues in Europe and the United States," *Insights Into Imaging*, vol. 9, no. 5, pp. 745–753, 2018.

[42] G. Chartrand, P. M. Cheng, E. Vorontsov et al., "Deep learning: a primer for radiologists," *Radiographics*, vol. 37, no. 7, pp. 2113–2131, 2017.

Hindawi
Scanning
Volume 2023, Article ID 9896168, 1 page
https://doi.org/10.1155/2023/9896168

Retraction

Retracted: Diagnostic Efficacy of CT Radiomic Features in Pulmonary Invasive Mucinous Adenocarcinoma

Scanning

Received 12 December 2023; Accepted 12 December 2023; Published 13 December 2023

This article has been retracted by Hindawi, as publisher, following an investigation undertaken by the publisher [1]. This investigation has uncovered evidence of systematic manipulation of the publication and peer-review process. We cannot, therefore, vouch for the reliability or integrity of this article.

Please note that this notice is intended solely to alert readers that the peer-review process of this article has been compromised.

Wiley and Hindawi regret that the usual quality checks did not identify these issues before publication and have since put additional measures in place to safeguard research integrity.

We wish to credit our Research Integrity and Research Publishing teams and anonymous and named external researchers and research integrity experts for contributing to this investigation.

The corresponding author, as the representative of all authors, has been given the opportunity to register their agreement or disagreement to this retraction. We have kept a record of any response received.

References

[1] A. Sheng, P. Zhou, Y. Ye, K. Sun, and Z. Yang, "Diagnostic Efficacy of CT Radiomic Features in Pulmonary Invasive Mucinous Adenocarcinoma," *Scanning*, vol. 2022, Article ID 5314225, 8 pages, 2022.

Hindawi
Scanning
Volume 2022, Article ID 5314225, 8 pages
https://doi.org/10.1155/2022/5314225

Research Article

Diagnostic Efficacy of CT Radiomic Features in Pulmonary Invasive Mucinous Adenocarcinoma

Aizhu Sheng,[1] **Pengfei Zhou**,[1] **Yizhai Ye**,[2] **Keda Sun**,[3] **and Zhenhua Yang**[4]

[1]*Department of Radiology, Hwa Mei Hospital, University of Chinese Academy of Sciences, Zhejiang 315000, China*
[2]*Department of Radiology, Ninghai First Hospital, Ningbo, Zhejiang 315600, China*
[3]*Department of Radiology, No. 2 Hospital of Yinzhou District, Ningbo, Zhejiang 315100, China*
[4]*Department of Thoracic Surgery, Hwa Mei Hospital, University of Chinese Academy of Sciences, Zhejiang 315000, China*

Correspondence should be addressed to Zhenhua Yang; 201904012241@stu.zjsru.edu.cn

Received 15 May 2022; Revised 6 June 2022; Accepted 14 June 2022; Published 25 June 2022

Academic Editor: Danilo Pelusi

In order to solve the problem of the effect of CT images on the diagnosis of lungs, the authors proposed a method for the diagnosis of invasive mucinous adenocarcinoma of the lungs based on CT radiomic features, and the modified method is found by reviewing past cases: among the 34 cases of primary pulmonary lymphoma, 12 cases were nodular mass type, 19 cases were nonnodular mass type, and 3 cases were mixed type; 13 cases involved bilateral lung lobes, 7 cases involved right lung, and 4 cases involved left lung example. There were 17 cases of tumor consolidation density shadow, 17 cases of mixed density shadow, the average CT value was about 32HU, 15 cases of cavitation sign, 6 cases of cavity, 9 cases of angiography sign, 30 cases of air bronchus sign, 22 cases of bronchiectasis, bronchial stenosis or amputation in 8 cases, pleural effusion in 12 cases, lymph node enlargement in 15 cases, and pleural metastasis in 2 cases. The final pathological results included 24 cases of membrane-associated lymphoid tissue (MALT) lymphoma, 9 cases of diffuse large B-cell lymphoma (DLBCL), and 1 case of T-cell lymphoma. The CT manifestations of primary pulmonary lymphoma (PPL) are diverse and do not have obvious specificity, the imaging manifestations are correlated with pathological types, and air bronchial signs, bronchiectasis, angiography signs, and other signs are used for the diagnosis of PPL. This is of great significance for the diagnosis of PPL.

1. Introduction

Lung cancer has become the malignant tumor with the highest morbidity and mortality in the world. In China, the incidence and mortality of lung cancer are increasing year by year, it has always been at the forefront, statistics from China's national cancer center show that there are about 800,000 new lung cancer patients in China every year, and 630,000 people died of lung cancer; among them, lung adenocarcinoma has also become the most common pathological type. In 2015, the World Health Organization (WHO) integrated multidisciplinary research on lung adenocarcinoma and revised its classification criteria, classifying lung adenocarcinoma into atypical adenomatous hyperplasia (AAH·carcinoma in situ), adenocarcinoma in situ (AIS), minimally adenocarcinoma, (MIA), and invasive adenocarcinoma (IAC); among them, atypical adenomatous hyperplasia and carcinoma in situ are classified as preinvasive lesions. With the continuous improvement of imaging equipment, technology and diagnostic capabilities, and the wide application of low-dose chest thin-layer CT for lung cancer screening, the detection rate of early-stage lung adenocarcinoma with ground-glass nodule (GGN) as the main manifestation has been greatly improved. Ground-glass nodules refer to nodules with a diameter of less than 30 mm and increased cloud-like density on CT thin-layer lung window images, with clear or blurred boundaries, and the original blood vessels and bronchial shadows in the nodules can still be identified. During the pathological progression of lung adenocarcinoma from preinvasive lesions to invasive lung adenocarcinoma, CT images can all appear as ground-glass density nodules, which lack specificity. According to relevant statistics, the 5-year disease-free survival rate of patients with preinvasive lesions after wedge resection is 100%. For

patients with minimally invasive lung adenocarcinoma, precise resection of lung segments or subsegments has a 5-year survival rate after surgery, which is nearly 100%. However, patients with invasive lung adenocarcinoma need to be treated with relatively invasive lobectomy and lymph node dissection, and the 5-year survival rate after surgery does not exceed 9. Therefore, the infiltration of ground glass nodules has a crucial impact on the choice of surgical approach. The traditional CT morphological features of ground-glass nodules have always played a pivotal role in clinical diagnosis, including the size, mean cT value, shape, lobulation sign, burr sign, vacuole sign, air bronchus sign, vascular bundle sign, and pleural depression sign; however, the diagnostic value of cT signs mainly depends on the experience of the diagnostic imaging doctor; so, there is a lot of subjectivity. The features of early-stage lung cancer are often atypical, which makes the differential diagnosis of lung adenocarcinoma subtypes more difficult. Due to the heterogeneity of the tumor or the limitations of the needle biopsy, the traditional preoperative lung biopsy, it often cannot accurately reflect the overall invasiveness of the lesion. And needle biopsy is an invasive examination, which not only brings pain to the patient but also may cause complications such as bleeding and pneumothorax, and there are certain operational risks. Therefore, if the infiltration degree of ground-glass nodule-type lung adenocarcinoma can be accurately and noninvasively identified before surgery, it will have extremely important guiding significance for the precise selection of clinical surgical methods and the individualized formulation of treatment plans.

2. Literature Review

Arai et al. said that lung cancer is currently the malignant tumor with the highest morbidity and mortality in the world [1]. Liu et al. said that the American Cancer Society predicts that there will be about 230,000 new cases in the United States in 2018, and the death toll from lung cancer will also be as high as 154,000, ranking first in the incidence and mortality of malignant tumors [2]. Babiy et al. said that the latest statistics in China in 2017 showed that the number of lung cancer cases was 730,000, the number of deaths was 590,000, and the two figures also topped the list [3]. Choi et al. said that known risk factors for lung cancer include smoking and air pollution, and the incidence of lung cancer is increasing year by year with the increase of tobacco abuse and environmental pollution worldwide [4]. Blackstone and El-Aini stated that surgical resection is the preferred treatment for early stage lung cancer, and it is mainly treated by a combination of surgery, radiotherapy, and chemotherapy [5]. Wang et al. said that in recent years, the statistics of lung cancer pathological types showed that lung adenocarcinoma has replaced lung squamous cell carcinoma as the type with the highest incidence and thus has received extensive attention [6]. Yuan et al. said that the three authoritative organizations of the International Association for the Study of Lung Cancer/American Thoracic Society/European Respiratory Society jointly released a new version of the pathological classification of lung adenocarcinoma in 2011, canceling the original "bronchioalveolar carcinoma (BAC)" statement, put forward new concepts such as "adenocarcinoma in situ (AIS" and "minimally invasive carcinoma (MIA"), and refined the diagnostic types of lung adenocarcinoma [7]. Shenoy et al. stated that lung adenocarcinoma has no specific symptoms in the early onset and is easily overlooked. When hemoptysis, chest pain, and other related symptoms appear, it means that the disease course has entered an advanced stage [8]. Qiu et al. said that the five-year survival rate of patients with stage IA lung adenocarcinoma can reach 90,070, and that of stage IB is 73,070. Most of the early-stage patients with pathological types have a good prognosis, but more than 20% of patients still have adverse prognostic events, such as local recurrence and distant metastasis [9]. The prognosis of patients with intermediate and advanced lung adenocarcinoma is generally poor. CT of early-stage lung adenocarcinoma can manifest as ground-glass density nodules (GGNs), which can be refined into pure ground-glass nodules (GGNs) by the presence or absence of solid components (pGGN) and mixed ground glass nodules (mGGN). The development process of lung adenocarcinoma can be regarded as a continuous process from atypical adenomatous hyperplasia (AAH) to invasive adenocarcinoma (IAC), and pGGN has a tendency to transform into mGGN. On imaging, it is generally believed that the presence of a solid component in GGN is related to the degree of infiltration, but many postoperative pathological results confirmed that pGGN appeared on CT, but the pathological results were infiltrative lesions. At present, the clinical tendency is to carry out long-term follow-up or limited lung resection for preinfiltrating lesions, in order to preserve more healthy lung tissue. Perre et al. say that preserving healthy lung tissue as much as possible can help patients recover from postoperative pulmonary function, especially in the elderly or patients with extremely poor cardiopulmonary function, and it is of great significance to improve the quality of life after surgery [10]. For invasive lesions, lobectomy and enlarged lymph node dissection should be selected more carefully to avoid the risk of postoperative recurrence and metastasis. And there is evidence that invasive adenocarcinoma has a higher risk of recurrence after surgery than noninvasive adenocarcinoma. If it is possible to determine whether there is infiltration of pGGN by CT examination, it can avoid the psychological burden and economic pressure brought by long-term follow-up observation to a certain extent and can also guide the clinical practice of timely surgical resection of invasive lesions, so as to avoid delaying the prognosis caused by the disease; in the process of diagnosis and treatment of lung cancer, CT has an irreplaceable status, no matter from the detection of the disease or the review during treatment. Currently, HRCT is more recommended for pulmonary GGN scanning, its advantage is that HRCT uses thin-layer bone algorithm scanning, which can display the fine structure of the lung more clearly, and HRCT is available in 512×512 or 1024×1024 matrix with spatial resolution in the range of 0.12-0.35 mm. It has definite advantages in showing the edge of the lesion, the internal structure, and the relationship with the small blood vessels and bronchioles. At the same time, compared with

conventional chest CT examination, it is more accurate in distinguishing the nature of nodules, especially in distinguishing the degree of infiltration of nodules. However, it is difficult for doctors to evaluate CT images with the naked eye to obtain the information contained in the pixels. Under such a background, the emergence of radiomics is expected to change this situation. Radiomics collects medical image information, extracts high-throughput data from it, and conducts in-depth mining of quantitative data to obtain quantitative information. In the era of advocating precision medicine, traditional medical imaging is highly subjective and provides limited quantitative information. Radiomics quantifies image data, the extracted nodule feature information far exceeds the signs obtained by naked eye observation and has high repeatability, and some of the obtained information has the predictive ability of tumor phenotype, which is in line with the concept of precision medicine. One of the key issues in radiomic analysis is the choice of a reliable and reproducible image assessment method, which requires accurate delineation of the edges of the lesion. There is a good natural contrast between lung nodules and lung fields, which can ensure accurate segmentation of lesions, making them ideal research subjects. Combining radiomics with pGGN is a noninvasive preoperative prediction of the degree of nodule invasion by automatically acquiring quantitative features of pGGN on HRCT images. At present, preoperative judgment of pGGN infiltration degree by noninvasive methods is a hot spot in foreign research. Conventional imaging diagnostic methods and radiomic methods, respectively, determine the degree of infiltration of pGGN and the excellent degree of diagnostic methods, in order to better assist clinical selection of reasonable treatment plans. By comparing the excellence of the two diagnostic methods at the same time, the authors hope to better assist the clinical selection of a reasonable treatment plan, as shown in Figure 1.

3. Methods

Paraffin-embedded specimens obtained after surgery in all cases were sectioned with 0.4 cm thick tissue sections, including the largest cutting plane of the tumor, and tissue sections were then stained with hematoxylin and eosin. All sections were studied by 2 pathology professors. When there is a dispute, the seniority in pulmonary pathology is taken as the standard. All cases were diagnosed and classified according to the WHO classification of lung adenocarcinoma, and the types of pathological diagnosis included the following: MIA and IAC. IHC staining was performed with Ki-67 protein antibody (Santa Cruz Biotechnology, Santa Cruz, CA, USA) at a dilution of 1 : 100. Cells with brown nuclei were considered positive. Select the three regions with the highest density of positive cells. Randomly count 100 cells in each area under high magnification and calculate the percentage of positive cells as the Ki-67 index. The Ki-67 index for the three regions was calculated and averaged. Analysis was performed using SPSS 24.0 statistical software (SPSS Inc., Chicago, IL, USA). In all variables, the mean ± standard deviation was used for normal distribution, and the median was used for nonnormal distribution. The differences in clinical and imaging characteristics of the MIA group and IAC group were compared. Count data were analyzed by chi-square test, measurement data with normal distribution were analyzed by Student's t-test, and nonnormal distribution was analyzed by Mann–Whitney U test. P value <0.05 was statistically significant [11]. A neural network model was established with variables with P value <0.05 in univariate analysis as input variables and factors, and the conjugate gradient optimization algorithm was used. Receiver operating characteristic curve C, ROC, was analyzed by MedCalc v19.0.2 software, and the area under the curve (AUC) was calculated and compared to evaluate the predictive value of IAC. A retrospective analysis was carried out in this study. Among 469 patients with pGGNs, 268 of them were MIA, and 201 were IAC. The mean age of the patients in the 0MIA group (54.90 ± 10.92 years) was lower than that in the IAC group (61.27 ± 9.12 years) ($P \leq 0.001$) and in the MIA group. The proportion of smoking patients was less than that in the IAC group ($P = 0.015$). Gender and lesion location were not statistically different between the two groups (specifically shown in Table 1). In this study, a total of 436 pGGNs were stained with ki-67, of which 246 were in the MIA group and 190 in the IAC group [12]. The ki-67 070 of the MIA group (5.00, 5.00-7.63) was lower than that of the IAC group (5.00, 5.00-10.00; ($P \leq 0.001$), as shown in Table 1.

In the morphological analysis of CT images, the lesions in the MIA group were more round-like than those in the IAC group ($P = 0.036$). The lesions in the MIA group had fewer imaging morphological signs (lobulation sign, vacuole sign, air bronchus sign, and vascular bundle sign) in the MIA group and in the IAC group (all $P < 0.050$) [13, 14]. In the quantitative analysis of CT images, the CT-LP and CT-W of the MIA group were lower than those of the IAC group; the diameter, volume, and mass of the MIA group were significantly lower than those of the IAC group (all $P \leq 0.001$), as shown in Table 2.

Among the 469 pGGNs, the AUCs of CT-LP, CT-W, lesion diameter, volume, and mass to determine IAC were 0.67, 0.67, 0.78, 0.77, and 0.81, respectively, as shown in Table 3.

Based on CT imaging features, the variables with P value <0.05 in univariate analysis were used as input variables and factors to establish a neural network model. The diagnostic performance analysis of neural network model to distinguish MIA and IAC showed that its AUC, accuracy, sensitivity, and specificity were 0.91, 83.55%, 82.09%, and 85.45%, respectively. CT-W, lesion diameter, volume, and mass showed the diagnostic efficacy of distinguishing MIA and IAC. The AUC value of the neural network model is significantly better than the latter prediction results (all $P < 0.050$), as shown in Figure 2.

WHO proposes a new classification system based on adherent growth pattern as a clinicopathological type, which clarifies the heterogeneity between different pathological types of lung adenocarcinoma, and the pathological manifestations, immunohistochemistry, growth rate, surgical plan, and prognosis were all the same; therefore, the authors retrospectively analyzed 469 pGGNs confirmed by pathology before surgery and established an effective neural

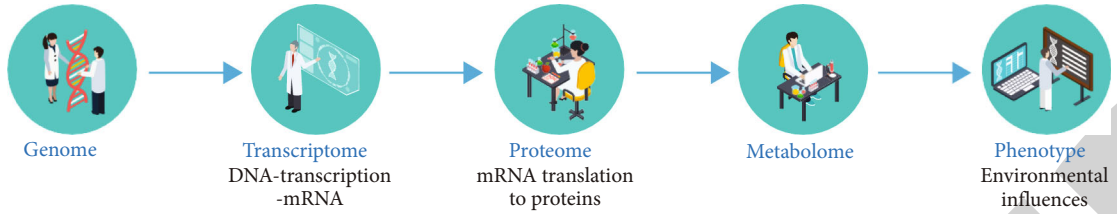

Figure 1: The diagnostic effect of CT radiomic features in pulmonary invasive mucinous adenocarcinoma.

Table 1: Summary of basic clinical data of the MIA group and IAC group.

Variable	All (n = 469 example)	MIA (n = 268 example)	IAC (n = 201 example)	P
Age				0.00
Mean ± standard deviation	57.63 ± 10.67	54.90 ± 10.92	61.27 ± 9.12	
Gender				0.90
Male (example)	146 (31.13%)	75 (27.99%)	71 (35.32%)	

Table 2: Differences of CT imaging features between the MIA group and IAC group.

Variable	All (n = 469 example)	MIA (n = 268 example)	IAC (n = 201 example)	P
Lesion shape				0.036
Round shape (example)	323 (68.87%)	195 (72.76%)	128 (63.68%)	
Irregular shape (example)	146 (31.13%)	73 (27.24%)	73 (36.32%)	
Lobography (example)	165 (35.18%)	81 (30.22%)	84 (41.79%)	0.010
Vacuolation sign (example)	84 (17.91%)	39 (14.55%)	45 (22.39%)	0.029
Air bronchus sign (example)	87 (18.55%)	41 (15.30%)	46 (22.89%)	0.037
Vascular bundle sign (example)	178 (37.95%)	53 (19.78%)	118 (58.71%)	≤0.001

Table 3: Diagnostic efficacy of quantitative imaging parameters of lesions in the MIA group and IAC group.

	AUC	95% CI	Optimal value	Sensitivity	Specificity
CT-LP, HU	0.67	0.62~0.71	-633.93	66.20%	61.90%
CT-W, HU	0.67	0.62~0.72	-656.28	61.70%	66.00%
Diameter, mm	0.78	0.74~0.82.	1.35	77.60%	65.70%
Volume, mm^3	0.77	0.73~0.81	681.30	78.10%	63.40%
Mass, mg	0.81	0.78~0.85	213.76	85.10%	63.80%

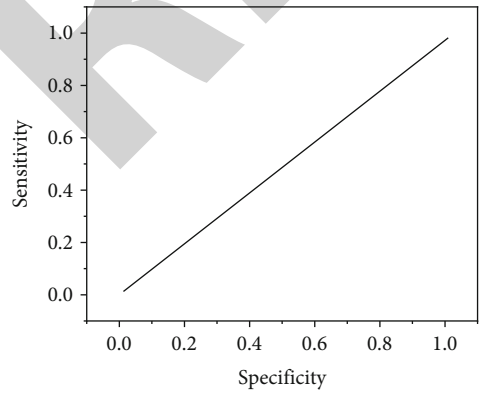

Figure 2: ROC curve analysis for predicting pGGN as IAC.

network model by using thin-slice CT imaging features, and the diagnostic performance for differentiating MIA and IAC presented as pGGNs was greatly improved. In the study, the age of the patients in the MIA group (54.90 ± 10.92 years) was lower than that in the IAC group (61.27 ± 9.12 years) ($P \leq 0.001$). In a study of 154 cases of subsolid pulmonary nodules < 5 mm, Ren et al. also found that the age of onset of MIA was lower than that of IAC ($P = 0.015$), which is basically similar to the results of this study [15]. This study also showed that the proportion of smokers in the MIA group was less than that in the IAC group ($P = 0.015$), but there was no statistical difference in gender and lesion location between the two groups. The shape and edges of pGGNs are determined by a combination of different cell growth rates and matrix responses, and most MIAs are oval (86.70070) [16]. In this study, the lesions in the MIA group

were more round-like (72.76070) than in the IAC group (63.68070), which was similar to previous results. At the same time, other imaging morphological features (lobulation sign, vacuole sign, air bronchus sign, and vascular bundle sign) of pGGNs in this study were statistically different between the two groups, and the IAC group was more than the previous literature results, which is also roughly the same. The bronchus of the same order is always accompanied by the pulmonary artery, when the vascular bundle sign and the air bronchus sign appear in pGGNs, the lesion may have more blood and oxygen supply, and it may reflect the accelerated growth and infiltration of tumor cells. Pathologically, the vacuolar sign refers to obstructive expansion of small airways, multiple ruptured alveolar fusion cavities, and lung tissue not occupied by tumor tissue. However, unlike most of the previous literature, there was no statistical difference between the two groups in the pleural stretch sign in this study. Due to human factors and experience differences in the cognition of conventional imaging signs, therefore, there may also be some degree of instability. The size and CT value of the lesions are of great significance for the diagnosis and identification of pGGNs. It is generally believed that the larger the pGGNs, the higher the grade of malignancy. In this study, the diameter, volume, and mass of the MIA group were significantly lower than those of the IAC group (all $P \leq 0.001$). Using quantitative CT histogram and FDG-PET analysis of 225 cases of c-0/I stage lung adenocarcinoma, it was found that the tumor diameter and volume in the IAC group were higher than those in the preinvasive lesion group. Meng's analysis of 145 cases of GGNs also showed that the tumor in the IAC group was significantly larger than that in the MIA group (12.84 vs. 9.0 scm, $P < 0.05$). It can be seen that the size of pGGNs is a more important distinguishing indicator. The CT value of the lesion can reflect more tumor cells growing along the alveolar septa, there is a strong negative correlation with the air gap retained in the tumor, and the CT attenuation value increases as the infiltrating component continues to spread and grow [17, 18]. In the study of 253 pGGNs, the CT value of preinvasive lesions was lower than that of IAC ($P = 0.020$), which was similar to our results. In this study, CT-LP and CT-W were lower in the MIA group than in the IAC group (-659.45 vs. -606.44: -677.96 vs. -634.19; all $P \leq 0.001$).

4. Experiments and Analysis

In recent years, the popularity of spiral CT has made the detection rate of pulmonary nodules higher and higher. Compared with conventional scanning, HRCT has clear advantages in displaying the internal and surrounding characteristics of nodules. Some studies have pointed out that the probability of malignant tumor in GGN is significantly higher than that in solid nodules, and the most common pathological type is lung adenocarcinoma. There is a real component in the ground glass density, indicating that the lesion has infiltration or fibrosis, and the progression is rapid. It is recommended to reexamine in a short period of 3-6 months. After the lesion enlarges or becomes consolidated, surgical resection should be taken for treatment [19]. However, whether the pure ground glass component lesions are inflammatory lesions or tumor lesions requires further observation and judgment. And according to the new version of lung adenocarcinoma classification in 2011, the judgment of AIS and MIA must be judged by a complete gross specimen, and there is a sampling position error in needle aspiration cytology, which causes differences in pathological results. If ground glass lesions are rashly surgically removed, the postoperative pathological results are confirmed to be benign, which may lead to controversy over overdiagnosis [20]. However, some scholars have continuously found that pGGN also has invasive components, and delaying preoperative diagnosis may lead to poor long-term prognosis. The 65 nodules in this study were all surgically resected pGGN, and there were also invasive lesions such as MIA and IAC, which also confirmed the above point of view. The authors analyzed the qualitative and quantitative characteristics of pGGNs < 30 mm in diameter on HRCT. Qualitative features included lobulation sign, burr sign, vacuole sign, vascular cluster sign, and nodule size and mean CT value in quantitative features, which were statistically significant between the two groups for preinvasive and invasive lesions ($P < 0.05$). There were no significant differences in gender, lesion location, shape, air bronchus sign, pleural traction sign, and tumor-lung interface ($P > 0.05$). Studies have shown that the lobulation sign and the spicule sign are more frequently present in invasive lesions, and our findings are consistent with those reported in the literature [21]. Lobulation and spicules are the edge features of nodular lesions. Some scholars believe that the proportion of spicule signs is higher in lung adenocarcinoma; lung adenocarcinoma lesions with few solid components are more prone to lobulation signs and spicules, which is consistent with our study. The results are consistent, and it is considered to be related to the invasion of tumor cells into the interstitial structure of the lung, resulting in uneven arrangement of tumor cells and differences in tumor cell growth rates [22]. The vascular bundle sign is an independent risk factor for judging the presence or absence of infiltrating components. The biological behavior of the tumor is also confirmed by the side, the degree of malignancy is positively correlated with its ability to proliferate, and vascular endothelial factor surges in the early stage of tumorigenesis, resulting in an increase in new blood vessels or vascular remodeling. Analysis of the blood vessels in the GGN showed that the tortuosity, thickening, and aggregation of the blood vessels in the lesions increased the blood supply in the lesions, which were more likely to appear in MIA and IAC lesions, which was consistent with our results. The study found that the degree of tortuosity of pulmonary veins in MIA was higher than that of preinvasive lesions, indicating that vascular changes can distinguish preinvasive and invasive pGGN to a certain extent. The vacuolar sign refers to the nontextured area within 1-2 mm in diameter of the pulmonary nodule, the vacuolar sign may be the lung tissue that is not filled by tumor cells in the lesion or the alveolar cavity and the remnant luminal structure of the bronchioles destroyed by tumor invasion, and it has been

reported in the literature that the vacuolar sign can be used in differentiating benign and benign pulmonary nodules. The degree of malignancy is significant, and there are many female patients in this study, but the gender comparison was not statistically significant between the two groups (expansion = 0.012, $P = 0.912$). At present, the incidence of lung adenocarcinoma in women is increasing year by year, especially in nonsmoking women. The cause is unknown, but it may be related to second-hand smoke and cooking fumes. Among the 65 nodules in this study, 41 cases of bilateral upper lobe lesions, accounting for 63% of the total, also showed a pattern of bilateral upper lobe predilection, but no relationship between bilateral upper lobe predisposition and pGGN was found. Relationship. In this study, no exact correlation was found between the distribution of lesions with or without invasion [23]. We divided the nodules into two groups: round/round-like and irregular. The round/round-like group was the majority (84.6%). There was no difference between the two groups ($P = 0.555$). The nodule morphology is related to benign and malignant nodules, but these conclusions are compared between the two groups of benign and malignant nodules, and this study is compared within the malignant pGGN; so, the conclusions are different. The morphology of malignant pGGN was also compared, and the conclusions obtained also support this study. There was no statistical significance in the air bronchus in this study ($P > 0.05$). It is believed that the appearance of the air bronchus sign in the lung adenocarcinoma nodule is related to the fibrosis within the lesion pulling the bronchus, but the research subjects in this study were all pGGN solid or subsolid. In terms of sexual nodules, the degree of fibrosis in pGGN lesions is lower; so, the conclusions are different. The pleural stretch sign is greatly affected by the location of the nodule, and lesions in the subpleural area are more likely to have pleural stretch signs. In this study, no definite statistical significance was found between the two groups ($P = 0.882$) [24]. The size of the nodule directly reflects the growth rate of the nodule. In this study, the average size of the nodule in the preinfiltration group was 11.16 ± 4.29 mm, and the infiltration group was 15.10 ± 5.35 mm. Previous studies have shown that the diameter of AIS in pGGN is significantly smaller than that of MIA and IAC, 10 mm was selected as the cut-off value for judging invasive lesions, and 13.6 mm was considered as the cut-off point for judging invasive lesions; there are differences in the grouping method used in this paper because of the errors caused by species or manual measurement or the classification of MIA as preinvasive lesions. Previous studies have shown that the size of CT value is considered as a method to distinguish different pathological types. The arrangement of tumor cells in invasive lesions changes. The higher the CT value, the higher the degree of malignancy. In the study, the analysis of pGGN also included the relationship between tube voltage and CT value was explored. For images scanned in the range of 120-140 kVp, the CT value was related to the degree of infiltration, while the low voltage of 40-110 kVp was not meaningful for identification. In this study, a high voltage of 140 kVp was also used for scanning, which ensured the reliability of CT value analysis. By analyzing the data, we obtained that the mean CT values of preinvasive and invasive lesions were -587.29 ± 78.86 HU and -494.78 ± 85.53 HU, there was a significant difference $P \leq 0.001$, the cut-off value was -533.50 HU, and the sensitivity was 0.704 and specificity 0.763. Considering the differences in CT value measurement methods and scanning parameters, the results were basically consistent with those reported in the literature. The high-quality images of HRCT play an important role in the diagnosis of GGN, but the information obtained by radiologists from medical images is limited. There is a lot of overlap in imaging features between preinvasive lesions and invasive lesions, and it is difficult to distinguish morphologically. Traditional CT images can only obtain simple quantitative information such as nodule size and CT value. The judgment of the degree of pGGN infiltration is mostly based on clinical experience, which is prone to missed diagnosis and misdiagnosis. At present, there is no definite quantitative information to distinguish whether there is an infiltrating component in pGGN, and it can only be judged by postoperative pathology. The emergence of radiomics provides a new idea to solve this problem [25]. Radiomic analysis of pulmonary nodules has been widely concerned, and its advantages lie in improving diagnostic specificity and sensitivity while minimizing the workload of radiologists [26, 27]. Omic analysis is to extract high-throughput information from CT images and quantify it to obtain morphological features, grayscale features, and texture features, and the extraction of these features is generally done automatically by computers. In addition, by analyzing image features and clinical data, radiomics can provide additional diagnostic information for the internal components, and lymph node metastasis and distant metastasis of lung adenocarcinoma, the observation and measurement of the morphology, nodule size, and average CT value of pGGN by conventional imaging diagnostic methods are limited to the naked eye. Detailed and three-dimensional, all images are delineated layer by layer to form a three-dimensional structure, which can more fully obtain the volume and morphological characteristics of the lesion. Secondly, the first-order histogram and high-order texture features obtained through the original DICOM image are based on the changes of different grayscale values in the image, the human eye can only distinguish 16-level grayscale changes, and it is often difficult to understand subtleties; there are many omissions, the identification of image grayscale through computer software is more detailed and accurate, and the judgment of infiltration components is more accurate. However, the infiltration degree analysis and long-term prognosis evaluation of pGGN by radiomics is still in its infancy, and it has not been widely used. In the future, we will incorporate images from more sources to validate and optimize the diagnostic performance of this omics model [28].

5. Conclusion

The qualitative and quantitative characteristics of pGGN of lung adenocarcinoma with a diameter of less than 30 mm on HRCT were analyzed by conventional imaging diagnostic

methods, and it was found that lobulation sign ($P \leq 0.001$, burr sign ($P = 0.008$), vacuole sign ($P = 0.047$, vascular sign), cluster sign ($P = 0.001$), nodule size ($P = 0.001$), and mean CT value ($P \leq 0.001$) were meaningful in distinguishing preinvasive and invasive lesions. The optimal cut-off values of nodule size and mean CT value were, respectively, 12.7 mm and -544.50 HU. The DICOM images of lung adenocarcinoma pGGN with HRCT diameter < 30 mm were analyzed by the radiomic method, the quantitative features of medical image data were deeply excavated to obtain two omics parameters of "dimension" and "sphericity," which were used to establish a group, a scientific model was established, and the validation of the model was meaningful for diagnosing the degree of pGGN infiltration. The quantitative diagnostic value of radiomics (AUC = 0.824) was higher than that of conventional imaging diagnostic methods (AUC = 0.740 and 0.784).

Data Availability

The data used to support the findings of this study are available from the corresponding author upon request.

Conflicts of Interest

The authors declare that they have no conflicts of interest.

Acknowledgments

This study was supported by the Health General Project of Zhejiang Province (2021KY291).

References

[1] K. Arai, T. Iwasaki, C. Tsuchiya, and A. Sonoda, "Annexin a2 expression in the aerogenous spread of pulmonary invasive mucinous adenocarcinoma with gastric lineage," *Case Reports in Oncological Medicine*, vol. 2020, Article ID 2492636, 9 pages, 2020.

[2] J. Liu, S. Zhang, and J. Luo, "Prognosis of early stage pulmonary mucinous adenocarcinoma with different treatments," *Translational Cancer Research*, vol. 9, no. 9, pp. 5182–5189, 2020.

[3] Y. Babiy, T. Sychova, and I. Dykan, "Radiological aspects of the new "international multidisciplinary classification of lung adenocarcinoma": methodological bases and own experience," *Radiation Diagnostics Radiation Therapy*, vol. 3, pp. 55–71, 2019.

[4] Y. Choi, K. H. Kim, B. H. Jeong et al., "Clinicoradiopathological features and prognosis according to genomic alterations in patients with resected lung adenocarcinoma," *Journal of Thoracic Disease*, vol. 12, no. 10, pp. 5357–5368, 2020.

[5] N. Blackstone and T. El-Aini, "Medical image of the month: mucinous adenocarcinoma of the lung mimicking pneumonia," *Southwest Journal of Pulmonary and Critical Care*, vol. 22, no. 1, pp. 8–10, 2021.

[6] L. Wang, Y. Hirano, G. Heng, T. Ishii, and S. Yamaguchi, "Mucinous adenocarcinoma as a high-risk factor in stage ii colorectal cancer: a propensity score-matched study from Japan," *Anticancer Research*, vol. 40, no. 3, pp. 1651–1659, 2020.

[7] H. J. Yuan, Z. B. You, G. Y. Li et al., "Clinical characteristics and treatment strategies of prostatic mucinous adenocarcinoma: a report of 10 cases and literature review," *National Journal of Andrology*, vol. 26, no. 12, pp. 1087–1091, 2020.

[8] V. Shenoy, M. Buckley, H. Hosseini, M. Ma, and A. Aggarwal, "S1710 signet ring cell mucinous adenocarcinoma of the colon manifesting as intermittent hiccups," *The American Journal of Gastroenterology*, vol. 115, no. 1, pp. S882–S883, 2020.

[9] T. Qiu, X. Ru, K. Yin, J. Yu, Y. Song, and J. Wu, "Two nomograms based on ct features to predict tumor invasiveness of pulmonary adenocarcinoma and growth in pure ggn: a retrospective analysis," *Japanese Journal of Radiology*, vol. 38, no. 8, pp. 761–770, 2020.

[10] S. V. Perre, L. Duron, A. Milon et al., "Radiomic analysis of htr-dce mr sequences improves diagnostic performance compared to bi-rads analysis of breast mr lesions," *European Radiology*, vol. 31, no. 7, pp. 4848–4859, 2021.

[11] M. Li, T. Chen, W. Zhao, C. Wei, and J. Shen, "Radiomics prediction model for the improved diagnosis of clinically significant prostate cancer on biparametric mri," *Quantitative Imaging in Medicine and Surgery*, vol. 10, no. 2, pp. 368–379, 2020.

[12] Z. Liu, Z. Jiang, L. Meng, J. Yang, and R. Zhou, "Handcrafted and deep learning-based radiomic models can distinguish gbm from brain metastasis," *Journal of Oncology*, vol. 2021, Article ID 5518717, 10 pages, 2021.

[13] J. M. Chen, Q. Wan, H. Y. Zhu, Y. Q. Ge, and Z. M. Ding, "The value of conventional magnetic resonance imaging based radiomic model in predicting the texture of pituitary macroadenoma," *Zhonghua Yi Xue Za Zhi*, vol. 100, no. 45, pp. 3626–3631, 2020.

[14] G. Montrucchio, T. Lupia, D. Lombardo et al., "Risk factors for invasive aspergillosis in icu patients with covid-19: current insights and new key elements," *Annals of Intensive Care*, vol. 11, no. 1, pp. 1–11, 2021.

[15] X. Ren, C. Li, X. Ma et al., "Design of multi-information fusion based intelligent electrical fire detection system for green buildings," *Sustainability*, vol. 13, no. 6, p. 3405, 2021.

[16] S. Shriram, J. Jaya, S. Shankar, and P. Ajay, "Deep learning-based real-time AI virtual mouse system using computer vision to avoid COVID-19 spread," *Journal of Healthcare Engineering*, vol. 2021, Article ID 8133076, 8 pages, 2021.

[17] K. Roy, S. Jana, S. K. Ghosh, B. Mahanty, and D. Mandal, "Three-dimensional MOF-assisted self-polarized ferroelectret: an effective autopowered remote healthcare monitoring approach," *Langmuir*, vol. 36, no. 39, pp. 11477–11489, 2020.

[18] L. Xin, L. Jianqi, C. Jiayao, Z. Fangchuan, and M. Chengyu, "Study on treatment of printing and dyeing waste gas in the atmosphere with Ce-Mn/GF catalyst," *Arabian Journal of Sciences*, vol. 14, no. 8, pp. 1–6, 2021.

[19] A. Avc, M. Korkut, A. F. Bekta, and S. Syüncü, "Thoracic fluid content measurement: diagnostic value of suspected pulmonary oedema in acute decompensate heart failure," *Eurasian Journal of Emergency Medicine*, vol. 19, no. 2, pp. 63–70, 2020.

[20] R. Huang, S. Zhang, W. Zhang, and X. Yang, "Progress of zinc oxide-based nanocomposites in the textile industry," *IET Collaborative Intelligent Manufacturing*, vol. 3, no. 3, pp. 281–289, 2021.

[21] J. A. Pegoraro, S. Lavault, N. Wattiez, T. Similowski, J. Gonzalez-Bermejo, and E. Birmelé, "Machine-learning based feature selection for a non-invasive breathing change detection," *Bio Data Mining*, vol. 14, no. 1, pp. 1–16, 2021.

Hindawi
Scanning
Volume 2023, Article ID 9890786, 1 page
https://doi.org/10.1155/2023/9890786

Retraction

Retracted: Unsupervised Hyperspectral Microscopic Image Segmentation Using Deep Embedded Clustering Algorithm

Scanning

Received 20 June 2023; Accepted 20 June 2023; Published 21 June 2023

This is article has been retracted by Hindawi following an investigation undertaken by the publisher [1]. This is investigation has uncovered evidence of one or more of the following indicators of systematic manipulation of the publication process:

(1) Discrepancies in scope

(2) Discrepancies in the description of the research reported

(3) Discrepancies between the availability of data and the research described

(4) Inappropriate citations

(5) Incoherent, meaningless and/or irrelevant content included in the article

(6) Peer-review manipulation

The presence of these indicators undermines our confidence in the integrity of the article's content and we cannot, therefore, vouch for its reliability. Please note that this notice is intended solely to alert readers that the content of this article is unreliable. We have not investigated whether authors were aware of or involved in the systematic manipulation of the publication process.

Wiley and Hindawi regrets that the usual quality checks did not identify these issues before publication and have since put additional measures in place to safeguard research integrity.

We wish to credit our own Research Integrity and Research Publishing teams and anonymous and named external researchers and research integrity experts for contributing to this investigation.

The corresponding author, as the representative of all authors, has been given the opportunity to register their agreement or disagreement to this retraction. We have kept a record of any response received.

References

[1] P. Ajay, B. Nagaraj, R. A. Kumar, R. Huang, and P. Ananthi, "Unsupervised Hyperspectral Microscopic Image Segmentation Using Deep Embedded Clustering Algorithm," *Scanning*, vol. 2022, Article ID 1200860, 9 pages, 2022.

Hindawi
Scanning
Volume 2022, Article ID 1200860, 9 pages
https://doi.org/10.1155/2022/1200860

Research Article

Unsupervised Hyperspectral Microscopic Image Segmentation Using Deep Embedded Clustering Algorithm

P. Ajay,[1] **B. Nagaraj**,[2] **R. Arun Kumar**,[3] **Ruihang Huang**,[4] **and P. Ananthi**[5]

[1]*Faculty of Information and Communication Engineering, Anna University, Chennai, India*
[2]*Department of ECE, Rathinam Technical Campus, India*
[3]*Rathinam Technical Campus, Department of Electronics and Communication Engineering, India*
[4]*Donghua University, Shanghai, China*
[5]*Department of Artificial Intelligence and Data Science, Rathinam Technical Campus, India*

Correspondence should be addressed to P. Ajay; ajaynair707@gmail.com

Received 18 April 2022; Accepted 23 May 2022; Published 6 June 2022

Academic Editor: Danilo Pelusi

Hyperspectral microscopy in biology and minerals, unsupervised deep learning neural network denoising SRS photos: hyperspectral resolution enhancement and denoising one hyperspectral picture is enough to teach unsupervised method. An intuitive chemical species map for a lithium ore sample is produced using *k*-means clustering. Many researchers are now interested in biosignals. Uncertainty limits the algorithms' capacity to evaluate these signals for further information. Even while AI systems can answer puzzles, they remain limited. Deep learning is used when machine learning is inefficient. Supervised learning needs a lot of data. Deep learning is vital in modern AI. Supervised learning requires a large labeled dataset. The selection of parameters prevents over- or underfitting. Unsupervised learning is used to overcome the challenges outlined above (performed by the clustering algorithm). To accomplish this, two processing processes were used: (1) utilizing nonlinear deep learning networks to turn data into a latent feature space (Z). The Kullback–Leibler divergence is used to test the objective function convergence. This article explores a novel research on hyperspectral microscopic picture using deep learning and effective unsupervised learning.

1. Introduction

Data-driven systems gain knowledge. Recommendations regarding, we need more of them. Data mining, big data, and machine learning are all used. Deep learning without supervision of data classification is a dataset or feature is classified by an application [1]. Data classification is used to make decisions in this circumstance. SVM, linear regression, and feature vectors are examples of data categorization algorithms. This decade, machine learning algorithms have played a critical role in data science. Nonlinear thinking is adapted to real-world problems using machine learning. In ANN (artificial neural network) applications, unsupervised learning is applied. ANN algorithms can learn and comprehend circumstances scientifically thanks to their iterative learning process. Data mining, on the other hand, is a branch of machine learning study that employs unsupervised learning. Predictive models such as SVM, decision trees, and linear discriminant analysis can be used to directly classify data. Even if machine learning for data classification produces improved outcomes, modern application requirements and innovations demand more precision. This new era of study began with the development of deep learning algorithms. Deep learning involves several ANN layers at different levels. So the data is thoroughly analyzed, revealing a huge feature that is transferred to the next layer. The procedure transforms the learnt features from the preceding layer into a high-level data abstraction. Hence, deep learning can be applied to multiclass classification [1, 2].

Many datasets and applications benefit from deep learning, yet its limits open up new research avenues.

(1) Deep learning algorithms are supervised learning algorithms. Supervised learning involves labeling or annotating datasets. However, to train and classify for real-time applications, the labeled dataset is expensive and requires a lot of manual labor to manually label

(2) Deep learning techniques require a lot of compute to process the huge amount of data. Also, through training on a huge dataset, the deep learning algorithm learns the pattern of comprehension. That is why when talking about deep learning algorithms, CPUs and GPUs come up

(3) However, clustering algorithms group data points or features with comparable properties. Unsupervised clustering techniques do this. Unlike supervised deep learning algorithms, it can process grouping and classification without a dataset. Many data applications employ soft or hard clustering methods. Due to the restrictions of the clustering technique, it is difficult to apply it to classification tasks

This study is aimed at improving the behavior and nature of deep learning by using a clustering technique so that deep learning systems can use unsupervised learning to efficiently classify data.

It is widely used to resolve ambiguity. Historical data solves these problems. Algorithms are for supervised machine and deep learning. But unsupervised learning has promise. Experimentation is encouraged. Discriminatory biases are inherent in supervised learning methods, where the set of rules is specified by a set of DOs and DONTs. In the absence of labeling, supervised learning requires a lot of manual work and time.

So the research's major objective is to enhance unsupervised deep learning. Methods for unsupervised learning (b) selecting acceptable and efficient deep learning methodologies and issues to verify and confirm the research findings (d) investigating the best deep learning strategy for data classification. This section's subjects elaborate on the research's goal [3–5].

2. Classification Difficulties

A data classification scheme is an integral part of a data security system. Data categorization helps with risk management and data protection. It also offers a natural data hierarchy. Depending on the application, context, content, and behavior, data are employed. Data categorization is used in many ways. In this approach, all segmentation is done manually on tiny datasets. (*b*) Equal intervals: this approach groups data (as desired by the user). (*c*) Quantities: quantity segmentation: a natural break happens when a collection of data changes. It specifies the geometric interval segmentation in each data type. Data are segmented using standard deviation intervals to characterize their attributes and quantify their departure from the normal. (*g*) Custom range: this strategy uses the user's input and may be changed to meet new needs [4, 6].

2.1. Implementing Data Classification

(1) Manual data classification by their personnel (or incharges) while storage would be significantly easier: this is not a simple operation if the data is created in large quantities. Today's entities recognize the value of classification and require their process managers to perform it prior to storing. However, their historical data requires modern algorithms and process segmentation/classification

(2) The researcher can use several traditional classification approaches, but most are linear and do not work well with data that lacks a pattern. Accuracy varies with dataset size

(3) The stated complexity allows for nonlinear techniques like machine learning. But again, machine learning requires labelled data, etc. But the precision is poor

(4) The ability of machine learning to operate on unknown data allows for deep learning research. Supervised learning requires a lot of data to train to be effective. Deep learning is important in today's AI. That being said, this platform requires a lot of processing power (GPU) (b) a large labelled dataset preventing over- or underfitting parameters [7, 8]

2.2. Implementing Data Classification Strategies. Using a suitable clustering technique, the research is aimed at improving deep learning in an unsupervised mode. The following is the deep learning unsupervised learning approach.

Deep learning is used instead of standard artificial neural networks because it can abstract deep features. The transformation is achieved using a nonlinear deep learning network. Z is smaller than X due to the transformation. The strategy then processes Z to produce k clusters by initializing and converging the random centroid. The deep network's clustering and reconstruction losses are determined during this step. It can be trained to minimize loss using the consolidated loss function (LR and LC). Unsupervised learning can be done with the final trained network. For this reason, unsupervised categorization is widely used. The implementation and study are described below [9].

2.3. Algorithms for Data. These goals are achieved by unsupervised learning. It looks into clustering methods like k-means and FCM. The goal function assigns the data convergent iterative clustering. Clustering loss is crucial in DL networks [10].

DL algorithms are essential in research. To comprehend deep learning algorithms, one must first comprehend ANNs. GDO and thresholding calculations are required. This research begins with autoencoders.

2.4. Operational Simulation Tools. TAn open-source Google Brain algorithm is used. That is not all. Applied deep learning requires it. This study uses numpy, pandas, and Scikit-learn to build a model. This research uses MATLAB (mathematical model) [11].

2.5. Datasets. It aids in deep learning. Module learning, testing, and validation datasets abound. A WordNet-organized image and vision research dataset is ImageNet. A massive dataset for deep learning, MNIST has 14 million data points. Handwritten NIST digits (7291 training and 2007 testing samples) in 16×16 size, quite a dataset. Algorithms for text categorization: this dataset has 80 million CIFAR-10 images in it. Ten classes of 6000 photos each. 50000 records per training and testing set language statistics (STL-10) 96×96 photos. They are useless without labels. These datasets are frequently used to validate proposed modules [12].

High-performance imaging applications like superresolution microscopy and cancer detection have made machine learning a potent general tool for scientific data processing: lung cancer diagnostic, human medium expression, and sample classification [13]. Deep learning was used to denoise SRS microscopy and spectra. DeepChem is a sophisticated customized SRS microscopy technology. While DeepChem can segment pictures without spectrally resolved data, it cannot properly identify species without such data. Previously, supervised deep learning was used for CRM image identification. Labeled training data is necessary for DeepChem's spectral resolution and picture and spectrum denoising, while delicate or uncommon biological samples may be collected.

On unsupervised deep learning for CRM image interpretation, unsupervised method finds and segments data. Supervised method: unsupervised model outperforms supervised nonlinear optic signature (HSI). That means it can describe any laser-based optical signal channel, a SRS vibrational spectrum. Other optical microscopy techniques could benefit [14–16].

We SRS-ed each pixel (a). We used two. It took 32 seconds to slice 256 pixels. First, hexadecane and water: C-H stretch resonance 2852 cm^1 802 nm pump, 1040 nm Stokes, interval between two beams 92 frames. High- and low-SNR ground truth photos were taken with identical laser input strengths (GT). Due to the high laser power input, hyperspectral, a pixel's local mean and standard deviation (5-pixel radius neighborhood). Using a reference time series, each pixel's PSNR was calculated [16].

Deep learning denoising and segmentation use unsupervised (spodumene, feldspar, and quartz). Its popularity has grown due to the rise of electric cars, AT4O8, where B = boron and T = silicon or aluminum (Al). Like quartz (SiO_2), a lot of SRS and NOR peaks! The pump beam was 70 mW at 929–998 nm. 909 frames were scanned [16, 17].

2.6. NN Models. They both used a neural network. Linked convolutional layer kernel arrays are in conv. Each convolutional layer had this layer (yellow). Encoding required latent space; 4 DE convolutional layer sample size increases with deconvolution. It was used in encoding and decoding (ReLU and leaky-ReLU). The number of fully connected nodes determines a parameter's size [18]. It modifies hyperparameters (hexadecane vs. lithium ore). Identical dataset structure (number and type of layers), a similar validation set optimized the loss. The SI provides model hyperparameters, datasets, and code, that is, supervised or not. It had a good SNR (ground truth). A classic neural network denoiser, our unsupervised method had no supervision. Encoding can only extract properties that are common to many pixels. Our loss was always msd. All pixels were treated as samples during training. Unlike model or hyper parameter data, using one eye improved transferability (supervised method): supervised hyperspectral resolution enhancement (unsupervised hyperspectral resolution enhancement and denoising). Prior algorithms custom PyTorch built on NVidia K80 GPU. It used a ten-layer convolutional auto encoder. It is similar [19].

2.7. Autosegmentation. It can classify and denoise spectral components (and, subsequently, image segmentation). Encoding reduces input data dimensionality. A method called *k*-means clustering may find comparable pixels inside an image. This technique is unsupervised, unlike earlier ones. The elbow technique is used in the *k*-means algorithm. The elbow method establishes. The number of components per cluster reduces as *k* grows. The elbow is the inflection point where *k* increases the most. Unsupervised segmentation method: it first projects hyperspectral image data into latent space (blue) (green). This space uses hyperdimensional clustering (*k*-means) to classify each image pixel. The trained autoencoder can automatically identify picture pixels based on hyperspectral properties. Using hyperspectral SRS, each sample constituent is allocated a unique vibrational spectroscopy-based chemical identification [20].

2.8. Algorithms for Deep Cluster. Many industries now struggle with data (which has been generated every second in a massive quantity). Deep learning algorithms are essential for research and modernization. Many issues can be solved with supervised learning. However, unsupervised learning may open new doors. But data mining systems' clustering techniques can structure unknown data. Data are clustered using knowledge discovery. Measuring distances is a common clustering: a deep learning and clustering [21] mix.

DEC surplus to unsupervised learning: supervised learning is extended in these ways; algorithms aided DEC core design using autoencoders, and DEC creates a feature space. The clustering technique affects the autoencoder training phase through loss limitations. DEC is a two-stage technique. Pretraining factors like cluster centers and convergence criteria are used to fine-tune the clustering process [22]. This level includes learning and grouping. DEC recommends the autoencoder for data reconstruction since it is simple and reliable (Figure 1). This section introduces DEC and its variants. As stated above, this part is about studying and analyzing algorithms.

Deep learning networks focus on low-dimensional input and learn its features. The autoencoder technique is popular in deep learning networks.

3. Loss Function-Deep Clustering

This is because the deep clustering method involves both nonlinear learning and clustering methodology.

3.1. Network Loss. Deep learning strategies solely analyze reconstruction loss when using an autoencoder network. Consider the vibrational loss and the adversarial loss when

using VAE and GAN. No matter the deep learning network's learning mode, this is required for training (supervised or the unsupervised) [23].

3.2. Clustering Loss. A clustering loss that measures algorithm, this study uses them. Adding data points results in a loss. It is estimated using the student t-distribution. k-means and agglomerative clustering are examples of this loss. It is a clustering loss. And it keeps discriminant information. Group sparsity loss and location loss are discussed [24].

3.3. Measuring Results. Metrics for evaluating existing systems and research contributions include measurements that were made using the tagged data from the standard datasets.

3.3.1. Unsupervised Clustering Accuracy (ACC). The ground truth (g) and the clustering assignment output (mp) (c): the unsupervised output has little chance of matching the ground truth labels.

$$\mathrm{ACC} = \max_{\mathrm{mp}} \frac{\sum_{j=1}^{n} 1\left(g_j = \mathrm{mp}(c_i)\right)}{n}, \tag{1}$$

where i and j are loop variables for identifying data points.

3.3.2. Normalized Mutual Information (NMI). Cluster assignments (c) and ground truth labels (l) have the same average entropy (H) (g). This study identifies the output's mutual information compared to the ground truth [25].

$$\mathrm{NMI}(g, c) = \frac{I(g, c)}{1/2[H(g) + H(c)]}. \tag{2}$$

3.3.3. Adjusted Rand Index (ARI). ARI calculates the similarity of two data clusters.

The algorithm's success rate is determined by this metric and its assessment. An example of the permutation model is presented below [26].

$$\mathrm{ARI} = \frac{\sum_{ij}^{\mathrm{k}} \binom{n_{ij}}{2} - \left[\sum_{i}^{\mathrm{k}} \binom{a_i}{2} \sum_{j}^{\mathrm{k}} \binom{b_j}{2}\right] / \binom{n}{2}}{1/2\left[\sum_{i}^{\mathrm{k}} \binom{a_i}{2} \sum_{j}^{\mathrm{k}} \binom{b_j}{2}\right] - \left[\sum_{i}^{\mathrm{k}} \binom{a_i}{2} \sum_{j}^{\mathrm{k}} \binom{b_j}{2}\right] / \binom{n}{2}}. \tag{3}$$

4. Results and Discussion

It was intended to demonstrate our autoencoder networks' image demising and reconstruction abilities. The trained autoencoder networks produced a hyperspectral image from a low SNR image. Figure 2 shows one shift of 2852 cm^1 near a peak in hexadecane. The dataset's maximum pixel reading is used to normalize the noisy input image, reducing the perceived dynamic range while resolving the noise. The images clearly reveal two phases, with the hexadecane phase having a stronger signal. SNR may be used to evaluate different neural networks' denoising abilities (Figure 3). The SNR for the GT image in Figure 2 is 31 dB in hexadecane and 10 dB in water.

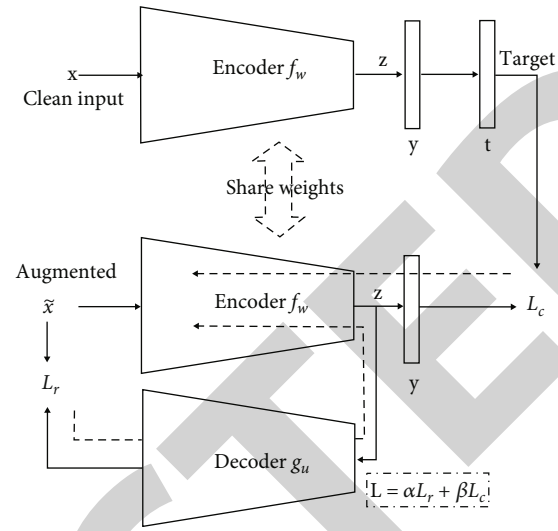

Figure 1: Deep clustering networks with stacked autoencoder.

In hexadecane, the SNR is 15 dB, whereas in water, it is 8 dB. We used the model to denoise two new hyperspectral imaging datasets (FOV 1 and FOV 2) for testing. We show examples from 2852 cm^1 of the denoised hyperspectral dataset. Photos with low SNR are in Figure 4 (20 mW input power).

The GT image was used to compare unsupervised method and supervised method results, not for training. The SNR is 15 dB for unsupervised method, supervised method, and GT and 4 dB for water. Water has an SNR of 86.6 dB, while hexadecane is 14. They both use spectral data to improve picture quality. Figure 2 shows a 15 m droplet in the FOV 2 ROI. It also shows more defined droplet boundaries. The PSNR of noisy GT data is 14, unsupervised method is 22, and supervised method is 25 dB [27].

Peak resolution is critical for SRS component categorization. Supervised method and unsupervised method denoise images across the entire spectrum (Figure 2). Supervised method denoises SRS spectra using a trained model on an unknown dataset. Figure 4 shows a low SNR image of hexadecane water with a spectrum around the C-H stretch. As shown in Figure 4, the supervised method output spectrum (red) is represented by a pixel in Figure 5. SNR GT spectrum (green) is in Figure 4 (60 mW input power). Suppressing GT data from input, supervised method, and unsupervised method spectra reduced spectral noise. Figure 5 shows the input, supervised method, and unsupervised method residuals for a pixel. To compute PSNR, we use the GT as a reference in Figures 4 and 6. The water-hexadecane phase boundary moved between high- and low-SNR recordings (60 mW input power). The input PSNR is 12.1 dB, while the supervised method output is 23.2 dB. Both processing methods improve hyperspectral contrast and reduce noise in unsupervised method [28].

SRS datasets often contain "stitched" spectral scan spectra. These two phenomena are nonlinear optical phenomena. The unsupervised method was tested on a complex lithium ore sample. Weak linear absorption reduces sample power. In this

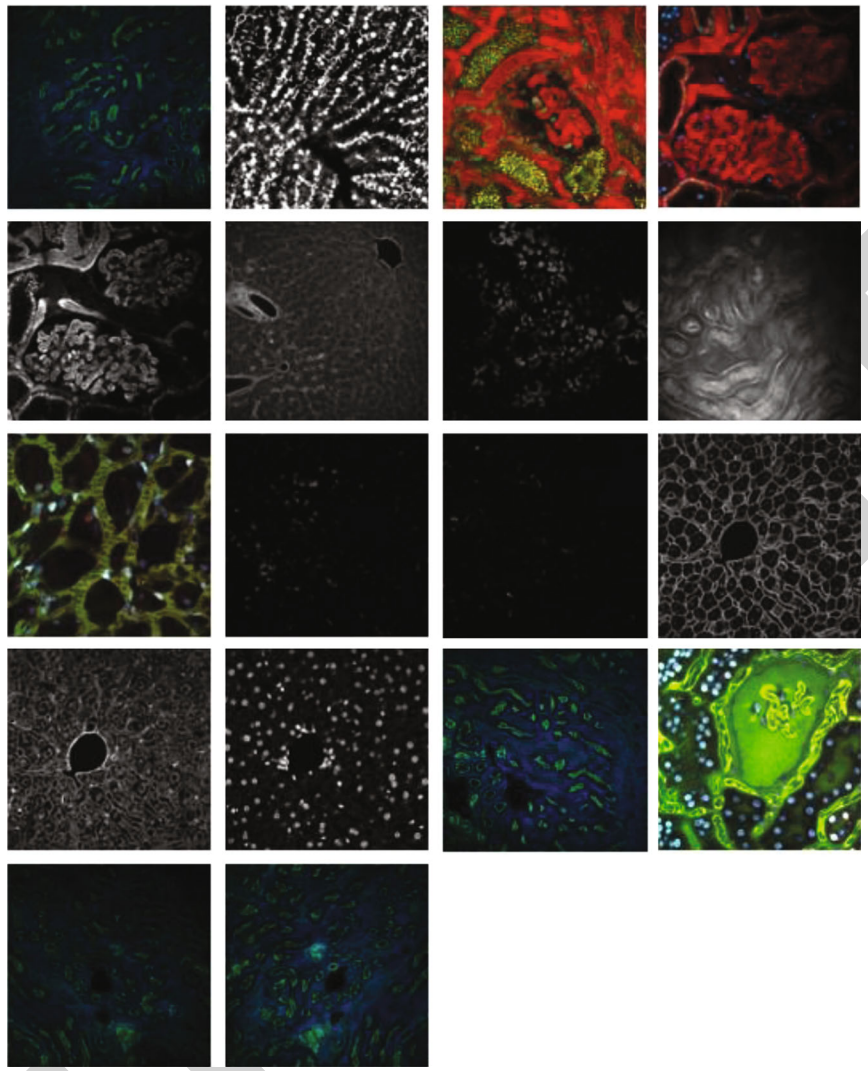

Figure 2: Microscopic dataset list.

sample, the diversity reduces collected signal. In a spectral focus scan, the SRS vibrational spectrum shows the Pump-Stokes delay. We also offer hyperspectral index maps (blue). Noisy image data unsupervised method model on lithium ore is not shown. Its output (red) is shown in Figure 5(a). This method improves SNR while maintaining spectral resolution, less spectral resolution and peak contrast. Then, a 10-pixel average filter (blue), smoothing reduces peak contrast and spectral resolution (b). A high absorption semiconductor material (pyrite) may be present in these mineral samples [29].

The encoder's latent space can be segmented using clustering. Compare directly with known mineral complex spectra [30]. Non-SRS modulation transfer signals are automatically segmented using k-means because they are saturated at the detector. Ingredient-specific unsupervised single-pixel spectra compared to Ref. (black dashed lines). These are the model's spectra. In this case, unsupervised + k-means works well. Easily create chemical species maps from images.

Y / X	Y_1	Y_2	Y_3	Y_4	.....	Y_s	*Sums*
X_1	n_{11}	n_{12}	n_{13}	n_{14}	.....	n_{1s}	a_1
X_2	n_{21}	n_{22}	n_{23}	n_{24}	.....	n_{2s}	a_2
⋮	⋮	⋮	⋮	⋮	⋱	⋮	⋮
X_r	n_{r1}	n_{r2}	n_{r3}	n_{r4}	.....	n_{rs}	a_r
Sums	b_1	b_2	b_3	b_4	.....	b_S	

Figure 3: Contingency matrix table.

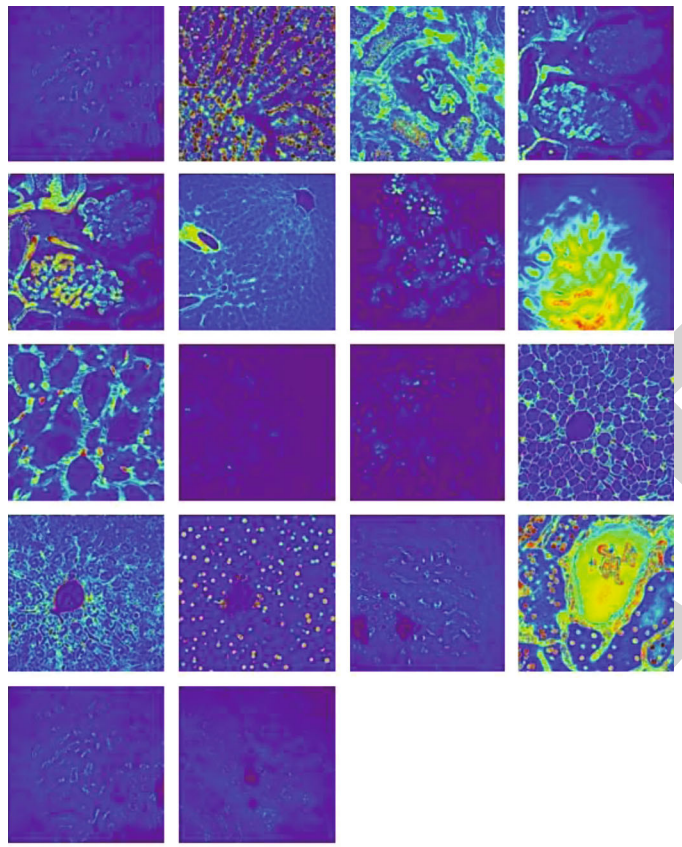

Figure 4: Microscopic segmented dataset list.

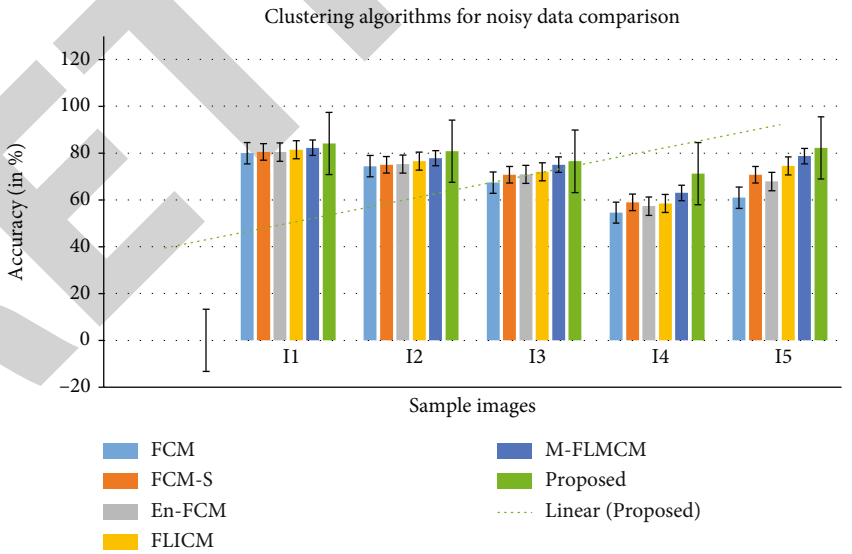

Figure 5: Comparison of clustering algorithms (for noisy data).

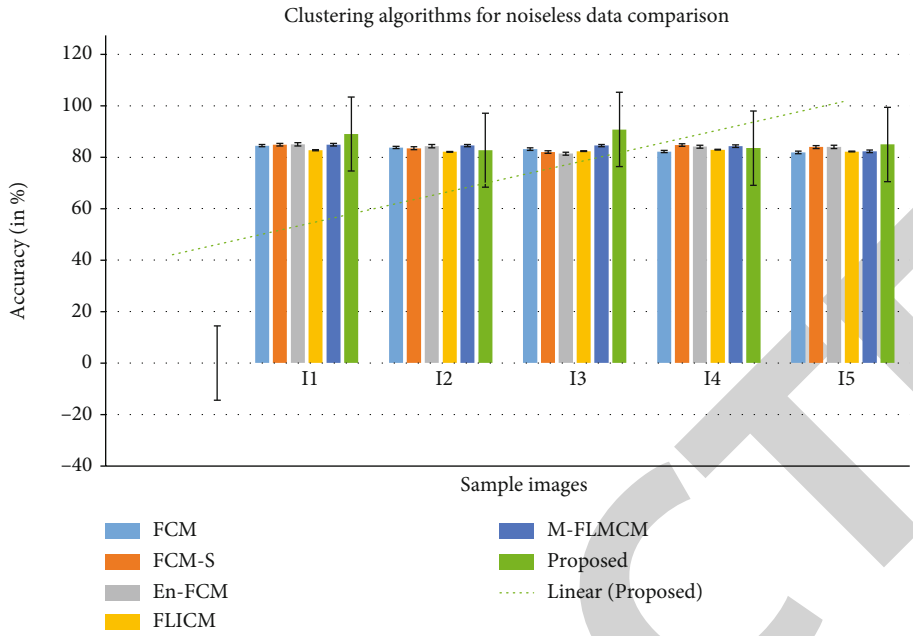

Figure 6: Clustering algorithms for noiseless data comparison.

Table 1: Noisy data comparison on clustering algorithms.

Data	FCM	FCM_S	En-FCM	FLICM	M-FLMCM	Proposed DEC
I1	62.71	72.30	67.22	75.25	81.25	83.10
I2	62.90	71.55	67.95	76.63	81.10	83.38
I3	61.85	73.82	67.12	75.53	80.01	82.86
I4	62.95	74.16	66.97	74.51	79.46	83.16
I5	60.98	70.80	67.86	74.58	78.75	82.25

Table 2: Noiseless data comparison on clustering algorithm.

Data	FCM	FCM-S	En-FCM	FLICM	M-FLMCM	Proposed DEC
I1	84.53	84.88	84.99	82.74	84.89	89.026
I2	83.81	83.52	84.28	82.13	84.56	82.726
I3	83.21	82.07	81.40	82.34	84.57	90.811
I4	82.24	84.79	84.13	82.91	84.31	83.563
I5	81.90	83.96	84.00	82.19	82.33	84.999

Table 3: Noisy variance data comparison on clustering algorithms.

Noise variance	FCM	FCM_S	En-FCM	FLICM	M-FLMCM	Proposed DEC
0.2	81.80	83.16	82.15	83.26	83.62	84.26
0.4	78.08	76.12	78.30	78.97	76.06	79.50
0.6	71.91	73.59	71.70	72.25	71.97	75.00
0.8	68.70	67.53	67.44	66.52	67.39	70.77

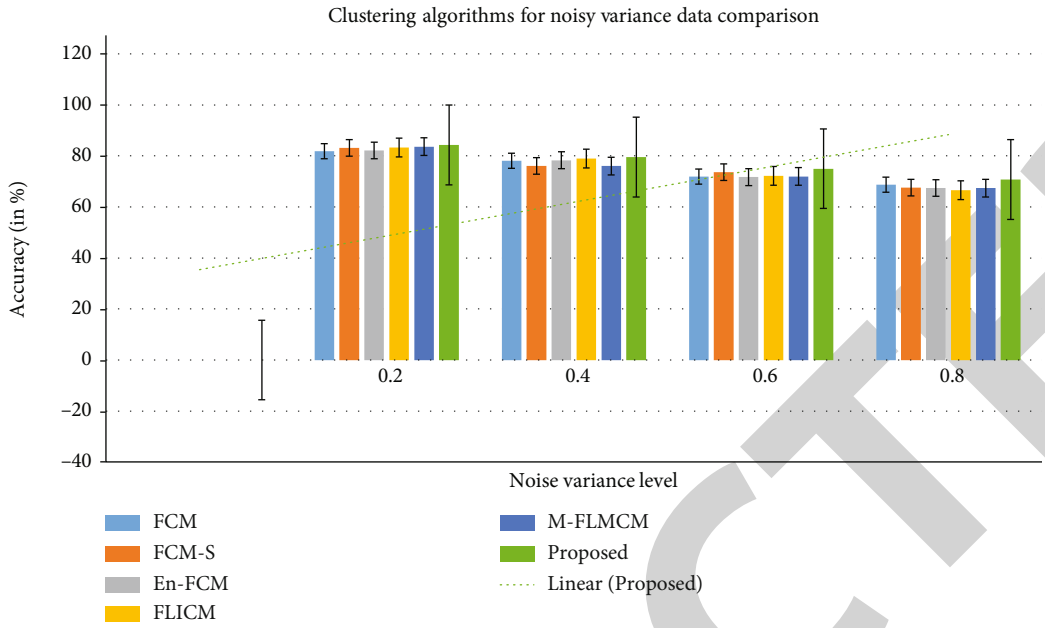

Figure 7: Clustering algorithms for noisy variance data comparison.

The proposed algorithm and FCM versions are tested on 300 samples from various datasets. The results were tested with both Table 1 noisy data and Figure 2 noiseless images to assess the proposed algorithm's property handedness. In the noisy mode of analysis, DEC outperforms other descendants of the FCM (except specific sample). Table 2 and Figure 2 show the proposed DEC comparison result.

The same comparison procedure with noiseless data in Table 3 and Figure 6 compares the DEC and FCM versions. The proposed DEC outperforms the other algorithms. In both noisy and quiet environments, the proposed DEC performs well (Figure 7). For the noise sensitivity test, the image was processed with various noise variances (such as 0.2, 0.4, 0.6, and 0.8).

5. Conclusion

In this work, deep learning was employed to improve contrast and identify chemical species. Index variable for any laser parameter, TL or CPM microscope spectra examples of SRS vibrational spectra SRS contrast enhancement supervised and unsupervised spectra (the latter recorded at high SNR). *k*-means clustering for unsupervised picture segmentation, this chemical species map has several applications. Harmonic generation, fluorescence, and thermal lensing are a few examples. Unsupervised picture denoising and material identification are available globally. Deep learning complements dimension reduction methods effectively. As a preprocessing unit, fraternal *K*-median clustering maintains and enhances the important information available in and via regularization utilizing dropout approach. But even if the dropout probability is larger, the SH-FE techniques are vital in boosting cluster values. The findings and discussions show that the technique devised offers the best outcomes in terms of time complexity and accuracy.

Data Availability

The data used to support the findings of this study are available from the corresponding author upon request.

Conflicts of Interest

The authors declare that they have no conflicts of interest.

Authors' Contributions

Mr. Ajay P was responsible for content development and research contributions. Dr. Nagaraj B was responsible for content development and research contributions. Dr. R. Arun Kumar was responsible for data implementation and processing. Mr. Ruihang Huang was responsible for data modification and image enhancements. Ms. Ananthi P was responsible for data and algorithm-based output result generation.

References

[1] Y. Ren, K. Hu, X. Dai, L. Pan, S. C. Hoi, and Z. Xu, "Semi-supervised deep embedded clustering," *Neurocomputing*, vol. 325, pp. 121–130, 2019.

[2] J. Xie, R. Girshick, and A. Farhadi, "Unsupervised deep embedding for clustering analysis," in *International conference on machine learning*, pp. 478–487, New York, New York, USA, 2016.

[3] Y. Zhang, L. Kang, I. H. Wong et al., "High-throughput, label-free and slide-free histological imaging by computational microscopy and unsupervised learning," *Advanced Science*, vol. 9, no. 2, article 2102358, 2022.

[4] T. D. McRae, D. Oleksyn, J. Miller, and Y. R. Gao, "Robust blind spectral unmixing for fluorescence microscopy using unsupervised learning," *PLoS One*, vol. 14, no. 12, article e0225410, 2019.

Hindawi
Scanning
Volume 2023, Article ID 9836370, 1 page
https://doi.org/10.1155/2023/9836370

Retraction

Retracted: Application of Scanning Magnetic Resonance Imaging in the Diagnosis of Prenatal Placental Implantation and Related Care

Scanning

Received 20 June 2023; Accepted 20 June 2023; Published 21 June 2023

This article has been retracted by Hindawi following an investigation undertaken by the publisher [1]. This investigation has uncovered evidence of one or more of the following indicators of systematic manipulation of the publication process:

(1) Discrepancies in scope

(2) Discrepancies in the description of the research reported

(3) Discrepancies between the availability of data and the research described

(4) Inappropriate citations

(5) Incoherent, meaningless and/or irrelevant content included in the article

(6) Peer-review manipulation

The presence of these indicators undermines our confidence in the integrity of the article's content and we cannot, therefore, vouch for its reliability. Please note that this notice is intended solely to alert readers that the content of this article is unreliable. We have not investigated whether authors were aware of or involved in the systematic manipulation of the publication process.

In addition, our investigation has also shown that one or more of the following human-subject reporting requirements has not been met in this article: ethical approval by an Institutional Review Board (IRB) committee or equivalent, patient/participant consent to participate, and/or agreement to publish patient/participant details (where relevant).

Wiley and Hindawi regrets that the usual quality checks did not identify these issues before publication and have since put additional measures in place to safeguard research integrity.

We wish to credit our own Research Integrity and Research Publishing teams and anonymous and named external researchers and research integrity experts for contributing to this investigation.

The corresponding author, as the representative of all authors, has been given the opportunity to register their agreement or disagreement to this retraction. We have kept a record of any response received.

References

[1] Q. Lin, B. Li, S. Chen et al., "Application of Scanning Magnetic Resonance Imaging in the Diagnosis of Prenatal Placental Implantation and Related Care," *Scanning*, vol. 2022, Article ID 4883989, 7 pages, 2022.

Hindawi
Scanning
Volume 2022, Article ID 4883989, 7 pages
https://doi.org/10.1155/2022/4883989

Research Article

Application of Scanning Magnetic Resonance Imaging in the Diagnosis of Prenatal Placental Implantation and Related Care

Qiuping Lin,[1] **Bizhu Li**,[1] **Shuyun Chen**,[1] **Cairu Lin**,[1] **Zhixia Lin**,[1] **Fengjiao Zhang**,[1] **Xiaojiao Luo**,[1] **Yulin Chen**,[1] **and Biyu Wu**[2]

[1]*Department of Obstetrics and Gynecology, The First Hospital of Quanzhou Affiliated to Fujian Medical University, Quanzhou, Fujian 362000, China*
[2]*The First Hospital of Quanzhou Affiliated to Fujian Medical University, Quanzhou, Fujian 362000, China*

Correspondence should be addressed to Biyu Wu; 1330304142@post.usts.edu.cn

Received 13 April 2022; Revised 8 May 2022; Accepted 13 May 2022; Published 1 June 2022

Academic Editor: Danilo Pelusi

In order to solve the problem of scanning magnetic resonance imaging in prenatal diagnosis, the application and research of placental implantation have been proposed. Placental implantation is a serious obstetric emergency, which refers to the abnormal attachment of placental villi caused by the dysplasia of decidual basal layer. A study from the United States showed that the incidence of placental implantation in pregnant women during delivery increased from 9.9/30000 to 11.6/20000 from 2006 to 2019, which increased the risk of prenatal or postpartum hemorrhage, hysterectomy, stillbirth, abdominal organ injury, and so on. Clinically, patients can show severe prenatal or postpartum hemorrhage, postpartum placental retention, uterine perforation, and secondary infection, which may seriously endanger the lives of pregnant mothers and fetuses. Placental implantation can also have no obvious symptoms before delivery, which leads to insufficient prenatal diagnosis. Gielchinsky retrospectively studied 410 patients with placental implantation and found that only 9 patients were detected by prenatal ultrasound or magnetic resonance imaging (MRI), and the detection rate was only 6.6%. It can be seen that if the accurate diagnosis of placental implantation can be made before prenatal or symptoms appear, clinical intervention treatment can be carried out in time to reduce the probability of hysterectomy and improve the examination means of patients' prerecovery. At present, studies at home and abroad suggest that it has good clinical application value and research prospect in the clinical diagnosis of placental implantation.

1. Introduction

Placental implantation is an abnormal placental implantation caused by the local deletion and interruption of the decidua fundus due to the hypoplasia or injury of the uterus, and the placental chorionic trophoblast invades the myometrium through the missing part, even breaks through the serosa, and involves the tissues and organs next to the uterus. According to the depth of placental villi implanted into the myometrium, they are divided into three types.

① Adherent placenta accreta refers to placental villi attached or adhered to the superficial muscle layer, but did not invade the deep muscle layer. ② Placenta implanta (placenta impleta) is that the placenta is implanted into the deep muscle layer without reaching the serosa layer. ③ Placenta perforta is the most serious type of placental villi penetrating the muscular layer and involving the serosa layer and even adjacent tissues and organs. The risk factors of placenta implantation are often related to endometrial trauma, endometrial dysplasia, and other factors. Because the cause of placental implantation may be endometrial damage, in addition to cesarean section, multiple uterine cleaning history, other intrauterine operation history, and intrauterine infection are also risk factors of placental implantation. Other studies have shown that older pregnancy (age > 35 years) is also one of the independent risk factors of placenta implantation. Some scholars have shown that assisted reproductive technology is another independent risk factor for placental implantation, as shown in Figure 1.

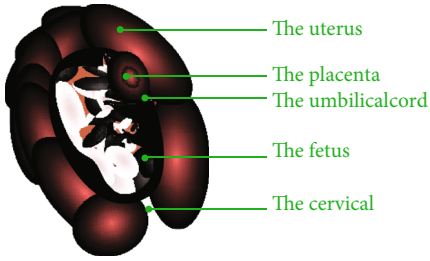

Figure 1: MRI diagnosis of placental implantation.

2. Literature Review

Placental implantation is a lesion caused by hypoplasia of uterine decidua and invasion of villous tissue into uterine myometrium. Pathologically, placental implantation without decidua as an intermediary is called placental implantation. Placental implantation can be classified according to the depth of placental villi invading the myometrium, which can generally be divided into three types. Adherent placenta refers to the villi attached to the myometrium of the uterus. This type may be stripped by itself. If part of the uterine cavity remains, it can be stripped manually. Placenta accreta is due to the invasion of villi into the myometrium. At this time, it is difficult for the placenta to peel off by itself. Generally, it cannot be peeled off manually, but the overall depth has not reached the serosa layer. Penetrating implantation means that the placental villi invade the myometrium and penetrate the serosa, invade the bladder or infiltrate the parauterine tissue, and the surrounding blood flow is rich. Usually, hysterectomy and even bladder repair are needed. Once placenta implantation occurs, it is a serious obstetric complication, an important cause of postpartum hemorrhage, puerperal infection, and uterine perforation and a great threat to the life and health of pregnant women and perinatal infants. 0'Brien and others reported that the incidence rate was about 2/640 to 1/920002 in 1997. But in recent years, the incidence rate of placenta accreta has increased due to the increase of age and age of uterus and the increase of intrauterine operation [1].

Prince and others believe that half-Fourier single excitation fast spin echo sequence (Haste) is the best sequence for the diagnosis of placental implantation, which is better than two-dimensional fast steady-state precession sequence (TrueFISP). The main reason is that it has fast scanning speed, reduces motion artifacts, and can obtain high-quality images [2]. Saunders and others believe that HASTE sequence signal is insensitive to fetal movement compared with TrueFISP sequence, produces less artifacts, and increases the resolution between tissues with different water content [3]. Some researchers also used single-shot fast spin echo (FSE), fast spin echo (TSE), and fast steady-state precession sequence to evaluate the placental position and the depth of invasion to the surrounding tissues. Others used T1 fat suppression sequence image to evaluate the situation of periplacental hemorrhage. Ghafoori and others did not find that diffusion weighted imaging can improve the accuracy of MRI in the diagnosis of placental implantation. Foreign scholars have found that the signal difference between placenta and uterine muscle wall of DWI sequence with $B = 1000\,\mathrm{s/mm^2}$ is more obvious than that of T2WI [4]. In the study of postpartum placental implantation, Terpos found that in DWI sequence, high-signal placenta and relatively low-signal uterine wall were more obvious than T2WI image [5]. Venkatasubramanian et al. proposed that the local bulge of bladder and the invasion of other tissues in pelvic cavity are also strong evidence of placental implantation. Aiming at the imaging signs of uneven signal in placenta, MD proposed that it may be related to the presence of bleeding, dark zone in placenta and increased blood vessels [6]. Ireland studies believe that the appearance of intraplacental dark zone is the strongest evidence of placental implantation, followed by the discontinuity of uterine myometrium and the invasion of adjacent pelvic organs [7]. Duncan believes that placental implantation has the following specific signs. ① The lower segment of the uterus is convex or swollen. ② The placental signal is obviously uneven. Prenatal manifestations during implantation can have different audiovisual characteristics [8]. Wang and others showed that the three-dimensional color Doppler ultrasound image of placental implantation had the following characteristics. ① The blood vessels around the placenta were increased and irregular. ② Pulse perfusion or turbulence is accompanied in the dark area of echo; that is, the blood flow of placental cavity is formed [9]. Yuan and others analyzed 8 patients with lacunar blood flow sonograms by ultrasound and confirmed that 7 cases were placenta accreta, which may be related to the abnormal microvascular dynamics in the villous space. The formation of lacunar blood flow may be due to the low decidual response of such placentas, resulting in the invasion of extravillous trophoblasts into the deep muscle layer. At this time, the blood vessels originally limited to the spiral arterioles expand and then extend to the larger arcuate artery. The high pulse pressure blood flow of the deep artery forms the lacunar blood flow under ultrasound [10].

Based on the current research, the application and research of placental implantation are proposed. Placenta accreta refers to the abnormal attachment of placental villi caused by the dysplasia of decidual basal layer. It is a serious obstetric emergency. In recent years, with the increase of intrauterine operation, the incidence of placental implantation is increasing year by year. Due to the differences in ethnic genetics and diagnostic level between regions, the current literature reports that the incidence of placental implantation ranges from 3/543 to 2/2205. Its complications mainly include injury of adjacent organs, intrauterine infection, and massive bleeding caused by incomplete separation of placenta during delivery. In addition, spontaneous uterine rupture in the second and third trimester of pregnancy, hemorrhagic shock, and intraperitoneal hemorrhage are also important causes of maternal death. Therefore, clinical correct and timely diagnosis of placental implantation is conducive to full prenatal preparation, reduce the complications caused by placental implantation, and then reduce the mortality of pregnant women and perinatal infants [11].

3. Application of Magnetic Resonance Imaging in the Diagnosis of Prenatal Placental Implantation and Related Nursing Research

3.1. Application of MRI in the Diagnosis of Placenta Previa and Placental Implantation. Placenta previa means that the lower edge of the placenta is close to the inner mouth of the cervix, and the distance is less than 3 cm. Placental implantation is decidual dysplasia, which leads to the invasion of placental villi into the myometrium, or serosa in severe cases, and may even involve the concave of adjacent pelvic organs. Placenta accreta is the main reason for maternal perinatal hemorrhage and postpartum hysterectomy. Placenta accreta is an important factor in incidence rate and mortality of pregnant women. The increasing prevalence of placental implantation may be related to the increasing proportion of elderly pregnant women and previous history of abortion and/or cesarean section. Accurate and timely diagnosis provides an important basis for the formulation of clinical operation plan. In the past, the imaging diagnosis of placental related diseases mostly relied on ultrasound, but there is an urgent need for an imaging that can provide more information [12].

3.1.1. Risk Factors of Placenta Previa and Placental Implantation. The specific etiology of placenta previa and placental implantation needs to be confirmed by further research, but a large number of studies have found that multiple intrauterine operations are high-risk factors. Cesarean section is an important risk factor. With the increase of cesarean section rate, placenta implantation incidence rate is also on the rise. The study found that the two independent risk factors of placental implantation were placenta previa and elderly pregnant women (age ≥ 36 years). Classification of placenta previa and pathological classification of placental implantation placenta previa is divided into three types according to the distance between the lower edge of placenta and the cervical opening. When the lower edge of the placenta is less than 3 cm away from the cervical opening but does not reach the cervical opening, it is called marginal placenta previa. When the lower edge of the placenta partially covers the cervical opening, it is called partial placenta previa, and when the lower edge of the placenta completely covers the cervical opening, it is called complete placenta previa. Placental implantation can be divided into three types according to the depth of villi infiltration into the myometrium: placental adhesion refers to the insertion of placental villi into the myometrium; placental implantation refers to the penetration of placental villi into the myometrium; penetrating placenta refers to the penetration of placental villous tissue into the serosa of the uterus [13].

3.1.2. Clinical Manifestations of Placenta Previa and Placental Implantation. Placenta previa is easy to cause painless vaginal bleeding in the second and third trimester of pregnancy. Generally speaking, the lower the position of placenta previa, the earlier the bleeding time and the more bleeding times. It can cause potentially life-threatening serious complications, including anemia, shock, disseminated intravascular coagulation, uterine rupture, and fetal distress [14].

Placental implantation is usually characterized by prolonged third stage of labor or partial placental residue, which can cause postpartum hemorrhage and infection. Placenta accreta is a high-risk factor for uterine varus. Placenta previa and placental implantation are important causes of perinatal bleeding [15].

3.1.3. Clinical Manifestations and Classification. According to the degree of placenta implantation into uterine myometrium, it can be divided into ① adherent placenta (shallow implantation), with only placental villi attached to the myometrium of the uterus; ② implantable placenta (deep implantation), the placental villi invaded the myometrium deeply; ③ penetrating placenta (deeper implantation), the placental villi invade deep into the serosa of the uterus and even penetrate the serosa to reach the bladder or rectum. In addition, according to the different degrees of placental attachment and its implantation and penetration area, it can be divided into partial placental implantation and complete placental implantation [16].

There are great differences in clinical manifestations according to the depth, scope, and location of placental implantation: pregnant women with shallow placental implantation depth and small implantation range may have no special manifestations during pregnancy. During delivery and after fetal delivery, some patients may have difficulty or even no placental stripping; pregnant women with deep placental implantation and a wide range of placentas are often characterized by nonseparation of the placenta and even active massive bleeding during delivery. More serious is the rupture of the uterus in the middle and third trimester of pregnancy, resulting in massive abdominal bleeding, which endangers the lives of mothers and infants [17].

3.2. Differential Diagnosis of Placenta Previa and Placental Implantation. Sagittal T2-weighted image is considered to be the main sequence to judge placenta previa. It mainly measures the distance between the lower edge of the placenta and the internal orifice of the cervix. It is easier to distinguish normal placenta or placenta previa and different types of placenta previa. The correct diagnosis of placental implantation is directly related to the choice of clinical treatment strategies, so the relevant differential diagnosis is very important. (1) Differentiation between normal placenta and slight placental implantation, i.e., placental adhesion: it mainly depends on whether the signal of uterine junction zone is continuous, but sometimes it must be distinguished by some indirect signs, such as the loss of normal pear shape in the lower segment of the uterus or the low-signal dark zone of T2-weighted image in placenta. (2) Identification of placental adhesion, placental implantation, and penetrating placental implantation: some scholars believe that it is extremely difficult to identify placental adhesion and placental implantation when there is no invasion of parauterine tissue. At this time, it mainly depends on the interruption of uterine wall signal. When there is parauterine infiltration and the most common bladder invasion, it indicates penetrating placental implantation. (3) The main distinguishing point between postpartum placental detachment and postpartum placental implantation is whether the uterine

junction zone is complete. When MRI plain scanning is difficult to distinguish, enhanced scanning is widely used as a better examination method. The blood supply of placenta accreta is rich, and obvious enhancement can be seen on enhanced scanning [18].

3.3. Relationship between Placenta Previa and Placental Implantation. Placenta previa and placenta accreta are common placental-related diseases. Accurate diagnosis plays an important role in improving the prognosis. Existing studies have not fully explained the causes of placenta previa and placental implantation, but existing studies have shown that the placental implantation rate of pregnant women with placenta previa is 9%, while that of pregnant women without placenta previa is reduced to 0.006%. It can be seen that placenta previa is a high-risk factor of placental implantation. In other words, there is no necessary connection between the two, but in this study, because the enrolled patients have been confirmed as cases of placenta previa, some data can be used as a reference for the exploration and research of placenta previa with placenta implantation [19].

In recent years, it has been called dangerous placenta previa with a history of cesarean section and placenta previa. The reason is that the probability of placenta implantation in this case is greatly increased, especially placenta accreta or even penetrating placenta implantation, which will be involved in the later discussion [20].

3.4. High-Risk Factors of Placenta Implantation. Studies have shown that the incidence of placental implantation in recent years has increased 13 times compared with that in the early 20th century, which increases the risk of prenatal or postpartum hemorrhage, hysterectomy, stillbirth, abdominal organ injury, and so on. Clinically, patients can show severe prenatal or postpartum hemorrhage, postpartum placental retention, uterine perforation, and secondary infection, which seriously endangers the safety of pregnant mothers and fetuses.

First, the occurrence of placental implantation may be related to previous endometrial injury. Washecka and others found through 23 pregnant women diagnosed with placental implantation induced abortion, excessive curettage, multiple abortion, intrauterine infection, high number of pregnancies and births, history of placental detachment by hand, endometritis, and other history that may damage the endometrium are closely related to the occurrence of placental implantation. In this study, 46 patients in the placenta implantation group had a history of curettage, myomectomy, and cesarean section, while only 46 patients in the nonplacenta implantation group had a history of endometrial injury, which also confirmed that endometrial injury may increase the risk of placenta implantation. The possible mechanism of this process is that the endometrial basal layer is destroyed due to the above operating factors, and the endometrial functional layer cannot be effectively repaired due to various reasons. When pregnancy occurs again, the basal decidua at the implantation site may be stunted or even absent. At this time, the villi will become an implantable placenta by directly implanting into the myometrium [21].

Table 1: Surgical diagnosis and pathological diagnosis.

Adhesiveness		Implantation	Pierce through	No PA	Total
Adhesiveness	12	5	7	2	0
Implantability	11	5	4	10	20
Penetrability	0	5	4	2	12
Total	23	15	15	14	22

Table 2: Comparative analysis of MRI abnormal signs in the PA group and the non-PA group.

Abnormal MRI findings	PIA group	Non-PIA group	X^2	P value
Intraplacental vessels	20	3	11.36	0.003
Uterine enlargement	16	1	2.36	0.062
Interruption of uterine boundary	14	5	3.23	0.23

Table 3: Comparison of MRI and ultrasound diagnosis of placenta previa.

MRI examination	Ultrasonic examination		
Consistent with postoperative diagnosis	46	12	58
Does not meet the postoperative diagnosis	1	2	1
Total	47	14	59

4. Experiment and Research

4.1. Comparison of Consistency between MRI Diagnosis of Placental Implantation and Surgical or Histopathological Results. In this study, method B has the highest diagnostic accuracy, so method B is compared with surgical and pathological results. Method B was used to diagnose 18 cases of PIA and 26 cases without PIA. There were 31 cases with PIA and 13 cases without PIA. The PIA diagnosis of MRI was statistically correlated with intraoperative diagnosis and histopathological diagnosis. The kappa coefficient test between them has good consistency (kappa = 0.624); that is, MRI diagnosis (method B) PIA has good consistency with surgical diagnosis and pathological diagnosis. Table 1 shows the cross list of MRI results (method B) and surgical pathological results.

4.2. Analysis of MRI Signs of Placental Implantation. There were 62 abnormal MRI signs in this group, of which 10 cases showed only one abnormal MRI sign, including 7 FP cases and 3 TP cases in method A. 61 signs appeared in the PIA group, including 16 cases of interruption of uterine boundary, 7 cases of interruption of myometrial signal, 4 cases of bladder changes (0 signs of invasion of other adjacent uterine tissues), 18 cases of intraplacental dark zone, 8 cases of intraplacental blood vessels, and 9 cases of uterine dilatation. 11 abnormal signs appeared in the non-PIA group, including 3 cases of intraplacental dark zone, 6 cases of interruption of uterine boundary, 2 cases of interruption of

Table 4: Comparison of MRI and color Doppler ultrasonography in diagnosis of placenta previa.

MRI examination	Color Doppler ultrasound examination		
Postoperative diagnosis of color Doppler ultrasound	12	16	7
Color Doppler ultrasound does not meet the postoperative diagnosis	3	3	1
Total	15	19	8

myometrial signal, 1 case of bladder change, 1 case of intraplacental blood vessel, and 2 cases of uterine dilatation. Fisher's exact probability method was used to compare the placenta implantation group with the nonimplantation group. It was found that there were statistically significant differences between the two groups in three signs: intraplacental dark zone, focal interruption of uterine boundary, and lower uterine enlargement, as shown in Table 2 [22].

4.3. Comparison between MRI and Ultrasound Diagnosis of Placenta Previa. In this study, 56 patients were diagnosed as placenta previa after cesarean section. The diagnostic coincidence rate of ultrasound was 79.36% (47/67), and the diagnostic coincidence rate of MRI was 99.00%. After comparison, the diagnostic coincidence rate of the two examination methods was statistically significant, that is, $P < 0.09$. In this study, 10 cases of complete placenta previa were misdiagnosed as marginal placenta previa and partial placenta previa by ultrasonography, and 1 case was missed. In contrast, there were no missed or misdiagnosed cases in MRI diagnosis, and the diagnostic coincidence rate was 99.00%. See Table 3 [23].

4.4. Analysis of MRI and Color Doppler Ultrasound in the Diagnosis of Placental Implantation. The pathological results (gold standard examination) of 77 patients with placental implantation (PIA) were confirmed in 28 cases and 27 patients without placental implantation. MRI showed that PIA was positive in 32 cases and negative in 24 cases; 9 cases of positive diagnosis were confirmed as normal placenta by the gold standard, and 24 cases of negative diagnosis were confirmed as normal placenta by the gold standard, so 9 cases were misdiagnosed without missed diagnosis. Color Doppler ultrasonography showed that 20 cases were PIA positive and 36 cases were negative; 4 positive cases were confirmed as normal placenta after operation, and 12 negative cases were confirmed as placenta implantation by gold standard, so 4 cases were misdiagnosed and 12 cases were missed. The coincidence rate of MRI in the diagnosis of placental implantation was 83.93%, and that of ultrasound in the diagnosis of placenta previa was 78.43% [24]. The comparison of MRI and color Doppler ultrasound diagnosis results of PIA is shown in Table 4.

4.5. Relationship between Diagnosis of Placental Implantation and Age Distribution of Patients. Age distribution of 104 patients with suspected placental implantation: 23 (46.1%) in the group without placental implantation and 11 (21.8%) in the group with placental implantation within the age range of 20-29; 17 (35.3%) in the group without placenta implantation and 21 (39.6%) in the group with placenta implantation within the age range of 30-34. There were 11 (22.6%) in the nonplacenta implantation group and 21 (37.6%) in the placenta implantation group. The relationship between diagnosis and age distribution of patients with placental implantation is shown in Table 5.

Table 5: Relationship between diagnosis and age distribution of patients with placental implantation.

Age	Placenta-free group	Placenta implantation group
30-39	24	15
40-49	15	23
>30	13	26

Table 6: MRI scanning parameters.

	SS-FS	FRIM	ERTA
Repetition time	Infinity	4.0	7
Layer thickness	80	1.9	4.9
Echo time	6	9	2
Number of layers	20-40	30-40	50

4.6. Research Object. From January 2017 to December 2018, 54 pregnant women with suspected placental implantation and prenatal MRI in Hulunbuir Hospital were selected as the research objects. The age of pregnant women was 24~41 years old, and the gestational weeks were 28~38 weeks at the time of MRI examination. In this group, 6 cases were primipara, the other 48 cases had one or more pregnancies, 26 cases had a history of cesarean section, 3 cases had a history of secondary cesarean section, and 0 cases had a history of three or more cesarean sections. 13 cases had a history of spontaneous labor. 27 cases had a history of one or more intrauterine operations such as curettage or hysteroscopy [25].

4.6.1. Preparations before Inspection. It is recommended that pregnant women hold their urine moderately to make the bladder in a semifilled state so that the urine can form a clear contrast with the bladder wall. It is not recommended to overfill, which will cause pregnant women unable to tolerate the examination or produce motion artifacts due to discomfort. Before the examination, eliminate the absolute contraindications and relative contraindications of MRI, remove the magnetic clothes and articles on the patient, inform the precautions, and appease the emotion so that the pregnant woman can better cooperate with the examination.

4.6.2. MRI Scanning Sequence and Parameters. Scanning orientation includes horizontal position, sagittal position, and

coronal position. MRI scanning sequences include coronal balanced steady-state acquisition (FIESTA), single-shot FSE (SSFSE), horizontal and sagittal balanced steady-state acquisition (FIESTA), and sagittal single-shot FSE (SS-FSE). In the fast version recovery motion inhibitory (firm) sequence, the coronal position was scanned first, the sagittal position was scanned parallel to the long axis of the placenta, and the axial position was scanned perpendicular to the long axis of the placenta. The positioning lines were copied between the sequences in the same direction.

As there are still some disputes about the safety of contrast medium to the fetus and there are no relevant technical guidelines or specifications for pregnant women to use contrast medium in China, enhanced scanning is not used as a routine examination in this study. The scanning parameters are shown in Table 6.

5. Conclusion

MRI provides a more accurate, objective, and comprehensive image diagnosis for the diagnosis of patients with placental-related diseases. Some scholars have proposed that MRI should be used as the routine examination P3 of placenta previa and suspected cases of placental implantation. It has broad application prospects in clinic and will better serve the majority of patients. In addition, pregnant women with intravesical hemorrhage and placental hemorrhage in the second trimester of pregnancy can also be caused by maternal shock and placental hemorrhage, which can also be harmful to pregnant women. MRI has become an important method for the diagnosis of placenta previa and placental implantation because of its high soft tissue resolution and large imaging range. The application of MRI can improve the accuracy of placenta implantation diagnosis. Through the continuous exploration of the image characteristics of MRI placental-related diseases, MRI will play an increasingly important role in the diagnosis of placenta previa and placental implantation, providing a broader space for clinical work.

Data Availability

The data used to support the findings of this study are available from the corresponding author upon request.

Conflicts of Interest

The authors declare that they have no conflicts of interest.

References

[1] R. Chana, A. Noorani, N. Ashwood, U. Chatterji, J. Healy, and P. Baird, "The role of MRI in the diagnosis of proximal femoral fractures in the elderly," *Injury extra*, vol. 37, no. 2, pp. 185–189, 2006.

[2] S. E. Prince, S. Woo, P. M. Doraiswamy, and J. R. Petrella, "Functional MRI in the early diagnosis of Alzheimer's disease: is it time to refocus?," *Expert Review of Neurotherapeutics*, vol. 8, no. 2, pp. 169–175, 2008.

[3] C. Saunders and D. Taylor, "Expanding the indications for MRI in the diagnosis and treatment of breast cancer: what is best practice?," *Journal of Medical Radiation Sciences*, vol. 62, no. 1, pp. 47–53, 2015.

[4] M. Ghafoori, "MRI in the diagnosis of diphallia: a case report," *Iranian Journal of Radiology*, vol. 5, no. S1, 2008.

[5] E. Terpos, V. Koutoulidis, S. Fontara et al., "Diffusion-weighted imaging improves accuracy in the diagnosis of MRI patterns of marrow involvement in newly diagnosed myeloma: results of a prospective study in 99 patients," *Blood*, vol. 126, no. 23, p. 4178, 2015.

[6] C. Venkatasubramanian, N. Fischbein, A. Finley-Caulfield et al., "Abstract 3220: does multimodality MRI have added benefit in the diagnosis and management of "classic" hypertensive intracerebral hemorrhage?," *Stroke*, vol. 43, suppl_1, 2012.

[7] R. Ireland, "How effective is ferumoxtran-10 MRI in the diagnosis of lymph node metastases?," *Nature Reviews Clinical Oncology*, vol. 3, no. 4, pp. 176-177, 2006.

[8] J. S. Duncan and J. D. Tisi, "MRI in the diagnosis and management of epileptomas," *Epilepsia*, vol. 54, pp. 40–43, 2013.

[9] M. Wang, H. Gong, and X. Xiao, "Evaluation of MRI and CT in the diagnosis of cholelithiasis: a comparative study," *Journal of Clinical Radiololgy*, vol. 22, no. 5, pp. 397–400, 2003.

[10] W. Yuan and L. Y. Dai, "MRI in the diagnosis of avascular necrosis of the femoral head," *Chinese Journal of Orthopaedics*, vol. 32, no. 9, p. 528, 1996.

[11] B. Francis, S. Pascale, B. Nathalie, B. Alexandra, and D. Yves, "MRI and fetal multidetector CT in the diagnosis of fetal malformations," *Bulletin De Lacadémie Nationale De Médecine*, vol. 192, no. 8, pp. 1573–1584, 2008.

[12] F. D. Paulis, A. Grossi, A. Cacchio, A. Barile, and A. D. Antoni, "The role of MRI in the early diagnosis of unilateral chondral overloading injuries of the athletic knee," *Operative Techniques in Sports Medicine*, vol. 8, no. 1, pp. 15–18, 2000.

[13] M. O. Rodríguez, A. Carbajal, R. M. G. Ramón, and R. C. Hevia, "Vein of galen malformation in an adult: MRI diagnosis," *Radiología*, vol. 49, no. 5, p. 347, 2007.

[14] A. Goyal, D. N. Srivastava, and T. Ansari, "MRI in de quervain tenosynovitis: is making the diagnosis sufficient?," *AJR American Journal of Roentgenology*, vol. 210, no. 3, pp. W133–W134, 2018.

[15] X. Shi, T. Du, D. Zhu, D. Ma, and Y. Yang, "The high-dose dexamethasone suppression test is inferior to pituitary dynamic enhanced MRI in the differential diagnosis of ACTH-dependent Cushing's syndrome," *Endocrine*, vol. 75, no. 2, pp. 516–524, 2022.

[16] M. S. Brown, S. Meraj, and D. Walz, "Reply to "MRI in de quervain tenosynovitis: is making the diagnosis sufficient?"," *American Journal of Roentgenology*, vol. 210, no. 3, pp. W135–W135, 2018.

[17] T. Nurm, P. Torres, and J. R. Ramaskandhan, "Is magnetic resonance imaging (MRI) reliable in the diagnosis of osteochondral lesions (ocl's)?," *Foot & Ankle Orthopaedics*, vol. 2, no. 3, p. 2473011417S0000, 2017.

[18] U. Baum and G. G. Grabenbauer, "Thin-layer spiral CT is superior to MRI in the diagnosis of local extent of pancreatic carcinoma," *Strahlentherapie und Onkologie*, vol. 175, no. 11, pp. 583-584, 1999.

[19] M. Fujii and J. Kanzaki, "The role of MRI for the diagnosis of recurrence of nasopharyngeal cancer," *Auris Nasus Larynx*, vol. 21, no. 1, pp. 32–37, 1994.

Hindawi
Scanning
Volume 2023, Article ID 9794806, 1 page
https://doi.org/10.1155/2023/9794806

Retraction

Retracted: Application of Color Doppler Ultrasound in Microscopic Imaging Diagnosis of Adenomyosis

Scanning

Received 20 June 2023; Accepted 20 June 2023; Published 21 June 2023

This article has been retracted by Hindawi following an investigation undertaken by the publisher [1]. This investigation has uncovered evidence of one or more of the following indicators of systematic manipulation of the publication process:

(1) Discrepancies in scope

(2) Discrepancies in the description of the research reported

(3) Discrepancies between the availability of data and the research described

(4) Inappropriate citations

(5) Incoherent, meaningless and/or irrelevant content included in the article

(6) Peer-review manipulation

The presence of these indicators undermines our confidence in the integrity of the article's content and we cannot, therefore, vouch for its reliability. Please note that this notice is intended solely to alert readers that the content of this article is unreliable. We have not investigated whether authors were aware of or involved in the systematic manipulation of the publication process.

In addition, our investigation has also shown that one or more of the following human-subject reporting requirements has not been met in this article: ethical approval by an Institutional Review Board (IRB) committee or equivalent, patient/participant consent to participate, and/or agreement to publish patient/participant details (where relevant).

Wiley and Hindawi regrets that the usual quality checks did not identify these issues before publication and have since put additional measures in place to safeguard research integrity.

We wish to credit our own Research Integrity and Research Publishing teams and anonymous and named external researchers and research integrity experts for contributing to this investigation.

The corresponding author, as the representative of all authors, has been given the opportunity to register their agreement or disagreement to this retraction. We have kept a record of any response received.

References

[1] J. Zhu, S. Liu, and D. Gao, "Application of Color Doppler Ultrasound in Microscopic Imaging Diagnosis of Adenomyosis," *Scanning*, vol. 2022, Article ID 2366871, 7 pages, 2022.

Hindawi
Scanning
Volume 2022, Article ID 2366871, 7 pages
https://doi.org/10.1155/2022/2366871

Research Article

Application of Color Doppler Ultrasound in Microscopic Imaging Diagnosis of Adenomyosis

Jianchang Zhu, Shuang Liu, and Dandan Gao

Ultrasonic Center, Huaibei Maternal and Child Health Hospital, Huaibei Anhui 235000, China

Correspondence should be addressed to Jianchang Zhu; 11233312@stu.wxic.edu.cn

Received 21 April 2022; Revised 8 May 2022; Accepted 13 May 2022; Published 31 May 2022

Academic Editor: Danilo Pelusi

In order to explore the value of color Doppler ultrasonography (TVCDS) in the diagnosis and differential diagnosis of adenomyosis. A total of 150 patients with adenomyosis admitted to a hospital from January 2020 to December 2021 were selected, taking transvaginal three-dimensional color Doppler ultrasound and abdominal ultrasound for examination, all results were compared with patient pathology or surgical results, in order to compare the accuracy of the two inspection methods. The positive predictive value of three-dimensional color Doppler ultrasonography was higher than that of abdominal ultrasonography, and the difference was statistically significant ($P < 0.05$). The coincidence rate, sensitivity, and specificity of three-dimensional color Doppler ultrasonography were higher than those of abdominal ultrasonography, while the misdiagnosis rate was lower than that of abdominal ultrasonography, and the differences were statistically significant (all $P < 0.05$). The imaging features of vaginal three-dimensional color Doppler ultrasound in patients with adenomyosis are mainly enlarged uterus, slightly stronger echoes in the myometrium with enhanced echogenic spots, and short or short branch blood flow signals in the lesions. After statistical analysis, there was a significant difference in the blood flow changes between benign and malignant endometrial echoes and abnormal echoes in the uterine cavity, $P < 0.05$. Normal endometrium and benign intrauterine lesions mainly showed no blood flow signal, while malignant lesions in the uterine cavity mostly showed changes in blood flow signal. Compared with abdominal examination, transvaginal color Doppler ultrasonography has obvious advantages in the diagnosis of adenomyosis. According to the characteristics of ultrasound images, blood flow distribution, frequency spectrum, etc., it can provide a more accurate basis for clinical timely, provide the identification points of uterine fibroids, and provide help for clinicians to choose a treatment plan.

1. Introduction

Uterine fibroids refer to a solid mass formed by the proliferation of smooth muscle cells, containing a small amount of fibrous connective tissue inside, with clear and smooth borders. In addition, there is a pseudocapsule composed of muscle fiber bundles and loose connective tissue. Adenomyosis is a common gynecological disease clinically, and it mostly occurred in multiparous women over 40 years old in the past, but in recent years, there is a tendency to be younger. The main cause is the invasion of endometrial glands and stroma into the myometrium, resulting in localized or diffuse lesions. Studies have shown that the disease is related to artificial abortion, cesarean section, and other surgeries [1]. There are many treatment methods for this disease, and it is necessary to choose an appropriate treatment method after comprehensive consideration of the patient's age, course of disease, reproductive requirements, and clinical symptoms. Therefore, accurate diagnosis of the disease is of great significance for physicians to choose scientific treatment methods. Clinically, histological examination and imaging examination can be used for the diagnosis of adenomyosis, histological examination is the most accurate method, imaging examination is the most effective method for preoperative diagnosis, and the process is shown in Figure 1. Clinically, the manifestations of patients with adenomyosis are quite different, a few patients do not have significant clinical features, and most patients have dysmenorrhea, therefore, it is difficult for physicians to make a diagnosis based on clinical symptoms alone [2]. Most patients

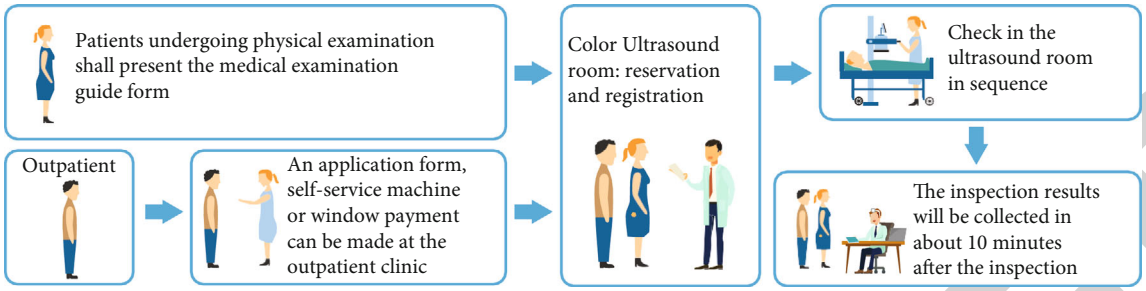

Figure 1: Flow chart of Doppler ultrasound.

with adenomyosis are found to have the disease during the process of receiving imaging tests for other diseases, or during a health check-up, for patients with adenomyosis, in the process of diagnosing adenomyosis using magnetic resonance imaging, due to its relatively high price, it has certain limitations. The three-dimensional color Doppler ultrasound has the characteristics of simplicity, convenience, and relatively low price and has gradually been widely used in clinical practice. The author mainly analyzes the clinical diagnostic value of color Doppler ultrasound for adenomyosis, aiming to provide scientific basis for the clinical examination of such diseases and provide reference value for clinical work [3].

2. Literature Review

Xu et al. indicated that adenomyosis is a relatively common gynecological disease in clinical practice, mostly in middle-aged multiparous women, and with the development of society in recent years, people's living environment is becoming more and more polluted, and work pressure is also increasing, which also leads to a younger trend of adenomyosis [4]. Mascaretti et al. stated that the etiology of adenomyosis has not yet been identified, and the consensus on the disease is that endometrial basal layer cells proliferate and invade the myometrium, accompanied by compensatory myometrial cells and hypertrophic hyperplasia [5]. Wei et al. believe that adenomyosis is related to genetics, uterine injury (cut and curettage and cesarean section), hyperestrogenemia, and other factors [6]. Cevoli et al. indicated that the clinical symptoms of adenomyosis are mainly menstrual disorders, dysmenorrhea, etc., and some patients have no obvious clinical symptoms [7]. SAFWAT and others believe that the diagnosis of adenomyosis currently mainly relies on two methods: histopathology and imaging, histopathology is the most accurate method, but its diagnosis is complex and invasive [8]. KHODAIR et al. indicated that imaging is the best preoperative diagnostic method for the disease, and transvaginal ultrasound has a high diagnostic accuracy. Magnetic resonance imaging is also a commonly used diagnostic method, which can more objectively diagnose the location and extent of lesions [9]. Shen et al. stated that the application value of ultrasonography in the diagnosis of obstetrics and gynecology diseases has been witnessed by history, and with the development of medicine and the continuous improvement of medical technology, new ultrasonography technology is widely used in various clinical disciplines. Doctors have brought convenience and speed to the diagnosis and identification of related diseases [10]. Zhi et al. stated that gynecological ultrasonography started from B-mode ultrasound, which could only be operated from the abdomen and developed to transvaginal ultrasound. The resolution of vaginal ultrasound is higher, and with the advent of color Doppler ultrasound, not only the shape of the lesions can be dynamically observed but also the blood flow in the lesions can be observed [11]. Aborizk et al. stated that in today's wide application of ultrasound examination technology and various gynecological diseases, it is essential for gynecologists to master ultrasound skills, not only the use of the final ultrasound diagnosis alone but also the characteristics of the respective ultrasound images of different uterine diseases should be able to be distinguished, which is very important for more accurate diagnosis of gynecological clinical diseases [12]. Le and others believe that in the diagnosis of gynecological diseases, ultrasound is often used as the first choice for diagnosing diseases, it can not only diagnose diseases but also a common screening method for women's health check-up, and organ diseases have high diagnostic value [13].

3. Methods

3.1. Research Overview. Color Doppler ultrasound, also known as color Doppler ultrasound, is a medical device that is suitable for ultrasound examination of various parts of the body, especially for the examination and diagnosis of the heart, limb blood vessels, and superficial organs, as well as the abdomen, obstetrics, and gynecology. Doppler ultrasound can be divided into five types: pulsed Doppler, continuous Doppler, high pulse repetition frequency Doppler, multipoint gated Doppler, and color Doppler flow imaging, among them, pulsed Doppler is the most widely used [14]. It is based on the Doppler principle and a series of electronic techniques in the case of two-dimensional echocardiography positioning, real-time display of a spectrogram of a certain volume (SV) blood flow at a certain point in the heart or great vessels. It is an atraumatic technique for detecting intracardiac shunts and regurgitation. Continuous Doppler can continuously emit pulses, so it has the ability to measure high-speed blood flow, which has obvious advantages for quantitative analysis of stenosis, regurgitation, and shunt lesions in the cardiovascular system. Its working principle

is based on the introduction of color Doppler technology on the basis of high-definition black and white B ultrasound. Color Doppler ultrasound blood flow images can be formed, which not only has the advantages of two-dimensional ultrasound structural images but also provides rich information on hemodynamics. It is clinically known as "non-invasive angiography" [15]. Color Doppler blood flow imaging technology is to display blood flow signals in color, and the pseudocolor coding is composed of three basic colors of red, blue, and green. Set red to represent blood flow towards the probe and blue to represent blood flow away from the probe. Blood flow velocity is related to color luminance, with high velocity, strong color luminance, and low velocity, weak color luminance [16]. For example, when the blood flow velocity towards the probe is low, the signal is dark red, and when the blood flow velocity away from the probe is low, the signal is dark blue, the brightness of the color signal is very weak, that is, the color is very dark, and it is difficult to distinguish from the fluorescent screen. At this time, a color intensifier was added to improve the brightness of color signals in low-velocity blood flow. In order to express the speed of blood flow accurately and quickly, sometimes, three colors are used to express the speed of blood flow, the blood flow towards the probe is represented by a signal ranging from dark red to bright red, if the blood flow is faster, it will change from red to yellow, then yellow to green, and the coexistence of the three colors indicates different flow rates. Faster flow rates of blood flow away from the probe are indicated in cyan and green. On the ultrasound instrument, the color map is set to two types: one for noncardiovascular blood flow detection has only two colors of red, yellow, blue, and cyan. The other for cardiovascular blood flow detection has two to three colors in each direction. AM patients (adenomyosis patients) complete transvaginal three-dimensional color Doppler ultrasound examination before surgery, according to the imaging manifestations, the surgeon can preliminarily judge the location, size, and invasion depth of AM lesions before surgery, so as to formulate individualized surgical plan. This study shows that preoperative transvaginal three-dimensional color Doppler ultrasonography has high accuracy in diagnosing localized and diffuse AM and has a high reference value in the differential diagnosis of AM and uterine fibroids. Laparoscopic hysterectomy is used in patients with limited AM, and the recent clinical effect is definite, which can effectively relieve clinical symptoms, and is worthy of clinical application and promotion. For patients with diffuse AM, the clinical indications for laparoscopic hysterectomy wedge resection are relatively strict, mainly due to the patient's age, urgent fertility requirements, CA125 determination, etc., it is worth trying clinically, but the long-term effect needs to be further observed [17]. Research shows, other treatments, such as high-intensity focused ultrasound therapy, can also be used as a treatment option to eliminate uterine disorders and alleviate the disease process. In conclusion, transvaginal three-dimensional color Doppler ultrasound has the advantages of noninvasive, clear, measurable, etc., and it can provide specific parameter basis for the accurate diagnosis of AM types and then provide important reference indicators for the optimal selection of clinical treatment plans and postoperative follow-up, which is worthy of further application and promotion.

3.2. Data Sources. A total of 150 patients who received adenomyosis treatment in a people's hospital from January 2020 to December 2021 were selected as the research objects. The age of the patients ranged from 23 to 65 years old, with an average of (43.2 ± 2.9) years old. Among them, 25 had a history of abortion, 17 had dysmenorrhea and were infertile, and 53 had normal or slightly more menstrual flow and anemia but no history of dysmenorrhea. 55 cases of secondary dysmenorrhea. Inclusion criteria: (1) all patients were confirmed to have adenomyosis by postoperative pathology; (2) the clinical data were complete; (3) informed and agreed to this study. Exclusion criteria: (1) patients with mental illness and cognitive dysfunction; (2) patients with missing clinical data; (3) withdrew from the researcher midway.

3.3. Research Methods

3.3.1. Ultrasound Examination. All patients underwent abdominal ultrasonography first, followed by 3D color Doppler ultrasonography, specifically: (1) abdominal ultrasound: using a color ultrasound instrument (manufacturer: Toshiba APlio, model 500), probe frequency: 5.0 ~ 9.0 MHz, before the examination, instruct the patient to drink an appropriate amount of water to ensure bladder filling, take the supine position, and test the transverse, oblique and longitudinal sections of the patient's uterus, and record the test results in detail. (2) Three-dimensional color Doppler ultrasound: put the condom on the probe and routinely sterilize it, the patient is instructed to empty the bladder before the examination, and then, the probe is slowly inserted into the patient's vagina, the oblique section, longitudinal section, and transverse section of the bladder stone were taken for examination, and the size, shape, muscle echo, endometrial thickness, and double appendages of the patient's uterus were carefully observed. Corresponding hematological tests were performed on the patients to detect the changes of blood flow in the myometrium and endometrium, and the hemodynamic index of malignant lesions was compared with the conventional hemodynamic index [18]. The above test results were analyzed and evaluated by 2 experienced laboratory personnel, and the results were compared with the surgical and pathological results.

3.3.2. Observation Indicator. Taking the surgical and pathological results as the gold standard for judgment, the positive predictive value, coincidence rate, sensitivity, and specificity of the two examination methods were compared, and the main calculation methods were as follows: positive predictive value = true positives/(true positives + false positives); sensitivity = true positives/(true positives + false negatives); specificity = true negatives/(false positives + true negatives); coincidence rate = (true positives + true negatives) negative)/total number of cases [19].

3.4. Statistical Analysis. SPSS 18.0 software was used for statistical analysis of the data, the count data was expressed as (case (%)), the x^2 test was used for data comparison, the

measurement data are represented by ($\bar{x} \pm s$), the t-test was used to compare the data, and $P < 0.05$ was considered statistically significant.

4. Results and Analysis

4.1. Comparison of Diagnostic Efficacy of Two Ultrasound Methods. Abdominal ultrasonography was consistent in 94 cases, misdiagnosed in 27 cases, and missed in 29 cases. Vaginal three-dimensional color Doppler ultrasonography was consistent in 131 cases, misdiagnosed in 11 cases, and missed diagnosis in 8 cases, as shown in Table 1, in 11 misdiagnosed patients, when performing vaginal three-dimensional color Doppler ultrasonography, it was found that there were localized echogenic lesions in the uterine wall, and the echo was hypoechoic, which was misdiagnosed as uterine fibroids. The sensitivity, specificity, accuracy, positive predictive value, and negative predictive value of vaginal three-dimensional color Doppler ultrasound were higher than those of abdominal ultrasound, as shown in Table 2.

Ultrasonographic images of patients with adenomyosis diagnosed by transvaginal three-dimensional color Doppler ultrasonography, with the following characteristics: (1) the uterus has different degrees of enlargement. In diffuse adenomyosis, the uterus shows spherical enlargement, and the uterus is round and blunt. (2) There is a slightly stronger echo inside the myometrium, and the echo is uneven. (3) In some patients, echo-enhanced light spots can be seen inside the myometrium, there are two types of light spots, one is the light spot with strong and thick echoes, and the other is the anechoic or low echo area in addition to the light spot echoes. (4) There is uneven thickening of the anterior or posterior wall of the uterus, and endometrial line displacement can be seen in some patients. (5) Hematological examination showed that in the lesion, short branch-like or short-stripe blood flow signals could be seen [20].

4.2. Negative and Positive Comparative Analysis. Pathologically confirmed, among 150 cases of cervical lesions diagnosed by ultrasound, 91 cases (60.67%) were benign cervical lesions, and 59 cases (39.33%) were cervical malignant lesions, as shown in Figure 2.

Among the 91 cases of benign cervical lesions, 15.4% (14/91) had no obvious abnormal echoes on ultrasound, 62.6% (57/91) had hypoechoic cases, and 22.0% (20/91) had hyperechoic pathology. Among the 120 cervical malignant lesions, 16.9% (10/59) had no clear abnormal echoes on ultrasound, 79.7% (47/59) were hypoechoic, and 3.4% (2/59) were hyperechoic. Comparing ultrasound diagnosis of benign cervical lesions and malignant lesions, there was a significant difference in echo types, $x^2 = 82.11$, $P < 0.05$, as shown in Figure 3.

Among the 91 cases of benign cervical lesions, 16 cases (17.6%), 73 cases (80.2%), and 2 cases (2.2%) showed no blood flow, punctate blood flow, and abundant blood flow, respectively, among the 59 malignant cervical lesions, there were 1 (1.7%), 19 (32.2%), and 39 (66.1%) cases with no blood flow, punctate blood flow, and abundant blood flow, respectively. After chi-square statistical analysis, there were significant differences in blood flow changes between benign cervical lesions and malignant lesions diagnosed by ultrasound, $x^2 = 169.56$, $P < 0.05$. Benign lesions are mainly characterized by punctate blood flow, followed by no blood flow, and occasionally, abundant blood flow. On the contrary, malignant lesions are mainly characterized by abundant blood flow and punctate blood flow, but there are still a certain proportion of patients with no blood flow found in the lesions, as shown in Figure 4.

4.3. Discussion. There are many kinds of reproductive tract diseases, which affect the physical and mental health of women to varying degrees, especially uterine diseases, which not only damage the female body but also seriously affect the reproductive health of women of reproductive age; it affects the reproduction of human offspring, but if detected early, it can improve disease prognosis, improve health, and improve reproductive quality. As a simple, easy-to-operate, noninvasive, and economical examination method, ultrasound is the first choice for the diagnosis and differential diagnosis of gynecological-related diseases. How to improve the accuracy of ultrasound diagnosis of gynecological diseases is the goal that ultrasound, and clinicians have been pursuing [21]. Statistically summarizes the ultrasound imaging characteristics of uterine diseases, namely, intrauterine lesions, uterine lesions, and cervical lesions, in order to improve the detection rate of diseases, it can reduce missed diagnosis and misdiagnosis, avoid unnecessary operations or operations, and at the same time, it can also detect precancerous or malignant lesions in a timely manner, provide a reference for clinical gynecologists to accurately diagnose, design appropriate treatment plans, and select appropriate treatment methods. Ultrasound is widely used in clinical diagnosis of gynecological diseases, abdominal ultrasound is greatly affected by external factors, such as obesity, flatulence, and uterine position, it is easy to miss and misdiagnose, while hysteroscopy, hysterography, and magnetic resonance imaging have a high coincidence rate for the diagnosis of uterine diseases, but due to their relatively expensive price, complicated operation, and invasive factors such as sex limit its universality in clinical applications, therefore, transvaginal ultrasonography is widely used in clinical practice because of its noninvasiveness, simple operation, relatively low price, and high diagnostic coincidence rate. Doppler ultrasound has high diagnostic value for intrauterine lesions, uterine lesions, and cervical lesions and can be used as the first choice for disease screening; however, for the high rate of missed diagnosis of cervical lesions, ultrasound should be combined with internal diagnosis or cervical screening. Ultrasonography did not differ from MRI in assessing cervical stromal or parametrial invasion. MRI is a widely accepted and reliable method for cervical cancer detection, with the development of new ultrasound technology in recent years, ultrasound examination is also gradually used for preoperative evaluation of cervical cancer. Furthermore, ultrasonography is superior to MRI in assessing residual lesions and parametrial invasion after cervical cancer biopsy. In addition, color Doppler ultrasound can also predict the efficacy of cervical radiotherapy and chemotherapy, and

Table 1: Comparison of positive rates of abdominal ultrasonography and vaginal three-dimensional color Doppler ultrasonography.

Abdominal ultrasound	Gold standard		Vaginal 3D color Doppler ultrasound	Gold standard	
	Positive	Negative		Positive	Negative
Positive	52	21	Positive	81	14
Negative	36	41	Negative	7	48
Total	88	62		88	62

Table 2: The diagnostic efficiency ratio of abdominal ultrasonography and vaginal three-dimensional color Doppler ultrasonography.

Method	Sensitivity	Specificity	Accuracy	Positive predictive value	Negative predictive value
Abdominal ultrasound	68.42	51.07	64.39	31.57	60.00
3D color Doppler ultrasound	81.06	90.11	82.47	90.27	80.00

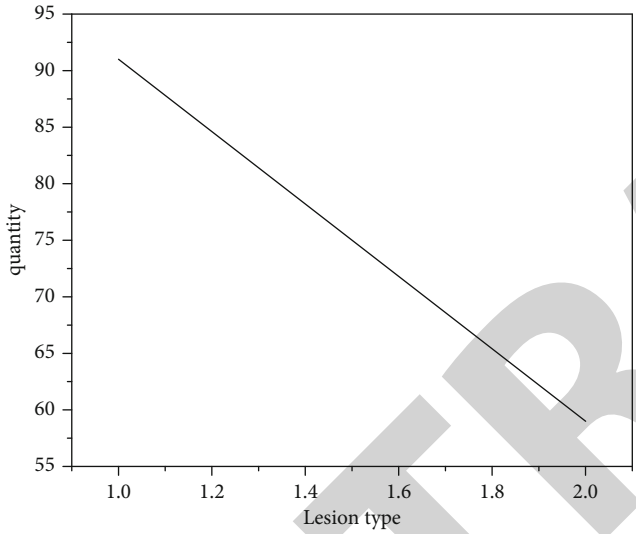

Figure 2: Lesion line chart.

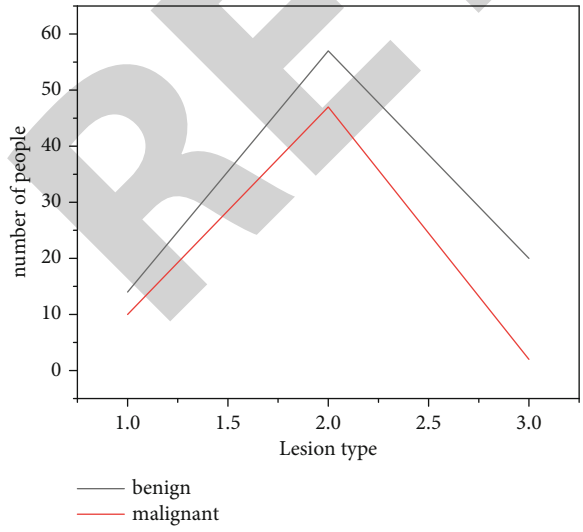

Figure 3: Line chart of benign and malignant lesions.

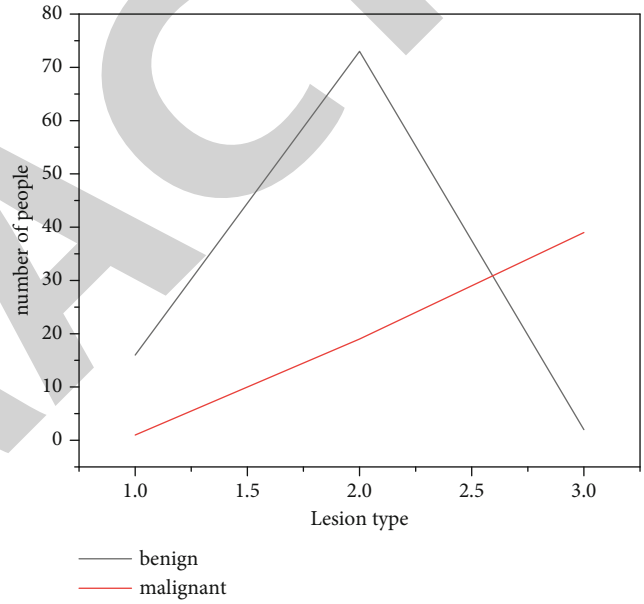

Figure 4: Comparison of bleeding spots in lesions.

not only cervical benign lesions but also cervical malignant lesions. It should be reminded that gynecological sonographers pay attention to the changes in the imaging characteristics of some cervical parts, especially the blood flow changes, which may improve the detection rate and reduce the missed diagnosis rate.

Transvaginal three-dimensional color Doppler ultrasound has the advantages of high resolution, noninvasiveness, sensitivity, and reproducibility, and the early diagnosis coincidence rate in AM is higher than that of abdominal color ultrasound. Transvaginal three-dimensional color Doppler ultrasound avoids factors such as excessive abdominal fat layer, uterine position, and severe pelvic gas and can accurately measure the shape, volume, muscle echo, local blood vessel distribution, and blood flow of the uterus. AM and uterine fibroids coexist in patients with localized AM (also known as adenomyoma). Ultrasound imaging features of uterine fibroids: there is a pseudocapsule around the lesion, the border of the fibroids is clear, and there may be annular blood flow signals

on the pseudocapsule. Some larger uterine fibroids are prone to imaging changes of degeneration or calcification [22]. Both uterine fibroids and AM patients have clinical manifestations such as increased menstrual volume and dysmenorrhea, which are prone to misdiagnosis and missed diagnosis. However, the principles of diagnosis and treatment are different, and a clear diagnosis is required before surgery to provide basis and technical support for rational clinical diagnosis and treatment.

5. Conclusion

Doppler ultrasonography has high diagnostic value for intrauterine lesions, uterine lesions, and cervical lesions, and it can be used as the first choice for disease census, but ultrasound has a high rate of missed diagnosis of cervical lesions, so it should be combined with internal diagnosis or cervical screening. The results of this study show that, patients diagnosed by abdominal ultrasonography and by vaginal 3D color Doppler ultrasonography, the accuracy was significantly different, the diagnostic accuracy of abdominal ultrasound was 62.67%, and the diagnostic accuracy of vaginal three-dimensional color Doppler ultrasound was 87.33%. Sometimes due to the limited distribution of ectopic endometrium, it shows a clearer boundary with the muscle wall, but there is no dark halo around it. The blood flow in adenomyosis lesions is sparse, with a few dot-shaped short rod-shaped blood flow signals, and there is no annular or semicircular blood flow around the localized lesions, spectral Doppler detected low-speed high-resistance blood flow spectrum RI > 0.7. The main characteristics of vaginal color ultrasound imaging are the uterus is enlarged to varying degrees. There is a strong echo inside the myometrium. The enhanced echo spot can be seen inside the myometrium. Hematology showed that short strips or short dendritic blood flow signals were seen in the lesions. In summary, vaginal three-dimensional color Doppler ultrasound has a high clinical diagnostic value for adenomyosis, adenomyosis can be more accurately diagnosed, and its accuracy is significantly higher than that of abdominal ultrasonography. And because vaginal three-dimensional color Doppler ultrasound is relatively inexpensive, simple to operate, and noninvasive, it is more easily tolerated by patients. The authors believe that, under the premise of conditions permitting, this method is worthy of clinical promotion and application.

Data Availability

The data used to support the findings of this study are available from the corresponding author upon request.

Conflicts of Interest

The authors declare that they have no competing interests.

References

[1] L. K. Chen, Y. W. Lai, P. C. Li, and S. S. Chen, "Significant relationship between parameters measured by transrectal color Doppler ultrasound and sexual dysfunction in patients with bph 12 months after turp," *BMC Urology*, vol. 21, no. 1, pp. 1–7, 2021.

[2] M. Li, Q. Li, Q. Yin, Y. Wang, J. M. Shang, and L. H. Wang, "Evaluation of color Doppler ultrasound combined with plasma mir-21 and mir-27a in the diagnosis of breast cancer," *Clinical and Translational Oncology*, vol. 23, no. 4, pp. 709–717, 2021.

[3] D. Li, X. Qian, R. Li et al., "High resolution adc for ultrasound color Doppler imaging based on mash sigma-delta modulator," *IEEE Transactions on Biomedical Engineering*, vol. 67, no. 5, pp. 1438–1449, 2020.

[4] Y. Xu, Y. Wu, R. Zhang, and C. Liu, "Application of color Doppler ultrasound combined with fibroscan scoring system in the diagnosis of chronic hepatitis b fibrosis," *Yingxiang Kexue yu Guanghuaxue/Imaging Science and Photochemistry*, vol. 39, no. 1, pp. 67–74, 2021.

[5] S. Mascaretti, C. Masciocchi, G. Mascaretti, E. Fascetti, and A. Serva, "Perineal color Doppler ultrasound of periurethral vascularization in women affected by urinary stress incontinence," *Eastern Journal of Medicine*, vol. 26, no. 3, pp. 354–361, 2021.

[6] Z. Wei, M. Mu, M. Li, J. Li, and Y. Cui, "Color Doppler ultrasound detection of hemodynamic changes in pregnant women with gdm and analysis of their influence on pregnancy outcomes," *American Journal of Translational Research*, vol. 13, no. 4, pp. 3330–3336, 2021.

[7] D. Cevoli, R. Vitale, W. Vandenberg, S. Hugelier, and C. Ruckebusch, "Design of experiments for the optimization of sofi super-resolution microscopy imaging," *Biomedical Optics Express*, vol. 12, no. 5, pp. 2617–2630, 2021.

[8] A. S. Mostafa, A. I. Gamal, M. Gadalla, and H. Sherine, "Diagnostic utility of color Doppler ultrasound for nuchal corddetection at term: a prospective study," *The Medical Journal of Cairo University*, vol. 89, no. 3, pp. 279–283, 2021.

[9] S. A. Khodair, A. A. Elsokary, and M. Z. Elabdien, "Antepartum evaluation of placenta accreta in women with placenta previa by color Doppler, power Doppler ultrasound and mri: a prospective study," *The Medical Journal of Cairo University*, vol. 88, no. 3, pp. 505–512, 2020.

[10] H. Guo, Z. Shen, N. Xu et al., "Evaluation of prognosis of brain function with early transcranial color Doppler ultrasound in patients after cardiopulmonary resuscitation," *World Journal of Cardiovascular Diseases*, vol. 10, no. 9, pp. 658–665, 2020.

[11] M. Zhi, M. Wang, W. Li, L. Ma, and Q. Lv, "Reliability of the application of transvaginal color Doppler ultrasound in the identification of pelvic tumors in women of childbearing age," *Annals of Translational Medicine*, vol. 8, no. 24, pp. 1662–1662, 2020.

[12] H. Eltyib, S. A. Aborizk, H. A. Albalawi, A. S. Almotairi, and A. H. Aidrus, "The diagnostic value of color Doppler ultrasound and grey scale sonography in predicting the malignancy of thyroid nodules," *Open Journal of Radiology*, vol. 10, no. 4, pp. 215–222, 2020.

[13] M. T. Le, D. N. Nguyen, T. Nguyen, V. Nguyen, and N. T. Cao, "Should scrotal color Doppler ultrasound be routinely indicated in fertility evaluation of non-azoospermic men?," *Current Urology*, vol. 14, no. 4, pp. 211–218, 2020.

[14] Y. T. Su, Y. Lu, J. Liu, M. Chen, and A. A. Liu, "Spatio-temporal mitosis detection in time-lapse phase-contrast microscopy image sequences: a benchmark," *IEEE Transactions on Medical Imaging*, vol. 40, no. 5, pp. 1319–1328, 2021.

Hindawi
Scanning
Volume 2023, Article ID 9831918, 1 page
https://doi.org/10.1155/2023/9831918

Retraction

Retracted: Prediction of Renal Function Damage in Patients with Essential Hypertension Based on Stepwise Regression Equation Scanning by AASI

Scanning

Received 20 June 2023; Accepted 20 June 2023; Published 21 June 2023

This article has been retracted by Hindawi following an investigation undertaken by the publisher [1]. This investigation has uncovered evidence of one or more of the following indicators of systematic manipulation of the publication process:

(1) Discrepancies in scope

(2) Discrepancies in the description of the research reported

(3) Discrepancies between the availability of data and the research described

(4) Inappropriate citations

(5) Incoherent, meaningless and/or irrelevant content included in the article

(6) Peer-review manipulation

The presence of these indicators undermines our confidence in the integrity of the article's content and we cannot, therefore, vouch for its reliability. Please note that this notice is intended solely to alert readers that the content of this article is unreliable. We have not investigated whether authors were aware of or involved in the systematic manipulation of the publication process.

In addition, our investigation has also shown that one or more of the following human-subject reporting requirements has not been met in this article: ethical approval by an Institutional Review Board (IRB) committee or equivalent, patient/participant consent to participate, and/or agreement to publish patient/participant details (where relevant).

Wiley and Hindawi regrets that the usual quality checks did not identify these issues before publication and have since put additional measures in place to safeguard research integrity.

We wish to credit our own Research Integrity and Research Publishing teams and anonymous and named external researchers and research integrity experts for contributing to this investigation.

The corresponding author, as the representative of all authors, has been given the opportunity to register their agreement or disagreement to this retraction. We have kept a record of any response received.

References

[1] Y. Wu, G. Ma, H. Sun, S. Zhang, and X. Li, "Prediction of Renal Function Damage in Patients with Essential Hypertension Based on Stepwise Regression Equation Scanning by AASI," *Scanning*, vol. 2022, Article ID 4728921, 6 pages, 2022.

Hindawi
Scanning
Volume 2022, Article ID 4728921, 6 pages
https://doi.org/10.1155/2022/4728921

Research Article

Prediction of Renal Function Damage in Patients with Essential Hypertension Based on Stepwise Regression Equation Scanning by AASI

Yaqiong Wu,[1] **Guangyu Ma**,[2] **Hongzhen Sun**,[1] **Sijie Zhang**,[1] **and Xingtao Li**[1]

[1]*The Department of Cardiology, Fourth Hospital of Hebei Medical University, Shijiangzhuang, Hebei 050011, China*
[2]*The Department of Haematology, Fourth Hospital of Hebei Medical University, Shijiangzhuang, Hebei 050011, China*

Correspondence should be addressed to Yaqiong Wu; 15035102210053@hainanu.edu.cn

Received 30 March 2022; Revised 1 May 2022; Accepted 9 May 2022; Published 28 May 2022

Academic Editor: Danilo Pelusi

Detection of arterial stiffness is an important method to predict the occurrence of hypertension complications and to screen patients with high cardiovascular risk. In order to predict the damage of AASI to the renal function of patients with essential hypertension, the prediction of AASI based on stepwise Regression equation scanning for renal function damage in patients with essential hypertension is proposed. Measure the 24 h ambulatory blood pressure of the selected subjects, establish a linear Regression equation scanning, and calculate the slope of the straight line, and finally, the slope is AASI. According to the quartiles, AASI is divided into four parts: group I < 0.53 ($n = 49$); 0.53 ≤ group II < 0.60 ($n = 51$); 0.60 ≤ group III < 0.69 ($n = 48$); group IV ≥ 0.69 ($n = 44$). Experiment result shows the following: with the increase of AASI, cystatin (CysC) also increased significantly, while CysC-eGFR decreased significantly ($P < 0.05$). Compared with groups I, II, and III, Scr and CysC in group IV increased ($P < 0.05$), and Ccr, CysC-eGFR, and (CKD-EPI)-eGFR all decreased ($P < 0.05$). AASI is positively correlated with CysC performance, and the correlation coefficient r is 0.637. It is negatively correlated with Ccr performance, and r is -0.361. It is negatively correlated with CysC-eGFR, and r is -0.698. And it is negatively correlated with (CKD-EPI)-eGFR, and r is -0.331. Age and 24 h PP also showed an increasing trend with the increase of AASI, and it suggests that age may be an influencing factor that promotes kidney damage caused by hypertension; it also suggests that AASI can be used as a new indicator of arterial compliance; AASI is linearly related to various indicators of renal damage and can be used as a predictive indicator of renal damage caused by essential hypertension; cystatin C and the estimated glomerular filtration rate CysC-eGFR based on cystatin C are better than other indicators reflecting glomerular filtration rate, more sensitively assess the degree of early renal damage. Obesity may also be a factor that promotes kidney damage caused by hypertension.

1. Introduction

Ambulatory blood pressure monitoring (ABPM) can reflect blood pressure levels and circadian rhythms; there is a good correlation with the damage degree of target organs such as heart, brain, and kidney. It also has important significance in studying the pathogenesis of hypertension-related complications [1]. The ambulatory blood pressure-related arteriosclerosis index is a series of indicators derived from ABPM that reflect the elastic function of arteries; the application scope of AB-PM in clinical has been further expanded [2]. Symmetrical Ambulatory Arterial Stiffness Index (S-AASI) is a new index derived from ABPM to assess arterial stiffness. In the current research, there are not many reports on the correlation between S-AASI and target organ damage in hypertension [3]. AASI is a new indicator of arteriosclerosis discovered by using a series of systolic and diastolic blood pressure values obtained by ABPM to perform function fitting [4]. In response to this research question, Kotecha et al. reported that AASI is positively correlated with PP, and it is less dependent on blood pressure value and blood pressure variability than PP; it is a good supplement to PP predicting arterial elastic function, and it is recommended that AASI.PP and blood pressure variability should be used

in combination in the evaluation of arteriosclerosis [5]. Couderc et al. pointed out that AASI is affected by factors such as the correlation between systolic and diastolic blood pressure, age, gender, PP, and nocturnal blood pressure when it reflects the degree of arteriosclerosis and predicts target organ damage; the measurement results are unstable [6]. Turner et al. believe that S-AASI is a newer and improved dynamic arteriosclerosis index; the calculation of S-AASI value is due to the introduction of the concept of symmetric linear Regression equation scanning and the use of r value for correction; it is believed to be able to detect arteriosclerosis more accurately; it may be better than AASI in evaluating the correlation with hypertension target organ damage; S-AASI has not been shown to be superior to AASI [7]. Therefore, the pros and cons of the abovementioned indicators for evaluating arteriosclerosis in clinical use are still controversial [8]. On the basis of the current research, the AASI based on the stepwise Regression equation scanning is proposed to predict the renal function damage of patients with essential hypertension. Measure the 24 h ambulatory blood pressure of the selected subjects, establish a linear Regression equation scanning, and calculate the slope of the straight line; finally, the slope is AASI. According to the quartiles, AASI is divided into four parts: group I < 0.53 ($n = 49$); 0.53 ≤ group II < 0.60 ($n = 51$); 0.60 ≤ III group < 0.69 ($n = 48$); IV group ≥ 0.69 ($n = 44$). Age and 24 h PP also showed an increasing trend with the increase of AASI; it suggests that age may be an influencing factor that promotes kidney damage caused by hypertension; it also suggests that AASI can be used as a new indicator of arterial compliance; AASI is linearly related to various indicators of renal damage; it can be used as a predictor of renal damage caused by essential hypertension; cystatin C and the estimated glomerular filtration rate CysC-eGFR based on cystatin C are better than other indicators reflecting glomerular filtration rate, more sensitively assess the degree of early renal damage. Obesity may also be a factor that promotes kidney damage caused by hypertension.

2. Method

2.1. Research Objects. A total of 192 patients with essential hypertension were selected for the outpatient department of the cardiology department of a university hospital; among them, there are 98 males and 94 females; the age fluctuates in the range of 40-81; the diagnoses of all selected subjects met the selection criteria of this experiment but did not meet the exclusion criteria.

(1) *Selection Criteria*. Diagnosed as a patient with essential hypertension, routine urine examination showed negative urine protein, those who did not take antihypertensive drugs within two weeks before seeing a doctor, and understand this experiment and give informed consent

(2) *Exclusion Criteria*. People with secondary hypertension, past liver and kidney dysfunction, urinary system diseases, pheochromocytoma, congenital heart disease, valvular disease, severe heart failure, myocardial infarction, atrial fibrillation, pleural or abdominal effusion, severe edema or malnutrition, diabetes, ketoacidosis, hyperthyroidism and hypothyroidism, gout, cerebrovascular accidents, and severe blood system diseases; those who take drugs that affect blood pressure measurement within 2 weeks; and those who have recently undergone glucocorticoid or hemodialysis treatment [9]

2.2. Experimental Method

2.2.1. Record Blood Pressure and Calculate AASI. All subjects wore 24 h ambulatory blood pressure monitors, using MOBI-0-GRAPH ambulatory blood pressure monitor. Set the blood pressure to be measured every half an hour from 6 : 00 in the morning, until 23 : 00 at night. Set again from 23 : 00 at night; blood pressure was measured every hour until 6 : 00 a.m. the next day. During the measurement, the patient is required not to stay up late to be consistent with daily life. Establish a linear Regression equation scanning and calculate the slope of the straight line, and finally, the slope is AASI. According to the quartiles, AASI is divided into four parts: group I < 0.53 ($n = 49$); 0.53 ≤ group II < 0.60 ($n = 51$); 0.60 ≤ III group < 0.69 ($n = 48$); IV group ≥ 0.69 ($n = 44$).

2.2.2. Calculate 24 h Pulse Pressure Based on Blood Pressure. Pulse pressure, also known as pulse pressure (PP), is the difference between systolic blood pressure (SBP) and diastolic blood pressure (DBP); it is a commonly used index to evaluate arterial compliance in clinical practice.

2.2.3. General Data Collection. Record the general condition of the patient, such as age, weight, height, and heart rate. And calculate its body mass index (BMI) based on weight and height and the patient's blood glucose, blood lipids, liver function, kidney function, blood routine, urine routine, electrolytes, and other biochemical indicators.

2.2.4. Indicators of Kidney Function. All subjects get blood from fasting veins in the morning, the particle-enhanced transmission immunoturbidimetric method was used to determine the serum cystatin C level of subjects, and bring the measured serum CysC into the corresponding formula for estimating glomerular filtration rate, MacIsaac modified formula: GFR = (77.30/CysC) + 2.32, and calculate CysC-eGFR.

2.3. Statistical Processing. The data of this study was processed using the SPSS17.0 statistical software package, statistical analysis adopts a two-sided test, and $P < 0.05$ means the difference is statistically significant, unless otherwise specified. The measurement data is statistically described in the form of mean ± standard deviation ($\bar{x} \pm s$). Counting data is expressed in frequency and percentage. The chi-square test was used for the statistical inference of the comparison between the count data groups, and the analysis of variance was used for the statistical inference of the comparison between the measurement data groups. Pearson

correlation analysis was used to compare the linear correlation between AASI and renal damage indexes. In addition, the multiple linear stepwise regression analysis method was used to take the kidney damage index as the dependent variable, and construct a model with base data as independent variables.

3. Results and Analysis

3.1. Baseline Data Analysis. According to the ambulatory blood pressure value measured at 24 h, take systolic blood pressure and diastolic blood pressure as the abscissa and ordinate, respectively, draw a scatter plot, establish a linear Regression equation scanning, calculate the slope of the straight line, and finally get the AASI with 1-the slope, and according to the quartiles, AASI is divided into four parts: group I: 49 cases, AASI < 0.53; group II: 51 cases, $0.53 \leq$ AASI < 0.60; group III: 48 cases, $0.60 \leq$ AASI < 0.69; and group IV: 44 cases, AASI $\geq$ 0.69. After analysis of variance for each group: heart rate between 4 groups, there was no statistically significant difference in BMI comparison ($P > 0.05$), the age difference between the groups was statistically significant ($P < 0.05$), and it is suggested that as the AASI level increases, age is also increasing. The difference in 24 h PP between the groups was statistically significant ($P < 0.05$), suggesting that with the increase of AASI level, 24 h PP also gradually increased.

3.2. Single Factor Analysis. Among the indicators of kidney damage, the four groups of data were first analyzed by variance analysis between groups, and the results showed that the differences between the index groups were statistically significant ($P < 0.05$). Then, use the Bonferroni test method to compare the two within the group; the results are as follows: in Scr indicators, there were statistically significant differences between group II and group I, group III and group I, and group IV, group II, and group III ($P < 0.05$). In the CysC index, group II is compared with the group I, and group III is compared with group I and group II; there was a statistically significant difference between group IV and group I, group II, and group III ($P < 0.05$). In the Ccr index, group II is compared with group I, and group III is compared with group I; there was a statistically significant difference between group IV and group I, group II, and group III ($P < 0.05$). In the CysC-eGFR index, group II is compared with group I, and group III is compared with group I and group II; there was a statistically significant difference between group IV and group I, group II, and group III ($P < 0.05$). In the (CKD-EPI)-eGFR index, group II is compared with group I, and group III is compared with group I; there was a statistically significant difference between group IV and group I, group II, and group III ($P < 0.05$). The tip is as follows: as AASI increases, cystatin (CysC) also increased significantly, while CysC-eGFR decreased significantly ($P < 0.05$). Compared with groups I, II, and III, both Scr and CysC in group IV increased ($P < 0.05$), and Ccr, CysC-eGFR, and (CKD-EPI)-eGFR all decreased ($P < 0.05$).

3.3. The Linear Correlation between Various Indexes of Renal Function and AASI. The indicators of kidney damage are as follows: creatinine clearance, cystatin C, CysC-eGFR, and (CKD-EPI)-eGFR, respectively, and AASI after linear correlation analysis by Pearson correlation analysis method, AASI is positively correlated with CysC, the correlation coefficient r is 0.637; it is negatively correlated with Ccr performance, and r is -0.361; it is negatively correlated with CysC-eGFR performance, and r is -0.698. It is negatively correlated with (CKD-EPI)-eGFR, and r is -0.331. After adjusting for age factors, after partial correlation analysis, AASI is positively correlated with CysC performance and negatively correlated with the performance of Ccr, CysC-eGFR, and (CKD-EPI)-eGFR, the correlation coefficients are as follows, and the P values are all <0.05, as shown in Figure 1.

3.4. Multiple Linear Regression Analysis of Each Index and AASI

(1) Taking CysC as the dependent variable, then use age, heart rate, BMI, and AASI as independent variables, and the multiple linear stepwise regression analysis is shown in Table 1. The result shows the following: the Regression equation scanning of cystatin C and AASI is as follows: $\text{CysC} = 0.657 + 2.111 \times \text{AASI}$.

(2) Taking Ccr as the dependent variable, then use age, heart rate, BMI, and AASI as independent variables; the multiple linear stepwise regression analysis is shown in Table 2. The Regression equation scanning of creatinine clearance rate and AASI, age, and BMI is as follows: $\text{Ccr} = 120.012 - 39.885 \times \text{AASI} - 0.898 \times \text{age} - 1.211 \times \text{BMI}$.

(3) Taking CysC-eGFR as the dependent variable, then use age, heart rate, BMI, and AASI as independent variables; the multiple linear stepwise regression analysis is shown in Table 3; the result shows the following: the Regression equation scanning of CysC-eGFR and AASI is as follows: $\text{CysC} - \text{eGFR} = 121.598 - 157.968 \times \text{AASI}$.

(4) Taking (CKD-EPI)-eGFR as the dependent variable, then use age, heart rate, BMI, and AASI as independent variables; the multiple linear stepwise regression analysis is shown in Table 4; the result shows the following: the Regression equation scanning of (CKD-EPI)-eGFR, AASI, and age is as follows: $(\text{CKD-EPI}) - \text{eGFR} = 130.011 - 35.010 \times \text{AASI} - 0.603 \times \text{age}$.

The kidneys can regulate blood pressure; it can also be damaged by persistent high blood pressure. There is an interaction between high blood pressure and the kidneys;

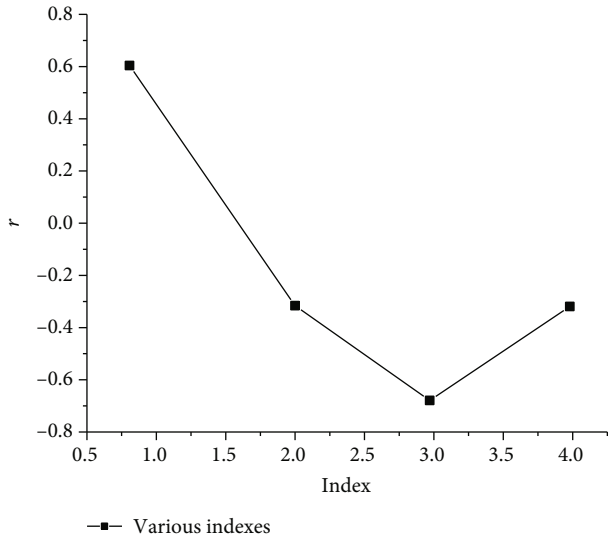

Figure 1: The linear correlation between various indexes of renal function and AASI.

Table 1: Results of multiple linear regression with CysC as the dependent variable.

X	*B* value	Standard error	Beta	*P*
Constant	0.657	0.080	-	$P < 0.001$
AASI	2.111	0.145	0.633	$P < 0.001$

Table 2: Results of multiple linear stepwise regression with Ccr as the dependent variable.

X	*B* value	Standard error	Beta	*P*
Constant	120.012	10.120	-	$P < 0.001$
AASI	-39.012	7.111	-0.259	$P < 0.001$
Age	-0.898	0.079	-0.551	$P < 0.01$
BMI	-1.211	0.229	-0.320	$P < 0.05$

actively control benign hypertension (especially moderate to severe benign hypertension); it is very important to prevent kidney damage caused by hypertension. How does the kidney perform the task of regulating blood pressure? First of all, the kidneys regulate the balance of water and electrolytes in the body; if the kidneys are damaged, water and sodium cannot be excreted from the body; it will cause increased blood vessel pressure and blood pressure. Secondly, the endocrine function of the kidney, the renin, and angiotensin that it secretes are involved in regulation, human blood pressure, and once the kidney is damaged, the imbalance of these endocrine hormones can cause vascular tension and cause high blood pressure. Kidney damage caused by long-term high blood pressure, it is also due to the continuous state of high blood pressure, which continuously damages the blood vessel wall, gradually lead to arteriosclerosis, and after arteriosclerosis,

Table 3: Results of multiple linear stepwise regression with CysC-eGFR as the dependent variable.

X	*B* value	Standard error	Beta	*P*
Constant	121.598	4.149	-	$P < 0.001$
AASI	157.968	9.910	-0.721	$P < 0.001$

Table 4: Results of multiple linear stepwise regression with (CKD-EPI)-eGFR as the dependent variable.

X	*B* value	Standard error	Beta	*P*
Constant	130.011	7.972	-	$P < 0.001$
AASI	-35.010	6.729	-0.282	$P < 0.001$
Age	-0.603	0.072	-0.420	$P < 0.01$

changes in hemodynamics, less blood flowing into the kidneys, eventually cause kidney damage [10].

This study found that the dynamic arteriosclerosis index (AASI) is linearly related to various indicators of renal damage [11]. As a new indicator of arteriosclerosis, AASI predicts changes in vascular disease earlier and more sensitively than pulse pressure; it mainly reflects the degree of arteriosclerosis. As mentioned earlier, the higher the degree of arteriosclerosis, the closer the AASI is to 1. The better the arterial elasticity, the closer the AASI is to 0 [12]. The pulse pressure mainly depends on the ejection rate of the left ventricle, the stroke volume of the heart, and factors such as the compliance of the large arteries and the pressure reflection waves of the peripheral blood vessels, and as the pulse pressure increases, its damage to blood vessels is also strengthened; the tube wall is in a state of high tension for a long time; it is easy to fatigue and break, and the factor that regulates the vasoconstriction and relaxation function is out of proportion, and vascular endothelial dysfunction strengthens the progression of vascular sclerosis; therefore, pulse pressure has a certain role in reflecting the degree of arteriosclerosis [13]. As obtained from this experiment, according to the AASI grouping, as the AASI level increases, 24 h PP is gradually increasing, but the stability of PP is weaker than that of AASI and is susceptible to changes in blood pressure fluctuations and other factors and affects the accuracy of prediction, so the AASI in this study has become the most suitable indicator for predicting arteriosclerosis [14].

According to the results of this experimental study, AASI can be used as a predictor of renal damage in patients with essential hypertension; at present, a large amount of data has proved that AASI can predict the damage of target organs; for example, it can predict cardiovascular and cerebrovascular diseases, especially the predictive value of stroke is greater. The ambulatory arteriosclerosis index (AASI) is calculated from ambulatory blood pressure monitoring, and ABPM is since the 1960s, one of the important results of studying hypertension; it is required that in daily life, according to the set time interval, it can automatically measure blood pressure, and the series of blood pressure values

obtained include daytime activity and night sleep; it objectively reflects the dynamic changes of human blood pressure [15]. Hypertensive target organ damage (TOD) is a possible result in the development of hypertension; therefore, actively predict the target organ damage caused by hypertension, and intervene in a timely manner; it is of great significance to delay the occurrence of target organ damage [16]. According to research findings, AASI has been confirmed as a predictor of renal damage caused by essential hypertension. AASI is greatly affected by age, the systolic and diastolic blood pressure of normal people slowly increase with age, mainly because the peripheral resistance of blood vessels also increases with age, and for the elderly, the increase in systolic blood pressure is mainly caused by the gradual hardening of the aorta with age and the gradual decrease in the vascular volume of the elastic large arteries; its diastolic blood pressure is reduced, mainly because the amount of blood injected into the periphery from the heart during systole increases, at the beginning of diastole, as the amount of blood remaining in the aorta decreases, and the elasticity of the arteries is weakened, and diastolic blood pressure decreases [17]. And get older with age, human aging, the thickness of the media in the aorta increases, and the elastic fibers become thinner, increasing the stiffness of the aorta; therefore, the results of this study are significantly due to the focus on the predictive value of the dynamic arteriosclerosis index on the renal damage caused by essential hypertension; to summarize the results of this research, AASI is positively correlated with CysC performance and negatively correlated with Ccr, CysC-eGFR, and (CKD-EPI)-eGFR performance. It shows that with the influence of long-term hypertension, the AASI gradually increases, that is, the compliance of the arteries gradually decreases, and the degree of hardening gradually increases, and kidney damage is also gradually getting worse. After adjusting for age factors, after partial correlation analysis, AASI is positively correlated with CysC performance and negatively correlated with Ccr, CysC-eGFR, and (CKD-EPI)-eGFR performance; the P values are all <0.05, indicating the error that may be caused by excluding the age factor, and AASI and renal damage indicators are correlated [18]. Further analyze the multiple linear stepwise regression model, and the result shows that for every 0.01 increase in AASI, cystatin C increased by 0.02 mg/L, creatinine clearance decreased by 0.40 mL/(min · 1.73m^2), CysC-eGFR decreased by 1.58 mL/(min · 1.73m^2), and (CKD-EPI)-eGFR decreased by 0.35 mL/(min · 1.73m^2) (all P values < 0.05), and controlling the confounding factors of age and body mass index, it further illustrates that AASI can be used as an independent predictor of renal damage in patients with essential hypertension. But in this multiple linear stepwise regression analysis, we also found that the creatinine clearance rate decreases by 0.90 mL/(min · 1.73m^2) for every 1 year increase in age, (CKD-EPI)-eGFR decreased by 0.60 mL/(min · 1.73m^2) (all P values < 0.05), and this also suggests that age may also be a factor that promotes kidney damage caused by primary hypertension. In addition, we also found that for every increase in body mass index (BMI) by 1 unit, creatinine clearance decreased by 1.21 mL/(min · 1.73m^2); this also shows that obesity may also be a factor that promotes kidney damage caused by primary hypertension. And Table 4 of the results of this study also shows that AASI has the strongest correlation with cystatin C and CysC-eGFR ($r = 0.637$; $r = -0.698$); tip in the experiment is only in the indicators of cystatin C and CysC-eGFR that the differences in each group were statistically significant.

4. Conclusion

Propose the prediction of renal damage in patients with essential hypertension based on AASI stepwise Regression equation scanning, select qualified subjects to measure 24 h ambulatory blood pressure to calculate AASI, AASI is linearly related to various indicators of renal damage, and it can be used as a predictor of renal damage caused by essential hypertension. Age and 24 h PP also showed an increasing trend with the increase of AASI, it suggests that age may be an influencing factor that promotes kidney damage caused by hypertension, and it also suggests that AASI can be used as a new indicator of arterial compliance. Obesity may also be a factor that promotes kidney damage caused by hypertension. Cystatin C and the estimated glomerular filtration rate CysC-eGFR based on cystatin C are more sensitive to assess the degree of early renal damage than other indicators reflecting glomerular filtration rate.

Data Availability

The data used to support the findings of this study are available from the corresponding author upon request.

Conflicts of Interest

The authors declare that they have no conflicts of interest.

Acknowledgments

The research was funded by the Hebei Provincial Finance Department (2705002).

References

[1] D. W. Kim, S. K. Yoon, D. H. Ha, M. J. Kang, J. H. Lee, and S. Choi, "Ct-based assessment of renal function impairment in patients with acute unilateral ureteral obstruction by urinary stones," *Abdominal Imaging*, vol. 40, no. 7, pp. 2446–2452, 2015.

[2] F. H. Mose, J. M. Jensen, S. Therwani et al., "Effect of nebivolol on renal nitric oxide availability and tubular function in patients with essential hypertension," *British Journal of Clinical Pharmacology*, vol. 80, no. 3, pp. 425–435, 2015.

[3] D. Watanabe, H. Fujii, N. Matsuhashi, H. Iihara, and A. Suzuki, "Dose adjustment of oxaliplatin based on renal function in patients with metastatic colorectal cancer," *Anticancer Research*, vol. 40, no. 4, pp. 2379–2386, 2020.

[4] M. Usman, O. R. Frey, and G. Hempel, "Population pharmacokinetics of meropenem in elderly patients: dosing simulations based on renal function," *European Journal of Clinical Pharmacology*, vol. 73, no. 3, pp. 1–10, 2016.

Hindawi
Scanning
Volume 2023, Article ID 9819368, 1 page
https://doi.org/10.1155/2023/9819368

Retraction

Retracted: Scanning Imaging Study of Patients with Parkinson's Disease Lower Urinary Tract Dysfunction Based on Linear Equation

Scanning

Received 3 October 2023; Accepted 3 October 2023; Published 4 October 2023

This article has been retracted by Hindawi following an investigation undertaken by the publisher [1]. This investigation has uncovered evidence of one or more of the following indicators of systematic manipulation of the publication process:

(1) Discrepancies in scope

(2) Discrepancies in the description of the research reported

(3) Discrepancies between the availability of data and the research described

(4) Inappropriate citations

(5) Incoherent, meaningless and/or irrelevant content included in the article

(6) Peer-review manipulation

The presence of these indicators undermines our confidence in the integrity of the article's content and we cannot, therefore, vouch for its reliability. Please note that this notice is intended solely to alert readers that the content of this article is unreliable. We have not investigated whether authors were aware of or involved in the systematic manipulation of the publication process.

In addition, our investigation has also shown that one or more of the following human-subject reporting requirements has not been met in this article: ethical approval by an Institutional Review Board (IRB) committee or equivalent, patient/participant consent to participate, and/or agreement to publish patient/participant details (where relevant).

Wiley and Hindawi regrets that the usual quality checks did not identify these issues before publication and have since put additional measures in place to safeguard research integrity.

We wish to credit our own Research Integrity and Research Publishing teams and anonymous and named external researchers and research integrity experts for contributing to this investigation.

The corresponding author, as the representative of all authors, has been given the opportunity to register their agreement or disagreement to this retraction. We have kept a record of any response received.

References

[1] Y. Liu, J. Han, X. Guo, L. Fang, and T. Liu, "Scanning Imaging Study of Patients with Parkinson's Disease Lower Urinary Tract Dysfunction Based on Linear Equation," *Scanning*, vol. 2022, Article ID 9506328, 6 pages, 2022.

Hindawi
Scanning
Volume 2022, Article ID 9506328, 6 pages
https://doi.org/10.1155/2022/9506328

Research Article

Scanning Imaging Study of Patients with Parkinson's Disease Lower Urinary Tract Dysfunction Based on Linear Equation

Yong Liu,[1] **Jiasheng Han**,[2] **Xuguang Guo**,[2] **Lei Fang**,[3] **and Ting Liu**[2]

[1]*Neurology Department, The 80th Group Army Hospital of the People's Liberation Army, Weifang, Shandong 261021, China*
[2]*Urinary Surgery, The 80th Group Army Hospital of the People's Liberation Army, Weifang, Shandong 261021, China*
[3]*School of Public Health, Weifang Medical College, Weifang, Shandong 261021, China*

Correspondence should be addressed to Ting Liu; 11133147@stu.wxic.edu.cn

Received 21 March 2022; Revised 1 May 2022; Accepted 9 May 2022; Published 27 May 2022

Academic Editor: Danilo Pelusi

A predictive method based on a linear equation was proposed to study the factors influencing lower urinary tract dysfunction in Parkinson's disease. A 10-month follow-up of 200 selected Parkinson's patients from January to December 2020 used a linear regression equation to analyze whether depletion function was associated with a specific nonmotor function loss, and a linear regression equation was used for analysis. A loss of emptiness function was used to determine whether there are complications associated with lower motor function and cognitive function. The experimental results showed that dysuria in Parkinson's disease was related to the following nonmotility disorders: gastrointestinal dysfunction (OR 2.52, 95% CI 1.57-3.92, $P < 0.001$), cardiovascular dysfunction (OR 2.31, 95% CI 1.23~4.11, $P = 0.014$), respiratory dysfunction (OR 1.72, 95% CI 1.32~3.24, $P = 0.029$), cutaneous autonomic dysfunction (OR 1.91, 95% CI 1.15~3.08, $P = 0.023$), and sleep disorders (OR 2.01, 95% CI 1.32~3.14, $P = 0.001$). In addition, dysuria was associated with higher UPDRS-III (regression coefficient 1.74, 95% CI 0.56-2.67, $P = 0.001$). Thus, nonmotor disorders have been shown to be associated with early impairment.

1. Introduction

Parkinson's disease (PD) is a progressive degenerative disease of the central nervous system; its typical symptom is motor dysfunction, which mainly includes motor retardation, muscle rigidity, resting tremor, and ataxia. For a long time, the treatment of PD is mainly to improve motor symptoms [1]. A large-scale epidemiological survey showed that, for 206 cases in 2019, 304 cases in 2018, and 404 cases in 2017, the incidence of lower urinary tract dysfunction in PD patients is as high as 27.0% to 63.9%, mainly including overactive bladder (OAB), nocturia, urge incontinence (UI), and detrusor overactivity [2]. In addition, some patients will have slight urinary tract obstruction. Lower urinary tract function involves the regulation of multiple nerve pathways, and the mechanism of lower urinary tract dysfunction in PD patients is complicated; the current study believes that it may be due to basal ganglia disease in PD patients, interfering with the function of the pontine voiding center. Studies have shown that about 90% of Parkinson's patients will have some degree of speech disorder; therefore, it is more convenient and effective to directly collect voices for research through noncontact methods, such as array microphones, compared with other diagnostic methods. This has caused great attention on the research on voice-based Parkinson's diagnosis and treatment programs. With the rapid development of computer technology, in recent years, people have applied many diagnosis and treatment programs based on machine learning algorithms to study Parkinson's disease, in order to completely replace clinical decision-making [3]. These diagnosis and treatment plans are mainly classified into two categories: (1) determining whether the user has Parkinson's disease, that is, realizing the diagnosis of Parkinson's disease (the common one is based on the linearly separable and nonlinear separable data and linear SVM and nonlinear SVM application for research); (2) predicting the severity of Parkinson's disease patients, that is, tracking the progress of Parkinson's disease by predicting UPDRS (unified Parkinson's disease rating scale) [4].

24-month follow-up data showed that the prevalence of early urinary dysfunction in Parkinson's is stable at about

50%. In the study, the lowest rate of patients with urination disorders was 47.86% (T1) and the highest was 51.28% (T2); it is basically consistent with the research results of Picillo et al. The above data shows that urination disorders can appear in the early stage of the disease and basically remained stable as the disease progressed; it further supports that Parkinson's disease dysuria may be related to early autonomic nerve damage [5]. However, Senol's statistical study showed that Parkinson's patients with urinary dysfunction accounted for 63.9%. The reason for the difference in the above data may be that Picillo et al. and this study are both the results of the statistics of Parkinson's early urinary dysfunction; the entire natural history of the development and evolution of urination disorders is not covered [6]. Research by Lindsay et al. showed that patients with Parkinson's urinary dysfunction had more nonmotor symptoms than those without urinary dysfunction [7]. Based on this, the study conducted a 10-month follow-up observation of 200 Parkinson's disease patients selected from January to December 2020; linear regression equation was used to analyze whether urinary dysfunction is related to specific nonmotor dysfunction and to analyze whether urinary dysfunction is related to lower motor function and cognitive function. Prospective data analysis was used in order to clarify the marker role of Parkinson's early urination disorder in the progression of dysfunction (nondyskinesia and dyskinesia).

2. Prediction of Parkinson's Disease UPDRS Based on GBDT

2.1. Data Set Description. This article uses the remote Parkinson's data set in UCI, which contains 42 speech samples with Parkinson's disease; the sample is derived from the continuous vowel/a/voice collected from the patient once a week, collected 6 pieces each time, lasting 6 months, at a total of 5875 samples. Through the speech signal processing algorithm, the total number of features extracted from these speech samples is 16; among them, the characteristics that measure the change of the fundamental frequency are as follows: jitter (%), jitter absolute value (Abs), relative amplitude perturbation jitter (RAP), 5-point period perturbation entropy jitter (PPQ5), and absolute difference of the period and the average period ratio jitter (DDP); the characteristics that measure the amplitude change are as follows: local flicker (dB) shimmer (dB), 3-point amplitude perturbation entropy shimmer (APQ3), 5-point amplitude perturbation entropy shimmer (APQ5), 11-point amplitude perturbation entropy shimmer (APQ11), average absolute difference of the amplitude difference between adjacent period shimmer (DDA), noise harmonic ratio (NHR), harmonic noise ratio (HNR), cyclic period density entropy (RPDE), trend fluctuation analysis (DFA), and pitch period entropy (PPE). And finally, a sample set of$5875 * 16$is obtained [8].

2.2. Data Set Division. Computers can use machine learning to construct various linear regression equations to solve the same or similar problems. However, for the establishment of a good linear regression equation, in addition to relying on a suitable algorithm, the computing power of the computer also requires data preprocessing for the data set. Using the remote

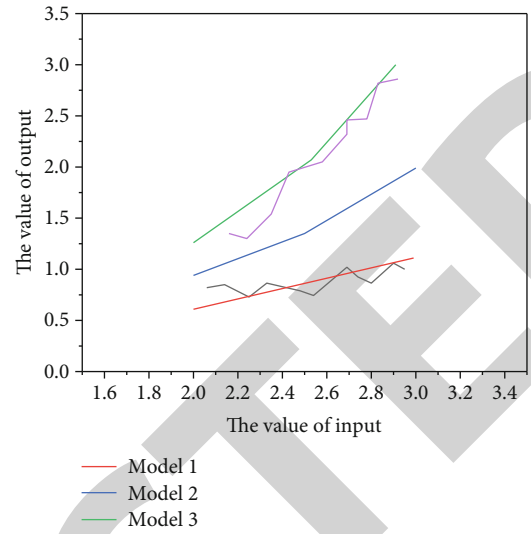

Figure 1: Regression training model.

Parkinson data set in UCI and using LS to train the prediction model, a certain prediction effect has been achieved. In this article, two different data sets are taken as examples, using ordinary least squares to train a regression prediction model, model 3, as shown in Figure 1. Taking into account the distribution of sample data, obviously, model 3 has made a compromise in order to fit object samples in two different domains; the real prediction effect of this model is not very satisfactory. The learning of the regression model is to calculate the square error between the predicted value and the true value of all data, and the error is accumulated so that the positive difference and the negative difference cancel each other out. This will lead to regression prediction on sample data sets with different distributions, that is, different domains, but the same model can be obtained. The concept of data set distribution is more complicated; in general, the sample size of each type should be conducive to the establishment and evaluation of the model [9]. According to the principle of Occam's razor, when choosing a model, a very simple model that can interpret the known data well is the most suitable model [10]. Analyzing the remote Parkinson data set, the model 3 built on these two objects is obviously underfitting, but if the two objects are divided into two domains of data according to a certain prior knowledge and then the original model is decomposed on the two domains, then the model 1 and model 2 established on the two domains can fit the data in the respective domains well, as shown in Figure 1. Therefore, the data set is divided according to the gender and age of the object, and linear regression equations are established on different data sets to achieve effective decomposition [11]. In practical applications, the user's voice is collected, and according to the user's age and gender, a suitable model is given through the recommendation system to realize the prediction of the user's UPDRS. The principle is shown in Figure 2.

2.3. Iterative Decision Tree. Integrated learning can significantly improve the generalization ability of the learning system; it has received extensive attention from the linear

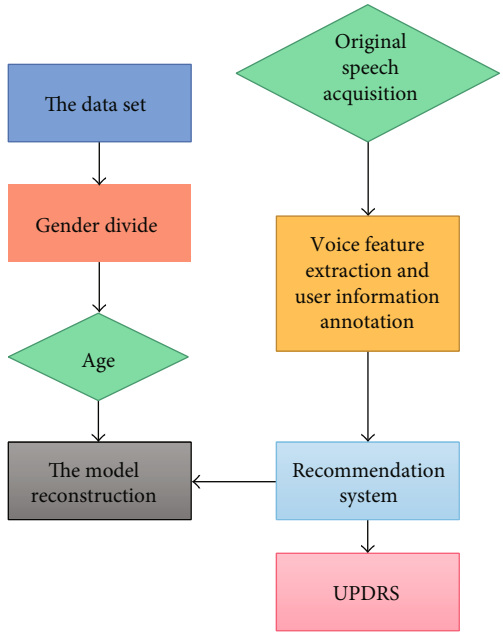

Figure 2: Implementation process.

regression equation community. GBDT is an integrated learning algorithm; a strong learner is generated by the combination of multiple weak learners. The algorithm is continuously iterated by multiple decision trees; through iteration, the linear regression and residuals of all trees are equal to or approaching 0, and a high-accuracy prediction model is finally obtained.

Assume that the initially obtained learner is

$$F_0(x) = agr \min_a \sum_{i=1}^{n} L(y_i, a). \tag{1}$$

Among them, $L(y_i, a)$ is the loss function of model $f(x)$. $((x_i, y_i))_{i=1}^n$ is the sample training set, x_i is the feature, and the corresponding result is y_i.

First, according to the current data, the loss function is minimized, and the initial loss function model is obtained. The number of iterations is set to M; each iteration produces a model, in order to minimize the loss function of the model generated in each iteration to the training set, according to equation (1); in each iteration, the loss function is made smaller and smaller by moving to the negative gradient direction of the loss function, to get more and more accurate models. The main steps of algorithm iteration are as follows.

The first step is to calculate the residual r_a.

Use the initial model $F_0(x)$ to calculate the negative gradient, as shown in equation (2). The negative gradient of the loss function is used as the residual for the current model $F_0(x)$ value. For the square loss function, this value is the residual, and for the general loss function, this value is the estimated value of the residual.

$$r_{i1} = -\left[\frac{\partial L(y_i, F_0(x_i))}{\partial F_0(x_i)}\right], \quad i = 1, 2, \cdots, n. \tag{2}$$

The second step is to train a linear regression equation and get the decision tree $h_1(x)$ composed of leaf nodes.

The third step is to find a suitable step length. In the gradient descent used in the GBDT algorithm, the step size is obtained by calculation. The calculation rule is to minimize the $F_1(x)$ loss function β_1 value of the new learner.

$$\beta_1 = agr \min_a \sum_{i=1}^{n} L(y_i, F_0(x_i) + ah_1(x_i)). \tag{3}$$

The fourth step, according to the gradient and step length, is to iteratively obtain the regression tree model $F_1(x)$, as shown in the following equation:

$$F_1(x) = F_0(x) + \beta_1 h_1(x). \tag{4}$$

Through the above four steps, the second model $F_1(x)$ can be optimized from the initial model $F_0(x)$. Iterate these four steps $M - 1$ times to get the final GBDT model.

3. Experimental Analysis

3.1. Data Preprocessing. Data preprocessing generally includes operations such as feature selection and data cleaning. Feature selection refers to selecting a subset of important features from the original feature set. Feature selection can remove redundant or irrelevant features, in order to achieve the purpose of improving the generalization ability of the model. The feature selection algorithm used in this article is Relief [12]. The earliest Relief algorithm was used to solve the problem of two classifications, the algorithm designs a relevant statistical vector to evaluate the importance of each feature, each component of the vector is the evaluation value of one of the initial features, the importance of a feature subset is the sum of relevant statistics of all features in the subset, and this correlation statistic is regarded as the weight of each feature; that is, Relief belongs to a feature weighting algorithm. The formula is as follows:

$$W(f_j) = \frac{1}{q}\sum_{i=1}^{q}\left\{-\frac{1}{|NH(X_i)|}\cdot\sum_{X_n\in NH(X_i)}\|x_{i,j} - x_{n,j}\| + \sum_{y_l\neq y_i}\frac{1}{|NM(X_i)|}\cdot\frac{p(y=y_l)}{1-p(y=y_l)}\cdot\sum_{X_n\in NH(X_i)}\|x_{i,j} - x_{n,j}\|\right\}. \tag{5}$$

Among them, $W(f_j)$ represents the weight of the j-th feature, q represents the number of samples randomly selected, X_i represents a data sample, $|NH(X_i)|$ represents the number of similar samples closest to sample X_i, $|NH(X_i)|$ represents the number of different types of samples closest to the sample X_i, and $\|\cdot\|$ represents the distance measurement, commonly using the Euclidean distance or Manhattan distance. Use the Relief algorithm to get feature weights; the importance of the features is sorted according to the weight, and the top 13 important features are selected. After the feature selection is completed, the data cannot be directly used for calculation; in many cases, some basic

processing of the data is required [13]. These basic processing includes the processing of missing values, the processing of nondigital feature values, and the processing of outliers; the remote Parkinson data set has been cleaned up.

3.2. Statistical Methods. Perform a normal distribution test on the collected data; subsequently, the data of PD-UD and PD-NUD groups were subjected to χ^2 test, t test, and one-way analysis of variance (ANOVA) according to the situation. The results are expressed in percentage (%), mean, and standard deviation (SD) ($x \pm s$). To examine the relationship between nonmotor dysfunction and early urination disorders, multivariate mixed-effect linear regression equations were used to control independent variables such as age and UPDRS-III. To examine the relationship between motor function, cognitive function, and early voiding dysfunction, multiple mixed-effect linear regression analysis was performed, with gender and age as covariates, and covariance analysis was performed. All covariates were tested for multicollinearity. When the variance inflation factor is less than 5, all predictors can be considered independent. The analysis result is expressed by odds ratio (OR) and regression coefficient. The study used 95% confidence interval (CI); $P \leq 0.05$ as the difference was statistically significant [14].

3.3. Experimental Method. Each patient undergoes 3 data collections: T1 (baseline value), T2 (3 months), and T3 (9 months). During the follow-up period, if the patient develops other diseases (such as cerebral infarction, cerebral hemorrhage, and cerebellar atrophy) that may affect motor, nonmotor functions, and urinary symptoms, and if it is difficult to distinguish symptoms that affects the accuracy of the data, the sample will be eliminated. Each data collection includes the following:

(1) Collect samples for urination disorders. Those who have one of the following symptoms and last for more than 3 months can be considered as combined urination disorders: (1) urgency, (2) frequent urination (≥1 time/2 h), and (3) nocturia. Patients with positive results were classified into the urinary dysfunction group (PD-UD), and the rest were classified into the nonurinary dysfunction group (PD-NUD).

(2) Investigate the following 6 nonmotor dysfunctions through face-to-face interviews: gastrointestinal dysfunction, cardiovascular dysfunction, sleep disorders, respiratory dysfunction, mental disorders, and skin lesions. Each NMS includes several specific questions, and the answers are all divided into two parts ("yes" or "no").

(3) The motor function level of the samples was evaluated by the unified Parkinson's disease rating scale 3.0 (UPDRS-III). The higher the UPDRS-III score, the lower the patient's motor function level

4. Experimental Results

A total of 204 of 324 Parkinson's patients passed the screening. During the 9-month observation period, 4 cases were excluded due to new cerebral infarction, and the final sample count was 200 cases [15]. During the entire observation period, the lowest prevalence of urination disorders was T147.86%, and the highest was T251.28%. Data are shown 3 times, the PD-UD group is usually older and more male, and the UPDRS-III score is higher than that of the PD-NUD group. The prevalence of almost all nonmovement disorders in the PD-UD group was higher than that in the PD-NUD group, and the difference was statistically significant ($P < 0.05$) [16]. After linear regression analysis, the following nonmotility disorders may be associated with early voiding disorders: gastrointestinal dysfunction (OR 2.52, 95% CI 1.57-3.92, $P < 0.001$), cardiovascular dysfunction (OR 2.31, 95% CI 1.23-4.11, $P = 0.014$), sleep disturbance (OR 2.01, 95% CI 1.32~3.14, $P = 0.001$), respiratory dysfunction (OR 1.72, 95% CI 1.32~3.24, $P = 0.029$), and autonomous skin disease (OR 1.91, 95% CI 1.15-3.08, $P = 0.023$). Figure 3 shows a comparison of the degree of motor function between PD-NUD and PD-UD during the observation period. In the three sets of data, both T1 and T2 showed that there was no statistical difference in the relationship between mental disorders and urinary system diseases. Multiple linear regression analysis showed that compared with PD-NUD, early voiding disturbance was associated with higher UPDRS-III (regression coefficient 1.74, 95% CI 0.56-2.67, $P = 0.001$) [17].

Figure 4 Comparison of the cognitive function of PD-NUD and PD-UD during the observation period, It can be clearly seen from Figure 3 that the reduction in motor function level in the PD-UD group was more significant within 9 months. A recent domestic study shows that the untreated Parkinson's overactive bladder symptom score (OABSS score) was positively correlated with the UP-DRS-III score and the hypoactive rigidity score. The study also showed that the degree of dyskinesia and the use of levodopa in Parkinson's patients with urinary dysfunction increased significantly after 24 months. Consistent with the above conclusions, the study also confirmed the link between early urination disorders and lower levels of motor function [18]. The study also showed that early urination disorders are related to the following nondyskinesias through linear regression equation analysis, including gastrointestinal dysfunction (OR 2.52, 95% CI 1.57~3.92, $P < 0.001$), cardiovascular dysfunction (OR 2.31, 95% CI 1.23~4.11, $P = 0.014$), respiratory dysfunction (OR 1.72, 95% CI 1.32~3.24, $P = 0.029$), autonomic skin disorders (OR 1.91, 95% CI 1.15~3.08, $P = 0.023$), and sleep disturbance (OR 2.01, 95% CI 1.32~3.14, $P = 0.001$). Among them, gastrointestinal dysfunction, cardiovascular dysfunction, skin lesions, and urination disorders are all autonomic nerve dysfunction. Studies have shown that the cause of urinary disturbance and sleep disturbance may be related to brainstem lesions in the early stage of the disease [19]. As can be seen from Figure 4, the score of the PD-UD group decreased more significantly than that of the PD-NUD group within 9 months, and linear regression analysis also showed dysuria (regression coefficient -0.21, 95% CI -0.87~0.22, $P = 0.043$), the research conclusions were inconsistent (regression coefficient -0.34, 95% CI -0.92~0.24, $P = 0.251$), and there was

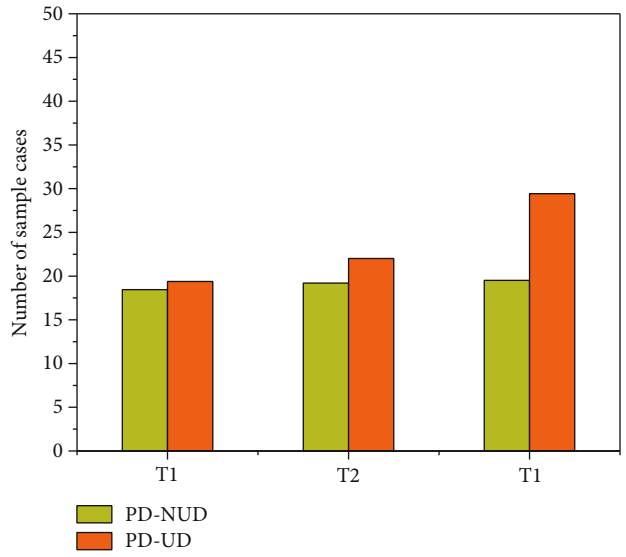

Figure 3: Comparison of the degree of motor function between PD-NUD and PD-UD during the observation period.

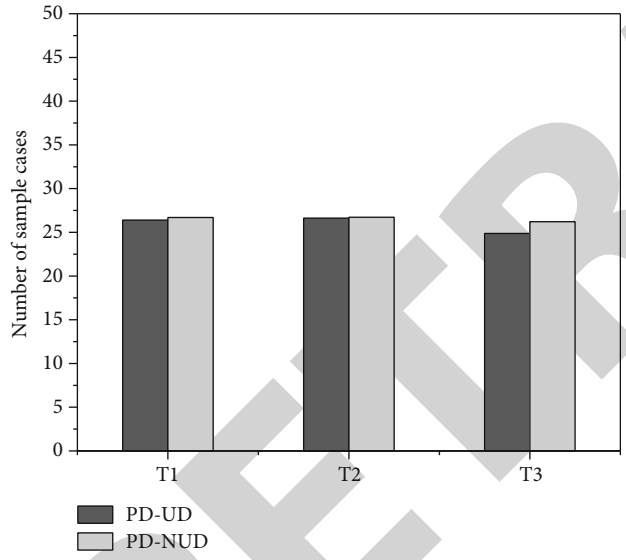

Figure 4: Comparison of the cognitive function of PD-NUD and PD-UD during the observation period.

no statistical difference between the two. Therefore, the correlation between early Parkinsonian urinary dysfunction and cognitive function level still needs high-level research to continue [20].

5. Conclusion

Studies have shown that urinary dysfunction in Parkinson's disease can be used as an early clinical indicator of the progression of dyskinesia and nondyskinesia. Experimental results show that the final prediction effect is more than half that of the ordinary decision tree; at the same time, it has been further verified that Parkinson's disease is greatly affected by age and gender. Gender and age belong to prior knowledge; using these kinds of prior knowledge to decompose prediction models not only is simple and efficient but also has certain practical guiding significance. Of course, in addition to gender, there are many other kinds of a priori knowledge of life, such as the patient's health status, loss of gastrointestinal function, cardiovascular dysfunction, skin lesions, and sleep disorders. Many of these are associated with loss of autonomic function, which to some extent supports the classification of nonmotor symptoms of Parkinson's disease. The functional classification is long. Sufficient classification of Parkinson's disease, in particular, a comprehensive assessment system covering motor and nonmotor functions, is needed.

Data Availability

The data used to support the findings of this study are available from the corresponding author upon request.

Conflicts of Interest

The authors declare that they have no conflicts of interest.

References

[1] P. Sulzer, A. Bumer, H. G. Hoang, S. Becker, and I. Liepelt-Scarfone, "Assessment of cognitive-driven performance-based activities of daily living dysfunction in Parkinson's disease," *Journal of the International Neuropsychological Society*, vol. 26, no. 4, pp. 430–440, 2019.

[2] K. R. Chaudhuri, "Thirty years of research on autonomic dysfunction, non-motor features, and endophenotypes in Parkinson disease," *Clinical Autonomic Research*, vol. 31, no. 1, pp. 37–39, 2021.

[3] H. Li, S. Liang, Y. Yu, Y. Wang, and X. Tong, "Clinical experience of comprehensive treatment on the balance function of Parkinson's disease," *Medicine*, vol. 99, no. 19, article e20154, 2020.

[4] S. K. Kim, K. H. Kim, S. H. Kim, S. J. Yoo, and Y. W. Jeong, "Health-related quality of life in adult males with lower urinary tract symptoms," *Quality of Life Research*, vol. 28, no. 9, pp. 2419–2428, 2019.

[5] I. Stefanova, A. C. Currie, R. C. Newton et al., "Systematic review and meta-analysis of the impact of bariatric surgery on lower urinary tract symptoms in males," *Obesity Surgery*, vol. 31, no. 7, pp. 3151–3158, 2021.

[6] S. Tonyali, "Alpha-blockers are widely used in medical expulsion therapy for ureteral stones besides management of lower urinary tract symptoms," *World Journal of Urology*, vol. 37, no. 9, pp. 1981–1981, 2019.

[7] L. H. Keir and D. P. Breen, "New awakenings: current understanding of sleep dysfunction and its treatment in Parkinson's disease," *Journal of Neurology*, vol. 267, no. 1, pp. 288–294, 2020.

[8] L. Zhang and J. Zhu, "1121 nonmotor symptoms affect sleep quality in early-stage Parkinson's disease patients with or without cognitive dysfunction," *Sleep*, vol. 43, Supplement_1, pp. A427–A427, 2020.

[9] C. Lina, J. Ana, F. Reginaldo, S. Carolina, and S. Genoile, "P063 manometric study and the role of the perianal disease and the clinical activity in anorectal dysfunction in Crohn's disease,"

Hindawi
Scanning
Volume 2023, Article ID 9823960, 1 page
https://doi.org/10.1155/2023/9823960

Retraction

Retracted: The Pathogenesis and Influencing Factors of Adult Hypertension Based on Structural Equation Scanning

Scanning

Received 20 June 2023; Accepted 20 June 2023; Published 21 June 2023

This article has been retracted by Hindawi following an investigation undertaken by the publisher [1]. This investigation has uncovered evidence of one or more of the following indicators of systematic manipulation of the publication process:

(1) Discrepancies in scope

(2) Discrepancies in the description of the research reported

(3) Discrepancies between the availability of data and the research described

(4) Inappropriate citations

(5) Incoherent, meaningless and/or irrelevant content included in the article

(6) Peer-review manipulation

The presence of these indicators undermines our confidence in the integrity of the article's content and we cannot, therefore, vouch for its reliability. Please note that this notice is intended solely to alert readers that the content of this article is unreliable. We have not investigated whether authors were aware of or involved in the systematic manipulation of the publication process.

In addition, our investigation has also shown that one or more of the following human-subject reporting requirements has not been met in this article: ethical approval by an Institutional Review Board (IRB) committee or equivalent, patient/participant consent to participate, and/or agreement to publish patient/participant details (where relevant).

Wiley and Hindawi regrets that the usual quality checks did not identify these issues before publication and have since put additional measures in place to safeguard research integrity.

We wish to credit our own Research Integrity and Research Publishing teams and anonymous and named external researchers and research integrity experts for contributing to this investigation.

The corresponding author, as the representative of all authors, has been given the opportunity to register their agreement or disagreement to this retraction. We have kept a record of any response received.

References

[1] Y. Wu, G. Ma, N. Feng, Z. Zhang, S. Zhang, and X. Li, "The Pathogenesis and Influencing Factors of Adult Hypertension Based on Structural Equation Scanning," *Scanning*, vol. 2022, Article ID 2663604, 6 pages, 2022.

Hindawi
Scanning
Volume 2022, Article ID 2663604, 6 pages
https://doi.org/10.1155/2022/2663604

Research Article

The Pathogenesis and Influencing Factors of Adult Hypertension Based on Structural Equation Scanning

Yaqiong Wu,[1] **Guangyu Ma**,[2] **Nana Feng**,[1] **Zhiqiang Zhang**,[1] **Sijie Zhang**,[1] **and Xingtao Li**[1]

[1]*The Department of Cardiology, Fourth Hospital of Hebei Medical University, Shijiazhuang, Hebei 050011, China*
[2]*The Department of Haematology, Fourth Hospital of Hebei Medical University, Shijiazhuang, Hebei 050011, China*

Correspondence should be addressed to Yaqiong Wu; 15035102210053@hainanu.edu.cn

Received 30 March 2022; Revised 1 May 2022; Accepted 9 May 2022; Published 27 May 2022

Academic Editor: Danilo Pelusi

Explore the pathogenesis and influencing factors of adult hypertension based on structural equation scanning. Using a multistage random sampling method, randomly select 2 community health service centers in each administrative area of a certain city and conduct a sample survey of residents in the community. According to the predetermined sample size n, multiply by 1.3 ($1.3n$) to draw a sample. Community doctors and medical students who have been uniformly trained form an investigation team draw up a questionnaire by consulting the literature, seek expert opinions, and then make changes based on the questions in the preinvestigation. Experiment result shows that the average systolic blood pressure of the experimental subjects was 126.13 + 15.36 mmHg and the average diastolic blood pressure was 79.52 + 8.81 mmHg; males are higher than females and increase with age. The prevalence rate of hyperemia is 26.3%, and the prevalence rate of prehypertension among the survey subjects is 55.4%; that of males (62.6%) is higher than that of females (49.2%). The prevalence of isolated systolic hypertension was 7.5%, and that of men (6.9%) was lower than that of women (7.9%). The awareness rate of hypertension was 66.5%, and the treatment rate of hypertension was 62.7%; the control rate of hypertension was 13.2%, and the control rate of hypertension treatment was 25.7%; all the abovementioned rates are higher for women than for men, and they all tend to increase with age which proved that being overweight is a risk factor for hypertension, dyslipidemia, and hypertension. Hypertension, dyslipidemia, and family history of hypertension are risk factors for hypertension. There is a positive correlation between hypertension and dyslipidemia.

1. Introduction

Hypertension refers to the increase in systemic arterial blood pressure (systolic blood pressure and/or diastolic blood pressure) (systolic blood pressure ≥ 140 mmHg (1 mmHg = 0.133 kPa), diastolic blood pressure ≥ 90 mmHg) which is the main feature; it may be accompanied by clinical syndromes of organ function or organic damage such as that in the heart, brain, and kidney. Hypertension is currently one of the main diseases threatening human health, it not only caused serious physical, mental, and economic damage to patients but also brings a significant economic burden of disease to all mankind. Hypertension is a disease caused by multiple causes; according to research, hypertension is affected by the interaction of genetic, social, and lifestyle factors, with the improvement of living standards; the choice of diet has increased; obesity among adolescents is also increasing; as a result, hypertensive patients are gradually becoming youthful, which further makes hypertension an important public health problem [1]. In addition, the complications caused by high blood pressure cannot be ignored; in China, hypertension combined with coronary heart disease is more common. As a kind of high blood pressure, it has obvious characteristics of high blood pressure; the quality of life of patients can be improved by improving living habits after the onset of disease. With the development of social economy and the progress of urbanization, with the increase in life expectancy, the problem of population aging has become more and more serious [2]. According to the China Health Service Survey, the prevalence of hypertension

in middle-aged and elderly people is gradually increasing and the phenomenon of multiple types of hypertension in the elderly is becoming more and more serious; it has become a major public health problem in China. There are many factors that affect the number of hypertension in the elderly; previous studies only analyzed the direct effects of related influencing factors on the number of hypertension; the interaction between factors and the indirect effects on outcome variables are ignored. Structural equation scanning modeling can incorporate multiple variables into the model at the same time and observe the interaction between various variables and the direct or indirect effects on the outcome variables; it can fully explain the influence of research factors on outcome variables.

With the rapid increase in the prevalence of hypertension, the disability, death, and related diseases caused by it have greatly threatened the health and social and economic development of Chinese residents. What is more worrying is that among hypertensive patients, less than 50% of hypertensive patients know that they are sick; only 25% of those are taking medication and control blood pressure to less than 10% of the normal range. The high prevalence, low awareness, treatment, and control rates of hypertension have become the bottleneck for the prevention and treatment of cardiovascular disease in China [3]. In response to this research question, according to Duarte and others, being overweight or obesity is one of the important factors for elevated blood pressure, regardless of whether children or adults; body weight is highly correlated with blood pressure. Relevant information shows that those who are overweight and have a family history of hypertension may have a dual effect, which will have a synergistic effect [4]. The body mass index of most individuals has a significant correlation with the percentage of body fat; it can better reflect the degree of obesity of the body. Increased body mass index is an independent risk factor for hypertension. Wang et al. believe that dietary factors are the most important environmental factors related to cardiovascular disease [5]. Although the Chinese diet is low in fat compared to the Western diet, low saturated fat and low cholesterol help to keep serum cholesterol and body mass index at a low level, but at the same time, China's low-calcium, low-potassium, and low-animal protein diets also promote the blood pressure effect of sodium. Therefore, the Chinese diet based on plant foods has many factors that promote blood pressure and has a lack of protective factors; this may be the reason why the Chinese population who has been exposed to high sodium for a long time has a greater slope of blood pressure with age than other populations. The influence of dietary factors on blood pressure is the result of the combined effect of many factors [6]. According to Diederichs and Neuhauser, the main risk factors for male hypertension are BMI and salt intake; the main risk factors for women are serum total cholesterol, age, and BMI; the content of total cholesterol in serum is affected by the intake of meat, fish, and green vegetables. Salt intake is positively correlated with high blood pressure in men, but there is no such relationship in women [7].

Based on the current research, this paper investigates the influence of social and economic background on overweight, hypertension, dyslipidemia and hypertension through individual lifestyle behaviors, such as smoking, drinking, exercise and salt intake, through a sample survey of community residents in a city. The main findings are as follows: family history of hypertension, dyslipidemia, hypertension, overweight, and lifestyle behavior (salt intake, active exercise, drinking, and smoking) are risk factors for hypertension.

2. Method

2.1. Experimental Subjects. The survey object is the permanent population of a certain urban area, aged 18–80 years. Two community health service centers were randomly selected from each district, and samples were drawn according to the predetermined sample content n, multiplied by 1.2 ($1.2n$). The respondent was asked to sit and rest for 5 minutes before measuring blood pressure and asked if they smoked or drank within half an hour before the measurement; those who smoked or drank within half an hour were excluded and included in the analysis; all respondents signed an informed consent form.

2.2. Principle of the Structural Equation Scanning Model. Structural equation scanning modeling introduces path analysis into hidden variables; at the same time, using the method of factor analysis, the hidden variables and the observed variables are effectively combined and the multivariate statistical analysis method is proposed [8]. It is an analysis method that combines factor $H_0 : F_A = F_B$ analysis and path analysis; compared with traditional analysis methods, it can handle the relationship between multiple dependent variables and independent variables at the same time and clarify the relationship structure between factors [9].

The structural equation scanning model consists of two parts, the measurement model and the structural model.

The measurement model is equivalent to factor analysis, which can explain the subordination between the measured variable and the latent variable of its response, and its equation is expressed as

$$\begin{aligned} x &= A_x \xi + \delta, \\ y &= A_y \eta + \varepsilon. \end{aligned} \tag{1}$$

x, y represent exogenous and endogenous measurement variables, respectively, ξ, η are exogenous and endogenous latent variables, respectively; A_x, A_y are the relationship between exogenous measured variables and latent variables and endogenous measured variables and latent variables; A_x is the factor loading matrix of the exogenous index on the exogenous latent variable, and A_y is the factor loading matrix of the endogenous index on the endogenous latent variable; δ and ε are the error terms of exogenous and endogenous measurement variables. Exogenous means that the factor only affects other factors; it is not affected by other factors. Endogenous means that the factor is affected by other factors and can affect other factors [10].

The structural model is equivalent to path analysis, explaining the relationship between the latent variables, and its equation is expressed as

$$\eta = B\eta + r\xi + \zeta. \quad (2)$$

η is the endogenous latent variable, ξ is the exogenous latent variable, and B is the relationship between the endogenous latent variable; r is the influence of exogenous latent variables on endogenous latent variables; ζ is the residual term of the structural equation scanning, reflecting the part that η cannot be explained in the equation [11].

The fitting of the structural equation scanning model requires 8 matrices; in addition to the 4 matrices $A_x A_y Br$ appearing in the abovementioned two models, the other 4 matrices are Φ (covariance matrix of exogenous latent variable ξ), Ψ (covariance matrix of error variable ζ), Θ_ε (the covariance matrix of the endogenous observation variable error term ε), and Θ_δ (exogenous indicator variable error term δ covariance matrix). Through the transformation of these eight matrices, a new variance covariance matrix S about Y and X can be obtained; compare the original data variance covariance matrix with the newly generated matrix S, to judge the fitting effect; the closer the two are, the better the fitting effect [12].

The basic principles of the structural equation scanning model can be summarized as two types of variables (explicit variables and latent variables), two models (measurement model and structural model), and two pathways (path between latent and explicit variables and the path between latent variables). Structural equation scanning models can also fit multiple sets of data at the same time. This function is mainly used to test the applicability of the same model among different sample data [13]. At this time, the first thing to check is whether the shape of the model is consistent between different groups (forms)$H_0 : F_A = F_B$, including the number of index variables and latent variables in the model, the subordination relationship, and the structural relationship between the latent variables, only if this condition is met, in order to continue to check whether the covariance matrices of the model parameters are equal (covariance matrices) $H_0 : \Sigma_A = \Sigma_B$. Among the various parameters, we must first test the consistency of the load between the latent variable and the index variable (A_X, A_y). On this basis, it can be tested in turn according to the essence of the research question:

$$H_0 : B_A = B_B,$$
$$r_A = r_B,$$
$$H_0 : B_A = B_B,$$
$$r_A = r_B,$$
$$\Phi_A = \Phi_B,$$
$$H_0 : B_A = B_B,$$
$$r_A = r_B,$$
$$\Phi_A = \Phi_B,$$
$$\Psi_A = \Psi_B. \quad (3)$$

In the abovementioned formula, Φ is the variance and covariance of the measurement error and Ψ is the variance and covariance of the regression residual. The abovementioned layers are assumed to be nested relationships, based on $H_0 : F_A = F_B$; when the first hypothesis is rejected, the later hypothesis does not need to be tested [14]. When the previous hypothesis is true, it can be tested by the likelihood ratio, that is, the difference of X^2 between two adjacent hypothetical models (ΔX^2) and the difference of degrees of freedom (Δdf) to determine; set whether there is a difference between the new model formed by an equal part of the parameters and the previous model. If the likelihood ratio result is significant, it means that there are differences between the two models with nested relationships and the research hypothesis corresponding to the second model is rejected [15].

The evaluation of the structural equation scanning model is mainly based on the index of goodness of fit that cannot meet the corresponding standard. The test of the goodness of fit of the structural equation scanning model is not as straightforward as other multivariate statistical analysis methods, because there is no indicator that can tell whether the model fits correctly, but researchers can compare the goodness of fit of different models based on these indicators. In other words, although the structural model does not provide the final answer to the model setting but it provides the flexibility to form and test various hypothetical models, make the analysis result more fully explain the relationship contained in the data. The goodness of fit test indicators provided by different statistical analysis software are also different.

3. Results and Analysis

3.1. Smoking. Among the respondents in this survey, the difference in smoking rates between males and females was statistically significant; the smoking rate of men is much higher than that of women. Among men, the smoking rate is highest in middle-aged age and lowest in old age. Among women, the elderly have the highest smoking rate and the young are the lowest. See Table 1 for details.

3.2. Prevalence of Hypertension. Among the respondents in this survey, 33.5% of the respondents had a family history of hypertension, the prevalence rate of hypertension was 11.2%, and the rate of dyslipidemia was 5.5%; those with cerebrovascular disease accounted for 4.3%, and those with cardiovascular disease accounted for 7.3%; the prevalence of various types of hypertension in the survey subjects is shown in Table 2 for details.

3.3. Effect Decomposition of Factors Affecting Hypertension in Male Population. The standardized total effect shows that the effects of risk factors for hypertension in descending

Table 1: Analysis of smoking status among study subjects of different ages and genders.

Age group	Man		Women	
	Number of people	Smoking rate	Number of people	Number of people
Youth	4975	45.8	5335	2.8
Middle aged	4720	55.2	5324	5.1
Elderly	2120	27.1	2360	13.5

Table 2: The prevalence of various types of hypertension in the study subjects.

Hypertension	Number of patients	Prevalence (%)
Hypertension	2585	11.2
Dyslipidemia	1431	5.5
Hypertensive nephropathy	108	0.6
Impaired kidney function	66	0.2
Ischemic stroke	662	2.9
Cerebral hemorrhage	140	0.8
Transient ischemic attack	122	0.6
Myocardial infarction	260	1.2
Angina pectoris	725	3.2
Coronary revascularization	391	1.8
Congestive heart failure	252	1.1
Peripheral vascular disease	40	0.5

order are as follows: family history of hypertension, overweight, dyslipidemia, hypertension, salt intake, drinking, and active exercise [16]. The effect of the protective factors of hypertension is as follows: high GDP level, high SES level, and smoking. See Figure 1.

3.4. Effect Decomposition of Factors Affecting Hypertension in Female Population. The standardized total effect shows that the effects of the risk factors for hypertension, from large to small, are as follows: family history of hypertension, overweight, dyslipidemia, high blood pressure, salt intake, active exercise, and smoking. The effects of the protective factors of hypertension in descending order are as follows: high GDP level, high SES level, and alcohol consumption [17]. See Table 3 for details.

4. Discussion

Based on further understanding of prehypertension that the etiological factor model proposes, the causes of diseases include external causes (such as socioeconomic factors, lifestyle, and living environment) and internal proximate causes (such as the pathophysiological changes of the body) [18]. Although these factors are independent of each other but they interact with each other to form a causal chain, that is, a certain factor can be the cause of the change of other factors or it can be the result of other factors, these causal links form the structure of the cause network [19]. Hypertension is a disease caused by the combined action of many factors, and its influencing factors can be divided into personal characteristics (gender, age), socioeconomic background (living environment, culture, and income level), behavioral factors (smoking, drinking, insufficient exercise, and high-salt diet), and health factors (hyperglycemia, dyslipidemia, and obesity). These factors are connected to each other and have an effect on human health [20]. In the relationship between life behavior style and hypertension involved in this study, the direct effect of salt intake on hypertension is statistically significant; however, the direct effects of active exercise, smoking, and drinking on hypertension were not statistically significant. This situation may be due to the structural equation scanning model analysis; the relationship between a certain factor and the disease includes two parts, a direct effect and an indirect effect; when other mediating factors are included in the model, the direct effects will be weakened or even disappear. In addition to the direct effect of lifestyle on hypertension in this study, it also has an indirect effect on high blood pressure through being overweight, high blood pressure, and dyslipidemia; it may be that these indirect effects through intermediary factors which explain part of the relationship between lifestyle and hypertension. In addition, although community residents' awareness, treatment, and control of hypertension have improved but for blood pressure prevention and control, we still have a lot of work to do and need to further strengthen the health education of hypertension-related knowledge; in the future, further research will be conducted on related factors affecting blood pressure control to help patients control blood pressure levels more effectively [21].

Studies have found that the sleep quality, as a variable factor, has a protective effect on the number of hypertension. Gender, age, and ethnicity have a direct or indirect effect on the number of hypertension; the path coefficients of these factors are small, which still suggests that in the prevention and control of hypertension, corresponding intervention measures should be taken for the relevant behavioral risk factors among elderly people of different ages, ethnicities, and genders. Studies have found that with increasing age, the proportion of the elderly who lack physical activity has increased. At the same time, as the age increases, the socioeconomic status of the elderly declines; it is a risk factor for the increase in the number of hypertension. Therefore, in the prevention and control of hypertension, for the elderly, the government should increase subsidies, improve the economic conditions of the elderly while strengthening social support, pay attention to family care of the elderly, improve the emotional and physical state of the elderly, improve the quality of sleep, and encourage the elderly to exercise properly. For female obesity, the central obesity rate is high, the socioeconomic status is low, and the influence of

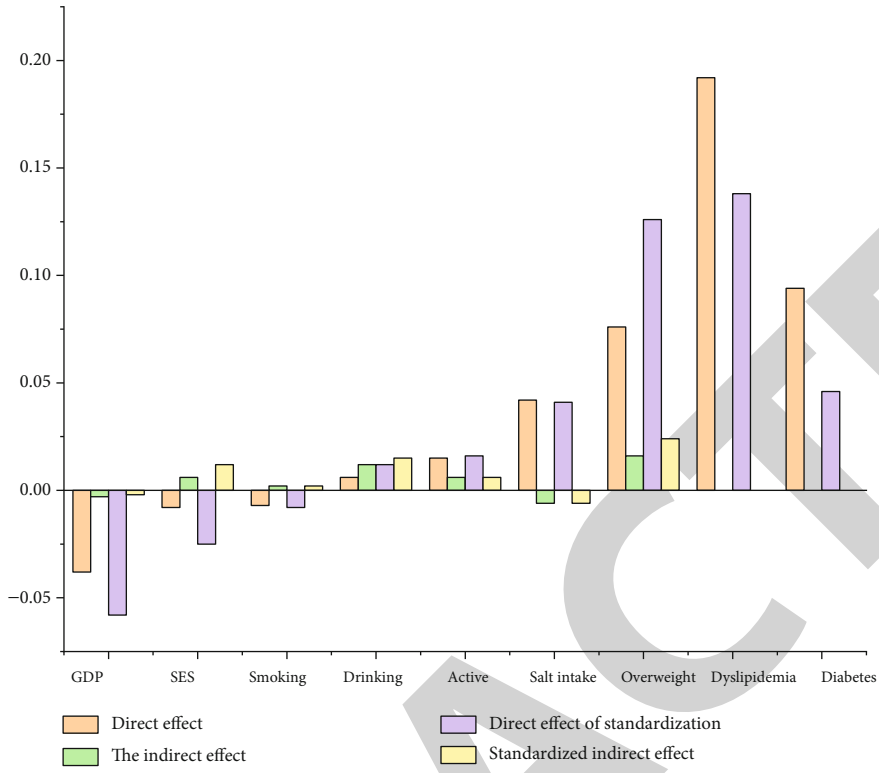

Figure 1: Decomposition of effects of factors affecting hypertension in males.

Table 3: Effect decomposition of factors affecting hypertension in female population.

Variable	Direct effect	Indirect effect	Standard direct effect	Standard indirect effect
CDP	−0.019	−0.002	−0.026	−0.005
SES	−0.012	—	−0.030	−0.002
Smoking	0.022	−0.006	0.013	−0.004
Drinking	−0.006	0.004	−0.002	0.005
Active exercise	0.004	0.005	0.005	0.006
Salt intake	0.018	0.002	0.021	0.002
Overweight	0.082	0.015	0.142	0.020
Dyslipidemia	0.168	—	0.122	—
Hypertension	0.148	—	0.078	—

these pathways has led to an increase in the number of hypertension. Therefore, in rural survey areas, elderly women with low socioeconomic status and obesity or central obesity are the key populations for the prevention and control of hypertension; in the prevention and control of hypertension, this group should be targeted, carry out health education, improve the welfare of the elderly, and prevent the occurrence of hypertension [22].

5. Conclusion

The results of a sample survey of residents aged 18–80 years in a certain city's community showed that, in the structural equation scanning by gender, the model has the same appearance between the male and female groups but the path coefficients are not consistent. SES and GDP indirectly affect hypertension through behavior and health status; it also has a direct impact on the distribution of hypertension; it suggests that external socioeconomic background factors also play an important role in the development of the disease. The socioeconomic background affects being overweight, hypertension, dyslipidemia, and hypertension through personal lifestyle behaviors such as smoking, drinking, exercise, and salt intake. The main findings are as follows: family history of hypertension, dyslipidemia, hypertension, overweight, and lifestyle behavior (salt intake, active exercise, drinking, and smoking) are risk factors for hypertension. The hypothesis that external causes (social and economic background) affect the occurrence of diseases through internal proximate causes (behavior, health status) is verified.

Hindawi
Scanning
Volume 2023, Article ID 9760450, 1 page
https://doi.org/10.1155/2023/9760450

Retraction

Retracted: Observation on the Effect of MRI Image Scanning on Knee Pain in Football Injury

Scanning

Received 12 December 2023; Accepted 12 December 2023; Published 13 December 2023

This article has been retracted by Hindawi, as publisher, following an investigation undertaken by the publisher [1]. This investigation has uncovered evidence of systematic manipulation of the publication and peer-review process. We cannot, therefore, vouch for the reliability or integrity of this article.

Please note that this notice is intended solely to alert readers that the peer-review process of this article has been compromised.

Wiley and Hindawi regret that the usual quality checks did not identify these issues before publication and have since put additional measures in place to safeguard research integrity.

We wish to credit our Research Integrity and Research Publishing teams and anonymous and named external researchers and research integrity experts for contributing to this investigation.

The corresponding author, as the representative of all authors, has been given the opportunity to register their agreement or disagreement to this retraction. We have kept a record of any response received.

References

[1] W. Yu, "Observation on the Effect of MRI Image Scanning on Knee Pain in Football Injury," *Scanning*, vol. 2022, Article ID 7348978, 6 pages, 2022.

Hindawi
Scanning
Volume 2022, Article ID 7348978, 6 pages
https://doi.org/10.1155/2022/7348978

Research Article

Observation on the Effect of MRI Image Scanning on Knee Pain in Football Injury

Weidong Yu

College of Physical Education, Fuyang Normal University, Fuyang, Anhui 236037, China

Correspondence should be addressed to Weidong Yu; 201704413@stu.ncwu.edu.cn

Received 13 April 2022; Revised 4 May 2022; Accepted 10 May 2022; Published 25 May 2022

Academic Editor: Danilo Pelusi

To study the effect of football injury on knee pain based on MRI image scanning, in this paper, a total of 31 knee injuries of 29 male professional football players from December 2012 to April 2015 were used as the experimental group. The players were 23.6 ± 3.5 years old and received professional football training time 15.3 ± 3.6 years; 31 outpatients of the same age group with acute knee joint acute injury were randomly selected as the control group; both groups were imaged with a 1.5 TMR scanner and knee joint standard array coil imaging, and 2 senior radiation surgeons evaluate knee cartilage, meniscus, ligaments, tendons, bone marrow, infrapatellar fat pad, and joint effusions. Pearson's chi-squared test and nonparametric test for two independent samples were used for statistical testing of the evaluation results. The experimental results showed that there were significant differences in the incidence of articular cartilage, lateral collateral ligament, tendon or ligament injury, multiligament or tendon injury, and bone marrow edema between the two groups ($P < 0.05$). There was no significant difference in the incidence of medial collateral ligament injury, infrapatellar fat pad edema, and joint effusion. MRI shows that knee injuries in male professional football players often involve ligaments or tendons, mostly multiligament or tendon injuries. The lesions of articular cartilage and meniscus are more common and serious, and bone marrow edema is also more common in football injuries. MRI has high diagnostic accuracy for various clinical knee injuries, and it belongs to a noninvasive examination method. It can not only reflect the pathological changes and changes of the knee joints of patients but also provide information for the formulation of clinical programs and the judgment of prognosis, for timely, accurate, and comprehensive imaging reference.

1. Introduction

As we all know, in football, players often need to start quickly and in high-speed running, change speed, change direction, stop suddenly, take off, collide, etc. The results of the knee biomechanics study show that the knee strength is the greatest when the knee joint is 30°-50°, so almost all running and jumping movements are also "forced" when the knee is flexed at a 30°-50° angle. In football events where the lower limbs are the main activity, players are required to maintain this position from time to time, the force point is concentrated, and the patellar cartilage surface bears a lot of pressure. At this angle, the contact range of the patella joint is the largest, and the knee is stable at this time. It is mainly maintained by the patella [1]. These anatomical and physiological characteristics have become potential factors for patellar cartilage injury in the semisquatting position. Violent impact and pulling will damage the meniscus and cruciate ligament, causing collateral ligament injury, etc.

As the main weight-bearing joint of the human lower limbs, the knee joint is prone to strain, and with the increase of age, the elderly with chronic diseases have a greater burden on the knee joint and are prone to bone and soft tissue damage (Figure 1) [2]. When people exercise or have a car accident, it is easy to cause injury. The knee joint is a weight-bearing joint in the whole body and is also the most commonly injured joint. With the increase of accidents and injuries, more and more people are injured in the knee joint, but in most people, insufficient attention is paid to knee joint injuries, and the disease is often delayed, so that patients are only admitted to the hospital for treatment when the knee joint function is affected later. At this time, only when the

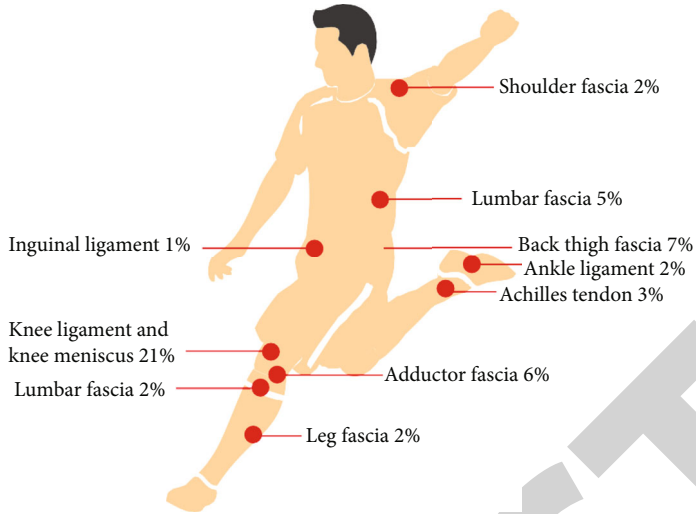

Figure 1: Knee sports injury.

condition of the patient's knee joint is clear can a suitable treatment plan be determined, and the patient's normal knee joint function can be gradually restored. In the diagnosis of knee joint disease, imaging has always been the preferred examination method. Conventional X-ray and CT examinations are more sensitive to bone injuries, but there are many soft tissues around the knee joint, and patients are prone to soft tissue injuries due to accidents. It can not only clarify the patient's bone injury but also better display the soft tissue injury such as the meniscus and the ligaments around the knee joint [3], which is helpful for clinicians to refer to. Among knee joint diseases, MRI gradually shows its incomparable position.

2. Literature Review

Malta et al. believe that football is one of the sports with a higher incidence of injury; this is because many technical movements in football, such as strong shooting, falling to the ground, and dribbling, require physical and various muscles. These parts are coordinated and completed together. In addition, the physical confrontation in football is fierce, and the sudden stop and start, jumping, and variable speed running will cause repeated and high-intensity wear and tear to the body, so the sports injury rate in football is relatively high [4]. Endstrasser et al. pointed out in the study that the characteristics of football sports are high intensity, high confrontation, and physical contact. Through the investigation, it is found that the incidence of football injury is from high to low: stomping joint, knee joint, thigh, calf, and medullary joints. Most of the injuries are minor, among which knee stomping joint sprain, thigh muscle strain, and contusion are the most common [5]. Yoon et al. mentioned that the research found that the causes of football players' injuries are mainly caused by insufficient training levels, human factors, and objective factors. Moreover, the incidence of football injuries is on the rise, which should be paid great attention to by athletes and coaches [6]. Anne-Priscille et al. found through a survey of the athletes in the men's football match at the Jilin Provincial University Games that sports injuries in football are mostly concentrated in the lower extremities, of which the stomping joint and knee joint are the parts with a higher incidence of injury, followed by the head, neck, and waist. Fractures mostly occur in the calf; strain in the knee joint and contusion in the lower extremity are relatively high [7]. According to Derouin and others, knee joints are one of the most vulnerable joints in football. Domestic scholars pay more attention to common knee injuries such as medial and lateral collateral ligament injury, meniscus injury, knee cartilage injury, and cruciate ligament injury. The research rate is high [8]. Huang et al. investigated knee injuries in 147 female soccer players from 8 national women's soccer teams in 2006. The results showed that meniscal and knee ligament injuries accounted for the top two cases of total injuries among all female football players participating in the competition [9]. Zhong and Zhu investigated the sports injuries of 8 women's football teams in spring training in 1997 and found that the top three common knee injuries of female football players were knee soft tissue contusion, knee ligament injury, and bone strain [10]. Sun et al. found in their study of football teaching that athletes lack self-protection awareness, lax protection thinking, fail to protect themselves under intense collisions, and also cause knee joint injuries. In football, the force of the knee joint is in the flexion position, and the ligaments of the knee joint are relatively loose in this situation [11]. Pan et al. also studied the injury of the medial and lateral collateral ligaments. The medial and lateral collateral ligaments play a role in stabilizing the knee joint. Compared with the lateral collateral ligaments, the medial collateral ligament has a higher injury rate in football. Direct violence is the main cause of the injury, such as physical confrontation, scramble, and excessive tackle in football games. The athlete's thigh is adducted and internally rotated, and the calf is suddenly abducted and externally rotated. At this time, the medial collateral ligament of the knee joint will be torn or strained. The lateral collateral ligament, on the other hand, is caused by the adduction and internal rotation of the calf and the paradoxical movement of the thigh [12].

3. Experimental Analysis

3.1. Research Objects. From December 2012 to April 2015, 29 male professional football players (31 knee joints), aged 17 to 29 years, with an average age of 23.6 ± 3.5 years, received professional training for 15.3 ± 3.6 years, all due to knee pain and swelling after training or competition injury, combined with different degrees of dysfunction (experimental group). 31 male patients (31 knee joints, control group) aged 18-30 who underwent MRI examination in the outpatient department of our hospital due to knee joint trauma from May to October 2013 were randomly selected. There was no significant difference in age between the two groups ($F = 0.01$, $P = 0.971$). Those with a history of knee surgery, a diagnosis of knee fracture, or combined systemic diseases (such as rheumatoid arthritis and blood diseases) were not included in this study.

3.2. Inspection Method. All subjects were scanned with a 1.5 T dual gradient MR whole-body scanner (Achieva, Philips, The Netherlands), an 8-channel phased coil in the knee joint, and a fast spin echo sequence and a short-time inversion recovery sequence, specifically: sagittal TSE T2WI (TR 3600 ms, TE 100 ms), PD-SPIR (TR 3000 ms, TE 30 ms), coronal TSE T1WI (TR 500 ms, TE17 ms), PD-SPIR (TR 3000 ms, TE30 ms), axial PD-SPIR T2WI (TR3000 ms, TE30ms), slice thickness 5.0 mm, slice spacing 0.5 mm, matrix 512×512, and field of view (FOV) 220 mm × 220 mm. The sagittal scan direction is parallel to the running direction of the anterior cruciate ligament, the coronal scan direction is parallel to the femoral condyle, and the axial scan direction is perpendicular to the long axis of the knee joint [13].

3.3. Image Analysis. The scanned images were analyzed by 2 experienced radiologists to judge articular cartilage injury, meniscus injury, ligament and tendon injury, bone marrow edema, infrapatellar fat pad edema, joint effusion, etc. For grading, when assessing articular cartilage damage and bone marrow edema, the anatomical sites, namely, lateral tibial plateau, medial tibial plateau, lateral femoral condyle, medial femoral condyle, femoral trochlea, and patella, were analyzed; articular cartilage grading was assessed using the revised Outerbridge grading criteria [14]. The meniscus is divided into medial and lateral meniscus anterior and posterior horns, and the changes are classified into 4 grades using Stoller's criteria. Ligament injuries are classified into three grades: normal ligaments including degenerated ligaments (grade 0), partial ligament tears (grade 1), and completely torn (grade 2). Bone marrow edema is defined as a localized ill-margined signal increase in the bone marrow on lipid-suppressive sequences and a localized ill-defined signal-decreased area on T1WI. Infrapatellar fat pad edema is defined as a hyperintense area with ill-defined margins in the infrapatellar fat pad on T2WI fat-suppressed or proton density-weighted fat-suppressed sequences. The evaluation criteria for joint effusion are that the thickness of the suprapatellar bursa fluid in the anterior-posterior direction on the sagittal plane image is greater than 10 mm, that is, the presence of pathological joint effusion [15].

3.4. Statistical Methods. Pearson's chi-squared test was used to compare the knee articular cartilage, meniscus, anterior cruciate ligament, medial collateral ligament, lateral collateral ligament, tendon or ligament injury, multiple ligament or tendon injury, bone marrow edema, and infrapatellar fat pad in the experimental group and the control group. The incidence of edema, joint effusion, and the number of lesions were compared. When $T < 1$, or $n < 40$, or the value obtained after the chi-squared test is close to the test level, the exact probability method is used. The severity of articular cartilage, meniscus, ligament, or tendon lesions was analyzed and compared using nonparametric tests of two independent samples. $P < 0.05$ considered the difference to be statistically significant [16].

4. Result Analysis

For the incidence of knee joint injuries, the incidence of articular cartilage, lateral collateral ligament, tendon or ligament injury, multiple ligament or tendon injury, and bone marrow edema in the experimental group was higher than those in the control group. The difference between the two groups was statistically significant, but the meniscus, anterior cruciate ligament injury, medial collateral ligament injury, infrapatellar fat pad edema, and the incidence of joint effusion were not significantly different from the control group (Table 1). For the injury degree, the damaged area (number of lesions) of articular cartilage, meniscus, and tendon in the experimental group was significantly higher than that in the control group. In addition, the degree of articular cartilage and meniscus damage in the experimental group was more serious than that in the control group (Tables 2–4).

From Tables 1–4, it can be seen that knee joint injury seriously affects the training and game quality of football players and even makes some elite athletes end their sports careers prematurely [17–19]. At present, the replantation of articular cartilage is only in the clinical trial stage, and the clinical effect is not exact; it is difficult to recover through conservative treatment after meniscus tear, and it is easy to recur after repair; ligaments and tendons have no regeneration ability and poor healing ability and affect the rupture joint mobility and stability. From Figure 2, timely and accurate diagnosis is helpful for early rehabilitation or surgical treatment, preventing the aggravation of lesions and restoring knee joint function as soon as possible. MRI is used to examine acute and chronic sports-related injuries such as knee cartilage, meniscus, ligaments, and tendons. Check with high consistency.

Football is intense, and the activities and load of the knee joint are large, so it is easy to be damaged. The knee joint is the largest and most complex joint in the human body. The traditional X-ray and CT diagnostic value are limited. Magnetic resonance imaging has high resolution on soft tissue and can image with multiple parameters, multiple orientations, and multiple sequences. The normal meniscus shows a low signal in each sequence. When the meniscus degenerates and tears, it can absorb the synovial fluid in the joint cavity. When the synovial fluid penetrates into the degenerated and torn meniscus, the local proton concentration is

Table 1: Comparison of the incidence of knee joint injury between the experimental group and the control group (case (%)).

Group	Meniscus	Cartilage	Anterior cruciate ligament	Medial collateral ligament	Lateral collateral ligament	Hamstrings
Test group	16	11	12	17	14	6
Control group	11	4	14	13	5	1
P value	0.200	0.038	0.607	0.309	0.013	*

Table 2: Statistical table of the distribution of knee cartilage injury in the experimental group and the control group (cases (%)).

Group	Lateral tibial plateau	Medial tibial plateau	Lateral malleolus of femur	Medial malleolus of femur	Femoral trochlea
Test group	6	6	4	4	4
Control group	2	2	0	2	0
P value	*	*	*	*	*

Table 3: Statistical table of the distribution of knee meniscus injury in the experimental group and the control group (cases (%)).

Group	Medial meniscus		Lateral meniscus		Total
	Front corner	Rear corner	Front corner	Rear corner	
Test group	4	8	18	4	34
Control group	1	2	7	5	15
P value	*	0.038	0.004	0.718	0.002

increased. T1 and T2 are shortened, so T1 weighting and proton density weighting are more sensitive to meniscus damage [20]. Evaluation of the meniscus is mainly on the sagittal plane on T1 or proton images. Three-dimensional magnetic resonance imaging of the meniscus can clearly show the shape of the meniscus and the location of the injury. The magnetic resonance imaging of meniscus tear shows the following types: (1) oblique meniscus tear: it is the most common type of meniscus tear, and it is generally better in the coronal view than in the sagittal plane; (2) horizontal tear: generally relatively rare, often accompanied by meniscus cysts; (3) barrel-handle tear: more common in young patients with severe trauma, it is a complex tear, and generally, three-dimensional magnetic resonance can show its shape well; (4) radial tear: the direction of tear is perpendicular to the direction of the long axis of the meniscus, and it usually occurs in the lateral meniscus, and it is more common in the inner 1/3 of the meniscus; and (5) longitudinal tear: the direction of the tear is consistent with the direction of the long axis of the meniscus. According to literature reports, with arthroscopy as the standard, the accuracy of MRI diagnosis of meniscus is 90% to 100%.

As a noninvasive examination, MRI has high tissue resolution and can correspond to pathology and arthroscopic grading. The meniscus injury is divided into three grades according to its shape and degree: the first grade is an amorphous or spherical high signal shadow; the second grade is a linear high signal shadow, neither of which extends to the articular surface; and the third grade is linear or diffuse hyperintensity extending into the articular surface representing an arthroscopic tear [21]. In order to reduce the false-positive rate, a high-intensity shadow extending to the meniscus surface must be seen on both the coronal and sagittal planes to diagnose a tear. Among ligament injuries, the anterior cruciate ligament is more common than the posterior cruciate ligament, and the medial collateral ligament is more common than the lateral collateral ligament. Common MRI findings of ligament tears include the following.

4.1. Direct Signs. (1) No normal ligaments can be seen on the coronal and sagittal planes, (2) the ligaments are interrupted and discontinuous, (3) the ligaments are thickened with irregular or wavy edges, and (4) there is a localized or diffuse high signal in the ligaments.

4.2. Indirect Signs. The indirect signs are (1) avulsion fracture at the ligament attachment, (2) local cartilage defect or with meniscus tear, and (3) bone contusion and bone marrow edema.

In addition, it may be accompanied by bursae effusion, subcutaneous tissue, fascial edema, and disappearance of nearby fat shadows. The presence or absence of edema in the ligament and its adjacent soft tissues is the main basis for identifying acute and chronic injuries. In judging the bone condition after trauma, plain X-ray still has an irreplaceable role, but MRI has certain advantages in showing the hidden lesions of the knee bone structure because it can select a variety of sequences [22]. It can be used as an important supplement to determine the bone condition of X-ray plain film. The MRI of occult bone lesions of the knee joint can be divided into five types: type I: long T1 and long T2 signal areas with blurred long T1 and long T2 signals in the bone or metaphysis, with unclear boundary and irregular shape, which reflect the bone marrow edema of pure bone contusion [23, 24]. Type II: line-like structures with mixed signals of high and low signals are seen in type I lesions and extend to the cortex, and the corresponding cortical lines are slightly staggered, reflecting an occult fracture. Type III: there is a patchy, fuzzy high signal area on T1WI and T2WI immediately under the articular cartilage, and a line-like structure extending to the cartilage can be seen, indicating an osteochondral joint injury. Type IV: T1WI and T2WI are hypointense lesions immediately under the articular cartilage, with clear borders, and the thickness,

Table 4: Statistical table of grading of knee articular cartilage, meniscus, and tendon lesions in experimental group and control group (cases).

		Level 0	Level 1	Level 2	Level 3	Level 4	P value
Articular cartilage	Test group	158	12	9	3	4	0
	Control group	179	2	3	2	0	
Meniscus	Test group	90	11	12	11	—	0
	Control group	109	3	3	9	—	
Tendon or ligament	Test group	—	52	13	—	—	—
	Control group	—	35	9	—	—	

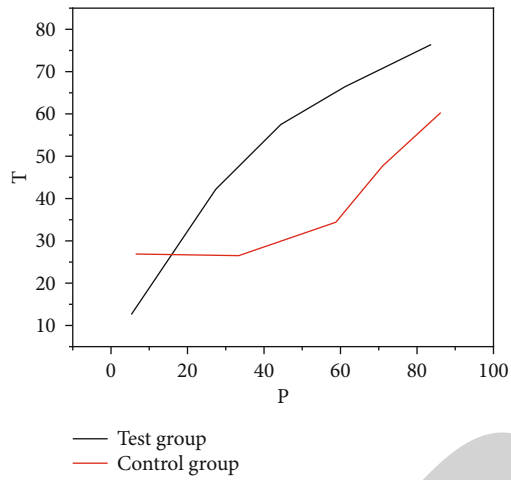

Figure 2: The relative P value of the knee joint of the experimental group and the control group (cases).

shape, and signal of the upper cartilage may have different degrees of change, suggesting subosseous bone sclerosis. Type V: the subchondral bone structure of the articular cartilage shows a low signal on T1WI, T2WI shows a central high-peripheral low signal shadow, with clear boundary and abnormal changes in the cartilage on the lesion, because the structure is continuous with the diseased cartilage, so it may be due to a cartilage break invasion of synovial fluid and synovium. Types I to III are more common in acute injuries, and types IV to V are more common in chronic injuries. Among the hidden intraosseous lesions, the tibia is the most common site and is often associated with articular ligament injury, especially the anterior cruciate ligament. MRI can clearly show the effusion of the knee joint cavity and can distinguish the composition of the fluid according to the different signals [25]. In this article, there are 3 cases of lipemia in the joint cavity, which is caused by the simultaneous entry of adipose tissue and blood from the bone marrow cavity or the torn periosteum into the joint cavity after trauma, and the fat floats on the synovial fluid, and the blood submerged under the synovial fluid; MRI showed three layers of joint effusion with different signals.

5. Conclusion

The injury of the meniscus and articular cartilage of the knee joint of football players is more serious and involves multiple structures of the knee joint, which is consistent with the research of other scholars. Cartilage signal changes were seen in 11 joints in the athletes in this group, of which 4 had full-thickness loss of cartilage and exposed subchondral bone. In addition to articular cartilage damage, these 4 were combined with severe damage to other structures, while none of the control group had joints. For full-thickness exfoliation of cartilage, articular cartilage damage is considered to be the core pathological change of osteoarthritis, which is more common in middle-aged and elderly people, but repeated and intense trauma can also cause articular cartilage rupture and peeling in adolescents. Among the 31 knee joints in the experimental group, there were 11 knee joints with third-degree injury of the meniscus, 12 with second-degree injury, and 9 with first-degree injury. Since the course of the knee joint is mostly acute, it is recommended that for acute knee joint injury, early diagnosis and early treatment must be performed, so that the injury can heal as soon as possible and to prevent the acute injury from turning into a chronic injury.

To sum up, MRI imaging examination for knee joint injury can reduce the radiation to the patient and can clearly identify the pathological changes in the knee joint of the patient. The evaluation of late prognosis provides imaging reference, which is worthy of promotion and application in clinical practice.

Data Availability

The data used to support the findings of this study are available from the corresponding author upon request.

Conflicts of Interest

The author declares that they have no conflicts of interest.

Acknowledgments

The author acknowledges the (1) 2019 Key Projects of Universities and Humanities and Social Sciences in Anhui Province: Research on Campus Football Teachers (sk2019a1159); (2) Key Research Project of Humanities and Social Sciences in Anhui Universities in 2020: Research on the Revision and Improvement of Physical Education Professional Evaluation Index System under the Vision of Core Literacy (2020jyxm1989); (3) 2020 Provincial Quality Engineering Project of Higher Education in Anhui Province: New Liberal Arts,

Hindawi
Scanning
Volume 2023, Article ID 9864261, 1 page
https://doi.org/10.1155/2023/9864261

Retraction

Retracted: Clinical Observation of MRI Image in Floating Needle Therapy for Cervical Spondylosis of Cervical Type

Scanning

Received 20 June 2023; Accepted 20 June 2023; Published 21 June 2023

This article has been retracted by Hindawi following an investigation undertaken by the publisher [1]. This investigation has uncovered evidence of one or more of the following indicators of systematic manipulation of the publication process:

(1) Discrepancies in scope

(2) Discrepancies in the description of the research reported

(3) Discrepancies between the availability of data and the research described

(4) Inappropriate citations

(5) Incoherent, meaningless and/or irrelevant content included in the article

(6) Peer-review manipulation

The presence of these indicators undermines our confidence in the integrity of the article's content and we cannot, therefore, vouch for its reliability. Please note that this notice is intended solely to alert readers that the content of this article is unreliable. We have not investigated whether authors were aware of or involved in the systematic manipulation of the publication process.

In addition, our investigation has also shown that one or more of the following human-subject reporting requirements has not been met in this article: ethical approval by an Institutional Review Board (IRB) committee or equivalent, patient/participant consent to participate, and/or agreement to publish patient/participant details (where relevant).

Wiley and Hindawi regrets that the usual quality checks did not identify these issues before publication and have since put additional measures in place to safeguard research integrity.

We wish to credit our own Research Integrity and Research Publishing teams and anonymous and named external researchers and research integrity experts for contributing to this investigation.

The corresponding author, as the representative of all authors, has been given the opportunity to register their agreement or disagreement to this retraction. We have kept a record of any response received.

References

[1] X. Liu, Z. Tang, B. Wang, and Y. Chen, "Clinical Observation of MRI Image in Floating Needle Therapy for Cervical Spondylosis of Cervical Type," *Scanning*, vol. 2022, Article ID 1340192, 10 pages, 2022.

Hindawi
Scanning
Volume 2022, Article ID 1340192, 10 pages
https://doi.org/10.1155/2022/1340192

Research Article

Clinical Observation of MRI Image in Floating Needle Therapy for Cervical Spondylosis of Cervical Type

Xianqiang Liu,[1,2] **Zhenyi Tang**,[2] **Botao Wang**,[2] **and Yongshuai Chen**[2]

[1]*Gradute School, Tianjin University of Traditional Chinese Medicine, Tianjin 301617, China*
[2]*Department of Orthopedics, Tianjin Beichen Traditional Chinese Medicine Hospital, Tianjin 300400, China*

Correspondence should be addressed to Xianqiang Liu; 320045119106@stu.suse.edu.cn

Received 12 April 2022; Revised 4 May 2022; Accepted 10 May 2022; Published 24 May 2022

Academic Editor: Danilo Pelusi

In order to solve the problem of cervical spondylosis in the early stage of various cervical spondylosis, effective treatment can prevent the deterioration of the disease. This paper presents the results of a clinical trial examining magnetic resonance imaging in the treatment of cervical spondylosis with flotation therapy and selected 68 patients with cervical spondylosis. According to research commodity, using a rigorous randomized controlled trial, 34 cases were divided into a control group (acupuncture group). The needles were kept for 30 minutes once a day. The treatment group (acupuncture combined with floating acupuncture group) was treated with acupuncture on the 1st, 3rd, and 5th days and floating acupuncture on the 2nd, 4th, and 6th days, respectively. Both groups were treated for 6 consecutive days and rested for 1 day. After 2 weeks of treatment, the simplified McGill Pain Scale (MPQ), visual analogue scale (VAS), and neck pain scale (NPQ) were observed and recorded to compare the curative effects. Finally, Excel software is used to manage the data, and SPSS21.0 is used for statistical analysis. Measurements of gender, age, disease, VAS, simple MPQ, and NPQ of the two groups were compared in the two groups, $P > 0.05$, which was not significant and comparable. After treatment, VAS, simple MPQ, and NPQ of the two groups were compared in and between groups, the total $P < 0.05$, with the mean data. *Topics*. Acupuncture combined with float needle and acupuncture therapy can improve the pain and breathing of cervical spondylosis and improve the quality of life of patients, but acupuncture combined with needle float is more pronounced than acupuncture groups.

1. Introduction

Cervical spondylosis, tseem hu ua ligament joint capsule type cervical spondylosis, refers to a series of clinical syndromes caused by wind cold invading the local area; improper sleeping position or fatigue on the basis of acute and chronic injury of cervical muscles, joint capsule, and ligaments; dislocation of small joints; degeneration of intervertebral disc; and instability of vertebral body, resulting in excessive flexion or extension of cervical spine and compression or tension of some muscles, ligaments, or nerves in the neck. Most of the clinical manifestations are neck pain and limited activity. There are no obvious degenerative changes such as intervertebral space on X-ray films, but they can be accompanied by changes in cervical physiological curvature, vertebral instability, and mild hyperosteogeny. Most of them occur in the morning, the cold, or continuous fatigue, which is easy to ease naturally and occur repeatedly, and long-term repeated attacks will affect daily activities and quality of life. This type is very common in clinic and is the earliest stage of cervical spondylosis. In recent years, with the change of lifestyle, the number of long-term desk workers has increased, plus the incorrect posture of using the neck, resulting in the rising prevalence of cervical spondylosis, which has attracted more and more attention. The age of onset is also becoming younger. According to the survey, the incidence rate of cervical spondylosis among young and middle-aged is 19.22, while 29.1% of primary school students have abnormal cervical vertebra. This kind of patients' condition is light and heavy and easy to repeat, and many patients have insomnia, anxiety, and other symptoms. Some scholars believe that people with cervical spondylosis are prone to a lack of security and anxiety, which affects their physical and mental health. At the beginning of the disease, the

symptoms are mild and transient, mainly local symptoms, and occasionally transient, which can be alleviated and easy to be ignored, which may develop into other types of cervical thrust disease. Cervical spondylosis is the first stage of various cervical spondylosis, and it is also the best time to treat and prevent other types of cervical spondylosis. Therefore, the treatment of cervical spondylosis is very important for the prevention and treatment of cervical spondylosis at all stages. At present, acupuncture has been widely used in the treatment of clinical NTCS. This treatment can effectively correct the block of Qi and blood along the meridians, so as to improve people's essence, Qi, and spirit, so as to achieve the purpose of treatment. In the treatment of clinical NTCS, acupuncture has significant advantages, not only because of its significant analgesic effect and less adverse reactions but also because it is a green therapy without any pollution. However, in the process of treatment, there are sometimes body position restrictions and more acupoints, which leads to some patients' resistance during treatment, which is easy to cause the end of treatment and reduce the therapeutic effect to a great extent. Therefore, it is necessary to evaluate treatment in combination with actual treatment effects to overcome the above limitations and make it easier for patients to improve health benefits. In recent years, a number of studies have confirmed that the occurrence and progression of NTCS are related to the muscles around the cervix, and the state of the muscles around the cervical spine plays an important role in the diagnosis of cervical spondylosis. As a new acupuncture physical therapy, floating acupuncture has the following advantages: There is obvious analgesic effect. The affected muscle can be transformed into normal muscle. There are less acupoints and convenient operation. The curative effect can be evaluated after each treatment. There are no restrictions on body position. And its indications are mainly the pain caused by muscle and soft tissue injury. The introduction of floating needle therapy into the treatment of NTCS can reperfuse the damaged muscles around the neck, so as to change muscle damage and spasticity, so as to improve the symptoms and signs of neck pain, neck stiffness, and limited activity, as shown in Figure 1.

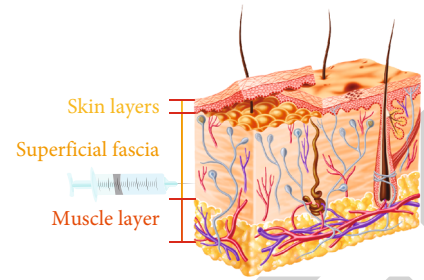

Figure 1: Clinical observation of image in floating needle therapy in the treatment of cervical spondylosis of cervical type.

2. Literature Review

Sheng-Lian and others said that cervical spondylosis (CS) refers to the syndrome with corresponding symptoms caused by the degeneration and proliferation of cervical intervertebral disc and various neck injuries or the prolapse of cervical intervertebral disc and the thickening of ligaments, which are squeezed into the adjacent spinal cord, cervical nerve, and cervical blood vessels [1]. Zheng and others think that according to the anatomical position of compression, it can be roughly divided into five types: nerve root type, vertebral artery type, spinal cord type, sympathetic nerve type, and neck type [2]. In recent years, Xu and others said that due to the rapid development of social economy, most people have changed in life, work, and learning methods, resulting in the incidence rate of spinal-related diseases being increased [3]. Xiao and others believe that this is due to the fact that the spine continues to maintain a fixed posture due to long-time sitting at the desk, resulting in the continuous fatigue of the whole spine, resulting in the occurrence of cervical spondylosis [4]. The incidence rate of incidence of cervical spondylosis is 3.8% and 17.6% and is related to occupation and age, with the incidence rate of 12%. Neck type cervical spondylosis (NTCS) belongs to the type with the lightest symptoms among all clinical types of cervical spondylosis. Its main clinical features are neck pain, neck stiffness, or limited activity. Me-Wu-Jia et al. said that the incidence rate of NTCS in the initial stage accounted for 40% to 60% of the total incidence rate of cervical spondylosis. If treatment is delayed or with improper treatment, it could develop into other types of cervical spondylosis. And studies showed that 80% to 90% of NTCS patients could be relieved of symptoms or even cured [5] by standard and systematic conservative treatment. Early prevention and treatment of NTCS are urgent. Ye and others said that cervical spondylosis belongs to the category of "arthralgia," "neck and shoulder pain," and "Xiang Qiang" in traditional Chinese medicine. There are various clinical treatment methods. Traditional Chinese medicine treatment includes oral administration, external application of traditional Chinese medicine, acupuncture, and massage, but most of them are comprehensive therapy [6]. Song and others think that acupuncture and moxibustion, as a green therapy, is widely accepted in clinic with better curative effect and less adverse reactions [7]. Xue and others said that in the process of clinical acupuncture treatment, doctors take more points and spend a long time on treatment, which not only increases patients' fear of acupuncture but also makes patients suffer a certain amount of pain in treatment [8]. The main methods of Western medicine treatment are symptomatic use of anti-inflammatory and analgesic drugs, physical therapy, and traction treatment. Its advantage is that it can alleviate symptoms relatively quickly, but with the recurrence of the disease, long-term use of analgesic and anti-inflammatory drugs will cause damage to liver and kidney function. Li and others said that in addition, incorrect operation of physiotherapy instruments or improper traction techniques may add additional pain to patients [9]. Yun and others feel that it is of great significance to explore a treatment scheme with convenient operation, rapid effect, and less pain [10]. Through the study of the experience of using a floating needle to treat various pain syndromes in clinic, it is observed that the floating needle has definite curative effect on the treatment of cervical

spondylosis, especially in the change of pain degree after the first treatment, which greatly increases the patient's trust in doctors, and the number of times required for floating needle treatment is less than that of ordinary acupuncture, which greatly reduces the patient's pain. Therefore, based on the tutor's experience in the clinical treatment of cervical spondylosis with floating needle therapy, this time designs clinical trials, research methods, efficacy evaluation, and data management, so as to provide clinicians and patients with cervical spondylosis with a more effective, safe, and acceptable treatment scheme.

3. Method

Refer to the guidelines for diagnosis, treatment, and rehabilitation of cervical spondylosis (2010 edition) to determine the diagnostic criteria of cervical spondylosis: clinical symptoms: stiff neck and pain, which can stretch the whole shoulder and back in severe cases. In case of acute attack, you cannot do activities such as nodding, turning your head, and raising your head. When turning your head, you need to rotate together with your trunk, and your neck is in an oblique position. Clinical examination: nodding and head raising activities are not allowed in the acute stage, the activity of the cervical spine is absolutely limited, the range of activity of the cervical spine in all directions is close to zero, and there is multiple tenderness in the cervical muscle group. Common tenderness points are mostly located in T1~T7 paravertebral muscle, trapezius muscle, supraspinatus muscle, infraspinatus muscle, sternocleidomastoid muscle, etc. If there is secondary spasm of anterior scalene muscle, it can be on the inner side of sternocleidomastoid muscle, which is equivalent to the level of transverse process of neck 3-neck 6. Buckle it to the spasmodic muscle and press it with a little force, then there will be radiation pain in shoulder, arm, and hand. Imaging findings: the physiological curvature of cervical spine is slightly changed or normal, slight stenosis can be seen in intervertebral space, and hyperosteogeny can occur in some patients [11]. Clinical trials of traditional Chinese medicine refer to the clinical trials of cervical spondylosis in the Guidelines for Clinical Trials of New Chinese Medicines, some of which are included in the classification of cervical spondylosis. Syndrome of cold obstruction and collaterals: cold in the neck, stiff neck, dysfunction, fear of wind, cold and pain in the neck and shoulders, warm and appropriate [12], light red tongue, thin and white moss, and tight pulse string. Qi stagnation and blood addiction syndrome: it occurs due to neck trauma or injury, with strong pain in the neck, such as acupuncture, refusal to press the pain, fixed pain points, dark tongue, and astringent pulse strings. Liver and kidney deficiency syndrome: sore neck, increased fatigue, dizziness, shortness of breath, weak waist and knee, pale tongue, white fur, and heavy and weak pulse. The exclusion criteria were only abnormal imaging findings without clinical symptoms of cervical spondylosis, cervical spondylosis which is mainly of other types, no other serious systemic diseases, those who have obvious fear of acupuncture and refuse to cooperate with treatment, pregnant and lactating women who are allergic to acupuncture and have damaged skin, and observer who has received other analgesic treatment affecting the analgesic effect index of this trial [13]. The technology roadmap is shown in Figure 2.

Compressed sensing (CS) is a sampling method that can compress data proposed by Donoho. Traditional sampling generally uses the Nyquist sampling theorem, that is, Shannon theory, to discretize the signal. This theorem stipulates that the maximum frequency of a signal is Jmax, and when the minimum sampling frequency is greater than or equal to 2Jmax, the original signal can be restored without distortion through the sampling signal. However, with the rapid development of science and technology, the signal bandwidth is increasing day by day, and people's requirements for information processing speed are increasing day by day. The traditional sampling methods encounter great resistance in processing problems. The proposal of compressed sensing theory can well meet the existing sampling requirements, greatly reduce the operation cost, and improve the information processing speed, which provides a new sampling idea for signal processing [8, 14]. Finally, it is pointed out that the sparse signal can be reconstructed into a low-dimensional signal by using the theory of compressibility. From this assumption, it can be seen that signal density does not necessarily depend on bandwidth, which affects signal variability and inconsistency. Compressed sensing uses sampled and compressed signal features. The operation of compressed sensing is shown in Figure 3.

In Figure 3, the compressed sensing processing process mainly has three steps. In the first step, assuming that the input original signals X, $X \in R^{n*1}$ has sparsity on orthogonal bases $\psi = [\psi_1, \psi_2, \cdots, \psi_n]$ and $\psi_i \in R^{n*1}$, the compressed signal is shown in

$$S = \psi^T X. \tag{1}$$

The second step is to select a matrix Φ, $\Phi \in R^{m*n}(m<<n)$ independent of the orthogonal basis and measure s linearly. The processing process is shown in

$$Y = \Phi S = \Phi \psi^T X = \Theta X, \tag{2}$$

where $\Theta = \Phi \Psi^T, \Theta \in R^{m*n}, Y \in R^{m*n}$, we call Θ the sensing matrix. The original signal s is observed through the observation matrix Φ to obtain m observation values. Since $m \ll n$, it is equivalent to transforming the high-dimensional signal into the low-dimensional signal. The third step is to solve the following objective function to obtain the reconstructed signal, as shown in

$$\begin{aligned} &\arg\min \left\| \Psi^T X \right\| \\ &\text{s.t.} \Theta X = \Phi S = Y. \end{aligned} \tag{3}$$

A sparse representation of a signal is the basis for compressed sensing applications. Only when the signal is small can it be guaranteed not to lose too much data after compression [15, 16]. The difference in the signal is easy to understand because there are few nonzeros in the signal, but the signal contained in the context is not complete, but approximately sparse in one exchange. In order to obtain

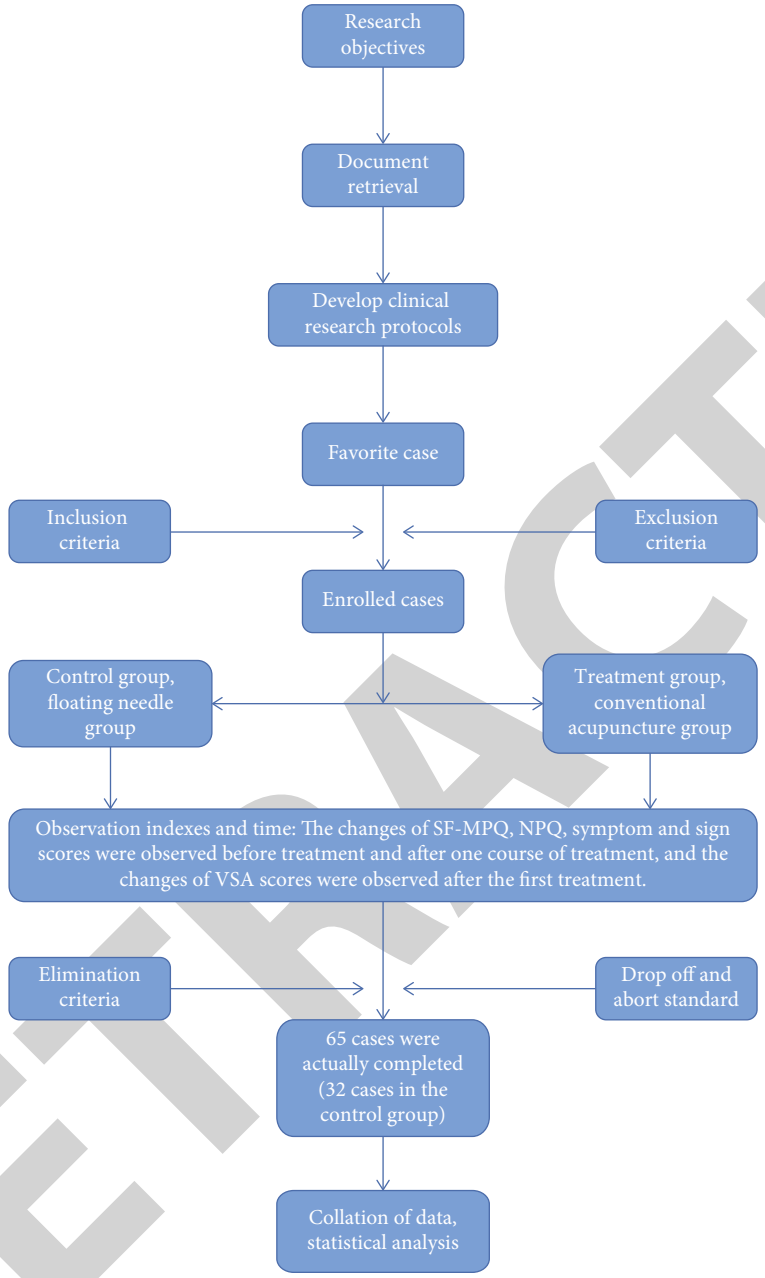

Figure 2: Technical circuit diagram.

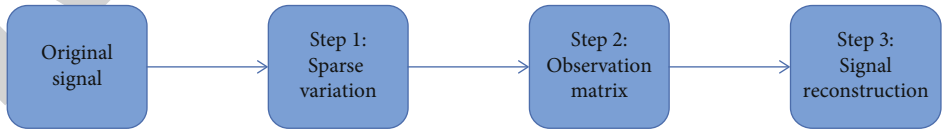

Figure 3: Compressed sensing processing flow.

different signal levels, it is important to find different representations. For any input signal Y, it can be expressed linearly as shown in

$$Y = \sum_{i=1}^{n} \varphi_i \sigma_i, \tag{4}$$

where φ_i is a set of sparse basis vectors and σ_i is the transformation vector of Y in the phosphorus domain. If the sparse representation of signal Y requires at most k basis vectors and $K \ll n$, the signal is said to be k-sparse. If most element values of vector σ_i are very small, the signal is said to be compressible. The traditional sparse representation of signals is mostly based on nonredundant orthogonal bases, such as

wavelet transform, Fourier transform, and discrete cosine change. However, because the orthogonal bases required by different signals are different and different orthogonal bases have different characteristics, the use of a single orthogonal basis will have some limitations. For example, although wavelet transform can effectively represent point singular signals, it cannot well represent the high-dimensional function of line surface singularity, and Fourier transform cannot represent the characteristics of signals in time and frequency. In order to solve this problem, some researchers have proposed a signal sparse representation method based on combined orthogonal basis. In recent years, representations based on redundant dictionaries have also become a research hotspot. Redundancy dictionary refers to the complete redundant function, which is used to replace the basic function. This method can select the identity of the orthogonal basis according to the characteristics of the signal. At present, the sparse representation based on redundant dictionary is mostly studied from two aspects: the construction of redundant dictionary and the design of sparse decomposition algorithm. At present, there are two common sparse decomposition algorithms: matching pursuit and base pursuit. Matching pursuit (MP) is a sparse decomposition algorithm proposed by Mallat and others. It uses greedy algorithm to iteratively select the atoms that best approximate the signal structure from the Atomic Dictionary, but it is difficult to expand the signal after determining the selected atoms, because the atoms selected by the algorithm are not orthogonal to each other [17]. In order to solve this problem, Patl and others proposed orthogonal matching pursuit (OMP), which mainly realizes the signal expansion by orthogonalizing the selected atoms. The basis pursuit (BP) algorithm is proposed by Chen and others. It transforms the l0 norm minimization problem into the H norm minimization optimization problem, which can simplify the signal sparse decomposition process [18]. The selection of observation matrix Φ is very important for the realization of compressed sensing. Its quality directly affects whether the signal can be reconstructed correctly and whether the signal can be compressed to a great extent. This is because the main role of the observation matrix is to convert a high-dimensional signal to a low-dimensional signal without losing data, so that the signal velocity and the algorithmically constructed signal are based on the projection data, the first signal and observation matrices in low-dimensional space. A good observation matrix needs to meet the restricted isometric property rip condition, which stipulates that for any matrix Φ, if it satisfies the following formula, it is shown in

$$(1-\partial_k)\|X\|_2^2 \le \|\Phi X\|_2^2 \le (1+\partial_k)\|X\|_2^2. \tag{5}$$

The matrix is said to meet the equidistant constraint, where x is the k-order sparse signal, ∂_k is a constant, and the value range is $(0, 1)$. Although the rip condition is of great significance, it is a necessary and insufficient condition, and it is impossible to directly verify whether the matrix meets this condition in practice. Based on this, Donoho and others proposed a more operable condition criterion, which stipulates that the observation matrix needs to meet the following conditions: the vector line of the observation matrix should be free and random; the vector line of the probe matrix must have some degrees of freedom, and the minimum value of the matrix containing it must be greater than the minimum value of the special matrix; the measured sparsity is in the h-norm minimal vector. The matrix meeting the above conditions can basically meet the rip condition; that is, it can be used as the observation matrix in compressed sensing. Common observation matrix construction methods include the following, based on orthogonal transformation, random sequence, binary matrix, specific signal, and polynomial. The specific introduction of each method is as follows. Based on the method of orthogonal transformation, this method mainly generates the observation matrix through the transformation of the orthogonal matrix. The specific steps are as follows: form an $N \times N$ -dimensional orthogonal matrix, then take M rows from the matrix to obtain an $M \times N$-dimensional matrix, and finally, normalize the column direction of the matrix to obtain the observation matrix [19, 20]. At present, the observation matrix obtained by this method is mainly composed of the partial Fourier observation matrix and partial Hadamard observation matrix. This method is relatively simple and has certain stability, but there are still some disadvantages; that is, the partial Fourier observation matrix cannot reflect the characteristics in the time domain, there are certain limitations, and some Hadamard observation matrices have certain requirements for the length of signal and the number of observations. Signal reconstruction is simply to reconstruct the original signal 2 by using the observation sample y and the observation matrix Φ, that is, to solve the equation $y = \Phi x$. Since the number of observation samples is lower than the dimension of the original signal, there are countless solutions to the equation. However, because the compressed sensing theory requires that the original signal must be sparse, the above equation can be transformed into sparse solution by using this characteristic. The solution formula is shown in

$$\begin{aligned} &\arg\min \|x\|_0 \\ &\text{s.t.} y = \Phi x. \end{aligned} \tag{6}$$

In formula (6), $\|x\|_0$ refers to the number of nonzero elements in the original signal. The model uses minimization. In theory, this method is feasible, but Donoho's research results show that to solve the above model, it is necessary to enumerate the arrangement of C_N^K nonzero elements, which is a NP hard problem, so this method is not practical. After that, some researchers found that when the observation matrix is not related to the orthogonal basis, it can be solved by minimizing l_1 norm instead of the above model. The formula is shown in

$$\begin{aligned} &\arg\min \|x\|_1 \\ &\text{s.t.} y = \Phi x. \end{aligned} \tag{7}$$

In this way, an NP problem can become a problem solving problem, and further simplification can become a linear programming problem. As research progresses, scientists demand more signal recovery algorithms. Several decorations are shown below. Greedy algorithms are prepared by reducing technical knowledge. Because the latter belongs to the NP complex problem, the direct solution will waste a lot of time, so some scientists solve the problem in the past. The greedy algorithm uses only the signal coefficients and support settings to iteratively compute the best solution. The algorithm allows some errors in reconstruction. The advantage of the greedy algorithm is that it is fast and can be done in real time in practice, but the accuracy of the algorithm is low and requires high observations. In view of the shortcomings of this algorithm, many improved algorithms have been proposed, such as the orthogonal matching pursuit algorithm, compressed sampling matching pursuit CoSaMP, and stage wise orthogonal matching pursuit algorithm. A convex optimization algorithm solves the minimum l_1 norm to reconstruct the original signal. This algorithm is also proposed to solve the problem of minimizing l_0 norm. It is found that when the observation matrix is not related to the orthogonal basis, the problem of minimizing l_0 norm can be transformed into the problem of minimizing l_1 norm; that is, it becomes a convex optimization problem. Finally, the original signal can be reconstructed by linear programming. The algorithm has the advantages of high precision and less observations, but it is not suitable for processing large-scale signals, and the running time of the algorithm is long. In addition, its search direction is easily affected by the observation matrix, so it is necessary to reasonably select the observation matrix for the algorithm. At present, common convex optimization algorithms include base tracking algorithm, gradient projection for sparse reconstruction (GPSR), and iterative hard threshold algorithm (IHT) [21]. The statistical optimization algorithm first generates a training set with the help of typical signals, then finds the optimal linear projection set through a certain learning algorithm, and finally uses the set to reconstruct the signal. Although the algorithm requires more observations than the convex optimization algorithm, it takes less time to run, which can achieve a good balance between the two. At the same time, the accuracy of the algorithm is high [22]. At present, the common statistical optimization algorithms are the algorithm based on Bayesian statistics and the statistical optimization algorithm based on training set learning. The combination algorithm mainly uses highly structured and group testing to obtain the support set of the signal. Compared with the convex optimization algorithm, it runs faster and requires less observations. However, the combination algorithm does not specifically limit the observation matrix, which makes it difficult to propose a new observation matrix. In addition, the accuracy of the algorithm cannot be fully guaranteed [23, 24]. At present, the more popular combination algorithms include chain pursuit (CP), Fourier sampling, and HHSP (heavy hitters on steroids pursuit). Signal reconstruction is very important in the process of compressed sensing. The error of the original signal reconstructed determines the performance of compressed sensing. At present, a large number of signal reconstruction algorithms have been proposed, but these algorithms still have some limitations. Therefore, how to obtain reconstruction algorithms with low time complexity and high precision is still a difficult and hot spot for researchers to solve. A compressed tracking algorithm is a robust tracking algorithm based on compressed sensing theory. It is simple and efficient and has been used in many fields. Compressed sensing theory points out that a random matrix satisfying the condition of compressed isometry property rip is used to randomly sample the sparse vector, and the sampled low-dimensional vector retains almost all the information of the original vector. CT algorithm samples and compresses high-dimensional features according to this theory, and its tracking process is shown in Figure 4.

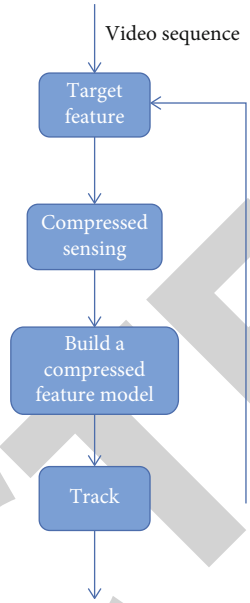

Figure 4: Basic flow of compression tracking.

Haar-like feature is used here. Haar-like feature is a common feature description operator in the field of computer vision. It uses a random matrix E with dimension $M \times N$ satisfying rip conditions to convert the high-dimensional feature vector X (n-dimensional) to the low-dimensional feature vector V (m-dimensional), where m is much less than n. The formula is shown in

$$V = EX. \tag{8}$$

The random matrix e is a very sparse matrix, and the values of the elements in row Z and column J are shown in

$$e_{i,j} = \sqrt{s} * \begin{cases} 1, & \text{the probability is } (2s)^{-1}, \\ 0, & \text{the probability is } 1\text{-}s^{-1}, \\ -1, & \text{the probability is } (2s)^{-1}. \end{cases} \tag{9}$$

When $s = O(n)$, matrix E satisfies the rip condition, and at most four nonzero elements in each row need to be

calculated, which can effectively improve the running speed of the algorithm. The CT algorithm uses the naive Bayesian classifier for classification and uses formula (8) to obtain the low-dimensional feature vector $V = (v_1, \cdots, v_m)^T$ of the sample image. Assuming that the components in the feature vector are independent of each other and the probability that each sample is a target or background is the same, the model of naive Bayesian classifier is shown in

$$H(v) = \sum_{i=1}^{m} \log\left(\frac{p(v_i|y=1)}{p(v_i|y=0)}\right). \tag{10}$$

When evaluating treatment outcomes, carefully consider any adverse or unexpected events (including the patient's symptoms and signs) and cause, make similar decisions, and write them down. In serious cases, the exam will be cancelled. For adverse events in the experiment, symptoms, signs, degree of occurrence, time of occurrence, timing, treatment, etc., shall be recorded on the case report form to evaluate their correlation with the test methods and acupoint selection, which shall be recorded in detail by the researcher, who shall sign and indicate the date of the event [25]. The possible adverse events in this test mainly include needle fainting, hematoma, and infection caused by the retention of floating needle hose. Judge the relevant conditions of adverse events in detail, such as occurrence time, main symptoms, duration, severity, treatment measures taken, and disappearance time. After evaluating the adverse reactions, judge whether to terminate the test according to the severity of the situation. According to the adverse reactions of different cases in this study, determine the safety classification and then count the number of cases in each safety classification of different treatment schemes. After statistical analysis, the safety of different treatment schemes can be evaluated [26]. The safety evaluation is graded as follows: Level 1: safe without any adverse reactions. Level 2: relatively safe, with adverse reactions, but to a lesser extent, and the treatment can be continued without any treatment. Level 3: safety concerns and adverse reactions. Degrees are average. Treatment can be continued after symptoms are treated. Grade 4: the study was postponed due to adverse reactions.

4. Experiment and Analysis

A total of 70 eligible studies were included in this study, including 35 cases in the experimental group and 35 cases in the control group. Among them, 3 cases were lost to follow-up due to personal reasons, and no circumstances were excluded. The final treatment included 34 cases in the experimental group and 32 cases in the control group, a total of 66 cases. See Table 1 for the completion status.

In the process of this study, there were 4 cases of abscission, and no cases were excluded, accounting for 4.41 of the total design samples. Among them, 1 case fell off in the floating needle group and 3 cases fell off in the conventional acupuncture group. The difference between the groups was not statistically significant by the χ^2 test, $P > 0.05$. Case rejection/shedding is shown in Table 2.

Table 1: Completion of two groups of cases.

Group	Number of cases	Removal/shedding	Complete
Treatment group	35	1	34
Control group	35	3	32
Total	70	4	66

Three cases did not complete the treatment plan, including 2 cases of noncompliance with the treatment due to occupation (4 cases in the treatment group and 7 cases in the control group) and 1 case of noncompliance, seeing a doctor due to inconvenience of transportation. The other cases were successfully treated according to the trial design steps, and the completion rate was 95.59%. The gender comparison between the two groups is shown in Table 3.

According to the statistical analysis of the gender distribution of the subjects in the test group and the control group, the χ^2 test shows that $\chi^2 = 0.365$, $P = 0.524 > 0.05$, so the gender distribution difference between the two groups is not statistically significant and comparable. The age comparison between the two groups is shown in Table 4.

The oldest in the medical group was 52 years old, and the youngest was 21 years old. On the board of directors, the oldest is 51 years old and the youngest is 25 years old. The age comparison of the two groups and the face test showed that $t = -0.123$, $P = 0.903 > 0.05$; the difference was not significant and significant. The comparison of the two groups of diseases is shown in Table 5.

The data did not follow a normal distribution after natural measures analysis compared to the disease categories of the two groups, so two independent examples without the use of a test (Mann-Whitney U test) were used. The test results showed that $Z = -0.539$, $P = 0.590 > 0.05$, the difference was not significant, and the two groups were compared. The comparison of symptoms between the two groups is shown in Table 6.

There was no significant difference in the distribution of TCM syndromes between the two groups ($P > 0.05$). After the first course of treatment and one course of treatment, the VAS scores of both groups were lower than those before treatment. Two discordant samples (Wilcoxon sign test scale) differed significantly ($P < 0.05$): test VAS scores after the first treatment compared with both groups. From the two noninvasive tests (Mann-Whitney U test), the difference was significant; after one course of treatment, the VAS scores of the two tests were not inconsistent (Mann-Whitney U test); the difference was not significant ($P > 0.05$), as shown in Figure 5.

Cervical spondylosis is the highest incidence rate in all types of cervical spondylosis, accounting for 4086. In recent years, with the incidence rate of cervical spondylosis increasing, the age of onset of cervical spondylosis is gradually younger. Therefore [27], many doctors are trying to explore in clinic to find a way to relieve pain and be convenient, simple, safe, nontoxic, and effective. Acupuncture and moxibustion therapy are the most widely used intervention for

Table 2: Summary of case rejection/shedding.

Group	Number	Removal/shedding	Reason	Time
Treatment group	12	1	Work	4th time
Control group	3/25	2	Inconvenient transportation	7th time

Table 3: Comparison of gender composition between the two groups.

Group	Number of cases	Male (%)	Female (%)
Treatment group	33	16 (48.5%)	17 (51.5%)
Control group	32	17 (53.1%)	15 (46.9%)

Table 4: Age comparison between the two groups.

Group	Number of cases	Average age (years)	t	P
Treatment group	33	33.39 ± 8.5	-0.123	0.903
Control group	32	33.63 ± 6.4		

Table 5: Comparison of course of disease between the two groups ($x \pm s$, month).

Group	Number of cases	Average course of disease (months)	Z	P
Treatment group	33	3.70 ± 1.45	-0.53	0.59
Control group	32	3.88 ± 1.29		

Table 6: Comparison of syndrome types between the two groups.

Group	Number of cases	Wind cold blocking collaterals	Qi stagnation and blood stasis	Deficiency of liver and kidney
Treatment group	33	10	17	6
Control group	32	9	16	7

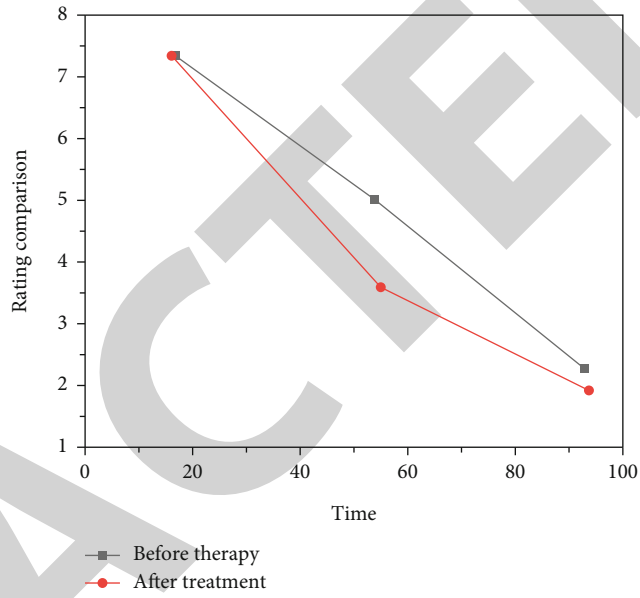

Figure 5: VAS score comparison.

cervical spondylosis of cervical type. The accuracy and safety of its efficacy have been confirmed by a large number of clinical applications and studies. Therefore, this study takes the conventional acupuncture group as the control group to explore the clinical application advantages of floating acupuncture therapy. Floating needle therapy is a new acupuncture technology invented by Professor Fu Zhonghua based on Ashi point theory and wrist manic needle theory. Because of its significant analgesic effect and convenience of operation, it is widely used by clinical doctors to treat various bone injuries, pain diseases, and medical miscellaneous diseases, especially for pain caused by muscle and soft tissue injury. The analgesic effect is immediate. Therefore, by comparing the overall efficacy, immediate analgesic effect, and impact on emotional life of acupuncture and floating needle therapy in the intervention of cervical spondylosis, this paper comprehensively analyzes the advantages of floating needle therapy, so as to provide guidance and basis for its further wide application in clinic.

5. Conclusion

In overall evaluation, acupuncture is based on the theory of Yu acupoints in the meridians, "the meridians pass through and the main treatment reaches," which plays a role in harmonizing Yin and Yang and dredging the meridians, so as to treat NTCS. Acupuncture plays an irreplaceable role in the treatment of NTCS and is widely used in clinic. In the treatment of NTCS, a floating needle mainly selects the affected muscle, which makes the target more accurate and avoids the disadvantage of blind selection. Moreover, the selection of points by floating needle is less than that by conventional acupuncture, which reduces the physical and mental pressure of patients to a certain extent. The floating needle has the advantages of quick effect and nontoxic side effects. In general, floating needle therapy has comprehensive advantages in the treatment of NTCS. Therefore, this study chose the complementary way of floating needle therapy and acupuncture therapy to improve the overall curative effect. This study combines the pathogenesis characteristics of NTCS and follows the principle of tendon disease following meridians, so as to achieve the purpose of treating NTCS. Both floating acupuncture and conventional acupuncture can

effectively improve the pain symptoms of cervical spondylosis, and the curative effects of both are equivalent. After the first treatment, floating acupuncture was significantly better than conventional acupuncture in improving the degree of pain, indicating that floating acupuncture has better immediate analgesic effect. Under the condition of considerable clinical efficacy, safety, and compliance, the number of treatment times required by floating needle is less than that of conventional acupuncture, which is conducive to reducing the pain of patients, saving the time cost of doctors and patients, and improving clinical efficiency.

Data Availability

The data used to support the findings of this study are available from the corresponding author upon request.

Conflicts of Interest

The authors declare that they have no conflicts of interest.

References

[1] S. L. Pan, S. L. Zheng, X. H. Zhou, and Q. L. Wang, "Acupuncture combined with Jingtong granule for nerve-root type cervical spondylosis and its effects on IL-6, TNF-α, IL-1β and hemorheological indexes," *Zhongguo Zhen jiu = Chinese Acupuncture & Moxibustion*, vol. 39, no. 12, pp. 1274–1278, 2019.

[2] H. Zheng, Z. G. Lü, W. C. Hu, W. Jing, H. Li, and W. L. Hou, "Clinical study on tuina for acute cervical radiculopathy," *Science*, vol. 17, no. 6, pp. 438–444, 2019.

[3] J. Xu, Z. F. Shen, Y. J. Wu, and X. D. Bian, "Clinical observation on warm needling moxibustion plus tuina for cervical spondylosis of vertebral artery type," *Journal of Acupuncture and Tuina Science*, vol. 17, no. 2, pp. 111–115, 2019.

[4] L. X. Xiao, C. S. Liu, S. Z. Zhong, and W. H. Huang, "Effect of a traction exercise neck brace on cervical spondylopathy radiculopathy: a clinical study and finite element analysis," *Evidence-based Complementary and Alternative Medicine*, vol. 2021, 10 pages, 2021.

[5] M. W. Maiji, Y. Zhao, Q. Wen, Y. Yang, J. Q. Lü, and N. Li, "Influence of different courses of electroacupuncture treatment on compliance and therapeutic outcome of patients with cervical type cervical spondylosis: a small-sample randomized controlled trial," *Zhen ci yan jiu = Acupuncture Research*, vol. 44, no. 11, pp. 835–839, 2019.

[6] Y. J. Ye, Y. X. Xie, T. W. Yan et al., "Rolling needle pricking-cupping therapy and traditional pricking-cupping therapy for cervical spondylosis of neck type: a randomized controlled trial," *Zhongguo Zhen jiu = Chinese Acupuncture & Moxibustion*, vol. 40, no. 12, pp. 1299–1303, 2020.

[7] Z. Y. Song, Z. M. Zhang, X. G. Qin, X. L. Fang, and X. Q. Yao, "Treatment of neck type cervical spondylopathy with zheng's jin gou diao yu (gold-hook-fishing) acupuncture method: a randomized controlled trial," *Journal of Acupuncture and Tuina Science*, vol. 17, no. 5, pp. 350–355, 2019.

[8] S. Y. Xue, C. Y. Wang, T. Li, S. M. Liu, and Y. Shi, "Therapeutic efficacy observation on moxibustion with moxa of different storage years for moderate-to-severe primary knee osteoarthritis," *Journal of Acupuncture and Tuina Science*, vol. 18, no. 5, pp. 345–351, 2020.

[9] C. Li, L. Tan, and W. Zhou, "Meta-analysis of clinical efficacy of metformin combined with chemotherapy in the treatment of ovarian cancer," *Journal of Clinical Medicine Research*, vol. 3, no. 1, pp. 25–30, 2022.

[10] X. Yun, C. Zhi-liang, L. Ying-han, L. Bi-dan, and Z. Wei, "Clinical observation on moxibustion therapy plus tuina in treating children with recurrent respiratory tract infections due to qi deficiency of spleen and lung," *Journal of Acupuncture and Tuina Science*, vol. 19, no. 5, pp. 371–377, 2021.

[11] X. Dong, J. Liu, and J. Bu, "The efficacy of modified posterior scleral reinforcement with round scleral patches in Chinese children with high myopia," *Clinical and Experimental Ophthalmology*, vol. 258, no. 7, pp. 1543–1547, 2020.

[12] L. W. Zhang, X. Fei, and Y. Song, "The clinical efficacy of novel vacuum suction ureteroscopic lithotripsy in the treatment of upper ureteral calculi," *World Journal of Urology*, vol. 39, no. 11, pp. 4261–4265, 2021.

[13] V. D. Zavoikin, O. P. Zelya, and N. I. Tumolskaya, "Clinical tolerance and efficacy of anti-parasitic treatment with albendazole in patients with alveolar echinococcosis: long-term follow-up observation in 117 patients," *Parasitology Research*, vol. 120, no. 10, pp. 3603–3610, 2021.

[14] T. L. Mao, Z. X. Wang, F. W. Tian, and X. Zhou, "Evaluation of the clinical efficacy of muscle regions of meridians needling method for refractory facial paralysis based on infrared thermal imaging technology," *Journal of Acupuncture and Tuina Science*, vol. 19, no. 6, pp. 449–456, 2021.

[15] W. Kun-xiu, L. Zhi-hui, Y. Peng et al., "Clinical efficacy observation of 'Tong Du Yun Pi' manipulation for infantile diarrhea in autumn," *Science*, vol. 19, no. 5, pp. 364–370, 2021.

[16] Y. Shimozono, Y. Yasui, E. T. Hurley, R. A. Paugh, T. W. Deyer, and J. G. Kennedy, "Concentrated bone marrow aspirate may decrease postoperative cyst occurrence rate in autologous osteochondral transplantation for osteochondral lesions of the talus," *Arthroscopy: The Journal of Arthroscopic & Related Surgery*, vol. 35, no. 1, pp. 99–105, 2019.

[17] D. B. Cardin, J. Whisenant, G. D. Ayers et al., "Pilot study to test safety and efficacy of avelumab in small bowel adenocarcinoma (SBA)," *Journal of Clinical Oncology*, vol. 38, 4_suppl, p. 797, 2020.

[18] C. Uzunköprü, Y. Beckmann, and S. Türe, "Long-term effectiveness of fingolimod for multiple sclerosis in a real-world clinical setting," *European Neurology*, vol. 84, no. 3, pp. 200–205, 2021.

[19] Y. Ji, W. Lou, and J. Ji, "Machine learning algorithm-based analysis of efficacy of pulmonary surfactant combined with mucosolvan in meconium aspiration syndrome of newborns through ultrasonic images," *Scientific Programming*, vol. 2021, 7 pages, 2021.

[20] Y. Huang, X. Ran, X. Xu et al., "Itraconazole oral solution for a case of infantile hemangioma: monitoring the efficacy by dermoscopy and MRI," *Dermatology and Therapy*, vol. 11, no. 5, pp. 1861–1866, 2021.

[21] M. K. Louvrou, I. Fragkioudakis, and L. Batas, "The use of lasers in peri-implant disease treatment and their efficacy in inflammation reduction: a narrative review," *Science*, vol. 6, no. 1, pp. 15–26, 2022.

[22] X. Xu, L. Li, and A. Sharma, "Controlling messy errors in virtual reconstruction of random sports image capture points for complex systems," *International Journal of Systems Assurance Engineering and Management*, pp. 1–8, 2021.

Hindawi
Scanning
Volume 2023, Article ID 9785215, 1 page
https://doi.org/10.1155/2023/9785215

Retraction

Retracted: Effect of Core Muscle Strength Training Combined with Taijiquan on Bone Mineral Density Measured by Quantitative CT Scanning in the Elderly

Scanning

Received 3 October 2023; Accepted 3 October 2023; Published 4 October 2023

This article has been retracted by Hindawi following an investigation undertaken by the publisher [1]. This investigation has uncovered evidence of one or more of the following indicators of systematic manipulation of the publication process:

(1) Discrepancies in scope

(2) Discrepancies in the description of the research reported

(3) Discrepancies between the availability of data and the research described

(4) Inappropriate citations

(5) Incoherent, meaningless and/or irrelevant content included in the article

(6) Peer-review manipulation

The presence of these indicators undermines our confidence in the integrity of the article's content and we cannot, therefore, vouch for its reliability. Please note that this notice is intended solely to alert readers that the content of this article is unreliable. We have not investigated whether authors were aware of or involved in the systematic manipulation of the publication process.

In addition, our investigation has also shown that one or more of the following human-subject reporting requirements has not been met in this article: ethical approval by an Institutional Review Board (IRB) committee or equivalent, patient/participant consent to participate, and/or agreement to publish patient/participant details (where relevant).

Wiley and Hindawi regrets that the usual quality checks did not identify these issues before publication and have since put additional measures in place to safeguard research integrity.

We wish to credit our own Research Integrity and Research Publishing teams and anonymous and named external researchers and research integrity experts for contributing to this investigation.

The corresponding author, as the representative of all authors, has been given the opportunity to register their agreement or disagreement to this retraction. We have kept a record of any response received.

References

[1] M. Zhong, "Effect of Core Muscle Strength Training Combined with Taijiquan on Bone Mineral Density Measured by Quantitative CT Scanning in the Elderly," *Scanning*, vol. 2022, Article ID 6942081, 7 pages, 2022.

Hindawi
Scanning
Volume 2022, Article ID 6942081, 7 pages
https://doi.org/10.1155/2022/6942081

Research Article

Effect of Core Muscle Strength Training Combined with Taijiquan on Bone Mineral Density Measured by Quantitative CT Scanning in the Elderly

Mingliang Zhong

Zhengzhou Preschool Education College, Zhengzhou, Henan 450000, China

Correspondence should be addressed to Mingliang Zhong; 1330304133@post.usts.edu.cn

Received 12 April 2022; Revised 8 May 2022; Accepted 13 May 2022; Published 23 May 2022

Academic Editor: Danilo Pelusi

Learn about the benefits of muscle strength training combined with tai chi for adult skeletal muscle in multiple CT scanning. The study included 182 people over the age of 60 with no long-term history of physical activity and exercise. They were divided into the Taijiquan group (52 people), student muscle strength group (45 people), student muscle group combined with Taijiquan group (45 people), and control group (40 people). The board of directors did not attend. The other three groups received tai chi (more than 4 times a week), muscle strength training, and muscle training combined with tai chi for 6 months. Lumbar spine (L1-4) BMD and Berg scores were approximately the same as those measured in adults before exercise and at 3 and 6 months after exercise. The results showed that there were significant differences in the scores of lumbar spine BMD and Berg Balance Scale between the Taijiquan group and students before and after exercise combined with muscle strength training ($P < 0.05$ or <0.01). The difference was statistically significant ($P < 0.05$). The scores of lumbar BMD and Berg Balance Scale in the core muscle strength training combined with Taijiquan group after 6 months of exercise were higher than those after 3 months of exercise ($P < 0.05$), and the CT value of lumbar vertebral bone calcium was significantly positively correlated with BMD (Pearson correlation coefficients of L5 vertebral body were $r = 0.704$, 0.683, 0.728, 0.673, and 0.686, $P < 0.01$). Single or combined training of core muscle strength or Taijiquan can improve lumbar bone mineral density and balance function in the elderly.

1. Introduction

In recent years, countries pay more and more attention to the research on the physique of the middle-aged and elderly, focusing on the influencing factors of the health of the middle-aged and elderly, especially the impact of exercise on the health of the middle-aged and elderly. The American Association of Sports Medicine (AESM) found through research that the elderly can effectively improve cardiovascular function and prolong life through regular endurance training. Regular exercise behavior can improve the bone health of middle-aged and elderly people, prevent osteoporosis [1], increase physical stability, reduce the risk of fracture, and slow down the aging of physiological function, especially the decline of muscle function. Nichols's experiment found that the lean weight of middle-aged and elderly people increased after regular exercise for a long time, and the body fat composition also decreased significantly. The respiratory function of the elderly decreased significantly. The respiratory muscle strength of elderly women is weakened, the alveolar fusion and the elasticity of lung tissue are weakened, the oxygen diffusion function begins to appear as an obstacle, the activity of the thorax becomes smaller, and the ventilation function of the lung decreases accordingly [2]. Therefore, in the process of strenuous exercise, if you want to improve lung ventilation, you can only be effective by increasing the frequency of breathing, rather than simply increasing the depth of breathing. Even if the respiratory system function decreases with aging, the lung ventilation reserve of healthy elderly people still has a considerable degree of accommodation. Pay attention to maintenance at ordinary times. Exercising more and prolonging

the health level of cardiopulmonary function will not cause too much problems.

With the aggravation of population aging in China, senile osteoporosis has become a problem of widespread concern, which seriously affects the daily life of the elderly. Domestic research on the health care function of traditional boxing exercises shows that Taijiquan can improve the brain function, physical strength, and balance function of the elderly, so as to prevent falls. Core muscle strength training stabilizes the spine and pelvis by controlling the trunk strength of the whole body, so as to improve the level of controlling the trunk balance function, improve the efficiency of limb coordination, reduce energy consumption, and prevent sports injury. However, there is no report on the relevant research on the combination of the two. This study observed the effect of regular core muscle strength training combined with traditional 24-style Taijiquan exercise on bone mineral density and balance function of the elderly for 6 months, so as to provide a more scientific and effective training method for the elderly to prevent falling and osteoporosis [3].

Noninvasive examination of large bone marrow and bone marrow is essential for early prevention and treatment of osteoporosis. Currently, there are several ways to measure bone mineral density (BMD) (Figure 1). The two most widely accepted methods are dual-energy X-ray absorptiometry (DXA) and quantitative computed tomography (QCT). In recent years, there have been a large number of studies on the two methods to measure BMD. Dual-energy CT (DECT) can detect the separation of substances through the difference of dual-energy index between different substances. It can pass through the cancellous bone and excessively separate the bone mineral and bone marrow in the bone tissue, so as to obtain a separate calcium map or bone marrow map, so as to realize the quantitative measurement of BMD. In this study, dual-energy CT scanning was used to measure BMD by using dual-energy material separation technology, and the BMD of the vertebral body was measured by comparing with single-energy QCT to evaluate the application value of DECT in the measurement of bone mineral density [4].

2. Literature Review

Wang and others believe that Taijiquan is a whole-body participatory exercise. During Taijiquan exercise, the knee joint is basically in a squat state, in order to stabilize the strength of the lower limbs. Even with the movement and center of gravity transfer, it is also required to keep the lower limbs stable, the transition is stable, and the footwall is stable before the movement is smooth. Standing with eyes closed and one foot is an effective method to evaluate the balance of the human body in a static state, which reflects the vestibular system function of the elderly [5]. Lin and others believe that Taijiquan exercise has a significant effect on the strength of quadriceps femoris and cochineal muscles in the elderly. Because in Taijiquan, the center of gravity of the body is always kept at a low position, the quadriceps femoris is in a state of alternating relaxation and tension for a long time, which stimulates the muscle, accelerates the metabolism, increases the opening of capillaries, increases the blood supply, enhances the absorption and storage capacity of nutrients such as protein, thickens the muscle fibers, increases the muscle volume, and then makes the muscle become stronger and stronger [6]. Gong and others believe that in terms of cardiopulmonary function, the maximum oxygen intake is a comprehensive index to evaluate cardiopulmonary function. It reflects the body's ability to transport oxygen and the efficiency of using oxygen and is an important factor to determine the exercise ability. The maximum oxygen intake decreases with age, and the cardiac output is positively correlated with the maximum oxygen intake [7]. Aas and others believe that the physical work ability PWC170 is an index recommended by the World Health Organization to evaluate the physical work ability of adolescents, while PWC130 is an index to evaluate the physical work ability of middle-aged and elderly people [8]. Tice and others believe that the maximum oxygen intake and body work ability of middle-aged and elderly women are significantly improved after long-term Taijiquan exercise, which shows that long-term Taijiquan exercise can effectively improve the heart function capacity and body work ability of the elderly [9]. Reis and others believe that the respiratory function of the elderly is gradually declining, the respiratory muscle function is impaired, the work efficiency is limited, the muscle strength and endurance are declining, and the respiratory reserve is significantly reduced. The maximum ventilation volume per minute reflects the maximum ventilation capacity of the lung and the reserve capacity of ventilation function under continuous ventilation. It is an index that can comprehensively reflect the function of the whole respiratory system [10]. Hwang and others believe that the maximum ventilation volume decreases rapidly with the increase in age. The maximum ventilation of the elderly is reduced due to the reduction of the contractility of respiratory muscles, the weakening of the compliance of the lungs and thorax, the increase in respiratory resistance, and the reduction of sensitive excitability of the respiratory center [11]. Hwang and others said that the maximum ventilation of middle-aged and elderly women who have participated in Taijiquan for a long time shows an upward trend, and the vital capacity (VC), forced vital capacity (FEV1), and airway obstruction (FEV1/FVC) are significantly increased, indicating that Taijiquan exercise can increase respiratory reserve, delay the degradation of ventilator energy caused by aging, significantly improve pulmonary elastic retraction, improve respiratory muscle strength, increase oxygen uptake, and ensure the body's demand for oxygen. After keeping the habit of Taijiquan exercise for a long time, the systolic blood pressure, diastolic blood pressure, and average arterial pressure of middle-aged and elderly women decreased significantly in a quiet state. The change of blood pressure ensures the coronary blood flow and myocardial blood supply .

3. Experimental Analysis

3.1. Research Object. 182 elderly people over 60 years old without long-term exercise history and exercise habits in

Figure 1: The main reasons for the effect of bone density.

the community were randomly divided into 4 groups: 52 cases in the core muscle strength training plus Taijiquan group (age: 68.41 ± 6.25 years; height: 163.07 ± 6.39 cm; and body weight: 63.06 ± 8.49 kg); 45 cases in the Taijiquan group (age: 68.15 ± 4.67 years; height: 165.19 ± 5.44 cm; and body weight: 66.06 ± 8.42 kg); 45 cases in the core muscle strength training group (age: 68.62 ± 6.47 years; height: 163.16 ± 6.45 cm; and body weight: 63.06 ± 8.49 kg); and 40 cases in the control group (age: 66.69 ± 4.11 years; height: 163.73 ± 5.49 cm; and body weight: 63.25 ± 7.07 kg). There was no significant difference in age, height, and body mass among the four groups ($P > 0.05$). Inclusion criteria were as follows: (1) those aged ≥60; (2) no long-term exercise history and no long-term Taijiquan practice history; (3) no diseases that seriously affect core muscle strength training and Taijiquan exercise, such as joint deformity, spinal joint-related diseases or severe pain, and serious cardiopulmonary diseases; (4) no other serious organic diseases; and (5) those who voluntarily cooperate with this study in core muscle strength training and Taijiquan exercise and can accept a questionnaire survey, bone mineral density (BMD) test, and Berg Balance Scale score test. Exclusion criteria were as follows: (1) those who cannot be trained for a long time (this test requires 6 months), (2) those with cognitive impairment [12], (3) serious mental illness, and (4) observers who are receiving other relevant treatment that may affect the effect indicators of this study.

3.2. Method

3.2.1. Taijiquan Group. Video teaching of Taijiquan shall be carried out first, and then, 24 simplified Taijiquan teaching training shall be carried out for the elderly by Taijiquan professionals. The training shall not be less than 4 times a week, and each training shall not be less than 30 minutes (not less than 5 times), and the training shall be continued for 6 months.

3.2.2. Core Muscle Strength Training Group. The core muscle strength training is guided by the rehabilitation therapist. Methods for the elderly are as follows: lift the back and hip and stretch the hip to increase the strength of the back and hip. (1) For the elderly, it is convenient to bend the hip at home. (2) For one leg bypass, in the supine position, bend the hip and knee of the left lower limb, straighten the right leg, exert force on the hip and waist back, lift the waist back, hip, and right lower limb, straighten the hip joints on both sides, and carry out alternately on both sides with only the shoulders and left foot as the fulcrum of the body. (3) For step in lying position, in the supine position, bend the hips and knees of both legs and step alternately with left and right feet. (4) For flat support, in the prone position, with both forearms and feet as the fulcrum, support the body and hang it in the air. The body is in a straight line to maintain the movement. (5) For diagonal support of the kneeling position, take the kneeling position, first support the body with both hands and knees, straighten both upper limbs, bend both hips and knees by 90°, then straighten the left upper limb forward, extend the right lower limb backward, form a straight line with the trunk, and only support the body with the right hand and left knee [13], alternating on both sides. Each action is repeated 10 times, each action lasts for 5~10 s, and the action interval is 5~10 s.

The five training movements were performed in two groups for a total of about 40 minutes (about 3 minutes for double leg bridging, about 5 minutes for bilateral alternation of single leg bridging, 3 minutes for treadmill in lying position, about 3 minutes for plate support, and about 5 minutes for bilateral alternation of diagonal support in the kneeling position). They were practiced at least 4 times a week for 6 months.

3.2.3. Core Muscle Strength Training plus Taijiquan Group. The training content includes core muscle strength and Taijiquan, which are completed in the morning and afternoon. The core muscle strength training and Taijiquan are not less than 30 minutes and not less than 4 times a week and practiced continuously for 6 months.

3.2.4. Control Group. The subjects lived according to their previous living habits without training.

In this study, a Norland XR~46 dual-energy X-ray BMD tester (Norland Company of the United States) was used to scan the lumbar spine (L1-4) for 5 times before the exercise intervention and 3 months and 6 months after the intervention. The following 14 items were evaluated according to the evaluation standard of the Berg evaluation scale: stand up from a sitting position, stand without support, sit without back but with both feet on the ground or on a stool, sit down from a standing position, transfer, stand with eyes closed without support, stand with both feet together without support, stretch forward and move forward when standing, pick up items from the ground when standing, turn back from the standing position, turn 360°, put one foot on a step or stool when standing without support, stand with one foot in front, stand without support, and stand on one leg. Each item has a minimum score of 0 and a maximum score of 4, with a total of 56. The test is generally completed within 20 minutes. According to the score, it is divided into three levels: 0~20 (wheelchair), 21~40 (auxiliary walking), and 41~56 (independent walking). A score lower than 40 indicates the risk of falling.

3.3. Statistical Methods. The data were analyzed by using SPSS 19.00 statistical software. The measurement data were expressed as mean ± standard deviation ($\bar{x} \pm s$). One-way ANOVA was used for intergroup comparison. For multiple comparisons within the group, the LSD-t method or SNK-q method was used when the variance was homogeneous, and Tamhane's T2 method was used when the variance was uneven. $P \leq 0.05$ means that the difference is statistically significant [14].

3.4. Result Analysis. All subjects in this study completed DECT and QCT bone mineral density measurements of lumbar vertebrae 1-5. The measurement results are shown in Table 1. According to the QCT bone mineral density diagnostic standard 4 recommended by experts of the International Society for clinical bone mineral density (ISCD) in 2007, 6 subjects in this study were diagnosed with osteoporosis, with a BMD of the 57.66 ± 13.75 mg/cc; 13 subjects were diagnosed with low bone mass [15], and the BMD was 103.44 ± 14.15 mg/cc. The bone mass of 37 subjects was normal, and the BMD was 135.74 ± 13.45 mg/cc.

Table 1: Bone calcium CT value, bone marrow CT value, and BMD value measured by QCT of lumbar vertebrae measured by DECT ($\bar{x} \pm s$).

Lumbar vertebrae	BMD value measured by QCT (mg/cc)	DECT bone calcium-related CT value (HU)
L1	124.92 ± 27.30	223.76 ± 38.18
L2	120.91 ± 28.68	221.80 ± 39.74
L3	114.92 ± 28.04	220.11 ± 36.01
L4	117.31 ± 29.69	225.71 ± 34.22
L5	130.32 ± 30.61	239.22 ± 36.09

There was a significant positive correlation between the bone calcium CT value of the lumbar spine (LS) vertebral body measured by DECT and the BMD value measured by QCT. The Pearson correlation coefficients were as follows: r lumbar 1 vertebral body = 0.715, r lumbar 2 vertebral body = 0.692, r lumbar 3 vertebral body = 0.739, r lumbar 4 vertebral body = 0.673, and r lumbar 5 vertebral body = 0.686, respectively ($P < 0.01$). There was a positive correlation between bone marrow CT value and BMD value. Pearson correlation coefficients were as follows: RL1 vertebral body = 0.343, RL2 vertebral body = 0.315, RL3 vertebral body = 0.439, RL4 vertebral body = 0.440, and RL5 vertebral body = 0.456, respectively. The difference was statistically significant (LS vertebral body, $P < 0.05$; the rest, $P < 0.01$).

There were significant differences in lumbar BMD before and after exercise in the core muscle strength training combined with Taijiquan group, Taijiquan group, and core muscle strength training group ($P < 0.05$ or <0.01). The lumbar BMD of the core muscle strength training combined with Taijiquan group, Taijiquan group, and core muscle strength training group after 6 months of exercise was higher than that before exercise [16]. The lumbar BMD of the core muscle strength training combined with Taijiquan group after 6 months of exercise was higher than that of 3 months of exercise ($P < 0.05$).

There was no significant difference in the BMD of the lumbar spine between the four groups before and 3 months after exercise ($P > 0.05$). The lumbar spine BMD of the core muscle strength training combined with Taijiquan group, Taijiquan group, and core strength training were all higher than those of the control group [17]. The lumbar spine BMD of the core muscle strength training combined with Taijiquan group was higher than that of the Taijiquan group and the core muscle strength group (total $P < 0.05$), as shown in Table 2.

After 6 months of the youth strength training combined with Taijiquan team, Taijiquan team, and students' muscle strength training, the Berg Balance Scale scores of the same group were higher than those before training ($P < 0.01$). Months later, exercise was higher at 3 months ($P < 0.01$). After 6 months of strenuous exercise, the strength of the Berg Balance Scale combined with Taijiquan group, Taijiquan group, and core muscle group in

Table 2: Changes of lumbar spine (L1-4) BMD of subjects in each group before and after exercise.

Group	n	Before exercise	Exercise for 3 months	Exercise for 6 months	F value	P value
Core muscle strength + Taijiquan group	50	43.1 ± 2.45	44.62 ± 1.09	47.5 ± 2.01	24.187	<0.01
Taijiquan group	50	44.2 ± 3.23	44.84 ± 3.16	45.0 ± 3.15	4.931	<0.05
Core muscle strength training group	47	45.15 ± 4.14	43.746 ± 2.98	44.87 ± 1.81	3.150	<0.05
Control group	45	41.2 ± 3.15	43.2 ± 3.05	43.2 ± 3.05	0	>0.05
F value		0.086	0.276	8.524		
P value		>0.05	>0.05	<0.01		

Table 3: Comparison of Berg Balance Scale scores of subjects in each group.

Group	n	Before exercise	Exercise for 3 months	Exercise for 6 months	F value	P value
Core muscle strength + Taijiquan group	50	0.751 ± 0.47	0.862 ± 0.22	1.061 ± 0.25	9.860	<0.01
Taijiquan group	50	0.721 ± 0.38	0.785 ± 0.28	0.984 ± 0.278	3.747	<0.05
Core muscle strength training group	47	0.841 ± 0.31	0.979 ± 0.23	0.991 ± 0.23	5.364	<0.01
Control group	45	0.828 ± 0.267	0.829 ± 0.226	0.824 ± 0.278	0	>0.05
F value		0.054	1.313	6.763		
P value		>0.05	>0.05	<0.01		

youth muscle strength training was higher than that of the control group ($P < 0.01$) [18]. After 6 months of exercise, the Taijiquan group had higher muscle training Berg Balance Scale scores than the Taijiquan group and the core muscle group ($P < 0.05$). See Tables 3 and 4.

Table 4 shows that after the test, the four indexes tested in the regular Taijiquan exercise group have significant differences compared with those in the nonexercise group ($P < 0.05$).

4. Discussion

With the aging of the world population, the incidence rate and disability rate of osteoporosis have been significantly improved, which has brought heavy burden to patients and society. Therefore, early diagnosis of osteoporosis is very important [19]. The main evaluation index of osteoporosis is bone mineral density (BMD). Dual X-ray absorptiometry (DXA) is a commonly used imaging diagnostic method for measuring bone mineral density. Although the measurement is simple and widely used in clinic, there are still many deficiencies. Because DXA is an area BMD measurement, the measurement results include the comprehensive measurement values of cancellous bone and cortical bone at the same time, and the early bone mass change of osteoporosis mainly occurs in cancellous bone, the measurement results of DXA cannot reflect the early bone mineral density change, and there are many factors affecting the measurement results, resulting in large measurement error. Compared with DXA, QCT measures the true volumetric bone mineral density, which can independently measure the bone mineral density of vertebral cancellous bone. The measurement results are generally not affected by bone size, shape, hyperosteogeny, and other factors, as shown in Figure 2. In recent years, the value of QCT in the early diagnosis of osteoporosis has attracted more and more attention, and there are more and more studies on the measurement of BMD by QCT [20]. Studies have shown that the detection rate of osteoporosis by QCT is higher than that by DXA, suggesting that measuring BMD by QCT can detect osteoporosis earlier, which is conducive to the early prevention and treatment of osteoporosis. However, because QCT measurement needs special calibration phantom and measurement software, its application is also limited.

With the increase in age, the body tissue of the elderly gradually shows physiological decline, resulting in bone metabolism disorder and bone absorption being greater than bone formation and finally leading to bone loss, which is prone to osteoporosis and even fracture. At the same time, with the decrease in activity, muscle strength, and physical stability, the physical exercise ability of the elderly decreases. Balance function is the ability of the body to adjust itself to prevent falling when the body posture is stable or under the action of external force. It is affected by many factors such as age, muscle strength, proprioception, and vision [21]. Long-term regular Taijiquan exercise and resistance training are helpful to improve the bone mineral density, muscle strength, balance, and posture control ability of the elderly. Research has confirmed that regular physical exercise can improve the bone mineral density of the elderly. It is an important means to delay the process of physical aging and improve the physique of the elderly. Taijiquan is a sport with the advantages of soothing, gentle, dynamic, and static combination, moderate exercise intensity, low risk, and not being easy to be injured. It is one of the preferred exercise methods for the elderly.

Generally speaking, bone mineral density is affected by many factors such as heredity, nutrition, hormones, and

Table 4: Effect of Taijiquan exercise on bone mineral density of the elderly.

Index	No exercise group ($n = 28$)	Exercise group ($n = 28$)
L2~L4	0.830 ± 0.153	0.813 ± 0.126*
Neck	0.873 ± 0.134	0.750 ± 0.144*
Ward's	0.469 ± 0.129	0.679 ± 0.143*
Torch	0.518 ± 0.147	0.658 ± 0.142*

physical exercise. Due to the frail adult body and poor bone metabolism, bone resorption exceeds bone formation, resulting in bone loss. Improper functioning of the bones can cause the bones to deform, which can lead to the synthesis of DNA and collagen in the bones, which can lead to bone loss [22]. On the contrary, when the mechanical stress decreases, the weight of the bone decreases with the decrease in stress. Moderate exercise can significantly increase the bone density of the human body, regulate the bone metabolism of the body, and moderately increase the total amount of bone in the body. As one of the main factors affecting bone mass, physical exercise cannot completely control the decrease in bone mineral content with age and menopause, but it plays a positive role in bone blood circulation, helps to prevent bone loss, and effectively stimulates the formation of bone cells, which plays a very important role in the prevention of osteoporosis. The results showed that the bone marrow level in the study group was higher than that in the four groups (L2-0, $P < 0.05$). Studies have shown that regular tai chi exercises can improve bone marrow function in older adults. This may be because Taijiquan integrates isotonic exercise and isometric exercise. It produces load through muscle contraction, which directly or indirectly acts on bone, changes the voltage in bone, and then stimulates the formation of osteoblasts. It can not only maintain bone mass or increase bone mineral density but also increase the elasticity of bone and enhance the ability of antibending, antiextrusion, and antitorsion. Secondly, Taijiquan's unique body method, step method, and gentle wave movement can massage the periosteum, improve the blood supply of bone tissue, and promote the absorption of bone nutrients. At the same time, Taijiquan belongs to aerobic exercise. Long-term aerobic exercise can increase muscle strength, coordination, and balance, repair bone structure and bone mass, stimulate osteoblast activity, and increase bone formation [23].

As an easy way to master aerobic exercise, Taijiquan has a good mass base in China's community. The exercise intensity is light and medium, the required site has no special requirements, and the physiological burden is small, safe, and feasible. It is not only suitable for exercise in groups but also suitable for individual physical exercise. The exercise should start from low intensity, step by step, and must be persistent in order to maintain the exercise effect and achieve the purpose of improving the middle-aged and elderly in the community, reducing the risk of cardiovascular and cerebrovascular diseases and preventing osteoporosis.

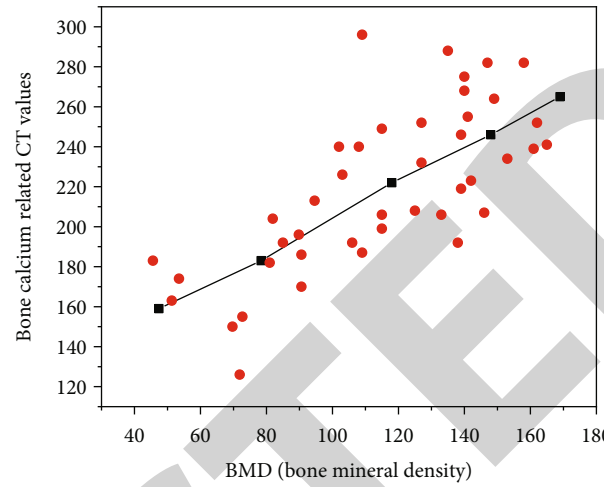

Figure 2: Correlation between vertebral QCT bone mineral density and DECT bone calcium CT value.

5. Conclusion

Taijiquan exercise can effectively improve the body composition of the elderly and increase bone mineral density. This has a positive effect on reducing the risk of cardiovascular and cerebrovascular diseases and preventing osteoporosis. Taijiquan entering the community has the needs of the times. It can exercise the body, enhance physique, promote mutual exchanges among community residents, enrich community cultural life, and enable more people to enjoy the health and happiness brought by Taijiquan in a harmonious society. Taijiquan has rich connotation and a unique way of movement. In the long-term development process, it is organically combined with Chinese traditional culture to form a boxing technique integrating self-cultivation, fitness, and medical treatment, which is not limited by venues and equipment. Research shows that Taijiquan exercise plays a positive role in improving calcaneal bone mineral density and preventing osteoporosis in middle-aged and elderly people. Taijiquan exercise plays a positive role in shortening the reaction time of middle-aged and elderly people and improving the sensitivity of middle-aged and elderly people. Taijiquan is a traditional sport with a long history. It has small exercise load and mellow, gentle, coherent, and natural movements. When exercising, we should relax physically and mentally without high physical and mental tension, which is very in line with the sports ability and physiological characteristics of the middle-aged and elderly and is very suitable for the middle-aged and elderly to practice. Therefore, we should vigorously encourage the middle-aged and elderly to perform Taijiquan exercise.

Data Availability

The data used to support the findings of this study are available from the corresponding author upon request.

Hindawi
Scanning
Volume 2023, Article ID 9803893, 1 page
https://doi.org/10.1155/2023/9803893

Retraction

Retracted: Observation on the Effect of Shoulder Pain Caused by Volleyball Training Injury Based on MRI Image Scanning

Scanning

Received 20 June 2023; Accepted 20 June 2023; Published 21 June 2023

This article has been retracted by Hindawi following an investigation undertaken by the publisher [1]. This investigation has uncovered evidence of one or more of the following indicators of systematic manipulation of the publication process:

(1) Discrepancies in scope

(2) Discrepancies in the description of the research reported

(3) Discrepancies between the availability of data and the research described

(4) Inappropriate citations

(5) Incoherent, meaningless and/or irrelevant content included in the article

(6) Peer-review manipulation

The presence of these indicators undermines our confidence in the integrity of the article's content and we cannot, therefore, vouch for its reliability. Please note that this notice is intended solely to alert readers that the content of this article is unreliable. We have not investigated whether authors were aware of or involved in the systematic manipulation of the publication process.

In addition, our investigation has also shown that one or more of the following human-subject reporting requirements has not been met in this article: ethical approval by an Institutional Review Board (IRB) committee or equivalent, patient/participant consent to participate, and/or agreement to publish patient/participant details (where relevant).

Wiley and Hindawi regrets that the usual quality checks did not identify these issues before publication and have since put additional measures in place to safeguard research integrity.

We wish to credit our own Research Integrity and Research Publishing teams and anonymous and named external researchers and research integrity experts for contributing to this investigation.

The corresponding author, as the representative of all authors, has been given the opportunity to register their agreement or disagreement to this retraction. We have kept a record of any response received.

References

[1] K. Li and N. Fu, "Observation on the effect of shoulder pain caused by volleyball training injury based on MRI image scanning," *Scanning*, vol. 2022, Article ID 4368871, 5 pages, 2022.

Hindawi
Scanning
Volume 2022, Article ID 4368871, 5 pages
https://doi.org/10.1155/2022/4368871

Research Article

Observation on the Effect of Shoulder Pain Caused by Volleyball Training Injury Based on MRI Image Scanning

Kesen Li[1] **and Nan Fu**[2]

[1]*Dianchi College of Yunnan University, Yunnan Kunming 650228, China*
[2]*Yunnan Technology and Business University, Yunnan Kunming 650217, China*

Correspondence should be addressed to Nan Fu; 11233302@stu.wxic.edu.cn

Received 13 April 2022; Revised 4 May 2022; Accepted 10 May 2022; Published 23 May 2022

Academic Editor: Danilo Pelusi

In order to observe the effect of MRI image scanning on shoulder pain caused by volleyball training injury, this paper proposes to analyze the value of MR arthrography and conventional MRI image scanning in the diagnosis of shoulder injury. Taking the female volleyball players in a no. 1 middle school for nearly ten years as the research object, the injury investigation and statistics were carried out. The shoulder joint injury was investigated using arthroscopy and no injury was found. All patients underwent MR arthrography and routine MRI image scanning after admission. All patients underwent MR arthrography and routine MRI image scanning after admission. The patient took the flat lying position and put their arms flat on both sides of the body, and the Philips Achieva 3.0T MRI image scanning and Sense Flex M soft coil for MRI image scanning detection were used. The plain scan included oblique sagittal, axial, and oblique coronal proton density weighted image sequences; echo chain ETL = 6, TR/TE 2300/25 ms; and oblique sagittal and oblique coronal SET1W1; TRTE is 400/10 ms. Comparison was made with regard to the sensitivity, specificity, Jordan index, and accuracy of MR arthrography versus conventional MRI imaging in the diagnosis of shoulder injuries. The results were 38 true positives, 19 true negatives, 1 false positive, and 2 false negatives; a normal MRI scan showed 33 true positives, 13 true negatives, 7 false positives, and 7 false negatives. MR arthrography is more accurate than MRI image scanners in the diagnosis of shoulder injuries.

1. Introduction

The shoulder joint is the most active in all the joints of the human body. Due to degenerative changes in different shoulder tissues (ligaments and rotator cuff), or trauma, excessive repeated use, and activities, the patient's shoulder joint will be damaged, and the tissues around the shoulder joint will be damaged [1]. Therefore, it has a serious impact on the normal life and work of patients. If it is not diagnosed and treated in time, it will easily lead to many serious complications [2]. In the clinical diagnosis and treatment plan, there are many examination methods used to determine whether shoulder joint injury occurs. The most commonly used ones are X-ray plain film and computerized tomography (CT). Traditional conservative treatment can avoid the trauma and risk of surgery but may cause serious obstacles to respiratory function and circulatory function. MSCT and MRI examination methods have the advantages of simple operation, convenience, noninvasiveness, and high detection rate. They have been gradually used in clinical diagnosis. Figure 1 shows the composition of the MRI imaging system [3].

2. Literature Review

In response to this research problem, Ba reported a 13-year follow-up experiment in which patients with rotator cuff injury diagnosed by MRI received conservative treatment. The treatment included range of motion training, strength training, and intra-articular steroid injection. In the final follow-up, 88% of patients had no slight pain and 72% of patients had no daily dysfunction [4]. Tang and Pan

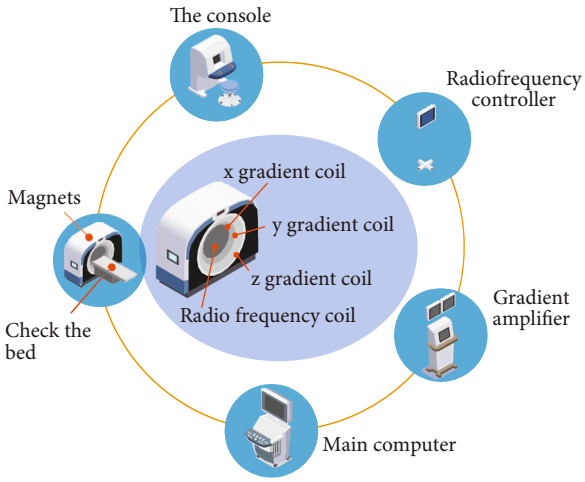

Figure 1: Composition of MRI imaging system.

reported 452 patients with noninvasive rotator cuff injury with an average age of 62 years. They underwent range of motion training and stretching exercises three times a day for 6~12 weeks. In the final follow-up, the patient reported a significant improvement in the outcome score at 6 and 12 weeks, and 75% of nonsurgical patients were effective after 2 years [5]. Hwang and others used ultrasound combined with acupuncture to treat 30 cases of calcified rotator cuff tendinitis. The research results have good clinical efficacy [6]. Chu and others reported the efficacy of acupuncture and moxibustion in the treatment of rotator cuff injury. There is evidence to support the effectiveness and safety of acupuncture and moxibustion in the treatment of chronic musculoskeletal diseases including shoulder pain. However, whether acupuncture and moxibustion are effective and safe for rotator cuff injury is still uncertain. The authors believe that part of the reason is the lack of high-quality basic research and systematic evaluation specifically for rotator cuff injury [7]. Krishnan and Rewale found that the activity was preserved, there was no impact sign, and there was slight ridge. The presence of superior muscle atrophy and supraspinatus tendon connection is an important predictor of the success of nonsurgical treatment. If three of the above four criteria are met, 87% of patients may be successful in conservative treatment [8]. Liu selected 70 patients with moderate irritation rotator cuff injury as the research object, through strict randomized controlled trials and rehabilitation training as the control group [9]. Pasquier and Andersson put forward corresponding prevention suggestions in combination with the causes of sports injury in relevant volleyball training [10]. Yang et al. Discussed the imaging diagnosis of shoulder pain caused by sports injury [11]. Xiong and others observed and analyzed the effect of multislice spiral CT and magnetic resonance imaging (MRI) in the joint diagnosis of shoulder injury [12]. Based on the current research, this paper proposes to analyze the value of MR arthrography and conventional MRI in the diagnosis of shoulder injury. Through the investigation and statistics of the sports injury of female volleyball players in a first middle school, this paper studies the causes and preventive measures of the injury in training and competition in volleyball. The results show that MRI has high soft tissue resolution, can well show the anatomical structure and histopathological changes of the shoulder, and can make multisequence and multidirectional imaging to clearly show the complex anatomical structure of the shoulder joint.

3. Method

3.1. Research Object. The research object is the female volleyball players in a first middle school for nearly ten years.

(1) *Documentation method.* Collect relevant data and literature on volleyball injury through the China Journal Network, China Sports Information Network, reference room, and other channels to provide reference for the conception, design, and research of this paper [13].

(2) *Questionnaire survey method.* An online questionnaire "volleyball injury" questionnaire was distributed to female volleyball players in a no. 1 middle school in recent ten years. 70 questionnaires were distributed and 60 were recovered. The effective rate of the questionnaire was 85%. In this process, the test-retest reliability method of the reliability analysis method is also used to analyze the reliability and sort out the investigated data and materials [14, 15].

(3) *Mathematical statistics.* The questionnaire star is used to summarize and count the results of the questionnaire and analyze and study the statistical data.

3.2. Findings of Investigation

3.2.1. Investigation and Statistics of Damaged Parts. The injured parts of athletes are shown in Table 1. Among the volleyball players investigated, the main injured parts are the ankle, knee, waist, and finger joints, accounting for 60%, 55%, 45%, and 45%, respectively; the shoulder joint accounts for 40% and the foot accounts for 15%. Arms and legs account for 10% and 5%, respectively. It is easy to get injured in the knee and ankle [16].

3.2.2. Investigation and Statistics of Damage Types. The injury types of athletes are shown in Table 2. The results show that the main injury types are joint sprain, accounting for 40%; muscle strain and lumbar muscle strain, each accounting for 20%; abrasion, accounting for 10%; fracture, accounting for 5%; and other types of injuries, accounting for 5%.

3.2.3. Investigation and Statistics of Damage Properties. The statistics of the nature of athletes' injuries are shown in Table 3. The results show that chronic injuries and acute injuries account for 50% of the nature of athletes' injuries.

3.2.4. Investigation and Statistics of Damage Causes. As can be seen from Table 4, carelessness and having no sense of protection; insufficient training level; violating the principle of scientific training; unscientific preparatory activities [17];

Table 1: Statistics of injury parts of volleyball players.

Damage site	Number of injured	Percentage (%)
Ankle joint	36	60
Knee joint	33	55
Waist	27	45
Finger joint	27	45
Shoulder joint	24	40
Foot	9	15
Arm	6	10
Lower leg	3	5

Table 2: Statistics of volleyball injury types of volleyball players.

Damage type	Number of injured (person)	Percentage (%)
Joint sprain	24	40
Muscle strain	12	20
Lumbar muscle degeneration	12	20
Scratch	6	10
Fracture	3	5
Other	3	5

Table 3: Statistics of volleyball injury types of volleyball players.

Damage property	Number of injured (person)	Percentage (%)
Chronic injury	30	50
Acute injury	30	50

neglecting relaxation activities; improper organization and arrangement of competition and training; poor competitive condition, clothing, protective equipment, and field equipment; bad equipment and natural environment; influence of seasonal environment; poor physical quality; insufficient muscle strength; and influence of personal physiological and psychological factors may cause unnecessary sports injury [18].

3.3. Detection Method. All patients underwent MR arthrography and routine MRI after admission. The patient took the flat lying position, put their arms flat on both sides of the body, and used the Philips Achieva 3.0T MRI and Sense Flex M soft coil for MRI detection. The plain scan included oblique sagittal, axial, and oblique coronal proton density weighted image sequences; echo chainETL = 6, TR/TE 2300/25 ms; and oblique sagittal and oblique coronal SET1W1; TRTE is 400/10 ms [19]. 15 ml of 1 : 200 magenweixian solution and 5 ml of 2% lidocaine were extracted, 20 ml of contrast medium was injected into the articular cavity, and then, enhanced scanning was performed after fully moving the shoulder joint, including oblique sagittal position, axial position, and oblique coronal position. Fat suppression SET1WI sequence, TR/TE was 650/10 ms. FOV is 18 cm × 18 cm, and the matrix is 320 × 256. Without knowing the diagnosis results of arthroscopy and the patient's medical history, one sports medicine doctor and one skeletal muscle system imaging doctor were asked to analyze the results of MR arthrography and routine MRI of all patients to evaluate whether there were rotator cuff injury and anterior glenoid lip injury [20].

3.4. Observation Indicators. Taking the arthroscopic results as the gold standard, the sensitivity, specificity, Jordan index, and accuracy of MR arthrography and conventional MRI image scanning in the diagnosis of shoulder injury were compared [21].

3.5. Statistical Methods. The data were analyzed using SPSS 21.0. The counting data were represented by $(x \pm s)$, t-test, n (%), and x^2 test, and $P < 0.05$indicated that the difference was statistically significant [22].

4. Results and Analysis

4.1. Comparison of MR Arthrography and Conventional MRI Diagnostic Results. Among the 60 patients, MR arthrography showed that 38 cases were true positive, 19 cases were true negative, 1 case was false positive, and 2 cases were false negative; conventional MRI diagnosis showed that 33 cases were true positive, 13 cases were true negative, 7 cases were false positive, and 7 cases were false negative, as shown in Figure 2.

4.2. Comparison of Various Indexes of MR Arthrography and Conventional MRI in the Diagnosis of Shoulder Injury. The diagnostic accuracy of MR arthrography in shoulder injury was higher than that of MRI, and the difference was statistically significant ($P < 0.05$) (see Table 5).

As the joint with the maximum range of motion of the human body, the shoulder joint is easy to injure after a wide range of complex movements because the humeral head is large and round, while the scapular pelvis is small and the joint capsule is relatively loose. The injury factors include acute or chronic trauma caused by the impact and friction of the coracoacromial arch by the rotator cuff and the acromial glider capsule and excessive exercise when the patient is doing zenith exercise or abduction exercise; if not diagnosed and treated in time, it will greatly affect the daily work and life of the patient. Therefore, more and more attention is paid to the diagnosis and treatment of shoulder injury. MRI has high soft tissue resolution, can well show the anatomical structure and histopathological changes of the shoulder, can be multisequence and multidirectional imaging, and clearly shows the complex anatomical structure of the shoulder joint [23, 24]. In addition, clinical studies have also found that MRI can provide surgeons with detailed information such as the location of rotator cuff tear, retraction degree of muscle waist junction, and partial or full-thickness rotator cuff tear, while it has relatively low sensitivity in the diagnosis of joint cavity stenosis and chronic injury. As one of the effective means to diagnose shoulder soft tissue injury, MR arthrography mainly injects iodine solution and

Table 4: Statistics of volleyball injury types of volleyball players.

Cause of damage	Number of injured (person)	Percentage (%)
Errors in detail actions	42	70
Unscientific preparation activities	33	55
Seasonal environmental factors	24	40
Site equipment factors	21	35
Excessive exercise load	15	25
Lack of awareness of sports injury protection	12	20
Poor physical fitness	9	15
Lack of muscle strength	9	15
Unscientific recovery after injury	6	10
Poor physical and psychological state	6	10

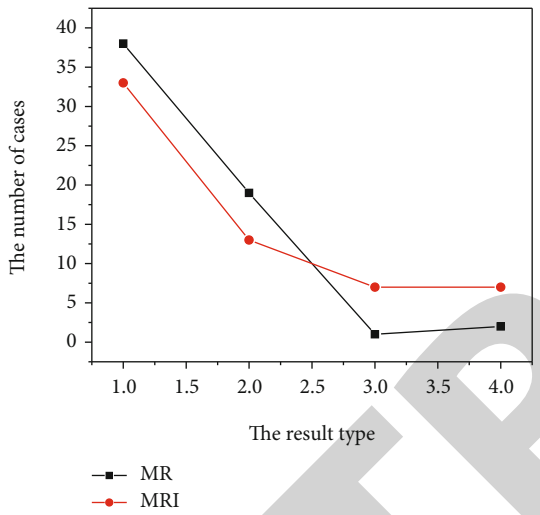

Figure 2: Comparison of MR arthrography and conventional MRI diagnosis results.

Table 5: Comparison of various indexes of MR arthrography and conventional MRI in the diagnosis of shoulder injury.

Diagnosis mode	Sensitivity	Specificity	Accuracy	Jordan index
MRI	85%	80.47%	83.1%	0.6761%
MR arthrography	95%	96.26%	95.48%	0.9348%
X^2 value	1.945	3.489	6.522	/
P value	0.159	0.05	0.022	/

paramagnetic contrast agent into the shoulder joint cavity, so as to fully expand the joint capsule and completely expose the position of shoulder injury. The purpose of diagnosis can be achieved through routine scanning. It is suggested that MR arthrography has a higher application value in the diagnosis of shoulder injury, which can improve the sensitivity and accuracy of diagnosis, minimize the risk of missed diagnosis or misdiagnosis, and carry out corresponding treatment in time in the early stage [25].

5. Conclusion

This paper puts forward the effect observation of shoulder pain caused by volleyball training injury based on MRI imaging. Through the investigation and statistics of the sports injury of a female volleyball player in a first middle school, this paper studies the causes and preventive measures of the injury in volleyball training and competition. Arthroscopic findings were used as the gold standard to compare the sensitivity, specificity, Jordan index, and accuracy of MR arthrography with conventional MRI in diagnosing shoulder injuries. The results show that MRI has high soft tissue resolution, can well show the anatomical structure and histopathological changes of the shoulder, and can make multisequence and multidirectional imaging to clearly show the complex anatomical structure of the shoulder joint. Although MRI is very sensitive for the diagnosis of acute shoulder injuries, it is relatively insensitive for joint stenosis and chronic injuries. In the future, multi-incision spiral CT and magnetic resonance imaging (MRI) could be used to study its role in the diagnosis of patients with shoulder injuries.

Data Availability

The data used to support the findings of this study are available from the corresponding author upon request.

Conflicts of Interest

The authors declare that they have no conflicts of interest.

References

[1] C. Tsarbou, N. I. Liveris, P. D. Tsimeas, G. Papageorgiou, and A. Tsiokanos, "The effect of fatigue on jump height and the risk of knee injury after a volleyball training game: a pilot study," *Biomedical Human Kinetics*, vol. 13, no. 1, pp. 197–204, 2021.

[2] R. L. Touche, A. Herranz-Gómez, F. Cuenca-Martínez, A. París-Alemany, and L. Suso-Martí, "Effect of brain training through visual mirror feedback, action observation and motor imagery on orofacial sensorimotor variables: a single-blind

Hindawi
Scanning
Volume 2023, Article ID 9809430, 1 page
https://doi.org/10.1155/2023/9809430

Retraction

Retracted: Diagnostic Value of Magnetic Resonance Susceptibility-Weighted Imaging Scanning in Different Types of Early Prostate Cancer

Scanning

Received 20 June 2023; Accepted 20 June 2023; Published 21 June 2023

This article has been retracted by Hindawi following an investigation undertaken by the publisher [1]. This investigation has uncovered evidence of one or more of the following indicators of systematic manipulation of the publication process:

(1) Discrepancies in scope

(2) Discrepancies in the description of the research reported

(3) Discrepancies between the availability of data and the research described

(4) Inappropriate citations

(5) Incoherent, meaningless and/or irrelevant content included in the article

(6) Peer-review manipulation

The presence of these indicators undermines our confidence in the integrity of the article's content and we cannot, therefore, vouch for its reliability. Please note that this notice is intended solely to alert readers that the content of this article is unreliable. We have not investigated whether authors were aware of or involved in the systematic manipulation of the publication process.

In addition, our investigation has also shown that one or more of the following human-subject reporting requirements has not been met in this article: ethical approval by an Institutional Review Board (IRB) committee or equivalent, patient/participant consent to participate, and/or agreement to publish patient/participant details (where relevant).

Wiley and Hindawi regrets that the usual quality checks did not identify these issues before publication and have since put additional measures in place to safeguard research integrity.

We wish to credit our own Research Integrity and Research Publishing teams and anonymous and named external researchers and research integrity experts for contributing to this investigation.

The corresponding author, as the representative of all authors, has been given the opportunity to register their agreement or disagreement to this retraction. We have kept a record of any response received.

References

[1] R. Gao, J. Liu, and H. Zhu, "Diagnostic Value of Magnetic Resonance Susceptibility-Weighted Imaging Scanning in Different Types of Early Prostate Cancer," *Scanning*, vol. 2022, Article ID 4884646, 6 pages, 2022.

Hindawi
Scanning
Volume 2022, Article ID 4884646, 6 pages
https://doi.org/10.1155/2022/4884646

Research Article

Diagnostic Value of Magnetic Resonance Susceptibility-Weighted Imaging Scanning in Different Types of Early Prostate Cancer

Ruihui Gao,[1] **Jiayuan Liu**,[1] **and Hengcheng Zhu**[2]

[1]*Department of Urology, People's Hospital, Dongxihu District, Wuhan, Hubei 430040, China*
[2]*Department of Urology, Wuhan University People's Hospital, Wuhan, Hubei 430060, China*

Correspondence should be addressed to Jiayuan Liu; 15071010110004@hainanu.edu.cn

Received 13 April 2022; Revised 4 May 2022; Accepted 10 May 2022; Published 23 May 2022

Academic Editor: Danilo Pelusi

To investigate the cost of MRI-sensitive imaging (SWI) for early-stage prostate cancer. In 2019, the research group included a total of 60 leukemia patients, all of whom were diagnosed with prostate-specific antigen (PSA). According to the range of PSA values, they were group A (18 cases), group A 0-44 mg/ml (18 cases), and group B 4-1010 mg/ml (26 cases). 10 mg/ml was divided into C group (16 cases). Another 60 patients with benign prostatic hyperplasia treated at the same time served as a control group. All patients underwent sensitive MRI scanning, followed by diagnostic and clinical evaluation of weighted MRI scanning to diagnose various types of prostate cancer. The results showed that there was no difference in Ve levels among the three groups ($P > 0.05$); the SUSE score and Ktrans and Kep levels of the patients in group C were higher in groups B, A, and A ($P < 0.05$). In patients with early leukemia, SUSE score was significantly correlated with Ktrans and Kep levels ($P < 0.05$), but not with Ve and $P > 0.05$ levels. Magnetic resonance imaging can be used to diagnose prostate cancer. It can differentiate and diagnose different types of prostate cancer early. This is important for evaluating the benefits of prostate cancer screening and treatment.

1. Introduction

Prostate cancer is a very common cancer in the male. It is mainly caused by the elderly and is a highly malignant reproductive system. The incidence rate of this disease is very high, which is next only to gastric cancer. With the development of aging society in recent years, the incidence rate and mortality of prostate cancer are increasing year by year [1]. Therefore, it is the key factor to ensure the rehabilitation of patients and guide various treatment plans by using appropriate regimen to diagnose patients. Magnetic resonance diffusion-weighted imaging is a very common clinical diagnostic scheme (see Figure 1); it mainly uses an image comparison formed by the difference of internal or local magnetic sensitivity in the magnetic field as the diagnostic scheme. The imaging basis of this diagnostic scheme is mainly high-resolution and three-dimensional complete flow compensated gradient echo sequence, which can clearly show the patient's intracranial lesions [2].

Prostate cancer mostly occurs in elderly men over the age of 60, and the periphery of the prostate is a frequent area of the disease. This disease will have a great impact on the normal life of elderly men, and most elderly patients will have a more serious psychological adverse state after the onset, which will have a great adverse impact on the normal life of elderly patients. In the traditional diagnostic scheme, patients are usually diagnosed by ultrasound or CT, but the diagnostic accuracy is often low. Puncture biopsy is an open diagnostic scheme, which has a certain adverse impact on patients. At the same time, elderly patients are often combined with patients with other systemic and organic diseases, which is not only painful but also prone to transfer and implant with the puncture needle path [3]. Dynamic enhanced scanning can clarify the cancerous tissue and microvessel status of patients to a certain extent. Because the vascular density in cancerous tissue is higher than that in normal tissue and is evenly distributed, the application of enhanced scanning can clarify the changes of cancerous tissue by observing vascular proliferation. Diffusion-weighted MRI has a good clinical diagnostic effect. This diagnostic scheme can diagnose the diffusion movement of water molecules in tissues. It is also the only diagnostic scheme that can play this effect in

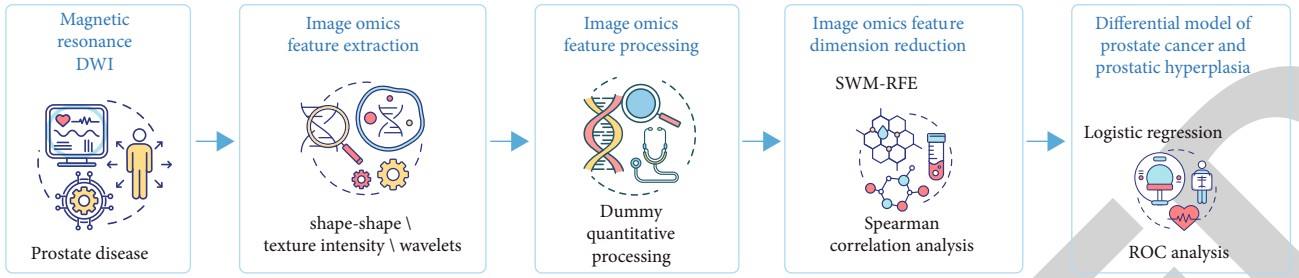

Figure 1: MRI susceptibility-weighted imaging scanning diagnosis.

clinic. Generally speaking, water molecules often have high degrees of freedom when diffusing in the human body, which belongs to diffusion type movement, and will be limited when the surrounding tissues change, which is called diffusion limitation. Diffusion-weighted MRI can effectively diagnose the diffusion degree and direction of water molecules and further reflect the microstructure of the tissue. When the patient's tissue is cancerous, the patient's normal tissue will be excluded and banned by cancerous tissue, and the water molecular weight contained in it will be reduced. Therefore, in this case, the content of water molecules in cancerous tissues will decrease, and cancerous tissues tend to be distorted and narrow in the process of proliferation. Therefore, diffusion-weighted can effectively clarify the cancer status and prostate tissue changes of patients in this situation, and this scheme belongs to noninvasive diagnosis scheme, which will not cause additional adverse effects on patients and has high diagnostic significance. According to the clinical stage obtained by MRI and the GS score obtained by the pathological results of biopsy tissue, the condition of patients with PCA can be evaluated comprehensively and accurately [4]. Some studies have shown that the preoperative pathological grading of prostate cancer plays a very important guiding role in clinical diagnosis and treatment, such as the low-risk cancer in the low-risk group with GS score ≤ 6. Clinically, local treatment and dynamic observation can often be adopted, and some inert cancer foci may be carried for life without any progress. Those with Gleason score > 6 are medium- and high-risk cancers, which need scientific and correct intervention and treatment. Therefore, blind treatment or overtreatment of some patients in clinic cannot achieve the expected effect and even cause serious adverse effects. It can be seen that early accurate diagnosis of PCA patients and accurate risk classification have important guiding significance for the treatment and prognosis of patients [5].

2. Literature Review

Seo et al. believe that magnetic resonance imaging (MRI) can provide important evidence for the clinical diagnosis, staging, and treatment of prostate cancer because of its high resolution of soft tissue and the advantages of multiparameter, multisequence, and multidirectional imaging. At present, it is considered to be one of the most ideal examination methods in the examination of prostate diseases. With the upgrading of magnetic resonance imaging equipment, the improvement of technology, and the enrichment of functional imaging methods, magnetic resonance imaging can provide more basis for the diagnosis and classification of prostate cancer and provide important evidence for the selection of clinical diagnosis and treatment of prostate cancer [6]. The proposal of pi-rads V2 in Trufanov et al. is mainly to diagnose prostate cancer according to the advantages of different sequences on different anatomical sites and tissue structures. High-resolution T2WI was the main diagnosis of cancer lesions in the central gland area; DWI sequence and ADC image are the main reference for the diagnosis of peripheral diseases; DCE sequence was used when the benign and malignant lesions could not be determined (the score was 3 points). In the junction area between the central area and the peripheral zone, T2WI is mainly used. When the benign and malignant cannot be determined, DWI sequence is supplemented [7]. Peeters et al. believe that according to the clinical stage obtained by MRI and the GS score obtained by the pathological results of biopsy tissue, the condition of patients with PCA can be evaluated comprehensively and accurately [8]. Conte et al. proposed that the preoperative pathological grading of prostate cancer plays a very important guiding role in clinical diagnosis and treatment. For example, for low-risk cancer in low-risk group with GS score ≤ 6, local treatment and dynamic observation can often be adopted clinically, and some inert cancer foci may be carried for life without any progress. Those with Gleason score > 6 are medium- and high-risk cancers, which need scientific and correct intervention and treatment [9]. The research of Antunes et al. shows that multiparameter magnetic resonance imaging (MP MRI) can provide more accurate and rich diagnostic information that is helpful to clinic. Other studies have shown that T2WI combined with magnetic resonance functional imaging sequences greater than or equal to two can significantly improve the sensitivity and specificity of image examination for PCA diagnosis and then improve the diagnostic efficiency [10]. Yildirim first used apt imaging technology to detect free proteins and amino acids in vivo in 2003. Under the principle of proton saturation and proton free exchange with water, the proton can be detected indirectly under the principle of proton saturation and proton free exchange with water [11]. Pinto et al. proposed that all prostate cancers $(CHO + CRE)/CIT \geq 0.86$. In the peripheral zone of prostate, when its value ≥ 0.75, it may be cancer [12]. Pecherkin et al. proposed that the diagnostic standard of prostate cancer in Chinese is >0.99 [13]. Eichhoff et al.

proposed that the diagnostic standard of prostate cancer in Chinese is >1.09/0.94 (before all/D stage), but when the cancer focus is small and limited, taking 0.94 as the standard has greater diagnostic significance. However, MRS is easily affected by the internal environment, and its parameters are prone to deviation. In the presence of inflammation, hyperplasia, and partial volume effect, its specificity and sensitivity are reduced. In matrix based gland hyperplasia, its metabolic characteristics are similar to those of prostate cancer, and its value overlaps to a certain extent, so it cannot be well identified [14].

Based on the current research, prostate cancer (PCA) is one of the common malignant tumors in elderly men. With the aggravation of China's aging population and the continuous improvement of examination technology, the detection rate of prostate cancer has a significant upward trend. Magnetic resonance imaging technology is an imaging examination method that has emerged in recent years. It occupies an important position in clinical examination with the advantages of high-resolution, multiplanar parameter imaging, and no radiation. At present, it has become the first choice for noninvasive diagnosis of prostate cancer. With the progress of imaging, the emergence of magnetic sensitivity-weighted imaging (SWI) further provides a reliable way for clinical diagnosis of diseases. It uses different magnetic sensitivities between different tissues to detect the distribution of blood vessels and mineral deposits in the lesions. This study examined SWI in patients with different types of early prostate cancer and benign prostatic hyperplasia in our hospital to explore the clinical diagnostic value of SWI in different types of early prostate cancer. The report is as follows.

3. Data and Methods

3.1. General Information. 60 patients with prostate cancer treated in 2019 were selected as the study group. All patients were tested for prostate-specific antigen (PSA). They were divided into different groups according to the range of PSA value, of which 0-4 mg/ml was group A ($n = 18$), 5-10 mg/ml was group B ($n = 26$), and > 10 mg/ml was divided into group C ($n = 16$). Procedures include (1) division and focal hypotension around the prostate; (2) MRI routine (T1WI, T2WI, DCE, and SWI); (3) patients have been diagnosed with prostate cancer through surgery, infection, or a blood test; (4) no relationship between diagnosis and treatment before MRI. Procedures: prost prostate cancer; and (5) before prostatectomy, the prostate needs to be biopsied. At this time, more than 60 patients with prostate hyperplasia who were admitted to our hospital were selected for the panel. The mean age of the patients in this study was 34-65 years, on average (49.6 ± 5.2). Patients on the control group were 60-66 years of age and of median age (50.2 ± 5.4). There were no significant differences between the two groups ($P > 0.05$) in the above data (sex and age).

3.2. Method

(1) SWI examination methods: the patients were examined by magnetic resonance sensitivity-weighted imaging with Siemens1.5TSkyra magnetic resonance scanner. The patient took the supine position and took the 2.0 cm above the pubic symphysis as the scanning center for the axial, sagittal, and coronal TSET2WI sequence scanning of the prostate [15]: TR 6500 ms, TE 104 ms, layer spacing 0 mm, layer thickness 3 mm, matrix384 × 607, average 2, and FOV180mm × 180 mm. SWI scanning parameters are as follows: TR 28 ms, TE 20 ms, turning angle 150, FOV 180 mm × 180 mm, layer thickness 3 mm, matrix 384 × 365, automatic generation of amplitude image, phase image, SWI image, and minimum density projection (MIP) image. After the second dynamic phase of dynamic contrast-enhanced scanning, the contrast agent GD DTPA was injected through elbow vein with high-pressure syringe at the injection rate of 2 ml/s and the dose of 0.2 mmol/kg, and then, 20 ml normal saline was injected intravenously at the same rate [16]

(2) Image analysis method SWI image processing and analysis: two senior doctors in the imaging department of our hospital jointly evaluate the film. Their opinions are not unified at one time, and a unified opinion is reached through negotiation [17]. According to the SWI image obtained by the patient, the internal bleeding focus of the focus was evaluated by SUSE score. SUSE scoring standard is as follows: 0: no bleeding; 1 point: there are 1-5 points and linear bleeding foci; 2 points: there are 6~10 points and thread mounted bleeding foci; and 3 points: more than 10 point and linear bleeding foci [18].

3.3. Observation Indicators. The levels of SUSE score, transport constant (Ktrans), extracellular space volume percentage (Kep), and rate constant (Ve) were observed, and the relationship between SUSE and the levels of Ktrans, Kep, and Ve in patients with prostate cancer was analyzed [19].

3.4. Statistical Treatment. SPSS18.0 statistical software was used. The counting data was expressed in percentage, x^2 test was used, and the measurement data was expressed in $\bar{x} \pm s$, and t test was used. The comparison between multiple groups was analyzed by analysis of variance, F-value test, and Spearman's analysis. $P < 0.05$ was the difference with statistical significance [20].

4. Experimental Results and Analysis

4.1. Comparison of SUSE Score and Ktrans, Kep, and Ve Levels in Each Group. There was no Ve phase difference between the four groups ($P > 0.05$); SUSE scores, Ktrans, and Kep were higher than group B, group B was higher than group A, and group A was higher (see Figure 2). The difference was significant ($P < 0.05$) (see Figures 3–6) [21].

4.2. Relationship between SUSE Score and Ktrans, Kep, and VE Levels in Patients with Early Prostate Cancer. SUSE score was positively correlated with the levels of Ktrans and Kep in

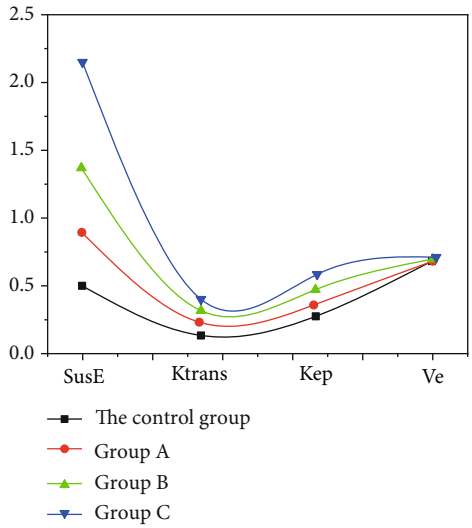

Figure 2: Comparison of SUSE scores and Ktrans, Kep, and Ve levels in each group of patients.

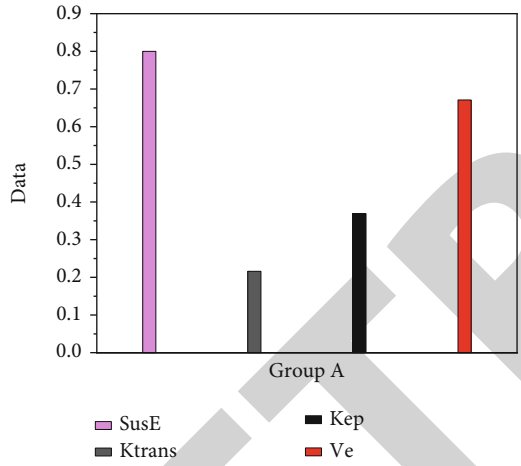

Figure 3: Comparison of SUSE score and Ktrans, Kep, and Ve levels of patients in group A.

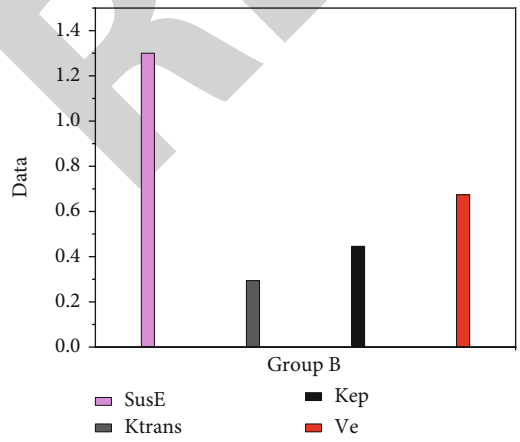

Figure 4: Comparison of SUSE score and Ktrans, Kep, and Ve levels in group B patients.

patients with early prostate cancer ($P < 0.05$). There was no correlation with Ve level, $P > 0.05$ (see Figure 7) [22].

4.3. Discussion. Prostate cancer is one of the common malignant tumors in men. With the aging of China's population, the detection rate of prostate cancer is higher and higher, with an obvious upward trend. Magnetic sensitivity-weighted imaging (SWI) is a technique in magnetic resonance imaging [23]. At present, it is used in the examination of various malignant tumors and is widely used in clinic. SWI mainly quantifies the difference through the difference of magnetic sensitivity between different tissues and reflects the variables of tissue characteristics. It is examined by high-resolution, three-dimensional complete flow compensated gradient echo sequence. In recent years, it has been found in the study of prostate cancer that the microvessel density and vascular growth factor level of prostate cancer tissue are significantly higher than those of benign prostate tumors, neovascularization is more prone to bleeding, and a large amount of deoxyhemoglobin can increase magnetic sensitivity [24]. Benign tumors are inflammatory reactions, which only cause accelerated blood flow, relatively complete blood vessel wall, and low magnetic sensitivity. Therefore, some scholars believe that SWI scanning plays an important role in differentiating prostate cancer and benign prostate tumor. SWI examination of patients with prostate cancer and benign prostatic hyperplasia in our hospital showed that SUSE score and Ktrans and Kep levels were different in patients with different types of prostate cancer. SUSE score and Ktrans and Kep levels in group C were higher than those in group B, group B was higher than that in group A, and group A was higher than that in the control group. Ktrans can reflect the important index of the diffusion rate of contrast agent from intravascular to extraluminal. Kep is an index reflecting the rate of contrast medium flowing back from the extracellular space to the lumen. In the results of this study, the levels of Ktrans and Kep in group C were the highest. Studies have shown that due to the relatively large number of neovascularization and incomplete vascular endothelial cells in malignant tumors, the contrast medium exudes faster during contrast examination. The results suggest that malignant tumor cells grow vigorously and have more neovascularization, and the vascular basement membrane is incomplete. Therefore, the contrast agent is easy to penetrate outside the blood vessel, and the penetration speed is faster. Similarly, the reflux speed of contrast agent from the extravascular space to the blood vessel is also significantly faster. Therefore, the levels of Ktrans and Kep in group C are higher. Benign tumor tissue has less neovascularization, relatively complete vascular endothelium, and relatively slow penetration and reflux of contrast medium. The degree of malignant transformation in group A and group B was lower than that in group C, so the levels of Ktrans and Kep were lower than those in group C. Ve is the volume ratio of extravascular cell space to the whole voxel, which mainly reflects the percentage of contrast agent staying in extravascular cell space. The results showed that there was no difference in VE Levels among the four groups, which may be due to the simultaneous increase of Ktrans and

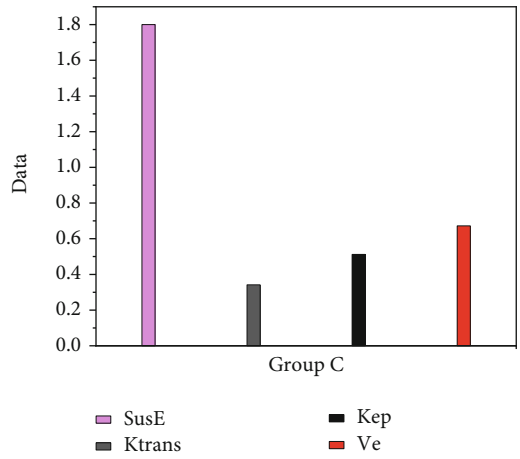

Figure 5: Comparison of SUSE score and Ktrans, Kep, and Ve levels of patients in group C.

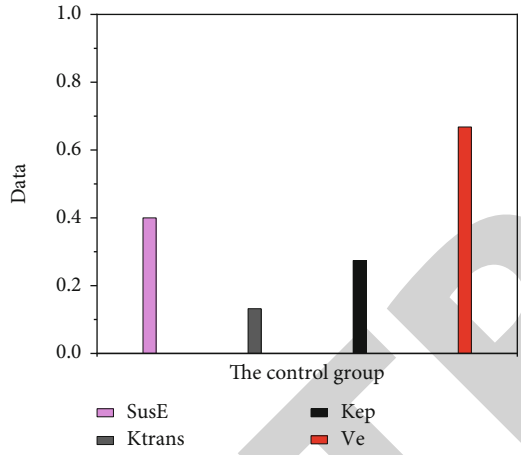

Figure 6: Comparison of SUSE score and Ktrans, Kep, and Ve levels in the control group.

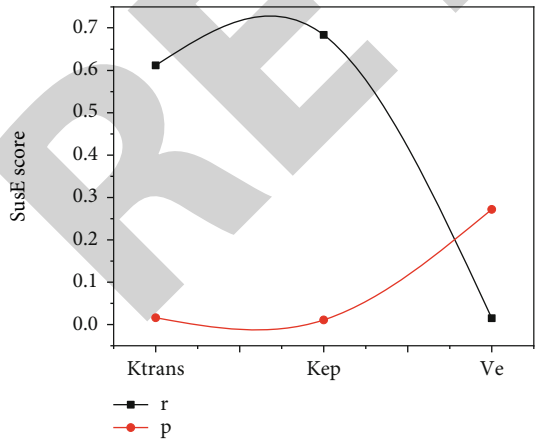

Figure 7: Comparison of SUSE scores and Ktrans, Kep, and Ve in each group of patients.

Kep levels in groups A, B, and C, Ve = Ktrans/Kep, so the Ve value was relatively stable. SUSE score is an index reflecting the bleeding focus of prostate diseases. The higher the malignant degree of malignant tumor cells, the more prone to bleeding. Therefore, SUSE score in group C is significantly higher than that in other groups and the lowest in the control group. When observing the relationship between SUSE score and Ktrans and Kep levels, it was found that SUSE score was significantly positively correlated with Ktrans and Kep levels. Therefore, the higher the SUSE score, the higher the Ktrans and Kep levels, and the higher the malignancy of prostate cancer [25, 26].

5. Conclusion

In conclusion, when diagnosing prostate cancer patients, the application of magnetic sensitive diffusion-weighted imaging can effectively identify the specific symptoms of patients. However, the type of diagnosis needs to be selected according to the specific disease of the patient. If necessary, it also needs to select a variety of diagnosis schemes or carry out diagnosis for many times in combination with the specific clinical symptoms of the patient. This is of positive significance for the rehabilitation of patients and is worthy of popularization and use.

Data Availability

The data used to support the findings of this study are available from the corresponding author upon request.

Conflicts of Interest

The authors declare that they have no conflicts of interest.

References

[1] S. J. Lim, C. H. Suh, W. H. Shim, and S. J. Kim, "Diagnostic performance of t2∗ gradient echo, susceptibility-weighted imaging, and quantitative susceptibility mapping for patients with multiple system atrophy–parkinsonian type: a systematic review and meta-analysis," *European Radiology*, vol. 32, no. 1, pp. 308–318, 2022.

[2] S. C. Mi, E. J. Lee, S. Kim, S. O. Kim, and J. S. Byun, "Wave-CAIPI susceptibility-weighted imaging achieves diagnostic performance comparable to conventional susceptibility-weighted imaging in half the scan time," *European Radiology*, vol. 30, no. 4, pp. 2182–2190, 2020.

[3] E. U. Pérez, E. S. Armentia, N. S. Priegue, A. V. Campos, and C. J. Basildo, "Should susceptibility-weighted imaging be included in the basic protocol for magnetic resonance imaging of the brain?," *Radiología (English Edition)*, vol. 62, no. 4, pp. 320–326, 2020.

[4] A. Kasenene, A. Baidya, S. Shams, and H. B. Xu, "Evaluation of tumor response to antiangiogenic therapy in patients with recurrent gliomas using contrast-enhanced perfusion-weighted magnetic resonance imaging techniques: a meta-analysis," *World Journal of Meta-Analysis*, vol. 7, no. 2, pp. 51–65, 2019.

[5] A. F. Delgado, D. Van Westen, M. Nilsson et al., "Diagnostic value ofalternative techniques to gadolinium-based contrast agents in mr neuroimaging—a comprehensive overview," *Insights Into Imaging*, vol. 10, no. 1, p. 84, 2019.

Hindawi
Scanning
Volume 2023, Article ID 9859742, 1 page
https://doi.org/10.1155/2023/9859742

Retraction

Retracted: The Diagnostic Value of Scanning in the Injury of Triceps Crus of Volleyball Players

Scanning

Received 3 October 2023; Accepted 3 October 2023; Published 4 October 2023

This article has been retracted by Hindawi following an investigation undertaken by the publisher [1]. This investigation has uncovered evidence of one or more of the following indicators of systematic manipulation of the publication process:

(1) Discrepancies in scope

(2) Discrepancies in the description of the research reported

(3) Discrepancies between the availability of data and the research described

(4) Inappropriate citations

(5) Incoherent, meaningless and/or irrelevant content included in the article

(6) Peer-review manipulation

The presence of these indicators undermines our confidence in the integrity of the article's content and we cannot, therefore, vouch for its reliability. Please note that this notice is intended solely to alert readers that the content of this article is unreliable. We have not investigated whether authors were aware of or involved in the systematic manipulation of the publication process.

In addition, our investigation has also shown that one or more of the following human-subject reporting requirements has not been met in this article: ethical approval by an Institutional Review Board (IRB) committee or equivalent, patient/participant consent to participate, and/or agreement to publish patient/participant details (where relevant).

Wiley and Hindawi regrets that the usual quality checks did not identify these issues before publication and have since put additional measures in place to safeguard research integrity.

We wish to credit our own Research Integrity and Research Publishing teams and anonymous and named external researchers and research integrity experts for contributing to this investigation.

The corresponding author, as the representative of all authors, has been given the opportunity to register their agreement or disagreement to this retraction. We have kept a record of any response received.

References

[1] J. Zhao and J. Liu, "The Diagnostic Value of Scanning in the Injury of Triceps Crus of Volleyball Players," *Scanning*, vol. 2022, Article ID 2203065, 7 pages, 2022.

Hindawi
Scanning
Volume 2022, Article ID 2203065, 7 pages
https://doi.org/10.1155/2022/2203065

Research Article

The Diagnostic Value of Scanning in the Injury of Triceps Crus of Volleyball Players

Jinfeng Zhao and Jianxin Liu

Pingdingshan University, Henan, Pingdingshan 467000, China

Correspondence should be addressed to Jianxin Liu; 20162103812@mails.imnu.edu.cn

Received 13 April 2022; Revised 8 May 2022; Accepted 12 May 2022; Published 23 May 2022

Academic Editor: Danilo Pelusi

The study goal is to solve the problem of the diagnosis of triceps crus injury of volleyball players, meet the needs of volleyball players and team doctors for the correct diagnosis of triceps crus injury scanning, make up for the deficiency that triceps crus injury scanning diagnosis is easy to make mistakes, and improve the efficiency and ability of triceps crus injury diagnosis scanning. Because the experiment involves the technical action of volleyball jump serve, DELSYSR Trignomobile wireless portable surface electromyography tester (16 leads) made in the United States is selected to test the surface electromyography of the main muscle groups of college male volleyball players in the process of jump serve. The German made simi-3D motion image system is used to conduct three-dimensional synchronous test of athletes' jump serve action. The data analysis software adopts EMG work analysis, EMG analysis software, and simi-3D motion image analysis system for postprocessing data. The original signal is filtered (400 Hz for low pass and 20 Hz for high pass) and rectified. Finally, IEMG, EMG contribution rate, and RMS were calculated. This ensures the accuracy of the experiment.

1. Introduction

In recent years, with the development of sports technology and the continuous improvement of training level, volleyball has gradually developed rapidly in the form of height, speed, strength, technology, and team cooperation and the competition among sports teams is becoming more and more fierce. "Every ball must be fought" has become an important goal for the team to carry out tactics and technology. All volleyball powers in the world have made deliberate research on how to improve the attack of their own team and strengthen the defense ability of the other team [1]. Serving skill is one of the basic skills of volleyball. It is the beginning of volleyball match and the beginning of attack of sports team. As an important offensive way in volleyball competition, serving can effectively destroy the stability of the opponent's first pass, interfere with the opponent's offensive ability, reduce the pressure of blocking or defense, and create favorable conditions for the team's attack. Therefore, with the increasingly fierce and competitive volleyball competition, volleyball service technology has gradually evolved to be more and more aggressive [2].

Although the jump serve has the characteristics of fast ball speed, strong attack interferes with the opponent's rhythm and causes the opponent to receive the ball with a high error rate. However, the jumping service technology has very high requirements for athletes' sports technical level, psychological stability, and physical quality. Relevant research shows that when jumping serve, athletes need to have higher take-off height, higher hitting point, and larger horizontal displacement to ensure greater ball speed. Therefore, the action technical structure of jumping serve is more complex and more difficult than that of in situ serve. This requires athletes to have good explosive power, bouncing power, coordination, and ball control ability. It means that athletes are more likely to be injured. Therefore, the experimental analysis of athletes' triceps injury is carried out. We prepare the experimental equipment, complete the site layout and instrument erection, and set up and calibrate the instrument at the same time [3]. The experimental site is shown in Figure 1.

We conduct a preliminary experiment, inform the selected athletes of the experimental purpose, task, and

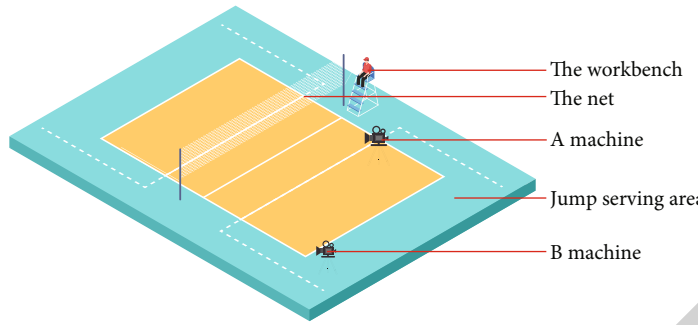

Figure 1: Experimental site.

Table 1: Basic information of preliminary research objects.

Gender	Quantity	Age (years)	Height (cm)	Weight (kg)	Training years
Experience group	10	21.6 ± 2.2	187.7 ± 4.5	78.5 ± 4.6	8.4 ± 3.1

experimental process, as well as the main precautions in the experimental process, and provide basic information such as athletes' height, weight, age, and position on the field. The basic information of the preliminary research object is shown in Table 1.

The preliminary study is for reference only.

2. Literature Review

Zhao et al. said that the core is a whole composed of waist, pelvis, and hip joint, which is the middle link of the human body [4], specifically, from the area below the shoulder joint to the area above the hip joint, including the pelvis, and the muscle groups covered include the back, abdomen, and all the muscle groups constituting the pelvis, with a total of 29. In 1996, Qu et al. first put forward the theory of trunk support force, which may be the earliest statement about core force [5]. In 2005, Sun et al. called the power to improve physical stability core power [6]. Since the 1990s, core strength training has been gradually applied to the field of competitive sports training in the United States. Sun et al. classified the muscles on the chest, back, abdomen, lumbosacral, and hip as core muscles [7]. They believe that the core muscle group not only includes rectus abdominis, transverse abdominal muscle, oblique abdominal muscle, back muscle, lower back muscle, and vertical muscle but also the muscles around the hip joint, and gluteus, hip rotator, and posterior femoral muscle group also belongs to the core muscle group of the human body. Zhu et al. put forward the core strength training method of raising and squatting [8] and analyzed the action essentials and precautions of this training method. It is considered that this training method can promote the coordinated strength of athletes' upper and lower limbs, stimulate the continuous contraction of deep muscles, and recruit more deep small muscles to participate in sports, which plays an important role in improving the balance and stability of the body. Xu et al. established the core strength training method based on the core training theory [9]. The scheme is mainly implemented and completed through four stages. The first stage allows athletes to master the methods of core strength training. The second stage allows athletes to practice slowly in a steady state. The third stage allows athletes to carry out static training in an unstable state. The fourth stage allows athletes to continue dynamic practice in an unstable state and let athletes slowly adapt to and master core strength training in a gradual process and feel the fitness value of core strength training. Yu et al. believe that core strength training can improve the transmission efficiency of strength between athletes' upper and lower limbs [10]. Facco et al. believe that the energy consumption of the upper and lower limbs is reduced during exercise, so as to improve the stability of the trunk [11].

With the increasing intensity of volleyball competition, the requirements of athletes' skills and tactics and various abilities related to competitive level are also increasing. At the same time, physical fitness is a prerequisite for all volleyball skills and has attracted more and more attention from researchers and coaches. An excellent volleyball team must keep coordination and progress in intelligence, psychological quality, volleyball field skills, and basic physical fitness [12]. Among the above five components of competitive ability, physical fitness is the basis and prerequisite for all skill performance. Exquisite technology and tactics can play a full role only with the support of good physical fitness. Without the advantage of physical level, there will be no chance to obtain more advanced competitive skills and field tactics. Therefore, physical factor is very important. It is the prerequisite for the formation of volleyball players' technology and the basis for mastering tactics and playing in the field. The ability of jumping and lower limb movement speed is also highly required in volleyball. At the same time, the arm swing action is required to be fast and powerful, which makes the special physical fitness training of volleyball becomes a hot issue that coaches and researchers have always paid attention to. In volleyball, training or competition on the field, athletes often use movements such as left and right forward and backward movement, bouncing, and arm swing. The mode composed of these three has become

the main sports mode of volleyball competition. For volleyball players, the special physical fitness of this sport is the ability to realize the above mode. Specific to the competition process, the special physical fitness is manifested in the movement, bouncing, smashing, blocking, and arm swing of athletes. Therefore, in order to improve the special physical fitness level of volleyball players, the core strategy should be to promote the ability of athletes in the three main movements and improve the strength, explosive level, action quality, action speed, and response sensitivity in the core area [13].

In recent years, the concept and training of core strength have been introduced into various sports. The effect of targeted training is very remarkable and has been popularized and applied in the field of sports training. Core strength first appeared in the field of sports rehabilitation, which is used to maintain the stability of the waist, pelvis, and hip. Each sport has its own core strength. Because in all sports, the coordination between muscle and bone is involved, and a specific central muscle group is connected to form a complete sports chain. In the process of sports, the human body needs to change or maintain a specific posture and transfer limb strength, and the core strength plays a key role in this process. In addition, athletes' learning of technical movements also depends on the core strength to a large extent. The lack of core strength will limit the play of tactics and skills in the field and become the bottleneck of athletes' professional level. The long-term practice in sports training has proved that only when the muscle strength reaches a certain threshold, athletes can realize the skilled operations such as flexibility, sensitivity, endurance, and explosive speed. In order to improve their sports skills and break through the bottleneck of comprehensive level, they need to forge enough muscle strength first. A good foundation of core strength can reduce the probability of sports injury, whether the core strength is sufficient and related to the realization and improvement of special skills and the basic protection of athletes [14].

Although there are still great disputes about the specific positioning of the "core," most experts and scholars define the position of the "core" around the lumbar spine, pelvis, and hip joint. On the basis of summarizing previous studies, this paper believes that the core is the center of the human body, which refers to the area below the shoulder joint and above the hip joint. It includes all the muscles of the back and abdomen, the deep muscles attached to the spine and around the hip joint, and all the muscle groups constituting the pelvis.

3. Method

3.1. Sports Injury. There is no unified standard for the definition of the concept of "sports injury." Scholars believe that the definition of injury depends on the time for athletes to receive sports guidance or rehabilitation, while some scholars believe that there are only two views on the effect of sports training on injury [15]. Gait is the behavior characteristic of human walking, which is affected by many factors. The control of walking is very complex, involving the coordinated movement of all joints and muscles of the whole body. The imbalance of any link may affect walking and gait, and the abnormality may also be compensated or covered up. After sports injury, the most obvious symptom is pain, which has a significant impact on gait. Pain is easy to lead to the shortening of gait support phase time and the prolongation of swing phase on the injured side. Hahn et al. concluded that the support phase time of patients with unilateral knee injury is shorter than that of patients without injury, so as to reduce the load of knee joint on the injured side, while the support phase time of patients with bilateral knee injury is prolonged, so as to increase the time of double support phase and reduce the load on one side of knee joint alone. Studies of patients with increased proprioceptive pain of the knee joint (and of patients with increased proprioceptive pain of the knee joint) seem to point out that the purpose of the study is to reduce the abnormal gait [16]. Many people have studied the time distribution of plantar pressure and ground vertical reaction force in patients with knee osteoarthritis (KOA). It is pointed out that due to pain, the time of single foot bearing period on the injured side of KOA patients is shortened, so as to reduce the time for the injured side to support weight alone. In addition, the pain will also make the heel dare not touch the ground, and the leg is weak when the foot is off the ground. Some studies have pointed out that the foot pressure center of gravity of athletes with repeated foot and ankle injury tends to shift to the front area of the foot, the time of front foot support is prolonged, and the time of rear foot support is reduced, which may be the protective mechanism adopted to reduce the load of foot and ankle joint on the injured side [17, 18].

Time domain characteristics regard muscle tone signal as a function of time, which can reflect the statistical characteristics of muscle tone signal in time domain. And because the calculation of time-domain characteristics does not need any conversion, it can be calculated directly from the original muscle tone signal sequence. Therefore, the calculation method is simple and the calculation speed is fast, which has been widely used in the field of signal analysis.

3.1.1. IMMG. IMMG is obtained by integrating the time series of muscle tone signal, and its expression is shown in

$$\mathrm{IMMG} = \frac{\sum_{i=1}^{N} |xi|}{N}. \tag{1}$$

3.1.2. MAV. MAV is the absolute mean value of muscle tone signal amplitude, and its calculation formula is shown in

$$\mathrm{MAV} = \frac{1}{n}\sum_{i=1}^{N} |xi|. \tag{2}$$

3.1.3. MAVI. MAVI is an extension of MAV. The introduction of weighted window function can improve the robustness of features. Its expression is shown in

$$\mathrm{MAVI} = \frac{1}{n}\sum_{i=1}^{N} wi|xi|. \tag{3}$$

3.1.4. SSI. SSI represents the energy of muscle tone signal, and its calculation formula is shown in

$$\mathrm{SSI} = \sum_{i=1}^{N} xi^2. \tag{4}$$

3.1.5. VAR. VAR represents the degree to which the signal deviates from the average value, and its expression is shown in

$$\mathrm{VAR} = \frac{1}{N-1}\sum_{i=1}^{N}(xi - \bar{x})^2. \tag{5}$$

3.1.6. TM3, TM4, and TM5. These three feature lengths are used for classification research, which can reduce the intra class interval. The calculation formula is shown in

$$\begin{aligned} \mathrm{TM3} &= \left|\frac{1}{N}\sum_{i=1}^{N} xi^3\right|, \\ \mathrm{TM4} &= \left|\frac{1}{N}\sum_{i=1}^{N} xi^4\right|, \\ \mathrm{TM5} &= \left|\frac{1}{N}\sum_{i=1}^{N} xi^5\right|. \end{aligned} \tag{6}$$

3.1.7. RMS. RMS represents the amplitude value at the maximum probability density of the signal, and its calculation formula is shown in

$$\mathrm{RMS} = \sqrt{\frac{1}{N}\sum_{i=1}^{N} xi^2}. \tag{7}$$

3.1.8. LRMS. LRMS is similar to RMS and further enlarges the spacing between features. Its expression is shown in

$$\mathrm{LRMS} = \log(\mathrm{RMS}). \tag{8}$$

Frequency domain characteristics are helpful to analyze the signal in frequency domain and understand the characteristic change trend of the signal in power spectrum. They are mainly used in the supplementary analysis of muscle fatigue and motor units. For the frequency domain analysis of muscle tone signal, firstly, the power spectrum of the signal needs to be obtained by Fourier transform, and the power spectral density is calculated. Then, the frequency domain characteristics of the signal are obtained by statistical method.

3.2. Relationship between Sports Injury and Stride Length. Stride length is another important parameter in gait characteristics. Stride length was significantly correlated with height. Generally speaking, the height is higher and the stride is longer. The stride length of female special students was significantly larger than that of ordinary female college students, and there was no significant difference between the two after standardization by dividing the stride length by height (female special students 0.76 ± 0.07, ordinary female college students 0.75 ± 0.05, $P > 0.05$). This shows that the stride difference between female special students and ordinary female college students may be related to height. Studies have shown that college students who often participate in physical exercise have fully developed their lower limb muscle strength and stability, so that the stride step of college students who participate in physical exercise for a long time is significantly larger than that of college students who do not participate in physical exercise. The height of male special students is significantly higher than that of ordinary male college students. At the same time, they also participate in sports training for a long time, and their physical quality and sports ability have been improved to varying degrees. However, there is no significant difference in stride between male special students and ordinary male college students. After standardization by dividing stride by height, there is still no significant difference between the two (male special students 0.73 ± 0.08, ordinary male college students 0.77 ± 0.02, $P > 0.05$). This shows that the stride characteristics of male students may be related to volleyball [19].

Many scholars pointed out in their research that the sagittal range of motion of the hip joint is the main factor affecting stride. The range of motion of the hip joint in sagittal plane is positively correlated with walking speed, and the range of motion of the hip joint and knee joint in sagittal plane increases with the increase of walking speed. Step length, stride length, and step frequency also increase with the increase of step speed. The walking speed of male special students is significantly lower than that of ordinary male college students. The walking speed is small, and the motion range of hip joint in sagittal plane is reduced, which may lead to the shortening of stride. In this study, the height of male special students is significantly higher than that of ordinary male college students, and there is no significant difference in stride between male special students and ordinary male college students, which may be related to the slow pace and insufficient hip flexion of male special students.

Hip joint is an important joint connecting the trunk and lower limbs, with complex structure and more weight-bearing. Hip joint not only supports the stability of human body upright but also coordinates the center of gravity of the body in the process of movement. It is one of the indispensable joints to maintain human body stability and complete body movements. Good hip flexion ability can improve sports performance and daily activity ability. The improvement of hip flexion flexibility can improve athletes' speed, strength, and explosive power to varying degrees. However, if hip flexion is limited, it may cause pain in other parts of the body, such as the back or knee, because many movements of the body need the cooperation of multiple joints, such as bending, which needs the cooperation of the lumbar spine, thoracic spine and hip joint. If the flexion of hip joint is limited, it will force the lumbar spine and thoracic spine to increase their range of motion to compensate for the reduced flexion range of the hip joint, so as to increase the risk of sports injury in other parts [20].

Table 2: Statistical table of injury questionnaire.

Survey object	Distribution (copy)	Recycling (copies)	Valid questionnaire	Recovery rate (%)	Effective rate (%)
Volleyball students	64	64	64	100	100

Table 3: Basic information of subjects (m ± SD).

Grouping	Gender	Number of people	Age (y)	Height (cm)	Weight (kg)	Years of professional sports (y)
Experimental group ($N = 64$)	Male	42	20.02 ± 1.14	184.00 ± 6.09**	74.57 ± 8.93**	6.31 ± 1.89
	Female	22	19.64 ± 1.33	172.55 ± 7.31##	61.91 ± 9.12##	6.14 ± 1.96
Control group($N = 64$)	Male	22	20.12 ± 0.93	170.00 ± 4.82##	61.88 ± 7.O9 ##	—
	Female	18	19.77 ± 0.73	160.69 ± 5.14**	49.31 ± 6.36**	—

The stride characteristics of male special students may be related to their insufficient hip flexion. Therefore, after strength training of hip extensor group in daily training, pay attention to fully stretch and relax the hip extensor group to avoid excessive tension of extensor group. At the same time, we also need to strengthen the strength training of hip flexor group, improve the flexion ability of hip joint, improve sports performance, reduce the risk of hip joint injury, and avoid the injury of waist or chest caused by compensatory hip joint flexion limitation.

4. Results and Analysis

Before the test, the questionnaire was distributed to the subjects on site, and the subjects filled it out on site. After filling it out, the researchers asked about the questionnaire and the actual situation of the subjects and recorded the inquiry results on the questionnaire [21]. The statistics of questionnaire distribution and recovery are shown in Table 2.

The gait data of the subjects are exported in Excel form from the gait view software, and the recovered sports injury investigation data are systematically classified and sorted. The data and data obtained from the investigation and test are processed and statistically analyzed with spss160, and the statistical results are expressed in the form of mean ± standard deviation (M ± SD) and histogram.

T-test was mainly used for the mean difference of gait parameters, and the significance level of *P* value was 0.05.

A total of 64 volleyball special students (experimental group) participated in the test, including 42 male special students and 22 female special students; a total of 40 ordinary college students (control group) participated in the test, including 22 boys and 18 girls, see Table 3 for the basic information of the subjects in the experimental group and the control group.

It can be seen from Table 3 that compared with female students, the male students involved in the test have the same age ($P > 0.05$), there is no significant difference in the years of Volleyball ($P > 0.05$), and there is a very significant difference in height and weight ($P < 0.01$). Compared with female college students, ordinary male college students are also the same age ($P > 0.05$), and there are very significant differences in height and weight ($P < 0.01$).

Table 4: Injury rate of special students of different genders in the injury group.

Gender	Number of injured	Number of people without injury	Damage rate (%)
Male	37	5	88.10
Female	16	6	72.73
Total	53	11	82.81

Compared with ordinary male college students, male special students are of the same age. The height and weight of male special students are significantly higher than those of ordinary male college students ($P < 0.01$). Compared with ordinary female college students, female special students are also the same age, and their height and weight are significantly higher than ordinary female college students ($P < 0.01$).

Before the gait test, the sports injuries of 64 volleyball special students were investigated, and the sports injuries of volleyball special students were counted. Among the 64 volleyball students, 53 had sports injuries, and the injury rate was as high as 82.81%. 37 male students had a history of sports injury, and the incidence of injury was 88.10%. There were 16 female students with a history of sports injury, and the incidence of injury was 72.73%. There was no significant difference in the incidence of sports injury between male and female students ($P > 0.05$), see Table 4. The triceps injury of lower leg is shown in Figure 2.

The results of this experiment show that there is no significant correlation between the incidence of waist injury and height and weight of volleyball students ($P > 0.05$), and there is a significant correlation with the number of years of exercise ($P < 0.05$). Therefore, it can be inferred that long-term high-intensity exercise training is one of the causes of waist injury [22].

Volleyball players often need to bend over, fish jump, roll over, and fall to the ground to save the ball. They have high speed, high intensity, and high requirements for body control. Therefore, the pressure on the waist is large, which is easy to cause pain or acute injury in the waist [23]. In addition, the requirements of serving and spiking on the waist and back muscles are quite high, which requires good muscle strength and explosive power in the waist and

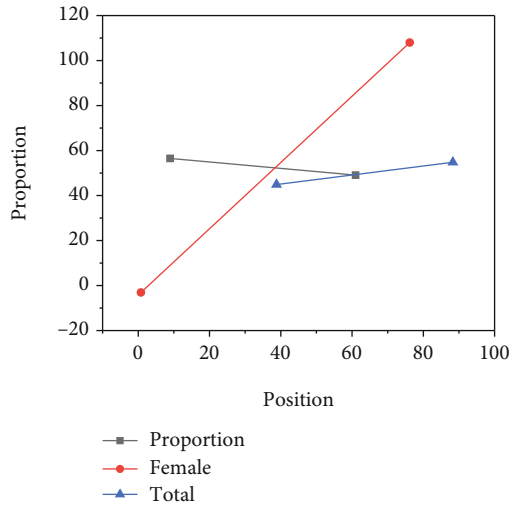

Figure 2: Distribution of triceps injury of the lower leg.

abdomen, and the intensity and amplitude of lumbar activity are overloaded, which is very easy to produce lumbar injury. When completing other basic technical movements of volleyball, the lumbar and abdominal muscles should also participate in work. In long-term heavy-load training and competition, the muscles and ligaments around the waist are prone to excessive fatigue. If they are not reasonably relaxed and rested, it is easy to cause chronic lumbar strain or aggravate the strain. The longer the years of sports training, the higher the risk of chronic lumbar strain [24].

In addition, insufficient preparation activities, incorrect take-off and landing movements, unstable landing, loss of center of gravity, insufficient strength of supporting legs when landing, no buffer on landing, increased impact on the waist, incorrect action during barbell strength training, unbalanced development of abdominal and back muscle strength, etc. are also easy to induce lumbar injury. Once the waist injury occurs, it is not easy to completely cure it. If the waist injury is not cured, training or competition will be arranged, and the injured part will not be well treated and recovered. In the long run, chronic strain will form, and the impact on the body will be more serious, forming a vicious circle [25].

Intervertebral disc is a fibrocartilage disc located between adjacent vertebral bodies, which has great elasticity and toughness. Due to the existence of intervertebral disc, the spine can perform forward flexion, backward extension, and lateral flexion [26]. The human lumbar intervertebral disc is the thickest, and the articular surface of the lumbar facet is almost sagittal, so the flexion and extension activities of the waist are flexible, but the rotation movement of the waist is limited, and the axial rotation range of the waist is small, only 5°. However, the overall range of axial rotation of the waist is large, which is due to the cooperative rotation of the thoracic spine and hip joint. In volleyball, the basic technique commonly used by athletes is cushion, which is the main technical action in receiving, defending, and dealing with all kinds of difficult balls. In the cushion action, the athlete needs to straighten and clamp his arms and close his abdomen with his chest. Such technical action basically locks the chest, thus limiting the axial rotation range of the chest. At the same time, when volleyball players do various technical movements, they are often in the hip flexion position, the hip joint is relatively fixed, and the axial rotation range of the hip joint is also relatively reduced. However, in volleyball, there is a high demand for the axial rotation range of the body. If the axial rotation range of the chest and hip joint is reduced, the pressure on the lumbar muscles and joints will increase, thus increasing the risk of lumbar injury. Therefore, it is necessary to increase the stretching activity of chest muscles in daily training to fully relax the chest in a state of tension for a long time [27].

In this experiment, the most damaged part of female students is the waist, which may be related to the physiological characteristics of women. The periodic changes of estrogen and progesterone levels in women have a certain impact on the joints and ligaments of women; when the estrogen level of women's body is high, the joint ligaments are relatively loose. If girls' waist is trained with high intensity during this period, it is easy to cause lumbar injury.

The experimental results show that the left side is significantly larger than the right side in the unilateral lumbar injury, suggesting that the pressure on the left waist of volleyball students may be greater than that on the right side, which should be paid attention to accordingly. Volleyball special students keep bending posture for a long time, the waist burden is too heavy, and the muscle tension increases, which destroys the coordination of lumbar muscles, reduces the elasticity and toughness of lumbar muscles, and will cause lumbar muscle strain for a long time. In volleyball, the technical actions such as serving and spiking often require waist rotation. Repeated and single special movement training makes the lumbar muscles frequently squeezed or pulled, and the local training intensity is too large, which is easy to lead to lumbar injury on one or both sides [28].

5. Conclusion

It is proved that it is feasible to apply the calculation of time-domain characteristics to the diagnosis of triceps crus injury of volleyball players. It can effectively solve the problem of cumbersome diagnosis of triceps crus injury of volleyball players, meet the needs of rapid diagnosis of sports injury of professional volleyball players, make up for the lack of slow diagnosis of sports injury before, and improve the efficiency of timely detection of volleyball players after injury. In this experiment, the right hand is the favorable hand of most volleyball students. When serving and spiking, the waist needs to exert force to drive the arm to turn to the right, and the left waist is prone to injury due to long-term extrusion, which may be one of the reasons why the left waist injury of volleyball students is significantly greater than that of the right.

Data Availability

The data used to support the findings of this study are available from the corresponding author upon request.

Hindawi
Scanning
Volume 2023, Article ID 9896178, 1 page
https://doi.org/10.1155/2023/9896178

Retraction

Retracted: Diagnostic Value of Spiral CT and Magnetic Resonance Imaging Scanning in Gastric Cancer and Precancerous Lesions

Scanning

Received 20 June 2023; Accepted 20 June 2023; Published 21 June 2023

This article has been retracted by Hindawi following an investigation undertaken by the publisher [1]. This investigation has uncovered evidence of one or more of the following indicators of systematic manipulation of the publication process:

(1) Discrepancies in scope

(2) Discrepancies in the description of the research reported

(3) Discrepancies between the availability of data and the research described

(4) Inappropriate citations

(5) Incoherent, meaningless and/or irrelevant content included in the article

(6) Peer-review manipulation

The presence of these indicators undermines our confidence in the integrity of the article's content and we cannot, therefore, vouch for its reliability. Please note that this notice is intended solely to alert readers that the content of this article is unreliable. We have not investigated whether authors were aware of or involved in the systematic manipulation of the publication process.

In addition, our investigation has also shown that one or more of the following human-subject reporting requirements has not been met in this article: ethical approval by an Institutional Review Board (IRB) committee or equivalent, patient/participant consent to participate, and/or agreement to publish patient/participant details (where relevant).

Wiley and Hindawi regrets that the usual quality checks did not identify these issues before publication and have since put additional measures in place to safeguard research integrity.

We wish to credit our own Research Integrity and Research Publishing teams and anonymous and named external researchers and research integrity experts for contributing to this investigation.

The corresponding author, as the representative of all authors, has been given the opportunity to register their agreement or disagreement to this retraction. We have kept a record of any response received.

References

[1] Y. Zhen, Q. Xie, and L. Liu, "Diagnostic Value of Spiral CT and Magnetic Resonance Imaging Scanning in Gastric Cancer and Precancerous Lesions," *Scanning*, vol. 2022, Article ID 3627385, 6 pages, 2022.

Hindawi
Scanning
Volume 2022, Article ID 3627385, 6 pages
https://doi.org/10.1155/2022/3627385

Research Article

Diagnostic Value of Spiral CT and Magnetic Resonance Imaging Scanning in Gastric Cancer and Precancerous Lesions

Yaolan Zhen, Qing Xie, and Lei Liu

Oncology Department, Xianning Center Hospital, Xianning, Hubei 437100, China

Correspondence should be addressed to Lei Liu; 2013062222@stu.zjhu.edu.cn

Received 12 April 2022; Revised 4 May 2022; Accepted 10 May 2022; Published 23 May 2022

Academic Editor: Danilo Pelusi

In order to explore the diagnostic value of spiral CT and magnetic resonance imaging scanning in gastric cancer and precancerous lesions, the author selected 56 gastric cancer patients treated in a medical center (group) as the experimental subjects, and all patients underwent MRI, multislice spiral CT scan, and enhanced CT scan two weeks before surgery; at the same time, the gastric cancer staging results of patients were diagnosed according to surgical pathology. All patients were examined under the condition of knowledge and performed breath-holding exercise before examination. The status, location, and extent of tumor lesions were evaluated. In comparison of T staging of gastric cancer patients with magnetic resonance scanning imaging and postoperative pathological examination results, among them, T staging of 3 patients did not match the results of pathological examination, the accuracy rates of T staging on magnetic resonance scanning imaging were T1 = 94.7%, T2 = 87.6%, T3 = 91.2%, and T4 = 94.7%, and the total accuracy was 92.1%. Comparison of helical CT scan imaging and postoperative pathological examination results is as follows. Among them, T staging of 8 patients did not match the results of pathological examination, 3 patients were ulcerative, 5 were protuberance, the accuracy rates of T staging in spiral CT scan imaging were T1 = 90.8%, T2 = 82.2%, T3 = 76.9%, and T4 = 87.6%, and the total accuracy was 84.5%. The total accuracy rate of imaging N staging was 77.5%, and the total accuracy rate of spiral CT scanning imaging N staging was 80.8%. The accuracy rates of M0 and M1 staging in magnetic resonance imaging were 100.0% and 96.5%, respectively, and the accuracy rates of M0 and M1 staging in spiral CT scan imaging were 96.5% and 96.5%, respectively. The accuracy rate of magnetic resonance imaging for the diagnosis of gastric cancer N staging was 77.4%, and the reason for the low accuracy rate was mainly because the enhancement effect was not obvious due to insufficient enhancement. The accuracy rate of spiral CT in diagnosing N staging of gastric cancer was 80.9%, which was mainly due to the small diameter of the middle celiac artery lymph nodes. Magnetic resonance and spiral CT scans have high value in the early diagnosis and staging of gastric cancer.

1. Introduction

Gastric cancer is a common disease in oncology, and men over the age of 50 are the high-risk group. As a malignant tumor, the incidence of gastric cancer is extremely high, there are obvious regional differences, and the incidence of gastric cancer in the northern region is significantly higher than that in the southern region [1]. With the change of people's life and diet structure and the increasing pressure of life, the current incidence of gastric cancer is increasing year by year, and it is getting younger and younger. When the patient has onset, the early symptoms are not obvious, some patients are often accompanied by nausea, belching, abdominal discomfort, and other symptoms, and serious complications such as pathological tissue changes, upper gastrointestinal symptoms, melena, perforation of tumor ulcers, and jaundice may occur in patients with advanced disease. To this end, it should be detected and treated early [2]. The direction of preoperative evaluation of gastric cancer mainly includes lymph node metastasis and tumor invasion depth. With the development of imaging, a variety of imaging detection methods are used to evaluate the development of gastric cancer before surgery, including MRI, CT, EUS, B-ultrasound, gastroscope, and PET-CT Figure 1 shows the principle of MRI instrument [3]. Gastroscopy is mostly used for the qualitative diagnosis of gastric cancer and is the gold standard for preoperative diagnosis of

gastric cancer; however, gastroscope cannot be used to evaluate lymph node metastasis and tumor invasion depth. B-ultrasound shows better sensitivity for diagnosing enlarged lymph nodes, but the disadvantage is that it is easily disturbed by abdominal gas or fluid; although to a certain extent, it can indicate the existence of lymphadenopathy, but it is impossible to make a qualitative diagnosis of lymph node metastasis, and B-ultrasound is rarely used to evaluate the stage of lymph node metastasis. Endoscopic ultrasonography shows good diagnostic value for the depth of tumor invasion and has good specificity for the diagnosis of lymph node metastasis but poor sensitivity; therefore, the diagnostic value of lymph node staging is poor. PET-CT has shown good diagnostic value for various tumors, but it is expensive and time-consuming; therefore, PET-CT is rarely used for preoperative evaluation in clinical practice. MRI scans, especially DWI imaging, show good specificity for the diagnosis of lymph node metastasis. Considering the evaluation value of gastric cancer, MRI is often used as an alternative to MDCT examination, and MRI is less directly used to assess the development of gastric cancer [4]. A number of previous studies have shown that MDCT has good sensitivity and specificity for evaluating lymph node metastasis, and it is also the most commonly used preoperative evaluation method in clinical practice.

2. Literature Review

In response to this research question, Gustinucci et al. stated that in the diagnosis of gastric cancer, research on the characteristics and accuracy of multislice spiral CT and 3.0 T magnetic resonance imaging provides a more reliable basis for the evaluation of subsequent clinical manifestations [5]. Bartpho et al. compared the value of multislice spiral CT and magnetic resonance imaging (MRI) in the diagnosis of gastric cancer N staging [6]. Zullo et al. stated that in the examination of primary gastric cancer lesions, CT and magnetic resonance imaging diagnostic methods can be used to detect lesions, a certain examination efficiency can be obtained, the application of the magnetic resonance examination method is as follows, the effect is more obvious, and the advantages are more significant; in the application of the corresponding spiral detection method for judgment, the corresponding treatment method can also be formulated through this effective treatment plan, in terms of its role. Its targeted use requirements also meet the actual use reference value [7]. Yi et al. showed that MRI is also more sensitive than CT imaging in detecting perineural spread and pathological lymph nodes [8]. He et al. showed that perineural dissemination and pathological lymph nodes were significantly associated with clinical treatment and prognosis [9]. Gopi et al. analyzed the MRI findings of 9 palatal tumors and found that MRI had significant advantages in assessing structures surrounding malignant tumor infiltration [10]. Aló et al. summarized the typical CT and MRI imaging findings of different histological types of palatal tumors and tumor-like lesions and found that conventional MRI signs can help narrow the range of differential diagnosis [11]. Cesare et al. studied the apparent diffusion coefficient (ADC) value of 32 salivary gland tumors (17 benign and 15 malignant) examined by preoperative

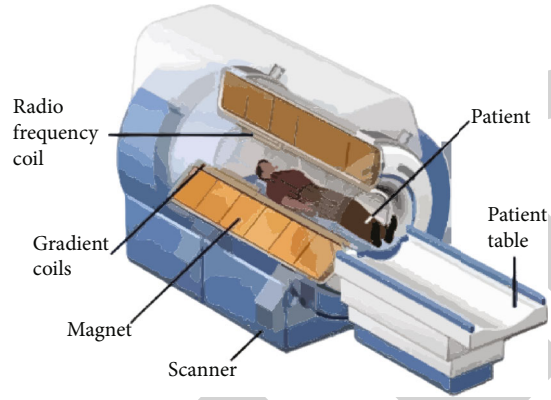

Figure 1: Principle of MRI instrument.

diffusion-weighted imaging (DWI), they found that the ADC value could not reliably distinguish benign and malignant salivary gland tumors, and they speculated that the possible reason was that some salivary gland malignancies such as acinar cell carcinoma contained rich extracellular matrix, which led to the increase of the corresponding ADC value [12]. Simo et al. stated that retrospective imaging of 42 patients with parotid adenocarcinoma with conventional MRI and DWI showed that the sensitivity of DWI in the differential diagnosis of critical and benign disease with an ADC value of $1.02 \times 10 - 3\ \mathrm{mm}^2/\mathrm{s}$. Cancers were as follows: 87.5% and specificity 75.0%. Compared with conventional MRI, DWI was nontoxic and did not significantly improve the differential diagnosis of cancer, suggesting that conventional MRI remains the most valuable diagnostic tool for palate cancer [13]. On the basis of the current research, the author selected 56 gastric cancer patients treated in a medical center (group) as the experimental subjects, and all patients underwent MRI, multislice spiral CT scan, and enhanced CT scan two weeks before surgery; at the same time, the gastric cancer staging results of patients were diagnosed according to surgical pathology. All patients were examined under the condition of knowledge and performed breath-holding exercise before examination. The reason for the low accuracy rate is mainly because the enhancement is not enough; so, the effect after enhancement is not obvious: the accuracy rate of spiral CT in diagnosing N staging of gastric cancer was 80.9%, which was mainly due to the small diameter of the middle celiac artery lymph nodes.

3. Methods

3.1. General Information. Fifty-six gastric cancer patients were treated at the medical center (group). All patients were diagnosed with gastric cancer by gastroscopy, and all patients underwent surgery voluntarily [14]. Among the 56 gastric cancer patients, 36 were male and 20 were female; the age ranged from 45 to 68 years, with an average of (55.7 ± 4.2) years old. Among them, 12 cases were gastric corpus cancer, 18 gastric fundus and cardia cancers, 12 gastric body and gastric cardia cancers, 9 gastric antral hilum cancers, and 5 gastric antral hilum and gastric corpus cancers.

Table 1: Comparison of magnetic resonance scan imaging and postoperative pathological examination results.

Magnetic resonance imaging	Sensitivity	Specificity	Positive predictive rate	Negative predictive rate	Accuracy
T1	85.8	95.8	75.1	97.8	94.7
T2	83.4	88.1	45.6	97.9	87.6
T3	92.8	90.6	76.6	97.5	91.2
T4	91.8	95.6	84.7	97.8	94.7

Table 2: Comparison of helical CT scan imaging and postoperative pathological examination results.

Spiral CT imaging	Sensitivity	Specificity	Positive predictive rate	Negative predictive rate	Accuracy
T1	75.1	92.1	42.8	97.8	90.8
T2	80.1	82.72	50.1	95.1	82.2
T3	70.1	80.67	66.8	82.8	76.9
T4	83.4	88.75	66.8	95.2	87.6

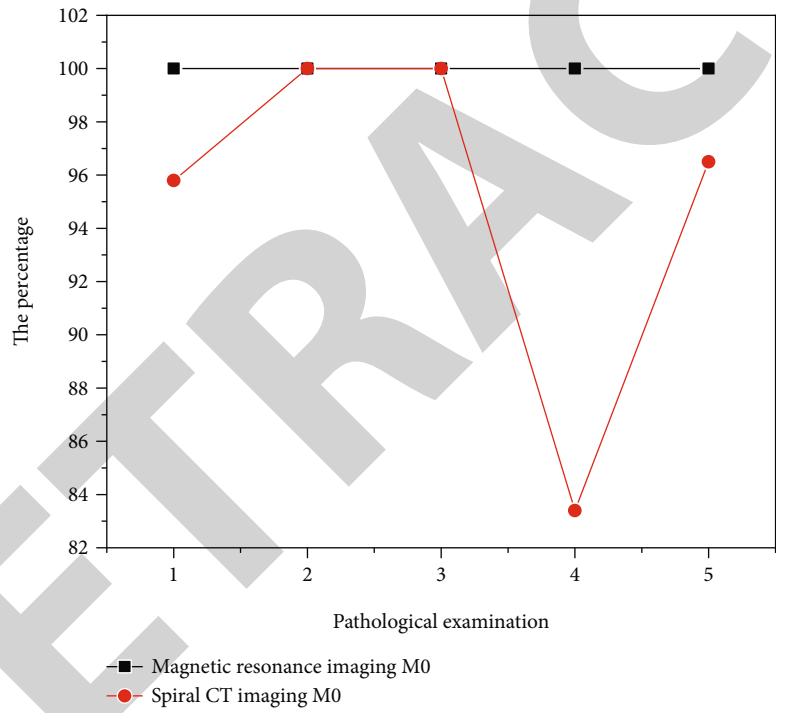

Figure 2: Comparison of the results of MRI and spiral CT in the diagnosis of gastric cancer M0 staging and pathological detection.

Table 3: Comparison of the results of magnetic resonance and spiral CT in the diagnosis and pathological examination of N stage of gastric cancer.

Method	Staging	Sensitivity	Specificity	Positive predictive rate	Negative predictive rate	Accuracy
Magnetic resonance imaging	N0	69.3	90.8	69.3	90.8	85.8
	N1	61.6	73.4	66.8	68.9	67.8
	N2	46.8	90.3	63.7	80.5	78.7
Spiral CT imaging	N0	71.5	80.8	55.7	89.6	78.7
	N1	80.1	77.5	74.2	82.9	78.7
	N2	73.4	90.3	73.4	90.3	85.8

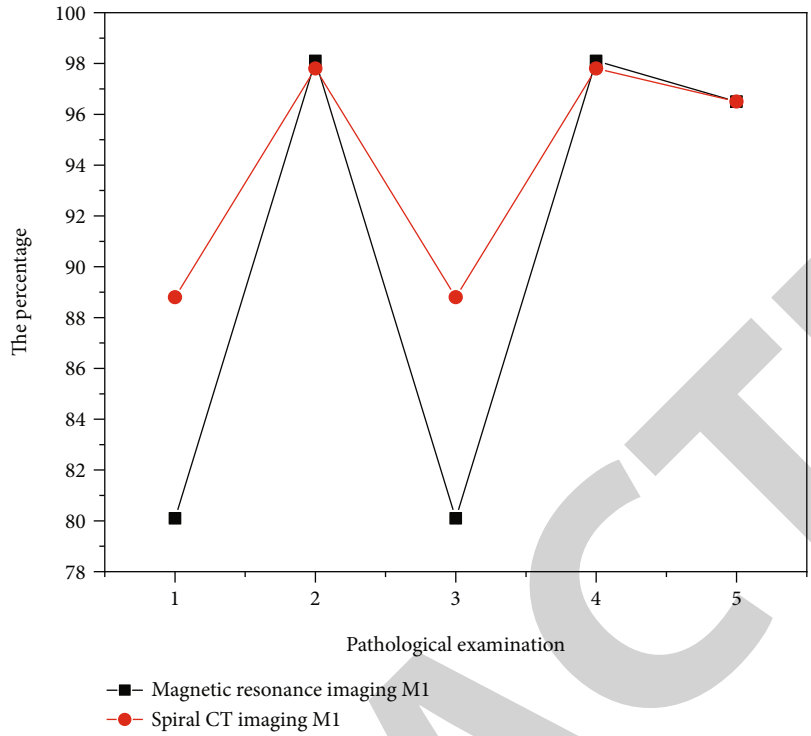

Figure 3: Comparison of the results of MRI and spiral CT in the diagnosis and pathology of gastric cancer M1 stage.

Table 4: Comparison of the results of magnetic resonance and spiral CT in the diagnosis of gastric cancer M staging and pathological detection.

Method	Staging	Sensitivity	Specificity	Positive predictive rate	Negative predictive rate	Accuracy
Magnetic resonance imaging	M0	100	100	100	100	100
	M1	80.1	98.1	80.1	98.1	96.5
Spiral CT imaging	M0	95.8	100	100	83.4	96.5
	M1	88.8	97.8	88.8	97.8	96.5

3.2. Methods. All patients underwent magnetic resonance imaging, multislice spiral CT scan, and enhanced CT scan two weeks before surgery; at the same time, the gastric cancer staging results of patients were diagnosed according to surgical pathology. Patients underwent informed examinations and performed breath-holding exercises before examinations [4, 15], using Philips GvmscanIntera1.5 T superconducting MR instrument and 4-channel and 8-channel body phased array coil. The sense technology was used to examine the patient, and the patient fasted for 8 hours and drank plenty of water (about 400 ml); before the examination, intramuscular injection of anisodamine (15 mg) and 250 ml of warm water were performed, the patient was lying down, an 8-channel imaging coil was selected for magnetic resonance imaging, and the coronal and transverse planes were mainly scanned. Accelerated dynamic acquisition enhanced scan of gastric volume, slice thickness 5 mm, and slice interval 1 mm. The patient was given an intravenous injection of 1.5 ml/s of 15 ml of meglumine spray, and all data were input to the ADW4.5 processing station for high-density and multiplanar projection imaging [2, 16]. The patient was scanned with a GE Lightspeed QX/ICT scanner, the tube voltage was 120 kV, the tube current was adjusted according to the actual situation of the test (250~300 mA), the layer thickness was 1.0 mm, the pitch was 3, and the scanning time was 8 ~ 10 s. Half an hour before the multispiral CT scan, 20 mg of intramuscular anisodamine hydrochloride muscles prevents the normal peristalsis of the gastrointestinal tract, and none of the patients had the stomach inflated through a gastric tube. Upload the data to the workstation and perform reconstruction analysis on the images. 3 radiologists with rich clinical experience above the deputy chief physician analyze the scan results, and the 3 radiologists jointly judge that the patient is gastric cancer [9].

3.3. Diagnostic Criteria. The status, location, and extent of tumor lesions were evaluated. The depth of invasion (T) is divided into four grades from T1 to T4: T1 means the lesion is not obvious or not detected, T2 means full-thickness gastric wall infiltration but no infiltration at the outer boundary, T3 means full-thickness gastric wall infiltration but irregular infiltration at the outer boundary, and T4 indicates that all surrounding organs are infiltrated [17, 18]. Lymph node

metastasis (N) is divided into five criteria: Nx, NO, N1, N2, and N3: Nx means no evaluation, N0 means no obvious metastasis, N1 means 1 ~ 6 metastasis values, N2 means 7 ~ 15 metastasis values, and N3 means >15 transfer values. Distant metastasis (M) is divided into three criteria: Mx, M0, and M1. Mx means no metastasis: metastasis, M0 means 3 metastasis values, and M1 means >12 metastasis values [19].

4. Results and Analysis

4.1. Comparison of T Staging of Gastric Cancer Patient Comparison of Magnetic Resonance Imaging and Postoperative Pathological Examination Results. Among them, T staging of 3 patients did not match the results of pathological examination. The accuracy rates of T staging on magnetic resonance scanning imaging were T1 = 94.7%, T2 = 87.6%, T3 = 91.2%, and T4 = 94.7%, and the total accuracy was 92.1%, see Table 1.

Comparison of helical CT scan imaging and postoperative pathological examination results is as follows: among them, T staging of 8 patients did not match the results of pathological examination, 3 patients were ulcerative, 5 were protuberance, the accuracy rates of T staging in spiral CT scan imaging were T1 = 90.8%, T2 = 82.2%, T3 = 76.9%, T4 = 87.6%, and the total accuracy was 84.5%, see Table 2.

4.2. Comparison of N Staging of Gastric Cancer Patients with MRI Scan. The total accuracy rate of imaging N staging was 77.5%, and the total accuracy rate of spiral CT scanning imaging N staging was 80.8%, see Table 3.

4.3. Comparison of M Stage of Gastric Cancer Patients. The accuracy rates of M0 and M1 staging in magnetic resonance imaging were 100.0% and 96.5%, respectively, and the accuracy rates of M0 and M1 staging in spiral CT scan imaging were 96.5% and 96.5%, respectively, see Table 4 and Figures 2 and 3.

5. Discussion

Gastric cancer is a malignant tumor with a high incidence in the digestive system. Different infiltration depths seriously affect the therapeutic effect of gastric cancer. In the past, CT scan, fiberoptic gastroscope, and X-ray gastrointestinal gas barium double angiography were commonly used in the diagnosis of gastric cancer; however, due to its slow imaging speed and magnetic resonance imaging, it is easily affected by factors such as respiration and gastrointestinal motility and has not been used clinically [20, 21]. In this study, spiral CT combined with enhanced scanning can show the thickness of gastric wall and the depth of invasion in patients with gastric cancer, as well as the TNM staging of gastric cancer. There are many factors that affect the results of the gastric wall test, including differences in patients' own physical constitution, testing equipment, and contrast agents [22]. During the magnetic resonance imaging examination, the author found that the signal of T1-weighted imaging was equal and slightly higher, and the signal of T2-weighted imaging was slightly higher and higher; at the same time, the folds on the gastric mucosa could be seen. In the early stage of gastric cancer, the use of enhanced scanning can detect the extent of the patient's lesions and tumors, and the use of enhanced scanning in the delayed phase is beneficial for tumor staging and diagnosis. The reason for the low accuracy rate is mainly because the enhancement is not enough; so, the effect after enhancement is not obvious: the accuracy rate of spiral CT in diagnosing N staging of gastric cancer was 80.9%, which was mainly due to the small diameter of the middle celiac artery lymph nodes.

6. Conclusion

The authors proposed the diagnostic value of spiral CT and magnetic resonance imaging in gastric cancer and precancerous lesions and evaluated the early diagnosis and TNM staging of gastric cancer by observing spiral CT and magnetic resonance imaging. Early diagnosis of gastric cancer and assessment of TNM staging include gastric cancer, precancerous spiral CT, and magnetic resonance imaging. A total of 56 gastric cancer patients underwent multi-incision helical tomography and magnetic resonance imaging before surgery. The preoperative staging of gastric cancer patients was evaluated according to the scanning images, and the postoperative pathological results were analyzed. Results. Compared with surgical and pathological diagnosis, the accuracy of MRI T-phase was 92.1%, the total accuracy of spiral CT was 84.5%, the accuracy of N-phase MRI was 77.5%, the general accuracy of spiral CT was 80.8%, the accuracy rate of MRM in detecting gastric cancer was 100.0%, and the accuracy rate of multislot spiral CT was 96.5%. Conclusion. Magnetic resonance imaging and spiral tomography are of great significance in the diagnosis of gastric cancer. Cancer patient. Due to the small number of cases in this study, the results of this study are limited, and further analysis and discussion are needed.

Data Availability

The data used to support the findings of this study are available from the corresponding author upon request.

Conflicts of Interest

The authors declare that they have no conflicts of interest.

References

[1] J. Sun, Y. Yue, R. Li, Q. Sun, and Q. Guan, "Detection of hpv e6/e7 mrna in the diagnosis of cervical cancer and precancerous lesions after kidney transplantation," *American Journal of Translational Research*, vol. 13, no. 6, pp. 7312–7317, 2021.

[2] C. X. Zhang, C. T. Wu, L. Xiao, and S. H. Tang, "The diagnostic and clinicopathological value of trefoil factor 3 in patients with gastric cancer: a systematic review and meta-analysis," *Biomarkers*, vol. 26, no. 2, pp. 95–102, 2021.

[3] R. K. Rothman, J. Weinreb, W. Zucconi, and A. Malhotra, "Diagnostic value of ct of chest, abdomen, and pelvis in patients with solitary and multiple brain lesions," *American Journal of Roentgenology*, vol. 214, no. 3, pp. 636–640, 2020.

[4] X. Zan, Q. Guo, R. Ji, Z. Chen, and Y. Zhou, "Mo1068 screening biomarkers associated with gastric cancer and precancerous lesions in high-risk area: cross-sectional study

Hindawi
Scanning
Volume 2023, Article ID 9892518, 1 page
https://doi.org/10.1155/2023/9892518

Retraction

Retracted: Balance Analysis of Peripheral Neuropathy in Type 2 Diabetes Mellitus Based on Logistic Regression Equation

Scanning

Received 12 December 2023; Accepted 12 December 2023; Published 13 December 2023

This article has been retracted by Hindawi, as publisher, following an investigation undertaken by the publisher [1]. This investigation has uncovered evidence of systematic manipulation of the publication and peer-review process. We cannot, therefore, vouch for the reliability or integrity of this article.

Please note that this notice is intended solely to alert readers that the peer-review process of this article has been compromised.

Wiley and Hindawi regret that the usual quality checks did not identify these issues before publication and have since put additional measures in place to safeguard research integrity.

We wish to credit our Research Integrity and Research Publishing teams and anonymous and named external researchers and research integrity experts for contributing to this investigation.

The corresponding author, as the representative of all authors, has been given the opportunity to register their agreement or disagreement to this retraction. We have kept a record of any response received.

References

[1] L. Zhang, Q. Du, M. Yao, M. Wang, and B. Ge, "Balance Analysis of Peripheral Neuropathy in Type 2 Diabetes Mellitus Based on Logistic Regression Equation," *Scanning*, vol. 2022, Article ID 2113758, 7 pages, 2022.

Hindawi
Scanning
Volume 2022, Article ID 2113758, 7 pages
https://doi.org/10.1155/2022/2113758

Research Article

Balance Analysis of Peripheral Neuropathy in Type 2 Diabetes Mellitus Based on Logistic Regression Equation

Lixin Zhang,[1] **Qianqian Du**,[2] **Manman Yao**,[3] **Mai Wang**,[2] **and Bing Ge**[4]

[1]*Nursing Department, The Second Hospital of Shijiazhuang, Hebei 050000, China*
[2]*Department of Endocrinology, The Second Hospital of Shijiazhuang, Hebei 050000, China*
[3]*Department of Obstetrics and Gynecology, The Second Hospital of Shijiazhuang, Hebei 050000, China*
[4]*Pediatrics Department, The Second Hospital of Shijiazhuang, Hebei 050000, China*

Correspondence should be addressed to Lixin Zhang; 201812210203034@zcmu.edu.cn

Received 26 February 2022; Revised 11 April 2022; Accepted 19 April 2022; Published 18 May 2022

Academic Editor: Danilo Pelusi

This paper analyzes the factors of peripheral neuropathy in type 2 diabetes mellitus and puts forward a balanced analysis of peripheral neuropathy in type 2 diabetes mellitus based on logistic regression equation. A total of 1192 eligible patients were selected as the study subjects. All selected patients underwent 75 g oral glucose tolerance test to measure fasting blood glucose and insulin and 2-hour postprandial blood glucose and 2-hour postprandial insulin, as well as neuroelectrophysiological examination. The results showed that the OR values of age, course of disease, fingertip blood glucose immediately after admission, and 2-hour blood glucose were greater than 1, and the P values were all less than 0.05, which were the risk factors of diabetic peripheral neuropathy. OR value of β cell function index (HBCI) is less than 1. P is less than 0.05, and it is a protective factor of diabetic peripheral neuropathy. Laboratory indicators are as follows: 75 g OGTT: 0-hour blood glucose, 2-hour blood glucose, and glycosylated hemoglobin; serum creatinine; glutamate transaminase; fibrinogen; ten items of hemoglobin; and indexes reflecting islet function: islet β is thin, and there are significant differences in cell function index, insulin resistance index, and insulin secretion index between the non-DPN group and DPN group. Age, course of disease, fingertip blood glucose immediately after admission, and blood glucose within 2 hours after admission were the risk factors for diabetic peripheral neuropathy. Islet β cell function index (HBCI) is a protective factor of diabetic peripheral neuropathy.

1. Introduction

Diabetic neuropathy refers to the damage of the nervous system caused by chronic hyperglycemia of diabetes and various pathophysiological changes caused by it, which can affect any part of the whole nervous system. It is one of the common and serious complications of diabetes and can affect 50%-90% of diabetic patients [1]. The most common diabetic neuropathy is peripheral neuropathy, the pathogenesis of this disease is complex, and its clinical manifestations are varied. It can not only occur in the late stage of diabetes, but also, 8% of newly diagnosed diabetic patients have found neuropathy [2]. Diabetic peripheral neuropathy is a hidden, gradual, and slow process, which is nonspecific and difficult to reverse. It is an important risk factor for diabetic foot and other critical diseases. It is the most common cause of non-traumatic amputation. Once diabetic patients have neuropathy, it is extremely difficult to treat them [3]. If we can find diabetic peripheral neuropathy early, actively and effectively control blood sugar and give symptomatic treatment [4], and carry out some necessary foot care, serious consequences such as ulcer, gangrene, and amputation of the foot may be avoided [5]. In view of this research problem, Younger and others reported that the course of diabetes is the influencing factor of DPN [6]. Studies by Dixit et al. show that hyperglycemia is one of the most important causes of DPN. Effective control of hyperglycemia in the early stage of DPN can regenerate the nerve fibers that have lost their functions and restore some functional fovea. However, if hyperglycemia is not well controlled for a long time, it will lead to irreversible damage of the peripheral nerve, which will gradually worsen [7]. Malone found that abnormal

insulin signal may be an important initiating factor of DPN and play an important role in the occurrence and development of DPN [8]. On the basis of the current research, this paper proposed the balance analysis of peripheral neuropathy in type 2 diabetes based on logistic regression equation. The results showed the analysis of influencing factors of peripheral neuropathy in elderly patients with type 2 diabetes, the baseline age and disease course; fingertip blood glucose immediately upon admission; laboratory indicators: 75 g OGTT: 0 h blood glucose, 2 h blood glucose, and HbA1c; serum creatinine; alanine aminotransferase; and fibrinogen. There were significant differences in 10 items of hemoglobin and the indexes reflecting the function of shadow islet: islet β-cell function index, insulin resistance index, and insulin secretion index in non-DPN group and DPN group ($P < 0.05$). Further multifactor analysis showed that the influencing factors of senile type 2 diabetic peripheral neuropathy included age, course of disease, blood glucose 2 hours after meals, fingertip blood glucose immediately after admission, and islet β cell function index.

2. Methods

2.1. Research Object. All the inpatients in the Department of Endocrinology and Geriatrics of the Staff General Hospital of a coal-fired power group company selected 1216 eligible elderly patients with type 2 diabetes, of which 24 were rejected because of incomplete data, and 1192 patients with complete data were selected as the research objects. All selected patients were tested by 75 g oral glucose tolerance test for fasting blood glucose, insulin, blood glucose, and insulin at 2 hours after meal and nerve electrophysiological examination. The youngest is 60 years old, and the oldest is 87 years old, with an average of 65.82±5.98 years old. There were 768 males (64.43%) and 424 females (35.57%) [9].

Inclusion criteria were as follows: confirmed type 2 diabetes (according to WHO 1999 diagnostic criteria) and age ≥ 60 years old.

Exclusion criteria were as follows: type 1 diabetes mellitus; patients with secondary diabetes; oral or inhaled corticosteroids were used during hospitalization or for a long time; and users of antipsychotic drugs.

2.2. Laboratory Inspection Items. Glycosylated hemoglobin (HbA1c); immediate fingertip blood glucose at admission; 75 g oral glucose tolerance test (OGTT): FPG, 2hPG, FINS, and 2hINS; total cholesterol (TC), triglyceride (TG), high-density lipoprotein-cholesterol (HDL-C), low-density lipoprotein-cholesterol (LDC-C); glutamate transaminase (ALT); total bilirubin (TBIL), conjugated bilirubin (DBIL); blood urea nitrogen (BUN) and serum creatinine (Cr); fibrinogen (FIB); and white blood cells (WBC), red blood cells (RBC), and platelets (PLT) were 19 items [10].

2.3. Neuroelectrophysiological Examination. The results of neuroelectrophysiological examination were collected, and the examination instrument was NDI-500P+ (Poseidon) neuroelectrodiagnostic instrument. The method of nerve electrophysiological examination was 18-9: specific measurement: motor nerve conduction velocity (MCV) and motor nerve action potential (CMAP) amplitude of the left and right median nerve (elbow→wrist), ulnar nerve (elbow→wrist), tibial nerve (popliteal→medial malleolus), and common peroneal nerve (below knee); sensory nerve conduction velocity (SCV) and sensory nerve action potential (SNAP) amplitude of median nerve (middle finger→wrist), ulnar nerve (little finger→wrist), peroneal nerve (lateral malleolus→calf); F wave; and H reflex.

2.4. Diagnosis and Exclusion Criteria of Diabetic Peripheral Neuropathy. For the diagnostic criteria of diabetic peripheral neuropathy (DPN), neuroelectric physiological examination is the "gold standard" to diagnose DPN, specifically

(1) a clear history of diabetes

(2) neuropathy occurring during or after diagnosis of diabetes

(3) the clinical symptoms and signs are consistent with the manifestations of diabetic peripheral neuropathy

(4) two or more items of nerve conduction velocity (NCV) slowed down

The diabetic peripheral neuropathy (DPN) exclusion criteria are as follows:

(1) Neuropathy caused by other causes, such as spinal neuropathy, nutritional deficiency, liver and kidney diseases, paraneoplastic syndrome, connective tissue diseases, and genetic diseases

(2) History of taking drugs (isoniazid, furazolidone) that can cause peripheral nerve damage and exposure to some toxic substances (such as heavy metals), anticholinergic drugs, and drugs that may affect autonomic main nerve function

(3) Diseases that can cause subjective sensory disorders (such as hysterical sensory disorders) and unable to cooperate with the inspection, such as low intelligence and difficult to understand

(4) Patients with special type diabetes and type 1 diabetes

2.5. Grouping. According to the results of neuroelectrophysiological examination (NET), 1192 hospitalized elderly patients with type 2 diabetes were divided into a simple diabetes group (non-DPN) and diabetic peripheral neuropathy group (DPN).

2.6. Statistical Analysis. All the data were verified and entered into the computer and analyzed by SPSS 16.0 statistical software. The measurement data were described by the standard deviation of mean soil,$\bar{x} \pm s$, using variance analysis. Chi-square test was used for counting data (x^2 test). Logistic regression analysis was used for multivariate analysis ($P < 0.05$ was statistically significant) [11].

2.7. Logistic Regression Equation. In logistic regression model analysis, some methods of variable screening can be used to control multicollinearity, and the logarithm of each value can be used to establish a general linear regression model of INX over $InX_1, InX_2 \cdots InX_6$.

3. Results and Analysis

3.1. Analysis of Influencing Factors of DPN in Elderly Patients with Type 2 Diabetes Mellitus

(1) The influence of age, course of disease, body mass index, and blood pressure on DPN

The analysis of variance showed that the average age, course of disease, and body mass index of patients in the non-DPN group were 63.33 ± 4.46 years, 2.69 ± 3.12 years, and 24.93 ± 4.12 kg/m^2, respectively. The mean systolic blood pressure was 125.60 ± 30.41 mmHg, and the mean diastolic blood pressure was 79.21 ± 51.18 mmHg. In the DPN group, the average age was 66.64 ± 6.18 years, the average course of disease was 8.10 ± 6.42 years, and the average body mass index was 24.55 ± 4.4.35 kg/m^2. The mean systolic blood pressure was 127.59 ± 38.73 mmHg, and the mean diastolic blood pressure was 75.0 ± 42.48 mmHg. Compared with the non-DPN group, the DPN group was older ($F = 71.83$, $P = 0.001$) and had a longer course of disease ($F = 193.67$, $P = 0.001$), and the difference was statistically significant. There was no significant difference in BMI, SBP, and DBP ($P > 0.05$) [12].

(2) The influence of gender and smoking on DPN

The chi-square test showed that there were 196 males (66.7%) and 98 females (33.3%) in the non-DPN group. In the DPN group, there were 572 males (63.7%) and 326 females (36.3%). There were 184 smokers in the non-DPN group, accounting for 62.59% of non-DPN patients, and 579 smokers in the DPN group, accounting for 64.48% of DPN patients. Different genders ($x^2 = 0.85$, $P = 0.356$) and smoking or not ($x^2 = 0.34$, $P = 0.556$) were not statistically significant between the non-DPN group and DPN group ($P > 0.05$) [13].

(3) The influence of blood sugar on DPN

The analysis of variance showed that the fingertip blood glucose (11.1 ± 4.72 mmol/L), fasting blood glucose (9.11 ± 2.52 mmol/L), 2-hour blood glucose (15.79 ± 6.46 mmol/L/L) and glycosylated hemoglobin (9.62 ± 2.55%) in the DPN group immediately after admission. Compared with the two groups, the indexes of blood glucose control in the DPN group were significantly worse than those in the non-DPN group, including fingertip blood glucose ($F = 53.80$, $P = 0.001$), fasting blood glucose ($F = 121.19$, $P = 0.001$), 2-hour blood glucose ($F = 64.12$, $P = 0.001$), and glycosylated hemoglobin (HbA1c). The difference was statistically significant [14].

(4) Effects of blood lipid and uric acid on DPN

The analysis of variance showed that the total cholesterol, triglyceride, high-density lipoprotein-cholesterol, and low-density lipoprotein-cholesterol in the DPN group were5.64 ± 16.19 mmoL/L/L, 2.11 ± 3.63 mmol/L, 1.21 ± 0.66 mmol/L, and 3.28 ± 7.71 mmol/L, respectively. Compared with the two groups, there was no significant difference in the total cholesterol ($F = 0.008$,$P = 0.927$), triglyceride ($F = 0.011$,$P = 0.916$), high-density lipoprotein-cholesterol ($F = l.100$,$P = 0.294$), and low-density lipoprotein-cholesterol ($F = 0.965$).

(5) Influence of liver function and kidney function on DPN

Analysis of variance showed that in the non-DPN group, the concentration of alanine aminotransferase was 25.84 ± 20.98 IU/L and the concentration of total bilirubin was 17.23 ± 7.92 μmol/L, the concentration of conjugated bilirubin was 3.53 ± 2.72 μmo1/L, and blood urea nitrogen concentration was 6.28 ± 4.23 mmol/L. Islet B Cell function index and insulin resistance index represent the effects on diabetes nephropathy. Analysis of variance showed that islets in the DPN group B Cell function index was 42.68 ± 41.62, insulin resistance index was 4.11 ± 4.63, insulin secretion index was 1.12 ± 1.05, insulin sensitivity index was 0.02 ± 0.02, islet B Cell function index $F = 54.633$ ($P = 0.001$), and insulin secretion index $F = 15.327$ ($P = 0.001$), and the above indexes were lower than those in the DPN group. In the DPN group, alanine aminotransferase (29.13 ± 18.73 IU/L/L), total bilirubin (17.03 ± 7.34 μmol/L/L), combined bilirubin (3.93 2.93 μmol/L), blood urea nitrogen (6.37 2.72 mmol/L), serum creatinine (78.07), and serum creatinine ($F = 7.248$, $P = 0.007$) reflecting renal function were higher than those in the non-DPN group, and the difference was statistically significant ($P < 0.05$). There was no significant difference in total bilirubin ($F = 0.343$, $P = 0.558$), conjugated bilirubin ($F = 0.282$, $P = 0.596$), and urea nitrogen ($F = 1.977$, $P = 0.16$) [15].

(6) The effects of leukocyte, hemoglobin, platelets, and fibrinogen on DPN

Analysis of variance showed that the DPN group had leukocytes $(6.63 \pm 2.84) \times 10^9$/L, hemoglobin 154.10 ± 44.84 g/L, platelet $(190.41 \pm 67.85) \times 10^9$/L, and fibrinogen 4.02 ± 1.92 g/L. Compared with the two groups, the DPN group had higher WBC ($F = 0.328$, $P = 0.567$), but there was no significant difference between the two groups. The fibrinogen was high ($F = 8.458$, $P = 0.004$), and the difference between the two groups was statistically significant. Hemoglobin was low ($F = 6.422$, $P = 0.011$), and the difference between the two groups was statistically significant. Platelet was low ($F = 1.356$, $P = 0.245$), and there was no statistically significant difference between the two groups ($P > 0.05$).

(7) The effects of islet β cell function index and insulin resistance index on DPN. ANOVA showed that the islet β cell function index (42.68 ± 41.62), insulin resistance index (4.11 ± 4.63), insulin secretion index (1.12 ± 1.05), and insulin sensitivity index (0.02 ± 0.02) in the DPN group and the islet β cell

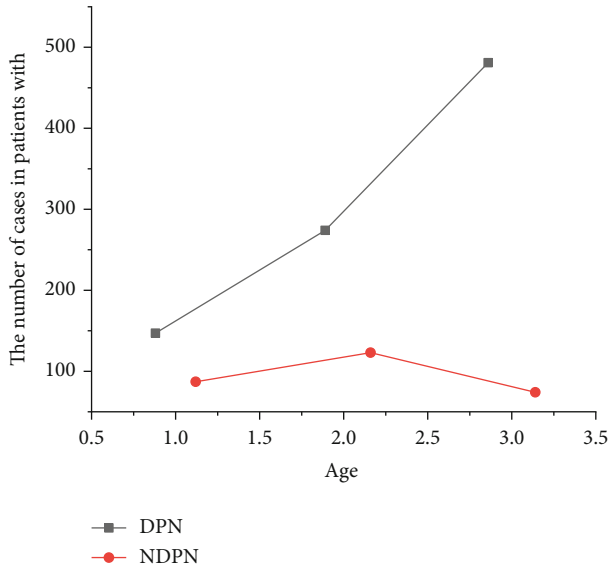

Figure 1: Relationship between age and DPN.

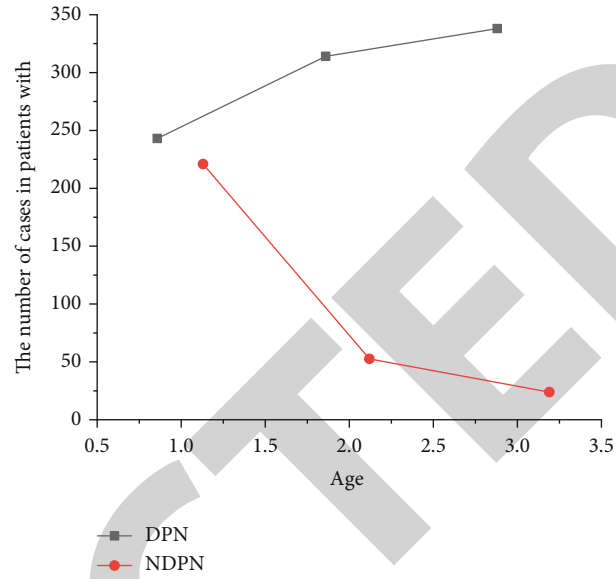

Figure 2: Relationship between course of disease and DPN.

function index ($F = 54.633, P = 0.001$) and insulin secretion index ($F = 15.327, P = 0.001$) were lower in the DPN group, and the differences between the two groups were statistically significant. The DPN group had higher insulin resistance index ($F = 11.276$, $P = 0.001$), and the difference was statistically significant. Insulin sensitivity index ($F = 0.919$, $P = 0.338$) showed no significant difference between the two groups

3.2. Stratified the Age, Course of Disease, and Glycosylated Hemoglobin Affecting Diabetic Peripheral Neuropathy and Understood Its Influence on DPN

(1) The influence of different ages on DPN

The chi-square test showed that the incidence of DPN was 6.5% in the 60-year-old group, 30.4% in the 60-64-year-old group, and 53.1% in ≥65 groups ($x^2 = 65.621$, $P = 0.001$); with the increase of age, the incidence of DPN increased gradually, and there were statistical differences between the two groups in three age groups ($P < 0.05$) (see Figure 1 for details).

(2) The influence of different courses of disease on DPN

The chi-square test showed that the incidence of DPN was 27.6% in the group with a course of less than 3 years, 34.7% in the group with a course of 3-9 years, and 37.6% in the group with a course of more than 10 years ($x^2 = 2.301E2$, $P = 0.001$), suggesting that with the prolongation of the course of disease, the incidence of DPN increased significantly, and there was a statistical difference between the two groups ($P < 0.05$), as shown in Figure 2 [16].

(3) Effects of different glycosylated hemoglobin on DPN

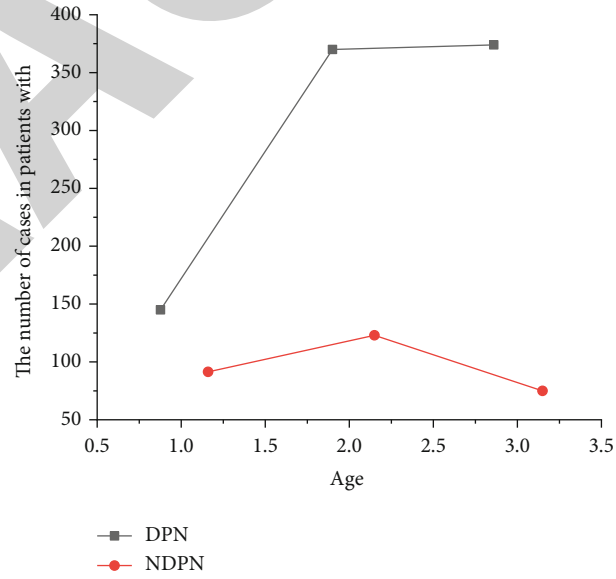

Figure 3: Relationship between HbA1c and DPN.

The chi-square test showed that glycosylated hemoglobin was divided into three layers, and the incidence of DPN increased with the increase of glycosylated hemoglobin ($x^2 = 37.01$, $P = 0.001$), and there was a statistical difference between the two groups ($P < 0.05$) (see Figure 3 for details).

3.3. Multivariate Logistic Regression Analysis of DPN in Type 2 Diabetes Mellitus. In the analysis of logistic regression model, sometimes, the multicollinearity can be controlled by variable screening. In addition to deleting the independent variable f that has no significant impact on the dependent variable Y, several variables that have a significant impact on the dependent variable Y can also be screened from the collinear relationship of group A variables to overcome the problem

Table 1: Multivariate logistic regression analysis of diabetic peripheral neuropathy.

Influence factor	B	SE	Wald	P values	The OR value
Course of disease	0.257	0.024	103.933	0.001	1.233-1.35
Fingertip blood glucose immediately upon admission	0.11	0.026	17.112	0.001	1.061-0.178
2-hour postmeal blood glucose	0.098	0.024	15.264	0.001	1.052-1.161
HBCI	-0.006	0.002	13.833	0.001	0.991-0.998

of collinearity. In order to use the forward method, the OR values of age, course of disease, fingertip blood glucose immediately after admission, and blood glucose within 2 hours should be greater than 1. However, for some practical problems, even if there is collinearity between independent variables, it is still expected to establish the regression between Y and a given independent variable. The general linear regression model of INX to $InX_1, InX_2 \cdots InX_6$ is established by the logarithm of each value, as shown in the following formula:

$$InY = InA + \alpha InX_1 + \beta InX_2 + \gamma InX_3 + \theta InX_4 + \lambda InX_5 + \omega InX_6. \quad (1)$$

In order to further analyze the influence of the above factors on diabetic peripheral neuropathy, the presence or absence of diabetic peripheral neuropathy (none = 0, yes = 1) was taken as dependent variable, and the age, course of disease, immediate fingertip blood glucose, fasting blood glucose, 2-hour blood glucose and glycosylated hemoglobin at admission, serum creatinine, glutamate transaminase, fibrinogen, hemoglobin, the 13 influencing factors of islet cell function index, insulin resistance index, and insulin secretion were analyzed by multivariate logistic regression. According to the standard of$a = 0.05$, forward method was selected for analysis. As a results, the OR values of age, course of disease, fingertip blood glucose immediately after admission, and blood glucose within 2 hours are greater than 1, and the P values are all less than 0.05, which are the risk factors of diabetic peripheral neuropathy. The OR value of β cell function index (HBCI) is less than 1; P is less than 0.05, which is the protective factor of diabetic peripheral neuropathy [17] (as shown in Table 1).

3.4. Peripheral Neuropathy in Elderly Patients with Type 2 Diabetes Mellitus Is the Result of Comprehensive Influence of Many Factors. DPN is the result of many factors. The main risk factors include age, sex, waist-hip ratio, course of disease, blood glucose drift, postprandial blood glucose, and low income. However, there are relatively few large sample studies on the elderly. In this study, when analyzing the influencing factors of peripheral neuropathy in elderly patients with type 2 diabetes mellitus, we found that the patient's age, course of disease, immediate fingertip blood glucose at admission, 2-hour blood glucose, glycosylated hemoglobin, serum creatinine, glutamic transaminase, fibrinogen, hemoglobin, and the indicators reflect islet function. This study found that elderly patients with type 2 diabetes peripheral neuropathy were affected by the following factors: first, compared with those in hospital, OGTT fasting blood glucose in patients with diabetes was relatively stable; for blood glucose after intervention, the result may be low and the impact on DPN may be reduced. Islet β is thin, and there are significant differences in cell function index, insulin resistance index, and insulin secretion index between the non-DPN group and DPN group ($P < 0.05$). And further multifactor analysis, the influencing factors of peripheral neuropathy in elderly patients with type 2 diabetes include age, course of disease, blood glucose 2 hours after meal, fingertip blood glucose immediately after admission, and islet β cell function index [18].

3.5. Age and the Incidence of DPN. The results of this study showed that the incidence of DPN was 75.34%. With the increase of age, the incidence of DPN increased gradually, which was 6.5% in 60-year-old group, 30.4% in 60-64-year-old group, and 53.1% in ≥65 groups. The abnormal rates of motor nerve conduction velocity (MNCV) and sensory nerve conduction velocity (SNCV) in patients with type 2 diabetes were 71.76% and 58.47%, respectively. 28% of 70-79 years old and 35% of ≥80 years old suffered from peripheral neuropathy. Aging can decrease the function of islet β cells in rats. Age is an independent risk factor for DPN. With the increase of age and the prolongation of disease course, the function of islet β cells gradually declines, which leads to the related complications of diabetes. Middle-aged and elderly people have become a high-risk group of diabetes due to the increase of age and genetic and environmental factors. However, during the development of glucose metabolism disorder, the function of islet β cells decreased gradually.

3.6. Incidence of Fingertip Blood Glucose and DPN Immediately after Admission. The results showed that fingertip blood glucose, fasting blood glucose, 2-hour blood glucose, and glycosylated hemoglobin were all risk factors of peripheral neuropathy in elderly patients with type 2 diabetes mellitus. Step-by-step multivariate logistic regression analysis showed that fingertip blood glucose was the risk factor of peripheral neuropathy in elderly patients with type 2 diabetes immediately after admission. The reasons were analyzed: immediate fingertip blood glucose can better reflect the out-of-hospital blood glucose control status of patients and represents the normal blood glucose control level. However, the long-term blood glucose control status is involved in the occurrence and development of peripheral neuropathy in type 2 diabetes mellitus. In related studies, there are few studies on immediate fingertip blood glucose and diabetic complications, but as a means of monitoring blood glucose, because its convenience, simplicity, popularity, and operability are of great help to clinical practice. Dynamic blood glucose detection (CGMS) has

good correlation, accuracy, and consistency with venous blood glucose and fingertip blood glucose.

3.7. Incidence of Blood Glucose and DPN 2 Hours after Meal. The results showed that OGTT 2-hour blood glucose was significantly correlated with DPN, which was a risk factor for diabetic peripheral neuropathy. Compared with young patients, elderly patients may have abnormal action of dual hormones with organ degeneration, that is, decreased insulin secretion and delayed peak insulin secretion after meals, while glucagon does not decrease, resulting in continuous increase of postprandial blood sugar. After 2 hours, it still increased significantly or reached its peak. According to the comprehensive analysis of the influence of blood sugar on DPN, whether it is fingertip blood sugar immediately after admission or blood sugar 2 hours after meals, the mechanism of DPN is still oxidative stress caused by hyperglycemia.

3.8. Influence of Other Factors on the Incidence of DPN. In this study, not in multivariable logistic regression analysis, it was found that in fasting plasma glucose and the elderly with type 2 diabetes peripheral neuropathy, the following factors were considered: first, the fasting blood sugar for diabetes patient is relatively stable after OGTT fasting glucose, in contrast to the hospital at that time; for the blood sugar of blood glucose after intervention, the result may be on the low side, and the effect on DPN is reduced. In addition, compared with fasting state, postprandial state lasts longer, so postprandial blood glucose may be more involved in the occurrence and development of DPN. In this study, no relationship was found between smoking and peripheral neuropathy in the elderly with type 2 diabetes. The reasons for this analysis were as follows: smoking was not stratified during data statistics, and only smoking was considered. Therefore, the influence of smoking on complications was ignored.

4. Conclusion

In this paper, a balanced analysis of peripheral neuropathy in type 2 diabetes mellitus based on logistic regression equation was proposed, and 1192 patients with complete data were selected as research objects. After testing and analyzing the related items, the results show that in the analysis of influencing factors of peripheral neuropathy in elderly patients with type 2 diabetes, the baseline age and course of disease; immediate fingertip blood glucose at admission; laboratory indicators: 75 g OGTT: 0-hour blood glucose, 2-hour blood glucose, and glycosylated hemoglobin; serum creatinine; glutamate transaminase; fibrinogen; ten items of hemoglobin; and indexes reflecting islet function: islet β is thin, there are significant differences in cell function index, insulin resistance index, and insulin secretion index between non-DPN group and DPN group ($P < 0.05$). Further multifactor analysis showed that the influencing factors of senile type 2 diabetic peripheral neuropathy included age, course of disease, blood glucose 2 hours after meals, fingertip blood glucose immediately after admission, and islet β cell function index.

Data Availability

The data used to support the findings of this study are available from the corresponding author upon request.

Conflicts of Interest

The authors declare that they have no conflicts of interest.

Acknowledgments

This study was financially supported by Key Subject Guidance Projects of Medical Science Research in Hebei Province (20201347).

References

[1] N. Tentolouris, S. Liatis, I. Moyssakis, P. Tsapogas, and N. Katsilambros, "Aortic distensibility is reduced in subjects with type 2 diabetes and cardiac autonomic neuropathy," *European Journal of Clinical Investigation*, vol. 33, no. 12, pp. 1075–1083, 2003.

[2] D. Afshari, N. Moradian, E. Rahmanian, and M. Mohammadi, "Prevalence of neuropathy in patients with type 2 diabetes in Iran," *Wiener Klinische Wochenschrift*, vol. 133, no. 7, pp. 222–228, 2020.

[3] S. Yu, Y. Chen, X. Hou et al., "Serum uric acid levels and diabetic peripheral neuropathy in type 2 diabetes: a systematic review and meta-analysis," *Molecular Neurobiology*, vol. 53, no. 2, pp. 1045–1051, 2016.

[4] J. Gastoł, P. Kapusta, A. Polus et al., "Epigenetic mechanism in search for the pathomechanism of diabetic neuropathy development in diabetes mellitus type 1 (T1DM)," *Endocrine*, vol. 68, no. 1, pp. 235–240, 2020.

[5] T. Xu, Z. Weng, C. Pei et al., "The relationship between neutrophil-to-lymphocyte ratio and diabetic peripheral neuropathy in type 2 diabetes mellitus," *Medicine*, vol. 96, no. 45, article e8289, 2017.

[6] D. S. Younger, G. Rosoklija, A. P. Hays, D. W. Trojaborg, and N. Latov, "Diabetic peripheral neuropathy: a clinicopathologic and immunohistochemical analysis of sural nerve biopsies," *Muscle & Nerve*, vol. 19, no. 6, pp. 722–727, 1996.

[7] S. Dixit, A. Maiya, B. A. Shastry, and V. Guddattu, "Analysis of postural control during quiet standing in a population with diabetic peripheral neuropathy undergoing moderate intensity aerobic exercise training," *American Journal of Physical Medicine & Rehabilitation*, vol. 95, no. 7, pp. 516–524, 2016.

[8] J. I. Malone, "Diabetic central neuropathy: CNS damage related to hyperglycemia," *Diabetes*, vol. 65, no. 2, pp. 355–357, 2016.

[9] H. Urabe, T. Terashima, F. Lin, H. Kojima, and L. Chan, "Bone marrow-derived TNF-α causes diabetic neuropathy in mice," *Diabetologia*, vol. 58, no. 2, pp. 402–410, 2015.

[10] M. Yokomoto-Umakoshi, I. Kanazawa, S. Kondo, and T. Sugimoto, "Association between the risk of falls and osteoporotic fractures in patients with type 2 diabetes mellitus," *Endocrine Journal*, vol. 64, no. 7, pp. 727–734, 2017.

Hindawi
Scanning
Volume 2023, Article ID 9817461, 1 page
https://doi.org/10.1155/2023/9817461

Retraction

Retracted: Research on Influencing Factors of Clinical Efficacy of Meniscus Resection Based on Logistic Regression Analysis

Scanning

Received 20 June 2023; Accepted 20 June 2023; Published 21 June 2023

This article has been retracted by Hindawi following an investigation undertaken by the publisher [1]. This investigation has uncovered evidence of one or more of the following indicators of systematic manipulation of the publication process:

(1) Discrepancies in scope

(2) Discrepancies in the description of the research reported

(3) Discrepancies between the availability of data and the research described

(4) Inappropriate citations

(5) Incoherent, meaningless and/or irrelevant content included in the article

(6) Peer-review manipulation

The presence of these indicators undermines our confidence in the integrity of the article's content and we cannot, therefore, vouch for its reliability. Please note that this notice is intended solely to alert readers that the content of this article is unreliable. We have not investigated whether authors were aware of or involved in the systematic manipulation of the publication process.

In addition, our investigation has also shown that one or more of the following human-subject reporting requirements has not been met in this article: ethical approval by an Institutional Review Board (IRB) committee or equivalent, patient/participant consent to participate, and/or agreement to publish patient/participant details (where relevant).

Wiley and Hindawi regrets that the usual quality checks did not identify these issues before publication and have since put additional measures in place to safeguard research integrity.

We wish to credit our own Research Integrity and Research Publishing teams and anonymous and named external researchers and research integrity experts for contributing to this investigation.

The corresponding author, as the representative of all authors, has been given the opportunity to register their agreement or disagreement to this retraction. We have kept a record of any response received.

References

[1] X. Mao, Q. Hong, R. You, Y. Lu, and F. Zhao, "Research on Influencing Factors of Clinical Efficacy of Meniscus Resection Based on Logistic Regression Analysis," *Scanning*, vol. 2022, Article ID 4606139, 2022.

Hindawi
Scanning
Volume 2022, Article ID 4606139, 6 pages
https://doi.org/10.1155/2022/4606139

Research Article

Research on Influencing Factors of Clinical Efficacy of Meniscus Resection Based on Logistic Regression Analysis

Xiaocheng Mao, Qingnan Hong, Ruijin You, Yizhe Lu, and Feng Zhao

Bone and Joint Ward, Joint Logistic Support Force Hospital 910, Hefei Anhui 230000, China

Correspondence should be addressed to Feng Zhao; 1430701121@post.usts.edu.cn

Received 26 February 2022; Revised 11 April 2022; Accepted 19 April 2022; Published 18 May 2022

Academic Editor: Danilo Pelusi

In order to solve the factors affecting the clinical efficacy of meniscus resection, a method based on logistic regression analysis is proposed. From May 2019 to May 2020, 60 patients with discoid meniscus who underwent arthroscopic surgery in the Joint Department of the Second Hospital of a certain city were selected as the research objects; the surgical methods are divided into partial meniscus excision and plasty and total meniscus resection. The Lysholm function score was used to evaluate the clinical efficacy of arthroscopic surgery for discoid meniscus injuries before and 3, 6, and 12 months after surgery and postoperative application of Ikeuchi score and Tegner exercise ability score to assess age, gender, body mass index (BMI), duration of symptoms, and the influence of meniscus injury types and surgical methods on the efficacy of arthroscopic surgery for discoid meniscus injuries. Experimental results show that Ikeuchi's assessment of the excellent and good rate of arthroscopic knee joints was significantly higher than that of the control group, the incidence of postoperative pain was significantly lower than that of the control group, and the difference was statistically significant ($P < 0.05$). Postoperative pain and premature weight-bearing of discoid meniscus injury of knee joint, factors such as noncold compress after operation, articular cartilage damage, age, and time from onset to operation are closely related; the difference was statistically significant ($P < 0.05$). Postoperative evaluation according to Ikeuchi score: excellent in 38 cases, good in 14 cases, 8 cases were poor, and the excellent and good rate was 86.7%. The patient's age, type of meniscus tear, and duration of symptoms have a certain impact on the postoperative clinical efficacy of discoid meniscus injury; BMI and surgical methods have no significant impact. Logistic regression analysis results show that postoperative pain and premature weight-bearing of discoid meniscus injury of the knee joint, no cold compress after operation, accompanied by articular cartilage damage, age, and factors such as onset to operation time are closely related; the difference was statistically significant ($P < 0.05$). It proves that arthroscopic surgery for discoid meniscus injury has the advantages of less damage and faster recovery, it is the first choice for the treatment of discoid meniscus injury, and the postoperative effect is significant in young patients and those with short duration of symptoms; mixed tears have a greater impact on the postoperative recovery of patients with discoid meniscus injury; therefore, patients with discoid meniscus injury should undergo surgery as soon as possible and perform active rehabilitation exercises after the operation.

1. Introduction

The discoid meniscus of the knee joint is also known as discoid cartilage; it means that its meniscus is thicker and larger than normal, and its shape is abnormal, especially on the body; it is disc-shaped, often on the lateral meniscus; it is a rare clinical meniscus deformity, and the high-risk population is male young adults [1]. The disc-shaped meniscus of the knee joint is mostly caused by torsional external force; there is pain and discomfort in the meniscus of the knee joint. Bounce occurs in the complete type with complex damage and extensive damage, while the complete type is less likely to be interlocked. Studies have pointed out that arthroscopic treatment of discoid meniscus injury of the knee joint significantly improves the patient's joint function; premature weight-bearing, postoperative noncold compress, and articular cartilage damage are closely related to postoperative pain and other factors [2].

Arthroscopic meniscus plasty can maximize the preservation of the load transmission capacity of the meniscus; at

the same time, the horizontal shear force is eliminated to promote the local biomechanics of the knee joint to return to normal; during the operation, the meniscus was removed under arthroscopic monitoring; it is helpful to accurately assess the scope of resection and prevent blind resection or residual damage. So far, the etiology of discoid meniscus is still controversial at home and abroad [3]. Zheng put forward the hypothesis of growth arrest; he believes that the disc shape is normal during embryonic development, but during the fetal period, its central part is not completely absorbed; this leads to the occurrence of congenital discoid meniscus [4]; Wu found that the ultrastructure of the outer disc-shaped meniscus is significantly different from that of the normal meniscus; the reduction and imbalance of discoid meniscus collagen fibers increase the incidence of discoid meniscus tears. In addition, the relatively weak attachment of the posterior horn of the disc-shaped meniscus to the joint capsule, the increase in thickness of the meniscus, and the insufficient blood supply are also factors that cause the disc-shaped meniscus to be easily damaged. With the movement of the knee joint, the meniscus will also show adaptive fretting, and the normal meniscus has the ability to bend and contract deformity [5]. Elagib found by MRI imaging that, compared with normal meniscus, the discoid meniscus is thick and lacks ligament restriction; as a result, the deformability of the disc-shaped meniscus is weakened. At the same time, the lateral discoid meniscus often merges with lateral intercondylar crista dysplasia, changes such as knee inversion and valgus; this causes the disease of the discoid meniscus; this may be one of the mechanisms of discoid meniscus injury. At present, the etiology research of discoid meniscus mainly focuses on two kinds of congenital and acquired factors; most scholars believe that congenital factors play an important role in the discoid meniscus [6]. It is very important to analyze the clinical effect of arthroscopic treatment of the discoid meniscus of the knee joint and the factors affecting postoperative pain; therefore, this study selected patients with discoid meniscus injury of the knee joint who were treated from May 2019 to May 2020; the arthroscopic treatment was performed, and the clinical effects and factors affecting postoperative pain were analyzed; the results are satisfactory. The current research is as follows.

2. Materials and Methods

2.1. General Information. A total of 60 patients with lateral discoid meniscus injury who were treated from May 2019 to May 2020 were selected; all were unilateral injuries, including 29 males, accounting for 48.3%; 31 cases were female, accounting for 51.7%. There were 27 cases on the left knee, accounting for 45%, and 33 cases on the right knee, accounting for 55%; the age was 18-50 years old, with an average of 32.04 years old. All patients had knee-related symptoms before surgery, such as pain, snapping, locks, and restricted movement; no relevant treatment was given. X-ray and magnetic resonance imaging (MRI) examinations of the affected limbs were performed before the operation and the Watanabe classification: 24 cases of complete type, accounting for 40%; 36 cases of incomplete type, accounting for 60%, 0 cases of Wrisberg ligament type. Meniscus tear types: 19 cases of horizontal tear, accounting for 31.7%; 20 cases of longitudinal or radial tear, accounting for 33.3%. There were 21 cases of mixed tear, accounting for 35%. According to the severity of meniscus injury, it was divided into meniscus total resection group and meniscus resection group, 30 cases in each [7].

2.2. Surgical Methods. The patient takes a supine position, place an airbag tourniquet on the upper 1/3 of the affected femur, and perform epidural anesthesia; and after the anesthesia takes effect, perform routine iodophor disinfection of the surgical area, and spread sterile towels and sheets; the affected limb will be bleeding, the tourniquet will be inflated, and the affected limb will be abducted and hung under one side of the operating table; bend the knee 90° and perform standard anteromedial and anterolateral surgical approaches, inject normal saline into the joint to expand the joint cavity, and insert the probe; a comprehensive exploration of the knee joint with the assistance of the probe hook, the sequence is as follows: the suprapatellar capsule, the patellofemoral joint surface, the medial and lateral condyles, and the medial and lateral spaces. Put the "4" position to explore the lateral meniscus and lateral space, bend the knee 30° and turn the knee joint out to explore the medial meniscus and medial space, exploring and removing hyperplastic synovial tissue at the same time, take out the loose body in the joint to fully expose the field of vision, and carefully observe the degree, extent, and type of damage to the disc-shaped meniscus [8]. For those with a small torn meniscus, a lighter degree of damage, and most of the red zone and the red-white junction area, partial meniscus excision and plasty; use blue forceps to bite away the free part of the meniscus injury, the planing knife trims the edge of the meniscus and absorbs free meniscus fragments, ensure that the edge is smooth, the periphery is thickened, and the free edge becomes thinner, to form a slope to adapt to the shape of the femoral condyle, try to preserve the synovial margin 6-8 mm, and finally loosen the adhesion tissue in the joint. And for the severe degree of meniscus tear, involving the peripheral tissues of the meniscus, at the same time as the torn meniscus is removed, part of the peripheral tissue of the meniscus is removed, and all meniscus fragments are removed; a total meniscus surgery was performed. After the operation, after confirming that there is no residue in the joint cavity and the stump is smooth, wash the joint cavity with a large amount of normal saline and flex and extend the knee joint, check the bounce, whether the symptoms such as strangulation disappear, leave a negative pressure drainage tube, full-layer sutures on both sides of the wound, covered with sterile accessories, compression bandage with elastic bandage, digital chuck adjustable brace fixes the affected limb in the straight position. After the operation, the affected knee can be iced for 24 to 48 hours to reduce bleeding and relieve pain [9].

2.3. Postoperative Rehabilitation Exercise. After 24 hours, you can perform quadriceps strength exercises and ankle pump exercises on the bed to promote blood circulation in the lower limbs; it is beneficial to reduce the swelling of

Table 1: Comparison of Lysholm scores before and after surgery in 60 patients ($x \pm s$, points).

Group	n	Preoperative	3 months after surgery	6 months after surgery	12 months after surgery
Meniscus plasty	30	62.85 ± 18.42	82.20 ± 12.40	90.28 ± 7.19	91.17 ± 5.31
Total meniscus surgery	30	64.37 ± 17.29	90.63 ± 4.99	91.33 ± 4.32	91.75 ± 4.70
P		0.643	0.001	0.335	0.525

the affected limb and prevent the formation of deep vein thrombosis in the lower limbs. On the second day after surgery, quadriceps strength exercises and straight leg raising exercises are available, and the digital chuck adjustable brace is used to passively move the knee joint. Limit passive flexion to 90° within 2 weeks after operation, while avoiding active flexion. Increase by 10° per week, 4 weeks of joint flexion and extension to 90°, 8 weeks to restore normal flexion angle. Partial weight-bearing can be carried out in 3 weeks after operation, and the weight-bearing weight can be gradually increased, and full weight-bearing can be carried out in 6 weeks. Knee joint function will gradually improve in 3-9 months, but within 4-6 months after surgery, weight-bearing exercises such as knee rotation, squatting, and large flexion should be avoided. [10]

2.4. Postoperative Functional Evaluation. All patients were followed up effectively after the operation, and the Ikeuchi score was used for evaluation after the operation. Excellent: normal range of motion, no mechanical symptoms (snap, lock), no pain; good: normal range of motion, no mechanical symptoms (snap, lock), and occasional mild pain during or after exercise; possible: normal range of motion, mechanical symptoms (snap, lock), mild pain during or after exercise; poor: limited range of motion, mechanical symptoms (snap, lock), pain during rest and exercise. At the same time, the Lysholm function score was used before surgery and 3, 6, and 12 months after surgery to evaluate the clinical efficacy of arthroscopic surgery for discoid meniscus injuries; the Tegner exercise performance score was used to evaluate the functional recovery of the knee joint after surgery [3].

2.5. Statistical Analysis. Use SPSS 17.0 statistical analysis software for statistical analysis, and use the χ^2 test for count data; the measurement data was measured by t-test, and logistic regression analysis was performed on the related factors of postoperative pain in patients with knee discoid meniscus injury; take the occurrence of postoperative pain as the dependent variable, and the basic data of the patient as the independent variable; multicategorical variables were set as subvariables, and $P < 0.05$ was used as the standard for screening variables in stepwise regression [11].

3. Results

All 60 patients were followed up effectively, and the knee joint function was improved to varying degrees after surgery; there were no serious complications such as knee joint infection and no cases of surgical revision. There was no significant difference in Lysholm score before arthroscopic partial meniscus resection and arthroscopic total meniscus resection ($P > 0.05$). The difference was statistically significant at 3 months after operation ($P < 0.05$). There was no significant difference between 6 months and 12 months after operation ($P > 0.05$); see Table 1. According to the Ikeuchi score, 38 cases were excellent, 14 cases were good, and 8 cases were poor; the excellent and good rate was 86.7%. The patient's age, type of meniscus tear, and duration of symptoms have a certain impact on the postoperative clinical efficacy of discoid meniscus injury: the younger the patient's age, the shorter the duration of symptoms, and the single type of meniscus tear, the better the recovery of knee joint function after surgery. However, gender, BMI, and surgical methods have no significant effects on postoperative clinical results. See Tables 2–6 and Figure 1.

3.1. Logistic Regression Analysis Results. The postoperative pain of discoid meniscus injury of the knee is closely related to factors such as premature weight-bearing, no cold compress after operation, articular cartilage injury, age, and time from onset to surgery; the difference was statistically significant ($P < 0.05$).

4. Discussion

4.1. Classification and Clinical Significance of Discoid Meniscus. There are many ways to classify discoid meniscus. According to the shape of the inner edge of the meniscus, the axial plane can be divided into "cape-shaped" or "bay-shaped"; the coronal plane can be divided into "plate shape" or "wedge shape." According to the tear form of discoid meniscus, it can be divided into simple tear, complex tear, horizontal tear, radial tear, degenerative tear, and compound tear. At present, the most widely used is the Watanabe classification, in which based on the Watanabe classification discoid meniscus can be divided into complete types. The meniscus is disc-shaped, thick, and large and completely covers the lateral articular surface of the tibial plateau, and it is connected to the posterior joint capsule, and the thickness of the inner and outer edges is not much different. Incomplete type: it also has a disc shape and is also connected to the posterior joint capsule; it is different from the complete type; the meniscus does not completely cover the lateral articular surface of the tibial plateau; the free edge of the medial side presents a double concave notch; there is a protrusion protruding to the center of the joint between the two depressions. Wrisberg type: the structure of the meniscus is similar to that of the normal meniscus, but the middle part is significantly wider, and it is not connected with the posterior joint capsule, only connected by the Wrisberg ligament. Among them, the complete type is the most common type, and the Wrisberg type is relatively rare [12].

Table 2: The effect of age on the treatment of discoid meniscus injury by arthroscopic surgery.

Group	n	Tegner athletic ability score	Ikeuchi score		
			Excellent	Good	Poor
<20 years old	31	7.38 ± 1.49	21	8	2
20~40 years old	16	5.48 ± 1.72	9	4	3
>40 years old	13	4.45 ± 1.63	8	2	3
P		0.001		0.548	

Table 3: The influence of gender on the curative effect of arthroscopic surgery for discoid meniscus injury.

Group	n	Tegner athletic ability score	Ikeuchi score		
			Excellent	Good	Poor
Man	29	5.52 ± 1.81	18	8	3
Women	31	5.13 ± 1.50	20	6	5
P		0.209		0.662	

Table 4: The effect of BMI on the curative effect of arthroscopic surgery for discoid meniscus injury.

Group	n	Tegner athletic ability score	Ikeuchi score		
			Excellent	Good	Poor
BMI < 24	33	4.43 ± 1.59	24	5	4
BMI ≥ 24	27	4.72 ± 1.37	14	9	4
P		0.297		0.201	

Table 5: The effect of duration of symptoms on the efficacy of arthroscopic surgery for discoid meniscus injury.

Group	n	Tegner athletic ability score	Ikeuchi score		
			Excellent	Good	Poor
<1 year	34	6.20 ± 2.58	25	6	3
>1 year	26	2.33 ± 1.52	13	8	5
P		0.001		0.168	

Table 6: The influence of surgical methods on the curative effect of arthroscopic treatment of discoid meniscus injury.

Group	n	Tegner athletic ability score	Ikeuchi score		
			Excellent	Good	Poor
Meniscus plasty	30	5.67 ± 1.67	21	6	3
Total meniscus surgery	30	5.82 ± 1.71	17	8	5
P		0.628		0.547	

In this group of data, 24 cases are of complete type, 36 cases are of incomplete type, and there is no Wrisberg type. There were 19 cases of horizontal tear, 20 cases of longitudinal or radial tear, and 21 cases of mixed tear. For patients with horizontal tears, due to their small injury range, partial meniscus resection and angioplasty are often used; for patients with severe radial tears and mixed tears, because of its serious degree of tear, involving the peripheral tissues of the meniscus, a total meniscectomy was used.

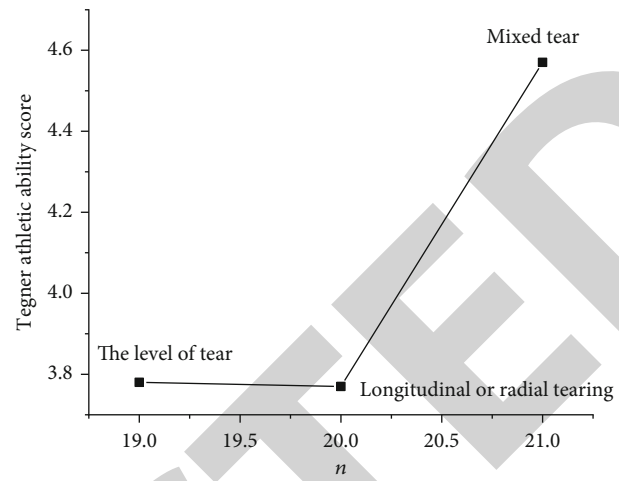

Figure 1: The influence of the type of meniscus injury on the curative effect of arthroscopic surgery for discoid meniscus injury.

4.2. Clinical Manifestations and Clinical Significance of Discoid Meniscus Injury. Discoid meniscus injury has no specific symptoms; pain is the most common symptom of discoid meniscus injury, followed by the knee joint flicking and snapping, swelling, joint locking, soft legs, and limited mobility. Joint space tenderness, quadriceps atrophy, and McMurray test and Apley test (+) are the more common signs of discoid meniscus injury [13]. Experiments show that male patients have a higher incidence of knee snapping, while female patients are more likely to have knee dysfunction. Most discoid meniscus are asymptomatic in childhood, and young patients may exhibit the typical "snapping knee syndrome"; it is painless at first, and then, mechanical symptoms and movement disorders appear. In clinical practice, most patients do not take effective and reasonable symptomatic treatment when they have knee discomfort; it has been sick for a long time when there are typical symptoms such as bounce and locks, and it has been accompanied by varying degrees of cartilage damage, which directly affects the clinical treatment effect [14].

4.3. The Clinical Efficacy and Influencing Factors of Arthroscopic Surgery for Discoid Meniscus Injury. Discoid meniscus injuries are mainly treated by nonsurgical treatment and surgical treatment. Among them, nonsurgical treatment mainly includes lower extremity fixation treatment, drug treatment, articular cavity puncture injection treatment, physical therapy, and Chinese medicine acupuncture treatment. Surgical treatment includes traditional cut and cut sac, meniscus surgery, and arthroscopic surgery. Patients with asymptomatic discoid meniscus injury can be treated conservatively first; if conservative treatment fails, surgical treatment is feasible. For patients with symptomatic discoid meniscus injury and no obvious symptoms but with

a clear discoid meniscus tear, surgical resection should be performed as soon as possible. Traditional surgery due to the reduction in the contact area of the tibiofemoral joint after the operation, excessive stress concentration, and softening of articular cartilage leads to narrowing of the joint space and osteophyte formation, which cause degenerative changes in the knee joint, leading to the early onset of osteoarthritis, so it has been seldom used. [15] At present, with the continuous development of arthroscopy technology, arthroscopic surgery for discoid meniscus injuries has become the most common orthopedic surgery; according to the type and location of the meniscus tear, the duration of symptoms, and the age of the patient, you can choose partial meniscus resection and plasty, meniscus suture repair, meniscus reconstruction, and meniscus talectomy; moreover, arthroscopic surgery has the advantages of less damage and faster recovery, so it has become the first choice for the treatment of discoid meniscus injury [16]. At present, there is no consensus on the research on the factors affecting the treatment of discoid meniscus injury by arthroscopic surgery. Wei et al. observed 198 patients with discoid meniscus injury who underwent arthroscopic surgery; it is believed that the patient's age, the duration of symptoms, the degree of cartilage damage, and the choice of surgical procedures have a greater impact on the efficacy of arthroscopic surgery for discoid meniscus injuries; the type of meniscus injury has no obvious effect. Through the follow-up of 97 patients with discoid meniscus injury, Yaxi et al. found that the patient's age and the duration of symptoms have a significant impact on the surgical effect; the gender, type of meniscus injury, and surgical procedure have no obvious influence. Through clinical observation of 21 patients with discoid meniscus injury, Wu et al. believed that the patient's age and meniscus classification affect the clinical efficacy of discoid meniscus to a certain extent. The choice of gender, trauma history, tearing method, and surgical method has no obvious influence [17, 18].

5. Conclusion

By assessing the impact of the patient's age, gender, BMI, duration of symptoms, type of meniscus injury, and surgical method on the efficacy of arthroscopic surgery for discoid meniscus injury, we found that age, type of meniscus tear, and duration of symptoms have a certain influence on the postoperative clinical efficacy of discoid meniscus injury; the younger the disease is, the shorter the duration of symptoms, and the single type of meniscus tear, the better the functional recovery of the knee joint after surgery; and the choice of patient's gender, BMI, and surgical method has no significant influence on the postoperative clinical effect. Therefore, for patients with discoid meniscus injury, arthroscopic surgery should be performed as soon as possible to achieve better clinical results.

Data Availability

The data used to support the findings of this study are available from the corresponding author upon request.

Conflicts of Interest

The authors declare that they have no conflicts of interest.

References

[1] W. Weng, S. Ding, J. Min, H. Tang, and S. Xing, "Logistic regression analysis of drug compliance and influencing factors in elderly osteoporosis patients," *Pakistan Journal of Pharmaceutical Sciences*, vol. 32, no. SI5, pp. 2399–2403, 2019.

[2] X. Tan, X. J. Zhao, J. X. Li, C. E. Xie, and X. X. Xue, "Study on the clinical mechanism of tong-xie-an-chang decoction in the treatment of diarrheal irritable bowel syndrome based on single-cell sequencing technology," *Medicine*, vol. 99, no. 52, article e23868, 2020.

[3] R. D. Farias, "Comment on "clinical study on the efficacy of led phototherapy for pain control in an orthodontic procedure"," *Lasers in Medical Science*, vol. 35, no. 2, pp. 1–1, 2019.

[4] Y. Zheng, S. Xu, Z. Zheng, L. Wu, and W. Zhan, "Ultrasonic classification of multicategory thyroid nodules based on logistic regression," *Ultrasound Quarterly*, vol. 36, no. 2, p. 1, 2019.

[5] L. Wu, L. Zhu, K. Xu, S. Zhou, and C. Y. Zee, "Clinical significance of site-specific metastases in pancreatic cancer: a study based on both clinical trial and real-world data," *Journal of Cancer*, vol. 12, no. 6, pp. 1715–1721, 2021.

[6] M. Elagib, R. Reddy, S. M. Al-Qahtani, N. A. A. Qahtani, and R. S. Raj, "Efficacy of pluronic f-127 gel containing green tea catechin extract on chronic periodontitis – a clinical study," *Tropical Journal of Pharmaceutical Research*, vol. 19, no. 2, pp. 427–432, 2020.

[7] A. R. Broderstad, S. Hansen, and M. Melhus, "The second clinical survey of the population-based study on health and living conditions in regions with sami and norwegian populations – the saminor 2 clinical survey: performing indigenous health research in a multiethnic landscape," *Scandinavian Journal of Public Health*, vol. 47, no. 6, article 1403494819845574-, 2019.

[8] F. Marmé, F. Hilpert, M. Welslau, J. P. Grabowski, and J. Sehouli, "Results of the second interim analysis of c-patrol: a non-interventional study on olaparib within german routine clinical practice," *Gynecologic Oncology*, vol. 154, no. 1, pp. 250-251, 2019.

[9] P. Giannatempo, L. Marandino, D. Raggi, F. Pierantoni, and M. D. Maio, "A multicenter, retrospective study on impact of immunotherapy in urothelial carcinoma with bone metastases (meet-uro01 study)," *Journal of Clinical Oncology*, vol. 39, 6_ suppl, pp. 401–401, 2021.

[10] X. Zhao, B. Huang, J. Ma, H. Chen, C. Wang, and Y. Lu, "Study on influencing factors and mechanisms of electro-assisted chemical conversion on titanium," *Materials Letters*, vol. 250, no. SEP.1, pp. 108–111, 2019.

[11] L. Huang, H. Guo, L. Xiu, and H. Wang, "Efficacy of individualized education in patients with type 2 diabetes mellitus: a randomized clinical study protocol," *Medicine*, vol. 99, no. 50, article e23625, 2020.

[12] F. L. Balci, C. Uras, and S. Feldman, "Clinical factors affecting the therapeutic efficacy of evening primrose oil on mastalgia," *Annals of Surgical Oncology*, vol. 27, no. 12, pp. 4844–4852, 2020.

[13] D. A. Restivo, E. Alfonsi, A. Casabona et al., "A pilot study on the efficacy of transcranial direct current stimulation applied to the pharyngeal motor cortex for dysphagia associated with

Hindawi
Scanning
Volume 2023, Article ID 9862750, 1 page
https://doi.org/10.1155/2023/9862750

Retraction

Retracted: Clinical Characteristics and Mathematical Analysis of Curative Effect of Hemodialysis in Curing Poisoning Caused by Snakebite

Scanning

Received 20 June 2023; Accepted 20 June 2023; Published 21 June 2023

This article has been retracted by Hindawi following an investigation undertaken by the publisher [1]. This investigation has uncovered evidence of one or more of the following indicators of systematic manipulation of the publication process:

(1) Discrepancies in scope

(2) Discrepancies in the description of the research reported

(3) Discrepancies between the availability of data and the research described

(4) Inappropriate citations

(5) Incoherent, meaningless and/or irrelevant content included in the article

(6) Peer-review manipulation

The presence of these indicators undermines our confidence in the integrity of the article's content and we cannot, therefore, vouch for its reliability. Please note that this notice is intended solely to alert readers that the content of this article is unreliable. We have not investigated whether authors were aware of or involved in the systematic manipulation of the publication process.

Wiley and Hindawi regrets that the usual quality checks did not identify these issues before publication and have since put additional measures in place to safeguard research integrity.

We wish to credit our own Research Integrity and Research Publishing teams and anonymous and named external researchers and research integrity experts for contributing to this investigation.

The corresponding author, as the representative of all authors, has been given the opportunity to register their agreement or disagreement to this retraction. We have kept a record of any response received.

References

[1] G. Huang, B. Chen, Y. Luo, L. Chen, S. Wu, and S. Wang, "Clinical Characteristics and Mathematical Analysis of Curative Effect of Hemodialysis in Curing Poisoning Caused by Snakebite," *Scanning*, vol. 2022, Article ID 2312972, 7 pages, 2022.

Hindawi
Scanning
Volume 2022, Article ID 2312972, 7 pages
https://doi.org/10.1155/2022/2312972

Research Article

Clinical Characteristics and Mathematical Analysis of Curative Effect of Hemodialysis in Curing Poisoning Caused by Snakebite

Guoliang Huang,[1] **Bingbing Chen**,[1] **Yi Luo**,[2] **Liming Chen**,[1] **Shaojie Wu**,[1] **and Shijun Wang**[3]

[1]*Department of Emergency Medicine, Emergency Medicine Department of the 910th Hospital of JLSF, Quanzhou Fujian 362000, China*
[2]*Department of Emergency Medicine, Liuzhou Traditional Chinese Medical Hospital, Liuzhou Guangxi 530021, China*
[3]*Fujian Provincial People Hospital, Fuzhou Fujian 350004, China*

Correspondence should be addressed to Shijun Wang; 2013041111@stu.zjhu.edu.cn

Received 26 February 2022; Revised 27 March 2022; Accepted 4 April 2022; Published 6 May 2022

Academic Editor: Danilo Pelusi

In order to explore the clinical characteristics of hemodialysis in curing poisoning from snakebites, a two-classification model of nuclear logistic neural network based on restricted Boltzmann machine is proposed. The model combines kernel logistic regression with artificial neural networks, enabling the model to both learn autonomously and handle linearly inseparable problems. The network first performs feature learning through unsupervised training of restricted Boltzmann machines and obtains the initial values of the parameters to be identified, which reduces the influence of the randomness of the initial parameters. The variable universe learning rate with scaling factor is used to learn the parameters to be identified, and the model convergence speed is improved by dynamic adjustment of the learning rate. Experimental results show the following: Compared with before treatment, patient's activated partial thromboplastin time (APTT) after treatment and the prothrombin time (PT) level decrease, fibrinogen (FIB) levels are elevated, aspartate transferase (AST) and creatine kinase isoenzyme (CK-MB) level decreased, and the differences were statistically significant ($p < 0.05$). It is proved that continuous hemodiafiltration combined with plasma exchange treatment can effectively improve the blood coagulation index and myocardial index of severe snakebite poisoning patients.

1. Introduction

Continuous renal replacement therapy is a method of extracorporeal blood purification based on hemodialysis. CRRT is hemodynamically stable and effectively removes medium and large molecules, improves inflammation, precisely controls the volume load, and adjusts the immune function and other advantages, for severe acute and chronic renal failure and its complications, acute poisoning, and heart failure, and the treatment of critical illnesses such as severe pancreatitis and crush syndrome has opened up new ways [1]. Continuous renal replacement therapy is a process that requires extracorporeal blood circulation, so the formulation of anticoagulation regimen is an important measure to ensure smooth CRRT treatment. Reasonable selection of anticoagulation regimens for blood purification is the key to ensuring and improving the success of continuous renal replacement therapy. Currently available anticoagulation methods for CRRT include the following categories: standard dose unfractionated heparin, regional citrate anticoagulation, low molecular weight heparin and heparinoid, regional heparinized anticoagulation, no anticoagulant, thrombin receptor antagonists, and platelet inhibitors, but no one anticoagulant regimen is suitable for all patients treated with CRRT, and the choice of anticoagula-

tion regimen should be individualized. Among a variety of anticoagulants, heparin is easy to use, economical, easy to monitor, and can antagonize protamine when overdose, it is currently the most widely used anticoagulant for CRRT [2]. Heparin is an anionic sulfated mucopolysaccharide with a molecular weight of 5 kDa to 100 kDa, it forms complexes with antithrombin III in the blood, and the serine proteases of blood coagulation factors I, IX, XI, and XII lead to the rapid inactivation of these factors and plays an anticoagulant effect. The half-life of heparin in the human body is 60 min, the half-life in AKI patients is 40-180 min. The main disadvantage of heparin is that it increases the risk of bleeding and causes heparin-related thrombocytopenia [3]. At present, in the dosage of heparin, the application method and the implementation of the individualized plan are still mainly based on the experience of the clinician, various research reports differ in the dosage and implementation of CRRT heparin anticoagulation.

As a classic research topic in classification problems, neural networks, in recent years, breakthrough research results have been achieved [4]. With a fast learning contrast divergence algorithm proposed by Hinton et al., and successfully applied it to deep belief network (DBN) training, the machine learning industry has set off an upsurge of research on deep learning theories and applications. The basic stacking unit of DBN restricted Boltzmann machine (RBM) is a kind of stochastic neural network and has been extensively studied [5]. Haar et al. gave the Chinese explanation of RBM, and RBM is a kind of unsupervised random neural network with two layers of visible layer and hidden layer without self-feedback and use the fast learning algorithm to unsupervised training the model [6]. Burn et al. proposed a new semisupervised learning algorithm for sentiment classification, and it is called a fuzzy deep belief network. First of all, on the training data, use semisupervised learning methods to train general DBNs, then design a fuzzy membership function, combine the previously trained DBN with the fuzzy membership function to get a new structured fuzzy DBN, and use a supervised learning algorithm to improve the classification accuracy of the model [7]. Wu et al., in order to improve the representation ability and robustness of the RBM model, proposed a new fuzzy restricted Boltzmann machine model. The weight threshold of the model connecting the visible layer and the hidden layer is taken as a fuzzy number [8]. The purpose of this study was to investigate the effect of continuous hemodiafiltration combined with plasma exchange on coagulation indexes and myocardial indexes in patients with severe snakebite poisoning. The results are reported as follows.

2. Nuclear Logistic Neural Network Based on Restricted Boltzmann Machine

Kernel Logistic Neural Network (KLNN) combines the self-learning, self-adapting, and generalization capabilities of artificial neural networks with the processing capabilities of nonlinear features of kernel logistic regression and is superior to general kernels in structure and performance. Logistic regression technology can handle two-class and multiclass problems very well. It uses restricted Boltzmann machine to initialize the parameters of each layer of the network, which reduces the influence of randomness of parameters and avoids the model falling into the local optimum improves the overall classification accuracy of the model [9].

Suppose the input sample data set is $X \in R^{N\times d}$, where N is the number of input samples, and d is the feature dimension of the input sample. In the binary classification, the output vector y is a binary vector, for each sample input, $x_i = [x_1^i, \cdots, x_d^i]^T$, where $i = 1, 2, \cdots, N$ is a row vector of X, its corresponding output $y_i = 1$ or $y_i = 0$. Suppose the number of hidden layer nodes of the neural network is H, and the output node is 1.

The specific functions of each layer for any piece of input data are as follows:

The first layer is the input layer, which mainly receives sample information from the outside and passes the input vector $x_i = [x_1^i, \cdots, x_d^i]$ directly to the next layer. The number of nodes in the input layer is the feature dimension d of the input sample, and the output of this layer is

$$f_i(x_i) = x_i. \tag{1}$$

The second layer is the conversion layer, and in this layer, the kernel function is added to the input sample, that is, each node of this layer is a kernel function, the input variable passed by the input layer is transformed into $K^0 = \varphi(x_i, x_j)$ after kernel transformation, where $x_i = [x_1^i, \cdots, x_d^i]$, $x_j = [x_1^j, \cdots, x_d^j]$, i, $j = 1, 2, \cdots, N$, and $\varphi(x_i, x_j)$ is the conversion function, and $K^0 \in R^{N\times N}$ is the input signal after adding the kernel function, it can be expressed as the following form:

$$K^0 = \begin{bmatrix} k_{11}^0 & k_{12}^0 & \cdots & k_{1N}^0 \\ k_{21}^0 & k_{22}^0 & \cdots & k_{2N}^0 \\ \cdots & \cdots & \cdots & \cdots \\ k_{N1}^0 & k_{N2}^0 & \cdots & k_{NN}^0 \end{bmatrix} = \left[k_1^0, k_2^0, \cdots, k_N^0\right]^T, \tag{2}$$

where $k_i^0 = [k_{i1}^0, k_{i2}^0, \cdots, k_{iN}^0]^T$ is line i of K^0, $i = 1, 2, \cdots, N$. There are many forms of conversion function when selecting, using linear kernel function and Gaussian kernel function.

As the addition of the kernel function makes the structure of the model more complicated, the introduction of high dimensions increases the noise of the data, and in order to reduce the amount of calculation, the principal component analysis (PCA) method is used to reduce the dimensionality of the input sample data of this layer, the first n principal components are selected as the output of the conversion layer [10].

After dimensionality reduction by PCA algorithm, new output sample data $K \in R^{N\times n}$ is obtained, where n is the dimension of the kernel matrix after dimensionality reduction, and the kernel matrix can be expressed as

$$K = \begin{bmatrix} k_{11} & k_{12} & \cdots & k_{1n} \\ k_{21} & k_{22} & \cdots & k_{2n} \\ \cdots & \cdots & \cdots & \cdots \\ k_{N1} & k_{N2} & \cdots & k_{Nn} \end{bmatrix} = [k_1, k_2, \cdots, k_N]^T, \quad (3)$$

where $k_i = [k_{i1}, k_{i2}, \cdots, k_{\text{in}}]^T$ is line i of K, $i = 1, 2, \cdots, N$. The output of this conversion layer can be expressed as

$$f_2(x_i) = PCA\left(\varphi\left(x_i, x_j\right)\right) = k_i. \quad (4)$$

The third layer is the hidden layer, receive the sample information after principal component analysis dimensionality reduction and pass it to the logistic regression layer. Suppose the number of neurons in this layer is H, connection weights and thresholds are ω_h, and $\theta, \omega_h \in R^{n\times H}$, is a matrix of $n \times H$, $\theta \in R^{H\times 1}$, is a vector of $H \times 1$. Enter the value $k_i = [k_{i1}, \cdots, k_{\text{in}}]^T$, $i = 1, 2, \cdots, N$, for each sample of this layer, and the corresponding output value G_i is expressed as

$$G_i = \sigma\left(\theta + \sum_{j=1}^{n} \omega_{jh} \cdot k_{ij}\right) = \sigma\left(\theta + \omega_h^T \cdot k_i\right). \quad (5)$$

For the activation function of the hidden layer, we take the Sigmoid function, and the output value of the $\sigma(u) = 1/1 + e^{-u}$ hidden layer can be expressed as

$$f_3(k_i) = G_i = \frac{1}{1 + e^{-\left(\theta + \omega_h^T \cdot k_i\right)}}. \quad (6)$$

The fourth layer is the logistic regression layer, and the logistic function is used to calculate the output information of the hidden layer. The input information of this layer is a vector G_i of $H \times 1$, the logistic regression parameter and threshold are β, α, respectively. Where $\beta \in R^{H\times 1}$ is a column vector of $H \times 1$, and θ is a constant. For two classifications, the probability formula for $y_i = 1$ can be obtained, that is, the logistic function:

$$\begin{aligned} P_i = P_i(y_i = 1) &= \sigma\left(\alpha + \sum_{h=1}^{H} \beta_h \cdot \sigma(\theta + \omega_h \cdot k_i)\right) \\ &= \sigma\left(\alpha + \sum_{h=1}^{H} \beta_h \cdot G_i\right) \end{aligned} \quad (7)$$

From this, the probability formula for $y_i = 0$ can also be obtained:

$$P_i(y_i = 0) = 1 - P_i(y_i = 1) = 1 - \sigma\left(\alpha + \sum_{h=1}^{H} \beta_h \cdot G_i\right). \quad (8)$$

For formula (7), take $\sigma(u) = 1/1 + e^{-u}$, so the output value of the logistic regression layer can be expressed as

$$\begin{aligned} f_4 = P_i &= \sigma\left(\alpha + \sum_{h=1}^{H} \beta_h \cdot \sigma(\theta + \omega_h \cdot k_1)\right) \\ &= \sigma\left(\alpha + \sum_{h=1}^{H} \beta_h \cdot G_i\right) = \frac{e^{\beta^T \cdot G_i + \alpha}}{1 + e^{\beta^T \cdot G_i + \alpha}}. \end{aligned} \quad (9)$$

The fifth layer is the output layer, and the output of the binary classification can be defined as

$$f_5 = y_i = \begin{cases} 1, \text{if} & P_i \geq 0.5, \\ 0, \text{if} & P_i < 0.5. \end{cases} \quad (10)$$

It can be seen from the binary classification model of the nuclear logistic neural network that the parameters that need to be optimized are the connection weight ω_h and threshold θ of the hidden layer and the regression parameter β and threshold α of the logistic regression layer. The following explains how to identify the parameters of the model. The KLNN-RBM learning algorithm is proposed to identify the parameters of the nuclear logistic neural network. The basic process of the algorithm is as follows: The restricted Boltzmann machine is used for unsupervised training of the initial weights and thresholds of the nuclear logistic neural network regression model, get the optimal initial value of the model parameters, and add the ridge regression regularization factor to the log-likelihood function in the logistic regression layer to estimate the maximum likelihood. On this basis, we use the stochastic gradient descent method with variable universe expansion factor to train the model parameters, by dynamically adjusting the learning rate to change the speed of training, improving the overall classification accuracy of the model [11].

3. Simulation Experiment

We selected 30 cases of severe snakebite poisoning patients who were admitted to a hospital from January 2019 to October 2020 and all meet the selection criteria: (1) inclusion criteria were as follows: ① meet the diagnostic criteria for severe snakebite poisoning; ② all were admitted to the hospital for treatment within 48 hours after being bitten; ③ this study was approved by the medical ethics committee, and the patient was informed of this study and signed a consent form; and ④ there is no contraindication to treatment. (2) exclusion criteria were as follows: ① patients with other blood system diseases; ② patients with damage to the heart, liver, and other organs; and ③ patients with coagulation dysfunction. Among the 30 patients, there were 17 males and 13 females; age ranged from 28 to 52 years old, with an average of39.69 ± 7.03years old. Snake species are as follows: 10 cases were bitten by Bamboo Leaf Green snake, 9 cases were bitten by silver ring snake, and 9 cases were bitten by cobra 11 cases; bite site is as follows: 11 cases of hand and arm, 13 cases of foot, and 6 cases of lower extremity. The local area of the bite was markedly swollen, and ecchymosis was visible under the skin, and the pain was severe. The data collected for each sample covers 19 physiological indicators,

such as the patient's gender, age, creatinine, albumin, hemoglobin, and survival time, and among them, the gender of the patient, whether the circulatory system has heart failure, whether the digestive system has nausea and vomiting, whether there is edema in the urinary system, whether the endocrine system suffers from diabetic nephropathy, six indicators, such as whether the nervous system suffers from uremic encephalopathy, are binary data, and the other 13 indicators are numerical data [12].

3.1. Conventional Treatment. After the patient was admitted to the hospital, the wound exudate, blood, etc. were detected by enzyme-linked immunosorbent assay from the patients who were bitten by an unknown species of snake to confirm the specie of the venomous snake. At the same time, conventional treatment was given, the wound was swollen and compressed with a bandage, the wound was debridement locally, and the corresponding antivenom serum was injected according to the type of venomous snake to stop bleeding, infection, etc. and the patient was instructed to keep quiet and not to panic to prevent the spread of the venom [13].

3.2. Continuous Hemodiafiltration Combined with Plasma Exchange Therapy

3.2.1. Plasma Exchange Treatment. For the application of plasma separator, use indwelling internal jugular vein or femoral vein catheter to establish vascular access and aseptically install extracorporeal circulation pipelines and plasma separators as required. First, flush the pipeline with saline, then rinse with 0.2 g/L heparin saline, and when the blood flow rate is 120 ml/min, choose 2500~3000 ml of fresh plasma and human albumin solution as the replacement fluid, replace once every 2.5 to 3 hours and once a day.

3.2.2. Continuous Hemodiafiltration Treatment. For continuous hemodiafiltration treatment, use the hemodialysis machine, select the continuous venous hemodiafiltration mode, establish a vascular access in the patient's central venous catheter, control the blood flow rate to 180 ml/min, adjust the temperature of the dialysate to 35~35.5°C, while drawing blood, instill 150 ml and 50% glucose solution at 20-30 drops/min. Decide whether to pump heparin for anticoagulation treatment according to the patient's condition, hemodiafiltration was performed 1 to 2 times, and each treatment was performed for 24 to 48 hours. After treatment, the patient's condition was stable and his vital signs were normal [14].

Since the collected sample data contains more indicator information, how to determine the key indicators that affect the relationship between dialysis timing and patient survival time, it is the main problem that needs to be solved. The proposed nuclear logistic neural network model based on the restricted Boltzmann machine analyzes the modeling data, and the classification results are used to mine the index variables used to establish the hemodialysis evaluation model. This section uses the training data set from 2019 to 2020 for analysis. The main input variables considered included patient's gender (Gen), patient's age at first dialysis (age), creatinine (Scr), albumin (Alb), urea (BUN), hemoglobin (Hb), serum phosphorus (P), serum potassium (K), heart failure (HF), diabetes (DM), nausea and vomiting (DIG), edema (URI), and uremic encephalopathy (NEU). The main consideration is based on the first 5 attributes, find the best combination of variables that affect the timing of hemodialysis. The output index is the survival time of the patient from the first dialysis, it is measured on a monthly basis. Figures 1–4, respectively, show the distribution line graphs of 4 numerical indicators [4, 15–17].

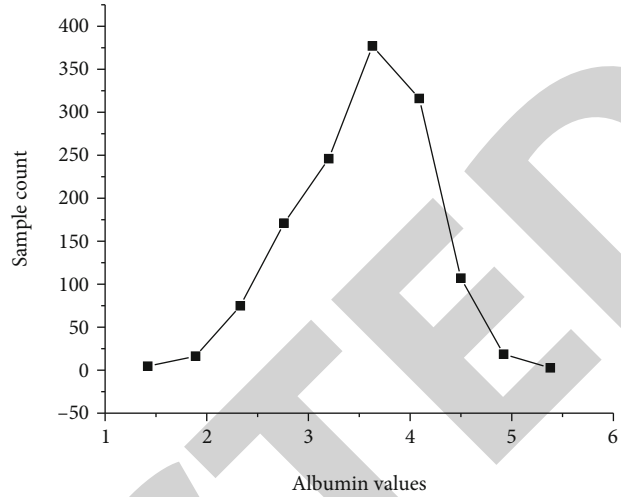

Figure 1: Line chart of the distribution of albumin index.

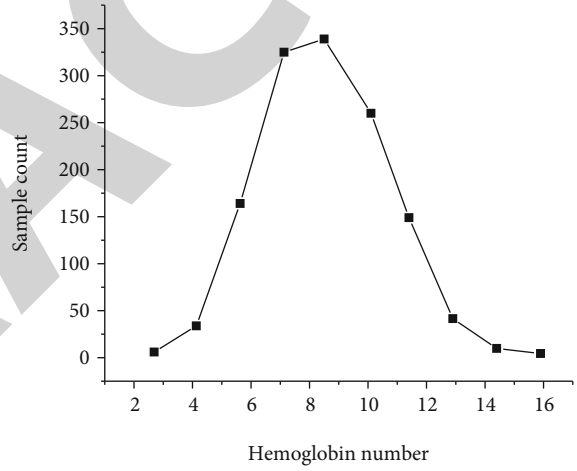

Figure 2: Line chart of the distribution of leucin indicators.

4. Results and Analysis

4.1. Comparison of Coagulation Indexes before and after Treatment. Compared with before treatment, the APTT and PT levels of patients after treatment are reduced, FIB levels increased, and the differences were statistically significant ($p < 0.05$). See Table 1.

4.2. Comparison of Myocardial Indexes before and after Treatment. Compared with before treatment, the AST and CK-MB levels of the patients after treatment decreased,

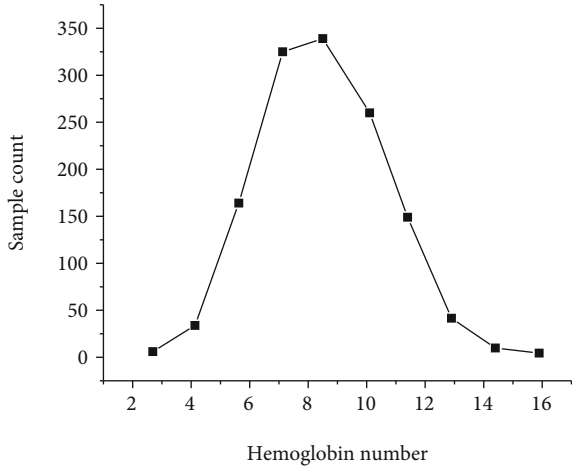

Figure 3: Broken line chart of the age distribution of patients on dialysis.

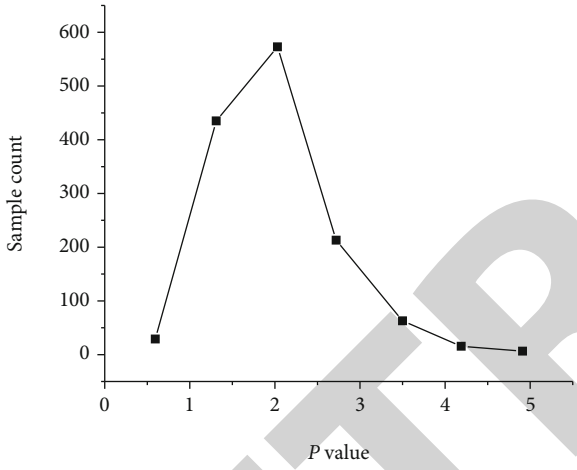

Figure 4: Line chart of the distribution of blood phosphorus indicators.

Table 1: Comparison of coagulation indexes before and after treatment.

Project	APTT	FIB	PT
Before therapy	44.67 ± 3.55	0.91 ± 0.46	18.29 ± 3.44
After treatment	29.61 ± 2.44	3.20 ± 0.68	10.06 ± 1.15
t value	30.953	15.724	21.040
p value	$p \leq 0.001$	$p \leq 0.001$	$p \leq 0.001$

and the difference was statistically significant (all $p < 0.05$). See Table 2.

5. Discussion

There are many kinds of snakes, cobras, green bamboo leaves, etc. are all common species; therefore, epidemiology shows that the fatality rate and disability rate of poisonous

Table 2: Comparison of myocardial indexes before and after treatment.

Project	AST	CK-MB
Before therapy	70.95 ± 12.58	49.49 ± 10.27
After treatment	21.52 ± 2.43	18.57 ± 2.63
t value	32.247	24.625
p value	$p \leq 0.001$	$p \leq 0.001$

snakebites are relatively high. Due to the large molecular proteins contained in snake venom, toxic substances such as small peptides quickly enter the bloodstream and can cause symptoms of systemic poisoning, and if not treated in time, it can cause damage to human liver and kidney function, even life-threatening. At present, the main principle of treating snakebite is to block the spread of snake venom in the body, to eliminate its harmful toxins, and to protect the function of important organs. Studies have shown that early treatment measures can effectively save the lives of patients.

The liver is the main organ for the body to synthesize blood clotting factors, and it plays a role in maintaining balance in the coagulation and anticoagulation system. After being bitten by a poisonous snake, snake venom entering the body can cause severe symptoms of poisoning, lead to damage to liver function, which in turn leads to a decrease in coagulation factors, abnormal blood clotting function. Clinical detection of elevated levels of AST and CK-MB indicators indicates that there is damage to liver cells or cardiomyocytes, so it is of great significance to detect coagulation indicators and myocardial indicators in patients with snakebite. The results of this study showed that compared with before treatment, the levels of APTT, PT, AST, and CK-MB in patients after treatment were decreased, and the level of FIB was increased, suggesting that continuous hemodiafiltration combined with plasma exchange therapy can effectively improve severe snakebite. Coagulation indexes and myocardial indexes of patients with trauma and poisoning analyze the reasons and believe that plasma exchange is a kind of extracorporeal circulation blood purification therapy, and its working principle is by drawing the patient's whole blood out of the body, separate plasma and cell components, discard the patient's plasma, then replace fresh plasma, albumin, and other substitutes at the same speed, back into the body, ultimately achieve the purpose of reducing disease damage. Since snake toxin enters the body, it can be combined with protein, blood lipids, etc. or dissolved in the plasma; plasma exchange can remove the poisonous substances from snake venom in the body in time, and at the same time, supplementation of coagulation factors can quickly play a role in the body, and the earlier the treatment, the more obvious the effect, conducive to improve the success rate of rescue and improve the clinical symptoms of patients bitten by poisonous snakes. Plasma exchange is used to treat venomous snakebites and can quickly remove toxins, improve the patient's blood hypercoagulability state, and improve the success rate of treatment. And the incidence of plasma exchange complications is relatively small,

common complications are mainly related to abnormalities in the patient's cardiopulmonary bypass, and fresh plasma is not related to factors such as discomfort and it can cause adverse reactions such as infection, bleeding, and hypotension [18]. Continuous hemodiafiltration can effectively maintain the body's water and electrolyte stability, remove toxins in the circulation, improve the nutritional status of patients, and facilitate the restoration of damaged cells; at the same time, it can promote hemodynamic stability and it is beneficial to maintain the body environment, to promote the recovery of patients and improve the survival rate [19]. Continuous hemodiafiltration combined with plasma exchange in the treatment of severe snakebite patients can play a synergistic effect, alleviate the insufficiency of single treatment, effectively remove snake toxins, improve blood coagulation and myocardial indicators, improve the success rate of treatment, and reduce the risk of death of patients. However, due to the small sample size, this study has certain limitations, and it is necessary to further increase the sample size to demonstrate the feasibility of this treatment plan.

6. Conclusion

A two-classification model and a multiclassification model of nuclear logistic neural network based on restricted Boltzmann machine are proposed. In the binary classification model of the nuclear logistic neural network, the input data is mapped from the low-dimensional feature space to the high-dimensional through a kernel function, solve the linear inseparability problem, and through principal component analysis to reduce the dimensionality of the data, avoid the amount of calculation caused by nuclear transformation. The network initializes the weights and thresholds of each layer through unsupervised learning RBM, it greatly improves the classification accuracy of the overall model; to reduce the influence of random parameters, the log-likelihood function with ridge regression regular term is used as the objective function for maximum likelihood estimation, and redundant features are eliminated to avoid overfitting. In snakebite, in addition to the acute renal failure caused by dialysis treatment, other system damage using dialysis treatment has not been reported, and the mechanism is unknown. In this group of cases, there were complications, such as respiratory failure, shock, heart failure, and renal failure, all of which were cured after conventional treatment. Therefore, we believe that dialysis has a definite effect on snakebite.

Data Availability

The data used to support the findings of this study are available from the corresponding author upon request.

Conflicts of Interest

The authors declare that they have no conflicts of interest.

References

[1] Y. C. Yavuz, Z. Biyik, D. Ozkul, S. Abusoglu, and L. Altintepe, "Association of depressive symptoms with 25 (OH) vitamin D in hemodialysis patients and effect of gender," *Clinical and Experimental Nephrology*, vol. 24, no. 2–3, pp. 1–10, 2019.

[2] Y. Zhao, Q. Liu, and J. Ji, "The prevalence of frailty in patients on hemodialysis: a systematic review and meta-analysis," *International Urology and Nephrology*, vol. 52, no. 1, pp. 115–120, 2020.

[3] H. Wang, J. Rong, C. Song et al., "Hemodialysis and risk of acute pancreatitis: a systematic review and meta- analysis," *Pancreatology*, vol. 21, no. 1, pp. 89–94, 2021.

[4] T. Hiyama, Y. Harada, and Y. Kiuchi, "Clinical characteristics and efficacy of methotrexate in japanese patients with noninfectious scleritis," *Japanese Journal of Ophthalmology*, vol. 65, no. 1, pp. 97–106, 2021.

[5] Y. H. Song, S. Y. Wang, J. H. Lang, Y. F. Xiao, and X. M. Chen, "Therapeutic effect of intravenous sodium thiosulfate for uremic pruritus in hemodialysis patients," *Renal Failure*, vol. 42, no. 1, pp. 987–993, 2020.

[6] N. Haar, C. Eijkelboom, L. Cantarini, R. Papa, and M. Gattorno, "Clinical characteristics and genetic analyses of 187 patients with undefined autoinflammatory diseases," *Annals of the Rheumatic Diseases*, vol. 78, no. 10, pp. 1405–1411, 2019.

[7] J. Burn, A. J. Sims, H. Patrick, L. G. Heaney, and R. M. Niven, "Efficacy and safety of bronchial thermoplasty in clinical practice: a prospective, longitudinal, cohort study using evidence from the UK Severe Asthma Registry," *BMJ Open*, vol. 9, no. 6, article e026742, 2019.

[8] C. Wu, L. Guo, L. Wang, J. Li, C. Wang, and D. Song, "Associations between short-term efficacy and clinical characteristics of infantile hemangioma treated by propranolol," *Medicine*, vol. 98, no. 6, article e14346, 2019.

[9] Y. Uemura, K. Takemoto, M. Koyasu et al., "Clinical outcomes of rotational atherectomy in severely calcified in-stent restenosis: a single-center, retrospective study," *Nagoya Journal of Medical Science*, vol. 81, no. 2, pp. 313–323, 2019.

[10] F. S. Shoshtari, S. Biranvand, L. Rezaei, N. Salari, and N. Aghaei, "The impact of hemodialysis on retinal and choroidal thickness in patients with chronic renal failure," *International Ophthalmology*, vol. 41, no. 5, pp. 1763–1771, 2021.

[11] J. Wu, J. Li, G. Zhu et al., "Clinical features of maintenance hemodialysis patients with 2019 novel coronavirus-infected pneumonia in Wuhan, China," *Clinical Journal of the American Society of Nephrology*, vol. 15, no. 8, pp. 1139–1145, 2020.

[12] J. Radford, B. Kahl, M. Hamadani, C. Carlo-Stella, and P. Caimi, "Analysis of efficacy and safety of loncastuximab tesirine (adct-402) by demographic and clinical characteristics in relapsed/refractory diffuse large b-cell lymphoma," *Hematological Oncology*, vol. 37, no. S2, pp. 93–95, 2019.

[13] G. Shi, B. Kaffenberger, Y. Semenov, J. Choi, and S. Kwatra, "468 clinical characteristics, etiology, and treatment of erythema multiforme at a tertiary care center," *Journal of Investigative Dermatology*, vol. 140, no. 7, p. S62, 2020.

[14] N. Y. Pshenichnaya, V. A. Bulgakova, N. I. Lvov, A. A. Poromov, and I. A. Leneva, "Clinical efficacy of umifenovir in influenza and ARVI (study ARBITR)," *Terapevticheskii arkhiv*, vol. 91, no. 3, pp. 56–63, 2019.

[15] Y. Wu, Q. Chen, K. Chen et al., "Clinical efficacy of ultrasound-guided injection in the treatment of olecranon

Hindawi
Scanning
Volume 2023, Article ID 9765738, 1 page
https://doi.org/10.1155/2023/9765738

WILEY | Hindawi

Retraction

Retracted: Effect of Rehabilitation Training Based on Automatic Extraction Algorithm on Knee Anterior Cruciate Ligament Injury Caused by Exercise

Scanning

Received 20 June 2023; Accepted 20 June 2023; Published 21 June 2023

This article has been retracted by Hindawi following an investigation undertaken by the publisher [1]. This investigation has uncovered evidence of one or more of the following indicators of systematic manipulation of the publication process:

(1) Discrepancies in scope

(2) Discrepancies in the description of the research reported

(3) Discrepancies between the availability of data and the research described

(4) Inappropriate citations

(5) Incoherent, meaningless and/or irrelevant content included in the article

(6) Peer-review manipulation

The presence of these indicators undermines our confidence in the integrity of the article's content and we cannot, therefore, vouch for its reliability. Please note that this notice is intended solely to alert readers that the content of this article is unreliable. We have not investigated whether authors were aware of or involved in the systematic manipulation of the publication process.

In addition, our investigation has also shown that one or more of the following human-subject reporting requirements has not been met in this article: ethical approval by an Institutional Review Board (IRB) committee or equivalent, patient/participant consent to participate, and/or agreement to publish patient/participant details (where relevant).

Wiley and Hindawi regrets that the usual quality checks did not identify these issues before publication and have since put additional measures in place to safeguard research integrity.

We wish to credit our own Research Integrity and Research Publishing teams and anonymous and named external researchers and research integrity experts for contributing to this investigation.

The corresponding author, as the representative of all authors, has been given the opportunity to register their agreement or disagreement to this retraction. We have kept a record of any response received.

References

[1] S. Zhu and J. Gao, "Effect of Rehabilitation Training Based on Automatic Extraction Algorithm on Knee Anterior Cruciate Ligament Injury Caused by Exercise," *Scanning*, vol. 2022, Article ID 8304071, 7 pages, 2022.

Hindawi
Scanning
Volume 2022, Article ID 8304071, 7 pages
https://doi.org/10.1155/2022/8304071

Research Article

Effect of Rehabilitation Training Based on Automatic Extraction Algorithm on Knee Anterior Cruciate Ligament Injury Caused by Exercise

Sibo Zhu and Jie Gao

China Swimming College, Beijing Sport University, Beijing 100084, China

Correspondence should be addressed to Jie Gao; 1621040596@stu.cpu.edu.cn

Received 23 February 2022; Revised 25 March 2022; Accepted 2 April 2022; Published 2 May 2022

Academic Editor: Danilo Pelusi

Objective. In order to explore the effect of rehabilitation training based on automatic extraction algorithm on knee anterior cruciate ligament reconstruction under arthroscopy.*Methods*. 81 patients with anterior cruciate ligament injury were randomly divided into observation group (42 cases) and control group (39 cases). The control group was given routine nursing, while the observation group was given rehabilitation training guidance based on automatic extraction algorithm. Lysholm score, HSS score, and range of motion of knee joint extension and flexion were used to evaluate the knee joint function before and after operation in the two groups. The quality of life of the two groups was evaluated by the concise health survey scale. The results showed that 50% of deep venous thrombosis occurred on the first day and 30% on the second day after operation. There was no significant difference in preoperative Lysholm score, HSS score, and knee flexion activity between the observation group and the control group ($P > 0.01$). After 1-month, 5-month, and 1-year follow-up, the effective rate of knee function recovery in the observation group was significantly better than that in the control group. Lysholm score, HSS score, and knee extension and flexion activity were significantly different from those in the control group ($P < 0.01$). The postoperative SF-36 quality of life score of the observation group was significantly higher than that of the control group, indicating that the quality of life of the observation group was significantly better than that of the control group. Therefore, early postoperative rehabilitation training guidance based on automatic extraction algorithm can improve local blood circulation and improve knee function and reduce pain, so as to promote the early recovery of patients.

1. Introduction

Anterior cruciate ligament (ACL) injury is a common and serious knee joint sports injury, which is a common disease in the field of sports and rehabilitation medicine. If not treated properly, it will easily lead to knee joint instability, articular cartilage, and meniscus injury and even secondary osteoarthritis, which will seriously affect the functional activities of the knee joint and significantly reduce the quality of life of patients [1, 2]. At present, arthroscopic anterior cruciate ligament (ACL) reconstruction is the preferred method to improve the instability of the knee joint after anterior cruciate ligament rupture. This technique can accurately restore the stability of the knee joint. It has the advantages of less trauma, shorter operation duration, and faster postoperative recovery. Effective rehabilitation training after surgery can further consolidate the surgical effect and promote the recovery of patient knee function, but irregular functional exercise will lead to ligament relaxation or elongated ligament after reconstruction or even rupture, so that the ligament cannot play its due function and directly affect the surgical effect [3, 4].

Anterior cruciate ligament injury occurs in children, adolescents, and adults. Once the ligament injury occurs, the knee joint function will be lost, resulting in instability of knee joint straight and rotation [5]. Arthroscopic ACL reconstruction has become the standard operation to repair the injured ligament and restore the knee joint activity [6].

However, ACL reconstruction can easily lead to muscle atrophy around the joint and severe cases complicated with joint stiffness, thus losing the opportunity of knee joint function recovery. Early postoperative knee function exercise is conducive to the recovery of knee joint function [7]. Compared with patients' independent functional exercise, joint loosening and continuous passive movement (CPM) can simulate the natural movement of the human body to make the continuous passive movement of the affected limb and accelerate the recovery of articular cartilage and surrounding tissues. Hadzovic et al.'s study determines the effect of exercise regimen on preventing injury to knee hip ligaments and knee ligaments in young female basketball players. To collect existing studies on the impact of the research prevention program on ACL damage prevention by young female basketball players, the following electronic databases were searched: PubMed, Scindeks, Pedro, J-Gate, Doaj, and Google Scholar. The analyzed study was published from 2003 to 2018, and the participants were young women's basketball players. According to the results of this study, the most commonly used training program is the neuromuscular program, whose structure includes several types of exercises and represents a combination of core strengthening exercises, strengthening lower limb muscles, agility exercises, flexibility exercises, and balancing exercises. Finally, the application of knee injury training programs leads to motor balance, sustained capacity balance, balance, flexibility, and biomechanical capabilities associated with ACL injury, thereby improving motor performance among female basketball players [8].

Based on this study, 81 patients with arthroscopy were randomly selected and a control study was conducted. Rehabilitation training guidance based on automatic extraction algorithm and control study were performed, and the effect was satisfactory. It is now reported as follows.

2. Research Methods

2.1. General Information. 81 patients with anterior cruciate ligament reconstruction under arthroscopy in a hospital were randomly selected as the research objects. Inclusion criteria are as follows: the patients had clear consciousness and had certain language communication ability. There was no history of drug dependence and mental illness. No serious complications such as heart, liver, and kidney were found. Informed consent was obtained from all participants [9]. There were 59 males and 22 females. The average age was 56.3 years (range, 14~72 years). Education level: 4 cases were illiterate, 7 cases were primary school, 45 cases were junior high school, 17 cases were senior high school (technical secondary school), and 8 cases were junior college or above. Marital status: 73 cases were married, 1 case was widowed, and 7 cases were divorced. Occupation is as follows: 46 workers, 21 farmers, and 14 cadres. The location of disease is as follows: left knee 48 cases and right knee 33 cases. The causes of injury are as follows: traffic injury in 39 cases, falling injury in 21 cases, and sports injury in 21 cases. There were 60 cases of simple anterior cruciate ligament injury, and there were 21 cases with joint injuries of medial meniscus, posterior cruciate ligament, medial collateral ligament, and lateral collateral ligament. There were 49 cases of acute injury and 32 cases of old injury. Clinical manifestations are as follows: knee joint swelling and pain with limited movement in patients with acute injury. Chronic injuries included knee pain, claudication, quadriceps atrophy, and limb weakness. The average length of stay was 8 ± 05 days. The course of disease was 3-67.5 days (21 ± 8 days). The selected cases were randomly divided into the observation group and control group, 42 cases in the observation group and 39 cases in the control group. There was no significant difference in age, gender, occupation, education level, lesion site, course of disease, operation method, and length of hospital stay between the two groups ($P > 0.05$). This clinical trial was approved by the ethics committee of our hospital.

2.2. Method

2.2.1. The Control Group Was Given Routine Nursing Care after Arthroscopic Anterior Cruciate Ligament Reconstruction. After the operation, the patient was not fully awake before the occipital supine position was removed, and the knee joint was elevated by 30 cm in the straight position, which was conducive to venous reflux and alleviating limb swelling, and the anterior cruciate ligament after transplantation was in the relaxation state with the minimum tension, so as to prevent the graft from shifting in the bone marrow tract; Elastic bandage was used to compress the knee joint, and sandbag was used to compress the knee joint; The vital signs, condition changes, sensory and motor function of the affected limbs, blood leakage of wound dressing, and quality and quantity of drainage fluid in wound cavity were closely observed; The self-made ice bag was used to completely close and cover the whole knee joint, and the ice compress lasted for 48-72 hours to achieve the effect of detumescence, hemostasis and pain relief. Targeted and personalized psychological care, diet guidance, symptomatic pain relief, health education, and functional exercise guidance were given [10].

2.2.2. On the Basis of Routine Nursing in the Control Group, the Observation Group Was Given Rehabilitation Training Guidance Based on Automatic Extraction Algorithm. The first stage was 1 day to 2 weeks after operation. The patients were instructed to perform systematic functional exercises according to ABCDE on the same day after operation. The purpose of functional exercise at this stage is to relax and contract muscles, promote blood circulation of lower limbs, reduce swelling of limbs, avoid deep venous thrombosis of lower limbs, and prevent adhesion and muscle atrophy. ① Patella pushing: on the first day after the operation, the patients were pushed up and down in four directions, and ice was applied for 10 minutes immediately after the activity, once a day for 3 days. ② Isometric contraction of quadriceps femoris is as follows: thigh muscle group contraction and patella upward lifting, 10 seconds each time, 10 times in each group, 6-7 groups per day. In order to make the muscles strong, sandbags can be added 10 cm above the patella. ③ Hamstring isometric contraction is as follows: toe down and heel down, lift the thigh slightly, 10 seconds each time,

10 times in each group, 6-8 groups per day. ④ Straight leg raising: the knee joint should be straightened and lifted 10~15 cm away from the bed surface, 3 groups a day, 10 times in each group, 10 seconds each time, to strengthen the stability of the knee joint. ⑤ Assisted knee flexion (closed chain exercise): hold 10 cm above the knee with both hands, lift it up slowly, and slide the heel slowly backward along the bed, gradually increasing from 15° to 30°, 45° to 60°, and 75° to 90°. Patients can reach 90° at 2 weeks after operation and then maintain 90° until 4 weeks after operation. In addition, continuous passive exercise (CPM) was given twice a day from 1 week after operation. The initial degree of CPM was 30° and increased by 5° to 10° every day. The exercise lasted for 30 minutes each time and was adjusted according to the patient's complaint.

The second stage was 2-4 weeks after operation. Continue to strengthen the muscle strength training of the first stage and gradually increase the weight-bearing walking training and further strengthen the muscle strength exercise of the affected limb and the active flexion and extension of the knee joint: walk on the ground with the toe tip, walk on crutches 2 weeks after the operation, and step forward with the crutches on the same line with the toes to keep up with the healthy legs. Three weeks after the operation, walk on crutches on the ground, and the affected leg should step forward and land on the sole of the foot. At the same time, double crutches should be placed in the same line with the toes, and the healthy legs should keep up with them.

The third stage was 4-6 weeks after operation. The purpose is to enhance the ability of knee joint motion control and strengthen various functional training. The range of motion of passive flexion and extension of joint should be 0° to 140°, and that of active knee joint should be 0° to 120°, in order to take off the crutch to walk, but should pay attention to avoid violent exercise and "stop and turn" and other actions. ① Walking gait practice: strengthen the lower limb muscle strength. From 4 to 6 weeks after surgery, gait training was strengthened to start walking under excessive double abduction protection to single abduction protection to 6 weeks after surgery, and the unbranch device walked normally. ② Stand against the wall: practice around the operation. The body stands against the wall, legs should be apart from shoulder-wide, and the tip becomes warped, 10 seconds per time, 10 times per group, 3 to 5 groups per day. ③ Squats against the wall: start exercising 4 weeks after surgery. The body should be against the wall, legs, and shoulder width, and the angle gradually increased (15, 30, 45, 60, 75, and 90); slowly slide down the calf to keep parallel to the wall, each action for 10 seconds, 10 times per group, 3 groups a day. ④ Up and down stair practice: practice up and down steps starting 5 weeks after the operation. When up the steps legs first, the bottom stable, knee straight after the leg up. When down the step, the leg first, heel steady, knee straight leg down. Each group lasted 10 times until the gait was normal and the activity stopped freely. ⑤ Arch step transfer: practice began 6 weeks after surgery. Angle gradually increased, with patient tolerance. Each was kept for 10 to 30 s, 10 each, 5 groups per day. So far, patients can work and live normally, and 8 weeks after practice fast walk, patients can walk in the swimming pool and can practice power bike, at 12 weeks, patients can practice jogging, rope skipping, and other activities and later gradually restore functional activities but should pay attention to avoid strenuous exercise and "emergency stop sharp turn" and other actions.

2.3. Rehabilitation Training Methods. Each kind of rehabilitation exercise is carried out under the supervision of professionals trained in rehabilitation medicine knowledge. The control group received routine rehabilitation training, including the following: (1) moderate joint range of motion training (2) According to the recovery of patients, different courses were carried out.

The specific method is as follows: straighten the legs, then straighten the knee joint, and then exercise the quadriceps femoris. When reaching the apex, keep relaxing for a few seconds and then continue to repeat after 10~30 seconds, four groups of actions per day. In addition to routine rehabilitation training, the study group completed proprioception training, including the following: (1) straight leg lift, side leg lift, and back leg lift training. Straight leg raising exercise: fully extend the leg and raise the heel to 15 cm away from the bed, and keep it until exhausted,10 times/group, 2~3 groups/d. Side leg lifting exercise: lying on the side, the abduction angle of the affected thigh is 45° and maintained until exhaustion, 10 times/group, 2-4 groups/D, 30 s rest between groups. Back leg raising exercise: in prone position, the affected leg is straightened and lifted backward until the toe is 5 cm away from the bed surface, 20 times/group, 2-3 groups/D, with 30 s rest between groups. (2) Adjust the function of knee joint, move under the protection of brace, and carry out static squat exercise against the wall under the protection of brace. Practice method is as follows: back against the wall, feet apart, shoulder width, gradually forward, and the body center of gravity forms a distance of about 40~50 cm. At this point, the body has shown a squat posture, so that the long axis of the lower leg is perpendicular to the ground. The angle between thigh and calf should not be less than 90 degrees. According to the action essentials, squat quietly until the pain and swelling around the knee joint, rest for 30 s, and then squat again. Repeat for 30 minutes. The number of static squat exercises against the wall is 1~3 times/d.

2.4. Automatic Extraction Algorithm of the Anterior Cruciate Ligament of the Knee Joint. The key to the automatic extraction of the ACL of the knee is the need to identify the cavity surface triangular slices from the three-dimensional model data of the knee. The extraction process can be summarized as follows: first, a triangular sheet of the cavity boundary surface on the femur and the tibia is selected as seeds, and the lower end surface of the femur and the upper end surface of the tibia are initially extracted using regional growth method; then, the holes on the two boundary surfaces are automatically detected, these holes are repaired, and finally, the surface edges are photoed smoothly.

2.4.1. The Intersection of the Normal Line and the Triangular Face Sheet Is Calculated. The intersection between the normal and adjacent anatomical structures is the condition for the selection of the seed, so the intersection of the normal triangular plane is calculated. This paper uses the method proposed by Moller and Trumbore to represent the vector as a basis point and directional vector as shown in formula (1):

$$L(t) = P + t\vec{d}. \quad (1)$$

A spatial triangle is simply defined as an ordered array of vertices $\{V_0, V_1, V_2\}$.

For any point Q within the triangle, we can represent the relative position of this point relative to the three vertices of the triangle as shown in Equation (2):

$$Q_{u,v,w} = wV_0 + uV_1 + vV_2. \quad (2)$$

Among these, $u + v + w = 1$. Triples (u, v, w) are called the center of gravity coordinates of Q, which can represent all points of the plane where the triangle lies, but at least one point outside the triangle is a negative number. Because $w = 1 - (u + v)$, we represent (u, v). By substituting Equation (1) into Equation (2), the intersection of the normal lines and the triangles is calculated as shown in the formula (3):

$$P + td = (1 - (u + v))V_0 + uV_1 + vV_2. \quad (3)$$

This formula can be extended as shown in formula (4):

$$[-dV_1 - V_0V_2 - V_0]\begin{bmatrix} t \\ u \\ v \end{bmatrix} = [p - V_0]. \quad (4)$$

After obtaining t, u, and v by formula above, we can determine whether the intersection Q of the normal and the triangle plane falls within the triangle (not elsewhere where the triangle is): if 0 u 1, 0 < v and v 1 and $u + v$ 1, the intersection Q falls within the triangle; otherwise, it is on the plane of the triangle, but outside the triangle.

2.5. Evaluation Method. Knee joint function score and Lysholm score were used to compare the knee joint function before and after operation. The extension and flexion range of motion was compared between the two groups before and after operation; SF-36 was used to compare the quality of life between the two groups. The knee joint percentage score system is the "gold standard" for the evaluation of knee joint function. The main contents of the study are as follows: extension and deficiency, whether brace is needed or not, and the degree of varus deformity. Among them, 6 items were scored items. The lighter the symptom was, the higher the score of each item was. The full score was 100 points. The higher the score, the better the functional rehabilitation.

2.5.1. Lysholm Score of Knee Joint. As shown in Table 1, concise health survey scale is widely used to measure the quality of life of general population. There are 36 items divided into 8 dimensions: physiological function, including 10 items: measuring whether health status hinders normal physiological activities; physiological function, including 4 items: measurement caused by physiological health problems, including 2 items: Measure the degree of pain and the effect of pain on daily activities; overall health, including five items: individual evaluation of their own health status and its development trend; vitality, including four items: measuring the subjective feelings of individuals on their own energy and fatigue; social function, including two items: measuring the impact of physical and mental health problems on the quantity and quality of social activities; emotion, including three items: measuring the limitation of functions caused by emotional problems; and mental health, including 5 items: measuring 4 kinds of psychology, health items are motivation, depression, behavior or emotion out of control, psychological subjective feeling, and a self-assessment of health change [11]. Each of the 36 items has 4~6 alternative answers representing different levels. According to different situations, give forward or reverse scores, first calculate the original scores, and then calculate the conversion scores with the standard formula. The higher the score, the lighter the functional damage, and the better the quality of life.

2.6. Statistical Analysis. The SPSS17.0 statistical software package is used for data processing, Chi-square test is used for counting data, and T-test is used for measuring data. $P < 0.05$ is statistically significant.

3. Result Analysis

This is the preoperative Lysholm score and HSS score between the knee function and the control group ($P > 0.05$). The Lysholm score, HSS score, and the range of motion of extension and flexion in the observation group were significantly better than those in the control group at different periods after knee function operation, and the difference was statistically significant ($P < 0.01$ and $P < 0.05$), as shown in Tables 2–4.

The scores of SF-36 of life in the observation group were significantly higher than those in the control group, and the difference between the two groups was statistically significant ($P < 0.05$), as shown in Figure 1.

4. Discussion

"Lingshu meridian tendon" said: "the knee is the house of tendons," and the knee is the collection of the tendons, closely connected around the knee joint. The modern anatomy refers to ligaments, muscles, joint capsule, synovial sac, cartilage, and tendons, and the anterior cruciate ligament and meniscus are the category of traditional Chinese medicine called "tendon." The tendon has the role of maintaining joint stability and maintaining joint function, such as "Class Sutra," and the tendon said: "the tendon strength is rigid, so it can restrain the bone, strong movement," and "impotence theory" said: "the main tendon bundle bone and benefit the organ also." As recorded in the ancient

Table 1: Lysholm score of knee joint.

Evaluation content	Limp	Need support	Interlock	Instable	Pain	Swell	Walk up and down stairs	Squat down
Score	5	5	15	25	25	10	10	5
Evaluation criterion	Excellent ≥ 90 points; good 80~89 points; generally 70~79 points; <70 points difference							

Table 2: Comparison of HSS function scores between two groups in different periods before and after knee joint operation (score, $\bar{x} \pm s$).

Group	n	Preoperative	After surgery		
			January	Mar.	December
Observation group	42	42.13 ± 10.37	50.11 ± 7.11	68.01 ± 5.1	84.64 ± 3.31
Control group	39	41.21 ± 10.43	47.31 ± 6.61	51.20 ± 5.1	70.10 ± 5.27

Note: Compared with the control group at different time after operation, $P < 0.01$.

Table 3: Comparison of Lysholm function scores between the two groups at different times before and after knee joint operation.

Group	n	Preoperative	After surgery		
			January	Mar.	December
Observation group	42	48.1 ± 4.3	62.1 ± 2.1	65.1 ± 3.4	84.6 ± 3.04
Control group	39	50.8 ± 5.2	60.3 ± 4.8	61.0 ± 5.2	70.1 ± 4.9

Note: Compared with the control group at different time after operation, $P < 0.05$.

Table 4: Comparison of knee flexion and extension activity between two groups ($\bar{x} \pm s$).

Group	n	Preoperative	After surgery		
			January	Mar.	December
Observation group	42	51.8° ± 5.8°	85.5° ± 2.1°	113.4° ± 7.5°	130.4° ± 5.3°
Control group	39	51.6° ± 6.4°	83.1° ± 5.8°	90.4° ± 13.1°	111.4° ± 6.8°

Note: Compared with the control group at different time after operation, $P < 0.05$.

Figure 1: Comparison of postoperative quality of life between two groups.

documents, etc., keep the normal operation of the original tendon, and it needs sufficient qi and blood, and appropriate rehabilitation training can play the role of dredge meridians, sis and qi and blood, anterior cruciate ligament, and meniscus injury after patients, and the knee structure was damaged, leading to the reinforcement loss of qi and blood, tendon meridian obstruction, tendon and clonture, and joint stiffness.

Rehabilitation training based on the automatic extraction algorithm is prone to knee anterior cruciate ligament injury caused by exercise, leading to knee joint instability, secondary joint cartilage, and meniscus wear and eventually causes joint degeneration and osteoarthritis, which seriously affects the joint function and then affects the patient's work and quality of life. Arthroscopic knee ligament reconstruction is one of the main treatment methods for anterior cruciate ligament injury. It has the advantages of less surgical trauma, quick recovery of knee joint function, and less postoperative complications, but the final postoperative effect depends on the correct postoperative rehabilitation training [12, 13]. ACL mainly improves the stability and joint function of knee joint. It is required to bear weight, stretch, and bend and has good stability after operation. If postoperative rehabilitation nursing and early functional exercise are not appropriate, knee flexion and extension are often unsatisfactory, and the recovery of knee function is an important factor to evaluate the curative effect of ACL surgery [14]. Nonstandard functional exercise after ACL reconstruction

can make the ligament after ACL reconstruction stretched, relaxed, or even broken, which cannot play its due role and seriously affect the surgical effect. The results showed that 50% of DVT occurred on the first day after operation. 30% occurred on the 2nd day after operation. Therefore, timely rehabilitation training guidance based on automatic extraction algorithm can improve local blood circulation, increase muscle strength around knees, prevent deep vein thrombosis of lower limbs, prevent adhesion and atrophy of joint capsule, soften scars, and increase joint mobility, thus preventing adhesion of tissues around joints, improving knee joint stability and joint function. Enhance ligament strength, restore muscle strength and balance ability of patients, promote functional rehabilitation, and significantly improve patients' quality of life. It also plays a very important role in the stability of knee joint and the recovery of motor function after ACL reconstruction under arthroscope, which not only ensures the safety of ligament reconstruction but also restores the affected knee to normal range of motion and stability [15, 16].

With the shift in biopsychological-social medical care mode and the gradual increase of patients undergoing arthroscopic anterior cruciate ligament (ACL) reconstruction, we need to further improve the quality of life while improving the functional activity of the knee joint. Lysholm score and HSS score as two current "gold standards" for knee function evaluation, their comprehensive evaluation can often better reflect the recovery of knee function of [17]. The results of this study show that there was no significant difference in the scores of preoperative Lysholm score, HSS score, and knee flexion activity between the observed and control patients ($P > 0.01$). Follow up in January, May, and 1 year after surgery. The observation group each stage of knee function recovery was significantly better than the control group, and Lysholm scores, HSS scores, and knee flexion activity were compared with control groups. The differences were all statistically significant ($P < 0.01$). Patients in the observed group had a significantly higher postoperative SF-36 QoL score than in the control group. The difference was statistically significant ($P < 0.01$). It shows that the observed quality of life was significantly better than the control group [18].

5. Conclusion

To sum up, rehabilitation training based on automatic extraction algorithm is effective for patients with knee anterior cruciate ligament injury caused by exercise. It can effectively reduce knee dysfunction and reduce pain, so as to promote the early recovery of patients and can provide strong support for clinical treatment, suitable for clinical promotion.

Data Availability

The data used to support the findings of this study are available from the corresponding author upon request.

Conflicts of Interest

The authors declare that they have no conflicts of interest.

References

[1] A. Derouin and J. R. Potvin, "The effect of functional knee braces on muscular contributions to joint rotational stiffness in anterior cruciate ligament-deficient and -reconstructed patients," *Journal of Applied Biomechanics*, vol. 35, no. 5, pp. 344–352, 2019.

[2] C. Clifford, C. Ayre, L. Edwards, S. Guy, and A. Jones, "Acute knee clinics are effective in reducing delay to diagnosis following anterior cruciate ligament injury," *The Knee*, vol. 30, no. 1, pp. 267–274, 2021.

[3] S. Zhang and Z. Lv, "Diagnosis and exercise rehabilitation of knee joint anterior cruciate ligament injury based on 3d-ct reconstruction," *Complexity*, vol. 2020, no. 7, Article ID 3690124, 13 pages, 2020.

[4] A. V. Korolev, A. P. Afanasyev, D. O. Il'In, D. O. Gerasimov, and P. M. Kadantsev, "Injury to the posterior cruciate ligament: biomechanics, diagnosis, treatment and prevention of secondary osteoarthritis," *Genij Ortopedii*, vol. 26, no. 3, pp. 413–419, 2020.

[5] S. R. Batchu, "Quantitative analysis of pivot shift test for anterior cruciate ligament injury of knee joint," *Journal of Evidence Based Medicine and Healthcare*, vol. 6, no. 41, pp. 2693–2696, 2019.

[6] S. J. Shultz and R. J. Schmitz, "Recent advances in prevention of primary and secondary anterior cruciate ligament injury: what does the future hold for optimizing knee-joint function?," *Kinesiology Review*, vol. 9, no. 1, pp. 1–7, 2019.

[7] T. Purevsuren, B. Khuyagbaatar, S. K. Lee, and Y. H. Kim, "Biomechanical factors leading to high loading in the anterior cruciate ligament of the lead knee during golf swing," *International Journal of Precision Engineering and Manufacturing*, vol. 21, no. 2, pp. 309–318, 2020.

[8] M. Hadzovic, P. Ilic, A. Lilic, and M. Stankovic, "The effects of a knee joint injury prevention program on young female basketball players: a systematic review," *Journal of Anthropology of Sport and Physical Education*, vol. 4, no. 1, pp. 51–56, 2020.

[9] E. A. Anastasieva, R. O. Simagaev, and I. A. Kirilova, "Surgical treatment of anterior cruciate ligament injury (review)," *Genij Ortopedii*, vol. 26, no. 1, pp. 117–128, 2020.

[10] M. Bére, Z. Svoboda, J. Gallo, R. Kalina, and J. Zapletalová, "Influence of anterior cruciate ligament reconstruction on gait kinematics," *Acta Chirurgiae Orthopaedicae et Traumatologiae Cechoslovaca*, vol. 87, no. 1, pp. 17–23, 2020.

[11] E. Hohmann, "*Editorial Commentary* : Stem Cells. They Are in the Fat Tissue, Bone Marrow, and Even in the Synovial Fluid of the Knee Joint," *Arthroscopy The Journal of Arthroscopic and Related Surgery*, vol. 37, no. 3, pp. 901-902, 2021.

[12] M. G. Mohamed, S. Shrinuvasan, and R. Chidambaram, "Role of magnetic resonance imaging in the evaluation of internal derangement of knee joint," *Journal of Evidence Based Medicine and Healthcare*, vol. 6, no. 4, pp. 234–241, 2019.

[13] U. Sudheer, C. Jayaprakash, and J. P. Ajay, "Evaluation of arthroscopic anterior cruciate ligament reconstruction using quadruple hamstring tendon graft," *Journal of Evidence Based Medicine and Healthcare*, vol. 6, no. 16, pp. 1277–1283, 2019.

[14] C. Nkanta, J. E. Nkanta, A. Ai, and O. Ndubuisi, "Hamstring autografts in arthroscopic anterior cruciate ligament

Hindawi
Scanning
Volume 2023, Article ID 9835940, 1 page
https://doi.org/10.1155/2023/9835940

Retraction

Retracted: Exploring the Clinical Point Selection Rules of Acupuncture and Moxibustion in the Treatment of Infantile Enuresis Based on Data Mining Technology

Scanning

Received 20 June 2023; Accepted 20 June 2023; Published 21 June 2023

This article has been retracted by Hindawi following an investigation undertaken by the publisher [1]. This investigation has uncovered evidence of one or more of the following indicators of systematic manipulation of the publication process:

(1) Discrepancies in scope

(2) Discrepancies in the description of the research reported

(3) Discrepancies between the availability of data and the research described

(4) Inappropriate citations

(5) Incoherent, meaningless and/or irrelevant content included in the article

(6) Peer-review manipulation

The presence of these indicators undermines our confidence in the integrity of the article's content and we cannot, therefore, vouch for its reliability. Please note that this notice is intended solely to alert readers that the content of this article is unreliable. We have not investigated whether authors were aware of or involved in the systematic manipulation of the publication process.

Wiley and Hindawi regrets that the usual quality checks did not identify these issues before publication and have since put additional measures in place to safeguard research integrity.

We wish to credit our own Research Integrity and Research Publishing teams and anonymous and named external researchers and research integrity experts for contributing to this investigation.

The corresponding author, as the representative of all authors, has been given the opportunity to register their agreement or disagreement to this retraction. We have kept a record of any response received.

References

[1] C. Ma, N. Li, and X. Zhang, "Exploring the Clinical Point Selection Rules of Acupuncture and Moxibustion in the Treatment of Infantile Enuresis Based on Data Mining Technology," *Scanning*, vol. 2022, Article ID 7928052, 6 pages, 2022.

Hindawi
Scanning
Volume 2022, Article ID 7928052, 6 pages
https://doi.org/10.1155/2022/7928052

Research Article

Exploring the Clinical Point Selection Rules of Acupuncture and Moxibustion in the Treatment of Infantile Enuresis Based on Data Mining Technology

Cuicui Ma, Nan Li, and Xu Zhang

Shijiazhuang Maternity and Child Healthcare Hospital, Shijiazhuang, Hebei 050000, China

Correspondence should be addressed to Cuicui Ma; 14095104210012@hainanu.edu.cn

Received 26 February 2022; Revised 27 March 2022; Accepted 4 April 2022; Published 27 April 2022

Academic Editor: Danilo Pelusi

In order to explore the clinical point selection rules of acupuncture and moxibustion in the treatment of infantile enuresis based on data mining technology, first, it introduces the principle of data mining technology, the global optimization strategy of information extraction + genetic search. In China Biomedical Literature Database, CNKI, Weipu, Wanfang. Use "enuresis," "enuresis," "leathering," "urinary discharge," "drowning," "bedwetting," "nocturia," "drowning," "moxibustion," "moxibustion," and "moxibustion" as search terms, take (enuresis + enuresis + urination + urination + addiction + bedwetting), (moxibustion + moxibustion + moxibustion)" as the retrieval style. The analysis of the use of moxibustion, the law of acupoint selection by different moxibustion methods, and the frequency analysis of meridian use show that most of the moxibustion methods are used (62 articles, of which 3 articles use 2 moxibustion methods), including non-suppurative moxibustion, ginger moxibustion, medicinal cake moxibustion, salt moxibustion, mild moxibustion, warm acupuncture moxibustion, bird pecking moxibustion, circling moxibustion, and warm moxibustion; among them, mild moxibustion has the highest frequency of use 24 and non-suppurative moxibustion and salt-separated moxibustion have the lowest frequency of use1; there are 4 non-moxibustion methods, which are medicated thread moxibustion methods. Different moxibustion methods for acupoint selection have their own emphasis. The 63 included literatures included 63 prescriptions for moxibustion, 11 prescriptions for acupoints. Analyzing the frequency of acupoint selection, a total of 18 ear acupoints are involved, and the total frequency of auricular acupoints is 54 times; 44 points are involved (including 1 odd point outside the meridian), the total frequency of acupoints is 300 times, and the total frequency of meridian points is 298, and the total frequency of Jingwaiqi acupoints (Sishencong) is 2. The results can provide great help for the clinical selection of acupuncture points for the treatment of infantile enuresis.

1. Introduction

The Pediatric Enuresis Treatment Association (1CCS) defines pediatric enuresis in this way, in children over 5 years of age, intermittent urinary control disorders occur during prolonged sleep at night. However, there is no consensus on the number of times to diagnose enuresis in children; However, in the survey, this standard is about once or more a month [1]. Enuresis is divided into the following four categories: primary, secondary, simple, and complex. The specific situation of secondary enuresis is that the child has been in intermittent urinary incontinence within 6 months of infancy; simple enuresis is after a bed-wetting period of more than 6 months, recurring urinary incontinence, and other situations [2]. Among these categories, children with enuresis are mostly primary simple enuresis. In response to this research question, Grevitt, M. found that children with normal family conditions have a significantly lower incidence of enuresis in children than children from abnormal families. So in social life, for example, the communicative relationship with classmates in school and the punishment of teachers, there are also fierce quarrels caused by the discord between the parents, or it may be due to poor parental management that children watch movies and TV shows that are not suitable for children. Although psychological factors are not directly related to pediatric enuresis, they are of great

significance in terms of prevention [3]. Lee, S. H. and Lim, S. believe that children with enuresis are mostly functional disorders, organic diseases do not account for a significant part of this disease, and organic disease is easy to find the cause, so it is not difficult to diagnose [4]. Chen, Q. and others believe that Western medicine has a very deep interpretation and understanding of the etiology and pathogenesis of children with enuresis, most of them are hypotheses that fail to achieve a unified understanding, so they are still in an embarrassing position in the treatment of the symptoms and not the root cause. However, in the treatment, the combination of Chinese and Western medicine should be used to treat children with enuresis, and the effect will be better [5]. At present, the clinical treatment of pediatric enuresis patients in need of medical treatment is still based on drugs, although traditional Chinese medicine has unique advantages in the treatment of children with enuresis; however, the decoction process of the drugs is relatively cumbersome, the high price and inconvenience of taking. Therefore, the study of non-drug treatments with less side effects is the main research direction and focus of current medical workers [6]. As a "green therapy," acupuncture has abandoned the disadvantages of drug treatment, it has the characteristics of safety, simplicity, effectiveness, and low price, and it has been widely used to treat enuresis in children. On the basis of current research, this topic is aimed at the disease of pediatric enuresis, a comprehensive collection and sorting of prescriptions for acupuncture and moxibustion in the treatment of infantile enuresis in recent literature, through information collection and data mining technology, analyze the acupuncture points and compatibility used in the treatment of infantile enuresis, sort out the frequency of use of acupoints and related characteristics and meridians, create a spectrum of optimal acupoints for children with enuresis, and provide theoretical support for the selection and application of acupoints for the clinical treatment of pediatric enuresis [7].

2. Method

2.1. Proposal of the Basic Principles

2.1.1. Simple Genetic Algorithm (or Serial Genetic Algorithm). GAs realize the transfer of relevant knowledge in the search process in a special form of 0/1; this allows it to be well applied in graph theory and combinatorial mathematics with 0/1 code as the result, the difficulty of genetic algorithm for global optimization problems lies in: selection of hybridization probability p_c and mutation probability p_m; the size of the group; encoding method and encoding length; how to control the convergence rate of several individuals in a group. If the convergence rate is too fast, the search process will fall into a local extreme trap, make the search process converge prematurely, and the phenomenon of "premature maturity" occurs; if the convergence speed is too slow, the search process degenerates into the traditional genetic algorithm of Monte-Carlo stochastic simulation process, genetic operations such as hybridization and mutation play an important role in the global traversal of the search process, people usually ignore the promotion of the traversal of feasible domains by the diversity of the population, and this results in blind and repetitive search [8].

2.2. Introduction of Data Mining Technology. In the basic operations of genetic algorithm initialization, hybridization, mutation, etc., people mostly realize the assignment of samples in a random way, identify the individuals involved in the cross and the location of the cross, the essence of the genetic optimization process of selecting the individuals to be mutated and the mutation position is the optimal allocation of samples in the search space of the Markov chain stability process based on the Bayesian optimal estimation principle, and it will greatly promote the stability of the Markov chain [9]. In order to realize the characterization of the search space by the sample, use the system information brought by individuals with higher fitness function values for further data mining, and make the genetic process search along the "pseudo-gradient" direction, the author combines the information extraction technology with the sampling rules in the SA method, improve the algorithm's ability to search and traverse the feasible region and the stability of the global optimal solution. The main principle of this method:

(1) It is the formation of the individual to enable the individual to effectively extract the effective information in the search space R^s, people often use random methods to generate larger samples, realize the characterization of R^s. This method is feasible to deal with the process synthesis problem in low-dimensional space, for the process synthesis problem in high-dimensional space, it is reluctant. In process system engineering, most of the comprehensive problems that people encounter are in multi-dimensional space, multivariate NLP (MINLP) problems with knowledge and experience constraints. A large number of rigid, high-order nonlinear constraints make the feasible region of the problem small, usually only occupies a small part of the variable value space. In order to enable the small sample set to fully express the effective information in the search space, avoid the generation of invalid individuals or repeated sampling of R^s, use the regular method to extract information in A [10].

(2) Mutation operation

Mutation operation is the main component of GAs; it provides the possibility for the algorithm to jump out of the local trap and realize the global traversal under the premise of ensuring the algorithm's global traversal, combine deterministic GAs with information extraction technology to realize data mining in search space.

2.3. Global Optimization Strategy of Information Extraction + Genetic Search. Under the condition of a small sample, in order to realize the effective solution of multivariate problems, the following solution strategies are adopted:

(1) In the search space, use information extraction technology to generate the initial individual set $po\ \mathrm{int}_m^d$

(2) for$(i = 0; i < m; i{+}{+})$

Centered on $po\ \mathrm{int}^d[i]$, $R[i]$ is the radius to construct the subspace $SubS^d[i]$ in S^d. In $SubS^d[i]$, a genetic algorithm based on information extraction technology is used to conduct sufficient data mining. Mark the final result of the search as $Best\_Generation[i]$.

Due to the limitations of mutation and hybridization operations, traditional GAs often fall into local extremes. It is unscientific to simply regard $\{Best\_Generation[i] | i = 1, \cdots, m\}$ as the final result of global optimization.

In order to prevent "population premature" and improve the search ability to jump out of the local extreme value trap, when the population steadily gathers in a certain area in some way, it can be considered that the system has obtained a credible global extremum solution. The generation of the information space depends on the information extraction of the search space by the initial samples. At the same time, in order to avoid the multi-peak and singularity of the objective function from causing the system to fall into a local extremum, a certain degree of information association and refinement are needed for the search results of the parallel information space. According to the characteristics of small sample information extraction, use knowledge association methods to exchange and associate information between parallel information spaces, provide guarantee for further data mining.

Specific steps are as follows:

Select n_t samples in R^s, its point set is $p_{n_t}^{(t)}$, if n_t is big enough, the point where the optimal value of the objective function on $p_{n_t}^{(t)}$ should approach the global optimal value $M.P_{n_t}^{(t)}$ can maximize the effective information in R^s under the condition of satisfying i, i, d.

Step 0: Let $t = 0$, $R^s \in R^{s,0}$, and make $x^{(-1)} = \{\phi\}$.

Step 1: The system information extraction technology is used to generate a point set $p_{n_t}^{(t)}$ with n_t points on $R^{s,t}$. Take the point in $p_{n_t}^{(t)}$ as the information center, construct the search subspace, perform deterministic and regular search for real GAs, and get the feasible solution set X_{n_t}.

Step 2: Find $x^{(t)} \in X_{n_t} \cup x^{(t-1)}$ and $M^{(t)}$ such that $M^{(t)} = f(x^{(t)}) \geq f(y), \forall y \in X_{n_t} \cup x^{(t-1)}$ here: $x^{(t-1)} = \{\phi\}$ is the empty set; $x^{(t)}$ and $M^{(t)}$ are currently the best approximations of x^* and M.

Step 3: Stop criteria: Let $r^{(t)} = \{\mathrm{r}_1^{(t)}, \cdots, \mathrm{r}_s^{(t)}\}$, $\mathrm{r}_i^{(t)}$ be the radius of the search subspace. If $\max r^{(t)} = \max(r_1^{(t)}, \cdots, r_s^{(t)}) < \delta$, here δ is a predetermined small positive number, then $R^{s,t}$ is small enough, $x^{(t)}$ and $M^{(t)}$ are accepted as approximate solutions, stop calculation. If $\max r^{(t)} \geq \delta 8$, go to the next step.

Step 4: Information association and exchange between different information spaces, in view of the small sample estimation characteristics of information extraction technology, the evolution result in the parallel search space is actually a noisy system output. Under inaccurate system output conditions, in order to avoid falling into the local extremum formed by the multi-peak and singularity of the function, improve search efficiency, adopt association rules based on deterministic information, and realize the exchange of information between different search spaces, in order to determine the information space for further searches.

Step 5: Take $x^{(t)}$ as the center and $\max r^{(t)}$ as the radius, define a new search space $R^{s,t+1}$ with a certain space shrinkage ratio, and return to step 1.

2.4. Information. China Biomedical Literature Database, CNKI, Weipu, Wanfang. Use "enuresis," "enuresis," "leathering," "urinary discharge," "drowning," "bedwetting," "nocturia," "drowning," "moxibustion," "moxibustion," and "moxibustion" as search terms, take (enuresis + enuresis + wetting + urination + addiction + bedwetting), (moxibustion + moxibustion + moxibustion) as the search formula [11].

2.5. Inclusion Criteria

(1) The document type is clinical randomized controlled or semi-randomized controlled trial

(2) The research subject was clearly diagnosed as enuresis; the diagnosis and efficacy evaluation system adopted are all recognized standards in China, such as the 1998 International Child Continence Society (ICCS) diagnostic criteria

(3) Mainly moxibustion therapy, with clear moxibustion prescription and definite curative effect

2.6. Data Extraction. Screen strictly according to the literature inclusion and exclusion criteria, if the literature involves syndrome differentiation and acupuncture points, it will be handled as 1 syndrome type and 1 prescription. Design documentation information extraction table, after the data is entered and saved, it is extracted and sorted. The data entry process was completed independently by two people and the consistency check was carried out.

3. Results and Analysis

3.1. Analysis of the Use of Moxibustion and Analysis of Acupoint Selection Rules of Different Moxibustion Methods. A total of 2528 articles were retrieved in this research; finally, a total of 63 articles were included. Analysis of the use of moxibustion found that moxibustion is mostly (62 articles, there are 3 articles using 2 kinds of moxibustion) including non-suppurative moxibustion, ginger moxibustion, medicinal cake moxibustion, salt moxibustion, mild moxibustion, warm acupuncture moxibustion, bird pecking moxibustion, circling moxibustion, and warm moxibustion; among them, mild moxibustion has the highest frequency of use 24 and non-suppurative moxibustion and salt-separated moxibustion have the lowest frequency of use1; there are 4 non-moxibustion methods, which are medicated thread moxibustion methods. Different moxibustion methods on acupoint selection have their own emphasis on acupuncture points [12]. See Table 1 for details.

Table 1: The law of selecting points for different moxibustion treatments for enuresis.

Moxibustion	Classification	Number of documents	The law of acupoint selection
Moxibustion	Non-suppurative moxibustion	1	Foot sun bladder meridian, the main acupoints on the lower waist of the Du Channel (Mingmen, Shenshu, Bladdershu, Guanyuanshu);
	Ginger moxibustion	4	① Ren Mai Zhongji, Guan Yuan is the main; ② the Backshu points (Shenshu, Bladdershu, etc.) of the waist under the foot sun bladder meridian are mainly; ③ Zusanli, the stomach meridian of foot Yangming, foot Taiyin, and spleen meridian Sanyinjiao dominate;
	Medicinal cake moxibustion	8	① Ren Mai Shenque is the master; ② Beishu acupoints (Shenshu, Bladdershu) at the waist under the foot sun bladder meridian are mainly;
	Salt moxibustion	1	Ren Mai Shenque is the master;
	Gentle moxibustion	24	① Ren Mai Zhongji and Guanyuan are the main ones; ② the Backshu points (Shenshu, Bladdershu, etc.) of the waist under the foot sun bladder meridian are mainly; ③ Footyangming stomach meridian Zusanli, foot Taiyin spleen meridian Sanyinjiao dominate, and Zushaoyin kidney meridian are dominated by Yongquan;
	Warm acupuncture	8	① Ren Mai Zhongji and Guanyuan are the main ones; ② foot Taiyin and spleen meridian are mainly Sanyinjiao; ③ the main points of Backshu (Shenshu, Bladdershu) in the lower waist of the full sun bladder meridian; ④ emphasize the selection of acupoints based on syndrome differentiation;
	Pecking moxibustion	5	① Ren Mai Guanyuan points are the main points; ② Beishu acupoints at the waist under the foot sun bladder meridian are the main points;
	Convolute moxibustion	2	① Ren Mai Zhongji, Guanyuan, and Qihai are the main ones; ② foot Taiyin and spleen meridian Sanyinjiao dominate;
	Moxibustion	9	① Ren Mai Zhongji, Guanyuan, and Qihai are the main ones; ② Beishu points (Shenshu, Bladdershu, Sanjiaoshu) at the waist under the foot sun bladder meridian are mainly; ③ Fooyangming stomach meridian Zusanli and Zutaiyin spleen meridian Sanyinjiao are the main ones;
Non-moxibustion	Medicinal thread moxibustion	4	① Governor Channel Baihui is the main one; ② Ren Mai Zhongji and guan yuan are the main ones; ③ Beishu acupoints (Shenshu, etc.) at the waist under the foot sun bladder meridian are mainly; ④ Fooyangming stomach meridian Zusanli, Zutaiyin spleen meridian Sanyinjiao are the main ones;

Table 2: Meridian analysis of moxibustion treatment of enuresis.

Meridian	Total frequency of acupoints	Frequency/%	Number of acupoints	Frequency/%
Ren Mai	104	34.9	7	15.9
Bladder Channel	77	26.1	13	29.6
Spleen Channel	33	11.4	2	4.6
Governor vessel	32	10.2	4	9.1
Stomach meridian	21	7.2	3	6.8
Stomach meridian	11	3.4	4	9.1
Heart sutra	4	1.2	1	2.3
Liver Channel	4	1.2	1	2.3
Gallbladder	2	0.7	2	4.6
Lung Channel	3	0.8	2	4.6
Large intestine meridian	2	0.7	2	4.6

3.2. Analysis of Frequency of Meridian Use. A total of 11 meridians are involved; the distribution of meridians is shown in Table 2. The meridian acupoints used are mainly concentrated in the Ren Channel and Zutaiyang Bladder Channel [13]. The acupoints belonging to Ren Mai shared 104 times, the acupoints belonging to the full sun bladder meridian share 73 times, the acupoints of the two meridians were used 177 times in total, accounted for 66.0% of the total

Table 3: Moxibustion treatment of enuresis, the top 12 acupoints used frequently.

Serial number	Acupoints	Frequency	Frequency
1	Guan yuan	46	74.5
2	Shenshu	31	47.8
3	Middle pole	27	44.3
4	Sanyinjiao	27	44.3
5	Bladdershu	21	32
6	Baihui	18	30
7	Zusanli	18	30
8	Qihai	15	25.2
9	Shenque	11	16
10	Pishu	7	12.5
11	Feishu	6	10.9
12	Yinlingquan	5	9.3

Figure 1: Moxibustion treatment of enuresis, the frequency of ear acupoint use, the first 9 acupoints.

frequency, and a total of 19 acupoints are used, accounting for 50.0% of the meridian acupoints used.

3.3. Analysis of Acupoints in the Treatment of Enuresis by Moxibustion. The 63 included literatures included 63 prescriptions for moxibustion, 11 prescriptions for acupoints. Analyze the frequency of acupoint selection, involving 18 ear acupoints, the total frequency of ear points is 54 times; 44 acupoints are involved (including 1 acupuncture point outside the meridian), and the total frequency of acupoints is 300 times, the total frequency of meridian points is 298, and the total frequency of meridian acupoints (Sishencong) is 2 [14]. Arrange the ear acupoints with the top 9 frequency of use and the 12 acupoints with the top 12 frequency of use in descending order. See Table 3 and Figure 1 for details.

Regarding NE, different countries have different diagnostic standards, the main difference is the frequency of enuresis and age. According to the definition established by the International Children's Continence Association in 2006, NE is age>5 years old, children without central nervous system disease, involuntary leakage of urine during sleep, at least twice a week for ≥3 months. According to different performance characteristics, enuresis is divided into single symptom nocturnal enuresis and compound symptom nocturnal enuresis; the enuresis discussed in this article is a kind of single-symptomatic nocturnal enuresis, refers to enuresis in which symptoms persist since childhood (the asymptomatic period does not exceed 6 months); it is representative and frequently occurs in clinical practice. Enuresis in Chinese medicine belongs to the category of "drowning," drowning was first seen in the "Internal Classics"; this name is still used in the "A-B Classic of Acupuncture and Moxibustion", or it is called enuresis, wetness, and urination [15]. The physician Wanquan of the Ming Dynasty believed that the physiological and pathological characteristics of children were more than two, "three deficiencies"; the liver often has surplus, and the spleen is often insufficient; the heart is often surplus, and the lungs are often insufficient; the kidney is often weak, and the lack of the lung, spleen, and kidney is more prominent. Children with enuresis are mostly with deficiency syndrome 0; therefore, the treatment is based on the principles of invigorating the kidney and cultivating vitality, replenishing qi and invigorating the spleen, the spleen qi can be raised, the lung qi can be lowered, the bladder can be restrained, and enuresis can be stopped. The results of this study suggest that there are many ways to treat enuresis with moxibustion, and the selection of acupoints is spread across many meridians and has obvious regularity; ear acupoints are widely used and the effect is obvious [16].

This study found that moxibustion used suspension moxibustion (including gentle moxibustion, bird pecking moxibustion, and circling moxibustion) in the treatment of enuresis, moxibustion points are based on the acupoints on the lower abdomen (Guanyuan, Qihai, etc.), the lower waist acupoints (Shenshu, Bladdershu, etc.) of the full sun bladder meridian are mainly used, and moxibustion heat can directly penetrate into the related viscera and play a direct therapeutic role. The compatibility of acupoints is an important part of the acupuncture treatment system; it has a direct impact on clinical efficacy. Faced with complex diseases, acupuncture is based on the theory, method, prescription, and acupoint theory of TCM acupuncture and moxibustion, that is, based on the differentiation of meridians and collaterals, guided by viscera differentiation, compatibility of acupoints for the cause and pathogenesis of the disease, a prescription for acupuncture and moxibustion that fits the disease syndrome is proposed for treatment. The analysis of association rules of acupoints shows that the highest support is Yidanshu, Baihui, Shenshu, Zhongji, Guanyuan, and Sanyinjiao. In terms of distribution, the meridian points used in moxibustion treatment of enuresis are mainly concentrated in Ren Channel, foot Taiyang bladder meridian, and foot Taiyin spleen meridian. The three meridians all pass through the trunk. Ren Mai and foot Taiyin spleen meridian connect to the abdomen, and the full sun bladder meridian is connected to the lower back [17]. Guanyuan, Shenshu,

Hindawi
Scanning
Volume 2023, Article ID 9872786, 1 page
https://doi.org/10.1155/2023/9872786

Retraction

Retracted: Predictive Model of Cerebral Vasospasm in Subarachnoid Hemorrhage Based on Regression Equation

Scanning

Received 20 June 2023; Accepted 20 June 2023; Published 21 June 2023

This article has been retracted by Hindawi following an investigation undertaken by the publisher [1]. This investigation has uncovered evidence of one or more of the following indicators of systematic manipulation of the publication process:

(1) Discrepancies in scope

(2) Discrepancies in the description of the research reported

(3) Discrepancies between the availability of data and the research described

(4) Inappropriate citations

(5) Incoherent, meaningless and/or irrelevant content included in the article

(6) Peer-review manipulation

The presence of these indicators undermines our confidence in the integrity of the article's content and we cannot, therefore, vouch for its reliability. Please note that this notice is intended solely to alert readers that the content of this article is unreliable. We have not investigated whether authors were aware of or involved in the systematic manipulation of the publication process.

In addition, our investigation has also shown that one or more of the following human-subject reporting requirements has not been met in this article: ethical approval by an Institutional Review Board (IRB) committee or equivalent, patient/participant consent to participate, and/or agreement to publish patient/participant details (where relevant).

Wiley and Hindawi regrets that the usual quality checks did not identify these issues before publication and have since put additional measures in place to safeguard research integrity.

We wish to credit our own Research Integrity and Research Publishing teams and anonymous and named external researchers and research integrity experts for contributing to this investigation.

The corresponding author, as the representative of all authors, has been given the opportunity to register their agreement or disagreement to this retraction. We have kept a record of any response received.

References

[1] J. Li, K. Zhou, L. Wang, and Q. Cao, "Predictive Model of Cerebral Vasospasm in Subarachnoid Hemorrhage Based on Regression Equation," *Scanning*, vol. 2022, Article ID 3397967, 6 pages, 2022.

Hindawi
Scanning
Volume 2022, Article ID 3397967, 6 pages
https://doi.org/10.1155/2022/3397967

Research Article

Predictive Model of Cerebral Vasospasm in Subarachnoid Hemorrhage Based on Regression Equation

Jianzhong Li, Kaiguo Zhou, Lei Wang, and Qiumei Cao

Department of Emergency, Beijing Tongren Hospital, Capital Medical University, 100176, China

Correspondence should be addressed to Qiumei Cao; 14211030609@stu.cpu.edu.cn

Received 24 February 2022; Revised 26 March 2022; Accepted 1 April 2022; Published 26 April 2022

Academic Editor: Danilo Pelusi

In order to explore the regression equation for the prediction model of subarachnoid hemorrhage and cerebral vasospasm, the nomogram prediction model of SCVS occurrence was established. This study is a retrospective analysis of 125 cases of aSAH admitted to a hospital; the patients were divided into SCVS group and non-SCVS group. Select SIRI as a simple and reliable marker of inflammation, analyze its correlation with SCVS and its predictive value, and analyze the predictive value of SIRI to SCVS through ROC curve. Based on the SIRI inflammation level and other related risk factors, a nomogram prediction model for the occurrence of SCVS was built. The experimental results show that the SIRI level of patients in the SCVS group was significantly higher than that of the non-SCVS group, and logistic regression analysis found that SIRI is an independent risk factor for SCVS. $SIRI = 3.63 \times 10^9/L$ is the best cutoff value for diagnosing the occurrence of SCVS. When TC = 2.24 mmol/L and SIRI = 3.63 × 10%/L, its Youden Index is the largest (0.312, 0.296) and is the best cutoff value for predicting the occurrence of SCVS; at the same time, its prediction accuracy (area under the ROC curve (AUC)), sensitivity, specificity, the positive predictive value, and negative predictive value are 0.743, 72.70%, 80.10%, 77.53%, and 94.24% and 0.725, 70.60%, 76.90%, 73.49%, and 93.59%. Nomogram prediction model establishment and evaluation combined with the results of multifactor analysis are used to build an individual nomogram prediction model. The model has good prediction consistency (C-index = 0.685, $P < 0.01$). ROC analysis results showed that the model that combined SIRI and other standard variables (AUC = 0.896, 95% CI was 0.803-0.929, $P < 0.001$) was better than the model that did not combine SIRI (AUC = 0.859, 95% CI was 0.759-0.912, $P < 0.001$) and the model based only on SIRI (AUC = 0.725, 95% CI was 0.586-0.793, $P = 0.001$) has better predictive value for SCVS. Joint SIRI will optimize the prediction performance of the nomogram model and improve the early recognition and screening capabilities of SCVS.

1. Introduction

Subarachnoid hemorrhage (SAH) is one of the diseases that seriously endangers human life and health. According to statistics, about 50~70% of SAH patients have cerebral vasospasm (CVS) complications, and about 19~46% of SAH patients progressed to delayed ischemic neurological deficit (DIND) seriously affect the prognosis of SAH [1]. Animal experiments and clinical studies have found that the incidence of CVS is biphasic, with two peak periods of early onset and late onset. A few minutes to a few hours after SAH is the first high-incidence period, mostly in the blood vessels surrounding the ruptured aneurysm with the significance of the location of the tumor-bearing artery. The second high-incidence period is usually 4-16 days after SAH, with 7-10 days being the most common; most of them are diffuse and multisegmental and have no positioning value for the tumor-bearing artery [2]. According to Poiseuille's law of hemodynamics, the blood flow per unit time is proportional to the 4th power of the vessel radius. When the blood vessel diameter changes slightly, it can produce obvious changes in cerebral blood flow [3]. In CVS patients, vasospasm, narrowing of the tube diameter, will produce symptoms of insufficient blood supply to the brain, such as increased consciousness disturbance, cerebral edema, and cerebral infarction. It is still a challenge to diagnose CVS in a timely and accurate manner. Transcranial Doppler (transcranial Doppler sonography, TCD) and angiography (digital

subtraction angiography, DSA) are currently recognized diagnostic methods, but there are still 1/4 to 1/3 of patients who cannot be diagnosed correctly; clinically, the diagnosis is often only after the deterioration of neurological function occurs; this has brought great passivity to the prevention and treatment. Therefore [4], it is very important to actively search for the risk factors of CVS and predict the occurrence of CVS. There are many risk factors for CVS that have been reported, including high blood pressure, diabetes, drinking, smoking, Hunt-Hess score, Fisher classification, fever, surgery, the total number of white blood cells, the total number of platelets, the location of the aneurysm, number of ruptures, and intraventricular hemorrhage; however, intracranial angiography is invasive and brings some risks [5]. The traditional clinical diagnosis method is based on the patient's clinical manifestations, the degree of SAH, the time after bleeding, and estimation of the weight of these objective factors such as TCD flow rate and Lindegaard rate [6]; and there are many studies focused on analyzing the relationship between TCD flow rate and CVS; however, these studies believe that only a very low or very high TCD flow rate can reliably predict CVS and did not fully consider the Lindegaard rate and VI; as a result, the diagnostic accuracy of CVS is not high. These studies also have limitations in statistical methods [7], most of the designs are retrospective studies, the appropriate statistical method should be a prospective cohort study, and a meaningful method has been used to integrate these factors and to meet the needs of clinicians to evaluate the risk of CVS in patients [8]. For more than 20 years, with the development of imaging technology, the performance of CT has improved a lot. In the current high resolution situation, grade 1 (no bleeding is seen) and grade 2 (bleeding thickness less than 1 mm) in the Fisher classification are rarely seen, and it is not exact to distinguish between grade 2 and grade 3 only by the thickness of the blood clot in the subarachnoid space [9]. Fisher classification has been unable to keep up with the needs of imaging progress. Especially when combined with intraventricular hemorrhage, the probability of concurrent CVS is high, and the Fisher classification cannot be well quantified. In 2001, Liang et al. revised the original Fisher classification, which is called the modified Fisher classification [10]. The modified Fisher classification is based on the thickness of blood in the subarachnoid space. As an independent risk factor for SCVS, the reason is presumed as follows: first, when the subarachnoid hemorrhage occurs, red blood cells are destroyed, producing a large amount of vasoconstrictors (oxyhemoglobin, adrenaline, norepinephrine, endothelin, etc.) to stimulate blood vessels, which causes strong and long-lasting spasms of blood vessels; secondly, the blood vessels running in the subarachnoid space, soaking in blood for a long time, can cause blood vessels to spasm. Furthermore, the blood clot in the subarachnoid space mechanically stretches and compresses the blood vessel wall, through nerve reflexes, etc. It can also cause vasospasm. Prolonged spasm further damages vascular endothelial cells, releasing more vasoconstrictors and creating a vicious circle and eventually SCVS. Many animal experiments and clinical studies have confirmed that the thickness and distribution range of hemorrhage determine the severity and range of vasospasm involvement to a certain extent; therefore, the modified Fisher classification, which is closely related to hemorrhage, can provide a good early warning of the occurrence of SCVS. Hunter-Hess classification is a commonly used indicator to reflect the severity of SAH patients [11]. Ryu et al. found that Hunter-Hess II~V level is an independent risk factor for SCVS [12]. According to Hsu et al., a multivariate analysis of 112 SAH patients found that Hunt-Hess IV-V grade and aging are independent risk factors for complication-like stroke [13]. The possible explanation is that there are many factors that affect Hunter-Hess classification, such as rebleeding, acute hydrocephalus, intracranial hypertension, fever, and electrolyte imbalance. Many factors can lead to a higher Hunter-Hess score; therefore, different statistical samples may draw different conclusions [14]. It shows that using Hunter-Hess classification to predict SCVS is less reliable. In addition to history of hypertension and location of aneurysm, there are differences between the two groups in 4-factor single factor analysis such as fever and ventricular hemorrhage; in the end, it failed to enter the multiple regression equation. The possible explanation is that their independent prediction of SCVS is still insufficient, not as sensitive as age and modified Fisher classification [15]. At the same time, it is not ruled out that some factors may be related to age and modified Fisher classification. Age and modified Fisher classification enter the equation; to a certain extent, it already contains information about the other 5 factors; this is exactly the advantage of using logistic regression. SCVS after subarachnoid hemorrhage is the result of multiple factors. Due to sampling errors, limited number of cases, etc., some possible risk factors have not been introduced. Therefore, to establish an accurate prediction model, it is still necessary to increase the sample size and continuously carry out prospective clinical verification. For patients with the above-mentioned risk factors in clinical work, the doctor should consider the poor clinical outcome. Diabetes in patients is due to relative or absolute lack of insulin, the organization's ability to use glucose decreases, lipoprotein lipase activity decreases, and elevated blood sugar and triglycerides gradually appear in vascular disease characterized by large and medium atherosclerosis, vascular endothelial dysfunction, and poor elasticity. The self-regulation function is impaired, resulting in ischemic or hemorrhagic cerebrovascular disease. At present, there is little literature on the relationship between diabetes history and CVS, and there is no conclusive conclusion. Most researches are on the relationship between blood glucose changes and CVS after SAH. It is generally believed that high blood sugar when SAH patients are admitted to the hospital is the result of a significant increase in catecholamines in the body and is a sign of SAH's serious condition, not a predictor of CVS. Based on the current research, in order to explore the regression equation for the prediction model of subarachnoid hemorrhage and cerebral vasospasm, the nomogram prediction model of SCVS occurrence was established. This study is a retrospective analysis of 125 cases of aSAH admitted to a hospital; the patients were divided into SCVS group and non-SCVS group. Select SIRI as a simple and reliable marker of

inflammation, analyze its correlation with SCVS and its predictive value, and analyze the predictive value of SIRI to SCVS through ROC curve. Based on the SIRI inflammation level and other related risk factors, a nomogram prediction model for the occurrence of SCVS was built. There are 19 cases of aSAH patients complicated with SCVS after operation; the incidence rate was 15.20% (19/125). In SCVS group and non-SCVS group, smoking, hypertension, Hunt-Hess classification at the hospital, and the number of aneurysms, combined with intraventricular hemorrhage (IVH), have significant differences in modified Fisher classification, triglyceride (TC), monocyte count, and SIRI level ($P < 0.01$). Multivariate logistic regression analysis shows that, complicated with hypertension, Hunt-Hess classification in hospital (level IV~V), combined IVH, modified Fisher classification (IV~V grade), and high TG level and SIRI level are independent risk factors for SCVS in aSAH patients ($P < 0.05$). It has been verified that the model has good prediction consistency (C-index = 0.685, $P < 0.01$). ROC analysis results show that the model that combines SIRI and other standard variables (AUC = 0.896, 95% CI is 0.803-0.929, $P < 0.001$) is better than the model that does not incorporate SIRI (AUC = 0.859, 95% CI is 0.759-0.912, $P < 0.001$) and the model based only on SIRI (AUC = 0.725, 95% CI is 0.586-0.793, $P = 0.001$) has better predictive value for SCVS. Further conduct AUC hypothesis test, and it was found that the difference between AUC combined with/not combined with SRI model and AUC Yige with SIRI model was statistically significant ($Z = 4.029$, $P < 0.001$; $Z = 3.734$, $P = 0.003$). SIRI is closely related to SCVS after aSAH, and combined with SIRI, a Nomogram model will optimize the prediction performance and improve the early recognition and screening ability of SCVS occurrence.

2. Method

2.1. Information. Retrospectively analyze the data of 125 aSAH cases admitted to a hospital; among them, there were 45 males and 80 females, aged 24-86 years old, with an average of 56.0012.00 years old. Admission criteria are as follows: admitted to the hospital within 24 hours of onset and patients who were diagnosed with aSAH after admission and underwent early surgery within 3 days. Exclusion criteria are as follows: accompanied by serious medical diseases or other central nervous system diseases and before the operation, there was cerebral vasospasm. For those who died during hospitalization or withdrew from the study, the basic information is shown in Table 1.

2.2. Method. The patients were divided into SCVS group and non-SCVS group. Collect the age, gender, and personal history of the 2 groups of patients (smoking: in the past year, smoking ≥1 cigarettes a day on average; drinking: drinking ≥1 times a day on average), comorbidities (hypertension and diabetes), body mass index, Hunt-Hess classification at admission, aneurysm parameters (aneurysm diameter, location, and number), timing of surgery (ultraearly stage: <24 h; early stage: >24-72 h), surgical methods (craniotomy, clipping, and vascular embolization), and other information. Based on the characteristics of the first CT, the patients were modified Fisher grading, and record the presence or absence of intraventricular hemorrhage (IVH). At the same time, all patients collected 6 mL of venous blood after hospitalization for related laboratory tests, record in detail the blood sample test time, triglyceride (TC) level, white blood cell count, neutrophil count, lymphocyte count and monocyte count, and other laboratory indicators, and calculate SIRI: SIRI = Monocyte count × neutrophil count/lymphocyte count.

2.3. Statistical Methods. Use SPSS23.0 for data analysis. First, perform a normality test on all measurement data, the measurement data conforming to the normal distribution are expressed by the mean and standard deviation, and the comparison between groups is by t test [16]. Measurement data that does not conform to the normal distribution are represented by $[M(Q_{25}, Q_{75})]$; the Mann-Whitney U nonparametric test was used for comparison. The counting data is represented by $(n(\%))$; the x-test is used for comparison. The variables of $P < 0.01$ are included in the multivariate logistic regression analysis, and determine the risk factors for SCVS. According to the results of multifactor analysis, the rms installation package in R3.4.0 software was used to establish the nomogram prediction model. Finally, draw the receiver operating characteristic (ROC) curve to evaluate the predictive value of SIRI and predictive models for the occurrence of SCVS with inspection level $a = 0.05$, two-sided inspection.

3. Results and Analysis

3.1. Comparison of Basic Data of the Two Groups of Patients. There are 19 cases of aSAH patients complicated with SCVS after operation, the incidence rate was 15.20% (19/125) with Hunt-Hess grade, number of aneurysms, combined IVH, modified Fisher grade, TG, and monocyte count at admission of SCVS group and non-SCVS group, and there is a significant difference in SIRI level ($P < 0.01$) (see Table 2).

3.2. Multifactor Analysis. Multivariate logistic regression analysis shows that, combined with hypertension, Hunt-Hess classification in hospital (level IV-V), combined with IVH, modified Fisher classification (Level IV-V), and high TG level and SIRI level are independent risk factors for SCVS in aSAH patients ($P < 0.05$) (see Table 3).

3.3. ROC Cutoff Value. Plot the ROC curve to determine the index cutoff value, convert continuous variables (TG, SIRI) into binary variables. The results show that when TC = 2.24 mmol/L and SIRI = 3.63 × 10%/L, its Youden Index is the largest (0.312, 0.296) and is the best cutoff value for predicting the occurrence of SCVS; at the same time, its prediction accuracy (area under the ROC curve (AUC)), sensitivity, specificity, positive predictive value, and negative predictive value are 0.743, 72.70%, 80.10%, 77.53%, and 94.24% and 0.725, 70.60%, 76.90%, 73.49%, and 93.59%. Nomogram prediction model establishment and evaluation combined with multifactor analysis results are used to build an individual nomogram prediction model [17]. It has been verified that the model has good prediction consistency (C-

Table 1: Comparison of general data of patients in SCVS group and non-SCVS group.

Factor		SCVS group	Non-SCVS group	$t/x^2/z$	P
Age		58.31 ± 13.415	55.37 ± 11.88	-0.976	0.331
Gender	Man	5 (26.31)	40 (37.75)	0.913	0.341
	Women	14 (73.69)	66 (62.24)		
Smoking	Yes	10 (52.62)	24 (22.63)	7.318	0.007
	No	9 (47.38)	82 (77.35)		
Drinking	Yes	7 (36.82)	24 (22.65)	1.742	0.187
	No	12 (63.14)	82 (77.38)		
Hypertension	Yes	15 (78.94)	36 (33.97)	13.499	0.001
	No	4 (21.051)	70 (66.07)		

Table 2: Comparison of various indicators between CVS group and non-SCVS group.

Factor		SCVS group	Non-SCVS group	$t/x^2/z$	P
Hunt-Hess classification	IV-V	11 (57.88)	28 (26.41)	7.439	0.007
	I-III	8 (42.12)	78 (73.57)		
Number of aneurysms	Multiple shots	5 (26.33)	12 (11.31)	3.082	0.078
	Single shot	14 (73.69)	94 (88.69)		
Merged IVH	Yes	11 (57.88)	23 (21.71)	10.662	0.001
	No	8 (42.10)	83 (78.32)		
Improved fisher classification	IV-V	12 (63.15)	25 (23.59)	12.109	0.001
	I-III	7 (36.86)	81 (76.43)		
TG		1.81 (1.39, 2.08)	1.28 (0.93, 1.64)	-3.414	0.001
Monocyte count		0.61 (0.51, 0.72)	0.41 (0.28, 0.63)	-3.231	0.001
SIRI		3.91 (1.94, 6.93)	2.39 (1.53, 4.54)	-2.282	0.021

Table 3: Multivariate analysis of SCVS in postoperative patients with aSAH.

Factor	β	Standard error	Woldx^2	OR value	95% CI	P value
Hypertension	2.298	0.853	7.172	4.653	1.847-23.584	0.006
Hunt-Hess classification	1.553	0.771	4.100	3.778	1.052-16.716	0.042
Merged IVH	2.305	0.956	5.807	4.035	1.538-20.453	0.017
Improved Fisher classification	2.566	0.967	7.055	5.021	1.959-28.554	0.009
TG	1.611	0.568	8.017	3.001	1.641-10.249	0.005
SIRI	0.332	0.163	4.075	1392	1.011-1.932	0.043

index = 0.685, $P < 0.01$). ROC analysis results show that the model that combines SIRI and other standard variables (AUC = 0.896, 95% CI is 0.803-0.929, $P < 0.001$) is better than the model without SIRI (AUC = 0.859, 95% CI is 0.759-0.912, $P < 0.001$) and only the model based on SIRI (AUC = 0.725, 95% CI is 0.586-0.793, $P = 0.001$) has better predictive value for SCVS [18] (see Figure 1). A further hypothesis test of AUC was performed, and it was found that the difference between the AUC combined with/not combined with SIRI model and the AUC model based on SIRI only was statistically significant ($Z = 4.029$, $P < 0.001$; $Z = 3.734$, $P = 0.003$); however, there was no statistically significant difference between AUC combined with SIRI model and AUC without SIRI model ($Z = 1.629$, $P = 0.1033$).

During the occurrence and development of SCVS, neuroinflammatory response is the first important driving force. Therefore, by examining various inflammation indicators and their dynamic changes, it is of great significance to understand the patient's condition and predict the occurrence of SCVS [19]. With the deepening of research, the key roles of nuclear transcription factors and interleukins have gradually been emphasized. However, these testing items require special instruments and equipment, and the price is relatively high, and the clinical application is restricted. SIRI is a new type of complex inflammation marker based on traditional inflammatory cell count, which can more comprehensively reflect the body's inflammatory state. At the same time, it has the advantages of convenient

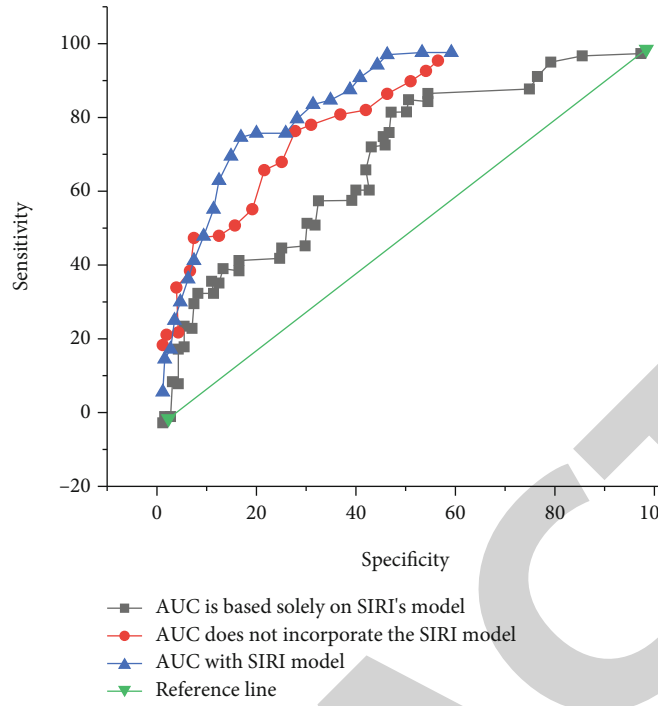

Figure 1: The ROC curve of SIRI predicting the occurrence of SCVS in aSAH patients after surgery.

detection, strong repeatability, and low price; it has become a good factor for predicting the occurrence, development, and prognosis of various diseases. In this study, SIRI was selected as a simple and reliable marker of inflammation, its correlation with SCVS and its predictive value have been analyzed, the results showed that the SIRI level of patients in the SCVS group was significantly higher than that of the non-SCVS group, and logistic regression analysis found that SIRI is an independent risk factor for SCVS. SIRI is a comprehensive index based on the absolute value of peripheral blood neutrophils, monocytes, and lymphocytes, representing different inflammatory and immune pathways in the body. The high SIRI state reflects the strong monocyte and neutrophil-mediated proinflammatory response and the weak or suppressed lymphocyte-mediated anti-inflammatory response; this aggravated the pathological degree of cerebral blood vessels after aSAH and induced the occurrence of SCVS. This study also analyzed the predictive value of SIRI to SCVS through the ROC curve. The results show that $SIRI = 3.63 \times 10^9/L$ is the best cutoff value for diagnosing the occurrence of SCVS. When $SIRI > 3.63 \times 10^9/L$, it can be considered that the patient has a high inflammation state; there is a risk of concurrent SCVS. At the same time, in order to further explore and visualize the predictive effectiveness of SIRI, in this study, a nomogram predictive model of SCVS was built based on the level of SIRI inflammation and other related risk factors. It has been verified that the C-index and the area under the ROC curve of the model are all good; it has reliable predictive efficiency and consistency and is suitable for clinical use. For example, a patient has a history of hypertension, Hunt-Hess grade IV-V at the time of admission, modified Fisher grade IV-V, combined with ventricular hemorrhage, $TG = 1.46mm ol/L$, and $SIRI = 4.85 \times 10^9/L$, through the nomogram model scoring line; the patient's total score is 365 points (94 + 73 + 98 + 87 + 0 + 39); the corresponding risk prediction value is 0.754; that is, the patient has a 75.4% probability of complicated SCVS. Nomogram can quickly and intuitively predict the probability of patients with SCVS and achieve individualized prediction [20].

4. Conclusion

Retrospectively analyze the data of aSAH patients admitted to a hospital, discuss the value of SIRI's assessment of SCVS, and based on the SIRI level to build a simple and reliable nomogram prediction model, nomogram can quickly and intuitively predict the occurrence probability of patients with SCVS and realize individualized prediction. SIRI is closely related to SCVS after aSAH, and the nomogram model constructed with SIRI will optimize the prediction efficiency and improve the ability of early identification and screening of SCVS.

Data Availability

The data used to support the findings of this study are available from the corresponding author upon request.

Conflicts of Interest

The authors declare that they have no conflicts of interest.

Hindawi
Scanning
Volume 2023, Article ID 9871261, 1 page
https://doi.org/10.1155/2023/9871261

Retraction

Retracted: Intervention of Fluency and Anxiety in Mindfulness Training of Shooting

Scanning

Received 3 October 2023; Accepted 3 October 2023; Published 4 October 2023

This article has been retracted by Hindawi following an investigation undertaken by the publisher [1]. This investigation has uncovered evidence of one or more of the following indicators of systematic manipulation of the publication process:

(1) Discrepancies in scope

(2) Discrepancies in the description of the research reported

(3) Discrepancies between the availability of data and the research described

(4) Inappropriate citations

(5) Incoherent, meaningless and/or irrelevant content included in the article

(6) Peer-review manipulation

The presence of these indicators undermines our confidence in the integrity of the article's content and we cannot, therefore, vouch for its reliability. Please note that this notice is intended solely to alert readers that the content of this article is unreliable. We have not investigated whether authors were aware of or involved in the systematic manipulation of the publication process.

In addition, our investigation has also shown that one or more of the following human-subject reporting requirements has not been met in this article: ethical approval by an Institutional Review Board (IRB) committee or equivalent, patient/participant consent to participate, and/or agreement to publish patient/participant details (where relevant).

Wiley and Hindawi regrets that the usual quality checks did not identify these issues before publication and have since put additional measures in place to safeguard research integrity.

We wish to credit our own Research Integrity and Research Publishing teams and anonymous and named external researchers and research integrity experts for contributing to this investigation.

The corresponding author, as the representative of all authors, has been given the opportunity to register their agreement or disagreement to this retraction. We have kept a record of any response received.

References

[1] W. Liu, "Intervention of Fluency and Anxiety in Mindfulness Training of Shooting," *Scanning*, vol. 2022, Article ID 6069561, 5 pages, 2022.

Hindawi
Scanning
Volume 2022, Article ID 6069561, 5 pages
https://doi.org/10.1155/2022/6069561

Research Article

Intervention of Fluency and Anxiety in Mindfulness Training of Shooting

Wei Liu

School of National Security, People's Public Security University of China, Beijing 100038, China

Correspondence should be addressed to Wei Liu; 31115207@njau.edu.cn

Received 26 February 2022; Revised 27 March 2022; Accepted 4 April 2022; Published 26 April 2022

Academic Editor: Danilo Pelusi

Introduction. Mindfulness cognitive therapy is based on mindfulness decompression, integrating the elements of cognitive behavioral therapy and related psychological education components, a set of mindfulness group courses designed. *Objective*. In order to explore the influence of mindfulness training on fluency and anxiety in shooting sports training. *Methods*. There are 22 athletes in a provincial shooting team, 12 in the experimental group and 10 people in the control group, grouped according to the random principle. A single-participant experiment design with multiple baseline levels of ABA was adopted. *Results*. The fluency state of the athletes has increased from 28.75 to 30.63; the average value before the intervention increased by 6.5%, PEM = 88%, explaining that the previous intervention has a moderate-intensity effect. The average value of athletes' sports competition anxiety state 205 before intervention was reduced to 171.25, reduced by 16.5%, PEM = 100%, showing that the intervention effect is very effective. *Conclusions*. After the shooting athletes received the intervention of the mindfulness cognitive intervention method MBCT, the state of fluency is improved, the level of competition anxiety is reduced, and the experimental intervention basically confirmed the research hypothesis. This study confirms the moderating role of emotion regulation self-efficacy between mindfulness and the fluency of shooters and provides further impetus for the refinement and development of a push-up spiral model that explains mindfulness mechanisms.

1. Introduction

Mindfulness-based cognitive therapy (MBCT) is based on mindfulness decompression, integrating the elements of cognitive behavioral therapy and related psychological education components, a set of mindfulness group courses designed. After MBCT was launched more than ten years ago, it has received a lot of clinical and laboratory research support [1]. Mindfulness cognitive therapy is built on two important sources: intensive mindfulness practice derived from eastern traditional wisdom and modern western cognitive behavioral therapy. Although the two belong to two systems, there are common goals: understand people's hearts and reduce or alleviate mental distress. People's susceptibility is an overreaction to low mood; this often manifests itself in two ways: experience avoidance—try to avoid unwanted experiences; rumination of the mind is to use the mind to solve the problem of the mood [2]. Shooting is a static, non-confrontational project, requiring a high degree of concentration. And the fluency state can get rid of distracting thoughts, a "peak experience" in which full attention is paid. In this state, athletes can devote themselves to the activities they engage in, in order to enter a state of personal stability, both internal and external interfering athletes can be automatically shielded. And it can let athletes in the process of training or competition immerse in the fun of the activity itself and have a sense of control over the action process [3, 4]. Many studies have shown that mindfulness helps promote fluency experience. Mindfulness includes awareness and conscious attention to the experience of the moment, in a way that does not require judgment and acceptance. Survey shows the challenge of a high degree of mindfulness and fluency experience—technical balance, clear goals, clear physical feedback, attention, awareness of action, and disinterestedness; these six dimensions are closely related [5]. These tasks are much simpler for athletes to understand

the concepts than they actually do, and mindfulness training can guide them through the mental skills they need to successfully build.

2. Method

2.1. Research Objects. 22 athletes were from a provincial shooting team (9 males and 13 females), 12 people in the experimental group and 10 people in the control group, grouped according to the random principle. Due to the loss of training athletes and the effectiveness of the athlete's questionnaire, the participation attitude issues lead to the loss of subjects; a total of 14 shooters (3 males and 11 females) completed the entire intervention plan. Age range is 15-31, with average age 22. The training period is 2-20, and the average training period is 9. The grouping situation is as follows: 8 people in the experimental group (2 males and 6 females, with an average age of 22.3 ± 5.7 and an average training period of 8.5 ± 5.6) and there were 6 people in the control group (1 male and 5 females, with an average age of 21.3 ± 6.9 and an average training period of 8.7 ± 6.1). There was no difference in the level of athletes between the experimental group and the control group.

2.2. Research Tools. Simplified dispositional flow scale (SDFS): there are 9 questions in this short form; each item is used to measure one of the 9 dimensions of fluency, through the fluency experienced by the subjects in a given situation (such as training and competition situations), and use the 5-point scoring method to answer. The internal consistency reliability of the scale is $a = 0.70$, and the test-retest reliability is $r = 0.70$.

2.3. Data Collection and Statistics. Respectively, on the first (start of intervention), third, fifth, seventh (end of intervention) [6], and fifteenth weeks (tracking test), use the Chinese Mindfulness Questionnaire (CMSS) for athlete training games, measure the participant's mindfulness level, use repeated measures analysis of variance to test the effect of the intervention, and analyze the changes in the level of mindfulness of shooting athletes.

2.4. Mindfulness Training Methods. During the seven weeks of mindfulness training, select the time points of the first, third, fifth, and seventh weeks, respectively; measure the mindfulness level of the shooter, and in the eighth week (that is, the fifteenth week) after the training, a follow-up test will be conducted. The Chinese Mindfulness Questionnaire (CMSS) was used to measure training and competitions for athletes. In the testing process of mindfulness training, according to the principle of voluntariness and balance, divide all athletes who participated effectively into an experimental group of 8 people and 6 people in the control group.

3. Results

3.1. Analysis of the Effectiveness of Mindfulness Training. The data will be measured in the first, third, fifth, seventh, and fifteenth weeks, stored in the data file with five variables $t1 \sim t5$, respectively, and in accordance with the method and procedure of repeated test analysis of variance, the analysis was carried out in the Chinese version of SPSS 18.0.

Table 1: Calculation results of the variation part between groups.

Source	Type IV sum of squares	df	Mean square	FS	Sig.
Intercept	111723.822	1	111723.822	1815.317	0.000
Grouping	18.404	1	18.404	0.217	0.473
Error	727.156	11	60.413		

First, the existence of a correlation between the repeated measurements was determined by the results of the spherical test.

Immediately after the second step, analyze the role of time and grouping factors and the interaction between time and grouping; the calculation results of the variation part in each body show that the time factor is statistically significant ($P < 0.05$), explaining that the measurement index has a tendency to change over time. But the interaction between time and grouping is close to significant ($P = 0.055$), explaining that the role of the time factor varies with different groups. The calculation results of the variation part between the groups are shown (see Table 1); the statistical significance of the grouping effect is not significant ($P > 0.05$), explaining that the grouping factor does not work; the difference of mindfulness intervention between the experimental group and the control group was not obvious.

With the help of the Plots submenu, the repeated measurement indicators of St are all trend graphs, which can intuitively see the change trend of the measurement index over time, as shown in Figure 1. It can be seen from the figure that starting from the third test (that is, the fifth week), compared with the control group, the experimental group has a significant improvement in the level of mindfulness; in the fourth test (that is, the seventh week), the level of mindfulness continued to be high.

In the follow-up test (the fifteenth week), the mindfulness level of the experimental group had a downward trend, while the control group did not change significantly.

3.2. The Role of Self-Efficacy in Emotional Regulation between Mindfulness and Fluency. The fluency score of the athletes is shown in Figure 2.

Figure 2 shows the scores of athletes in the trait fluency state. From the preintervention average of 28.75 to 30.63, increased by 6.5%, PEM = 88%, it shows that the previous intervention has a moderate-intensity effect. The score span has increased from 26-30 to 25-33; it shows that the fluency state of the athletes still fluctuates greatly during the 8 weeks of intervention. In particular, in the 4th week of the intervention, the fluency score dropped significantly, because that week the athlete's emotional dissatisfaction affected his mood. In the later follow-up investigation, the average value was 35.34, an increase of 22.9% compared to before the intervention, PEM = 100%; it shows that the intervention effect is significant. The score span has been shortened from 25-33 to 35-36, and the fluency state is more stable than

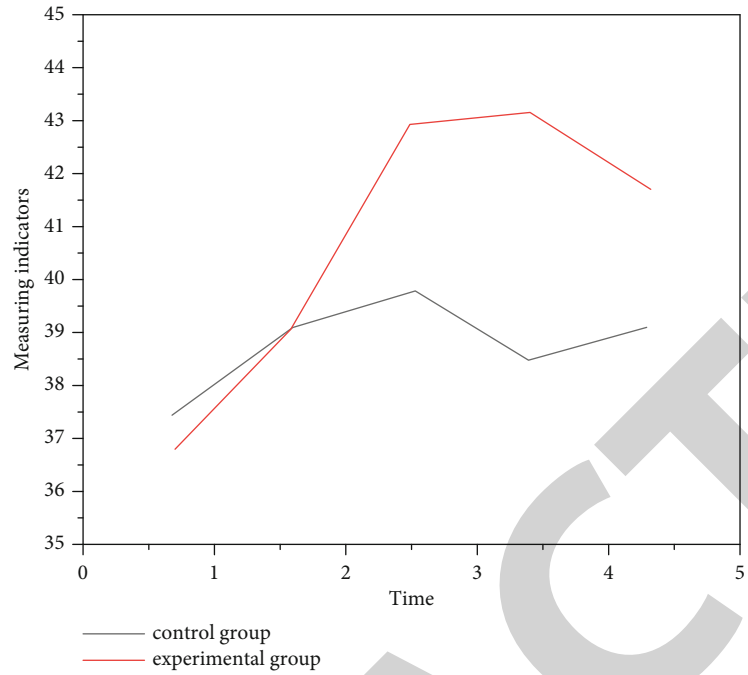

Figure 1: The trend chart of the mean change of the 5t repeated measurement index in each group.

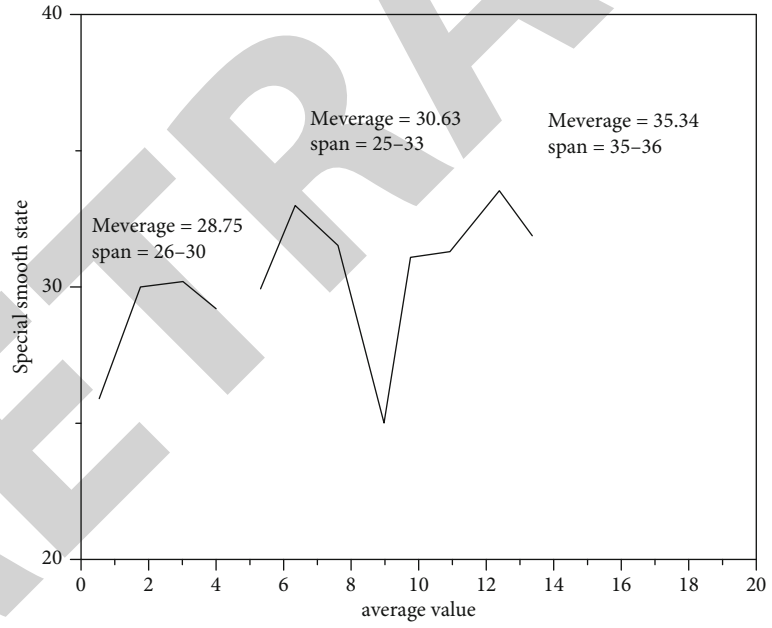

Figure 2: Fluency score.

expected. And the scores are higher than the baseline value, indicating that the intervention has a good sustained effect. The scores of athletes in the anxiety state of sports competitions are shown in Figure 3.

The scores of athletes in the anxiety state of sports competitions are shown in Figure 3. From the preintervention average 205 to 171.25, a decrease of 16.5%, PEM = 100%, showing that the intervention effect is very effective. The score span increased from 190-220 to 150-190; it shows that the athlete's anxiety state is relatively unstable during the intervention period; mood swings are greater. As shown in the figure, in the athletes in the first 3 weeks of the intervention, the effect of improving anxiety is not obvious; starting from the 4th week, the anxiety value has been greatly reduced and continues to maintain a stable state. In the follow-up survey, the average was 166.67; it was 18.7% lower than before the intervention, PEM = 100%, and the anxiety value is higher than the baseline value, indicating that the intervention effect is significant. The score span has been shortened from 150-190 to 160-170; it shows that the anxiety level maintains a relatively stable state, and the intervention has a good sustained effect.

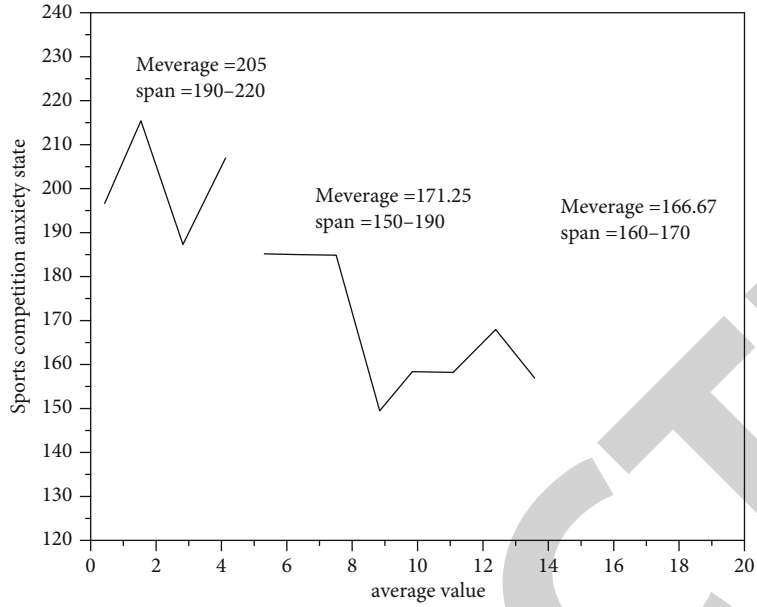

Figure 3: Score of anxiety state in sports competition.

4. Discussion

The above analysis results show that the level of mindfulness of shooting athletes has increased significantly, that is, the time factor is significant. The interaction between time and grouping is close to significant, indicating that grouping has a certain effect. And to examine the effect of grouping separately, it shows that the effect is not statistically significant [7, 8]. This shows that the whole seven weeks of mindfulness training has its effect, and to examine the effects of grouping factors separately, statistically significant, it may be due to the following reasons. (1) The control group was followed up with relevant questionnaires; athletes with strong learning and comprehension ability can also learn in the questionnaire; the measured level of mindfulness will increase; this is an invisible learning. (2) Due to the characteristics of athlete management, the control group members who get along day and night may inquire about learning related content in the experimental group members; this is a phenomenon similar to "stealing." (3) Although some mindfulness exercises will be done in the training class, the team members rarely did mindful breathing and body scanning exercises after class, so, at most, it is just a clarification of cognition in class, or the guidance of some adjustment methods is working, and the athletes did not experience the process of actively internalizing mindfulness practice, so as shown in Figure 1, in the follow-up test, the mindfulness level of the experimental group decreased, while that of the control group hardly changed [9]. This time between mindfulness and the fluency of shooting athletes introduce emotion regulation self-efficacy as a regulation variable, and the interaction with mindfulness affects the fluency state [10].

5. Conclusion

The author tries to examine shooting athletes through experiments; after receiving the mindfulness cognitive therapy intervention method, the fluency state can be improved, and the level of competition anxiety has been reduced. From the "simplified trait fluency scale" experimental data analysis, PEM effect analysis, and data analysis of social validity evaluation, all provided support for the intervention effect of this study, it shows that the intervention effect is significant and has good sustainability.

Data Availability

The data used to support the findings of this study are available from the corresponding author upon request.

Conflicts of Interest

The author declares that there are no competing interests.

Authors' Contributions

The author made significant contributions to this manuscript. Wei Liu was responsible for writing and performing surgeries, data analysis and performing surgeries, and article review and intellectual concept of the article.

References

[1] L. Smith, V. Argentina, J. Price, and C. O'Brien, "The mobile physical activity and cognitive training app for older adults," *Computers, informatics, nursing: CIN*, vol. 38, no. 11, pp. 537–542, 2020.

[2] M.-H. Cristina, L.-E. Fidel, M. J. Maria et al., "A pilot test for a one-year cognitive training intervention in elderly adults with mild cognitive impairment," *Biomedical and Environmental Sciences*, vol. 33, no. 10, pp. 66–72, 2020.

[3] J. Krans, G. Bosmans, E. Salemink, and R. De Raedt, "Cognitive bias modification of expectancies (CBM-E): effects on interpretation bias and autobiographical memory, and